

Synthesis of Co and Ni Complexes for Stereoselective Hydrogenation Catalysis

by

Dylan J. Hale

Submitted for partial fulfillment of the requirements
for the degree of Doctor of Philosophy

Dalhousie University
Halifax, Nova Scotia
April 2023

©Copyright by Dylan J. Hale, 2023

Table of Contents

Table of Contents	ii
List of Tables	vi
List of Figures	vii
List of Schemes	x
Abstract	xv
List of Abbreviations and Symbols Used	xvi
Acknowledgements	xvii
Chapter 1: Introduction	1
1.1 Overview	1
1.2 Base Metal Pincer Ligand Design	4
1.3 First Row Silyl Metal Pincer Complexes	12
1.4 First-Row Metal Catalyzed Asymmetric Hydrogenation.....	26
Chapter 2: Synthesis and Characterization of (Cy-PSiP)Co^I Complexes for Catalytic Alkene Hydrogenation	43
2.1 Introduction	43
2.2 Results and Discussion.....	49
2.2.1 Synthesis and Characterization of (Cy-PSiP)Co ^I Alkyne Complexes ...	49
2.2.2 (Cy-PSiP)Co Catalyzed Alkene Hydrogenation	54
2.2.3 DFT Mechanistic Investigation.....	56
2.3 Summary and Conclusions.....	60
2.4 Experimental	62

2.4.1 General Considerations	62
2.4.2 Synthetic Procedures and Characterization Data	62
Chapter 3: (PSiP)Ni-Catalyzed (<i>E</i>) – Selective Semihydrogenation of Alkynes with Molecular Hydrogen	67
3.1 Introduction	67
3.2 Results and Discussion.....	72
3.2.1 Substrate Scope.....	72
3.2.2 Mechanistic Inquiry	78
3.3 Summary and Conclusions.....	82
3.4 Experimental	83
3.4.1 General Considerations.....	83
3.4.2 Synthetic Procedures and Characterization Data	84
Chapter 4: Cobalt Catalyzed Asymmetric Hydrogenation of Dehydro-α- Amino Acids Enabled by Phen-DalPhos Ligation	86
4.1 Introduction	86
4.2 Results and Discussion.....	90
4.2.1 Ligand Synthesis.....	90
4.2.1 Synthesis of Co Complexes	91
4.2.2 Catalysis Optimization.....	94
4.2.3 Substrate Scope.....	96
4.2.4 Deuterium Labeling Studies	99

4.3 Summary and Conclusions	101
4.4 Experimental	101
4.4.1 General Considerations	101
4.4.2 Synthetic Procedures and Characterization Data	102
Chapter 5: Synthesis and Characterization of Chiral (Phosphino)Silyl Ligands for Asymmetric Hydrogenation Catalysis	109
5.1 Introduction	109
5.2 Results and Discussion.....	110
5.2.1 Synthesis of Chiral PSi Ligands	110
5.2.2 Synthesis of Chiral (PSi)Ni Complexes.....	115
5.2.3 (PSi)Ni-Mediated Asymmetric Hydrogenation of Enamides	117
5.2.4 Alternative Chiral PSi Ligation	120
5.3 Summary and Conclusions.....	128
5.4 Experimental	130
5.4.1 General Considerations.....	130
5.4.2 Synthetic Procedures and Characterization Data	131
Chapter 6: Conclusions and Future Work.....	142
6.1 Summary and Conclusions.....	142
6.2 Future Work	146
References	152
Appendix A: Crystallographic Experimental Details.....	178

Appendix B: Selected NMR Spectra and HPLC Chromatograms for Reported Compounds.....	194
Appendix C: Thermochemical Energies and Cartesian Coordinates for Computationally Modeled Compounds	402
Appendix D: Copyright Agreements.....	442

List of Tables

Table 3.2.1. Hydrogenation of alkenes catalyzed by 1-32 . ^a	73
Table 4.2.1. Pre-catalyst screen.....	95
Table 5.2.1. Catalyst screen of chiral P <i>Si</i> -supported Ni complexes for the asymmetric hydrogenation of <i>N</i> -(3,4-dihydro-1-naphthalenyl)acetamide	118
Table 5.2.2. Asymmetric hydrogenation results for <i>dehydro-N</i> -acetyl-phenylalanine and its methyl ester employing 5-4 and 5-5 as pre-catalysts.	120
Table 5.2.3. Asymmetric hydrogenation results for (<i>Z</i>)-2-acetamido-3-phenylacrylate catalyzed by 5-7	124
Table 5.2.4. Results for the asymmetric hydrogenation of <i>N</i> -(3,4-dihydro-1-naphthalenyl)acetamide catalyzed by 5-7	125
Table 5.2.5. Results for the asymmetric hydrogenation of <i>N</i> -(3,4-dihydro-1-naphthalenyl)- <i>tert</i> -butylamide catalyzed by 5-7 or a combination of Ni(COD) ₂ and 5-6	126

List of Figures

Figure 1.1.1. Common tridentate pincer ligand motifs.	2
Figure 1.1.2. Ligands employed in this work: the chemistry of Cy-PSiP A with Co is described in Chapter 2; the chemistry of ⁱ Pr-PSiP ^{Ind} B with Ni is described in Chapter 3; the chemistry of (<i>S</i>)-Ph-PhenDalPhos C with Co is described in Chapter 4; and the chemistry of (<i>R,R</i>)-IndolSi with Ni is described in Chapter 5.	3
Figure 1.2.1. (A) Examples of Fe and Co complexes featuring strong field ligands that support two-electron reactivity at the metal center. (B) Examples of Fe complexes supported by redox non-innocent PDI ligation	6
Figure 1.2.2. Structures of mono, bis, and tris(phosphino)silyl ligand precursors reported by Stobart, ³² Peters, ³³ and Turculet. ³⁶	11
Figure 1.3.1. Possible structural formulations for the species arising from exposure of 1-55 to an atmosphere of H ₂ . (Top) examples of Co ^{III} dihydride complexes (bottom) examples of nonclassical Co ^I dihydrogen complexes.....	23
Figure 2.1.1. Selected examples of homogeneous Co catalysts for the hydrogenation of alkenes featuring redox non-innocent ligands, ligands capable of engaging in metal-ligand cooperativity, and strong field ligands.	44
Figure 2.1.2. Ligand based H ₂ storage as a metal-ligand cooperative strategy.	46
Figure 2.2.1. (<i>Left</i>) Crystallographically determined structure of 2-1 , with thermal ellipsoids shown at the 30% probability level. Hydrogen atoms have been omitted for clarity. Selected interatomic distances (Å) and angles (°): Co-C(2) 1.8535(18), Co-C(3) 1.8976(18), C(2)-C(3) 1.3112(18), Co-P(1) 2.2091(5), Co-P(2) 2.1977(5), Co-Si 2.1884(5), C(1)-C(2) 1.492(3), C(2)-C(3) 1.296(3), C(3)-C(4) 1.495(3), Si-Co-C(2) 91.14(6), Si-Co-C(3) 107.90(6), P(1)-Co-P(2) 107.959(18), P(1)-Co-Si 88.879(17), P(2)-Co-Si 84.837(18), P(2)-Co-C(2) 102.69(6), P(1)-Co-C(3) 111.05(6), C(1)-C(2)-C(3) 138.13(19), C(2)-C(3)-C(4) 133.98(19). (<i>Right</i>) Crystallographically determined structure of 2-2 , with thermal ellipsoids shown at the 30% probability level. Hydrogen atoms have been omitted for clarity. Selected interatomic distances (Å) and angles (°): Co-C(2) 1.8817(13), Co-C(3) 1.8609(13), C(2)-C(3)	

1.296(3), Co(P1) 2.2091(4), Co-P(2) 2.2423(3), C(2)-C(3) 1.3112(18), C(2)-C(81) 1.4645(17), C(3)-C(71) 1.4636(17), Co-Si 2.2062(4), Si-Co-C(2) 110.12(4), Si-Co-C(3) 101.39(4), P(1)-Co-P(2) 114.731(14), P(1)-Co-Si 86.603(13), P(2)-Co-Si 84.808(13), P(1)-Co-C2 103.49(4), P(2)-Co-C(3) 100.69(4), C(3)-C(2)-C(81) 137.12(12), C(2)-C(3)-C(71) 137.46(12).....	51
Figure 2.2.2. Possible structures of a (Cy-PSiP)Co polyhydride species. Top: Complexes in the Co ^{III} oxidation state. Bottom: Complexes in the Co ^I oxidation state.....	52
Figure 2.2.3. (a) Computed ΔG and ΔH values for (Cy-PSiP)Co(H) ₄ isomers (kcal/mol). (b) The calculated kinetic barrier for isomer interconversion through metathesis.....	53
Figure 2.2.4. Lowest energy configurations calculated for (Cy-PSiP)Co and (Cy-PSiP)Rh polyhydride complexes. ⁸⁷	57
Figure 2.2.5. Proposed catalytic cycle highlighting relative free energies (kcal/mol) of intermediates and transition states calculated for the hydrogenation of propene mediated by (Cy-PSiP)Co(H) ₄	59
Figure 2.2.6. Free energies (kcal/mol) of intermediates and transition states calculated for the hydrogenation of propene mediated by (Cy-PSiP)Co(H) ₄	60
Figure 3.1.1. Ni catalysts for the (<i>E</i>) – selective semihydrogenation of alkynes with H ₂	68
Figure 3.2.1. Crystallographically determined structure of 3-1 with thermal ellipsoids drawn at the 30% probability level. Most hydrogen atoms are omitted for clarity. Selected interatomic distances (Å) and angles (deg): Ni–P1 2.1785(5), Ni–P2 2.1714(4), Ni–Si 2.2125(4), Ni–C51 1.9691(14), C51–C52 1.346(2), P1–Ni–P2 152.644(19), P1–Ni–Si 84.035(17), P1–Ni–C51 97.67(5), P2–Ni–Si 84.847(16), P2–Ni–C51 98.71(4), Si–Ni–C51 167.12(5), Ni–C51–C52 133.04(12).....	80
Figure 4.2.1. Crystallographically determined structure of 4-2 with thermal ellipsoids shown at the 50% probability level; hydrogen atoms have been omitted for clarity. Selected interatomic distances (Å) and angles (deg): Co-P1 2.2171(17), Co-P2 2.1250(15), Co-C45 2.009(6), Co-C47 2.017(6), C45-Co-C47 90.3(3), C45-Co-P2 176.6(2), C47-	

Co-P2 91.20(19), C45-Co-P1 91.8(2), C47-Co-P1 177.44(19), P2-Co-P1 86.66(6).....	93
Figure 4.2.2. Crystallographically determined structure of 4-3 with thermal ellipsoids shown at the 50% probability level; hydrogen atoms and the BAr ^F ₄ anion have been omitted for clarity. Selected interatomic distances (Å) and angles (deg): Co-P1 2.1570(11), Co-P2 2.0914(11), Co-Centroid 1.360, P2-Co-P1 86.26(4).....	94
Figure 5.1.1. Selected examples of privileged bis(phosphine) ligands that have been employed in base metal catalyzed asymmetric hydrogenation.....	109
Figure 5.2.1. Overlay of ³¹ P{ ¹ H} NMR (121.5 MHz) spectra for 5-6 at 298 K and 353 K.	122
Figure 5.2.2. Overlay of ¹ H NMR (300 MHz) spectra for 5-6 at 298 K and 353 K.	123
Figure 5.2.3. Overlay of ³¹ P{ ¹ H} NMR (121.5 MHz) spectra for the reaction of 5-6 with Ni(COD) ₂ in THF (spectra acquired in benzene- <i>d</i> ₆).....	127

List of Schemes

Scheme 1.2.1. (A) Dearomatization/aromatization of a pyridine based (PNP)Fe complex (1-5) enabled by deprotonation of the methylene linker. (B) Proposed catalytic cycle for metal-ligand cooperative hydrogenation of ketones employing ligand dearomatization/aromatization. (C) Metal-ligand cooperative H ₂ cleavage across an Fe – amido bond (1-8).	7
Scheme 1.2.2. Metal-ligand cooperative cleavage of H ₂ to afford borohydride species capable of hydrogenating non-polar bonds (<i>i.e.</i> , terminal alkenes, styrenes).	8
Scheme 1.2.3. (A) Oxidative addition of ammonia by Cy-PSiP supported Ir ^I . (B) Unusual 4-coordinate, trigonal pyramidal geometry enforced by PSiP ligation.	11
Scheme 1.3.1. Reversible rearrangement of 1-16 to 1-17 involving multiple Si-C cleavage steps. ⁴¹	12
Scheme 1.3.2. Synthesis of group 10 complexes featuring η^2 -(SiH) interactions (Ni, Pd) and possible SiH oxidative addition (Pt) reported by Iwasawa and co-workers.	13
Scheme 1.3.3. Synthesis of the 1-24 and 1-25 from 1-22 and 1-23 . ⁴⁴	14
Scheme 1.3.4. Equilibrium between terminal (Cy-PSiP)Ni ^{II} silyl hydride and dinitrogen adducts of (Cy-PSi ^H P)Ni ⁰	15
Scheme 1.3.5. Synthesis of group 10 ^{iPr} PSiP ^{Ind} complexes.	16
Scheme 1.3.6. Coordination chemistry involving complex 1-32	17
Scheme 1.3.7. Synthesis of a (PSiP)Co complex featuring an η^1 -(Si-H) interaction and the subsequent transformations it can undergo with (bottom) or without (top) base. ⁴⁹	19
Scheme 1.3.8. (A) Synthesis of Co complexes supported by N-heterocyclic PSiP, and (B) Kumada cross-coupling of chlorobenzene with <i>p</i> -tolylmagnesium bromide. ⁵⁰	21
Scheme 1.3.9. Synthesis of Fe and Co dinitrogen complexes supported by (Cy-PSiP) ligand variants. ⁵¹	21
Scheme 1.3.10. Synthesis of (Cy-PSiP)Fe hydride complexes facilitated by PMe ₃ coordination.	24

Scheme 1.3.11. Synthesis of (Cy-PSiP)Fe hydride complexes lacking exogenous phosphine donors.....	25
Scheme 1.4.1. (a) Asymmetric alkene hydrogenation enabled by 1-65 . (b) Chiral DuPhos supported Co catalyzed asymmetric hydrogenation of prochiral acrylamides discovered by high-throughput experimentation. (c) Ni catalyzed asymmetric hydrogenation of α,β -unsaturated esters discovered by high-throughput screening.	29
Scheme 1.4.2. Co catalyzed asymmetric hydrogenation of a pharmaceutically relevant enamide enabled through single electron reduction as shown by Chirik and co-workers. (a) Asymmetric hydrogenation mediated by isolated pre-catalysts 1-66 and 1-67 in the +1 and 0 oxidation state respectively. (b) <i>In-situ</i> generated pre-catalyst for the large-scale asymmetric hydrogenation of <i>dehydro</i> -levetiracetam.	30
Scheme 1.4.3. Top: Synthesis of cationic Co ^I complexes reminiscent of Schrock-Osborn type catalyst for asymmetric hydrogenation. Bottom: Asymmetric hydrogenation of methyl 2-acetamidoacrylate and methyl 2-acetamido-3-phenylacrylate mediated by complexes 1-69 , 1-70 , and 1-71	32
Scheme 1.4.4. Asymmetric hydrogenation of alkenes featuring various substitution patterns mediated by Co. (a) Asymmetric hydrogenation of vinylsilane reported by Huang and co-workers. (b) Asymmetric hydrogenation of α/β -unsaturated carboxylic acids reported by Zhang and co-workers. (c) Asymmetric hydrogenation of α/β -unsaturated carboxylic acids reported by Chirik and co-workers. (d) Asymmetric hydrogenation of α - <i>dehydro</i> amino acids reported by Chirik and co-workers.....	36
Scheme 1.4.5. Highly chemo- and enantioselective hydrogenation of conjugated enynes enabled by the use of a base-metal catalyst as reported by Zhang and co-workers.	37
Scheme 1.4.6. Co-catalyzed asymmetric hydrogenation of carbocyclic tri-substituted enamides as reported by de Vries and co-workers.	38
Scheme 1.4.7. Top: Synthesis of cationic (PP)Co ^I arene complexes <i>via</i> one-electron oxidation-induced reductive elimination from	

a Co ^{II} starting material. Bottom: Co-catalyzed asymmetric synthesis of Sitagliptin using 1-71 as the pre-catalyst.	40
Scheme 1.4.8. Ni-catalyzed asymmetric hydrogenation of 2-amidoacrylates as reported by W. Zhang and co-workers.	41
Scheme 2.1.1. Synthesis of the trihydride complex (BIAN)Co(H) ₃ from (BIAN)CoBr ₂ . ⁸⁰	46
Scheme 2.1.2. Substrate scope and conditions previously employed in the catalytic hydrogenation of alkenes by 1-55 . ⁹	48
Scheme 2.2.1. Synthetic route for the preparation of 2-1 and 2-2	50
Scheme 2.2.2. Substrate scope for the hydrogenation of alkenes with 2-2 . Reaction conditions: alkene (0.5 mmol), 2-2 (specified mol %), 1 atm H ₂ , benzene- <i>d</i> ₆ (volume to achieve 0.5 mL total volume), 25 °C, 4 h. Yield of product determined on the basis of ¹ H NMR integration vs. 1,3,5-trimethoxybenzene internal standard (0.5 mmol; average of two runs); a relaxation delay of 60 s was used to ensure accurate integrations. ^a Reaction performed on a 1.0 mmol scale, isolated yield in parentheses. ^b Reaction performed at 50 °C under 10 atm H ₂	55
Scheme 3.1.1. Interconversion of complex 1-32 between a terminal silyl Ni hydride and η ² – silane through coordination of L donors (N ₂ , PMe ₃).	72
Scheme 3.2.1. Substrate scope for the semihydrogenation of alkynes with 1-32 . Reaction conditions: alkyne (0.2 mmol), 1-32 (specified mol%, 40 mmol/L stock solution), 1 atm H ₂ , benzene- <i>d</i> ₆ (volume required to attain 200 μL total volume), 25 °C, 4 h. Conversion to product determined on the basis of ¹ H NMR integration vs. 1,3,5-trimethoxybenzene internal standard (0.2 mmol; average of two runs); a relaxation delay of 60 s was used to ensure accurate integrations. Isolated yields provided in parentheses. ^a Reaction performed at 50 °C. ^b Reaction performed at 90 °C. ^c For reaction run with 1 mol% 1-32 , 50 °C, benzene- <i>d</i> ₆ , and <i>E/Z</i> > 1:99. ^d All starting material consumed.	77
Scheme 3.2.2. Mechanistic experiments.	79
Scheme 3.2.3. Proposed catalytic cycle for the (<i>E</i>) – selective semihydrogenation of alkynes.	82

Scheme 4.1.1. Examples of chiral pharmaceutical targets synthesized via transition metal catalyzed asymmetric hydrogenation of unsaturated carboxylic acid derivatives.	87
Scheme 4.1.2. Previous notable examples of asymmetric hydrogenation of unsaturated carboxylic acid derivatives, including (a) Nobel prize winning work on Rh-mediated asymmetric hydrogenation of <i>dehydro-α</i> -amino acids, and (b, c) subsequent Co- and Ni-catalyzed examples.....	88
Scheme 4.1.3. (a) Previous example of Co-catalyzed asymmetric hydrogenation of <i>dehydro-α</i> -amino acids, and (b) this work, (<i>S</i>)-(Ph-PhenDalPhos)Co mediated asymmetric hydrogenation of <i>dehydro-α</i> -amino acids.	89
Scheme 4.2.1. (a) Synthesis of (<i>S</i>)-Cl(Phen). (b) Synthesis of (<i>S</i>)-Ph-PhenDalPhos (1). (c) Crystallographically determined structure of 1 with thermal ellipsoids drawn at the 50% probability level. Hydrogen atoms have been omitted for clarity.....	91
Scheme 4.2.2. Synthetic route for the preparation of 4-1 , 4-2 , and 4-3	92
Scheme 4.2.3. Substrate scope for the asymmetric hydrogenation of <i>dehydro-α</i> -amino acids catalyzed by 4-3 . Reaction conditions: substrate (0.2 mmol), 4-3 (specified mol %), 10 atm H ₂ (unless otherwise noted), THF (1 mL), 50 °C, 18 h. Conversion to product was determined on the basis of ¹ H NMR spectroscopy (isolated yield in parentheses). [a] Reaction performed under 20 atm H ₂ . [b] Reaction performed for 48 h.....	97
Scheme 4.2.4. Proposed mechanism for asymmetric alkene hydrogenation mediated by (<i>S</i>)-(Ph-PhenDalPhos)Co ⁺	100
Scheme 5.2.1. Synthetic route for the preparation of enantiopure secondary phosphine borane (<i>R</i>)-(^t Bu)(Me)PH(BH ₃) and the family of phosphino(silyl) ligands (<i>S</i>)-(P*Si ^R)H.....	111
Scheme 5.2.2. (a) Previous synthetic route employed by the Turculet group for the synthesis of bidentate PSi and tridentate PSiP ligands. (b) Synthetic route employing monolithiation of <i>o</i> -dibromobenzene to sequentially install a phosphorus-based donor followed by a silicon donor. (c) Synthetic route employing monolithiation of <i>o</i> -dibromobenzene to sequentially install a silicon-based donor followed by a phosphorus-based donor.....	112

Scheme 6.2.1. Potential synthetic route towards (PSiP)Co ^{III} complexes for bond activation chemistry.	147
Scheme 6.2.2. Proposed mixed phosphine/phosponite ligands for Co-catalyzed asymmetric hydrogenation.	149
Scheme 6.2.3. Proposed synthesis of chiral P <i>Si</i> -supported Co ^I and Co ^{II} complexes.	150
Scheme 6.2.4. Proposed derivatives of the chiral (phosphino)silyl framework.	151

Abstract

The chemistry of PSiP pincer complexes of second- and third-row transition metals has been well established within the context of bond activation chemistry and catalysis. Recent developments have begun to establish the chemistry of the first-row transition metals in conjunction with PSiP ligation, with examples of Fe, Co, and Ni demonstrating capable catalytic performance in a variety of hydrofunctionalization reactions. This document details the development of PSiP and bidentate PSi supported Co and Ni complexes for highly active catalytic hydrogenation. Additionally, an example of mixed phosphino-phosphonite ligation is shown to support Co catalyzed asymmetric hydrogenation.

In terms of (PSiP) Co chemistry, work in this document has improved on previously reported alkene hydrogenation catalysis through the synthesis of (PSiP)Co complexes supported by alkyne ligation. These complexes are shown to be active catalysts for a broad scope of functionalized alkenes under mild conditions (1 atm H₂, room temperature). A computational study into the mechanism of alkene hydrogenation by these complexes suggests that the silyl donor can act in a non-innocent manner to improve catalyst turnover.

A (PSiP)Ni hydride complex has been shown to act as a catalyst for the (*E*)-selective semihydrogenation of alkynes. This catalyst operates under exceptionally mild conditions (1 atm H₂, 1 mol % Ni, room temperature) and demonstrates excellent selectivity for (*E*)-selective semihydrogenation of alkynes across a broad substrate scope. A brief mechanistic investigation reveals facile insertion of alkynes into the Ni-H bond, and that electron withdrawing substituents on the substrate hinder the reaction.

A mixed phosphine-phosphonite ligand was coordinated to a series of Co complexes that could support the asymmetric hydrogenation of α -dehydroamino acid derivatives. A cationic Co^I complex was synthesized and applied towards this transformation where it was found to provide high enantioselectivity across a broad, functionalized, substrate scope. Deuterium labeling experiments provide evidence for a dihydride mechanism resulting from oxidative addition of dihydrogen.

Lastly, a new class of chiral ligand featuring chirality at Si has been developed and applied towards the Ni catalyzed asymmetric hydrogenation of functionalized enamides. Chiral phosphino(silyl) (PSi) ligation is shown to induce enantioselectivity and high catalytic turnover for the asymmetric hydrogenation of a dehydroamino acid methyl ester and a tri-substituted carbocyclic alkene. An *in situ* generated species is shown to provide the highest activity and enantioselectivity.

List of Abbreviations and Symbols Used

Å = Angstrom	L = two electron donor (neutral electron counting formalism)
η = hapticity (contiguous donor)	X = single electron donor (neutral and anionic electron counting formalism)
κ = denticity (non-contiguous donor)	s = singlet
μ_B = Bohr magneton	d = doublet
μ_{eff} = effective magnetic moment	t = triplet
Anal. Calcd = Analysis calculated	q = quartet
br = broad	m = multiplet
COD = 1,5-cyclooctadiene	δ = chemical shift (ppm)
DFT = density functional theory	ppm = parts per million
dme = 1,2-dimethoxyethane	acac = acetylacetonato
ENDOR = electron nuclear double resonance	py = pyridine
ee = enantiomeric excess	Mes = mesityl (2,4,6-trimethylphenyl)
er = enantiomer ratio	NHC = N – heterocyclic carbene
h = hour	BAr^F₄ = tetrakis(3,5-bis(trifluoromethyl)phenyl)borate
Hz = hertz	SISHA = secondary interaction between silicon and hydrogen atom
NMR = Nuclear Magnetic Resonance	TOF = turnover frequency
COSY = Homonuclear Shift COrrelation Spectroscopy	TON = turnover number
DEPT = distortionless enhancement by polarization transfer	equiv = equivalents
HMBC = Heteronuclear Multiple Bond Correlation	HPLC = High pressure liquid chromatography
HSQC = Heteronuclear Single Quantum Correlation	HBPIn = 4,4,5,5-tetramethyl-1,3,2-dioxaboralane
HMQC = Heteronuclear Multiple Quantum Correlation	ORTEP = Oak Ridge thermal ellipsoid plot
$^nJ_{XX'}$ = n bond coupling constant between atoms X and X'	

Acknowledgements

First and foremost, I would like to thank my supervisor, Dr. Laura Turculet, for her mentorship, guidance, and many laughs over the years. Laura provided the opportunities for me to pursue what I was interested in and always pushed me to excel. I will always be grateful to her. I would also like to thank the other members of the Turculet group and the 4th floor crew, past and present, for all their support and good times. In particular, the future Drs. Erin Welsh, Tyler Saunders, and Joe Bedard, as well as Drs. Fabien Lindeperg, Helia Hollenhorst, Blake Huchenski, and Luke Murphy are acknowledged for their friendship.

I would also like to thank the members of my supervisory committee, Drs. Mark Stradiotto, Alex Speed, and Norman Schepp for their continued mentorship and insights. My external examiner, Dr. Tom Baker, is also thanked for taking the time to evaluate my work. Additionally, Drs. Michael J. Ferguson and Katherine Robertson from the University of Alberta and Saint Mary's University respectively are acknowledged for their contributions concerning X-ray data collection and solution refinement. Dr. Mike Lumsden is also acknowledged for his help with NMR and funny interludes in the NMR facility. Mr. Xiao Feng is also thanked for his help with HPLC and MS.

Finally, I would like to thank my family. My wife, Lina, who has always believed in me and provided me with the most love and support a person can give. My parents, Glenn and Kim, who have always encouraged me to do my best and whose pride I've always felt. My brother, Ryan, who is one of my best friends, as well as Bryce Martin and Dr. Brad Acott, who have been like brothers.

This thesis is dedicated to Clarrie, who I wish could have seen it.

Chapter 1: Introduction

1.1 Overview

The ability of transition metal complexes to catalyze chemical transformations has become one of the fundamental applications of organometallic chemistry. In particular, homogeneous catalysis has been widely recognized as a useful application of organometallic complexes, as demonstrated by the 2001¹⁻³, 2005⁴⁻⁶, and 2010⁷ Nobel Prizes in Chemistry awarded for asymmetric catalysis, olefin metathesis, and Pd-catalyzed cross-coupling, respectively. Efforts continue today towards the discovery of new transition metal complexes capable of improving on these catalytic transformations, as well as the development of new methodologies and further applications for organometallic complexes.

Despite the high activity and low catalyst loadings afforded by the use of platinum group or 'noble' metals (*i.e.*, Ru, Rh, Ir, Pd, Pt), their low abundance and high cost has made their continued use prohibitive. In an effort to develop more sustainable synthetic methods, there has been increased global interest in the development of the organometallic chemistry of the much more abundant first-row transition or 'base' metals.⁸ The lower activity of many first-row transition metal catalysts as well as the propensity for often undesired single electron chemistry represent serious issues to be considered when developing complexes of these metals to be used as catalysts. These issues can hinder the adoption of first-row transition metal catalysts for large scale applications, as the economic benefit of employing a cheaper metal is quickly offset by the amount of catalyst required, and/or the cost of specialized ligands.

Ancillary ligand design represents the most straightforward way to overcome the inherent limitations of base metal catalyst performance due to the ability of ligands to

modify the coordination environment about the metal center. Improvements can be made through rational modification of the ligand scaffold to afford control of the steric and electronic features of the metal complexes. Ligands capable of coordinating in a tridentate ‘pincer’ fashion (typically meridional) are particularly useful, as they have multiple tuneable sites to tailor the reactivity of a metal complex to the desired transformations.

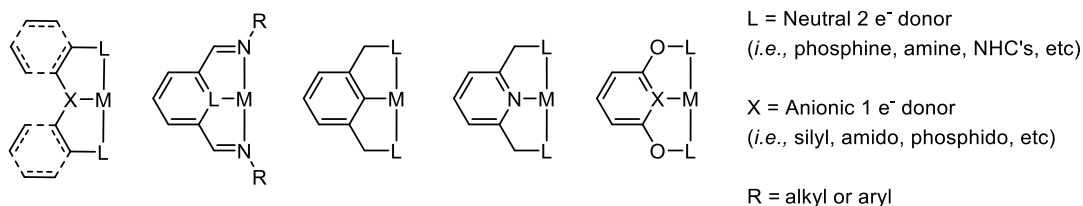


Figure 1.1.1. Common tridentate pincer ligand motifs.

The research outlined in this document builds on previous work done in the Turculet group exploring the ability of bis(phosphino)silyl (PSiP) first-row transition metal pincer complexes for the catalytic reduction of unsaturated substrates (Figure 1.1.2). Chapter 2 describes the synthesis of bis(phosphino)silyl (Figure 1.1.2 A) supported Co^I alkyne complexes that display excellent reactivity for alkene hydrogenation under mild reaction conditions. Previous work by former Turculet group student, Dr. Luke Murphy, established the ability of a (PSiP)Co^I complex supported by exogenous phosphine ligation to support alkene hydrogenation catalysis.⁹ The work described in Chapter 2 improves on this through the synthesis of alkyne supported (PSiP)Co^I complexes that were found to be exceptionally active toward alkene hydrogenation. An investigation into the potential mechanism was performed employing DFT methods and supports the hypothesis that the silyl donor can act in a cooperative manner with the metal center.

Chapter 3 describes the application of bis(phosphinoindolyl)silyl (Figure 1.1.2 B) supported Ni complexes in alkyne semihydrogenation catalysis. Previous work from the

Turculet group established the ability of (PSiP)Ni complexes to catalyze the selective hydroboration of CO₂ to the formaldehyde level of reduction using HBPIn as the reductant.¹⁰ The reactivity of these complexes could be extended to support (*E*)-selective alkyne semihydrogenation under mild conditions across a broad scope of diarylacetylenes and TMS protected terminal phenylacetylenes.

Chapter 4 investigates the utility of mixed phosphine/phosphonite ligands (Figure 1.1.2 C) in supporting Co catalyzed asymmetric hydrogenation of α -dehydroamino acids. This work builds upon the PhenDalPhos class of ligands previously employed in Ni catalyzed C-N cross coupling by the Stradiotto group.¹¹ In enantiopure form, this ligand platform was found to support Co^{II} and Co^I complexes that were capable of mediating highly selective asymmetric hydrogenation across a scope of substituted α -dehydroamino acids. Finally, Chapter 5 details the synthesis of chiral bidentate (indolylphosphino)silyl ligands (Figure 1.1.2 D) that are capable of supporting the Ni mediated asymmetric hydrogenation of functionalized enamides. This work combines the high catalytic reactivity observed in base metal supported bis(phosphino)silyl catalysis with high enantioselectivity through ligand design.

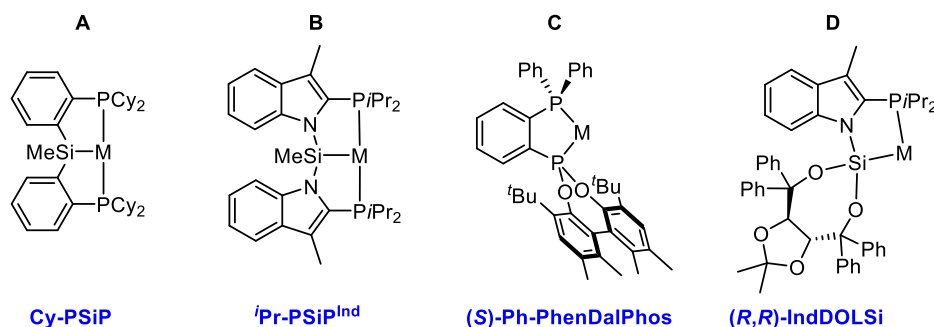


Figure 1.1.2. Ligands employed in this work: the chemistry of Cy-PSiP **A** with Co is described in Chapter 2; the chemistry of ⁱPr-PSiP^{Ind} **B** with Ni is described in Chapter 3; the chemistry of (*S*)-Ph-PhenDalPhos **C** with Co is described in Chapter 4; and the chemistry of (*R,R*)-IndDOLSi with Ni is described in Chapter 5.

1.2 Base Metal Pincer Ligand Design

While second and third row transition metals favor two-electron chemistry such as oxidative addition and reductive elimination, the propensity of first-row metal complexes to undergo one electron chemistry can lead to complex and often undesirable reactivity. In this regard, ligands featuring strong-field donors that enable low-spin ground state configurations have been shown to promote desirable reactivity. Studies by the Chirik¹² and Fout¹³ groups have demonstrated the efficacy of strong field ligands (Figure 1.2.1 A) to enable noble-metal like reactivity in base metal catalysis. Chirik and co-workers showed that a bis(arylimidazol-2-ylidene)pyridine ligand in conjunction with Fe (**1-1**) can facilitate the hydrogenation of challenging tri- and tetrasubstituted alkenes under mild conditions (4 atm H₂, 23 °C, 5 mol % catalyst).¹² Work by Fout and co-workers further demonstrates the effectiveness of strong field ligands in base metal hydrogenation catalysis through application of their monoanionic bis(mesityl-benzimidazol-2-ylidene)phenyl ligand (^{Mes}CCC) in Co mediated catalysis (complex **1-2**).¹³ Through extensive NMR studies they determined that it was likely that the catalysis proceeded by a Co^I/Co^{III} redox cycle, and found the catalysis to also proceed under mild conditions (4 atm H₂, room temperature, 2 mol % catalyst).

In addition to ligands that incorporate strong-field donors, ancillary ligands that become directly involved in the chemistry being performed at the metal center (termed ‘non-innocent’) have emerged in recent years as a key tool to control the reactivity of base metal complexes.¹⁴ Non-innocent ligands are capable of aiding reactivity through metal-ligand electron transfer (*i.e.*, redox non-innocence) or through tandem metal-ligand substrate bond

breaking (*i.e.*, metal-ligand cooperativity). Due to the strong chelate effect and their modular nature, k^3 -pincer ligands capable of engaging in either redox non-innocent behavior or metal-ligand cooperativity have emerged as capable ligands for first row transition metal catalysis.¹⁵

The redox non-innocent pyridine diimine (PDI) ligands extensively studied by the Chirik group have become a privileged class of ligands for Earth abundant metal catalysis (Figure 1.2.1 B).¹⁶ Work by Chirik and co-workers has established that PDI complexes of Fe and Co are competent catalysts for [2+2] cycloaddition,¹⁷ hydroboration,¹⁸ and alkene hydrogenation reactions.¹⁹⁻²² The ability of these ligands to act as an ‘electron reservoir’ during catalysis enables the metal to perform in a manner that resembles a more traditional two electron pathway (Figure 1.2.1 A). By contributing one electron the ligand allows the metal to supply an electron in a single electron oxidation process that is more favorable for the first-row metals.²³

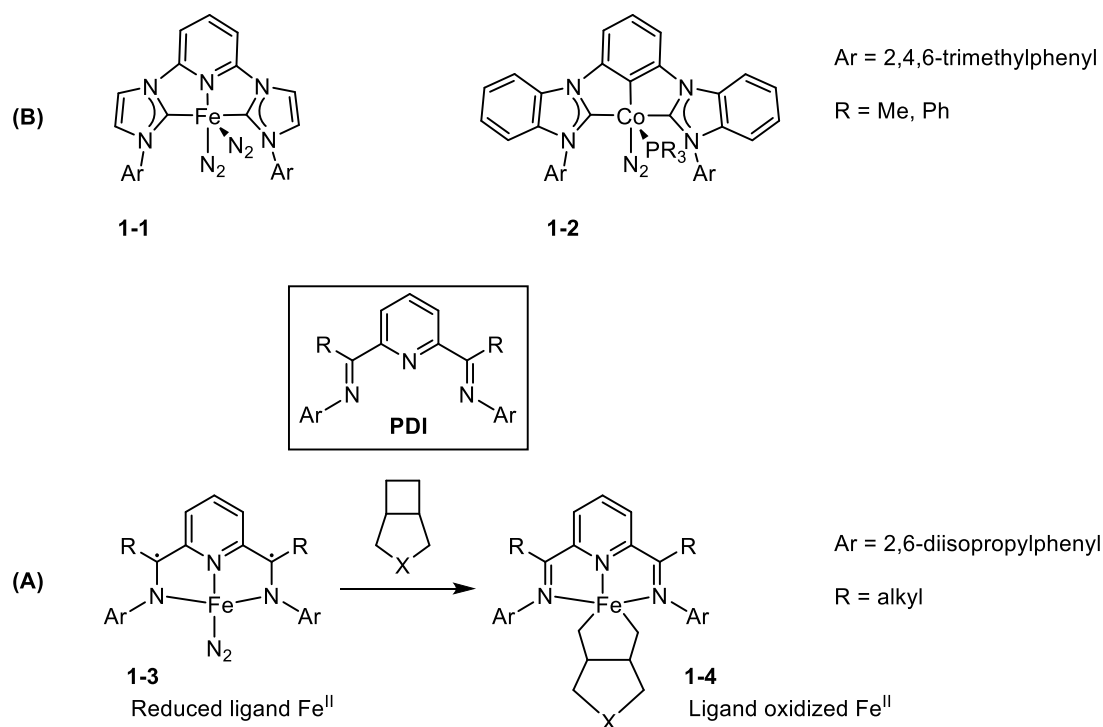
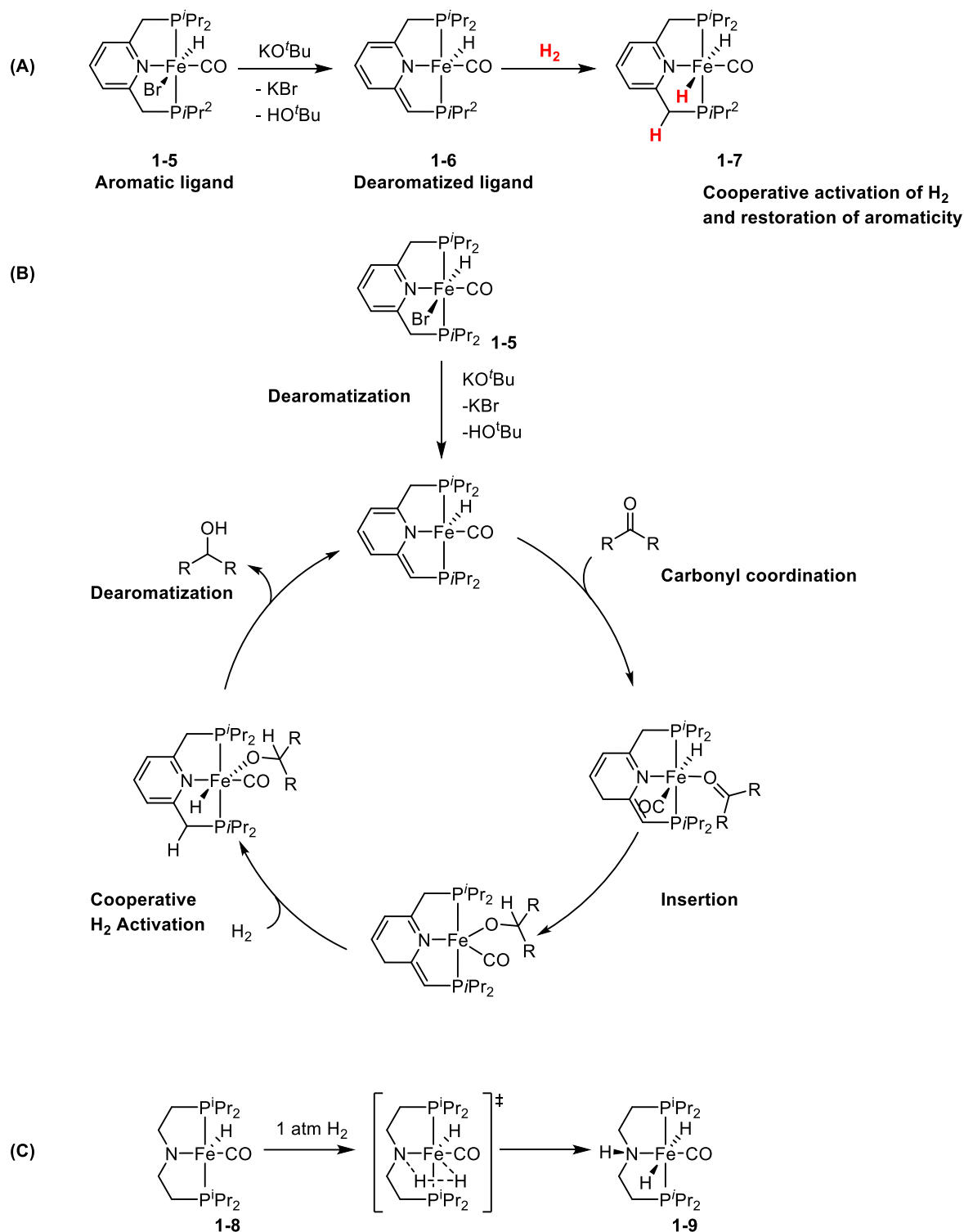


Figure 1.2.1. (A) Examples of Fe and Co complexes featuring strong field ligands that support two-electron reactivity at the metal center. (B) Examples of Fe complexes supported by redox non-innocent PDI ligation

Ligands that engage in metal-ligand cooperative substrate cleavage have also found popularity in base metal catalysis.²⁴ Such cooperativity typically features ligand – metal proton transfer processes. The Milstein group has established the use of ligand aromatization/dearomatization via ligand – metal proton transfer as a means to cleave substrates and form new bonds,²⁵ and they have utilized this concept to perform the Fe catalyzed hydrogenation of ketones²⁶ and CO₂ (Scheme 1.2.1 A).²⁷ In Fe catalyzed hydrogenation examples, Milstein and co-workers employed bis(phosphino)pyridine (PNP) tridentate pincer ligands featuring relatively acidic protons in the methylene linker (pK_a in THF of approximately 35). By employing a catalytic amount of strong base, they were able to deprotonate this linker and disrupt the aromaticity of the pyridine donor. Under hydrogenation conditions H₂ is split cooperatively into a proton (H⁺) and a hydride (H⁻) by the ligand and the metal respectively, restoring aromaticity and furnishing an Fe hydride capable of inserting a coordinated carbonyl. Deprotonation of the linker by the ensuing alkoxide is proposed to once again de-aromatize the ligand and turn the catalytic cycle over (Scheme 1.2.1 B).

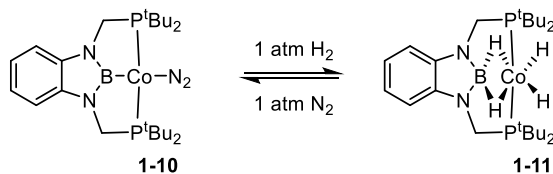


Scheme 1.2.1. (A) Dearomatization/aromatization of a pyridine based (PNP)Fe complex (1-5) enabled by deprotonation of the methylene linker. (B) Proposed catalytic cycle for metal-ligand cooperative hydrogenation of ketones employing ligand

dearomatization/aromatization. (C) Metal-ligand cooperative H₂ cleavage across an Fe – amido bond (**1-8**).

Metal-ligand cooperativity can also be achieved by incorporating amido groups in the ligand framework. For example, work from Hazari and co-workers has demonstrated that employing an amido group as a central donor in a (PNP)Fe complex allowed H₂ to be cooperatively split into a proton at the amido donor and a hydride at the metal center (complex **1-8**, scheme 1.1.2 C).²⁸ This allowed them to catalytically hydrogenate CO₂ with high turn over frequencies and low catalyst loadings.

In a reversal of the strategy where the ancillary ligand functions as a proton reservoir, the Peters group has demonstrated that by incorporating a boryl group into the ancillary ligand it is possible to transfer a hydride equivalent to the ligand in a cooperative fashion.²⁹⁻³⁰ This type of metal-ligand cooperativity was shown through use of a bis(phosphino)boryl (PBP) type ligand in conjunction with Co (Scheme 1.2.2). The reaction of a reduced Co^I dinitrogen complex (**1-10**) with two equivalents of H₂ led to the formation of a σ -borate complex (**1-11**) which features two terminal Co hydrides and two bridging hydrides. This reaction was reversible, and upon exposure to an atmosphere of N₂ **1-11** converts back to **1-10**. Complex **1-10** is an active precatalyst for the hydrogenation of terminal alkenes and styrene derivatives, as well as amine-borane dehydrocoupling and transfer hydrogenation, all of which are suggested by the authors to go through mechanisms involving reactivity at the ligand boryl group. This boryl mediated reactivity has not been further explored.



Scheme 1.2.2. Metal-ligand cooperative cleavage of H₂ to afford borohydride species capable of hydrogenating non-polar bonds (*i.e.*, terminal alkenes, styrenes).

The utility of metal-ligand systems designed to take advantage of hydride transfers has thus far remained an underexplored area of study. The utility of such ligands featuring electropositive hydride acceptor fragments with first-row metals offers an untapped area of chemistry that could lead to more active catalysts. Silicon is another example of an electropositive element that can be employed in ligand design as a hydride acceptor. In this regard, PSiP silyl pincer ligation has the potential to engage in metal-silyl cooperativity, which may facilitate reactivity involving E-H bond activation/cleavage for catalytic applications such as alkene/alkyne hydrofunctionalization. The feasibility of such metal-silyl cooperativity has not been rigorously demonstrated, although the formation of Si-H σ -complexes is well established.³¹ Such σ -complexes are especially favorable for 1st row metal complexes due to the orbital mismatch between the contracted metal d orbitals and the Si-H σ^* orbital. The Turculet group is broadly interested in developing and studying the utility of metal-silyl cooperativity in base metal catalyzed hydrofunctionalization reactions, with the goal of accessing new reactivity manifolds as well as increasingly efficient catalysis. Tridentate PSiP silyl pincer ligation developed in the Turculet groups offers both strong-field donor groups (P and Si) that have proven effective at promoting low-spin configurations, as well as the possibility for metal-silyl cooperative reactivity. The work described in this document as part of our ongoing studies in this regard.

Although silyl ligands are well-precedented in transition metal chemistry, such ligands have typically been studied as reactive ligands in transformations such as hydrosilylation.³¹ By comparison, the utilization of silyl fragments in multidentate ancillary ligands is less developed. A tridentate bis(phosphino)silyl ligand featuring a benzylic backbone was first synthesized in the 1990's by Stobart and co-workers in an effort to rigidify previously

studied bidentate phosphinosilyl “PSi” ligands (Figure 1.2.2).³² The lack of steric hindrance in the bidentate systems led to unreactive bis(ligated) complexes, while tetradentate tris(phosphino)silyl (P₃Si) systems were found to provide too much steric hindrance and thus were unreactive in catalysis.

Peters and co-workers synthesized a variant of tetradentate P₃Si wherein they replaced the benzylic linkers present in the Stobart with *o*-phenylene linkers.³³ This effectively removed the possibility of β -hydride elimination in the ligand backbone, while simultaneously increasing the rigidity of the ligand. This tris(phosphino)silyl framework has proven to be particularly robust, and has been extensively studied in the context of base metal coordination chemistry with an emphasis placed on the stoichiometric and catalytic reduction of N₂.³⁴⁻³⁵

Turculet and co-workers introduced a tridentate PSiP ligand featuring *o*-phenylene linkers (Figure 1.2.2).³⁶ This once again served to remove the possibility of β -hydride elimination, and rigidified the ligand to reduce the amount of conformational flexibility. The Turculet group has established that the PSiP ligand platform supports electron rich, coordinatively unsaturated complexes of the second- and third-row platinum group metals capable of performing challenging bond activation chemistry and can enforce unusual geometries. For example, an Ir^I species supported by Cy-PSiP (Cy-PSiP = [κ^3 -(2-Cy₂PC₆H₄)₂SiMe]) ligation generated from (Cy-PSiP)IrHCl (**1-12**) could perform facile N-H bond oxidative addition of ammonia to furnish the amido hydride species (Cy-PSiP)IrH(NH₂) (**1-13**) (Scheme 1.2.3 A).³⁷⁻³⁸ Furthermore, Cy-PSiP ligation was found to enforce an unusual 4-coordinate trigonal pyramidal geometry at Ru as a result of the strongly σ -donating silyl donor (complexes **1-14** and **1-15**, scheme 1.2.3 B).³⁹

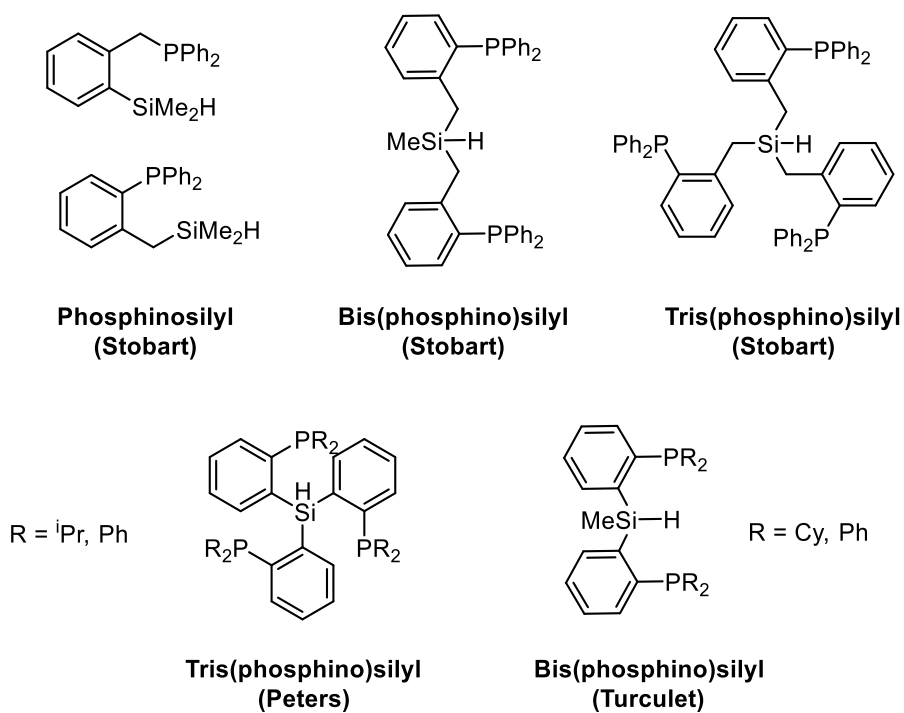
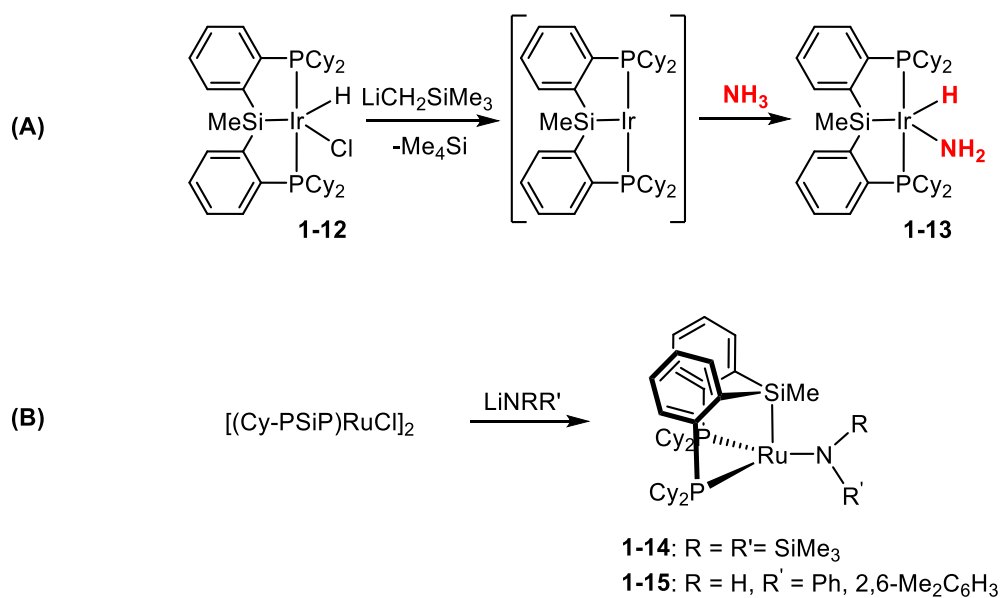


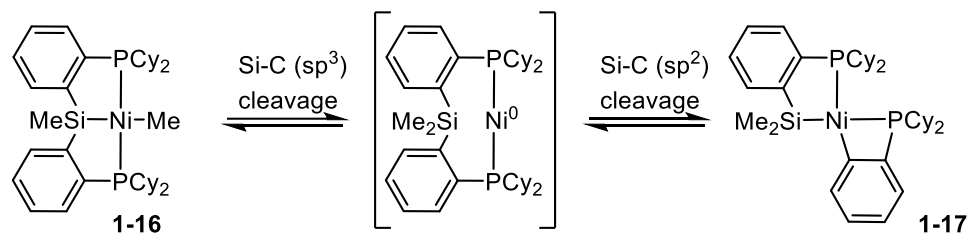
Figure 1.2.2. Structures of mono, bis, and tris(phosphino)silyl ligand precursors reported by Stobart,³² Peters,³³ and Turculet.³⁶



Scheme 1.2.3. (A) Oxidative addition of ammonia by Cy-PSiP supported Ir^I. (B) Unusual 4-coordinate, trigonal pyramidal geometry enforced by PSiP ligation.

1.3 First Row Silyl Metal Pincer Complexes

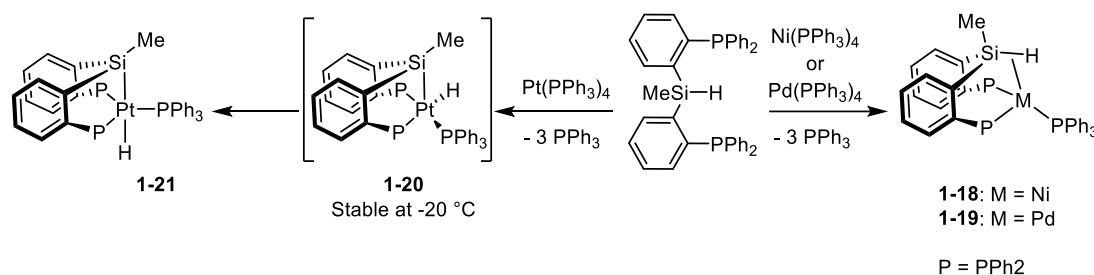
The reactivity of 3d-metal silyl pincer complexes has only recently become an area of interest.^{9-10, 40-41} The majority of such studies have focused on the chemistry of (PSiP)Ni species.^{10, 42-46} In 2009 Turculet and co-workers described the first example Ni supported by PSiP ligation.⁴¹ Previous investigations into the coordination chemistry of Pt had led to the isolation of square planar (Cy-PSiP)Pt^{II} complexes with silyl, aryl, or alkyl substituents *trans* to the central silyl donor. However, attempts to prepare analogous Ni alkyl complexes led to a mixture of products consisting of the terminal Ni alkyl complex (**1-16** for alkyl = Me) and the rearranged species **1-17** resulting from Si-C(sp²) cleavage in the ligand backbone. Complexes **1-16** and **1-17** undergo chemical exchange in solution, which implicates reversible Si-C(sp²) and Si-C(sp³) bond cleavage processes. This reactivity was proposed to involve a net Si-Me reductive elimination from complex **1-16** to afford a Ni⁰ intermediate that can then undergo either reversible Si-C oxidative addition of the Si-C(sp²) phenylene linkage in the ligand backbone to afford complex **1-17** or Si-C(sp³) oxidative addition to reform **1-16**. Such reversible Si-C bond cleavage reactivity is unprecedented.



Scheme 1.3.1. Reversible rearrangement of **1-16** to **1-17** involving multiple Si-C cleavage steps.⁴¹

Further investigation into group 10 hydride complexes supported by Ph-PSiP (Ph-PSiP = [κ^3 -(2-Ph₂PC₆H₄)₂SiMe]) ligation by Iwasawa and co-workers led to the isolation of η^2 -(SiH) complexes of Ni⁰ (**1-18**) (Scheme 1.3.2).⁴⁷ Solution NMR studies (¹H and ²⁹Si

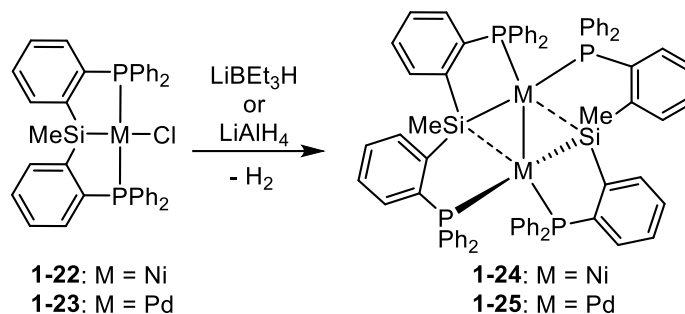
spectroscopy) support the assignment of η^2 -(SiH) coordination in solution, as indicated by the observation of coupling of the Si-H proton to both phosphorus nuclei, as well as to the methyl protons on silicon. Furthermore, the J_{SiH} coupling constants of 110 Hz was consistent with an η^2 -(SiH) assignment while an analogous Pd complex (**1-19**) was also isolated, this phenomenon was not observed in the case of Pt, where the trigonal bipyramidal complex (Ph-PSiP)PtH(PPh₃) (**1-21**) was isolated instead (Scheme 1.3.2). This reactivity suggests that the intermediacy of σ -SiH complexes in catalytic transformations involving PSiP – ligated 3d-metal complexes is indeed viable.



Scheme 1.3.2. Synthesis of group 10 complexes featuring η^2 -(SiH) interactions (Ni, Pd) and possible SiH oxidative addition (Pt) reported by Iwasawa and co-workers.

Nova and Hazari subsequently reported their attempts to synthesize variants of the Ni (and Pd) hydride complexes reported by Iwasawa and co-workers without triphenylphosphine as a co-ligand.⁴⁴ Treatment of (Ph-PSiP)MCl **1-22** (M = Ni), **1-23** (M = Pd) with LiAlH₄ or LiBEt₃H did not afford the expected hydride complexes, but instead led to the evolution of H₂ and formation of the unusual dinuclear complexes **1-24** and **1-25** that feature pentavalent silicon (Scheme 1.3.3). Complexes **1-24** and **1-25** both exhibit square pyramidal coordination geometry in the solid state, as well as inequivalent silicon atoms with one long and one short Si-M contact. These complexes represent an example of 4-center-2-electron (4c-2e) bonding involving the Si-M-M-Si core. The ²⁹Si NMR spectra of these complexes each feature two resonances corresponding to the inequivalent

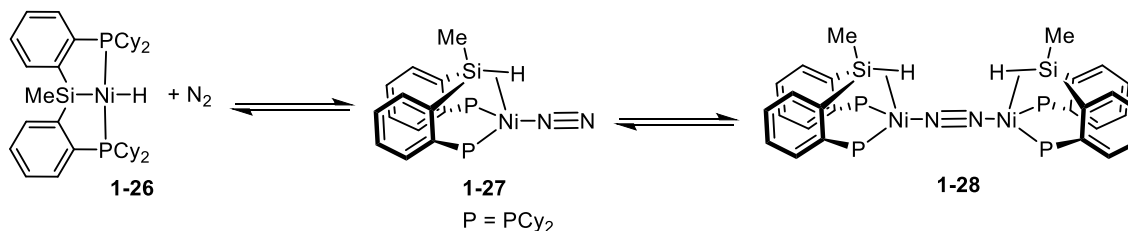
Si atoms while the $^{31}\text{P}\{^1\text{H}\}$ NMR spectra contain 2 broad resonances. Decoalescence was observed at $-60\text{ }^\circ\text{C}$, with the inequivalence being attributed by the authors to slight changes in the orientation of the ligand backbone and the phenyl substituents of the ligand.



Scheme 1.3.3. Synthesis of the **1-24** and **1-25** from **1-22** and **1-23**.⁴⁴

Further work by Hazari has shown that the use of alkylphosphino donors in place of aryl phosphino groups allows isolation of (PSiP)Ni hydrides without subsequent decomposition.^{42, 46} It was found that treatment of (Cy-PSiP)NiCl with LiBEt₃H afforded the expected product (Cy-PSiP)NiH (**1-26**) in moderate yield. Upon coordination of dinitrogen, it was found that this complex underwent reversible reductive elimination of the Si – H unit to afford a formally Ni⁰ N₂ – bridged dimer featuring two η²-(SiH) interactions (Scheme 1.3.4, **1-28**). The authors investigated this dynamic process through kinetic analysis, DFT, NMR, and X-ray crystallography. Together, these data demonstrate that in the presence of a donor such as N₂ or CO interconversion between a Ni^{II} silyl hydride species and Ni⁰ silane complex is facile (Scheme 1.3.4). The authors concluded that under an N₂ atmosphere at ambient temperature the two dominant species in solution are the N₂ – bridged dimer **1-28** and the terminal silyl hydride **1-26** (Cy-PSiP)NiH while the monomeric N₂ adduct **1-27** (Cy-PSi^HP)Ni(N₂) can be observed only under a large pressure of N₂ (*ca.* 14 atm).

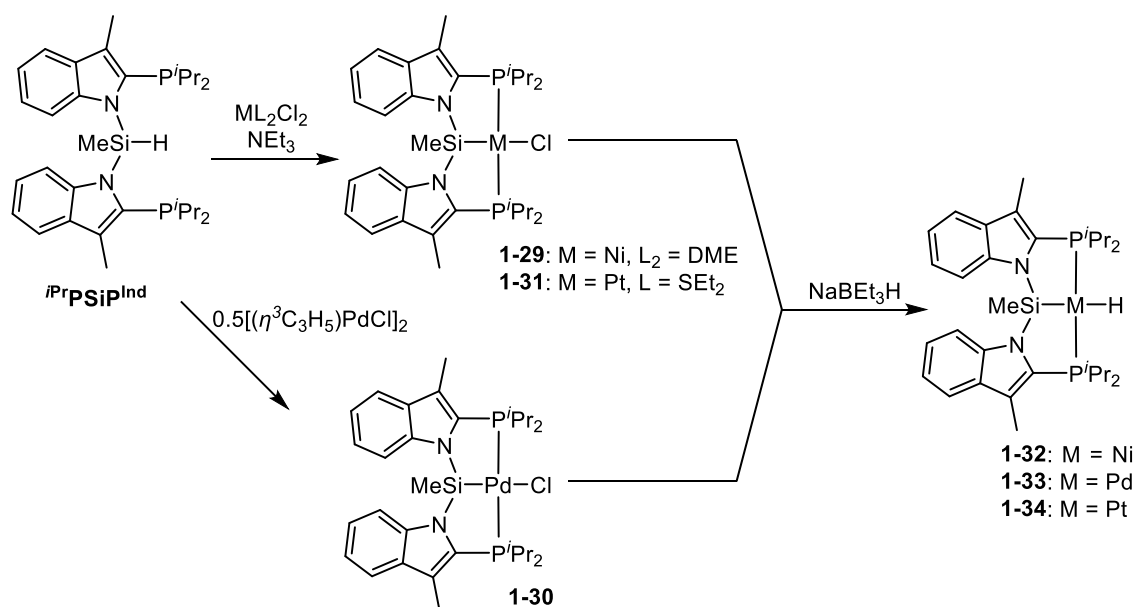
The ^{29}Si NMR chemical shift of **1-26** and **1-28** proved characteristic of the H-Ni-Si coordination mode. An examination of the $^{29}\text{Si}\{^1\text{H}\}$ NMR of a solution of **1-26** and **1-28** under 1 atm of N_2 showed chemical shifts of 60.7 ppm and -11.8 ppm respectively. The authors note that these values are in good agreement with ^{29}Si chemical shift values for group 10 metal complexes supported by PSiP ligands, and that for complexes in the M^{II} oxidation state the ^{29}Si chemical shifts typically range from 55 to 66 ppm while complexes in the M^0 oxidation state typically feature chemical shift values around 0 ppm. Furthermore, in the absence of ^1H decoupling, a $^1J_{\text{Si-H}}$ coupling constant of 101.3 Hz can be measured for the resonance at -11.8 ppm while no $J_{\text{Si-H}}$ coupling could be resolved for the peak at 60.7 ppm.



Scheme 1.3.4. Equilibrium between terminal (Cy-PSiP) Ni^{II} silyl hydride and dinitrogen adducts of (Cy-PSi $^{\text{H}}$ P) Ni^0 .

In 2017, the Turculet group disclosed the synthesis of a bis(indolyl)phosphino silyl $i^{\text{Pr}}\text{PSiP}^{\text{Ind}}$ ligand and its coordination chemistry with group 10 metals (Figure 1.1.2, C).¹⁰ Hydride complexes of the type $(i^{\text{Pr}}\text{PSiP}^{\text{Ind}})\text{MH}$ ($\text{M} = \text{Ni}, \text{Pd}, \text{Pt}$) were targeted as potential pre-catalysts for the reduction of CO_2 . The chloride complexes $(i^{\text{Pr}}\text{PSiP}^{\text{Ind}})\text{MCl}$ (**1-29** $\text{M} = \text{Ni}$, **1-30** $\text{M} = \text{Pd}$, **1-31** $\text{M} = \text{Pt}$) were first synthesized and subsequently treated with one equivalent of NaBEt_3H to afford the corresponding metal hydride species **1-32**, **1-33**, and **1-34** (Scheme 1.3.5). Like **1-26**, **1-32** was found to undergo reversible reductive elimination of the Si-H upon coordination of N_2 to afford the dinuclear $\text{Ni}(0)$ silane adduct

1-35 (Scheme 1.3.6). The major species in solution at ambient temperature and pressure was determined to be the Ni^{II} silyl hydride **1-32** as shown by the ²⁹Si NMR chemical shift of 59.8 ppm, with **1-35** present in small amounts (²⁹Si NMR chemical shift = -10.5 ppm). Both complexes display spectroscopic features similar to **1-26** and **1-28** respectively (*vide supra*), with no *J*_{Si-H} coupling observed for **1-32** while **1-35** features a ¹*J*_{Si-H} coupling constant of 89 Hz. Further support for the assignment of **1-35** is shown by the solid-state Raman spectrum which displays a relatively intense band at 2073 cm⁻¹ which is assigned as coordinated N₂.

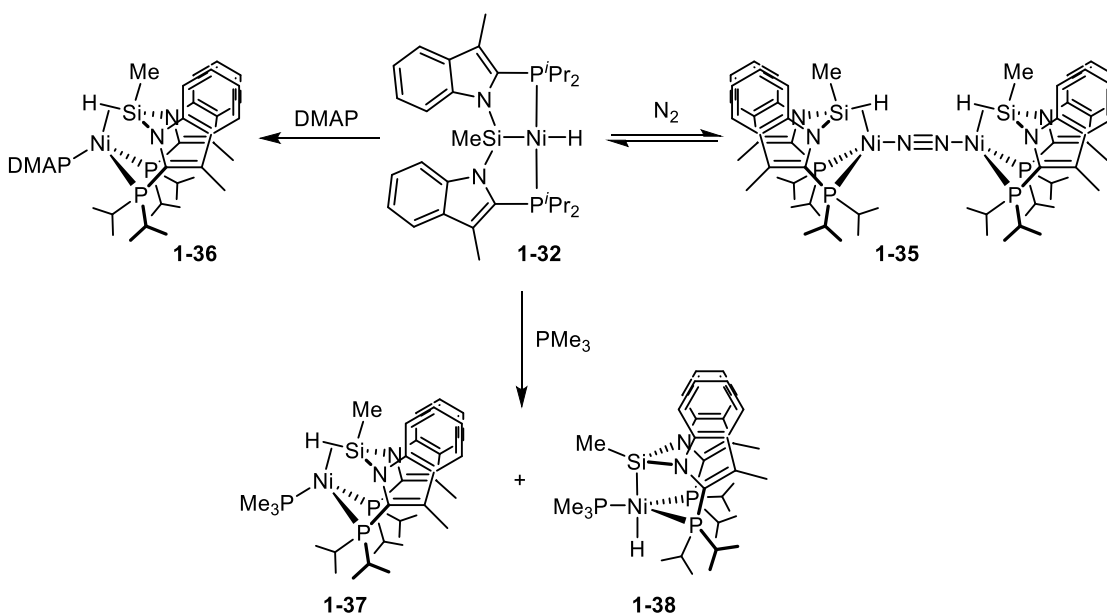


Scheme 1.3.5. Synthesis of group 10 *iPrPSiP^{Ind}* complexes.

To further corroborate the assignments of **1-32** and **1-35** the coordination chemistry of **1-32** was investigated through addition of L-donors (Scheme 1.3.6). Upon addition of one equivalent of DMAP, clean conversion to the corresponding Ni⁰ complex **1-36** was observed. Complex **1-36** features η^2 -(SiH) coordination and adopts a distorted tetrahedral

geometry in the solid state. The ^{29}Si NMR shift of -24.1 Hz and $^1J_{\text{Si-H}}$ coupling constant of -69 Hz are consistent with these structural features.

By contrast, the addition of one equivalent of PMe_3 to **1-32** led to a 2:1 mixture of the Ni^0 η^2 -(SiH) and Ni^{II} silyl hydride complexes **1-37** and **1-38**. The major product, **1-37**, features similar geometric features in the solid state as **1-36** and displays a ^{29}Si NMR resonance of 6.3 ppm and a $^1J_{\text{Si-H}}$ coupling constant of -82 Hz. The minor product, **1-38**, however, displays spectroscopic and geometric features that are similar to the trigonal bipyramidal Pt complex **1-21** reported by Iwasawa and co-workers (*vide supra*). This assignment is further supported by the solid-state structure of **1-38** which shows a distorted trigonal bipyramidal structure with the hydride oriented trans to the silyl donor, as well as the ^{29}Si NMR chemical shift of 65.7 ppm and $^1J_{\text{Si-H}}$ coupling constant of -81 Hz. This data further supports the hypothesis that the ^{29}Si NMR chemical shift can act as a predictor for the extent of Si-H interaction for P*Si*P-supported group 10 metal hydrides, with complexes that feature an η^2 -(SiH) interaction displaying relatively upfield ^{29}Si NMR resonances.



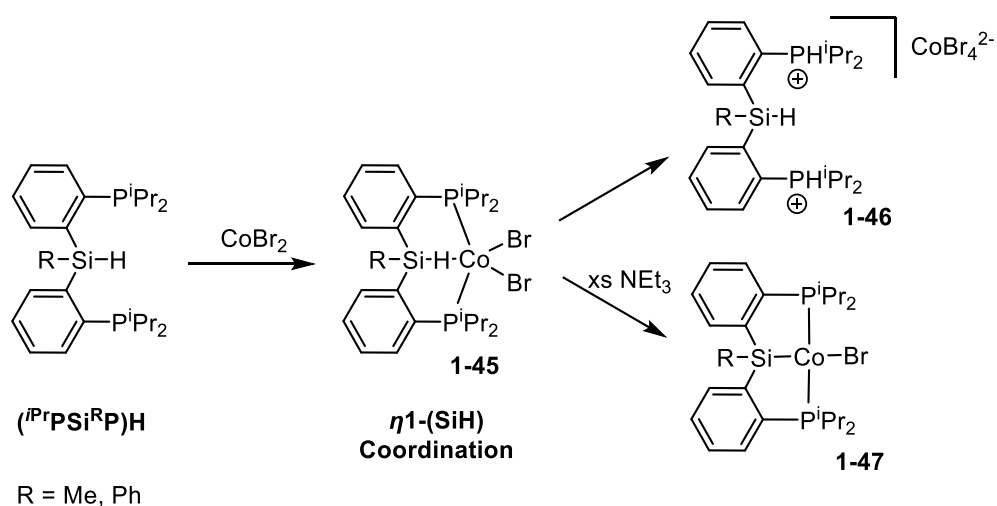
Scheme 1.3.6. Coordination chemistry involving complex **1-32**.

The utility of complexes **1-32**, **1-33**, and **1-34** as pre-catalysts for the hydroboration of CO₂ was subsequently investigated. While the Pd and Pt derivatives (**1-32** and **1-33** respectively) proved to be poor pre-catalysts in this regard, the Ni complex **1-32**, was found to be both highly reactive and selective with 84% conversion of CO₂ to the bis(boryl)acetal product arising from reduction with two equivalents of HBPIn. Optimization of the catalytic conditions led to 97% conversion to the bis(boryl)acetal product after 4 h at room temperature employing only 0.2 mol% **1-32**. These results are notable as no products arising from further reduction to the methoxyborane product were observed and establish **1-32** as the most selective catalyst for the reduction of CO₂ to the bis(boryl)acetal level of reduction.

While the chemistry of PSiP-supported first row metal complexes has been largely dominated by Ni, examples featuring Fe and Co have become more prominent in recent years. Examples of Fe and Co PSiP complexes were first reported by Sun and co-workers, who prepared complexes of the form (Ph-PSiP)M(PMe₃)_nH (n = 1 for **1-39** M = Co, n = 2 for **1-40** M = Fe) from the corresponding M(PMe₃)₄ precursors. Their efforts led to further isolation of the complexes (Ph-PSiP)CoCl(PMe₃) (**1-41**), (Ph-PSiP)CoHCl(PMe₃) (**1-42**), (Ph-PSiP)CoHI(PMe₃) (**1-43**), and (Ph-PSiP)Co(PMe₃)₂ (**1-44**) which highlight the ability of PSiP ligation to support Co in a range of oxidation states from Co^I to Co^{III}. The Fe^{II} complex **1-40** was used to catalyze the hydrosilylation of a small scope of aldehydes and ketones (1 mol % catalyst, 1.5 equiv. triethoxysilane, 1-6 h reaction time).⁴⁸

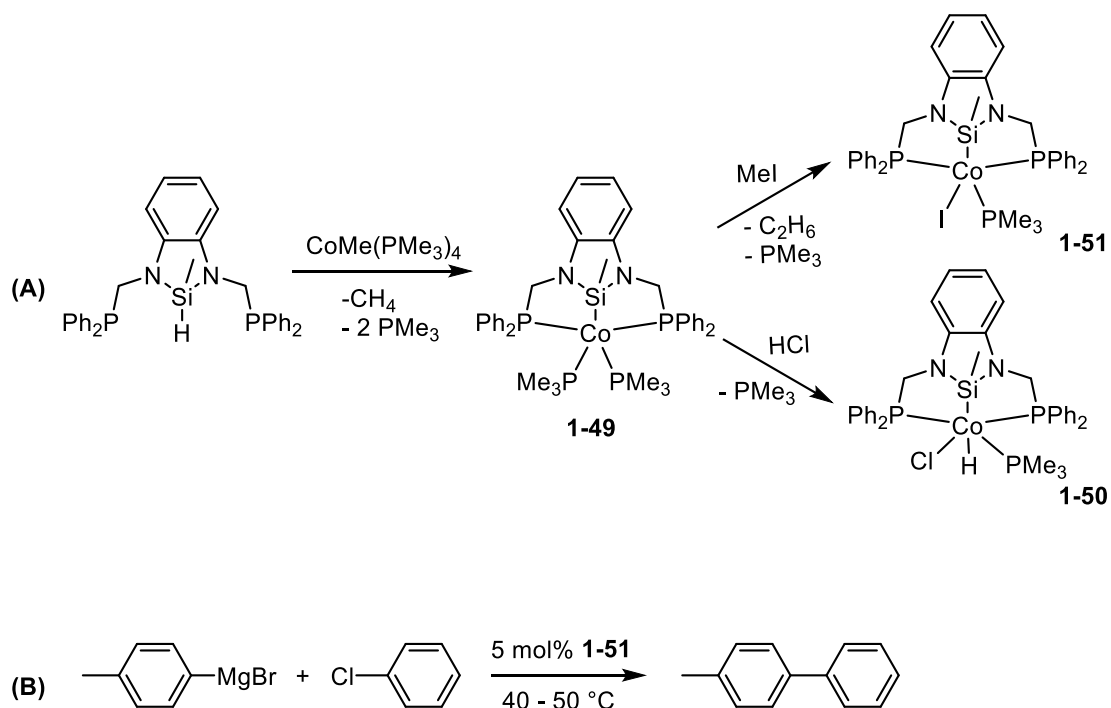
Another recent example of (PSiP)Co chemistry was reported by Kim, Lee, and co-workers⁴⁹ and highlighted an unusual example of an η¹-(Si-H)-Co interaction. The authors investigated the reaction of tertiary silanes (ⁱPrPSi^RP)H (^{Pr}PSi^RP = [κ^3 -(2-ⁱPr₂PC₆H₄)₂Si^R]⁻),

R = Me, Ph) with CoBr₂, finding that the initially formed species **1-45** is a complex wherein the PSiP ligand has coordinated to the Co center through both phosphorus donors as well as through an η^1 -(Si-H) interaction (Scheme 1.3.7). The authors were able to crystallographically characterize this complex and they further support their assignment of an η^1 -(Si-H) interaction with data from both ENDOR and DFT studies. Complex **1-45** subsequently reacted to afford complex **1-46**, in which both phosphorus donors are protonated. In the presence of an excess of NEt₃, **1-45** reacts to form the cyclometalated Co(II) silyl pincer complex **1-47**. This reactivity highlights an important aspect of PSiP complexation involving first-row transition metals. While Si-H oxidative addition is facile in the case of platinum group metals, it proves more challenging in the case of 3d-metals such as Co and Fe. Unlike E-H fragments that feature an acidic H, Si-H groups are hydridic and cannot be readily deprotonated to facilitate coordination to a metal center. However, pre-coordination of the Si-H bond to the metal (*e.g.*, via the formation of η^1 -(Si-H) species) may render it acidic, such that a simple amine base can readily deprotonate it, thereby leading to the formation of a metal silyl.



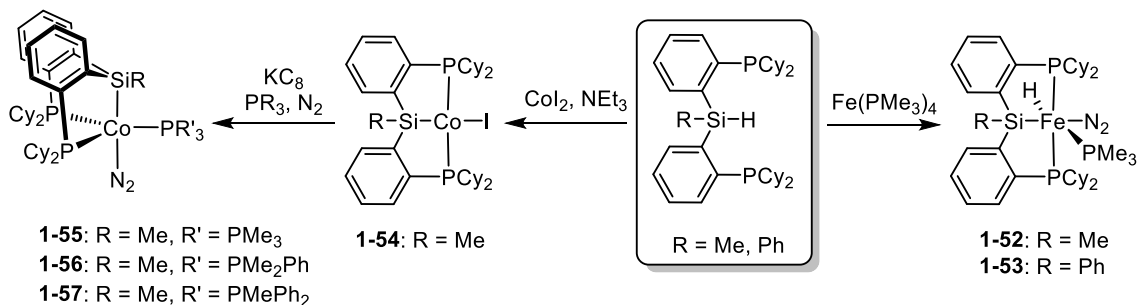
Scheme 1.3.7. Synthesis of a (PSiP)Co complex featuring an η^1 -(Si-H) interaction and the subsequent transformations it can undergo with (bottom) or without (top) base.⁴⁹

A recent report from Sun & co-workers details the synthesis of Fe and Co complexes supported by N-heterocyclic silyl PSiP ligation and their use as catalysts for Kumada cross couplings (Scheme 1.3.8).⁵⁰ Treatment of the neutral silane with $\text{Fe}(\text{PMe}_3)_4$ afforded $(\text{PSiP})\text{FeH}(\text{PMe}_3)_2$ (**1-48**) whereas $\text{CoMe}(\text{PMe}_3)_4$ gave $(\text{PSiP})\text{Co}(\text{PMe}_3)_2$ (**1-49**), which could be converted into $(\text{PSiP})\text{CoHCl}(\text{PMe}_3)$ (**1-50**) upon treatment with HCl, or $(\text{PSiP})\text{CoI}(\text{PMe}_3)$ (**1-51**) upon treatment with MeI (Scheme 1.3.8 A). It was noted that the Fe complex performed more poorly in hydrosilylation catalysis than the previously discussed **1-40**, which the authors attribute to the electronegative nitrogen atoms bound to silicon, which renders the dissociation of PMe_3 unfavorable, making the generation of a vacant coordination site for catalysis less feasible. Only **1-50** was a competent pre-catalyst for the desired Kumada cross couplings, and the authors found that it was capable of coupling a variety of aryl chlorides, bromides and iodides to several aryl Grignards in moderate yields employing 5 mol % catalyst at 40-50 °C (Scheme 1.3.8 B).



Scheme 1.3.8. (A) Synthesis of Co complexes supported by N-heterocyclic PSiP, and (B) Kumada cross-coupling of chlorobenzene with *p*-tolylmagnesium bromide.⁵⁰

Iwasawa, Nishibayashi, and co-workers further expanded the chemistry of Fe and Co with PSiP ligation through synthesis of complexes supported by Cy-PSi^RP ligands (Cy-PSi^RP = [κ^3 -(2-Cy₂PC₆H₄)₂SiR]⁻, R = Me, Ph) (Scheme 1.3.9).⁵¹ In similar fashion to Sun and co-workers,⁴⁸ the authors treated (Cy-PSi^RP)H ligands with Fe(PMe₃)₄ to afford complexes of the type (Cy-PSi^RP)FeH(N₂)(PMe₃) (**1-52** R = Me, **1-53** R = Ph). While related Co complexes could not be prepared by a similar route, (Cy-PSi^RP)CoI (**1-54** R = Me) was synthesized by treatment of the silane ligand precursor with CoI₂ in the presence of excess triethylamine (Scheme 1.3.9). Subsequent KC₈ reduction in the presence of a phosphine under an N₂ atmosphere afforded the Co(I) complexes of the type (Cy-PSi^RP)Co(PR₃)(N₂) in low yields (Scheme 1.3.9, complexes **1-55** – **1-57**). The Fe and Co dinitrogen complexes were investigated as catalysts for the reduction of N₂ to ammonia with KC₈ as a reductant and [H(OEt)₂][B(C₆F₅)₄] as a proton source. Only 1.2 equiv. of ammonia was generated using this method. Catalytic silylation employing Na as the reductant and Me₃SiCl as the silylating agent proved more viable, generating 15-26 equiv. of N(SiMe₃)₃ for Fe and 23-41 equiv. of N(SiMe₃)₃ for Co at a 0.2 mol% loading of each pre-catalyst, respectively.



Scheme 1.3.9. Synthesis of Fe and Co dinitrogen complexes supported by (Cy-PSiP) ligand variants.⁵¹

Work by the Turculet group has further expanded the scope of catalytic Fe and Co chemistry supported by Cy-PSiP (Cy-PSiP = [κ^3 -(2-Cy₂PC₆H₄)₂SiMe]⁻) ligation in two recent publications.^{9, 40} Having improved the synthesis of the Co complex **1-55** by using Mg as the reductant, subsequent exposure of **1-55** to H₂ was observed to afford a new diamagnetic Co hydride product featuring two broad ³¹P{¹H} resonances. The ¹H NMR spectrum revealed a broad hydride resonance at -13.51 ppm integrating to two hydrogens. This complex proved stable for several days under an atmosphere of H₂ and regenerated **1-55** when exposed to an atmosphere of N₂. Given that this complex could have the formulation of a Co^{III} dihydride or a nonclassical Co^I dihydrogen species (Figure 1.3.1), ¹H $T_{1(\text{min})}$ measurements as well as measurement of the ¹J_{HD} coupling constant of the partially deuterated complex were undertaken in an effort to further characterize the product resulting from addition of H₂. While the $T_{1(\text{min})}$ was low (less than 35 ms) and therefore consistent with a nonclassical dihydrogen complex, the proximity to nuclei with a high gyromagnetic ratio like Co can lead to misleadingly low relaxation times.⁵²⁻⁵⁴ The ¹J_{HD} coupling constant can thus be a better indicator in such a situation, as values between 15-35 Hz are consistent with a nonclassical formulation and have been correlated to H-H bond distances of the coordinated H₂.⁵⁵⁻⁵⁸ Upon preparation of the partially deuterated complex by treatment of **1-55** with HD gas two broad overlapping resonances were observed between -13 and -14 ppm by ¹H NMR analysis, however no discernible HD coupling could be observed, which is in line with a Co dihydride formulation. Variable temperature NMR experiments were also performed. Complex coalescence/decoalescence phenomena were observed for this complex in both the ¹H and ³¹P{¹H} NMR spectra over the range of +80 - -80 °C, which highlights the dynamic nature of this Co hydride species and suggests that

multiple hydride/dihydrogen species may be rapidly equilibrating in solution (Figure 1.3.1). The utility of **1-55** as a precatalyst for catalytic alkene hydrogenation was subsequently evaluated. It was found that complex **1-55** was capable of hydrogenating terminal alkenes under moderate conditions (10 atm H₂, 5 mol % Co, 60 °C, 4 h) but struggled with internal alkenes and those featuring carbonyl moieties.⁵¹

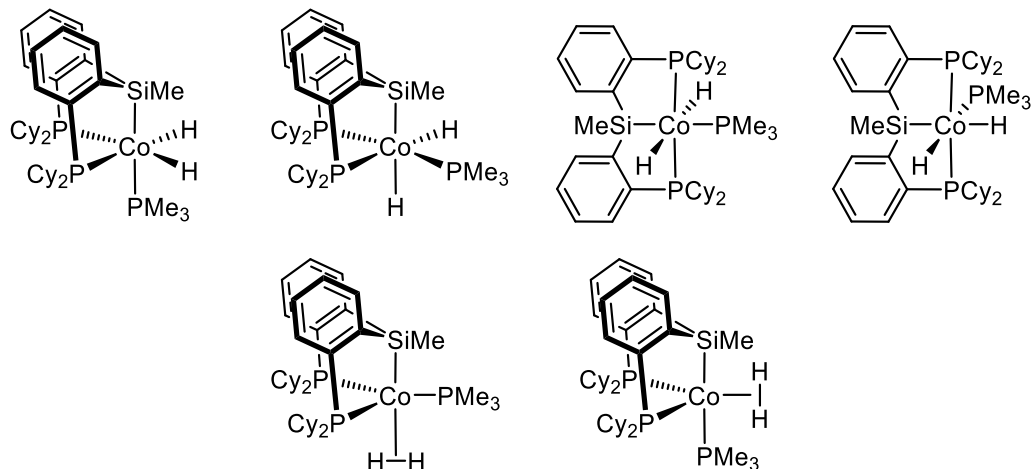
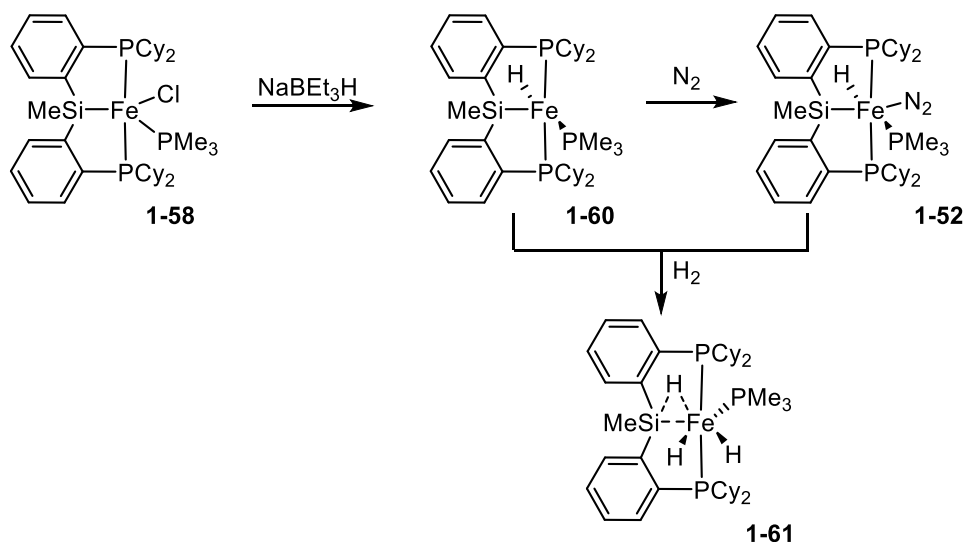


Figure 1.3.1. Possible structural formulations for the species arising from exposure of **1-55** to an atmosphere of H₂. (Top) examples of Co^{III} dihydride complexes (bottom) examples of nonclassical Co^I dihydrogen complexes.

Subsequent work from the Turculet group targeted the synthesis of low-coordinate (Cy-PSiP)Fe complexes.⁴⁰ Initial attempts to prepare four coordinate halide complexes of the type (Cy-PSiP)FeX (X = Cl, Br) by treatment of FeX₂ precursors with (Cy-PSiP)H in the presence of base gave rise to mixtures of products including, an Fe^{III} dihalide complex that was crystallographically characterized. These results highlight the potential for single electron transfer in this chemistry. Analogous reactions with the addition of donor ligands such as PMe₃ and CO led to the isolation of the Fe^{II} complexes (Cy-PSiP)FeCl(PMe₃) (**1-58**) and (Cy-PSiP)FeCl(CO)₂ (**1-59**) in high yields. Treatment of **1-58** with NaBEt₃H under an atmosphere of N₂ afforded (Cy-PSiP)FeH(PMe₃) (**1-60**), which upon standing converted to the previously reported complex **1-52**.⁵¹ Further reactivity was observed if these hydride

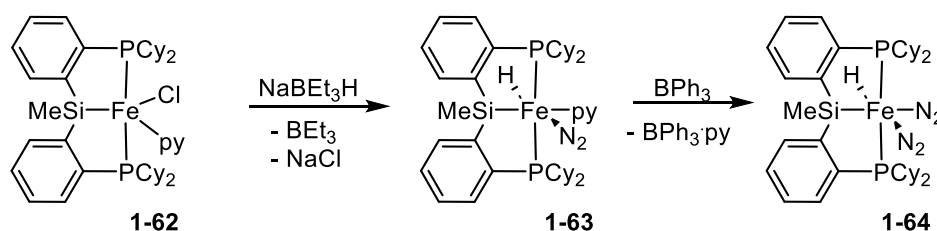
complexes were allowed to stand in solution, giving rise to a third diamagnetic hydride complex, **1-61**, featuring three broad hydride resonances in the ^1H NMR spectrum of the reaction mixture. Direct synthesis of **1-61** was achieved if the reaction of **1-58** and NaBEt_3H was performed under an atmosphere of H_2 . X-ray crystallographic analysis revealed the structure of **1-61** to be $(\text{Cy-P}(\eta^2\text{-(SiH)})\text{P})\text{Fe}(\text{H})_2(\text{PMe}_3)$ which features two terminal Fe hydrides and a third apparent $\eta^2\text{-(Si-H)}$ interaction ($^1J_{\text{SiH}} = 65$ Hz) (Scheme 1.3.10). NMR studies including NOESY, ^1H - ^{29}Si HMBC, and variable temperature experiments facilitated the unambiguous characterization of **1-61** in solution.



Scheme 1.3.10. Synthesis of $(\text{Cy-PSiP})\text{Fe}$ hydride complexes facilitated by PMe_3 coordination.

Complexes without stabilization from additional phosphine donor ligands were subsequently targeted. Towards this end, $(\text{py})_4\text{FeCl}_2$ and $(\text{Cy-PSiP})\text{H}$ were reacted in the presence of BnMgCl to generate the paramagnetic complex $(\text{Cy-PSiP})\text{FeCl}(\text{py})$ (**1-62**) in moderate yield. Treatment of this complex with NaBEt_3H led to the formation of the diamagnetic hydride complex $(\text{Cy-PSiP})\text{FeH}(\text{py})$ (**1-63**), which could be further reacted with triphenylborane to abstract the pyridine donor and afford $(\text{Cy-PSiP})\text{FeH}(\text{N}_2)_2$ (**1-64**)

in good yield (Scheme 1.3.11). X-ray crystallographic analysis of **1-64** revealed octahedral coordination geometry at the Fe center featuring two N₂ ligands as well as a hydride bound *cis* to the silyl donor. The acute Si-Fe-H angle of 78.8(7)°, relatively short Si-H distance of 2.44 Å (less than the sum of the van der Waals radii of 3.4 Å for H and Si), and ²J_{SiH} coupling constant of 70 Hz are all indicative of a nonclassical Si-H interaction (*i.e.* η²-(Si-H) interaction). However, the downfield ²⁹Si shift of 69.0 ppm as well as the Fe-H stretching frequency of 2012 cm⁻¹ by IR spectroscopy are more in line with a traditional metal silyl hydride complex. As such, the Si-H interaction is likely best formulated as a secondary Si-H interaction.⁵⁹



Scheme 1.3.11. Synthesis of (Cy-PSiP)Fe hydride complexes lacking exogenous phosphine donors.

As **1-64** can be viewed as a surrogate for the low coordinate (Cy-PSiP)FeH it was evaluated as a pre-catalyst for the hydrogenation of alkenes. Catalytic conditions were optimized to 10 atm H₂, 5 mol % Fe, 65 °C, and 4 h reaction time. Terminal alkenes, *cis/trans* internal alkenes, 1,1-disubstituted alkenes, and an example of a trisubstituted alkene were all hydrogenated with near quantitative conversions. Furthermore, the functional group tolerance was expanded to include examples featuring ether and ester functionalities. An alkyne was also semi-hydrogenated to the corresponding *trans* alkene under these conditions, with full hydrogenation being observed when the temperature was increased to 90 °C for 6 h. This work represents a rare examples of Fe catalyzed alkene

hydrogenation and serves to expand the scope of PSiP supported first row transition metal catalysis.

Of the chemistry reported thus for base metal complexes supported by PSiP ligation, trends that emerge include: (1) low coordinate complexes are accessible although their synthesis can be challenging; (2) low coordinate complexes are generally more reactive in catalytic applications; and lastly (3) there is significant evidence for the formation of η^2 -(SiH) species. In an effort to advance the application of such phosphino(silyl) complexes in hydrofunctionalization catalysis, this document describes the utility of PSiP supported Co^{I} alkyne complexes in alkene hydrogenation catalysis as shown in Chapter 2. Chapter 3 describes how PSiP Ni-H species can perform alkyne semihydrogenation catalysis while the work in Chapter 5 achieves the Ni mediated asymmetric hydrogenation of carbocyclic enamides through the development of chiral (indolylphosphino)silyl ligation.

1.4 First-Row Metal Catalyzed Asymmetric Hydrogenation

Transition metal catalyzed asymmetric hydrogenation of prochiral alkenes remains one of the most effective methods to access single enantiomer compounds. This fact was recognized in 2001 as Knowles and Noyori were awarded the Nobel Prize in Chemistry for their work on asymmetric hydrogenation.¹ Until recently, however, this reaction has been restricted to the platinum group metals due to their high catalytic activity, high enantioselectivity, and well-established ligand design.

As noted previously in this chapter (*vide supra*), the utility of the first-row transition metals is offset by their propensity to undergo single electron transfers, adopt multiple oxidation states, and their difficulty in performing two-electron chemistry such as oxidative addition. Ligand design that incorporates redox non-innocent motifs and heteroatoms that

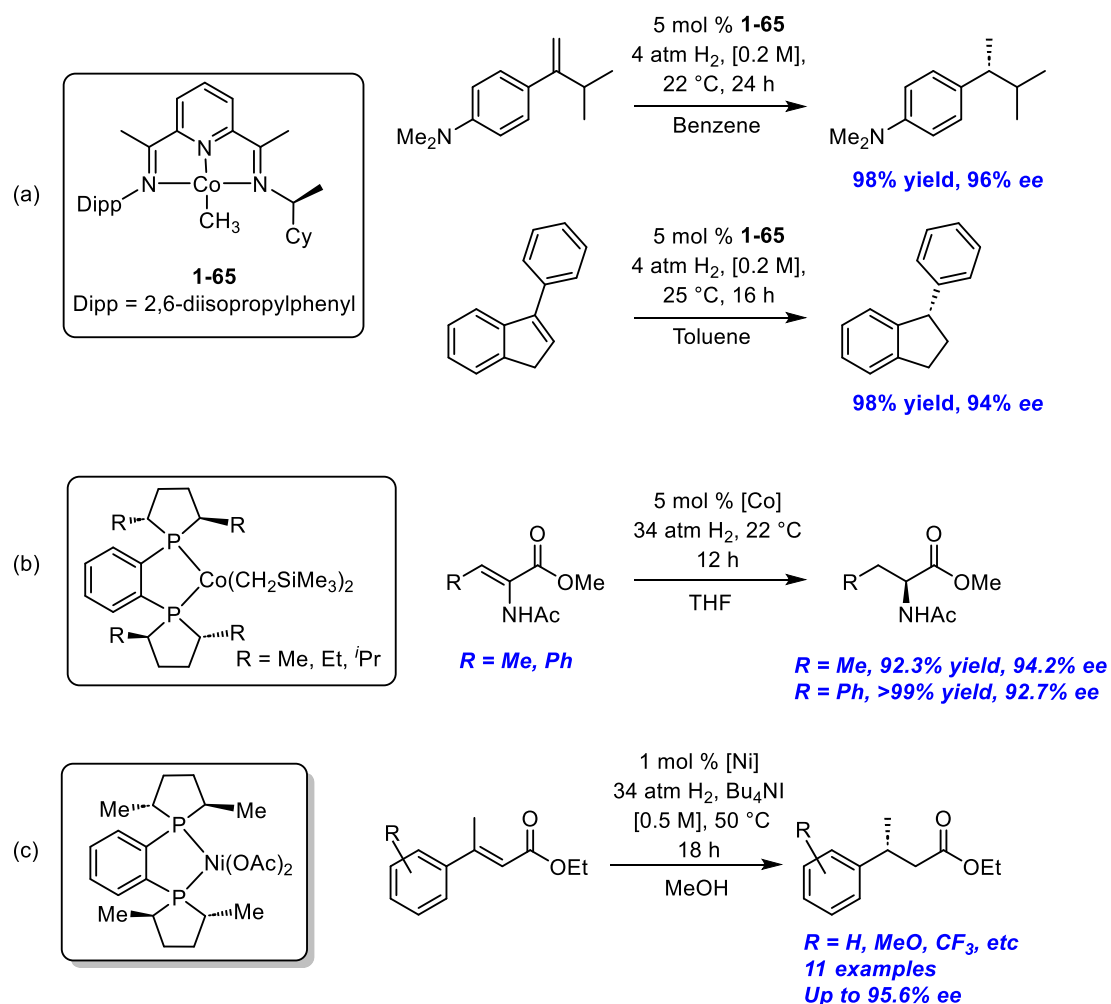
facilitate metal-ligand cooperativity have emerged as potent strategies to offset this behavior. These strategies have proven useful for a variety of catalytic reactions,^{14, 16, 60} but have not been applied towards the asymmetric hydrogenation of alkenes. Instead, a common strategy has been to employ rigid pincer ligands that incorporate chiral motifs or to repurpose privileged chiral bis(phosphines) that have been used in Rh catalyzed asymmetric hydrogenation.

The first example of highly selective base-metal catalyzed asymmetric hydrogenation of alkenes was reported in 2012 by Chirik and co-workers.¹⁹ By incorporating chiral amines into the bis(imino)pyridine ligand architecture Chirik and co-workers were able to synthesize several (PDI)CoCH₃ complexes that could perform the asymmetric hydrogenation of geminal-disubstituted alkenes. Complex **1-65**, which features an (*S*)-cyclohexylmethylamine moiety, could hydrogenate a small scope of styrene derivatives with *ee*'s as high as 96% (Scheme 1.4.1 (a)). Complex **1-65** was also shown to support the asymmetric hydrogenation of minimally functionalized alkenes such as 1-phenyl-1-indene and α -tetralone derived alkenes.²⁰ This work was notable as minimally functionalized alkenes are challenging substrates owing to their lack of coordinating functionality.

In 2013 the Chirik group disclosed the use of chiral bis(phosphines) commonly employed in Rh catalyzed asymmetric hydrogenation as ligands for Co catalyzed asymmetric hydrogenation. High-throughput screening identified several chiral bis(phosphines) that could support the Co catalyzed asymmetric hydrogenation of methyl 2-acetamidoacrylate, methyl 2-acetamido-3-phenylacrylate, and α -acetamidostyrene (Scheme 1.4.1 (b)).⁶¹ Ligands such as (*R,R*)-QuinoxP*, (*R,R*)-BenzP*, (*S,S*)-*i*Pr-DuPhos, and (*R,R*)-Et-DuPhos were shown to support highly enantioselective hydrogenation for

these substrates when combined with catalytic amounts of CoCl_2 and $\text{LiCH}_2\text{SiMe}_3$ as an activator.

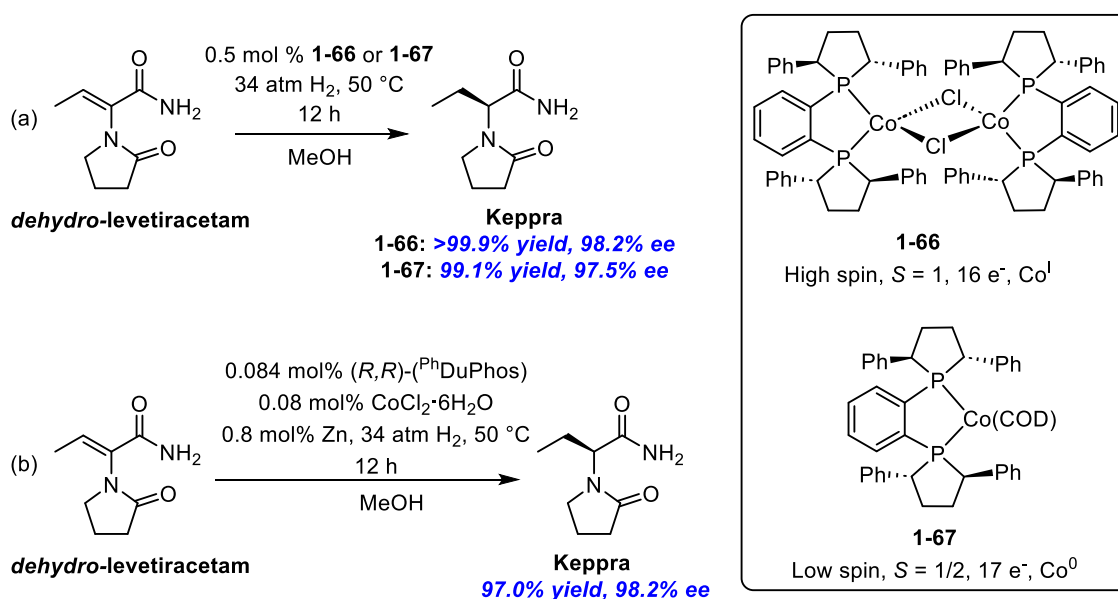
Further work from the Chirik group demonstrated the capability of Ni to effect asymmetric hydrogenation.⁶² High-throughput screening of a library of chiral bis(phosphines) identified the combination of $\text{Ni}(\text{OAc})_2$ and (*S,S*)-Me-DuPhos as capable of hydrogenating a scope of α,β -unsaturated esters with high conversion and moderate to good enantioselectivity (11 examples, 85-99% yield, 72-96% *ee*, Scheme 1.4.1 (c)). An investigation into the mechanism of this transformation identified the role of intermediate Ni carboxylates in facilitating heterolytic cleavage of dihydrogen. Furthermore, MeOH (the solvent) was found to be a proton source to complete product formation. This work demonstrates that first-row transition metals can employ non-traditional mechanisms while still achieving good enantioselectivity.



Scheme 1.4.1. (a) Asymmetric alkene hydrogenation enabled by **1-65**. (b) Chiral DuPhos supported Co catalyzed asymmetric hydrogenation of prochiral acrylamides discovered by high-throughput experimentation. (c) Ni catalyzed asymmetric hydrogenation of α,β -unsaturated esters discovered by high-throughput screening.

The Co pre-catalysts discussed thus far have all featured the Co^{II} oxidation state. While this has proven effective for catalysis, the Chirik group became interested in accessing the Co^I oxidation state due to its potential similarity to the Rh^I oxidation state found in privileged catalysts.⁶³ By once again employing high-throughput screening, Chirik and co-workers discovered that *in-situ* reduction of Co^{II} salts in the presence of a chiral bis(phosphine) in MeOH afforded rapid reduction to Co^I complexes that could support enantioselective hydrogenation catalysis. Furthermore, they discovered that catalytically

relevant low-spin Co^0 complexes stabilized by diene coordination could be accessed through further reduction. Complexes **1-66** and **1-67**, Co^{I} and Co^0 complexes of (*R,R*)-Ph-DuPhos, respectively, were isolated and shown to perform the asymmetric hydrogenation of *dehydro*-levetiracetam to provide levetiracetam (Keppra), a medication for the treatment of epilepsy. The active species could also be generated *in-situ* and applied to the 200-gram scale synthesis of Keppra in 97% isolated yield and 98.2% *ee* using only 0.084 mol% (*R,R*)-Ph-DuPhos and 0.08 mol% CoCl_2 in tandem with 0.8 mol% Zn dust (Scheme 1.4.2).

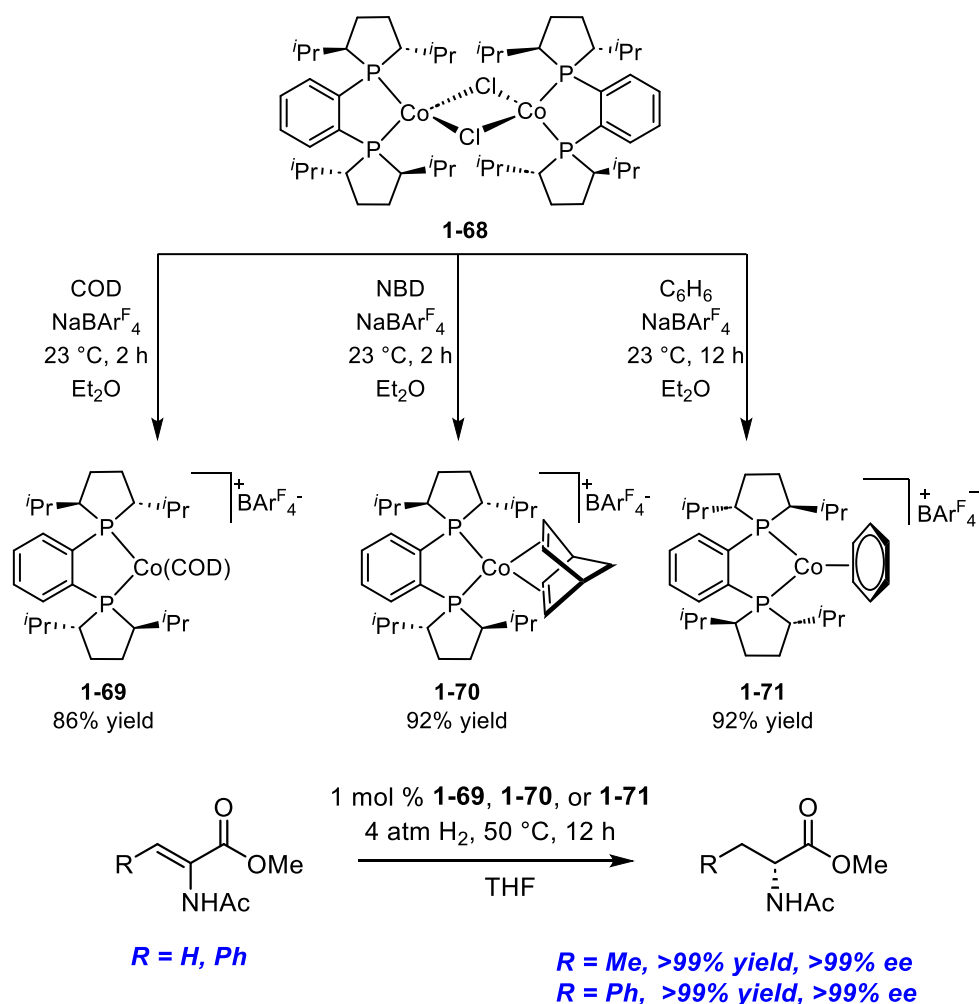


Scheme 1.4.2. Co catalyzed asymmetric hydrogenation of a pharmaceutically relevant enamide enabled through single electron reduction as shown by Chirik and co-workers. (a) Asymmetric hydrogenation mediated by isolated pre-catalysts **1-66** and **1-67** in the +1 and 0 oxidation state respectively. (b) *In-situ* generated pre-catalyst for the large-scale asymmetric hydrogenation of *dehydro*-levetiracetam.

The Chirik group next targeted cationic Co^{I} complexes as analogs of the Schrock-Osborn type η^2, η^2 -diene complexes that are privileged catalyst architectures within asymmetric hydrogenation.⁶⁴ Starting from complex **1-68**, the (*R,R*)-iPr-DuPhos analog of complex **1-66**, halide abstraction by $\text{NaBAR}^{\text{F}}_4$ in the presence of several dienes led to the formation of complexes **1-69**, **1-70**, and **1-71**, which featured 1,5-cyclooctadiene (COD),

norbornadiene, and η^6 - benzene ligation, respectively (Scheme 1.4.3). These complexes were found to be diamagnetic, 16-electron, Co^{I} cations and were characterized by multinuclear NMR spectroscopy as well as X-ray crystallographic analysis.

When complexes **1-69**, **1-70**, and **1-71** were evaluated as pre-catalysts for the asymmetric hydrogenation of methyl 2-acetamidoacrylate and methyl 2-acetamido-3-phenylacrylate quantitative conversions and essentially complete enantioselectivities were observed. The conditions employed (4 atm H_2 , 1 mol % Co) were mild when compared to the previously reported asymmetric hydrogenation of the same substrates mediated by a Co^{II} pre-catalyst (*vide supra*). Moreover, the enantioselectivity was higher (>99% *ee*) as was the conversion. A 2-acetamidoacrylate bound intermediate was isolated and exposed to 1 atm of H_2 wherein the authors observed liberation of the (*S*)-hydrogenation product, the opposite that was observed under catalytic conditions. The authors proposed a Curtin-Hammett regime wherein substrate coordination is fast and reversible as compared to the oxidative addition of H_2 .



Scheme 1.4.3. Top: Synthesis of cationic Co^I complexes reminiscent of Schrock-Osborn type catalyst for asymmetric hydrogenation. Bottom: Asymmetric hydrogenation of methyl 2-acetamidoacrylate and methyl 2-acetamido-3-phenylacrylate mediated by complexes **1-69**, **1-70**, and **1-71**.

Since the seminal reports by Chirik and co-workers establishing the ability of Co and Ni to perform highly enantioselective asymmetric hydrogenation, continued research in this area has lent further support for the utility of Co- and Ni-based hydrogenation catalysts that can operate across a range of oxidation states. Furthermore, unique reactivity can be achieved due to the smaller size and different oxidation states available to the first-row metals.

Huang and co-workers described the Co-catalyzed asymmetric hydrogenation of vinylsilanes with a chiral PNO phosphine-pyridine-oxazoline ligand.⁶⁵ The corresponding Co^{II} halide complex **1-72** was shown to react with NaBHET₃ to generate the catalytically active species that could, in turn, hydrogenate a broad scope of aryl-substituted vinyl silanes with moderate to high enantioselectivity (46-99% *ee*) under 2 atm H₂ at room temperature. The enantioenriched products were then further derivatized into optically active silolanes *via* Ru-catalyzed C-Si bond formation (Scheme 1.4.4 (a)).

The utility of Co in the asymmetric hydrogenation of α/β -unsaturated carboxylic acids was demonstrated by Zhang and co-workers.⁶⁶ These substrates are exceptionally challenging when compared to α/β -unsaturated esters due to the stability of the intermediate metallalactone that can form upon carboxylate coordination. Nonetheless, Zhang and co-workers were able to demonstrate that by employing Co(acac)₂ in the presence of (*S,S*)-Ph-BPE and Zn dust under 40 atm H₂ at room temperature, high yields and enantioselectivities could be achieved for a broad scope of α/β -unsaturated carboxylic acids (Scheme 1.4.4 (b)). This included the synthesis of the enantiomer of Naproxen, a nonsteroidal anti-inflammatory drug, in 99% yield with 96% *ee*.

When investigating the mechanism through deuterium labeling experiments the authors found that no deuterium incorporation occurred when isopropanol-*d*₈ was used as the solvent. Furthermore, when 40 atm of D₂ was used in place of H₂, the corresponding deuterium-labeled product was obtained with no evidence of proton incorporation from the solvent (MeOH). No reaction occurred when the hydrogenation of an ethyl ester was attempted, indicating that for this system the intermediate metal carboxylate is required for high activity. Finally, the authors propose a mechanism wherein the catalyst is activated

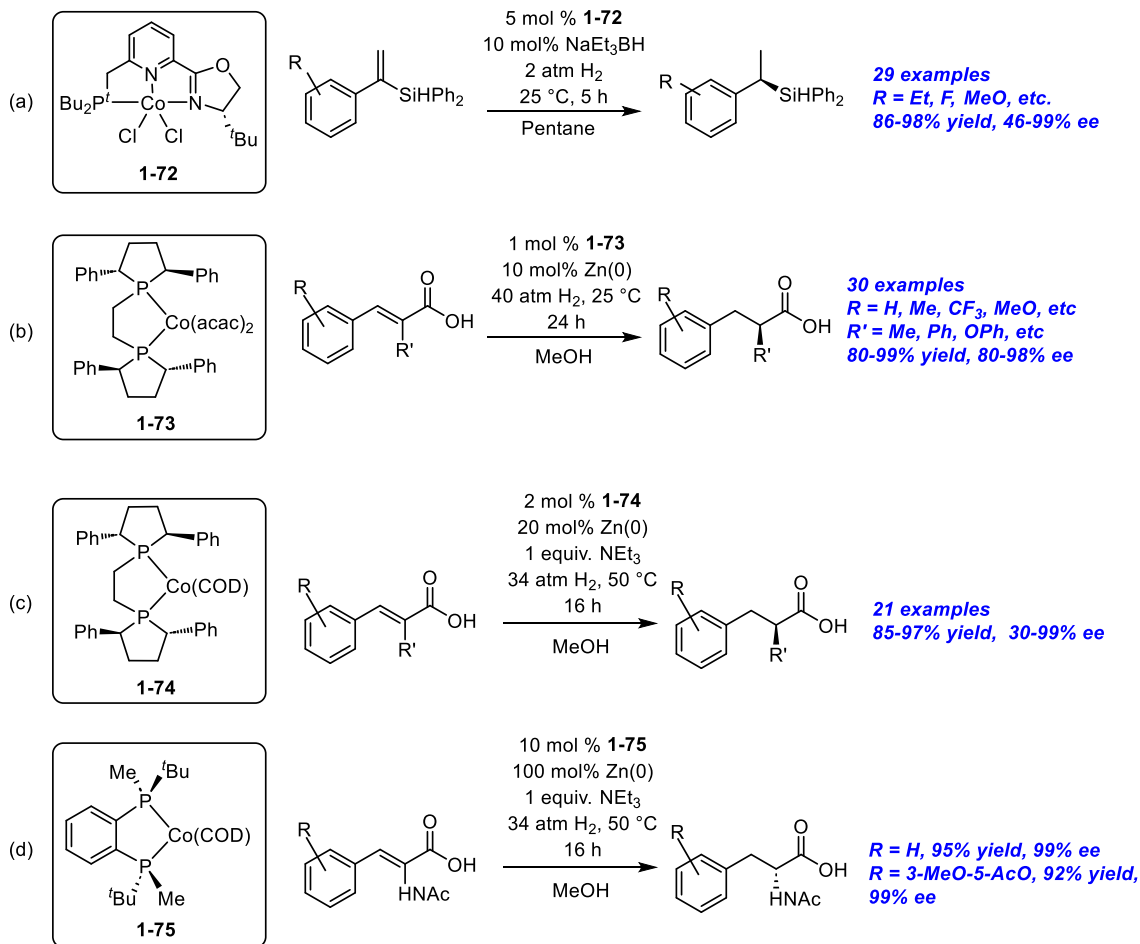
via carboxylate-assisted hydrogen deprotonation followed by subsequent migratory insertion to the substrate, sigma-bond metathesis of the intermediate alkyl, and substrate turnover that is assisted by protonation of the intermediate Co carboxylate by another equivalent of substrate.

Chirik and co-workers also reported on the Co catalyzed asymmetric hydrogenation of α/β -unsaturated carboxylic acids simultaneously with the Zhang group's disclosure.⁶⁷ While the Chirik group also identified (*R,R*)-Ph-BPE as the optimal ligand for this transformation, the oxidation state, operative mechanism, and reaction conditions differed from those reported by Zhang. Employing 2 mol % of complex **1-74**, a Co⁰ complex of the form (*R,R*)-(Ph-BPE)Co(COD), 20 mol % Zn dust, and one equivalent of NEt₃ under 34 atm of H₂ at 50 °C in MeOH, Chirik and co-workers were also able to achieve high isolated yields and enantioselectivity for the asymmetric hydrogenation of α/β -unsaturated carboxylic acids (Scheme 1.4.4 (c)). Pharmaceutically relevant compounds such as Naproxen, and (*S*)-Flurbiprofen were isolated with *ee* values of 99% and 97%, respectively.

The authors were also able to perform the asymmetric hydrogenation of *dehydro- α* -amino acids such as (*Z*)-*dehydro-N*-acetylphenylalanine and (*Z*)-*dehydro-N*-acetyl-(4-acetoxy-3-methoxy) phenylalanine when the Co⁰ complex (*R,R*)-(BenzP*)Co(COD) (**1-75**) was used instead (Scheme 1.4.4 (d)). The products for both substrates were isolated in high yield (95% and 92% yield, respectively) with almost perfect enantioselectivity (99% *ee*). The asymmetric hydrogenation of (*Z*)-*dehydro-N*-acetyl-(4-acetoxy-3-methoxy) phenylalanine is particularly notable, as the product is the precursor to *D*-DOPA, the biologically inactive enantiomer of the drug *L*-DOPA that is used in the treatment of Parkinson's disease. Knowles' work on the asymmetric hydrogenation of *dehydro- α* -amino

acids led to the first commercial synthetic route for the direct synthesis of enantiopure *L*-DOPA. The prevalence of such amino acid motifs in the pharmaceutical industry renders such *dehydro- α* -amino acid substrates desired targets for base-metal catalysts.

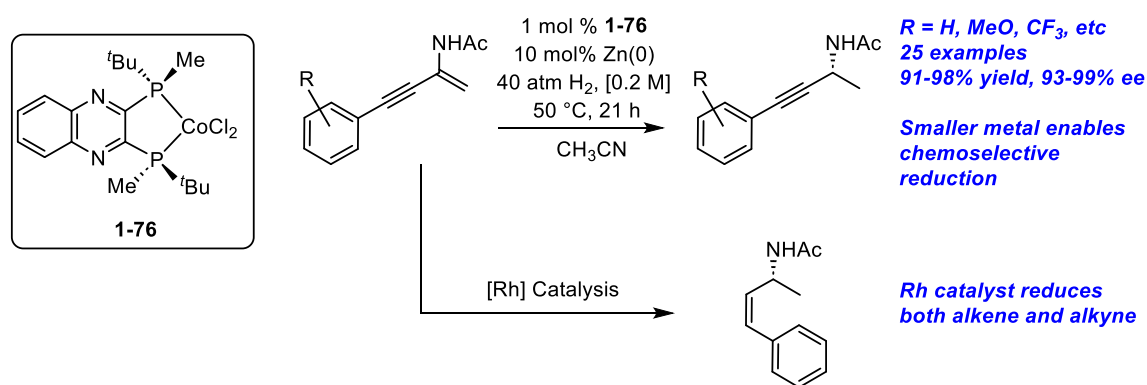
A probe into the mechanism of (*R,R*)-(Ph-BPE)Co-catalyzed asymmetric hydrogenation by the Chirik group provided support for a different pathway than was reported by Zhang and co-workers (*vide supra*). Like Zhang, Chirik did not observe any proton incorporation into the product arising from the methanol solvent, and deuterium was only included in the products when D₂ was used. Additionally, when no triethylamine or Zn dust was added, the same deuterium incorporation was observed, suggesting that the intermediacy of Zn or ammonium carboxylates is unlikely. These could not be definitively ruled out, however, as under catalytic conditions minute amounts of these species may be unobserved and can aid in catalyst turnover. The authors also proposed that homolytic cleavage of H₂ by the Co⁰ complexes was generating a transient Co^{II} dihydride, although this could not be observed by EPR spectroscopy due to the relatively low pressures of hydrogen employed for the spectroscopic experiment (4 atm). Migratory insertion of the alkene followed by C-H reductive elimination would afford the observed products.



Scheme 1.4.4. Asymmetric hydrogenation of alkenes featuring various substitution patterns mediated by Co. (a) Asymmetric hydrogenation of vinylsilane reported by Huang and co-workers. (b) Asymmetric hydrogenation of α/β -unsaturated carboxylic acids reported by Zhang and co-workers. (c) Asymmetric hydrogenation of α/β -unsaturated carboxylic acids reported by Chirik and co-workers. (d) Asymmetric hydrogenation of α -dehydroamino acids reported by Chirik and co-workers.

The Zhang group has also disclosed an example of the unique selectivity that can be achieved when using a base-metal catalyst system.⁶⁸ When (*R,R*)-QuinoxP* was used in conjunction with catalytic amounts of CoCl_2 (**1-76**) and Zn dust, both chemo- and enantioselective hydrogenation of conjugated enynes could be achieved (Scheme 1.4.5). The authors targeted conjugated enynes bearing amide functionality, as this class of substrates is difficult to reduce chemoselectively. Well established Rh catalysts were found to be incapable of selecting for reduction of the alkene, affording only the conjugated

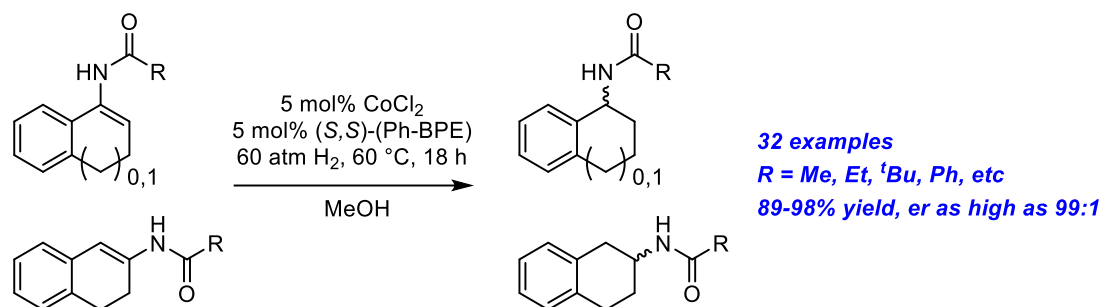
enamide products due to the large atomic size of Rh. With the use of Co, however, excellent enantioselectivity, chemoselectivity, and isolated yields were obtained for the chiral propargylamine products. A small mechanistic study concluded that the active oxidation state was likely a cationic Co^{I} species, as no reaction occurred in the absence of Zn. Furthermore, when $\text{CoCl}(\text{PPh}_3)_3$ was used as the Co source, no reaction occurred unless a catalytic amount of ZnCl_2 was also included to the reaction as a means of halide abstraction. Deuterium incorporation was found exclusively at the positions resulting from alkene reduction when D_2 was used.



Scheme 1.4.5. Highly chemo- and enantioselective hydrogenation of conjugated enynes enabled by the use of a base-metal catalyst as reported by Zhang and co-workers.

Another class of substrates that has proven to be particularly challenging for platinum group metal catalysts is carbocyclic tri-substituted enamides. The chiral products of these reactions are important structural motifs in pharmaceuticals such as Tametraline (norepinephrine-dopamine reuptake inhibitor), Sertraline (antidepressant), Rotigotine (dopamine agonist), and Rasagiline (anti Parkinson's therapeutic). Work by de Vries and co-workers sought to access Co-catalyzed asymmetric hydrogenation of these substrates, as existing catalysts based on precious metals struggled to achieve high enantioselectivity.⁶⁹

De Vries and co-workers found that by employing 5 mol% CoCl₂ in the presence of 5 mol% (*S,S*)-Ph-BPE under 60 atm H₂ at 60 °C in MeOH high enantioselectivity could be achieved for a broad scope of α - and β -cyclic enamides (Scheme 1.4.6). Six and seven membered rings as well as those bearing heteroatom substitution could be hydrogenated with good to excellent enantioselectivity. As with the examples discussed previously (*vide supra*), the use of MeOD-*d*₄ as solvent did not lead to deuterium incorporation into the products while the use of 60 atm D₂ did for both α - and β -cyclic enamide substrates. Through the use of EPR spectroscopy and mass spectrometry the authors identified plausible substrate bound intermediates and proposed a mechanism wherein the oxidation state of Co remains as Co^{II}, with substrate turnover occurring through a sigma-bond metathesis pathway. The authors were able to isolate 1,2,3,4-tetrahydronaphthalen-1-amine on a gram scale following deprotection of the amide, with full retention of configuration.



Scheme 1.4.6. Co-catalyzed asymmetric hydrogenation of carbocyclic tri-substituted enamides as reported by de Vries and co-workers.

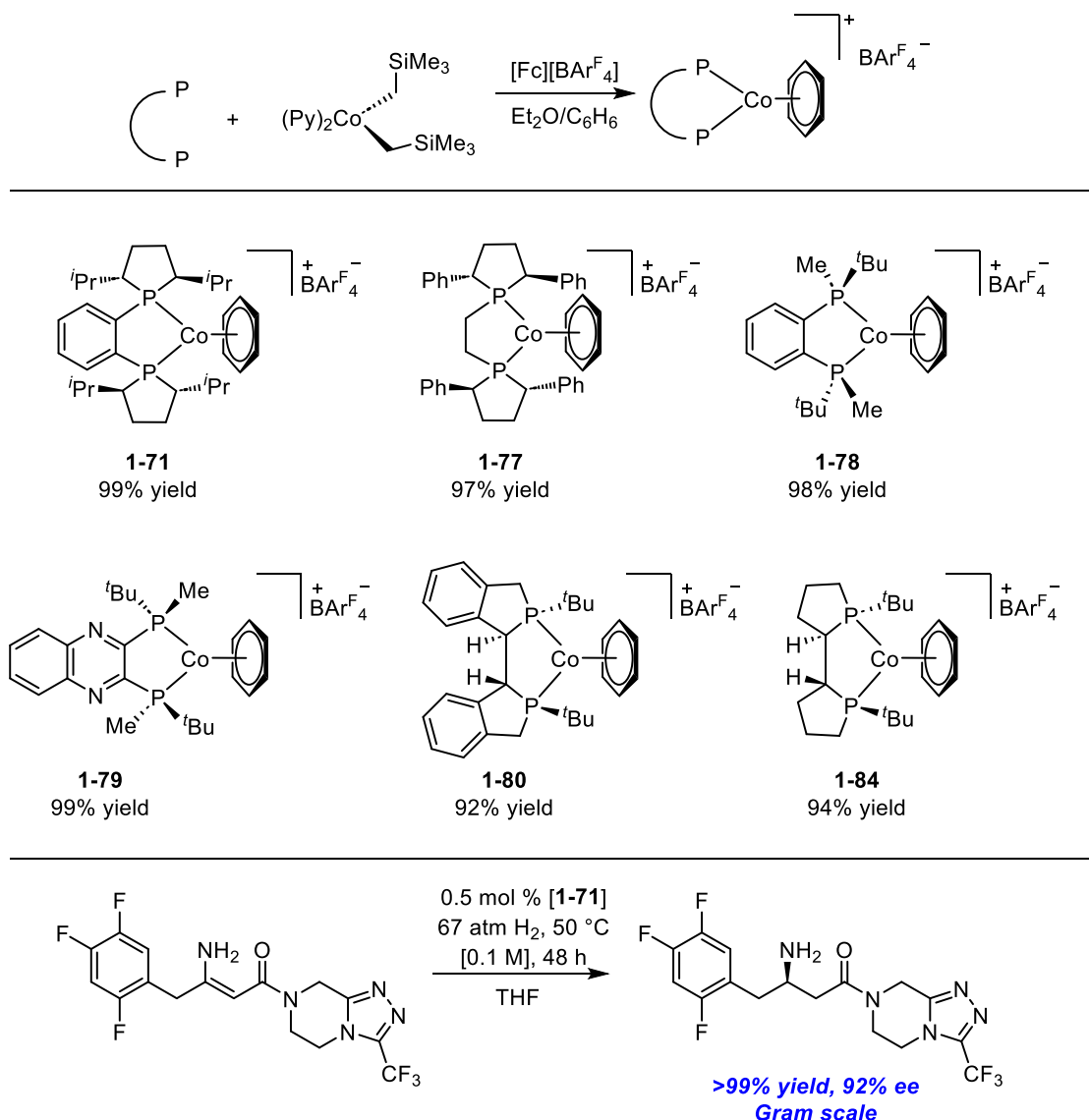
The examples discussed thus far have shown that Co can support asymmetric hydrogenation across a range of oxidation states. However, few examples employ well defined pre-catalysts, instead opting for the generation of the active species *in situ* and determining the active oxidation state after the fact. The Chirik group sought to expand synthetic methodology to access cationic Co^I species in a reliable way such that they could

be rapidly screened with a library of chiral ligands.⁷⁰ As a result, the Chirik group established a general reaction sequence that could be performed to access cationic $\text{Co}^{\text{I}}\eta^6$ -arene complexes of the form $[(\text{PP})\text{Co}(\eta^6\text{-arene})][\text{BAr}^{\text{F}}_4]$.

When $\text{bis}(\text{pyridine})\text{Co}(\text{CH}_2\text{SiMe}_3)_2$ was oxidized from Co^{II} to Co^{III} by ferrocenium tetrakis(3,5-bis(trifluoromethyl)phenyl)borate ($[\text{Fc}][\text{BAr}^{\text{F}}_4]$) in the presence of a bis(phosphine), diethyl ether, and arene, the corresponding Co^{I} cation could be isolated in high yield. These Co^{I} species arise through one-electron oxidation-induced reductive elimination from the resulting Co^{III} dialkyl complexes, which are then trapped by arene coordination (Scheme 1.4.7, top). This method was found to be general for most chiral bis(phosphines) except for those bearing ferrocene substitution, such as the JosiPhos family, where the ligand was oxidized instead. This method afforded the previously discussed complex **1-71** in high yield as well as the new complexes **1-77** - **1-84**. All complexes were found to be diamagnetic, crystalline solids that were characterized by multinuclear NMR spectroscopy as well as X-ray crystallography.

These complexes were screened as pre-catalysts for the asymmetric hydrogenation of *dehydro*-Sitagliptin which features an unprotected enamine. The Rh catalyzed asymmetric synthesis of Sitagliptin (a treatment for type II diabetes) was a transformative advancement in the field of homogeneous asymmetric hydrogenation catalysis and has been a so-called “holy grail” for base-metal catalysts.⁷¹ While all Co pre-catalysts provided some degree of enantioselectivity for this transformation, complex **1-71** provided >99% yield of Sitagliptin with near perfect enantioselectivity (97% *ee*) under screening conditions (0.5 mol% **1-71**, 68 atm H_2 , room temperature, [0.03 M], THF). When this reaction was performed on a

gram-scale a similarly high yield was obtained, albeit with a slight loss of enantioselectivity (92% *ee*) (Scheme 1.4.7, bottom).

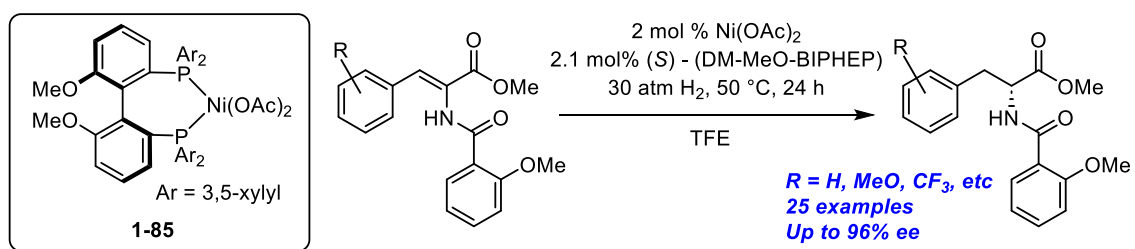


Scheme 1.4.7. Top: Synthesis of cationic (PP)Co^I arene complexes *via* one-electron oxidation-induced reductive elimination from a Co^{II} starting material. Bottom: Co-catalyzed asymmetric synthesis of Sitagliptin using **1-71** as the pre-catalyst.

When compared to Co, the use of Ni in the direct catalytic asymmetric hydrogenation of alkenes is relatively underdeveloped. X. Zhang and co-workers were able to achieve the diastereoselective hydrogenation of tetrasubstituted fluorinated enamides using a mixture of Ni(OAc)₂ and (*S*)-Binapine under 50 atm of H₂ at 80 °C using trifluoroethanol as the

solvent.⁷² Exceptionally high enantioselectivity was observed (96-99% *ee*) for all substrates, as was selectivity for *syn*-hydrogenation. The authors found that use of acidic solvent (trifluoroethanol) was crucial, as the reaction rate and diastereoselectivity decreased significantly when the less acidic methanol was used instead.

W. Zhang and co-workers disclosed a similar transformation wherein Ni(OAc)₂ in conjunction with an axially chiral ligand (*S*)-DM-MeO-BIPHEP was able to perform the asymmetric hydrogenation of 2-amidoacrylates across a broad substrate scope (Scheme 1.4.8).⁷³ This work also identified the crucial role of trifluoroethanol in achieving high catalyst turnover, and demonstrated that when deuterated trifluoroethanol was employed as the solvent deuterium was incorporated into the 2-position of the hydrogenation product. The authors surmised that the proton incorporated into the 1-position originates from H₂ while the proton in the 2-position originates from H⁺ in the reaction medium (trifluoroethanol and/or catalytic amounts of acetic acid derived from the acetate ligand). Furthermore, the authors identified complex **1-85** as the pre-catalyst species while also observing an off-cycle species resulting from bis-ligation of the bis(phosphine) ligand that was not catalytically competent.



Scheme 1.4.8. Ni-catalyzed asymmetric hydrogenation of 2-amidoacrylates as reported by W. Zhang and co-workers.

The examples outlined above represent nearly all of the recent reports on Co- and Ni-catalyzed asymmetric hydrogenation of alkenes. As such, there is significant opportunity

to expand the space of ligands that can support this transformation, as well as increase the scope of functionalized alkenes that can be hydrogenated with high selectivity by 3*d*-metals. Almost all the examples outlined above take the approach of repurposing privileged bis(phosphines) that have been employed in Rh-catalyzed asymmetric hydrogenation for base-metal catalysis. Work described in Chapter 4 of this document describes the development of a chiral mixed phosphine/phosphonite ligand that is readily prepared from a commercially available chiral diol. This ligand was applied towards the Co-catalyzed asymmetric hydrogenation of a broad scope of α -dehydroamino acids with high enantioselectivity.

Work described in Chapter 5 of this document further expands the space of ligands that can support base-metal catalyzed asymmetric hydrogenation and achieves a long-standing goal of research in the Turculet group—to combine the reactivity of (phosphino)silyl-ligated 3*d*-metal complexes in hydrofunctionalization catalysis with high enantioselectivity. Work in this chapter details the development of a new class of chiral ligands that can support the Ni-catalyzed asymmetric hydrogenation of functionalized enamides.

Chapter 2: Synthesis and Characterization of (Cy-PSiP)Co^I Complexes for Catalytic Alkene Hydrogenation

2.1 Introduction

As outlined in Chapter 1 of this document, base-metal complexes supported by tridentate pincer ligands have been shown to be exceptionally reactive in a variety of catalytic applications. Ligands incorporating redox non-innocent motifs¹⁴ or basic heteroatoms to facilitate metal-ligand cooperativity²⁴ have emerged as powerful tools to control the reactivity of first-row transition metal complexes. By comparison, the synthesis and catalytic application of first-row metal complexes supported by bis(phosphino)silyl (PSiP) ligation have been relatively unexplored until recently. In particular, reports of isolable (PSiP)Co complexes have been limited to a small number of examples from the Sun,^{48, 50} Lee,⁴⁹ Nishibayashi,⁵¹ and Turculet groups.⁹ The incorporation of silyl donors in the coordination sphere of Co has the potential to give rise to metal-silyl cooperativity involving the formation of σ -Si-H complexes via the transfer of hydride equivalents between Co and the electropositive Si center. Such reactivity could, in principle, allow Co to maintain a preferred lower oxidation state in the course of E-H bond activation processes (E = main group element) and may facilitate turnover in hydrofunctionalization catalysis.

In this context, this Chapter targets the synthesis of new, coordinatively unsaturated Co complexes supported by Cy-PSiP (Cy-PSiP = κ^3 -(2-Cy₂PC₆H₄)₂SiMe) for application in alkene hydrogenation catalysis. Alkene hydrogenation is one of the most important and widely employed catalytic reactions known, and has applications ranging from petrochemistry to fine chemical synthesis.⁷⁴ Traditional catalysts for this transformation are dominated by the platinum group metals, however recent advances have been made in

the development of earth abundant metal catalysts capable of performing this transformation.¹⁵ Cobalt in particular has come to the forefront as a capable metal for alkene hydrogenation catalysis, and has seen extensive development in recent years (Figure 2.1.1).

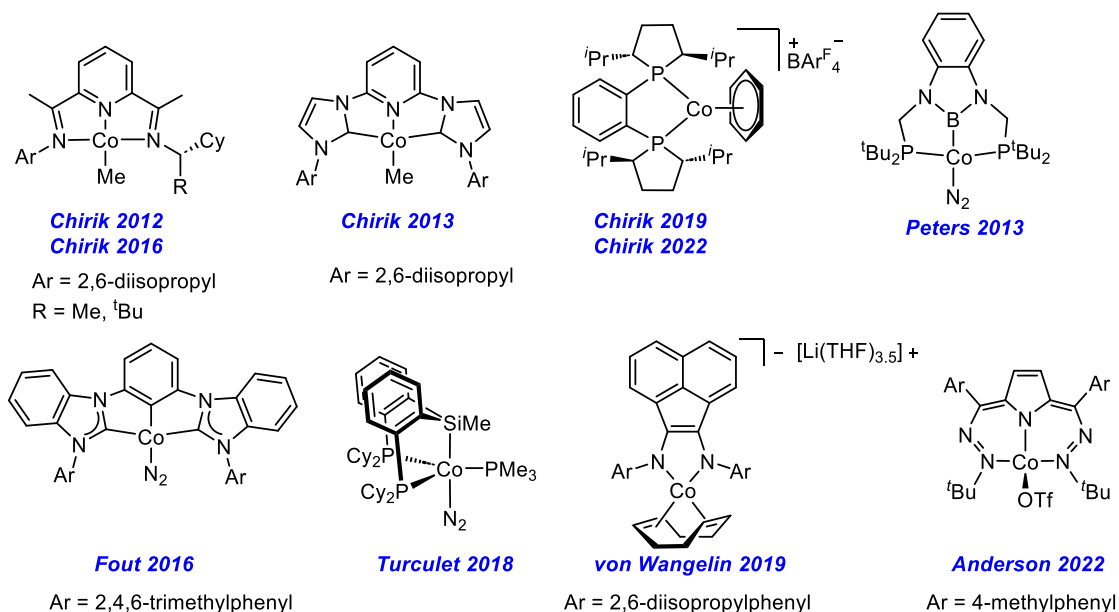
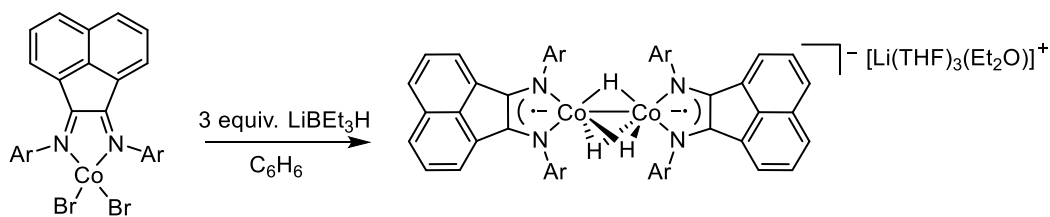


Figure 2.1.1. Selected examples of homogeneous Co catalysts for the hydrogenation of alkenes featuring redox non-innocent ligands, ligands capable of engaging in metal-ligand cooperativity, and strong field ligands.

Work from the Chirik group has shown that bidentate bis(phosphines) as well as tridentate pyridine(diimine) and bis(carbene)pyridine ligands are all capable of supporting alkene hydrogenation at Co (Figure 2.1.1).^{19-20, 64, 67, 70, 75-77} Notably, this has led to active catalysts capable of hydrogenating sterically hindered alkenes such as 1,2-dimethylbutene,⁷⁵ indene derivatives, and stilbene derivatives under exceptionally mild conditions (4 atm H₂, 5 mol% Co, 25-50 °C, 18 h).²⁰ The Fout group has shown that strong-field ligands that do not engage in metal-ligand cooperativity can also support hydrogenation catalysis at Co, including both alkene hydrogenation and alkyne semihydrogenation (Figure 2.1.1).^{13, 78-79} A phenyl bis(carbene) (CCC) supported Co(I)

triphenylphosphine complex $(\text{CCC})\text{Co}(\text{N}_2)(\text{PPh}_3)$ was shown to hydrogenate a small scope of alkenes under mild conditions (4 atm H_2 , room temperature, 2 mol% Co) while an increase in temperature to 60 °C was required to hydrogenate cyclic alkenes. Exposure of the $(\text{CCC})\text{CoN}_2(\text{PR}_3)$ complexes to an atmosphere of H_2 led to the reversible formation of the non-classical dihydrogen complex $(\text{CCC})\text{Co}(\text{H}_2)(\text{PR}_3)$, the formulation of which was confirmed via extensive NMR studies. Further mechanistic investigation was performed through use of parahydrogen induced polarization (PHIP) transfer which determined that substrate coordination and oxidative addition of H_2 occurred in a concerted manner and was reversible.

Work from von Wangelin and co-workers has shown that a redox non-innocent bis(imino)acenaphthalene ligand (BIAN) can support highly reduced Co(-I) complexes that displayed good activity for olefin hydrogenation as well as the hydrogenation of imines and quinolines (Figure 2.1.1).⁸⁰ Catalysis was performed under generally mild conditions (2-10 bar H_2 , 3 mol % Co, 20-60 °C, 24 h) and included challenging substrates such as substituted 1-cyclohexene derivatives, a tri-substituted α/β -unsaturated ester, conjugated imines, and substituted quinolines. An investigation into the mechanism allowed for isolation of a tri(hydrido)Co dimer $[(\text{BIAN})\text{Co}(\text{H})_3]_2$ that the authors speculated was a catalyst resting state (Figure 2.1.2). Despite the highly reduced nature of the Co center, the authors propose a homogeneous catalysis mechanism as evidenced by immediate catalysis onset, steady conversion, and a zero-order rate with respect to substrate. Furthermore, a plot of the initial rates versus catalyst concentrations showed a first order rate in Co and the attempted amalgamation of the catalyst with 300 equiv. Hg had only a small effect on the rate.



Ar = 2,6-diisopropylphenyl

Scheme 2.1.1. Synthesis of the trihydride complex (BIAN)Co(H)₃ from (BIAN)CoBr₂.⁸⁰

Anderson and co-workers have recently disclosed a dihydrazonopyrrole (DHP) ligand that is capable of supporting hydrogenation at Co through ligand-based storage of dihydrogen (Figure 2.1.2).⁸¹ The authors found that exposing the triflate complex (DHP)Co(OTf) to an atmosphere of dihydrogen gave rise to an unstable complex formulated as the doubly protonated (DHP-H₂)Co(OTf) complex that arises from protonation of the hydrazone linkage. (DHP)Co(OTf) was an active catalyst for the hydrogenation of a small scope of alkenes under mild conditions (1-10 mol% Co, 1-4 atm H₂, room temperature). The complex was largely intolerant of substrates that did not feature terminal alkenes.

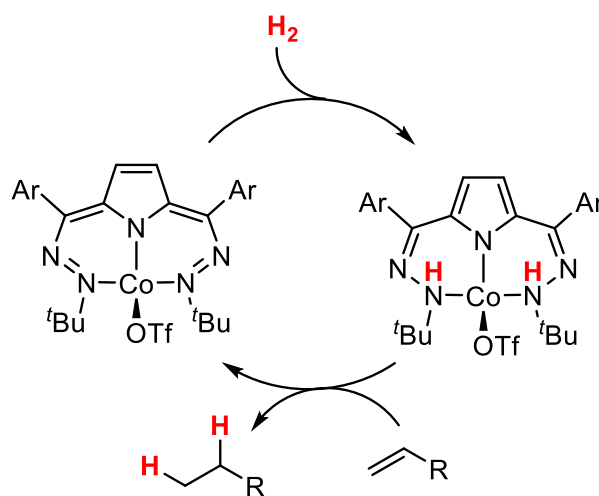
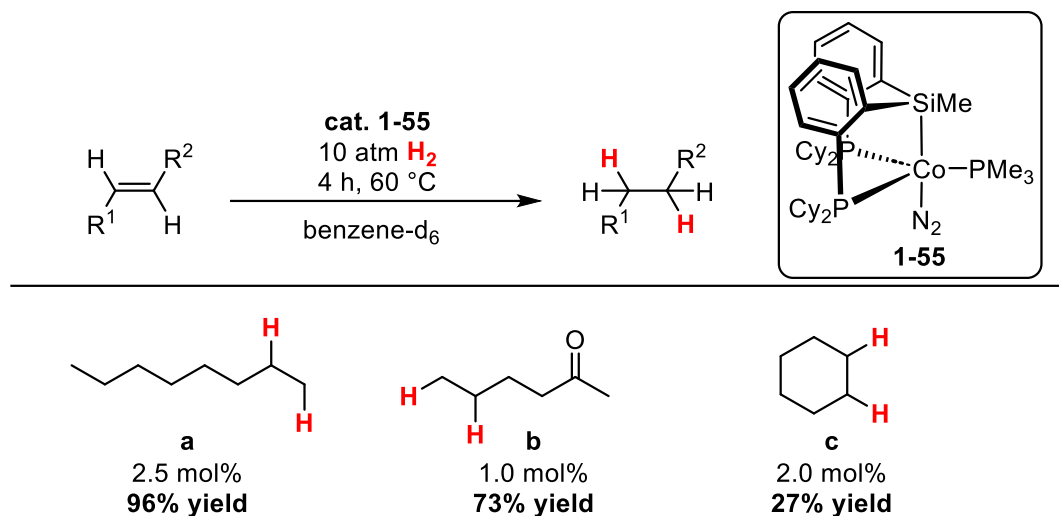


Figure 2.1.2. Ligand based H₂ storage as a metal-ligand cooperative strategy.

The utility of electronegative elements embedded in the framework of ligands has been well established in the literature as shown by the above examples (*vide supra*). Conversely, the utility of incorporating electropositive elements into the architecture of ligands has only recently begun to be explored as a possible means to leverage metal-ligand cooperativity. The Peters group has shown that an anionic bis(phosphino)boryl ligand was capable of supporting catalytic alkene hydrogenation at both Co and Ni,²⁹⁻³⁰ while work from the Turculet group has begun to establish the utility of bis(phosphino)silyl supported base metal complexes as active catalysts for hydroelementation transformations (Figure 2.1.1).^{9-10, 40, 82}

Previous work from the Turculet group has established the ability of (Cy-PSiP)CoN₂(PMe₃) (**1-55**) to react with H₂ and perform the catalytic hydrogenation of terminal alkenes.⁹ The catalysis required moderate pressure and temperature to afford good conversion (10 atm H₂, 2.5-5.0 mol% Co, 60 °C, 18 h, Scheme 2.1.2), and the scope was limited to terminal alkenes with little functional group tolerance. The authors hypothesized that the lack of lability associated with the PMe₃ co-ligand prevents its dissociation and thereby inhibits catalytic turnover.



Scheme 2.1.2. Substrate scope and conditions previously employed in the catalytic hydrogenation of alkenes by **1-55**.⁹

In this chapter, the synthesis of $(\text{Cy-PSiP})\text{Co}^{\text{I}}$ complexes lacking exogenous phosphine donors is reported. A reliable protocol to synthesize $(\text{Cy-PSiP})\text{Co}^{\text{I}}$ alkyne complexes in good yields and high purity is disclosed, as is the application of these complexes in the catalytic hydrogenation of alkenes bearing a variety of functional groups. The high catalytic activity of these species allows for the use of 1 atm of H_2 at room temperature employing low catalyst loading. Furthermore, an investigation into the relative stability of $(\text{Cy-PSiP})\text{Co}$ hydride species as well as a potential mechanism for catalytic hydrogenation employing DFT methods is reported. The apparent involvement of $\sigma\text{-Si-H}$ and secondary interactions between silicon and hydrogen atoms (SISHA) in the transfer of hydride equivalents to the substrate lends support to the notion that PSiP ligands have the potential to act in a cooperative manner in such hydrofunctionalization reactivity.

2.2 Results and Discussion

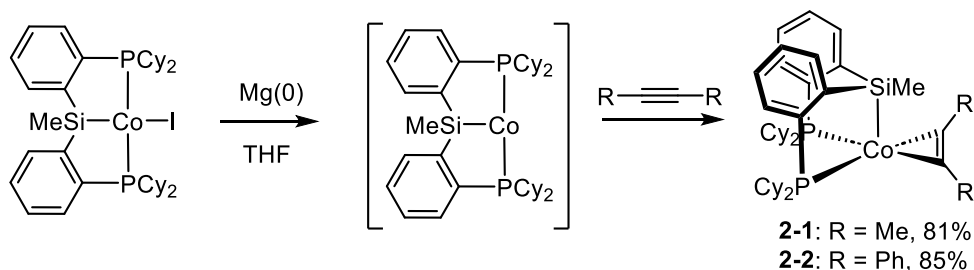
2.2.1 Synthesis and Characterization of (Cy-PSiP)Co^I Alkyne Complexes

Previous work towards the synthesis of (PSiP)Co^I complexes led exclusively to coordinatively saturated, 18-electron species that typically feature exogenous phosphine donors.^{9, 48, 50-51, 83-84} While such phosphine coordination is useful for stabilizing the Co(I) center, the lack of lability associated with their coordination can be a hindrance to catalysis. To improve upon the catalysis previously disclosed by the Turculet group (*vide supra*) this work sought to synthesize (Cy-PSiP)Co complexes that did not feature phosphines, CO, or other non-labile donors as co-ligands.

Single electron reduction of (Cy-PSiP)CoI (**1-54**) with excess Mg⁰ was performed in the presence of a variety of L-donor ligands. Reduction in the absence of additional donor ligands was attempted prior to this, however this led to intractable mixtures of paramagnetic products from which no clean material could be isolated. Pyridine and 4-(dimethylamino)pyridine were unsuccessful at supporting (Cy-PSiP)Co^I, as were acetonitrile and 2,6-(dimethylphenyl)isocyanide. The previously reported synthesis of the Ir^I ethylene complex (Cy-PSiP)Ir(C₂H₄)³⁷ prompted investigation into a possible Co analogue. Mg⁰ reduction of (Cy-PSiP)Co^I under an atmosphere of ethylene led to a color change from dark red to dark blue. Analysis of the crude reaction mixture by ³¹P and ¹H NMR revealed the likely formation of a diamagnetic ethylene complex of the type (Cy-PSiP)Co(C₂H₄) after 18 h at room temperature. A single resonance was observed in the ³¹P {¹H} NMR spectrum at 69.0 ppm, and the ¹H NMR spectrum revealed a singlet at 2.39 ppm integrating to 4 protons that likely corresponds to coordinated ethylene. However, in the absence of ethylene, the complex rapidly decomposed to form paramagnetic products

and could not be isolated. Mg^0 reduction of $(\text{Cy-PSiP})\text{CoI}$ in the presence of 1,5-cyclooctadiene and *cis*-stilbene led to the formation of paramagnetic species that could not be successfully isolated.

By comparison, Mg^0 reduction in the presence of the alkynes 2-butyne or diphenylacetylene led to the formation of isolable diamagnetic complexes formulated as $(\text{Cy-PSiP})\text{Co}(2\text{-butyne})$ (**2-1**) and $(\text{Cy-PSiP})\text{Co}(\text{diphenylacetylene})$ (**2-2**) in 81% and 85% yield, respectively (Scheme 2.2.1). For both complexes, X-ray crystallographic analysis revealed a distorted square pyramidal geometry at Co in the solid state (Figure 2.2.1), with Si occupying the apical position *trans* to a vacant coordination site and *cis*-disposed PCy_2 donors in the basal plane. Significant distortion of the alkyne $\text{C-C}\equiv\text{C}$ bond angles from the idealized 180° to $138.13(19)^\circ/133.98(19)^\circ$ and $137.12(12)^\circ/137.46(12)^\circ$ for **2-1** and **2-2**, respectively, suggests significant π -backbonding into the π^* antibonding orbitals of the alkynes. Furthermore, the elongated $\text{C}\equiv\text{C}$ bond distances of 1.3112(18) and 1.296(3) Å (for **2-1** and **2-2**), respectively, deviate significantly from the idealized $\text{C}\equiv\text{C}$ bond distance of 1.20 Å, with values closer to the idealized $\text{sp}^2\text{-sp}^2$ bond distance of 1.34 Å typical for an alkene.



Scheme 2.2.1. Synthetic route for the preparation of **2-1** and **2-2**.

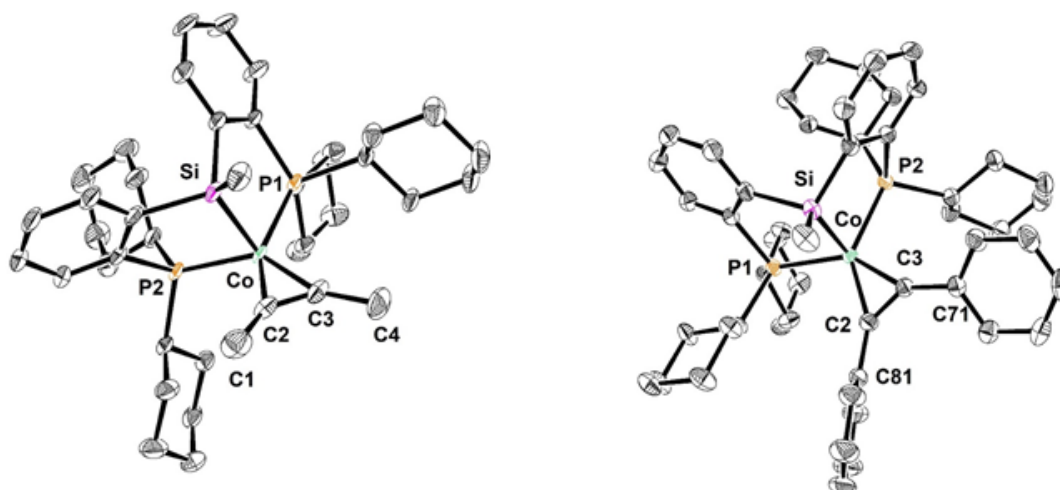


Figure 2.2.1. (Left) Crystallographically determined structure of **2-1**, with thermal ellipsoids shown at the 30% probability level. Hydrogen atoms have been omitted for clarity. Selected interatomic distances (Å) and angles (°): Co-C(2) 1.8535(18), Co-C(3) 1.8976(18), C(2)-C(3) 1.3112(18), Co-P(1) 2.2091(5), Co-P(2) 2.1977(5), Co-Si 2.1884(5), C(1)-C(2) 1.492(3), C(2)-C(3) 1.296(3), C(3)-C(4) 1.495(3), Si-Co-C(2) 91.14(6), Si-Co-C(3) 107.90(6), P(1)-Co-P(2) 107.959(18), P(1)-Co-Si 88.879(17), P(2)-Co-Si 84.837(18), P(2)-Co-C(2) 102.69(6), P(1)-Co-C(3) 111.05(6), C(1)-C(2)-C(3) 138.13(19), C(2)-C(3)-C(4) 133.98(19). **(Right)** Crystallographically determined structure of **2-2**, with thermal ellipsoids shown at the 30% probability level. Hydrogen atoms have been omitted for clarity. Selected interatomic distances (Å) and angles (°): Co-C(2) 1.8817(13), Co-C(3) 1.8609(13), C(2)-C(3) 1.296(3), Co-P(1) 2.2091(4), Co-P(2) 2.2423(3), C(2)-C(3) 1.3112(18), C(2)-C(81) 1.4645(17), C(3)-C(71) 1.4636(17), Co-Si 2.2062(4), Si-Co-C(2) 110.12(4), Si-Co-C(3) 101.39(4), P(1)-Co-P(2) 114.731(14), P(1)-Co-Si 86.603(13), P(2)-Co-Si 84.808(13), P(1)-Co-C(2) 103.49(4), P(2)-Co-C(3) 100.69(4), C(3)-C(2)-C(81) 137.12(12), C(2)-C(3)-C(71) 137.46(12).

With the alkyne complexes **2-1** and **2-2** in hand, their reactivity with H₂ was investigated. Exposure of a degassed solution of either complex to an atmosphere of H₂ in a sealed J-Young NMR tube led to a rapid color change from the respective dark purple or blue to yellow. Analysis by use of ¹H and ³¹P{¹H} NMR spectroscopy revealed complete conversion to a new diamagnetic product within minutes in both cases, with concomitant formation of the fully hydrogenated alkane product (butane or 1,2-diphenylethane, respectively). In both cases, a broad resonance at 100 ppm corresponding to a new (Cy-PSiP)Co-containing product was observed by ³¹P{¹H}, while the ¹H NMR spectrum

(benzene-*d*₆) showed a single, broad, hydride resonance at -8.64 ppm integrating to four hydrides. Variable temperature NMR studies were conducted, with no decoalescence phenomena observed down to -80 °C. Increasing the temperature to 80 °C led to no observable differences in the ¹H and ³¹P{¹H} NMR spectra of the reaction mixture, and no decomposition was observed upon cooling the sample back to room temperature. Attempts to isolate the observed polyhydride complex formulated as (Cy-PSiP)Co(H)₄ have thus far been unsuccessful as rapid decomposition occurs upon removal of the H₂ atmosphere.

Given the highly fluxional nature of the observed (Cy-PSiP)Co(H)₄ complex several formulations featuring a Co^I or Co^{III} oxidation state are possible (Figure 2.2.2). Co(III) dihydride species, non-classical dihydrogen adducts, as well as species that feature σ-Si-H interactions, are all possible isomers to consider. Our inability to isolate this complex coupled with a lack of observed decoalescence by variable temperature NMR spectroscopy prompted the use of DFT calculations to probe the potential energy surface.

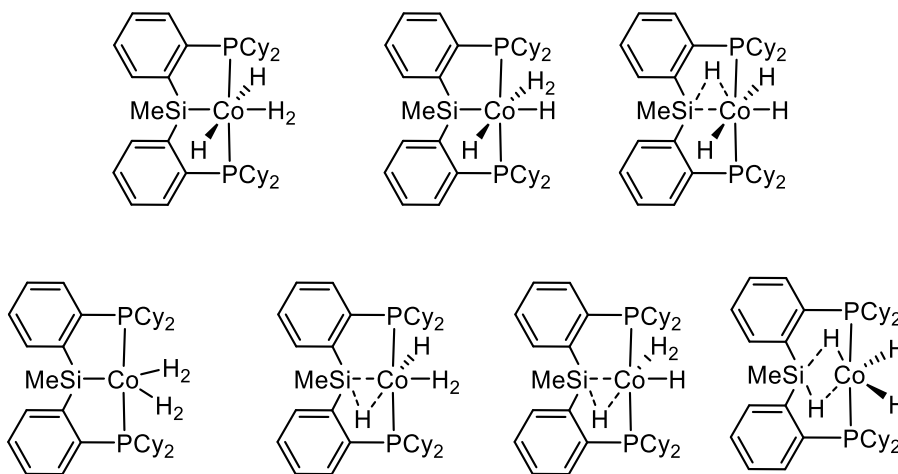


Figure 2.2.2. Possible structures of a (Cy-PSiP)Co polyhydride species. Top: Complexes in the Co^{III} oxidation state. Bottom: Complexes in the Co^I oxidation state.

Geometry optimization and frequency calculations using the B3LYP-XDM⁸⁵⁻⁸⁶ method led to several possible formulations for (Cy-PSiP)Co(H)₄. Three (Cy-PSiP)Co^{III}

polyhydride isomers within $\Delta G_{\text{rel}} = \pm 2.8$ kcal/mol of one another were found (Figure 2.2.3), while no local minima corresponding to Co^{I} complexes were identified. The lowest energy isomer (Figure 2.2.3 (a) **A**) features two *cis*-disposed terminal hydride ligands and a coordinated molecule of dihydrogen with a meridionally-coordinated PSiP ligand. However, an isomer featuring two *trans*-disposed terminal hydrides and a dihydrogen molecule coordinated *trans* to silicon was only +0.4 kcal/mol relative to **A** (Figure 2.2.3, (a) **B**). A third isomer featuring a σ -(Si-H) interaction and three terminal Co hydrides (isomer **C**) was found to be +2.4 kcal/mol relative to the isomer **B**. The barrier for the interconversion of these isomers through a metathesis process features $\Delta G^{\ddagger} = +4.38$ kcal/mol (Figure 2.2.3 (b)). These data suggests that it is possible that all three of these isomers are in equilibrium when a large excess of hydrogen is employed experimentally.

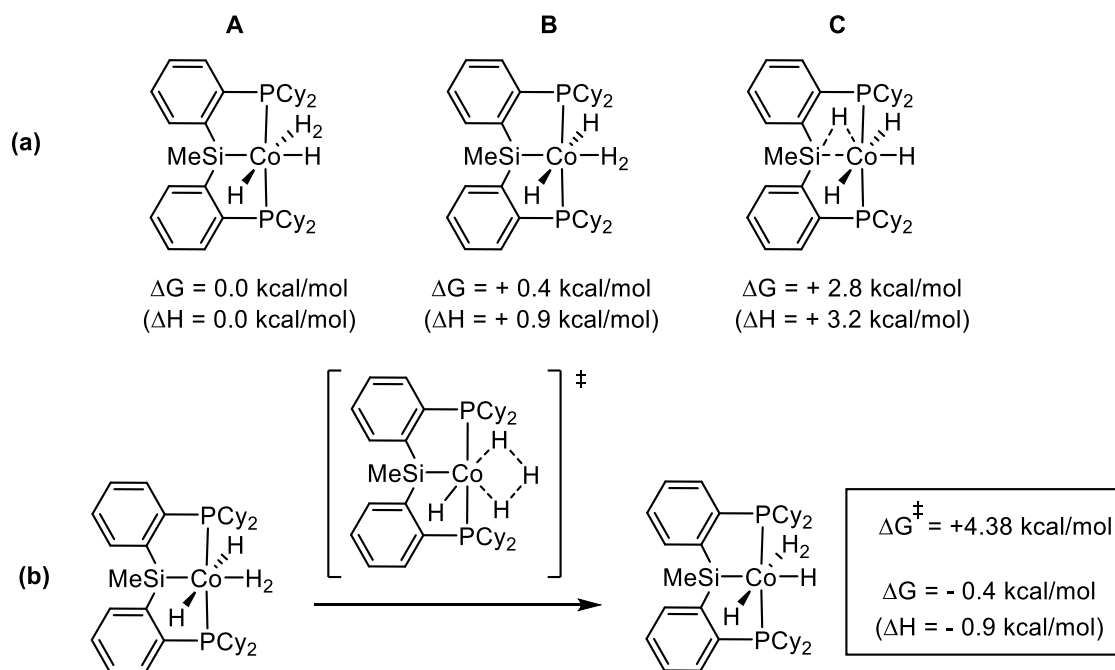
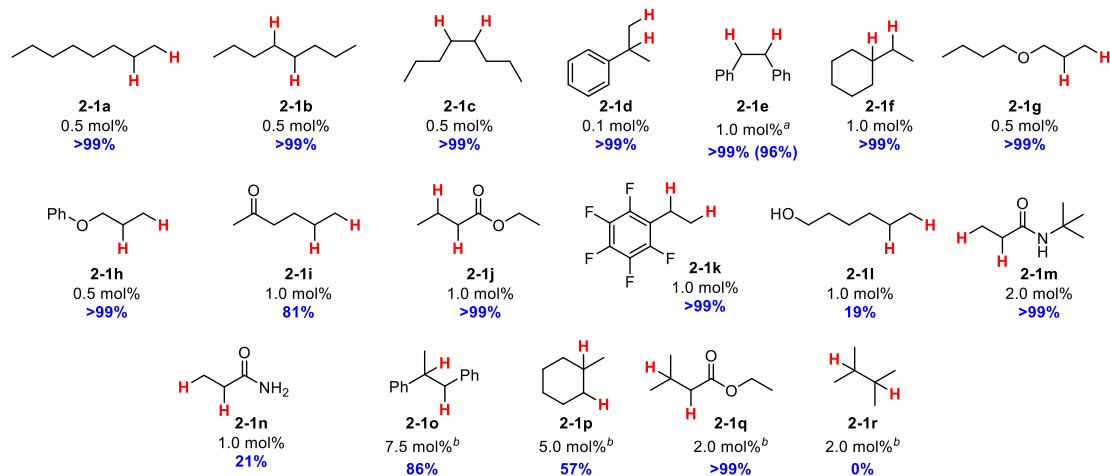
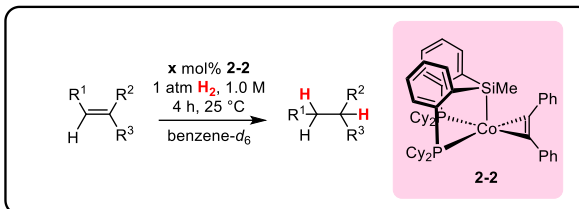


Figure 2.2.3. (a) Computed ΔG and ΔH values for $(\text{Cy-PSiP})\text{Co}(\text{H})_4$ isomers (kcal/mol). (b) The calculated kinetic barrier for isomer interconversion through metathesis.

2.2.2 (Cy-PSiP)Co Catalyzed Alkene Hydrogenation

With the pre-catalysts **2-1** and **2-2** in hand, their effectiveness in alkene hydrogenation was evaluated. In initial studies, 1-octene was employed as a model substrate to compare the reactivity of **2-1** and **2-2** to that of **1-55** (*vide supra*). Using 5 mol% of either alkyne complex under 5 atm H₂ led to complete conversion to octane after 4 h at 60 °C. Due to the ease with which **2-2** could be purified relative to **2-1**, subsequent optimization was done exclusively with the former pre-catalyst. Optimization of conditions with **2-2** for the hydrogenation of 1-octene (**2-1a**) led to the use of 0.5 mol % Co under 1 atm H₂ for 4 h at 25 °C to afford quantitative yields of octane (Scheme 2.2.2, **2-1a**). These conditions could be extended to include *cis*- and *trans*-4-octene and provided quantitative yields of octane (Scheme 2.2.2, **2-1b-c**). Furthermore, α -methylstyrene (**2-1d**) was hydrogenated to cumene in quantitative yields under the same conditions with a catalyst loading of 0.1 mol%, while an increased loading of 1 mol% was required for the hydrogenation of *cis*-stilbene and the tri-substituted alkene ethylidenecyclohexane (Scheme 2.2.2, **2-1e -f**). Performing the hydrogenation of *cis*-stilbene on a 1.0 mmol scale allowed for the isolation of 1,2-diphenylethane (96% yield) and demonstrates the efficacy of this catalyst on a larger scale.



Scheme 2.2.2. Substrate scope for the hydrogenation of alkenes with **2-2**. Reaction conditions: alkene (0.5 mmol), **2-2** (specified mol %), 1 atm H₂, benzene-*d*₆ (volume to achieve 0.5 mL total volume), 25 °C, 4 h. Yield of product determined on the basis of ¹H NMR integration vs. 1,3,5-trimethoxybenzene internal standard (0.5 mmol; average of two runs); a relaxation delay of 60 s was used to ensure accurate integrations. ^aReaction performed on a 1.0 mmol scale, isolated yield in parentheses. ^bReaction performed at 50 °C under 10 atm H₂.

The substrate scope was further expanded to assess the functional group tolerance of **2-2**. Allyl ethers were well tolerated with no observed C-O bond cleavage (Scheme 2.2.2, **2-1g-h**), as were ketones and esters with no observable reduction of the carbonyl (Scheme 2.2.2, **2-1i-j**). A secondary acrylamide featuring a bulky tert-butyl substituent was cleanly hydrogenated to the corresponding alkyl amide (Scheme 2.2.2, **2-1m**), however a primary acrylamide analogue afforded only 21% conversion (Scheme 2.2.2, **2-1n**). An alkene featuring an alcohol achieved similarly low conversion (19%, Scheme 2.2.2, **2-1l**) indicating the limitations of this catalyst.

Extending the substrate scope to include sterically hindered tri- and tetra-substituted alkenes was met with some success (Scheme 2.2.2, **2-1o-r**). *Trans*- α -methylstilbene was cleanly hydrogenated to the corresponding alkane with 86% conversion (with unreacted alkene comprising the remaining mass balance) but required an increase in catalyst loading (7.5 mol%) as well as increased temperature and pressure (10 atm H₂, 50 °C). Substrate **2-1p** 1-methyl-1-cyclohexene was similarly hydrogenated with 57% conversion using these conditions with 5 mol% **2-2** while 3,3-dimethylmethacrylate (**2-1q**) was hydrogenated in quantitative NMR yield. The tetra-substituted olefin **2-1r** afforded no conversion to the corresponding alkane and further identifies sterically demanding substrates as a difficult class for this catalyst.

2.2.3 DFT Mechanistic Investigation

The high catalytic activity of the (Cy-PSiP)Co^I alkyne complexes prompted an investigation into a potential mechanism using DFT methods, The potential mechanism by which (Cy-PSi^RP)Rh^I (R = OTf, Me) performs alkene hydrogenation was recently reported by Taylor and co-workers, where they observed that competitive σ -bond metathesis and reductive elimination pathways were operative.⁸⁷ Furthermore, they determined that a series of Rh dihydrogen and dihydride complexes are viable intermediates in the presence of H₂, and they demonstrated the potential for unusual bonding scenarios between the hydride ligand and the silyl donor. The authors also disclose a series of (Cy-PSiP)Rh^{III} polyhydride isomers similar to those reported above in above in section 2.2.2. The most stable isomer in this case was shown to be one that features *trans* disposed hydride ligands as well as a molecule of dihydrogen coordinated *trans* to silicon. In contrast, the lowest energy polyhydride isomer calculated for (Cy-PSiP)Co^{III} features *cis*-disposed terminal

hydride ligands and with a dihydrogen ligand coordinated *syn* to the Si methyl (Figure 2.2.4).

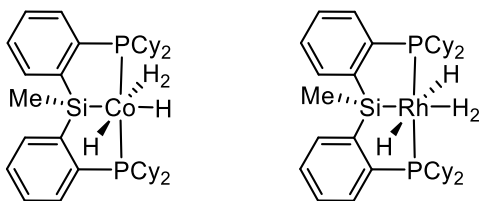


Figure 2.2.4. Lowest energy configurations calculated for (Cy-PSiP)Co and (Cy-PSiP)Rh polyhydride complexes.⁸⁷

When monitoring catalytic hydrogenation experiments it was noted that (Cy-PSiP)Co(H)₄ was the only species that could be observed by ³¹P {¹H} NMR and is likely the catalyst resting state. As the hydride ligands were observed to undergo rapid exchange under 1 atm of H₂ and the relative energies of the polyhydride isomers are close, (Cy-PSiP)Co(H)₄ isomer **B** (*vide supra*, Figure 2.2.3 (a)) was chosen as an entry point to the catalytic cycle due to the labile nature of the dihydrogen ligand *trans* to the silyl donor (Figure 2.2.5, **2-3**). Dissociation of H₂ was found to give intermediate **2** which displays two *trans* disposed hydride ligands and a vacant coordination site *trans* to silicon (Figure 2.2.5, **2-4**).

The hydride positioned *syn* to the Si methyl in **2-4** was calculated to possess an acute Si-Co-H angle of 69.3°, and an Si-H distance of 1.752 Å which is consistent with a secondary interaction between silicon and hydrogen atoms (SISHA).³¹ Sigma complexes of the form η^2 -(Si-H) can be viewed as a 3c-2-electron bond arising from reductive elimination of the Si-H moiety. SISHA, on the other hand, are noted as having values between 1.9 – 2.4 Å and can arise due to the tendency of Si to become hypervalent and engage in bonding interactions with both the metal and the hydride.⁵⁹ This becomes notable

when there are hydride ligands present on the metal center, leading to interactions between the Si, M, and H atoms that can be difficult to classify. While the Si-H distance in **2-4** is somewhat shorter than the range presented for SISHA, it is difficult to definitively assign in the absence of Si-H coupling constants from NMR spectroscopy.

The model substrate, propene, was found to coordinate to **2-4** through a barrierless transition state and led to the propenyl hydride complex **2-5**. The Si – H distance in **2-5** was calculated to be slightly longer than **2-4** (1.864 Å), albeit still within the range for SISHA. Migratory insertion of the alkene involving the hydride positioned *syn* to the Si methyl group in **2-5** was found to proceed through a low energy transition state **TS2**. Conversely, the barrier for migratory insertion involving the hydride ligand *anti* to the Si methyl was found to have a significantly higher barrier (**TS2'**, $\Delta G^\ddagger = +9.79$ kcal/mol), and led to the relatively unstable product **2-5'** ($\Delta G = +13.7$ kcal/mol). Further calculations from **2-5'** were not pursued. The lower barrier associated with **TS 2** could be due to the SISHA between the hydride *syn* to the Si methyl and the silyl donor. Subsequent coordination of H₂ to **2-6** was found to be barrierless and led to the slightly destabilized octahedral product **2-7**. The higher energy product is likely due to P*Si*P ligation favoring five-coordinate trigonal bipyramidal complexes as noted by Taylor and co-workers,⁸⁷ a result of the *trans* labilizing influence of the silyl donor. Subsequent sigma bond metathesis (**TS 4**) was found to possess a low barrier ($\Delta G^\ddagger = +1.59$ kcal/mol) and regenerates **2-4** as well as a molecule of propane. Unlike the (Cy-P*Si*P)Rh system described by Taylor and co-workers,⁸⁷ reductive elimination was not found to be a competitive pathway for substrate release (**TS 3'**), and instead was found to have a significantly higher barrier than sigma bond metathesis ($\Delta G^\ddagger = +8.64$ kcal/mol). These results further corroborate the claim by Taylor and co-

workers that the properties of PSiP ligated metal complexes favor metathesis elimination pathways.

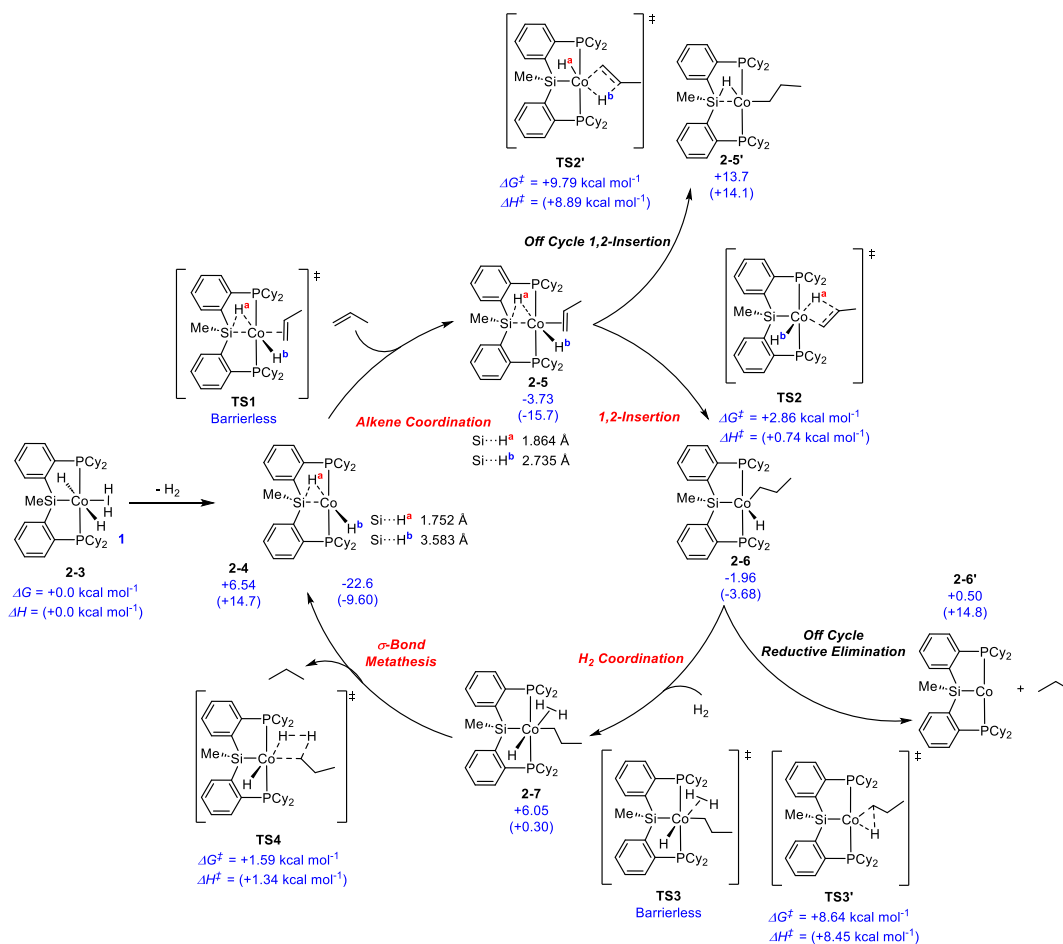


Figure 2.2.5. Proposed catalytic cycle highlighting relative free energies (kcal/mol) of intermediates and transition states calculated for the hydrogenation of propene mediated by (Cy-PSiP)Co(H)₄.

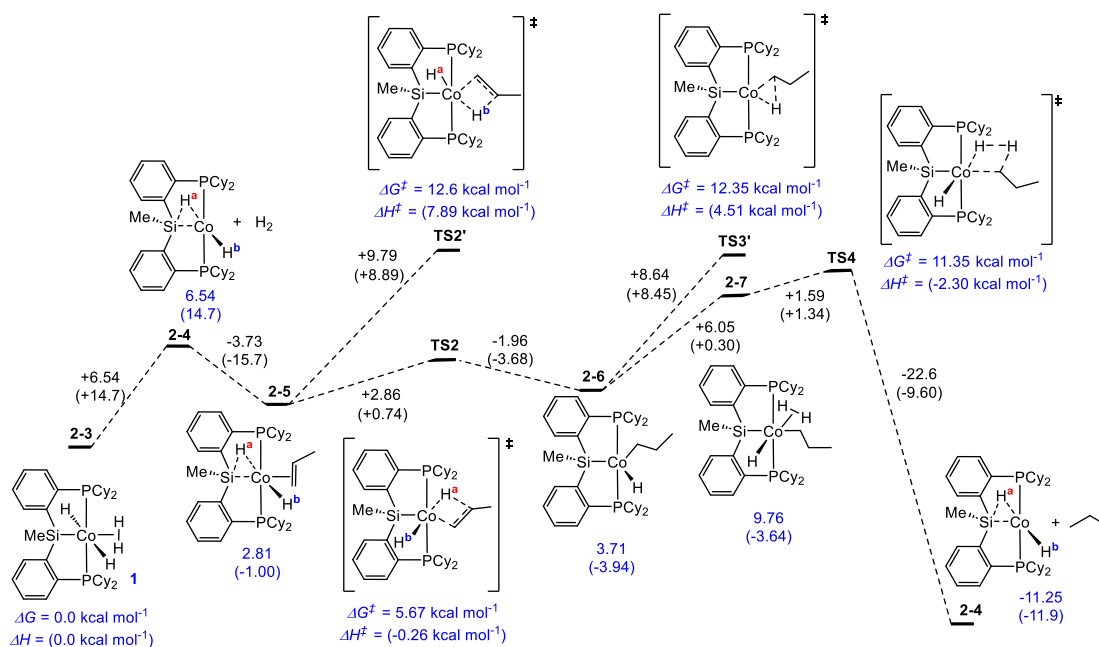


Figure 2.2.6. Free energies (kcal/mol) of intermediates and transition states calculated for the hydrogenation of propene mediated by (Cy-PSiP)Co(H)₄.

2.3 Summary and Conclusions

The results presented in this chapter detail the synthesis of reactive (Cy-PSiP)Co^I alkyne complexes that are uniquely primed for hydroelementation catalysis. The use of alkynes as stabilizing ligands for the electron rich Co^I metal center allows for the facile isolation of Co complexes that can act as a source of (Cy-PSiP)Co^I. The alkyne complexes **2-1** and **2-2** are both active pre-catalysts for alkene hydrogenation. The improved catalytic performance of the latter complex towards alkene hydrogenation relative to the previously reported **1-55** is remarkable. The utility of the **2-2** complex in hydrogenation catalysis was demonstrated through a diverse scope of substrates, including functionalized alkenes that contain ether, ester, ketone, and secondary amide groups. All such substrates were hydrogenated under exceptionally mild conditions, including room temperature and low hydrogen pressure (1 atm), as well as low catalyst loading (0.1 - 2.5 mol%). Employing

more forcing conditions (10 atm H₂, 5.0-7.5 mol% Co, 65 °C, 24 h) led to good conversion for sterically hindered tri-substituted alkenes such as *trans*- α -methylstilbene and 1-methyl-1-cyclohexene. The steric hindrance associated with the Cy-PSiP ligand likely inhibits coordination of bulky tri- and tetra- substituted alkenes, impeding catalysis in these instances. Despite such limitations involving especially bulky substrates, the (Cy-PSiP)Co^I pre-catalysts reported in this chapter are among the most reactive for the hydrogenation of simple terminal, internal *cis/trans*, and functionalized alkenes. The high yields and ease of purification associated with the alkyne complexes (Cy-PSiP)Co(alkyne) represent an important advance in the catalytic utility of PSiP-supported base metal complexes.

A DFT investigation into a potential mechanism for alkene hydrogenation as well as the potential non-innocence of the silyl donor was also explored. Universally low barriers complement the observed reactivity, and NMR studies combined with computational data corroborate several (Cy-PSiP)Co(H)₄ isomers as the resting state of the catalyst. Multiple species featuring Co \cdots H \cdots Si interactions were found to be catalytically relevant, including a dihydride species featuring SISHA that was implicated as the catalytically active species. The intermediacy of such Co \cdots H \cdots Si species appears to be crucial for catalytic turnover, consistent with the premise that metal-Si interactions in phosphino(silyl) ligated complexes play a key role in facilitating hydrofunctionalization reactivity. Substrate coordination, migratory insertion, and sigma bond metathesis all proceed with relatively low kinetic barriers to hydrogenate propene as the model substrate.

2.4 Experimental

2.4.1 General Considerations

All experiments were conducted under nitrogen in a glovebox or using standard Schlenk techniques. Tetrahydrofuran and diethyl ether were distilled from Na/benzophenone ketyl. Benzene, toluene, and pentane were first sparged with nitrogen and subsequently dried by passage through a double-column (one activated alumina column and one column packed with activated Q-5). All purified solvents were stored over 4 Å molecular sieves. Benzene- d_6 was degassed via three freeze-pump-thaw cycles and stored over 4 Å molecular sieves. The ligand precursor (Cy-PSiP)H³⁸ and (Cy-PSiP)CoI⁹ were prepared by previously reported methods. All other reagents were purchased from commercial suppliers and used without further purification. Unless otherwise stated, ¹H, ¹³C, ¹¹B, ³¹P, and ²⁹Si NMR characterization data were collected at 300K, with chemical shifts reported in parts per million downfield of SiMe₄ (for ¹H, ¹³C, and ²⁹Si), BF₃·OEt₂ (for ¹¹B), or 85% H₃PO₄ in D₂O (for ³¹P). ¹H and ¹³C NMR chemical shift assignments are based on data obtained from ¹³C{¹H}, ¹³C-DEPTQ, ¹H-¹H COSY, ¹H-¹³C HSQC, and ¹H-¹³C HMBC NMR experiments. ²⁹Si NMR assignments are based on ¹H-²⁹Si HMBC and ¹H-²⁹Si HMQC experiments. X-ray data collection, solution, and refinement were carried out by Drs. Michael J. Ferguson and Yuqiao Zhou at the University of Alberta X-ray Crystallography Laboratory, Edmonton, Alberta.

2.4.2 Synthetic Procedures and Characterization Data

Synthesis of (Cy-PSiP)Co(2-Butyne) (2-1). 2-Butyne (21.5 μL, 0.275 mmol) was added to a solution of (Cy-PSiP)CoI (0.195 g, 0.250 mmol) in ca. 5 mL THF and allowed to stir for 10 minutes. Magnesium powder (0.070 g, 2.50 mmol) was then added as a

suspension in ca. 2 mL of THF. Within minutes a color change was observed from dark red to black, and the reaction mixture was allowed to stir for 18 hours. The volatile components were then removed *in vacuo* and the resulting residue was triturated with 3 × 3 mL pentane. The residue was then extracted with 12 mL of cyclohexane and filtered through Celite to give a clear purple solution. The solvent was removed *in vacuo* and the resulting dark purple solid was washed with 2 × 1 mL of cold pentane to afford **2-1** (0.143 g, 81% yield) as a dark purple solid. Single crystals suitable for X-ray diffraction analysis were obtained from a concentrated diethyl ether solution at -35 °C. ¹H NMR (500 MHz, benzene-*d*₆): δ 7.66 (d, *J* = 7 Hz, 2H, *H*_{arom}), 7.58 (d, *J* = 7 Hz, 2H, *H*_{arom}), 7.16 (overlapping resonances, 2H, *H*_{arom}), 7.13 (t, *J* = 7 Hz, 2H, *H*_{arom}), 2.60 (m, 2H, PCy), 2.45 (s, 6H, CH₃), 2.13 – 0.94 (overlapping resonances, 42 H, PCy), 0.43 (s, 3H, SiCH₃). ¹³C{¹H} NMR (125.8 MHz, benzene-*d*₆): δ 157.9 (*C*_{arom}), 157.5 (*C*_{Butyne}), 147.8 (apparent d, *J* = 39 Hz, *C*_{arom}), 131.2 (m, *CH*_{arom}), 128.2 (*CH*_{arom}), 128.1 (*CH*_{arom}), 126.5 (*CH*_{arom}), 30.5 (CH₂Cy), 29.8 (CH₂Cy), 29.4 (CH₂Cy), 28.5 (CH₂Cy), 28.3 (m, CH₂Cy), 28.0 (m, CH₂Cy), 27.9 (m, CH₂Cy), 27.7 (m, CH₂Cy), 26.8 (CH₂Cy), 26.5 (CH₂Cy), 16.3 (t, ³*J*_{P-C} = 4.0 Hz, *Me*_{Butyne}), 3.16 (s, SiCH₃). ³¹P{¹H} NMR (202.5 MHz, benzene-*d*₆): δ 74.4. ²⁹Si NMR (99.4 MHz, benzene-*d*₆): δ 48.9. Anal. Calcd. for C₄₁H₆₁P₂SiCo: C. 70.06; H. 8.75. Found: C. 69.80; H. 8.39.

Synthesis of (PSiP)Co-(diphenylacetylene) (2-2). Diphenylacetylene (0.046 g, 0.257 mmol) was dissolved in ca. 4 mL of THF and added to a stirring solution of (PSiP)CoI (0.200 g, 0.257 mmol) in 5 mL of THF and allowed to stir for 10 minutes. Magnesium powder (0.063 g, 2.57 mmol) was then added as a suspension in ca. 3 mL of THF, and the resulting mixture was allowed to stir for 18 hours. The volatile components were

subsequently removed *in vacuo* and the residue was triturated with 3 × 3 mL of pentane. The residue was then extracted with 12 mL of a 1:1 pentane: cyclohexane mixture and filtered through Celite to give a clear, dark blue solution. The solvent was removed *in vacuo* and the resulting dark blue solid washed with 2 × 1 mL of cold pentane to afford **2-2** in 85% yield (0.218 g, 0.133 mmol). Single crystals suitable for X-ray diffraction analysis were obtained from a concentrated benzene solution. ¹H NMR (500 MHz, benzene-*d*₆): δ 7.76 (d, *J* = 7 Hz, 2H, *H*_{arom}), 7.54 (m, 2H, *H*_{arom}), 7.32, *J* = 7 Hz, 4H, *H*_{arom}), 7.22 (apparent t, *J* = 7 Hz, 2H, *H*_{arom}), 7.15 (apparent t, *J* = 7 Hz, 2H, *H*_{arom}), 7.06 (apparent t, *J* = 7 Hz, 4 H, *H*_{arom}), 6.98 (apparent t, *J* = 7 Hz, 2 H, *H*_{arom}), 2.56 (m, 2H, PCHCy), 2.32 (m, 2H, PCHCy), 2.07 (m, 2H, PCH₂Cy), 1.89 (m, 4H, PCH₂Cy), 1.75 (m, 2H, PCH₂Cy), 1.55 – 1.23 (overlapping resonance, 34H, PCH₂Cy), 0.77 (s, 3H, SiCH₃). ¹³C{¹H} NMR (125.8 MHz, benzene-*d*₆): δ 163.8 (m, C_{alkyne}), 158.7 (apparent d, *J* = 52 Hz, C_{arom}), 147.0 (apparent d, *J* = 38 Hz, C_{arom}), 141.2 (s, C_{arom}), 131.5 (apparent d, *J* = 20 Hz, CH_{arom}), 128.9 (s, CH_{arom}), 128.5 (s, CH_{arom}), 128.4 (s, CH_{arom}), 128.3 (s, CH_{arom}), 126.5 (s, CH_{arom}), 125.8 (s, CH_{arom}), 37.3 (m, CH_{Cy}), 37.0 (apparent d, *J* = 23 Hz, CH_{Cy}), 30.0 (s, CH₂Cy), 29.6 (s, CH₂Cy), 28.8 (s, CH₂Cy), 28.2 – 27.9 (overlapping resonance, CH₂Cy), 27.8 (apparent d, *J* = 9 Hz, CH₂Cy), 27.4 – 27.3 (overlapping resonances, CH₂Cy), 26.8 (s, CH₂Cy), 26.4 (s, CH₂Cy), 4.09 (s, SiCH₃). ³¹P{¹H} NMR (202.5 MHz, benzene-*d*₆): δ 73.5. ²⁹Si NMR (99.4 MHz, benzene-*d*₆): δ 51.5. Anal. Calcd. for C₅₁H₆₅P₂SiCo: C. 74.07; H. 7.92. Found: C. 73.82; H. 7.90.

General Procedure for Catalytic Hydrogenation of Alkenes. All hydrogenations were performed on a 0.5 mmol substrate scale using a 500 μL total reaction volume. **2-2** was dispensed as a stock solution into a 1-dram vial and the substrate added *via*

microsyringe. Benzene- d_6 was then added to bring the total reaction volume to 500 μL . The vial was then equipped with a stir bar and closed with a PTFE-sealed cap. A needle was then inserted through the septum to allow for introduction of H_2 gas. The vial was then transferred to a Parr reactor which was sealed and purged with H_2 and subsequently pressurized to 1 atm H_2 pressure (10 atm where specified). The Parr reactor was heated to 25 $^\circ\text{C}$ (50 $^\circ\text{C}$ where specified) in an oil bath for the duration of the reaction time. Afterward, the Parr reactor was removed from the oil bath and depressurized of H_2 . In the glovebox, 400 μL of a 1.25M stock solution of 1,3,5-trimethoxybenzene was added to the reaction mixture as an internal standard, and the mixture transferred to an NMR tube for data acquisition. For calculation of NMR conversion, a chosen diagnostic product signal was integrated relative to that of the internal standard. An excessively long (60s) relaxation delay was used to ensure accurate integrations.

Procedure for the Hydrogenation of *cis*-Stilbene and Isolation of 2-1e. A 1 dram vial was charged with 0.007 g **2-1** (0.01 mmol) and a magnetic stirbar and closed with a PTFE-sealed cap. *Cis*-Stilbene (178 μL , 1.0 mmol) and cyclohexane (1000 μL) were added *via* microsyringe, and a needle inserted through the seal to allow for introduction of H_2 gas. The vial was then transferred to a Parr reactor which was sealed and purged with H_2 and subsequently pressurized to 1 atm. The Parr reactor was heated to 25 $^\circ\text{C}$ in an oil bath for 4 hours, then removed from the bath and depressurized of H_2 . The reaction mixture was then exposed to air, diluted with 3 mL of hexanes, and filtered through a plug of silica gel. The filtrate was concentrated *in vacuo* to afford bibenzyl (**2-1e**) as a crystalline white solid (0.175 g, 96%).

General Computational Information. Geometry optimizations and frequency calculations were performed on all species with the B3LYP functional^{85-86, 88-89} and the XDM dispersion correction. A mixed basis set was used, consisting of 6-31G* for C and H and 6-31+G* for all other elements. Single-point energy calculations on the optimized geometries were carried out using the same B3LYP-XDM method with the 6-311+G(2d,2p) basis set. The XDM damping parameters were $a_1 = 0 \text{ \AA}$ and $a_2 = 3.7737 \text{ \AA}$ for the geometry optimizations and $a_1 = 0.4376 \text{ \AA}$ and $a_2 = 2.1607 \text{ \AA}$ for the single-point energies. All calculations were performed using the Gaussian 16⁸⁸ software package, along with the postg program for the dispersion energies. The postg program can be downloaded from <http://schooner.chem.dal.ca>

Chapter 3: (PSiP)Ni-Catalyzed (*E*) – Selective Semihydrogenation of Alkynes with Molecular Hydrogen

3.1 Introduction

The selective semihydrogenation of alkynes to alkenes is an important transformation for chemical synthesis, with applications ranging from the small-scale synthesis of fine chemicals to large-scale industrial processes.⁹⁰⁻¹⁰⁰ Controlling the stereo- and chemoselectivity of this reaction is challenging due to the competitive formation of both (*E*)- and (*Z*)-alkene isomers, as well as formation of over-reduced alkane products (Figure 3.1.1).¹⁰¹⁻¹⁰³ A number of approaches have been developed for achieving selective semihydrogenation, including examples of hetero-^{95, 104-107} and homogeneous^{91, 93} catalysis, as well as transfer¹⁰⁰ hydrogenation methods that utilize a range of hydrogen sources, such as silanes,^{21, 108-116} alcohols,^{109, 117-121} formic acid,¹²²⁻¹²⁶ water,^{109, 127-129} and amine boranes.¹³⁰⁻¹³⁴ Despite advances in the development of such transfer hydrogenation protocols, direct hydrogenation using molecular H₂ arguably offers a more efficient, atom economical approach to alkyne reduction. In this regard, the heterogeneous Pd-based Lindlar catalyst¹⁰⁴ is among the most commonly used catalysts for direct semihydrogenation to selectively afford (*Z*)-alkene products. Good selectivity for (*Z*)-alkenes can also be obtained using classic homogeneous hydrogenation catalysts such as Wilkinson's catalyst¹³⁵ and the Schrock/Osborn catalyst.^{136, 137-154} By comparison, the

stereocomplimentary semihydrogenation of alkynes to (*E*)-alkenes is more challenging, and is therefore underdeveloped.¹⁰²

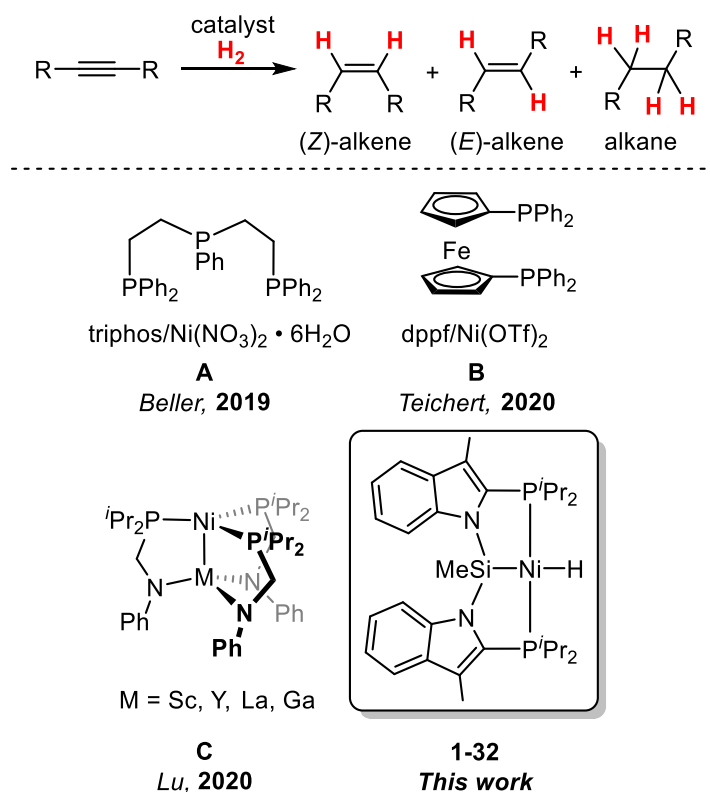


Figure 3.1.1. Ni catalysts for the (*E*) – selective semihydrogenation of alkynes with H_2 .

The most utilized method to access (*E*)-alkenes from alkynes is Birch-type reduction with Na/NH_3 as a stoichiometric reducing agent.¹⁵⁵ Such harsh reaction conditions are not compatible with many base-sensitive substrates, and as a result, this method suffers from a lack of functional group tolerance, as well as poor atom economy. A handful of catalytic systems have been developed for (*E*)-selective semihydrogenation of alkynes with H_2 .¹⁵⁶ As transition metal mediated H_2 addition to π -bonds typically involves suprafacial delivery of the two hydrogen atoms, with rare exception, (*E*)-alkene formation requires selective isomerization of the initially formed (*Z*)-alkene product. This additional step adds to the

complexity of developing catalytic (*E*)-selective semihydrogenation catalysis. To address this challenge, Furukawa and Komatsu¹⁵⁷⁻¹⁵⁸ developed a tandem catalytic system comprised of Pd₃Pb/SiO₂ for alkyne semihydrogenation and RhSb/SiO₂ for alkene isomerization. A heterobimetallic Ru/Ag catalyst,¹⁵⁹ as well as examples of homogeneous Ru-,¹⁶⁰⁻¹⁶² Pd-,¹⁶³ and Ir-catalyzed¹⁶⁴ (*E*)-selective semihydrogenation have also been reported. In addition, Fürstner and co-workers¹⁶⁵⁻¹⁶⁸ have developed Ru catalysts that operate via an unusual mechanism, whereby (*E*)-alkenes are formed directly without the need for an isomerization step.

While such examples of platinum group metal mediated reactivity are noteworthy, the development of increasingly sustainable catalysts based on abundant *3d*-transition metals is a current priority.^{60, 169-172} In this regard, efficient first row transition metal catalysts for the atom economical (*E*)-selective semihydrogenation of alkynes with H₂ are highly sought after. Yet only a small number of such catalysts have been reported. In 2013 Milstein and co-workers¹⁷³ disclosed an example of Fe-catalyzed reactivity, whereby a PNP complex of Fe catalyzed the semihydrogenation of diaryl alkynes at H₂ pressures of 4 – 10 bar (0.6 – 4 mol% Fe, 90 °C, 12 - 72 h). Ester, nitrile, and chloro substituents were tolerated, affording high yields with excellent (*E*)-selectivity. Several silyl-protected alkynes were also reduced effectively to afford the corresponding (*E*)-alkenes. More recently, Co-mediated semihydrogenation with H₂ has also been reported.^{78-79, 174} A pincer-supported Co^I-H₂ complex displayed excellent (*E*)-selectivity towards a small number of diaryl alkynes, as well as silyl-protected terminal alkynes, including several examples featuring heterocycle substitution (2-5 mol% Co, 4 atm H₂, 30 °C, 17 h).⁷⁹

Although catalysts employing Ni have been used both industrially and academically for

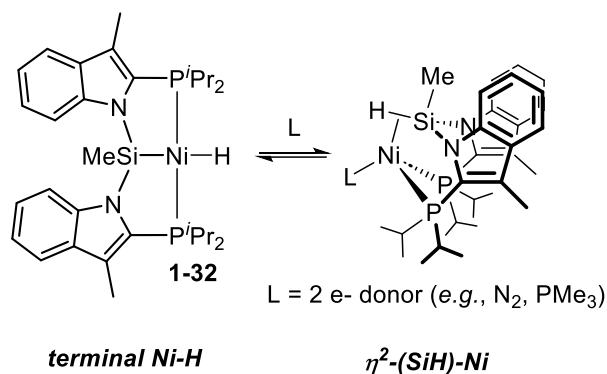
the hydrogenation of a variety of unsaturated substrates,^{105, 107, 175-183} it wasn't until very recently that the first example of Ni-catalyzed (*E*)-selective alkyne semihydrogenation with H₂ was reported by Beller and co-workers (Figure 3.1.1 A).¹⁸⁴ This work detailed a stereodivergent system wherein a Ni(NO₃)₂/triphos system (4 mol% Ni) afforded selectivity for the (*E*)-alkene, while Ni(NO₃)₂ in the absence of the phosphine ligand generated nanoparticles capable of producing the complementary (*Z*)-alkene isomer. Diaryl alkyne substrates containing both electron-donating and electron-withdrawing groups were reduced with high selectivity, and the catalyst proved tolerant of a variety of functional groups, such as hydroxy, halide, boronic ester, ketone, and nitrile groups. Although this system was selective and afforded high yields of the alkene products it required the use of rather forcing reaction conditions (120 °C, 30 bar H₂, 15 h) to do so. Subsequently, Teichert and co-workers¹⁸⁵ reported on a related semihydrogenation system featuring Ni(OTf)₂/dppf (Figure 3.1.1 B) that provided high (*E*)-selectivity for a variety of functionalized diaryl alkyne substrates, as well as alkyl/aryl, and cyclic dialkyl alkynes. As in the Beller system, the use of forcing reaction conditions (10 mol% Ni, 100 °C, 30 bar H₂, 18 h) was necessary for efficient reactivity. Evidence for over-reduction was observed after extended reaction times, which were necessary in some cases to achieve high (*E*)-selectivity. Alkyne cyclotrimerization was also noted as a side reaction in some instances, as in the case of terminal alkynes.

The use of well-defined, pre-formed Ni complexes as pre-catalysts was recently reported by Lu and co-workers.¹⁸⁶ A series of heterobimetallic Ni-M (M = Sc, Y, La, Ga; Figure 3.1.1, C) complexes were found to be active pre-catalysts for the (*E*)-selective semihydrogenation of alkynes at lower temperature and pressure (70 °C, 4.6 atm H₂) than

previously reported Ni systems. It was determined that the Ni–Y complex was the most effective at enabling the desired reactivity. High yields and (*E*)-selectivity were obtained for diphenylacetylene and one other diaryl alkyne substrate featuring *para*-boronic ester substitution. Several silyl-protected arylalkynes were also reduced effectively. These catalysts, while operating under comparatively mild conditions, did not demonstrate a broad scope or functional group tolerance, as only a relatively small group of substrates (*o*-Me, *o*-OMe, and *p*-F arene derivatives) was evaluated.

The Turculet group has developed considerable interest in the reactivity and catalytic applications of first row transition metal pincer complexes supported by bis(phosphino)silyl (PSiP) ligation.¹⁸⁷ In this context, the Turculet group has previously reported on the catalytic hydrogenation of alkenes mediated by Fe and Co complexes featuring [*k*³–((2-Cy₂PC₆H₄)₂SiMe)][–] (Cy-PSiP) ligation,^{9, 40} as well as the selective reduction of CO₂ to the formaldehyde level catalyzed by a bis(indolylphosphino)silyl-supported Ni hydride complex **1-32**.^{10, 48, 50, 84, 188-189} In the course of these studies, Turculet and co-workers observed the facile interconversion of hydrido-silyl Ni pincer species of the type (PSiP)NiH and [P(η^2 -Si-H)P]NiL (L = N₂, DMAP, PMe₃) complexes involving η^2 -SiH coordination (Scheme 3.1.1).^{10, 47, 190} Such an interplay can be envisioned to facilitate the (PSiP)Ni-mediated hydrofunctionalization of unsaturated species, such as alkenes and alkynes, by participating in the shuttling of hydride equivalents. Herein the catalytic utility of (^{*i*}Pr-PSiP^{Ind})NiH (**1-32**, Figure 3.1.1) for the (*E*)-selective semihydrogenation of internal alkynes is described. Complex **1-32** proved to be a highly effective pre-catalyst for this transformation across a broad substrate scope, using exceptionally mild conditions (1 atm H₂, 25 °C, 4 h), and low catalyst loadings (1-2.5 mol% Ni). The broad substrate scope, high

stereoselectivity, mild reaction conditions, and relative lack of side reactions, such as over-reduction, establish complex **1-32** as the state-of-the-art for this challenging transformation.



Scheme 3.1.1. Interconversion of complex **1-32** between a terminal silyl Ni hydride and η^2 – silane through coordination of L donors (N₂, PMe₃).

3.2 Results and Discussion

3.2.1 Substrate Scope

At the outset of this investigation the utility of the previously reported complex **1-32** as a catalyst for the hydrogenation of alkenes was probed. Initial studies demonstrated that **1-32** could effectively hydrogenate terminal alkenes such as 1-octene and pentafluorostyrene under mild conditions with low catalyst loading (Table 3.2.1, entries 1 and 4), but struggled to hydrogenate internal alkene substrates under comparable conditions (Table 3.2.1, entries 2 and 3). Surprisingly, upon expanding the substrate scope to include (*Z*)-stilbene (Table

3.2.1, entry 5), while no conversion to 1,2-diphenylethane occurred, quantitative isomerization to the (*E*)-isomer was observed prior to the addition of H₂.

Table 3.2.1. Hydrogenation of alkenes catalyzed by **1-32**.^a

1 mol% **1-32**
1 atm H₂, 1.0 M
4 h, 25 °C
benzene-*d*₆

entry	substrate	product	conversion (%) ^b
1		<i>n</i> -octane	>99
2		<i>n</i> -octane	11
3 ^c			64
4			>99
5 ^c			0 ^d

^aReaction conditions: alkene (0.2 mmol), complex **1-32** (40 mM/L stock solution), 1 atm H₂, benzene-*d*₆ (volume required to attain 200 μL total volume), 25 °C, 4 h. ^bConversion to product determined on the basis of ¹H NMR integration vs. 1,3,5-trimethoxybenzene internal standard (0.2 mmol; average of two runs); a relaxation delay of 60 s was used to ensure accurate integrations. ^cReaction employed 2 mol% of **1-32**. ^d>99% isomerization to (*E*)-stilbene observed.

With the knowledge that **1-32** could selectively isomerize (*Z*)-stilbene to (*E*)-stilbene the utility of **1-32** as a catalyst for alkyne semihydrogenation was evaluated. In light of the already observed reactivity of **1-32**, diphenylacetylene was chosen as an initial test substrate, as it was anticipated that semihydrogenation would proceed in a *cis*-fashion to afford (*Z*)-stilbene which could then be selectively isomerized to the (*E*)-isomer. Gratifyingly, the semihydrogenation of diphenylacetylene proceeded under mild conditions (1 mol% Ni, 1 atm H₂, 4 h, 25 °C) to afford (*E*)-stilbene with excellent selectivity (Scheme 3.2.1, **3-1a**; >99:1 selectivity). These reaction conditions were found to be general for a variety of substituted diaryl alkynes (Scheme 3.2.1, **3-1b** – **3-1n**), including those featuring

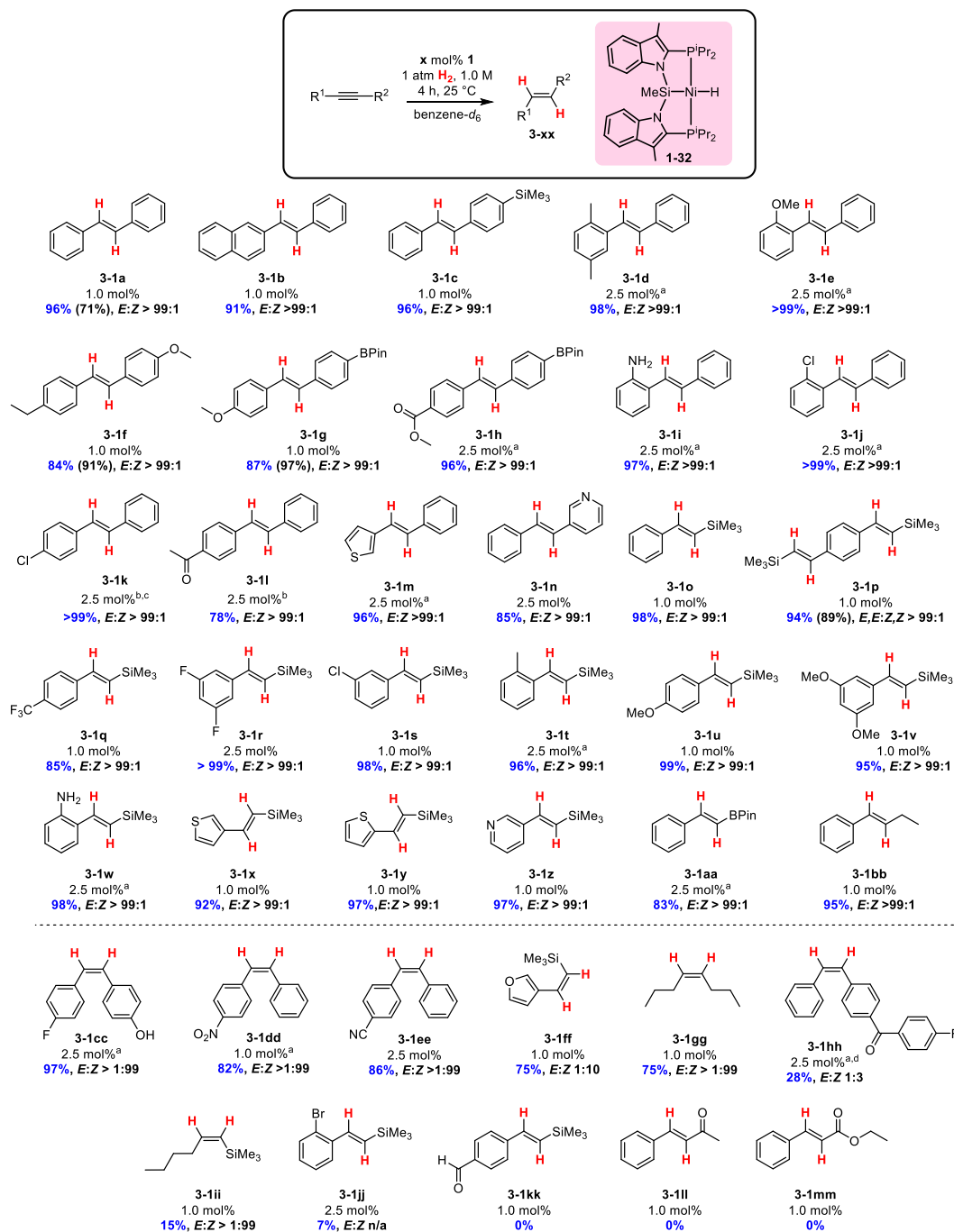
ether (**3-1e** – **3-1g**), ester (**3-1h**), and amino (**3-1i**) functional groups, as well as boronic esters (**3-1g**, **3-1h**), heterocycles (**3-1m**, **3-1n**), and polyaromatic groups (**3-1b**). In a few cases, an increase in catalyst loading to 2.5 mol% and/or an increase in reaction temperature to 50 °C were necessary in order to achieve high conversion to the alkene products. Remarkably, the corresponding (*Z*)-alkenes, as well as products resulting from overhydrogenation were not observed for these substrates. However, a reversal in selectivity to afford exclusively (*Z*)-alkene products was noted in the case of substrates featuring electron withdrawing aryl substituents in the para position, such as a *p*-chloro (**3-1cc**), *p*-fluoro (**3-1dd**), *p*-nitro (**3-1cc**), and *p*-nitrile (**3-1ee**) groups. This observation suggests that, in the case of less electron-rich substrates, the initially formed (*Z*)-alkene does not readily undergo subsequent insertion into the Ni-hydride to facilitate the presumptive *cis/trans*-isomerization step. In the semihydrogenation of 1-chloro-4-(2-phenylethynyl)benzene, an interesting temperature dependence was observed; while 90% conversion with >1:99 (*E*)/(*Z*) selectivity was obtained when the reaction was carried out at room temperature, increasing the temperature to 90 °C led to >99% conversion to the desired (*E*)-alkene **3-1k**. Furthermore, substrates featuring *para*-ketone substitution (**3-1l** and **3-1hh**) proved challenging at 50 °C, affording <50% conversion to the desired alkene products and poor (*E*)/(*Z*) selectivity. However, conversion to **3-1l** (78%) with high (*E*)-selectivity (99:1) was achieved at 90 °C. These observations suggest that for some substrates, temperature may be employed as a means of improving and/or inverting the observed selectivity.

In an effort to further expand the scope of semihydrogenation catalysis, the reactivity of trimethylsilyl protected terminal alkynes was investigated. Attempts to hydrogenate phenylacetylene, an unprotected terminal alkyne, led only to catalyst decomposition and

no observable hydrogenation products. When the trimethylsilyl protecting group is used, however, the corresponding (*E*)-alkenes are once again formed exclusively (Scheme 3.2.1, **3-1o** – **3-1z**). Both electron-donating and -withdrawing substituents (**3-1q** – **3-1w**) were tolerated with no decrease in stereoselectivity. In the case of **3-1p**, a substrate featuring two trimethylsilyl protected alkynes, stereoselectivity for the (*E,E*)-semihydrogenation was maintained, with no other observable hydrogenation products (by ¹H NMR analysis). Alkynes featuring heterocycles such as thiophene and pyridine could also be hydrogenated (**3-1x** – **3-1z**) to the corresponding (*E*)-alkenes, while the furan containing substrate **3-1ff** preferentially formed the (*Z*)-alkene isomer under the same reaction conditions. In the case of **3-1jj**, *ortho*-bromo substitution led to low conversion to the alkene product, possibly due to competing side reactions (*e.g.*, hydrodehalogenation) leading to catalyst deactivation. Aldehyde substitution was also found to be incompatible with the catalyst as shown in entry **3-1kk**, leading to catalyst decomposition and no observable hydrogenation products.

Lastly, internal alkynes featuring varied substitution were explored to further expand the scope of **1-32** in semihydrogenation reactivity. Substrates **3-1ll** and **3-1mm** (Scheme 3.2.1) featuring ketone and ester substitution on the alkyne, respectively, proved unreactive, demonstrating that direct carbonyl substitution on the alkyne is incompatible with catalytic turnover. For substrate **3-1aa**, which features a boronic ester in the terminal position, clean conversion to the (*E*)-alkene was achieved utilizing a 2.5 mol% loading of **1-32** and heating at 50 °C for 4 h. The mixed aryl/alkyl alkyne 1-phenyl-1-butyne could also be selectively hydrogenated to (*E*)-1-phenyl-1-butene (**3-1bb**) in high yield under the standard reaction conditions. Finally, the reactivity of alkyl substituted alkynes 4-octyne (**3-1gg**) and 1-

trimethylsilyl-1-hexyne (**3-1ii**) was evaluated. Both substrates were cleanly hydrogenated to the corresponding (*Z*)-alkenes, albeit in low conversion (15%) in the case **3-1ii**. This reversal of selectivity is preceded by the work of Lu and Ramirez¹⁸⁶ who observed a similar phenomenon. This suggests that, as in the case of diaryl alkenes featuring strongly electron-withdrawing groups (**3-1cc** – **3-1ee**), insertion of the alkyl-substituted (*Z*)-alkenes into the Ni-hydride does not readily occur, preventing *cis/trans*-isomerization subsequent to hydrogenation. This hypothesis is further supported by the attempted hydrogenation of *cis*-4-octene (Table 3.2.1, entry 2), which proceeded to only 11% conversion.



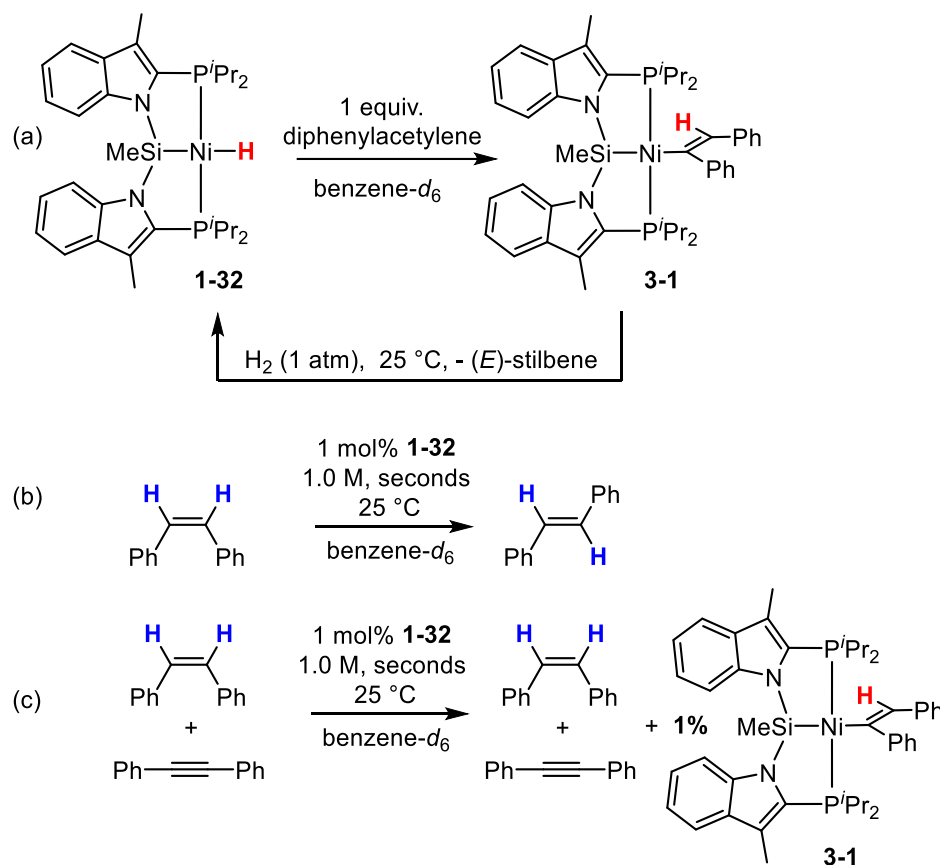
Scheme 3.2.1. Substrate scope for the semihydrogenation of alkynes with **1-32**. Reaction conditions: alkyne (0.2 mmol), **1-32** (specified mol%, 40 mmol/L stock solution), 1 atm H₂, benzene-*d*₆ (volume required to attain 200 μL total volume), 25 °C, 4 h. Conversion to product determined on the basis of ¹H NMR integration vs. 1,3,5-trimethoxybenzene internal standard (0.2 mmol; average of two runs); a relaxation delay of 60 s was used to ensure accurate integrations. Isolated yields provided in parentheses. ^aReaction performed at 50 °C. ^bReaction performed at 90 °C. ^cFor reaction run with 1 mol% **1-32**, 50 °C, benzene-*d*₆, and E/Z > 1:99. ^dAll starting material consumed.

The utility of **1-32** on a larger scale (1.0 mmol) was also evaluated. Isolated yields of (*E*)-alkenes proved comparable to conversions determined on the basis of ¹H NMR analysis (Scheme 3.2.1; **3-1a**, **3-1f**, **3-1g**, and **3-1p**). Product **3-1g**, obtained in 97% yield, is notable as it contains a boronic ester that can be used to rapidly build complexity through cross-coupling chemistry. Trimethylsilyl protected alkynes also proved amenable to scale-up, as indicated by the isolation of **3-1p** in 89% yield with excellent selectivity for the (*E,E*)-semihydrogenation product.

3.2.2 Mechanistic Inquiry

A series of catalytic and stoichiometric experiments provided insight into the mechanism of (*E*)-selective semihydrogenation involving **1-32**. Treatment of complex **1-32** with one equiv. of diphenylacetylene afforded quantitative (by ³¹P NMR) conversion to the corresponding alkenyl complex **3-1** upon mixing (Scheme 3.2.2 a). The ³¹P{¹H} NMR spectrum of complex **3-1** features a single resonance at 41 ppm, consistent with a *C_s*-symmetric complex in solution. In situ ¹H NMR (benzene-*d*₆) analysis of the reaction mixture revealed the disappearance of the Ni-*H* resonance associated with **1-32** at -4.81 ppm and the appearance of a new resonance at 6.82 ppm corresponding to the vinylic H in **3-1**. The solid-state structure of **3-1** was obtained by use of single crystal X-ray diffraction techniques and confirmed the formulation of this complex as a square planar alkenyl species (Figure 3.2.1). While the hydrogen atom attached to C52 could not be located in the difference map, the C51–C52 interatomic distance of 1.346(2) Å (*cf.* 1.198 Å in diphenylacetylene)¹⁹¹ is consistent with the alkenyl formulation. Adding H₂ (1 atm) to a degassed solution of alkenyl complex **3-1** at room temperature results in regeneration of

NiH **1-32** and formation of (*E*)-stilbene (Scheme 3.2.2 a).



Scheme 3.2.2. Mechanistic experiments.

Analysis of catalytic semihydrogenation reactions by use of ^1H and $^{31}\text{P}\{^1\text{H}\}$ NMR spectroscopy revealed that the only observable Ni-containing species in solution is complex **1-32** (in reactions that went to completion). In the case of catalytic reactions that did not proceed to completion, NMR spectroscopic analysis revealed the presence of Ni species giving rise to ^{31}P NMR resonances in the range of 30-40 ppm, as well as predominantly unreacted alkyne starting material. Having already confirmed that *cis/trans* isomerization of (*Z*)-stilbene could occur in the absence of H_2 (Table 2.2.1, entry 5), we further determined that this process is rapid, occurring upon mixing of 1 mol% of complex **3-1** and a 1.0 M benzene- d_6 solution of (*Z*)-stilbene, whereupon immediate precipitation of

(*E*)-stilbene was observed (Scheme 3.2.2 b). A ^1H NMR spectrum of the reaction mixture collected within <5 minutes of the catalyst addition confirmed the complete isomerization of (*Z*)-stilbene into (*E*)-stilbene. Analysis of the reaction mixture by $^{31}\text{P}\{^1\text{H}\}$ NMR spectroscopy also confirmed regeneration of **1-32** as the only observable Ni-containing species.

Lastly, a competition experiment wherein 1 mol% of complex **1-32** was added to an equimolar solution of (*Z*)-stilbene and diphenylacetylene in benzene- d_6 solution revealed no isomerization of the alkene, on the basis of ^1H NMR spectroscopy (Scheme 3.2.2 c). The $^{31}\text{P}\{^1\text{H}\}$ NMR spectrum of this mixture is consistent with the quantitative formation of **3-1**, indicating preferential insertion of the alkyne substrate prior to alkene isomerization.

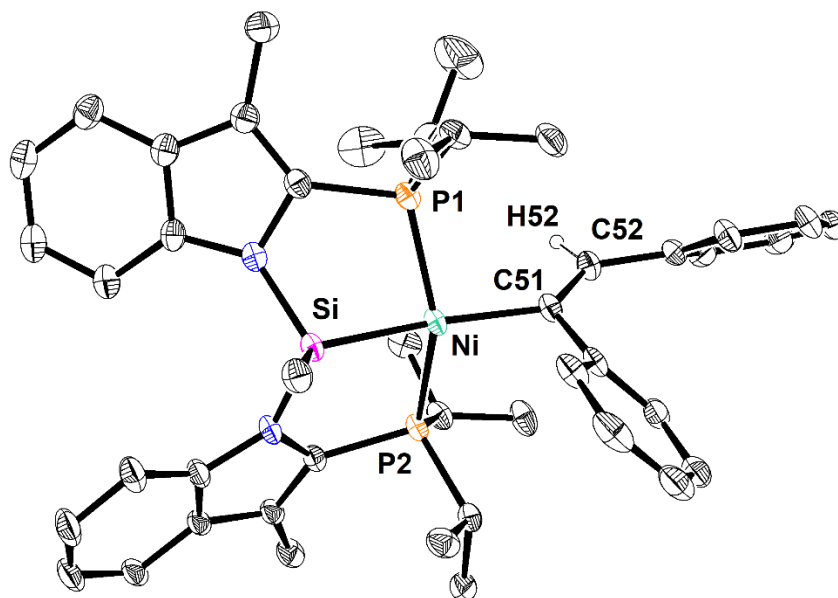
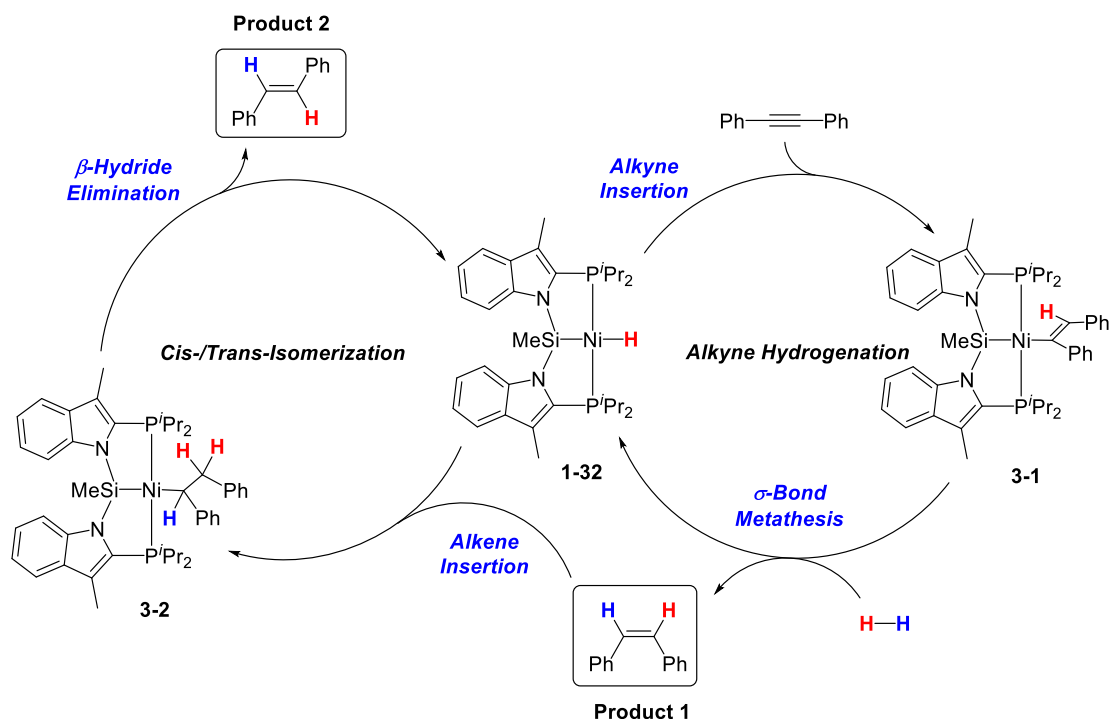


Figure 3.2.1. Crystallographically determined structure of **3-1** with thermal ellipsoids drawn at the 30% probability level. Most hydrogen atoms are omitted for clarity. Selected interatomic distances (Å) and angles (deg): Ni–P1 2.1785(5), Ni–P2 2.1714(4), Ni–Si 2.2125(4), Ni–C51 1.9691(14), C51–C52 1.346(2), P1–Ni–P2 152.644(19), P1–Ni–Si

84.035(17), P1–Ni–C51 97.67(5), P2–Ni–Si 84.847(16), P2–Ni–C51 98.71(4), Si–Ni–C51 167.12(5), Ni–C51–C52 133.04(12).

With the insights gained from the stoichiometric and catalytic experiments, a possible catalytic cycle for this semihydrogenation is proposed in Scheme 3.2.3. Following migratory insertion of the alkyne to yield complex **3-1**, reaction of the alkenyl complex **3-1** with H₂ liberates the (*Z*)-alkene and regenerates the nickel hydride complex **1-32**. This step could plausibly involve a σ -bond metathesis pathway, as H₂ oxidative addition to afford a Ni(IV) species is highly unlikely. Alternatively, we cannot rule out the intermediacy of [P(η^2 -Si-H)P]NiL (L = alkene or alkyne) species involving η^2 -SiH coordination in the catalytic cycle (Scheme 3.1.1). The (*Z*)-alkene can then re-enter the catalytic cycle, reacting with **1-32** to form an unobserved Ni-alkyl intermediate **3-2** that can undergo rotation about the alkyl C–C bond and generate the (*E*)-alkene product upon β -hydride elimination. This isomerization occurs quite readily, as demonstrated by the excellent selectivity observed in semihydrogenation catalysis for a broad range of substrates. Isomerization appears to be hindered only by the poor coordinating ability of very electron-poor alkenes that feature strongly electron-withdrawing substituents and sterically challenging internal alkenes such as *cis*-4-octene. The absence of over-

hydrogenated alkane products in all catalytic experiments suggests that β -hydride elimination in **3-2** occurs more readily than the reaction of the alkyl complex with H_2 .



Scheme 3.2.3. Proposed catalytic cycle for the (E) – selective semihydrogenation of alkynes.

3.3 Summary and Conclusions

In summary the PSiP-supported Ni hydride (iPr -PSiP^{Ind})NiH complex **1-32** has proven to be an efficient and selective catalyst for the atom economical (E) -selective semihydrogenation of alkynes using H_2 . Complex **1-32** operates under exceptionally mild conditions, including examples of room temperature reactivity using 1 atm of H_2 at low catalyst loadings. The substrate scope for this semihydrogenation reaction encompasses a variety of substituted diaryl alkynes and $SiMe_3$ -protected terminal alkynes, and is tolerant of a diverse range of functional groups. The broad scope of this reactivity, the high (E) -selectivity, and the mild reaction conditions establish complex **1-32** as the state-of-the-art

for this transformation.

Stoichiometric and catalytic experiments show that alkyne insertion into the Ni-hydride **1-32** and alkene isomerization mediated by **1-32** are facile processes. These results, coupled with the relative inability of complex **1-32** to hydrogenate internal alkenes, have led us to propose a simple catalytic cycle wherein complex **1-32** hydrogenates alkynes to the corresponding (*Z*)-alkenes, which are subsequently isomerized to the (*E*)-alkene products in a highly selective manner. The role of the PSiP ligand in the semihydrogenation process is currently under investigation.

3.4 Experimental

3.4.1 General Considerations

All experiments were conducted under nitrogen in a glovebox or using standard Schlenk techniques. Tetrahydrofuran and diethyl ether were distilled from Na/benzophenone ketyl. Benzene, toluene, and pentane were first sparged with nitrogen and subsequently dried by passage through a double-column (one activated alumina column and one column packed with activated Q-5). All purified solvents were stored over 4 Å molecular sieves. Benzene-*d*₆ was degassed via three freeze-pump-thaw cycles and stored over 4 Å molecular sieves. Complex **1-32** was prepared by previously reported methods.¹⁰ All other reagents were purchased from commercial suppliers and used without further purification. Unless otherwise stated, ¹H, ¹³C, ¹¹B, ³¹P, and ²⁹Si characterization data were collected at 300K, with chemical shifts reported in parts per million downfield of SiMe₄ (for ¹H, ¹³C, and ²⁹Si), BF₃·OEt₂ (for ¹¹B), or 85% H₃PO₄ in D₂O (for ³¹P). ¹H and ¹³C NMR chemical shift assignments are based on data obtained from ¹³C{¹H}, ¹³C-DEPTQ, ¹H-¹H COSY, ¹H-¹³C HSQC, and ¹H-¹³C HMBC NMR experiments. ²⁹Si NMR assignments are based on ¹H-²⁹Si

HMBC and ^1H - ^{29}Si HMQC experiments. X-ray data collection, solution, and refinement were carried out by Dr. Michael J. Ferguson at the University of Alberta X-ray Crystallography Laboratory, Edmonton, Alberta. Additional NMR characterization data and X-ray crystallographic parameters are provided in Appendices 1 and 2, respectively.

3.4.2 Synthetic Procedures and Characterization Data

General Procedure for the Catalytic Hydrogenation of Alkynes. The substrate (0.2 mmol) was weighed (or added via microsyringe for liquid substrates) into a 1-dram vial and benzene- d_6 was added to bring the total reaction volume to 200 μL (1.0M). Complex **1-32** was then added as a stock solution in benzene- d_6 and the vial was equipped with a stirbar and closed with a screw cap featuring a PTFE septum. A needle was then inserted through the septum to allow for the introduction of H_2 gas. The vial was then transferred to a Parr reactor which was sealed and purged with H_2 and subsequently pressurized to 1 atm H_2 pressure. The Parr reactor was heated to 25 $^\circ\text{C}$ (50 $^\circ\text{C}$ where specified) in an oil bath for the duration of the reaction time. Afterward, the Parr reactor was removed from the oil bath and depressurized. In the glovebox, 600 μL of a 0.33 M stock solution of 1,3,5-trimethoxybenzene was added to the reaction mixture as an internal standard, and the mixture was transferred to an NMR tube for data acquisition. For calculation of NMR yields, a chosen diagnostic product signal was integrated relative to that of the internal standard. A long (60 s) relaxation delay was used to ensure accurate integrations.

General Procedure for the Isolation of (*E*)-Alkenes 3-1f, 3-1g, and 3-1p. The substrate (1.0 mmol) was weighed into a 1-dram vial and 750 μL of benzene was added. Complex **1-32** was then added as a stock solution in benzene (1.0 mol%, 250 μL , 40.3 mM stock) and the vial was equipped with a stirbar and closed with a screw cap featuring a

PTFE septum. A needle was then inserted through the septum to allow for the introduction of H₂ gas. The vial was transferred to a Parr reactor which was sealed and purged with H₂ and subsequently pressurized to 1 atm H₂ pressure. The Parr reactor was heated to 25 °C in an oil bath for 4 h. Afterward, the Parr reactor was removed from the oil bath and depressurized of H₂. In the glovebox, the crude material was filtered through a plug of silica into a tared 4-dram vial. The solvent was removed in vacuo and the resulting residue was washed with cold pentane to afford the (*E*)-alkene product in the specified yield.

Synthesis of (*i*Pr-PSiP^{Ind})Ni(CPh=CHPh) (3-1). In a glovebox, complex **1-32** (0.033 g, 0.055 mmol) was weighed into a 1-dram vial and dissolved in ca. 0.7 mL of benzene-*d*₆. This solution was then transferred to a vial containing diphenylacetylene (0.010 g, 0.055 mmol) and the reaction mixture was agitated until the diphenylacetylene was completely dissolved. An immediate color change from dark orange to light orange was observed, and the contents of the vial were transferred to an NMR tube, whereupon complete conversion to **3-1** was observed by ³¹P{¹

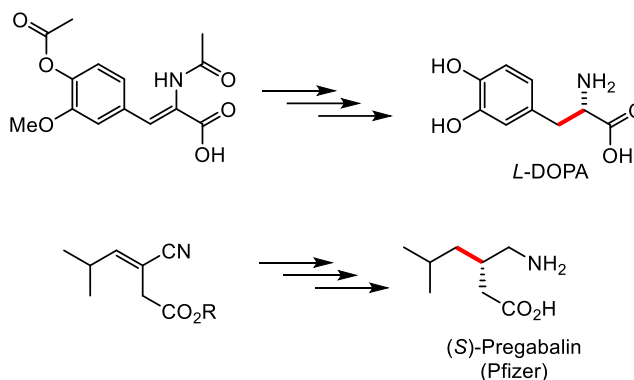
Chapter 4: Cobalt Catalyzed Asymmetric Hydrogenation of Dehydro- α -Amino Acids Enabled by Phen-DalPhos Ligation

4.1 Introduction

The transition metal catalyzed asymmetric hydrogenation of alkenes represents one of the most effective and atom economical methods for accessing single enantiomer compounds. Hydrogenation catalysts based on the second and third row transition metals Ru, Rh, and Ir have found widespread utility in the pharmaceutical, agrochemical, fragrance, and fine chemical industries, as well as in academic settings.^{1-2, 71, 192} In contrast, catalysts employing first row *3d*-transition metals (*i.e.*, Mn, Fe, Co, Ni) represent an attractive, yet underdeveloped, area of research owing to their relatively high abundance and low cost when compared to their second and third row congeners.^{60, 169-172} The last decade has seen an increased focus on the discovery of catalysts employing these Earth-abundant metals and has led to the development of several Co- and Ni-based catalysts that exhibit high hydrogenation activity and enantioselectivity.^{19-20, 61-68, 72-73, 76-77, 193-196} These advances notwithstanding, this area of research remains in its infancy, and the continued investigation of new strategies for facilitating *3d*-metal catalyzed asymmetric hydrogenation is key to the development of efficient synthetic protocols that can supplant platinum group metal based technology.

The asymmetric hydrogenation of unsaturated carboxylic acid derivatives is of particular interest due to the prevalence of such compounds in the pharmaceutical industry, with examples of drugs such as *L*-DOPA¹⁹⁷⁻¹⁹⁸ and Pregabalin,¹⁹⁹⁻²⁰⁰ whose synthesis is testament to the utility of transition metal catalysis for accessing such motifs in a streamlined fashion (Scheme 4.1.1). The synthesis of *L*-DOPA and *dehydro- α* -amino acids

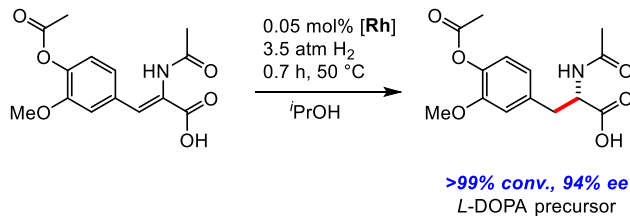
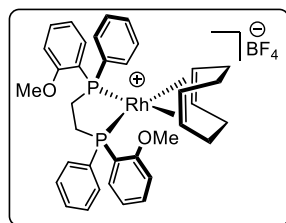
in general via Rh-catalyzed asymmetric hydrogenation was the basis of work by Knowles,^{1, 197-198} for which he was awarded the 2001 Nobel prize in Chemistry (3.1.2 (a)).



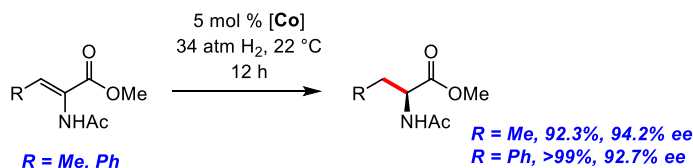
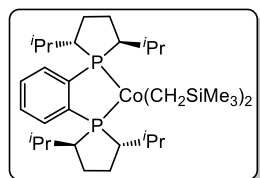
Scheme 4.1.1. Examples of chiral pharmaceutical targets synthesized via transition metal catalyzed asymmetric hydrogenation of unsaturated carboxylic acid derivatives.

While Rh- and Ru-based bis(phosphine) asymmetric hydrogenation catalysts dominated this area in subsequent years, seminal work by Chirik and co-workers in 2013 disclosed the asymmetric hydrogenation of acetamido acrylates mediated by a family of (DuPhos)Co(II) dialkyl complexes with good enantioselectivity (Scheme 4.1.2 (b)).⁶¹ Subsequent work from the Chirik group led to improved enantioselectivity for these substrates employing cationic Co(I)⁶⁴ as well as neutral Co(0)⁶⁷ complexes supported by related chiral bis(phosphine) ligands. Furthermore, work from the Zhang group demonstrated the ability of an axially chiral bis(phosphine)-supported Ni complex to mediate the asymmetric hydrogenation of benzoyl-protected acetamido acrylates with high enantioselectivity (Scheme 4.1.2 (c)).⁷³

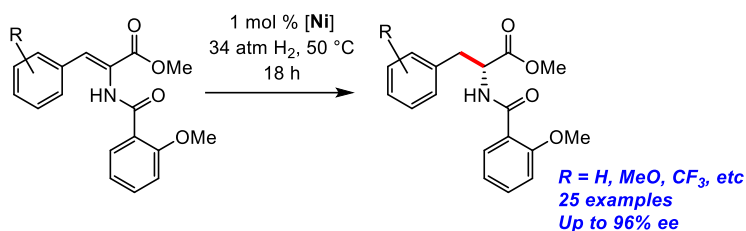
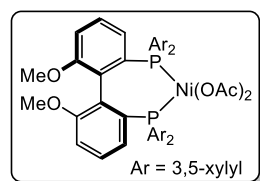
(a) Knowles, 1975



(b) Chirik, 2013



(c) Zhang, 2020

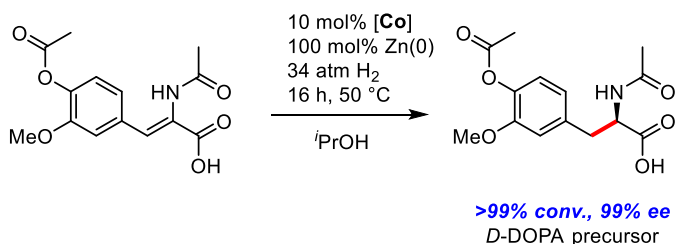
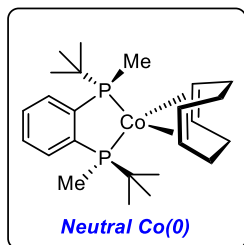


Scheme 4.1.2. Previous notable examples of asymmetric hydrogenation of unsaturated carboxylic acid derivatives, including (a) Nobel prize winning work on Rh-mediated asymmetric hydrogenation of *dehydro-α*-amino acids, and (b, c) subsequent Co- and Ni-catalyzed examples.

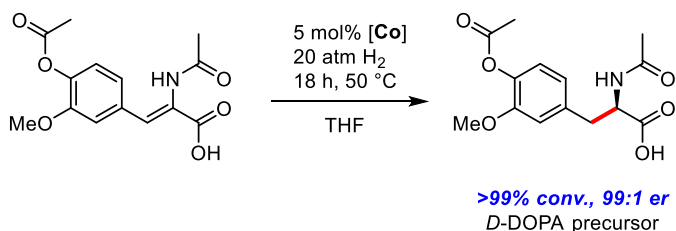
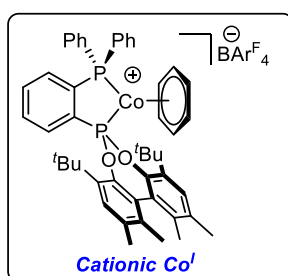
While these latter 3*d*-metal based catalysts are capable of achieving high conversion and enantioselectivity only the (*R,R*)-(BenzP*)Co(COD) complex (**1-75**) reported by Chirik and co-workers in 2020 was shown to be capable of asymmetrically hydrogenating the *dehydro-α*-amino acid as opposed to the acetamido acrylate (Scheme 4.1.3 (a)).⁶⁷ This complex was shown to be capable of hydrogenating (*Z*)-*dehydro-N*-acetylphenylalanine to give (*R*)-*N*-acetylphenylalanine in 95% yield with 99% *ee*. Additionally, the asymmetric hydrogenation of (*Z*)-*dehydro-N*-acetyl-(4-acetoxy-3-methoxy) phenylalanine could be performed to give the precursor to *D*-DOPA in 92% yield with 99% *ee*. This result was noteworthy, as it parallels the Nobel-prize-winning work of Knowles on the synthesis of

L-DOPA and *dehydro-α*-amino acids in general via Rh-catalyzed asymmetric hydrogenation.^{1, 197-198}

(a) Chirik, 2020



(b) This work



- New ligand platform for base metal mediated asymmetric catalysis
- Co-catalyzed asymmetric hydrogenation of *dehydro-α*-amino acids
- 20 examples, *e.r.* values up to 99:1

Scheme 4.1.3. (a) Previous example of Co-catalyzed asymmetric hydrogenation of *dehydro-α*-amino acids, and (b) this work, (*S*)-(Ph-PhenDalPhos)Co mediated asymmetric hydrogenation of *dehydro-α*-amino acids.

The Turculet group has recently become interested in the development of new catalysts for hydrofunctionalization reactions based on Earth-abundant first row transition metals. In this regard, Ni complexes supported by indolyl derived bis(phosphino)silyl ligation were shown to catalyze the (*E*)-selective semihydrogenation of a broad scope of diarylacetylenes, as well as silyl-protected terminal acetylenes, under exceptionally mild conditions with high selectivity (>99:1 *E:Z*).⁸² In an effort to access asymmetric hydrogenation we sought to develop suitable new ligand platforms that could be readily synthesized from commercially available starting materials and include easily tuned steric and electronic properties. This effort led to the synthesis and characterization of a family

of Co complexes supported by the enantiopure phosphino-phosphonite ligand (*S*)-2-(diphenylphosphino)P(Phen) (Phen = 5,5',6,6'-tetramethyl-3,3'-di-tert-butyl-1,1'-biphenyl-2,2'-diol, (*S*)-Ph-PhenDalPhos, **L4-1**). The application of these complexes as pre-catalysts for the asymmetric hydrogenation of *dehydro-α*-amino acids is described herein. While all three complexes displayed catalytic activity and some degree of enantioselectivity, the cationic arene complex [(*S*)-(Ph-PhenDalPhos)Co(η^6 -C₆H₆)] [BAr^F₄] (**4-3**) (BAr^F₄ = tetrakis(3,5-bis(trifluoromethyl)phenyl) borate) afforded both high conversion and enantioselectivity for a broad scope of *dehydro-α*-amino acid substrates.

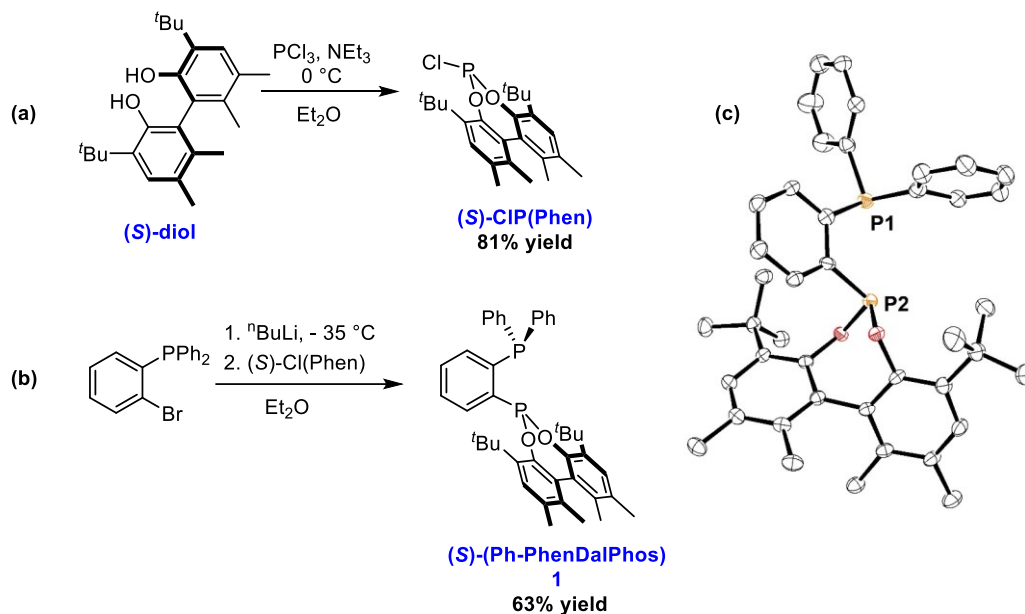
4.2 Results and Discussion

4.2.1 Ligand Synthesis

Prior to this work, the racemic family of ligands with the formula *rac*-(R-PhenDalPhos) (R = dicyclohexylphosphino, di(*o*-tolylphosphino)) had been reported for application in Ni-catalyzed C-N cross coupling.^{11, 201} The R-PhenDalPhos ligand platform was attractive for application in asymmetric catalysis as the enantiopure diol (*S*)-5,5',6,6'-tetramethyl-3,3'-di-tert-butyl-1,1'-biphenyl-2,2'-diol ((*S*)-diol) is commercially available and can be readily condensed with PCl₃ to afford the enantiopure chlorophosphine (*S*)-CIP(Phen) in good yield (Scheme 4.2.1 (a)). Furthermore, the synthesis of 2-R₂P-bromobenzene derivatives is well established and provides a useful handle for tuning the steric and electronic properties of the ligand by varying the R substituents on phosphorus.

The synthesis of the *C₁* symmetric variant (*S*)-Ph-PhenDalPhos (**L4-1**) was achieved in 63% yield via the lithiation of (2-diphenylphosphino)bromobenzene and subsequent reaction with the enantiopure chlorophosphine (*S*)-CIP(Phen) (Scheme 4.2.1). Compound

1 crystallizes in the chiral space group $P2_12_12_1$ and single crystal X-ray crystallographic analysis confirmed the connectivity in this molecule (Scheme 4.2.1 (c)).



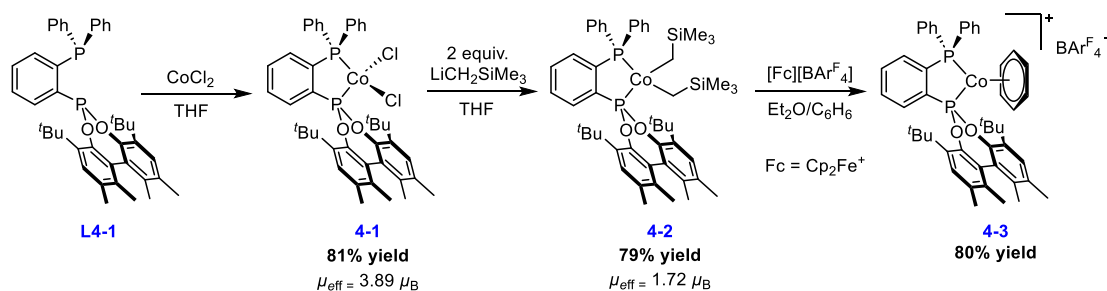
Scheme 4.2.1. (a) Synthesis of *(S)*-Cl(Phen). (b) Synthesis of *(S)*-Ph-PhenDalPhos (**1**). (c) Crystallographically determined structure of **1** with thermal ellipsoids drawn at the 50% probability level. Hydrogen atoms have been omitted for clarity.

4.2.1 Synthesis of Co Complexes

The ability of the first-row transition metals to support oxidation states that differ by only one electron has proven to be an added variable to be considered when designing and optimizing new catalysts. Neutral Co^{II} complexes, neutral or cationic $\text{Co}(\text{I})$ complexes, and neutral $\text{Co}(0)$ complexes have all displayed excellent catalytic activity and enantioselectivity for the asymmetric hydrogenation of substituted alkenes including 1,1-disubstituted alkenes,^{19, 193, 202} enamides,^{61, 63-64, 194-195} α,β -unsaturated carboxylic acids,⁶⁶⁻⁶⁷ and unprotected enamines.⁷⁰

To begin investigating the coordination chemistry of *(S)*-Ph-PhenDalPhos with Co, the Co^{II} chloride complex *(S)*-(Ph-PhenDalPhos) CoCl_2 (**4-1**) was prepared. Complex **4-1** was

obtained as a paramagnetic purple solid in 81% yield by treatment of a THF suspension of CoCl_2 with **L4-1** (Scheme 4.2.2). Solution magnetic moment measurements for **4-1** (Evans method, $\text{DCM-}d_2$, 300K) resulted in a calculated μ_{eff} value of $3.89 \mu_{\text{B}}$ ($S = 3/2$ ground state). Despite repeated attempts, single crystals of **4-1** suitable for X-ray diffraction could not be obtained. As a result, we tentatively assign the structure of **4-1** as a high spin tetrahedral complex on the basis of the observed magnetic susceptibility.



Scheme 4.2.2. Synthetic route for the preparation of **4-1**, **4-2**, and **4-3**.

Subsequent treatment of **4-1** with two equiv. of $\text{LiCH}_2\text{SiMe}_3$ in THF afforded the dialkyl complex (*S*)-(Ph-PhenDalPhos) $\text{Co}(\text{CH}_2\text{SiMe}_3)_2$ (**4-2**) as a paramagnetic red solid in 79% yield (Scheme 4.2.2). Solution magnetic moment measurements for **4-2** (Evans method, benzene- d_6 , 300K) resulted in a calculated μ_{eff} value of $1.72 \mu_{\text{B}}$ ($S = 1/2$ ground state), which is consistent with a low spin, square planar complex. The solid-state structure of **4-2** confirmed this assignment and displays the expected square planar geometry at Co (Figure 4.2.1). Despite the large steric profile of the phosphonite donor, the Co-P2 distance of 2.1250(15) Å in **4-2** was found to be shorter than the Co-P1 distance of 2.2171(17) Å involving the PPh_2 donor, possibly reflecting the π -accepting nature of the phosphonite moiety.²⁰³ Interestingly, there was relatively little difference in the interatomic distances for either of the Co-C bonds (Co-C45 2.009(6) Å vs. Co-C47 2.017(6) Å).

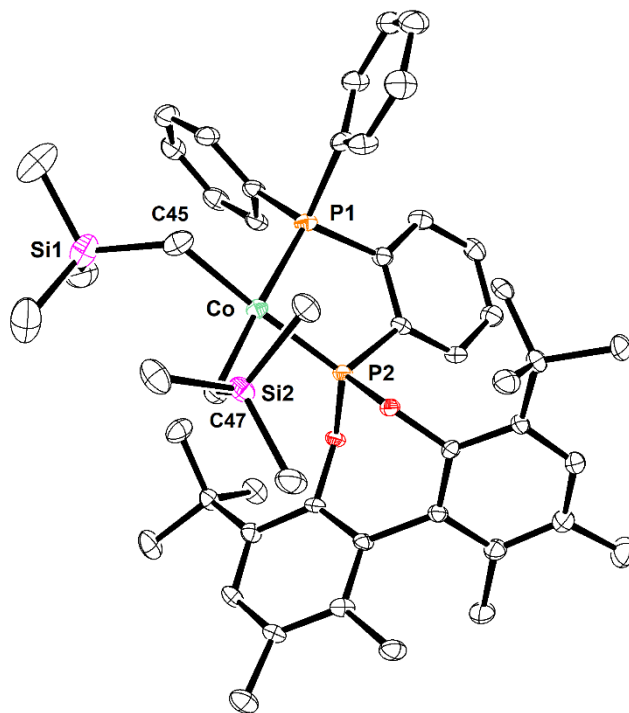


Figure 4.2.1. Crystallographically determined structure of **4-2** with thermal ellipsoids shown at the 50% probability level; hydrogen atoms have been omitted for clarity. Selected interatomic distances (Å) and angles (deg): Co-P1 2.2171(17), Co-P2 2.1250(15), Co-C45 2.009(6), Co-C47 2.017(6), C45-Co-C47 90.3(3), C45-Co-P2 176.6(2), C47-Co-P2 91.20(19), C45-Co-P1 91.8(2), C47-Co-P1 177.44(19), P2-Co-P1 86.66(6).

Although cationic bis(phosphine) Rh complexes are employed industrially as catalysts for asymmetric hydrogenation,^{198-200, 204} the Co analogs were unknown until recently due to the lack of synthetic methods to access them. Work from Chirik and co-workers has shown that cationic Co^I arene complexes can be accessed through oxidatively induced reductive elimination of *in-situ* generated bis(phosphine) Co^{III} dialkyl complexes.^{64, 70} In this regard, exposure of (py)₂Co(CH₂SiMe₃)₂ to a bis(phosphine) ligand in the presence of benzene, followed by the addition of ferrocenium salts of the type [Fc][X] (Fc = Cp₂Fe⁺, X = BAR^F₄⁻, BF₄⁻, PF₆⁻, or BPh₄⁻), was found to be a general method to access 18 electron complexes of the form [(P₂)Co(η⁶-C₆H₆)]⁺[X]. This protocol was successfully extended to **4-2**, such that treatment with the one electron oxidant [Fc][BAR^F₄] in a 1:1 mixture of diethyl ether and benzene afforded the corresponding cationic complex **4-3** as a

diamagnetic orange complex in 80% yield (Scheme 4.2.2). The X-ray crystal structure of **4-3** confirmed η^6 -coordination of the benzene ligand to the Co center and revealed a slight contraction of both Co-P bonds in comparison to **4-2** (Co-P1 2.1570(11) Å, Co-P2 2.0914(11) Å).

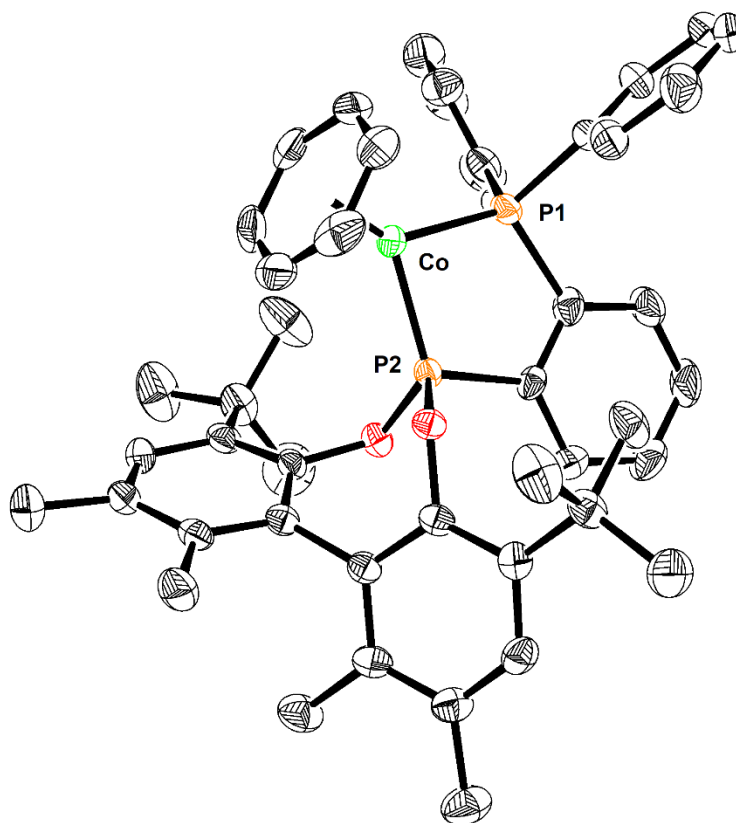


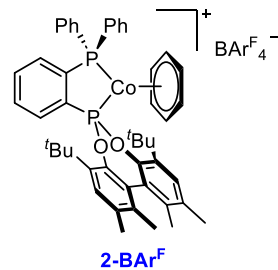
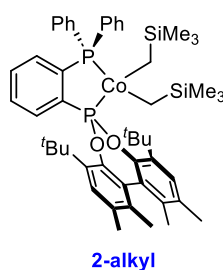
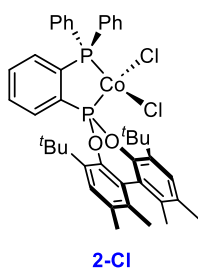
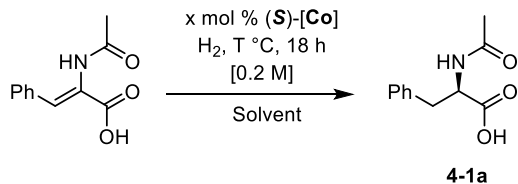
Figure 4.2.2. Crystallographically determined structure of **4-3** with thermal ellipsoids shown at the 50% probability level; hydrogen atoms and the BAr^{F}_4 anion have been omitted for clarity. Selected interatomic distances (Å) and angles (deg): Co-P1 2.1570(11), Co-P2 2.0914(11), Co-Centroid 1.360, P2-Co-P1 86.26(4).

4.2.2 Catalysis Optimization

The Co complexes **4-1**, **4-2**, and **4-3** were screened as pre-catalysts for the asymmetric hydrogenation of *dehydro-N*-acetyl-phenylalanine (Table 4.2.1). One equivalent of Zn(0) was employed as an additive when **4-1** was used as a pre-catalyst as this has been shown to promote increased catalytic activity and enantioselectivity.^{63, 66-68} While all three pre-

catalysts afforded good conversion to product, **4-3** gave both quantitative conversion and an *er* of 99:1 for (*R*)-*N*-acetyl-phenylalanine with a loading of 5 mol% Co after 18 h at 50 °C in ^tPrOH solution under 40 atm H₂ (Table 4.2.1, entry 3; absolute configuration determined relative to an authentic sample of (*R*)-*N*-acetyl-phenylalanine).

Table 4.2.1. Pre-catalyst screen.



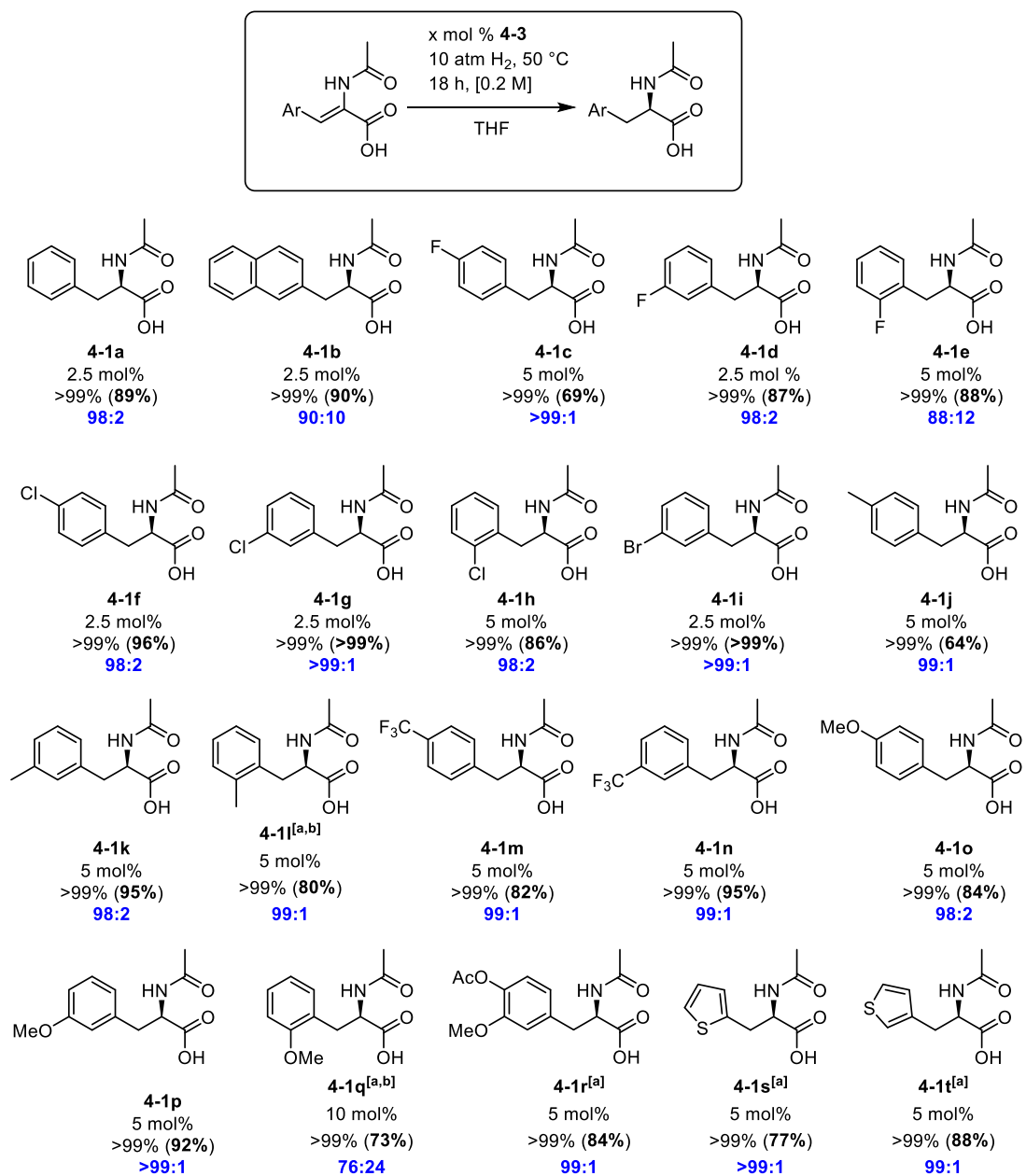
Entry	Pre-catalyst (mol%)	H ₂ (atm)	T (° C)	Solvent	Conv. (%) ^[a]	<i>er</i> ^[b]
1	4-1 (5 mol%) ^[c]	40	50	^t PrOH	>99	94:6
2	4-2 (5 mol%)	40	50	^t PrOH	78	76:2 4
3	4-3 (5 mol%)	40	50	^t PrOH	>99	99:1
4	4-3 (5 mol%)	10	50	^t PrOH	>99	99:1
5	4-3 (5 mol%)	10	50	TFE	53	98:2
6	4-3 (5 mol%)	10	50	THF	>99	99:1
7	4-3 (5 mol%)	10	50	CH ₃ CN	29	N/A
8	4-3 (5 mol%)	10	50	DCM	33	N/A
9	4-3 (2.5 mol%)	10	50	THF	>99	99:1
10	4-3 (1 mol%)	10	50	THF	67	99:1
11	4-3 (1 mol%)	40	50	THF	85	99:1
12	4-3 (0.5 mol%)	40	50	THF	60	99:1

[a] Determined by ¹H NMR spectroscopy. [b] Determined by chiral HPLC analysis on a chiral stationary phase. [c] With 100 mol% Zn(0) as additive.

Upon further optimization with **4-3** it was found that the H₂ pressure could be lowered from 40 to 10 atm with no loss in conversion or enantioselectivity (Table 4.2.1, entry 4). Furthermore, THF and *i*PrOH were found to be interchangeable as solvents, while 2,2,2-trifluoroethanol, acetonitrile, and dichloromethane did not afford high conversion (Table 4.2.1, entries 5,6,7, and 8). Lastly, the catalyst loading of **4-3** could be decreased to 2.5 mol% (Table 4.2.1, entry 9) with no degradation in conversion or enantioselectivity. However, reactions performed using 1 mol% **4-3** suffered from lower conversion (67%), albeit with similarly high enantioselectivity (Table 4.2.1, entry 10). Increasing the pressure to 40 atm in the presence of 1 or 0.5 mol% **4-3** increased conversion to 85% and 60% respectively, with no loss in enantioselectivity (Table 4.2.1, entries 11 and 12). The conditions employed in entry 9 were chosen as optimal for investigating the scope of the reaction owing to the balance of conversion and enantioselectivity with moderately reduced catalyst loading. Control experiments employing 5 mol% **L4-1** in the absence of Co under 10 atm H₂, 50 °C, in TFE for 18 h led to no conversion to product.

4.2.3 Substrate Scope

Having optimized catalysis conditions, a library of *dehydro-α*-amino acids was synthesized and subjected to asymmetric hydrogenation (Scheme 4.2.3). The optimized conditions could be extended to substrates bearing halogen (**4-1d** – **4-1j**) and polyaromatic substitution (**4-1b**). Substrates featuring electron donating groups (**4-1j**, **4-1k**, **4-1o**) or strongly electron withdrawing groups (**4-1c**, **4-1m**, **4-1n**) were found to require an increase in catalyst loading to 5 mol% to afford full conversion to product. In all cases the enantioselectivity remained high, with only **4-1b** showing an *er* of less than 98:2.



Scheme 4.2.3. Substrate scope for the asymmetric hydrogenation of *dehydro-α*-amino acids catalyzed by **4-3**. Reaction conditions: substrate (0.2 mmol), **4-3** (specified mol %), 10 atm H₂ (unless otherwise noted), THF (1 mL), 50 °C, 18 h. Conversion to product was determined on the basis of ¹H NMR spectroscopy (isolated yield in parentheses). [a] Reaction performed under 20 atm H₂. [b] Reaction performed for 48 h.

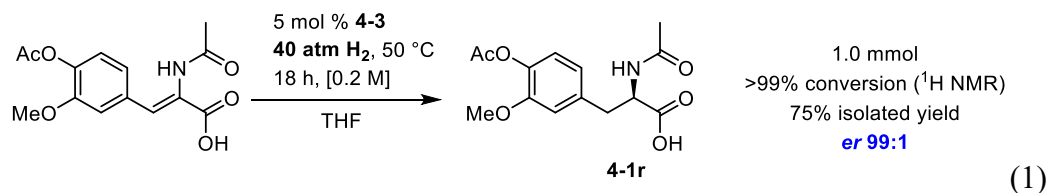
Substrates featuring *ortho*-substitution were found to be challenging for **4-3**. Substrate **4-1e**, which possesses *o*-fluoro substitution, proceeded to completion under the standard conditions at 5 mol%, but a decrease in enantioselectivity was observed, providing an *er*

of 88:12. Surprisingly, substrate **4-1h** (the Cl analogue of **4-1e**) was also completely hydrogenated under these conditions, yet afforded a higher *er* of 98:2. In the case of the *o*-tolyl derivative **4-1l** an increase in both the H₂ pressure (20 atm) and reaction time (48 h) were found to be necessary for the reaction to proceed to completion at 5 mol% loading of **4-3**. While **4-1l** displayed high enantioselectivity under these conditions (>99:1), the asymmetric hydrogenation of substrate **4-1q** (*o*-methoxy) was found to have an *er* of only 76:24 and required an even higher catalyst loading of 10 mol% to proceed to completion.

Heteroaryl substitution was found to be compatible with **4-3** as shown by substrates **4-1s** and **4-1t** which contain 2- and 3-substituted thiophene moieties, respectively. Under 20 atm H₂ the reactions were found to proceed smoothly with high enantioselectivity for both substrates (99:1). The asymmetric hydrogenation of substrate **4-1r** with Rh to produce the precursor to *L*-DOPA was a key reaction that Knowles performed in the work for which he was awarded the 2001 Nobel Prize in Chemistry (Scheme 4.1.2 (a)).^{1, 197-198} Through high-throughput experimentation Chirik and co-workers were able to demonstrate that a Co(0) complex supported by the chiral bis(phosphine) 1,2-bis(*t*-butylmethylphosphino)benzene ((*R,R*)-BenzP*) (**1-75**) could also achieve this hydrogenation with high conversion (>99%) and enantioselectivity (99% ee) to give the precursor to *D*-DOPA (Scheme 4.1.3(a)).⁶⁷ Applying **4-3** for the asymmetric hydrogenation of this same substrate proceeded with complete conversion and a similarly high enantioselectivity under 20 atm H₂ (99:1 selectivity for **4-1r**, precursor to *D*-DOPA).

The utility of **4-3** on a larger scale (1.0 mmol) was also evaluated (eq 1). Substrate **4-1r** was chosen for this experiment due to its historical importance and relevant status as a highly functionalized amino acid precursor. Pre-catalyst **4-3** was found to cleanly

hydrogenate **4-1r** on a 1.0 mmol scale to afford the precursor to *D*-DOPA in 75% isolated yield. The H₂ pressure was increased to 40 atm to ensure complete conversion with no accompanied degradation of the enantioselectivity. This is notable as increasing the H₂ pressure has led to a *decrease* in enantioselectivity for many bis(phosphine) supported Rh catalysts.²⁰⁵

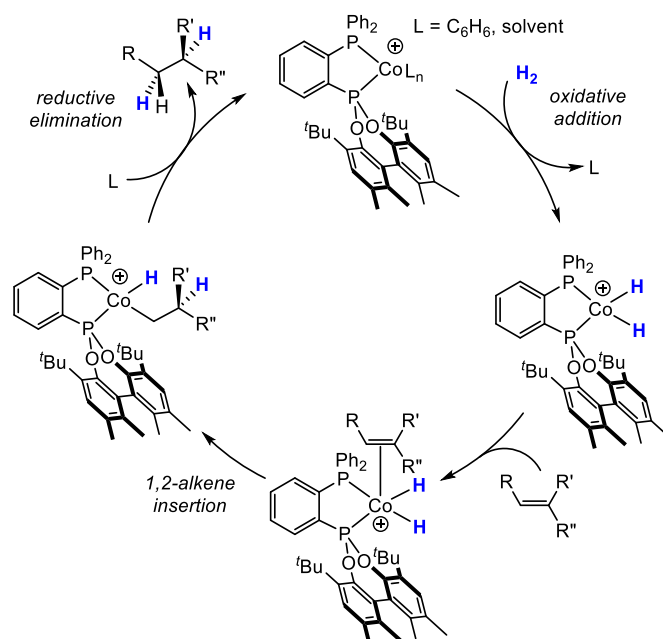
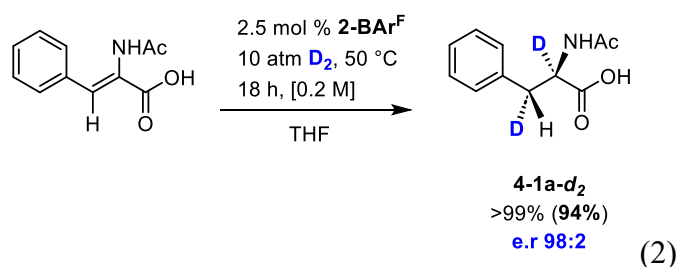


4.2.4 Deuterium Labeling Studies

Chirik and co-workers have recently shown that in the case of alkene hydrogenation mediated by bis(phosphine) Co(0) species a Co(II) dihydride mechanism is in effect.^{67, 194-195} Catalytic hydrogenation of (*Z*)-*dehydro-N*-acetyl-phenylalanine under 4 atm D₂ in the presence of natural abundance MeOH as solvent led exclusively to 1,2-*d*₂-incorporation in the product (**4-1a-d₂**). Moreover, of the two possible diastereotopic β-positions, deuterium incorporation only occurred at the position resulting from *cis*-D₂ addition. This resulted in a single isotopomer and is consistent with a dihydride mechanism similar to what has previously been invoked in Rh catalyzed asymmetric hydrogenation of the same substrate.²⁰⁶⁻²⁰⁷

The similarity of **4-3** to the cationic Rh(I) catalysts that have been historically employed as alkene hydrogenation catalysts led us to postulate that a similar dihydride mechanism to both the Rh(I) and Co(0) systems described previously may be possible.¹³⁶ Oxidative addition of H₂ by **4-3** would provide a cationic Co(III) dihydride intermediate that could then undergo alkene insertion and subsequent C-H reductive elimination to provide the

hydrogenated product (Scheme 4.2.4). When the hydrogenation of (*Z*)-*dehydro-N*-acetylphenylalanine was performed under 10 atm D₂ we observed exclusive 1,2-*d*₂ incorporation in the product **4-1a-d₂** (eq 2). Furthermore, deuterium incorporation in the diastereotopic β-position was confined to the position resulting from *cis*-D₂ addition. As a result, only a single isotopomer was observed, supporting the possibility of a Co(III) dihydride mechanism resulting from oxidative addition of H₂ to the cationic Co(I) complex **4-3**. To date, efforts to observe such a dihydride complex resulting from H₂ addition to **4-3** have not been successful.



Scheme 4.2.4. Proposed mechanism for asymmetric alkene hydrogenation mediated by (*S*)-(Ph-PhenDalPhos)Co⁺.

4.3 Summary and Conclusions

In summary, work in this chapter details the application of the readily prepared enantiopure ligand (*S*)-Ph-PhenDalPhos and corresponding Co complexes in the asymmetric hydrogenation of *dehydro- α* -amino acids. A series of such Co complexes varying in oxidation state between Co(I) and Co(II) were shown to be active catalysts for the hydrogenation of (*Z*)-*N*-acetyl-phenylalanine, with the cationic Co(I) complex **4-3** supporting highly enantioselective hydrogenation. We were able to extend this reaction to a broad scope of *dehydro- α* -amino acids displaying good functional group tolerance under relatively mild conditions (2.5-5.0 mol% Co, 10 atm H₂, 50 °C). The 1.0 mmol scale hydrogenation of (*Z*)-*dehydro-N*-acetyl-(*a*4-acetoxy-3-methoxy) phenylalanine also demonstrates the utility of **4-3** on larger scales, furnishing the precursor to *D*-DOPA **4-1r** in good isolated yield (75%) and high enantioselectivity (99:1 *er*). Moreover, this reaction could be performed under 40 atm H₂ to ensure complete conversion with no degradation in enantioselectivity. Deuterium labeling experiments suggest the plausibility of a Co(I/III) mechanism wherein H₂ undergoes homolytic cleavage by the Co(I) cation followed by alkene insertion into the Co – H bond and subsequent reductive elimination to furnish the hydrogenated product.

4.4 Experimental

4.4.1 General Considerations

All experiments were conducted under nitrogen in a glovebox or using standard Schlenk techniques. Tetrahydrofuran and diethyl ether were distilled from Na/benzophenone ketyl. Benzene, toluene, and pentane were first sparged with nitrogen and subsequently dried by passage through a double-column (one activated alumina column and one column packed

with activated Q-5). All purified solvents were stored over 4 Å molecular sieves. Benzene- d_6 was degassed via three freeze-pump-thaw cycles and stored over 4 Å molecular sieves. The chlorophosphine (*S*)-ClP(Phen) was prepared by previously reported methods.^{11, 201} (*Z*)-*dehydro-N*-acetyl-phenylalanine, *D/L-N*-acetyl-phenylalanine, and *L-N*-acetyl-phenylalanine were purchased from TCI. All *dehydro-α*-amino acids were synthesized according to literature procedure.²⁰⁸ All other reagents were purchased from commercial suppliers and used without further purification. Unless otherwise stated, ¹H, ¹³C, ¹¹B, and ³¹P NMR characterization data were collected at 300K, with chemical shifts reported in parts per million downfield of SiMe₄ (for ¹H and ¹³C), BF₃·OEt₂ (for ¹¹B), or 85% H₃PO₄ in D₂O (for ³¹P). ¹H and ¹³C NMR chemical shift assignments are based on data obtained from ¹³C{¹H}, ¹³C-DEPTQ, ¹H-¹H COSY, ¹H-¹³C HSQC, and ¹H-¹³C HMBC NMR experiments. X-ray data collection, solution, and refinement were carried out by Dr. Katherine N. Robertson at Saint Mary's University, Halifax, Nova Scotia.

4.4.2 Synthetic Procedures and Characterization Data

(*S*)-(Ph-PhenDalPhos) (L4-1). In a glovebox, (2-bromophenyl)diphenylphosphine (0.48 g, 1.41 mmol) was weighed into a 4-dram vial equipped with a stir bar. Diethyl ether (12 mL) was added and the resulting solution cooled to -35 °C. Simultaneously, the chlorophosphine (*S*)-ClP(Phen) (0.589 g, 1.41 mmol) was weighed into a separate 4-dram vial equipped with a stir bar, dissolved in diethyl ether (5 mL), and cooled to -35 °C. ⁿBuLi (0.564 mL, 1.41 mmol) was then added dropwise to the vial containing (2-bromophenyl)diphenylphosphine and the mixture allowed to warm to room temperature. The resulting suspension was allowed to stir at room temperature for 30 minutes before it was once more cooled to -35 °C. The cooled suspension was then added dropwise to the

vial containing the chlorophosphine. The mixture was then allowed to warm to room temperature and stir for 18 h after which it was filtered, triturated with pentane (3 x 3 mL), and washed with pentane (3 x 5 mL) to afford **L4-1** as a white solid (0.582 g, 0.902 mmol, 64% yield). ^1H NMR (500 MHz, benzene- d_6): δ 7.50 – 7.49 (m, 2 H, H_{arom}), 7.45 – 7.39 (overlapping resonances, 3 H), 7.22 (s, 1 H, H_{arom}), 7.19 (s, 1 H, H_{arom}), 7.16 (s, 1 H, H_{arom}), 7.13 – 7.05 (overlapping resonances, 7 H), 6.90 – 6.88 (m, 1 H, H_{arom}), 6.84 – 6.81 (m, 1 H, H_{arom}), 2.19 (s, 3 H, CH_3), 2.10 (s, 3 H, CH_3), 1.91 (s, 3 H, CH_3), 1.75 (s, 3 H, CH_3), 1.30 – 1.28 (overlapping resonances, 18 H, CMe_3). $^{13}\text{C}\{^1\text{H}\}$ NMR (125.7 MHz, benzene- d_6): δ 148.8 (s, C_{arom}), 146.4 (d, $J_{\text{C-P}} = 7.2$ Hz, C_{arom}), 145.1 – 144.2 (m), 138.4 (d, $J_{\text{C-P}} = 2.6$ Hz, C_{arom}), 138.3 (s, C_{arom}), 137.7 (s, C_{arom}), 137.6 – 137.5 (m), 135.2 (s, C_{arom}), 134.7 (d, $J_{\text{C-P}} = 16.7$ Hz, CH_{arom}), 134.7 – 134.5 (m, CH_{arom}), 133.2 (d, $J_{\text{C-P}} = 5.7$ Hz, C_{arom}), 132.9 (d, $J_{\text{C-P}} = 5.6$ Hz, C_{arom}), 132.7 (s, C_{arom}), 132.4 (d, $J_{\text{C-P}} = 2.3$ Hz, C_{arom}), 132.1 (s, C_{arom}), 131.6 (s, C_{arom}), 130.4 (apparent q, C_{arom}), 129.0 – 128.9 (overlapping resonances), 128.7 (s, CH_{arom}), 128.5 (s, CH_{arom}), 128.3 (s, C_{arom}), 35.3 (s, CMe_3), 34.9 (s, CMe_3), 31.7 (s, CMe_3), 31.4 (d, $J_{\text{C-P}} = 5.0$ Hz, CMe_3), 20.6 (s, CH_3), 20.4 (s, CH_3), 16.9 (s, CH_3), 16.5 (s, CH_3). $^{31}\text{P}\{^1\text{H}\}$ NMR (202.5 MHz, benzene- d_6): δ 160.6 (d, $^3J_{\text{P-P}} = 239.9$ Hz, PPhen), -11.4 (d, $^3J_{\text{P-P}} = 239.9$ Hz, PPh_2).

(S)-(Ph-PhenDalPhos)CoCl₂ (4-1). In a glovebox, CoCl_2 (0.157 g, 1.21 mmol) was weighed into a 4-dram vial equipped with a stir bar. THF (10 mL) was added and the resulting suspension stirred vigorously for 10 minutes until most of the CoCl_2 had dissolved. (S)-(Ph-PhenDalPhos) (0.782 g, 1.21 mmol) was then added as a THF solution (ca. 5 mL) and a color change from blue to dark purple observed. The resulting solution was stirred until all of the CoCl_2 was dissolved upon which the solvent was removed *in*

vacuo. The crude solid was washed with diethyl ether (3 x 10 mL) to afford **4-1** as a light purple solid (0.700 g, 0.895 mmol, 74% yield). ¹H NMR (300 MHz, CD₂Cl₂): δ 12.32, 10.84, 10.12, 9.52, 9.46, 9.34, 9.32, 8.55, 7.40, 7.06, 6.55, 5.36, 5.34, 5.32, 3.59, 3.44, 2.68, 2.56, 2.43, 0.87, 0.53, 0.23, 0.21. $\mu_{\text{eff}} = 3.89 \mu_{\text{B}}$ (S = 3/2). Anal. Calcd for C₄₂H₄₆Cl₂CoO₂P₂: C, 65.12; H, 5.99. Found: C, 61.44; H, 5.86. HRMS (ESI): calculated (M)⁺ [C₄₂H₄₆ClCoO₂P₂]⁺: 738.1988; found: 739.1994.

(S)-(Ph-PhenDalPhos)Co(CH₂TMS)₂ (4-2). Method A: In a glovebox, complex **4-1** (0.101 g, 0.130 mmol) was weighed into a 4-dram vial equipped with a stir bar and subsequently dissolved in 4 mL of THF. The solution was then cooled to -35 °C and LiCH₂TMS (0.050 g, 0.520 mmol) was added dropwise as a THF solution (ca. 2 mL) whereupon an immediate color change from purple to dark red was observed. The resulting solution was allowed to warm to room temperature and the volatile components were then removed *in vacuo*. The crude residue was triturated with pentane (3 x 3 mL), extracted with 12 mL of a 1:1 mixture of pentane: benzene, and filtered through Celite to afford a clear dark red filtrate. The solvent was removed *in vacuo* and the resulting red solid washed with cold (-35 °C) pentane (2x 0.5 mL) to afford **4-2** as a free-flowing red powder (0.072 g, 0.082 mmol, 63% yield). Single crystals suitable for X-ray crystallographic analysis were obtained from a concentrated diethyl ether solution at -35 °C.

Method B: CoCl₂ (0.034 g, 0.264 mmol) was weighed into a 4-dram vial equipped with a stir bar. THF (4 mL) was added, and the resulting suspension stirred vigorously for 10 minutes until most of the CoCl₂ had dissolved. (S)-(Ph-PhenDalPhos) (0.170 g, 0.264 mmol) was then added as a THF solution (ca. 3 mL) and a color change from blue to dark purple observed. The resulting was stirred until all of the CoCl₂ was dissolved upon which

the solution was cooled to -35 °C. LiCH₂TMS (0.050 g, 0.528 mmol) was added dropwise as a THF solution (ca. 2 mL) whereupon an immediate color change from purple to dark red was observed. The resulting solution was allowed to warm to room temperature and the volatile components were then removed *in vacuo*. The crude residue was triturated with pentane (3 x 3 mL), extracted with 12 mL of a 1:1 mixture of pentane: benzene, and filtered through celite to afford a clear dark red filtrate. The solvent was removed *in vacuo* and the resulting red solid washed with cold (-35 °C) pentane (2x 0.5 mL) to afford **4-2** as a free-flowing red powder (0.173 g, 0.198 mmol, 75% yield). ¹H NMR (300 MHz, benzene-*d*₆): δ 33.97, 19.96, 18.26, 17.53, 17.50, 15.37, 9.63, 5.91, 4.25, 4.05, 3.95, 2.77, 2.39, 2.22, 2.10, 2.08, 1.84, 1.70, 1.62, 1.49, 1.40, 1.30, -0.87, -1.08, -1.54, -2.00, -2.73. $\mu_{\text{eff}} = 1.72 \mu_{\text{B}}$ (*S* = ½). Anal Calcd for C₅₀H₆₈CoO₂P₂Si₂: C, 68.39; H, 7.81. Found: C, 65.16; H 7.42.

[(S)-(Ph-PhenDalPhos)Co(C₆H₆)] [BAr^F₄] (4-3). **4-2** (0.213 g, 0.242 mmol) was weighed into a 4-dram vial equipped with a stir bar and dissolved in 6 mL of a 1:1 mixture of diethyl ether: benzene. Ferrocenium tetrakis(3,5-bis(trifluoromethyl)phenyl) borate ([Fc][BAr^F]) was then added dropwise as an ether solution (ca. 2 mL) and the resulting mixture stirred for 30 minutes where a color change from dark red to dark orange was observed. The volatile components were removed *in vacuo*, and the crude mixture triturated with pentane (3 x 3 mL). The resulting oily solid was washed with pentane until all of the ferrocene was removed (as evidenced by the washes becoming colorless) and subsequently extracted with diethyl ether (ca. 12 mL) and filtered through celite to afford a clear orange solution. The solvent was removed *in vacuo* to afford **4-3** as a crystalline orange powder (0.318 g, 0.194 mmol, 80% yield). ¹H NMR (500 MHz, THF-*d*₈): δ 7.78 – 7.50 (overlapping resonances, 30 H), 7.35 (broad s, 1 H, *H*_{arom}), 6.93 (broad m, 1 H, *H*_{arom}), 5.96

(s, 6 H, η^6 -C₆H₆), 2.45 (s, 3 H, CH₃), 2.39 (s, 3 H, CH₃), 2.03 (s, 3 H, CH₃), 1.88 (s, 3 H, CH₃), 1.42 (s, 9 H, C(CH₃)₃), 1.18 (s, 9 H, C(CH₃)₃). ¹³C{¹H} NMR (125.7 MHz, THF-*d*₈): δ 162.5 (q, ¹J_{B-C} = 50.1 Hz, B[3,5-(CF₃)₂C₆H₃]₄), 147.6 (d, J_{C-P} = 14.4 Hz, C_{arom}), 146.1 (s, C_{arom}), 146.0 (s, C_{arom}), 145.5 (d, J_{C-P} = 37.7 Hz), 145.0 (d, J_{C-P} = 35.6, C_{arom}), 139.7 (apparent t, C_{arom}), 138.6 (s, C_{Phen}), 137.2 (s, C_{Phen}), 136.5 (d, J_{C-P} = 26.4 Hz, CH_{arom}), 135.3 (br s, B[3,5-(CF₃)₂C₆H₃]₄), 134.8 (d, J_{C-P} = 34.0 Hz, C_{arom}), 133.4 (d, J_{C-P} = 11.3 Hz, CH_{arom}), 132.9 (br s, C_{arom}), 132.8 (d, J_{C-P} = 11.2 Hz, CH_{arom}), 132.3 (br s, B[3,5-(CF₃)₂C₆H₃]₄), 131.7 (d, J_{C-P} = 19.7 Hz, C_{arom}), 131.2 (s, C_{arom}), 130.2 – 129.3 (overlapping resonances, B[3,5-(CF₃)₂C₆H₃]₄), 125.1 (q, ¹J_{C-F} = 272.5 Hz, B[3,5-(CF₃)₂C₆H₃]₄), 117.9 (s, CH_{arom}), 96.9 (s, η^6 -C₆H₆), 35.9 (s, C(CH₃)₃), 35.3 (s, C(CH₃)₃), 32.3 (s, C(CH₃)₃), 31.6 (s, C(CH₃)₃), 20.2 (s, CH₃), 20.1 (s, CH₃), 16.3 (s, CH₃), 16.2 (s, CH₃). ³¹P{¹H} NMR (202.5 MHz, THF-*d*₈): δ 192.9 (d, ³J_{P-P} = 97.4 Hz, PPhen), 77.8 (d, ³J_{P-P} = 97.4 Hz, PPh₂). ¹⁹F{¹H} NMR (376.5 MHz, THF-*d*₈): δ -63.4 (s, B[3,5-(CF₃)₂C₆H₃]₄). ¹¹B NMR (160.5 MHz, THF-*d*₈): δ -6.5 (s, B[3,5-(CF₃)₂C₆H₃]₄). Anal Calcd for C₈₀H₆₄BCoF₂₄O₂P₂: C, 58.41; H, 3.92. Found: C, 56.49; H, 4.04. HRMS (ESI): calculated (M)⁺ [C₄₈H₅₂CoO₂P₂]⁺: 781.2769; found: 781.2759. Calculated (M)⁻ [C₃₂H₁₂BF₂₄]⁻: 863.0654; found: 863.0643.

General Procedure for the Asymmetric Hydrogenation of *dehydro- α* -amino acids.

The substrate (0.2 mmol) was weighed into a 1-dram vial and 1 mL of a freshly prepared 0.005 M, 0.01 M, or 0.02 M THF stock solution of **4-3** was added via microsyringe (for 2.5 mol%, 5 mol%, and 10 mol% runs respectively). The vial was equipped with a stirbar and closed with a screw cap featuring a PTFE septum. A needle was then inserted through the septum to allow for the introduction of H₂ gas. The vial was subsequently transferred to a Parr reactor which was sealed and pressurized to 10 or 20 atm H₂ pressure. The Parr

reactor was heated to 50 °C in an oil bath for the duration of the reaction time. Afterward, the Parr reactor was removed from the oil bath and depressurized. The volatile components of the crude reaction were removed *in vacuo* and then treated with 0.1 M NaOH solution (2 equiv. NaOH to substrate). The aqueous solution was washed with ethyl acetate (3 × 10 mL), then acidified with 0.1 M HCl solution (3 equiv. HCl), and was subsequently extracted with 3 × 10 mL ethyl acetate. The combined ethyl acetate extracts were dried over MgSO₄, filtered, and the solvent was removed *in vacuo* to afford the hydrogenated product in the specified yield. Enantioselectivity was determined by chiral HPLC analysis on a Chiralpak AD-H column using the specified conditions.

Procedure for the Asymmetric Hydrogenation of (*Z*)-*dehydro-N*-acetyl-(*a*4-acetoxy-3-methoxy) phenylalanine. (*Z*)-*dehydro-N*-acetyl-(*a*4-acetoxy-3-methoxy) phenylalanine (0.293 g, 1.0 mmol) was weighed into a 4-dram vial and 5 mL of a freshly prepared 0.005M THF stock solution of **4-3** added via microsyringe. The vial was equipped with a stirbar and closed with a screw cap featuring a PTFE septum. A needle was then inserted through the septum to allow for the introduction of H₂ gas. The vial was subsequently transferred to a Parr reactor which was sealed and pressurized to 40 atm H₂ pressure. The Parr reactor was heated to 50 °C in an oil bath for the duration of the reaction time. Afterward, the Parr reactor was removed from the oil bath and depressurized. The volatile components of the crude reaction were removed *in vacuo* and then treated with 0.1 M NaOH solution (2 equiv. NaOH to substrate). The aqueous solution was washed with ethyl acetate (3 × 20 mL), then acidified with 0.1 M HCl solution (3 equiv. HCl), and was subsequently extracted with 3 × 20 mL ethyl acetate. The combined ethyl acetate extracts were dried over MgSO₄, filtered, and the solvent was removed *in vacuo* to afford (*R*)-*N*-

acetyl-(4-acetoxy-3-methoxy) phenylalanine as a white solid (**4-1r**, 0.221 g, 75% yield). Enantioselectivity was determined by chiral HPLC analysis on a Chiralpak AD-H column with a 91.5: 7.5: 1.0 Hexane: *i*PrOH: Formic acid mobile phase at a 1.0 mL/min flow rate. $t_{\text{major}} = 28.890$ min, $t_{\text{min}} = 31.222$ min. Enantiomeric ratio = 99:1.

Chapter 5: Synthesis and Characterization of Chiral (Phosphino)Silyl Ligands for Asymmetric Hydrogenation Catalysis

5.1 Introduction

As outlined in Chapters 1 and 4 of this document, asymmetric hydrogenation remains one of the most effective methods for the synthesis of single enantiomer compounds. Work in Chapter 4 details the (*S*)-(Ph-PhenDalPhos)Co-catalyzed asymmetric hydrogenation of *dehydro-α*-amino acids, while work in this chapter seeks to extend the scope of base metal catalyzed asymmetric hydrogenation by targeting new (phosphino)silyl ligation for such application. Asymmetric hydrogenation has wide utility in synthesis, particularly in the pharmaceutical industry, where catalyst development in this regard remains an active area of investigation. Examples of drugs such as Lyrica (pregabalin, Pfizer),¹⁹⁹⁻²⁰⁰ Januvia (sitagliptin, Merck),⁷⁰⁻⁷¹ and Keppra (levetiracetam, UCB)⁶³ all feature asymmetric hydrogenation in key bond forming steps in their syntheses.

Ligand design for the asymmetric hydrogenation of alkenes has largely converged on privileged chiral bis(phosphines), especially within the context of base metal mediated asymmetric hydrogenation. Examples from the Chirik group,^{19-20, 61-64, 67, 70, 77, 194-195, 209} W. Zhang group,^{68, 73} X. Zhang group,^{66, 72} and others,^{196, 210} have relied on repurposing ligands previously employed in platinum group metal mediated asymmetric hydrogenation. (Figure 5.1.1)

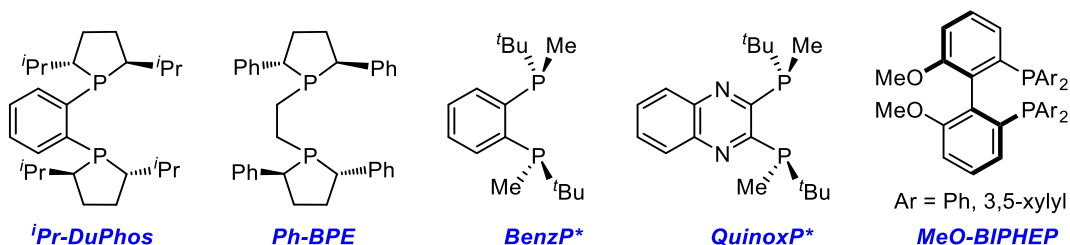


Figure 5.1.1. Selected examples of privileged bis(phosphine) ligands that have been employed in base metal catalyzed asymmetric hydrogenation.

The development of new, readily prepared, chiral ligands that can be employed in base metal mediated asymmetric catalysis is an area of great interest in the Turculet group. In this regard, we sought to develop a new class of chiral ligands that combines the high catalytic activity of our phosphino(silyl)-based pre-catalysts (described in Chapters 2 and 3 of this document) with readily prepared chiral components. Such ligands are anticipated to support catalysis under mild reaction conditions by taking advantage of metal-silyl cooperativity while providing high conversion to enantioenriched products with a broad functional group tolerance.

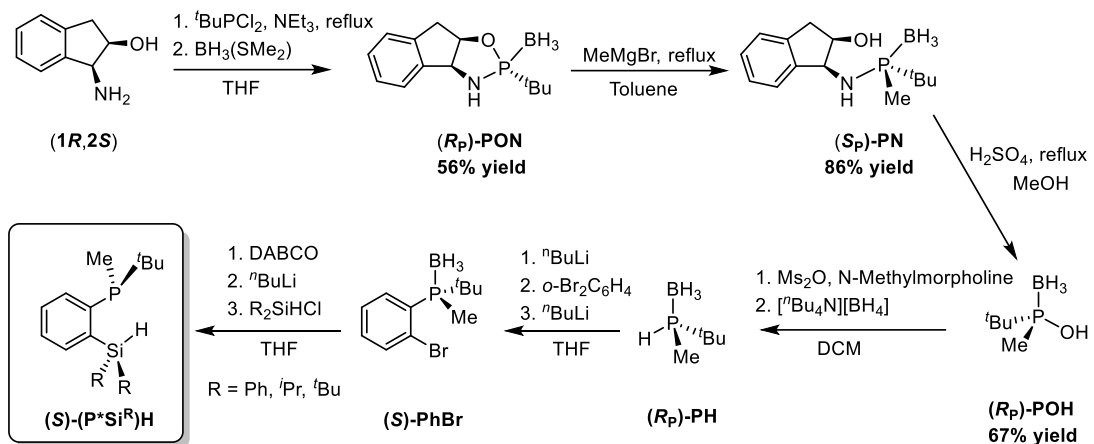
Research in this chapter details synthetic efforts that have been undertaken to develop this new class of chiral ligands. Ligand variants featuring chirality at phosphorus as well as at silicon are presented, as well as corresponding asymmetric hydrogenation catalysis results involving Ni-based pre-catalysts. While most of the pre-catalysts that were prepared afforded racemic hydrogenation products, the Ni complexes featuring the new indolyl-phosphino ligand (*R,R*)-(IndolSi)H (**5-6**) proved capable of supporting the asymmetric hydrogenation of a small scope of functionalized enamides. Prochiral enamides are an important class of substrates as their hydrogenation provides access to chiral amines, a prominent motif in pharmaceutical and fine chemical synthesis.

5.2 Results and Discussion

5.2.1 Synthesis of Chiral P*Si* Ligands

The ligands QuinoxP* and BenzP* served as initial inspiration for the development of a chiral phosphino(silyl) ligand platform.²¹¹ It was envisioned that the installation of enantiopure (*R*)-*tert*-butylmethylphosphine-borane on an *o*-bromophenylene unit would allow access to a modular family of P*Si* ligands *via* subsequent lithiation of the arene and

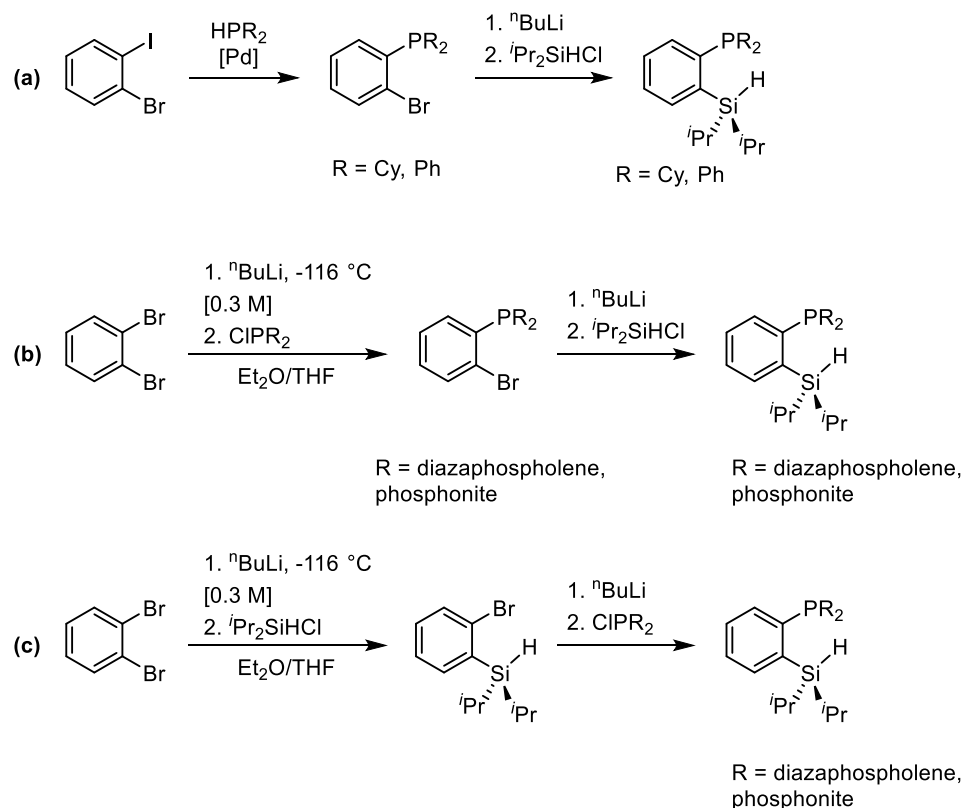
quenching with a chlorosilane (Scheme 5.2.1). Significant efforts by Salomo and co-workers have led to the development of the gram scale synthesis of (*R*)-*tert*-butylmethylphosphine-borane with high enantioselectivity through use of *cis*-1,2-aminoindanol as a chiral auxiliary.²¹²⁻²¹³ However, this reaction sequence was found to not be amenable to reaction scales beyond one gram and was not pursued further.



Scheme 5.2.1. Synthetic route for the preparation of enantiopure secondary phosphine borane (*R*)-(-*t*Bu)(Me)PH(BH₃) and the family of phosphino(silyl) ligands (*S*)-(P*Si^R)H.

For the next attempt to prepare chiral phosphino(silyl) ligands chiral diazaphospholenes and phosphonites were considered as potential phosphorus donors as they could be readily prepared on multi gram scales. The large scale synthesis of chiral diazaphospholenes and their application as catalysts for the asymmetric reduction of imines has been described by Speed and co-workers in recent years.²¹⁴⁻²¹⁵ Moreover, a collaboration between the Speed and Stradiotto groups led to the synthesis of mixed phosphine/diazaphospholene ligands that could support Ni-catalyzed C-N cross coupling catalysis.²¹⁶ The utility of chiral phosphonites in catalytic asymmetric hydrogenation was demonstrated in Chapter 4 of this document.

The synthesis of PSiP or PSi ligands that has been previously employed in the Turculet group involves installation of the phosphine donor through Pd catalyzed C-P cross-coupling to furnish the intermediate (2-bromophenyl)phosphine. Subsequent lithium-halogen exchange and quench with a substituted chlorosilane has been used to afford a variety of bidentate and tridentate phosphino(silyl) ligands (Scheme 5.2.2a).^{36-38, 41} As the phosphorus atom in a diazaphospholene or phosphonite is bound to nitrogen or oxygen, respectively, nucleophilic attack by the butyl anion during lithium-halogen exchange was anticipated as a possible side reaction. This precludes a synthetic route where the diazaphospholene or phosphonite moiety is installed prior to the silyl group (Scheme 5.2.2b). As such, the synthetic route shown in Scheme 5.2.2c was deemed the most likely to succeed and was pursued instead.



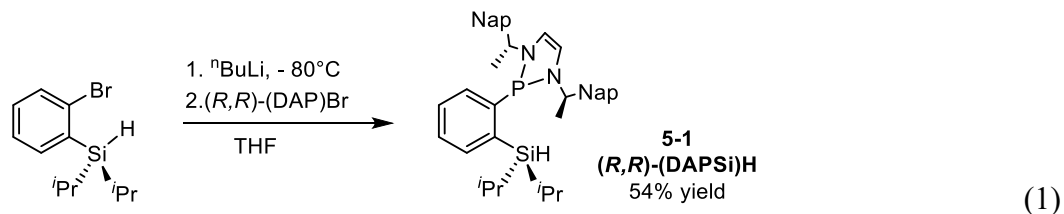
Scheme 5.2.2. (a) Previous synthetic route employed by the Turculet group for the synthesis of bidentate PSi and tridentate PSiP ligands. (b) Synthetic route employing

monolithiation of *o*-dibromobenzene to sequentially install a phosphorus-based donor followed by a silicon donor. (c) Synthetic route employing monolithiation of *o*-dibromobenzene to sequentially install a silicon-based donor followed by a phosphorus-based donor.

Monolithiation of *o*-dibromobenzene was used to install an electrophilic halo(silane).²¹⁷

The intermediate (2-bromophenyl)diisopropyl silane was targeted as the isopropyl substituents would provide reasonable steric bulk and afford an electron rich metal center. Employing the synthesis outlined in Scheme 5.2.2c, (2-bromophenyl)diisopropyl silane was isolated as a colorless oil in 89% yield. Analysis by ¹H NMR spectroscopy revealed the expected triplet resonance corresponding to the Si-*H* at 4.28 ppm with a ¹*J*_{Si-H} coupling constant of 94 Hz. The ²⁹Si chemical shift was determined to be 61.9 ppm.

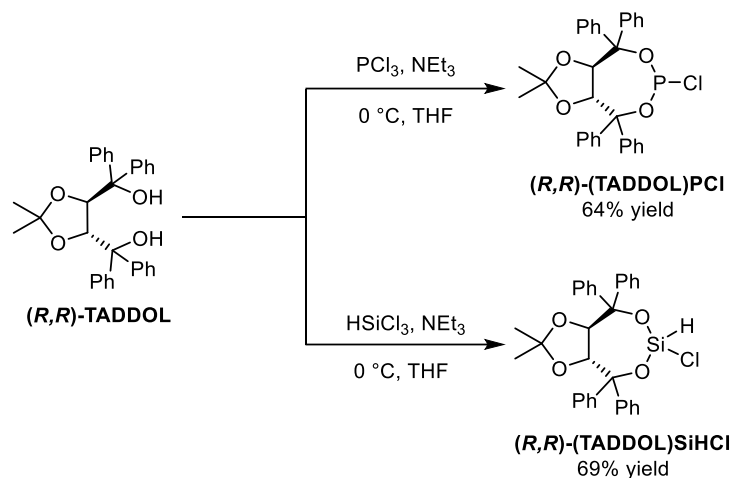
Ortho-lithiation of (2-bromophenyl)diisopropyl silane and subsequent quench with the enantiopure diazaphospholene 2-bromo-1,3-bis{(*R*)1-(naphthalen-1-yl)ethyl}-2,3-dihydro-1*H*-1,3,2-diazaphosphole ((*R,R*)-(DAP)Br) gave rise to the phosphino(silane) **5-1** (eq 1). Silane **5-1** was isolated as a viscous red oil in 54% yield and features a single resonance in the ³¹P{¹H} NMR spectrum at 86.6 ppm. Evaluation of the ¹H NMR spectra found a complex multiplet corresponding to the Si-*H* at 5.16 ppm and a ²⁹Si NMR chemical shift of 48.8 ppm.



Ligands derived from the readily prepared and commercially available TADDOL ($\alpha,\alpha,\alpha',\alpha'$ -tetraaryl-2,2-disubstituted 1,3-dioxolane-4,5-dimethanol) class of chiral auxiliaries were also targeted. TADDOL-derived ligands are attractive as TADDOL

derivatives can be easily prepared in high yield from the ethyl ester of tartaric acid.²¹⁸ In particular, TADDOL-derived phosphoramidites have found applications in asymmetric catalysis such as Rh-mediated asymmetric hydrogenation and Ni-mediated asymmetric cycloisomerization of dienes.^{205, 219-220}

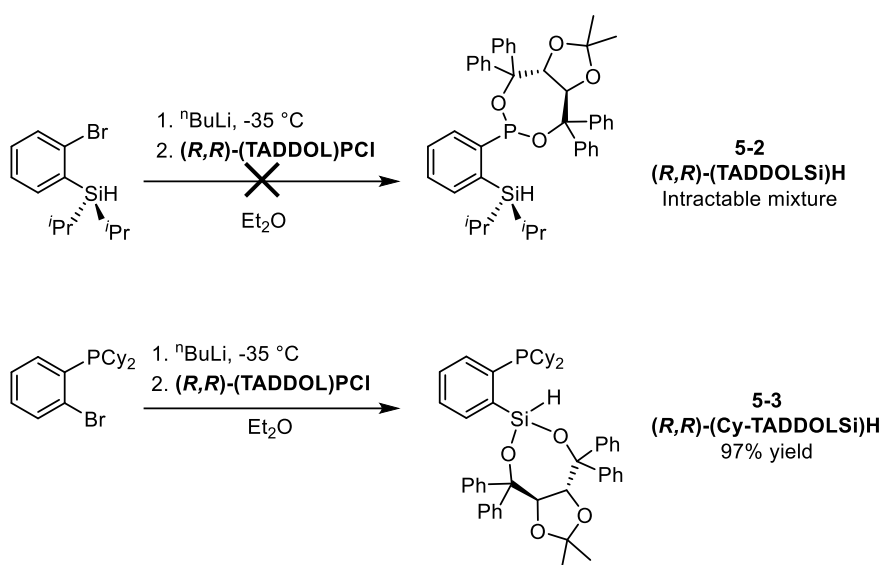
The chlorophosphine (*R,R*)-(TADDOL)PCl was prepared according to literature procedure in 64% yield (Scheme 5.2.3).²⁰⁵ The chiral chlorosilane (*R,R*)-(TADDOL)SiHCl was prepared in an analogous manner, whereby trichlorosilane was added to a cooled solution of (*R,R*)-(TADDOL) and excess triethylamine (Scheme 5.2.3). The ¹H NMR spectrum of (*R,R*)-(TADDOL)SiHCl features a characteristic resonance at 5.40 ppm corresponding to the Si-*H*. The corresponding ²⁹Si NMR resonance was observed at 198.2 ppm.



Scheme 5.2.3. Preparation of (*R,R*)-TADDOL derived precursors to P-Si ligands.

The TADDOL-derived (*R,R*)-(TADDOL)PCl and (*R,R*)-(TADDOL)SiHCl were subsequently utilized in attempts to prepare ligands **5-2** and **5-3** featuring chirality at either phosphorus or silicon, respectively (Scheme 5.2.4). The attempted synthesis of **5-2** led to an intractable mixture of products from which no pure material could be recovered. However, ligand **5-3** was successfully isolated as a white solid in high yield (97%) and is

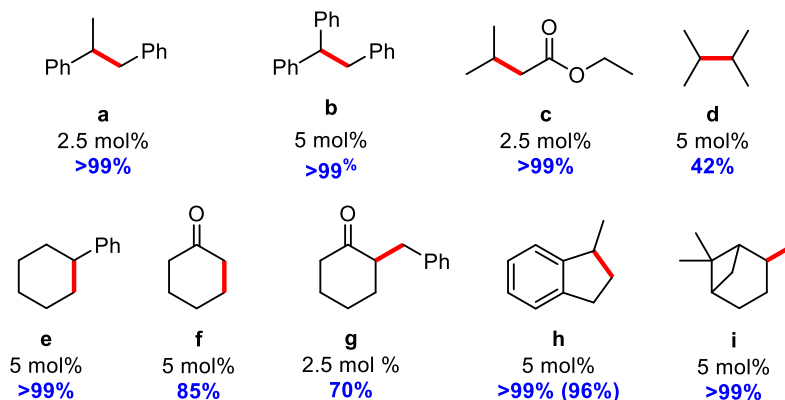
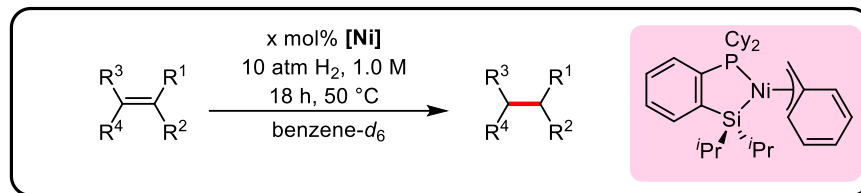
a unique example of a ligand that incorporates chirality at the silicon-derived donor. No other examples of chiral ligands featuring a chiral silyl donor have been reported to date. The scaffold that comprises **5-3** features multiple sites where the steric and electronic properties of the ligand can be tuned in a modular fashion for future iterations of such ligands. The phenylene backbone, the phosphorus substituents, and the aryl substituents of the TADDOL moiety can all be easily modified in this regard, as can the substituents that comprise the acetal moiety.



Scheme 5.2.4. Attempted synthesis of ligand **5-2** and synthesis of ligand **5-3**.

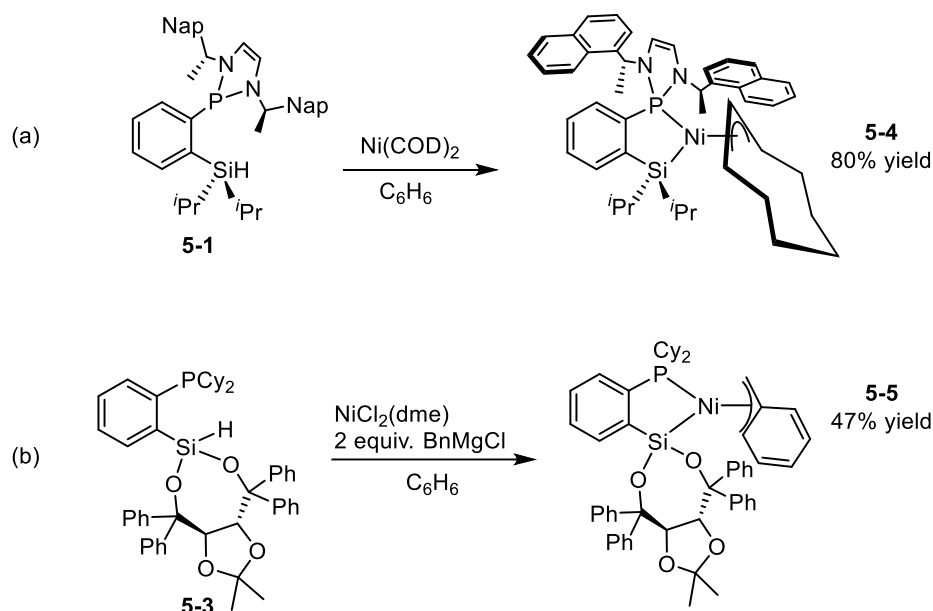
5.2.2 Synthesis of Chiral (PSi)Ni Complexes

Ongoing work by Turculet group member Tyler Saunders has shown that bidentate PSi ligation enables Ni-catalyzed alkene hydrogenation. Readily prepared complexes of the form $(\text{PSi})\text{Ni}(\eta^3\text{-benzyl})$ were shown to hydrogenate sterically hindered tri- and tetra-substituted alkenes under mild conditions (Scheme 5.2.5). Considering these results, related Ni complexes supported by the bidentate ligands described in section 5.2.1 (above) were targeted as pre-catalysts for asymmetric hydrogenation.



Scheme 5.2.5. Substrate scope for achiral (PSi)Ni(η^3 -benzyl) catalyzed hydrogenation of sterically hindered alkenes performed by Tyler Saunders. Reaction conditions: alkene (0.2 mmol), (PSi)Ni(η^3 -benzyl) (specified mol%), 10 atm H₂, benzene-*d*₆ (200 μ L), 50 °C, 18 h. Yield of product determined on the basis of ¹H NMR integration vs. 1,3,5-trimethoxybenzene internal standard (0.2 mmol; average of two runs); a relaxation delay of 60 s was used to ensure accurate integrations. Isolated yields shown in parentheses.

The treatment of **5-1** with one equivalent of Ni(COD)₂ in benzene was found to cleanly afford the corresponding cyclooctenyl complex **5-4** in 80% yield (Scheme 5.2.6a). η^3 -Cyclooctenyl complexes of Ni supported by (Ph-PSiP) ligation were first reported by Hazari and co-workers who found that they could act as a source of the unstable Ni hydride species (Ph-PSiP)NiH.⁴⁵ Complex **5-4** was found to exist as a 1:1 mixture of isomers that likely arise from coordination of the PSi ligand orthogonally to the cyclooctenyl ligand. The ³¹P{¹H} NMR spectrum displayed two singlets at 145.8 and 147.3 ppm corresponding to each isomer, respectively. Further characterization by multinuclear NMR spectroscopy found the expected disappearance of the resonance corresponding to the Si-*H* in **5-1**, and the two isomers of **5-4** gave rise to ²⁹Si NMR resonances at 60.4 and 61.5 ppm.



Scheme 5.2.6. (a) Synthesis of **5-4**, and (b) synthesis of **5-5**.

The coordination chemistry of ligand **5-3** with Ni was investigated next. It was found that reaction of **5-3** with Ni(COD)₂ proceeded slowly, affording only ca. 10% conversion to the corresponding cyclooctenyl complex after 24 h at room temperature. This is likely due to the large steric bulk associated with the TADDOL unit. Instead, η^3 -benzyl complexes akin to those described previously by the Turculet group (*vide supra*) were targeted. Addition of two equiv. of benzyl magnesium chloride to an equimolar suspension **5-3** and NiCl₂(dme) in benzene furnished the expected complex **5-5** in 47% yield (Scheme 5.2.6b).

5.2.3 (PSi)Ni-Mediated Asymmetric Hydrogenation of Enamides

The ability of complexes **5-4** and **5-5** to facilitate asymmetric hydrogenation was initially evaluated by targeting the catalytic hydrogenation of *N*-(3,4-dihydro-1-naphthalenyl)acetamide, a minimally functionalized cyclic enamide. Asymmetric hydrogenation of α -tetralone derived enamides would afford bioactive chiral aminotetralines, which few metal complexes have been capable of producing with high

enantioselectivity.^{211, 221} The first example of a first-row metal capable of performing the asymmetric hydrogenation of this class of substrates with high enantioselectivity was only reported recently by de Vries and co-workers.⁶⁹ This work employed a $\text{CoCl}_2/(\text{S,S})\text{-}(\text{Ph-BPE})$ catalyst system that was capable of achieving enantiomeric ratios as high as 99:1 for α - and β -substituted cyclic enamides, albeit it with forcing conditions (60 atm H_2 , 60 °C, 18-20 h). While enamides are less reactive substrates than α -dehydroamino acid esters, it was anticipated that the high reactivity of bidentate (PSi)Ni species could overcome this limitation and allow for the first example of Ni mediated asymmetric hydrogenation of an α -tetralone-derived enamide.

Unfortunately, while complex **5-4** displayed high activity toward the hydrogenation of *N*-(3,4-dihydro-1-naphthalenyl)acetamide, no enantioselectivity was observed (20 atm H_2 , 5 mol% Ni, 18 h, 50 °C; Table 5.2.1). Pre-catalyst **5-5** was not active at all under these conditions. As noted above, few catalysts are capable of performing the hydrogenation of this class of substrates with high enantioselectivity. Nonetheless, the high activity of **5-4** towards hydrogenation bodes well for further application in asymmetric catalysis.

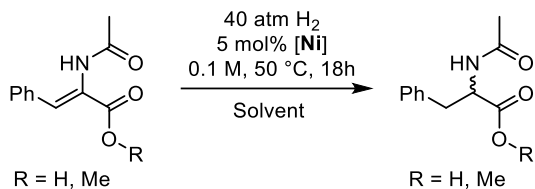
Table 5.2.1. Catalyst screen of chiral PSi-supported Ni complexes for the asymmetric hydrogenation of *N*-(3,4-dihydro-1-naphthalenyl)acetamide.

Entry	Pre-catalyst	Conversion (%) ^[a]	<i>er</i> ^[b]
1	5-4	>99	1:1
2	5-5	<5	n/a

[a] Determined by use of ^1H NMR spectroscopy. [b] Determined by use of chiral HPLC analysis on a chiral stationary phase.

Next, *dehydro-N*-acetyl-phenylalanine and (*Z*)-2-acetamido-3-phenylacrylate were chosen as test substrates, as α -dehydroamino acids and their methyl esters have become standard substrates for the evaluation of a new chiral ligands for asymmetric hydrogenation (Table 5.2.2).²¹¹ Disappointingly, neither complex **5-4** nor **5-5** could perform the hydrogenation of *dehydro-N*-acetyl-phenylalanine (40 atm H₂, 5 mol% Ni, 18 h, 50 °C; Table 5.2.2, entries 1 and 2), and the use of triethylamine as an additive did not promote further conversion (Table 5.2.2, entries 3-7). The addition of triethylamine was prompted by previous reports showing that it promotes carboxylate coordination to the metal center resulting in a metallalactone that can engage in cooperative H₂ cleavage.^{67, 222} When (*Z*)-2-acetamido-3-phenylacrylate was subjected to hydrogenation catalysis instead, full conversion to the hydrogenated product was observed when employing complex **5-4** in *i*PrOH but no enantioselectivity was induced (Table 5.2.2, entry 7). The use of THF as the solvent instead led to markedly decreased conversion (Table 5.2.2, entry 9). Complex **5-5** was found to be capable of supporting only moderate hydrogenation catalysis with (*Z*)-2-acetamido-3-phenylacrylate, with only 13% conversion to the hydrogenated product observed in *i*PrOH and 32% conversion in THF (Table 5.2.2, entries 8 and 10). In both cases the hydrogenation was found to proceed with no enantioselectivity, and consequently no further optimization was pursued with these pre-catalysts.

Table 5.2.2. Asymmetric hydrogenation results for *dehydro-N*-acetyl-phenylalanine and its methyl ester employing **5-4** and **5-5** as pre-catalysts.



Entry	Pre-catalyst	R	Solvent	Conversion (%) ^[a]	<i>er</i> ^[b]
1	5-4	H	^t PrOH	5	n/a
2	5-5	H	^t PrOH	5	n/a
3	5-4 ^[c]	H	^t PrOH	<5	n/a
4	5-5 ^[c]	H	^t PrOH	<5	n/a
5	5-4 ^[c]	H	THF	<5	n/a
6	5-5 ^[c]	H	THF	<5	n/a
7	5-4	Me	^t PrOH	>99	1:1
8	5-5	Me	^t PrOH	13	n/a
9	5-4	Me	THF	27	1:1
10	5-5	Me	THF	32	1:1

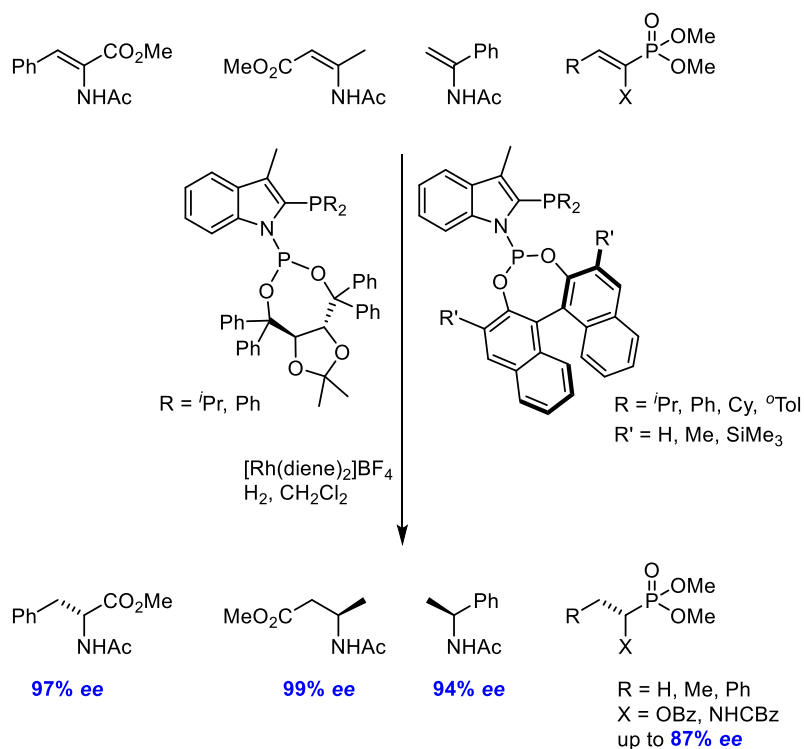
[a] Determined by use of ¹H NMR spectroscopy. [b] Determined by use of chiral HPLC analysis on a chiral stationary phase. [c] One equivalent of NEt₃ as additive.

5.2.4 Alternative Chiral PSi Ligation

The results obtained in section 5.2.3 prompted further investigation into modifications of the PSi ligand architecture to enable enantioselective hydrogenation. The Turculet group has previously employed the 3-methylindole derived diisopropyl(3-methylindolyl)phosphine as a modification to the supporting backbone of the PSiP ligand framework. As shown in Chapter 3 of this document, the resulting indolyl PSiP Ni hydride complex **1-32** can efficiently catalyze the (*E*)-selective semihydrogenation of alkynes under exceptionally mild conditions.

The synthesis of diisopropyl(3-methylindolyl)phosphine was originally developed by Reek and co-workers to establish a new library of mixed donor phosphine/phosphoramidite ligands referred to as IndolPhos (Figure 5.2.1).²²³⁻²²⁵ The IndolPhos family of ligands is

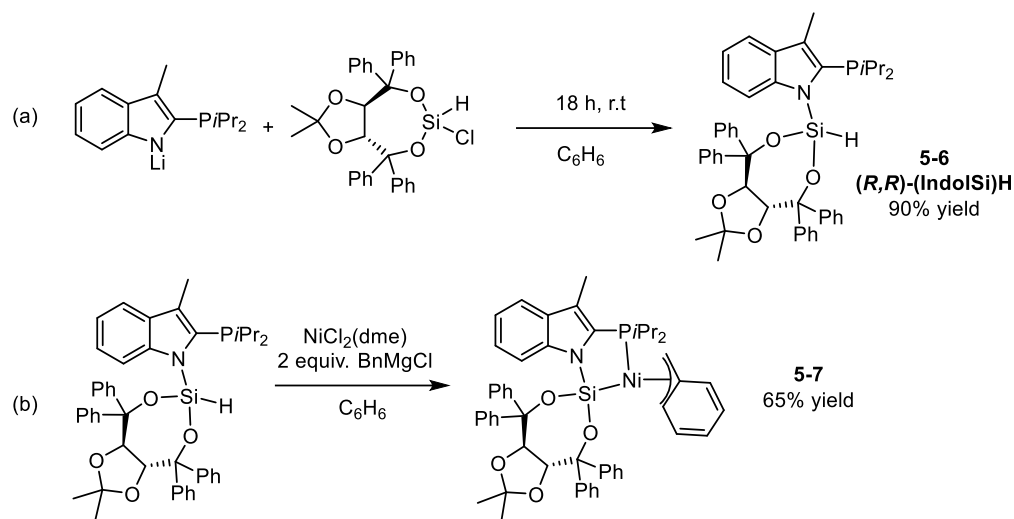
notable, as their synthesis is short and stems from commercially available 3-methylindole. The rigid nature of the 3-methylindole backbone encourages specific substrate coordination through two nonequivalent donor atoms leading to high enantioselectivity. The utility of these ligands in Rh-catalyzed asymmetric hydrogenation was established across a variety of substrates including α - and β -dehydroamino acid esters, α -arylenamides, as well as α -enamido and α -enol phosphonates (Scheme 5.2.7).



Scheme 5.2.7. Rh-catalyzed asymmetric hydrogenation of prochiral olefins supported by chiral IndolPhos mixed phosphine/phosphoramidite ligation, as reported by Reek and co-workers.²²³

As established in section 5.2.1, the chiral chlorosilane (*R,R*)-(TADDOL)SiHCl could be synthesized through condensation of (*R,R*)-(TADDOL) with HSiCl₃ (*vide supra*). Reacting this with one equivalent of the lithium salt of diisopropyl(3-methylindolyl)phosphine in benzene cleanly afforded the phosphino(silyl) pro-ligand **5-6** in 90% yield (Scheme 5.2.8a). Despite repeated attempts single crystals of **5-6** suitable for

X-ray crystallographic analysis could not be obtained. Compound **5-6** displays broad ^1H and $^{31}\text{P}\{^1\text{H}\}$ NMR features at room temperature, likely due to hindered rotation about the Si-N bond. Increasing the temperature to 80 °C allowed for resolution of these resonances (Figures 5.2.1 and 5.2.2).



Scheme 5.2.8. (a) Synthesis of **5-6**, and (b) synthesis of the corresponding Ni benzyl complex **5-7**.

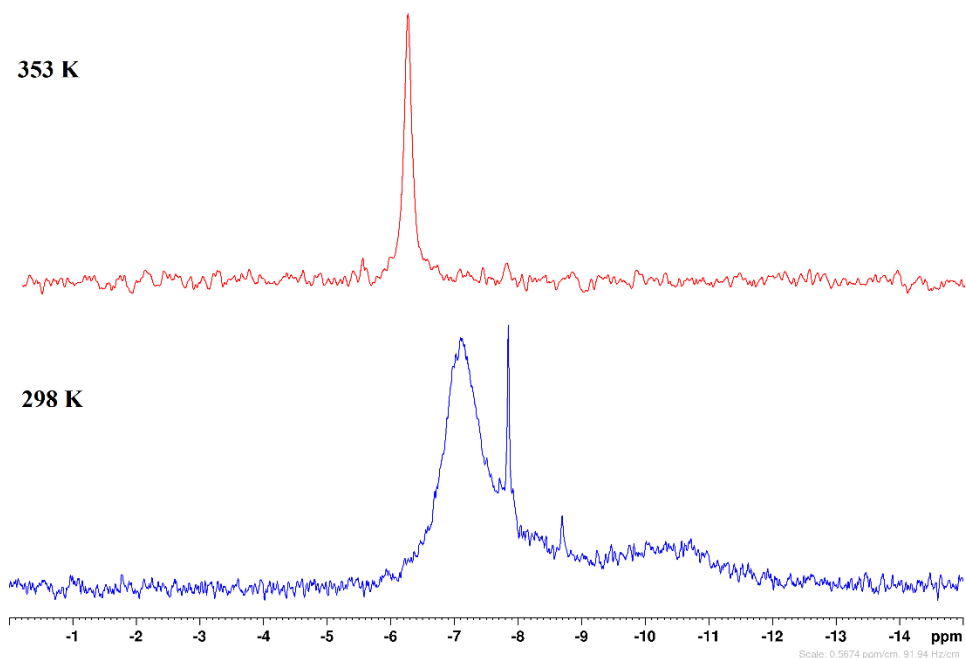


Figure 5.2.1. Overlay of $^{31}\text{P}\{^1\text{H}\}$ NMR (121.5 MHz) spectra for **5-6** at 298 K and 353 K.

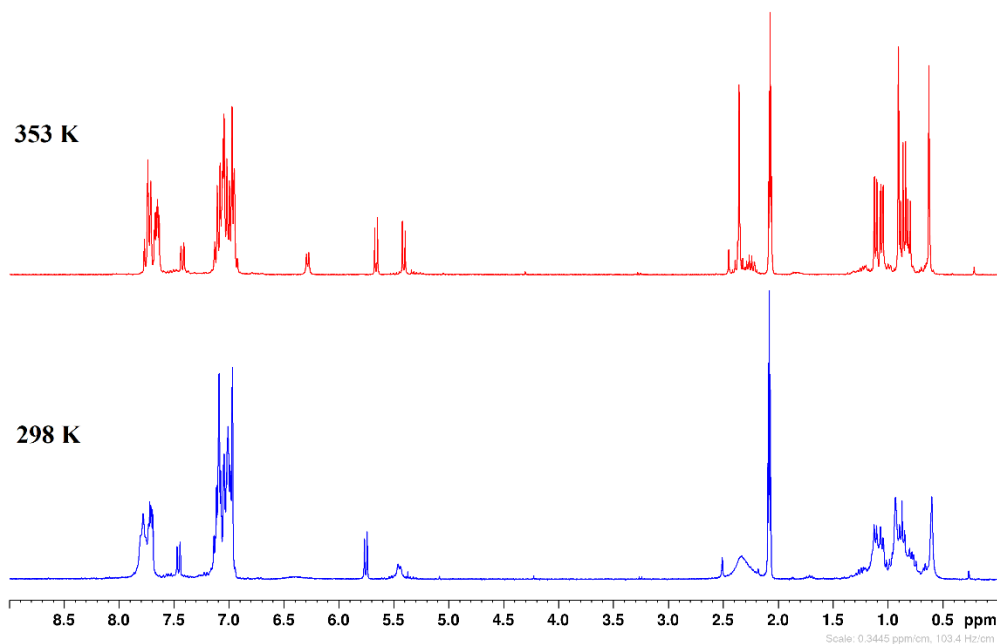
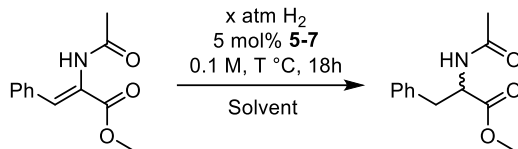


Figure 5.2.2. Overlay of ^1H NMR (300 MHz) spectra for **5-6** at 298 K and 353 K.

Next, a Ni benzyl complex (**5-7**) was synthesized employing the same procedure outlined for complex **5-5** (Scheme 5.2.8). Complex **5-7** was isolated in 65% yield as an orange solid. Employing 5 mol% **5-7** as a pre-catalyst for the asymmetric hydrogenation of (*Z*)-2-acetamido-3-phenylacrylate it was found that under 40 atm H_2 , 50 $^\circ\text{C}$, 18 h in $i\text{PrOH}$ full conversion to product was obtained with an *er* value of 94:6 (Table 5.2.3, entry 2). Evaluating other solvents (THF, MeOH, and THF) led to decreased conversion and enantioselectivity, identifying $i\text{PrOH}$ as the optimal solvent for this substrate. Decreasing the pressure to 20 atm resulted in a small decrease in enantioselectivity (Table 5.2.3, entry 5), while decreasing the temperature resulted in a marked decrease in conversion, albeit with similar enantioselectivity (Table 5.2.3, entry 6). When the pressure was increased to 60 atm H_2 full conversion was observed but with decreased enantioselectivity (Table 5.2.3, entry 7), identifying 40 atm H_2 as the optimal pressure.

Table 5.2.3. Asymmetric hydrogenation results for (*Z*)-2-acetamido-3-phenylacrylate catalyzed by **5-7**.



Entry	H ₂ (atm)	T (°C)	Solvent	Conversion (%) ^[a]	<i>er</i> ^[b]
1	20	50	THF	20	58:42
2	40	50	^t PrOH	>99	94:6
3	40	50	MeOH	<5	n/a
4	40	50	DCM	14	n/a
5	20	50	^t PrOH	>99	92:8
6	40	25	^t PrOH	42	93:7
7	60	50	^t PrOH	>99	91:9

[a] Determined by use of ¹H NMR spectroscopy. [b] Determined by use of chiral HPLC analysis on a chiral stationary phase.

Encouraged by these results, the asymmetric hydrogenation of *N*-(3,4-dihydro-1-naphthalenyl)acetamide was evaluated with **5-7** (Table 5.2.4). Across all conditions that were screened, the highest enantiomeric ratio achieved was 60:40 (40 atm H₂, 5 mol% Ni, 25 °C, 18 h; Table 5.2.4, entry 5). A recent report by de Vries and co-workers detailing the Co-catalyzed asymmetric hydrogenation of carbocyclic enamides found that the identity of the substituents on the amide protecting group can influence enantioselectivity.⁶⁹ Due to the large steric bulk of the TADDOL moiety in ligand **5-6**, it was hypothesized that introducing larger substituents on the amide may lead to improved enantioselectivity.

Table 5.2.4. Results for the asymmetric hydrogenation of *N*-(3,4-dihydro-1-naphthalenyl)acetamide catalyzed by **5-7**.

Entry	H ₂ (atm)	T (°C)	Solvent	Conversion (%) ^[a]	<i>er</i> ^[b]
1	20	50	THF	<5	n/a
2	20	50	MeOH	63	55:45
3	40	25	MeOH	22	56:44
4	20	50	<i>i</i> PrOH	57	57:43
5	40	25	<i>i</i> PrOH	46	60:40
6	60	50	MeOH	74	55:45
7	60	50	<i>i</i> PrOH	56	54:46

[a] Determined by use of ¹H NMR spectroscopy. [b] Determined by use of chiral HPLC analysis on a chiral stationary phase.

In an effort to improve the enantioselectivity observed in the hydrogenation of cyclic enamides, *N*-(3,4-dihydro-1-naphthalenyl)-*tert*-butylamide was synthesized and subjected to asymmetric hydrogenation (Table 5.2.5). At this point it was found that an exceptionally catalytically active species could be generated *in-situ* by simply combining catalytic amounts of Ni(COD)₂ and **5-6**. While the exact identity of the active species has remained elusive, this method is useful as it allows for rapid screening of ligand variants and substrates while obviating the synthesis of pre-catalysts that are often difficult to purify. While it is known that Ni(COD)₂ can catalyze alkene hydrogenation through decomposition to nanoparticles,¹⁸³ the observation of enantioselectivity suggests a homogeneous mechanism wherein **5-6** is ligated to a molecular species.

Table 5.2.5. Results for the asymmetric hydrogenation of *N*-(3,4-dihydro-1-naphthalenyl)-*tert*-butylamide catalyzed by **5-7** or a combination of Ni(COD)₂ and **5-6**.

Entry	Pre-catalyst	H ₂ (atm)	T (°C)	Solvent	Conversion (%) ^[a]	<i>er</i> ^[b]
1	5-7	60	60	MeOH	33	55:45
2	5-7	60	60	<i>i</i> PrOH	55	53:47
3	Ni(COD) ₂ / 5-6 ^[c]	60	60	MeOH	90	60:40
4	Ni(COD) ₂ / 5-6 ^[d]	60	60	MeOH	>99	83:17
5	Ni(COD) ₂ / 5-6 ^[e]	60	60	MeOH	>99	80:20
6	Ni(COD) ₂ / 5-6 ^[d]	60	40	MeOH	>99	97:3

[a] Determined by use of ¹H NMR spectroscopy. [b] Determined by use of chiral HPLC analysis on a chiral stationary phase. [c] 5 mol% Ni(COD)₂, 5 mol% **5-6**. [d] 5 mol% Ni(COD)₂, 7.5 mol% **5-6**. [e] 5 mol% Ni(COD)₂, 10 mol% **5-6**.

The combination of 5 mol% Ni(COD)₂ and 7.5 mol% **5-6** was determined to be optimal for the hydrogenation of *N*-(3,4-dihydro-1-naphthalenyl)-*tert*-butylamide, providing quantitative conversion and an *er* of 97:3 (60 atm H₂, 18 h, 40 °C; Table 5.2.5, entry 6). To further understand the potential identity of the active species a stoichiometric reaction between **5-6** and Ni(COD)₂ was performed in THF. It was observed that after 18 h at room temperature complete conversion to a 1:1 mixture of isomers occurred (determined by use of ³¹P{¹H} NMR spectroscopy, Figure 5.2.3). Heating this mixture to 65 °C for three hours led to conversion to a major product, albeit with some decomposition, as evidenced by the precipitation of Ni metal.

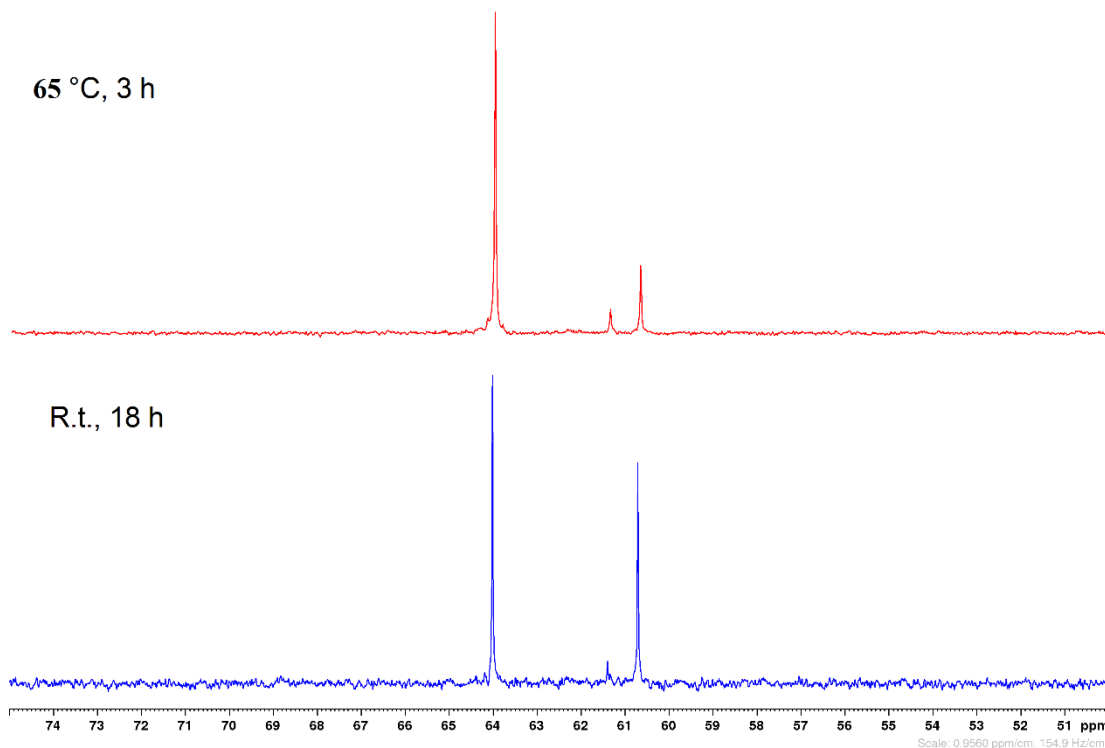
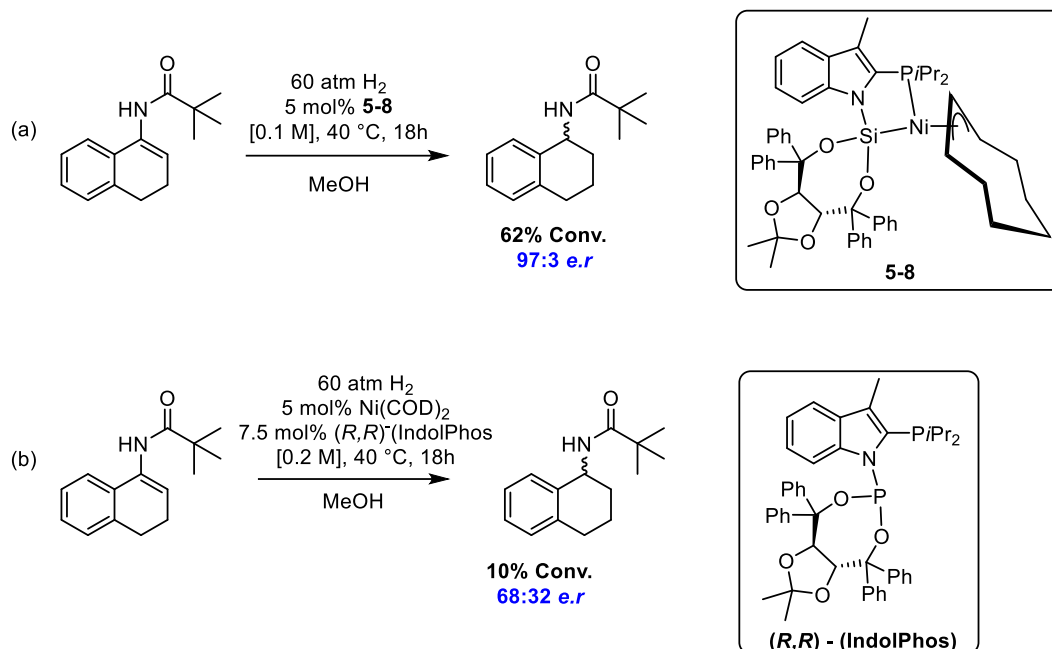


Figure 5.2.3. Overlay of $^{31}\text{P}\{^1\text{H}\}$ NMR (121.5 MHz) spectra for the reaction of **5-6** with $\text{Ni}(\text{COD})_2$ in THF (spectra acquired in benzene- d_6).

Attempts to purify this reaction mixture were unsuccessful, as all three products were found to have the same solubility properties. Attempts at recrystallization led to precipitation of material that was found to have the same product distribution. Regardless, this presumed mixture of cyclooctenyl isomers (tentatively formulated as complex **5-8**) was evaluated as a pre-catalyst for the asymmetric hydrogenation of *N*-(3,4-dihydro-1-naphthalenyl)-*tert*-butylamide. Complex **5-8** was found to provide slightly reduced conversion when compared to the *in-situ* generated catalyst (62% vs. >99%) but with the same enantioselectivity (97:3, Scheme 5.2.9a). The decreased conversion could be a result of incomplete catalyst activation due to low solubility in MeOH or due to minor impurities that form due to heating the reaction mixture in the absence of substrate.



Scheme 5.2.9. (a) Asymmetric hydrogenation of *N*-(3,4-dihydro-1-naphthalenyl)-*tert*-butylamide catalyzed by the presumed cyclooctenyl complex **5-8**. (b) *In-situ* generated catalyst employing (*R,R*)-(IndolPhos) in place of **5-6**.

Next, the function of the chiral silyl donor was probed, as outlined in Scheme 5.2.9b. The phosphine/phosphoramidite analog to **5-6**, (*R,R*)-(IndolPhos), was synthesized according to literature procedure²²³ and was employed under the optimized conditions for the hydrogenation of *N*-(3,4-dihydro-1-naphthalenyl)-*tert*-butylamide. It was found that the use of (*R,R*)-(IndolPhos) led to only 10% conversion and provided an *er* of 68:32. This result demonstrates that the silyl donor enables significantly improved reactivity when compared to the phosphorus analog, and also successfully facilitates enantioselectivity.

5.3 Summary and Conclusions

In summary, work in this chapter details the development of chiral phosphino(silyl) ligands for base-metal catalyzed asymmetric hydrogenation. Several bidentate ligand motifs incorporating a phenylene backbone were investigated such as variants featuring a diazaphospholene donor, a chiral phosphonite, and chiral siloxane, which led to the

synthesis of Ni complexes **5-4** and **5-5**. While these complexes were found to be active pre-catalysts for the hydrogenation of (*Z*)-2-acetamido-3-phenylacrylate and *N*-(3,4-dihydro-1-naphthalenyl)acetamide, they failed to induce enantioselectivity under any of the conditions that were screened. Reacting diisopropyl(3-methylindolyl)phosphine with the chiral siloxane (*R,R*)-(TADDOL)SiHCl gave rise to a rigid phosphino(silyl) pro-ligand (*R,R*)-(IndolSi)H (**5-6**). A (*R,R*)-(IndolSi)Ni(benzyl) complex (**5-7**) was found to provide high enantioselectivity (*er* = 94:6, >99% conversion) for the asymmetric hydrogenation of (*Z*)-2-acetamido-3-phenylacrylate. Generation of the active catalyst *in situ* from **5-6** and Ni(COD)₂ led to the highly selective hydrogenation of *N*-(3,4-dihydro-1-naphthalenyl)-*tert*-butylamide (*er* = 97:3, >99% conversion). While preliminary efforts to isolate the complex generated from treatment of Ni(COD)₂ with **5-6** were somewhat inconclusive, the product of this reaction is tentatively assigned as a mixture of isomers of the type (*R,R*)-(IndolSi)Ni(cyclooctenyl) (**5-8**). This isolated species was a viable pre-catalyst for the asymmetric hydrogenation of *N*-(3,4-dihydro-1-naphthalenyl)-*tert*-butylamide with similarly high selectivity (*er* = 97:3), albeit with lower conversion (62%). The (*R,R*)-(IndolSi)Ni catalyst was shown to outperform the P,P-phosphoramidite analog of this ligand, establishing PSi ligation with chirality at Si as a novel means to provide enantioselectivity and high catalytic turnover for base-metals complexes. Future work will focus on elaborating the scope of α -dehydroamino acids and cyclic enamides that can undergo (*R,R*)-(IndolSi)Ni-catalyzed asymmetric hydrogenation in order to establish the synthetic utility of this new catalyst system.

5.4 Experimental

5.4.1 General Considerations

All experiments were conducted under nitrogen in a glovebox or using standard Schlenk techniques. Tetrahydrofuran and diethyl ether were distilled from Na/benzophenone ketyl. Benzene, toluene, and pentane were first sparged with nitrogen and subsequently dried by passage through a double-column (one activated alumina column and one column packed with activated Q-5). All purified solvents were stored over 4 Å molecular sieves. Benzene-*d*₆ was degassed via three freeze-pump-thaw cycles and stored over 4 Å molecular sieves. All diazaphospholenes were prepared by Dr. Alex Speed using literature procedures.²¹⁴⁻²¹⁶ The chlorophosphine (*R,R*)-(TADDOL)PCl was prepared according to literature procedure.²¹⁹ (2-bromophenyl)dicyclohexylphosphine was prepared according to literature procedure.^{36, 38} *N*-(3,4-dihydro-1-naphthalenyl)acetamide was prepared through reduction of the corresponding oxime by iron in the presence of acetic anhydride.²²⁶ *N*-(3,4-dihydro-1-naphthalenyl)-*tert*-butylamide was prepared by TiCl₄ mediated condensation between α -tetralone and pivalamide.²²⁷ All other reagents were purchased from commercial suppliers and used without further purification. Unless otherwise stated, ¹H, ¹³C, ¹¹B, ³¹P, and ²⁹Si NMR characterization data were collected at 300K, with chemical shifts reported in parts per million downfield of SiMe₄ (for ¹H, ¹³C, and ²⁹Si), BF₃·OEt₂ (for ¹¹B), or 85% H₃PO₄ in D₂O (for ³¹P). ¹H and ¹³C NMR chemical shift assignments are based on data obtained from ¹³C{¹H}, ¹³C-DEPTQ, ¹H-¹H COSY, ¹H-¹³C HSQC, and ¹H-¹³C HMBC NMR experiments. ²⁹Si NMR assignments are based on ¹H-²⁹Si HMBC and ¹H-²⁹Si HMQC experiments.

5.4.2 Synthetic Procedures and Characterization Data

Synthesis of (2-bromophenyl)diisopropylsilane. **Note:** decomposition to benzyne is a possible side reaction and care must be taken to ensure the temperature is kept below -100 °C. Observation of a dark red color change during addition of either ⁿBuLi or the electrophile component is indicative of decomposition of the intermediate (2-bromophenyl)lithium. **Procedure:** A three-neck round bottom flask equipped with a pressure equalizing dropping funnel and a stir bar was charged with 3.02 mL of *o*-dibromobenzene (25.0 mmol) and a 1:1 mixture of diethyl ether and THF (83 mL total volume, 0.3 M). The mixture was placed in an ethanol bath and cooled to -116 °C (ethanol/liquid N₂ bath) whereupon ⁿBuLi (2.5 M, 10.0 mL, 25.0 mmol) was added dropwise over 15 minutes. The temperature was maintained at -116 °C and a white precipitate ((2-bromophenyl)lithium) was observed after 45 minutes (note that the time it takes for (2-bromophenyl)lithium to precipitate is variable and depends upon the rate of ⁿBuLi addition and overall temperature control). The precipitate was allowed to stir for an additional 5 minutes to ensure complete reaction, after which chlorodiisopropylsilane (4.27 mL, 25.0 mmol) was added dropwise over 15 minutes. The temperature was maintained at -116 °C for 1 hour after which the reaction was allowed to warm to room temperature. Hexanes (75 mL) and water (100 mL) were added and the crude reaction mixture was transferred to a separatory funnel under air. The organic phase was collected, and the solvent was removed under reduced pressure. The resulting crude material was redissolved in hexanes (100 mL) and filtered through a pad of silica to afford a colorless filtrate. The solvent was once again removed under reduced pressure to afford (2-bromophenyl)diisopropyl silane as a colorless oil (5.02 g, 18.5 mmol, 74% yield). ¹H NMR

(300 MHz, benzene- d_6): δ 7.37 – 7.34 (m, 2 H, overlapping resonances), 6.91 (m, 1 H, H_{arom}), 6.76 (m, 1 H, H_{arom}), 4.28 (t, 1 H, $^3J_{\text{H-H}} = 4.2$ Hz, Si – H), 1.40 (m, 2 H, CH(CH $_3$) $_2$), 1.12 (d, 6 H, $^3J_{\text{H-H}} = 7.4$ Hz, CH(CH $_3$) $_2$), 0.89 (d, 6 H, $^3J_{\text{H-H}} = 7.4$ Hz, CH(CH $_3$)). $^{13}\text{C}\{^1\text{H}\}$ NMR (75.5 MHz, benzene- d_6): δ 138.8 (s, CH $_{\text{arom}}$), 138.0 (s, C $_{\text{arom}}$), 132.9 (s, CH $_{\text{arom}}$), 131.2 (s, CH $_{\text{arom}}$), 130.9 (s, C $_{\text{arom}}$), 126.5 (s, CH $_{\text{arom}}$), 19.4 (s, CH(CH $_3$) $_2$), 19.3 (s, CH(CH $_3$) $_2$), 11.6 (s, CH(CH $_3$) $_2$). ^{29}Si NMR (59.6 MHz, benzene- d_6): δ 61.8.

Synthesis of 5-1 (*R,R*)-(DAPSi)H. A Schlenk flask equipped with a stir bar was charged with (2-bromophenyl)silane (0.616 g, 2.27 mmol) and 25 mL THF. The flask was cooled to -80 °C and $^n\text{BuLi}$ (0.908 mL, 2.27 mmol) was added dropwise. The resulting yellow solution was allowed to stir for 10 minutes at -80 °C and cannula transferred dropwise to a second Schlenk flask containing 2-bromo-1,3-bis{(*R*)-1-(naphthalen-1-yl)ethyl}-2,3-dihydro-1*H*-1,3,2-diazaphospholene (1.08 g, 2.27 mmol) in THF (30 mL) that had been pre-cooled to -80 °C. The temperature was maintained at -80 °C for an additional hour and then allowed to warm to room temperature, which afforded a clear red solution. The volatile components of the reaction mixture were removed *in vacuo* and the crude material was subsequently extracted with 50 mL pentane and filtered through a pad of silica under a N $_2$ atmosphere. The pentane filtrate (which contained an unidentified silane by-product) was discarded. Diethyl ether (ca. 50 mL) was then used to elute the ligand from the silica pad, affording a clear, red filtrate. The solvent was removed *in vacuo* to afford **5-1** as an orange oil (0.718 g, 1.22 mmol, 54% yield). ^1H NMR (500 MHz, benzene- d_6): δ 8.50 (m, 1 H, H_{arom}), 8.14 (m, 1 H, H_{arom}), 7.88 (m, 1 H, H_{arom}), 7.67 (m, 1 H, H_{arom}), 7.59 (m, 1 H, H_{arom}), 7.52 – 7.47 (overlapping resonances, 4 H), 7.42 (m, 1 H, H_{arom}), 7.29 – 7.26 (overlapping resonances, 2 H) 7.22 – 7.10 (overlapping resonances, 5

H), 7.06 (m, 1 H, H_{arom}), 5.64 (m, 1 H, CH), 5.48 (m, 1 H, CH), 5.36 (m, 1 H, CH), 5.24 (m, 1 H, CH), 5.16 (m, Si – H), 1.57 (d, 3 H, ${}^3J_{\text{H-H}} = 6.9$ Hz, CH_3), 1.46 (d, 3 H, ${}^3J_{\text{H-H}} = 6.9$ Hz, CH_3), 1.38 (m, 2 H, $\text{CH}(\text{CH}_3)_2$), 1.18 – 1.14 (overlapping resonances, 6 H), 1.09 (d, ${}^3J_{\text{H-H}} = 7.4$ Hz, $\text{CH}(\text{CH}_3)_2$), 1.01 (d, ${}^3J_{\text{H-H}} = 7.40$ Hz, $\text{CH}(\text{CH}_3)_2$). ${}^{13}\text{C}\{^1\text{H}\}$ NMR (125.7 MHz, benzene- d_6): δ 152.5 (d, $J_{\text{C-P}} = 36.4$ Hz, C_{arom}), 140.2 (d, $J_{\text{C-P}} = 4.0$ Hz, C_{arom}), 139.5 (d, $J_{\text{C-P}} = 4.6$ Hz, C_{arom}), 136.9 (s, C_{arom}), 136.4 (s, C_{arom}), 135.6 (d, $J_{\text{C-P}} = 12$ Hz, CH_{arom}), 134.5 (d, $J_{\text{C-P}} = 12.0$ Hz, C_{arom}), 133.9 (s, C_{arom}), 132.1 (s, C_{arom}), 131.8 (s, C_{arom}), 131.1 (s, CH_{arom}), 130.4 (s, CH_{arom}), 129.3 (s, CH_{arom}), 129.1 (s, CH_{arom}), 128.9 (s, CH_{arom}), 128.9 (s, CH_{arom}), 128.4 (s, CH_{arom}), 128.2 (s, CH_{arom}), 127.9 (s, CH_{arom}), 127.5 (s, CH_{arom}), 126.0 (s, CH_{arom}), 125.9 (s, CH_{arom}), 125.5 (s, CH_{arom}), 125.5 (s, CH_{arom}), 124.6 (s, CH_{arom}), 124.5 (s, CH_{arom}), 124.3 (s, CH_{arom}), 124.2 (s, CH_{arom}), 124.1 (s, CH_{arom}), 121.4 (s, CH_{arom}), 118.4 (d, $J_{\text{C-P}} = 5.8$ Hz, $\text{HC}=\text{CH}$), 117.5 (d, $J_{\text{C-P}} = 6.3$ Hz, $\text{CH}=\text{CH}$), 54.9 (d, $J_{\text{C-P}} = 25.6$ Hz, CH), 54.0 (d, $J_{\text{C-P}} = 25.0$ Hz, CH), 21.5 (d, $J_{\text{C-P}} = 7.8$ Hz, CH_3), 21.1 Hz (d, $J_{\text{C-P}} = 9.6$ Hz, CH_3), 19.7 (s, CH_3), 19.4 (s, CH_3), 19.3 (s, CH_3), 18.3 (s, CH_3), 12.2 (d, $J_{\text{C-P}} = 4.0$ Hz, $\text{CH}(\text{CH}_3)_2$), 12.1 (d, $J_{\text{C-P}} = 4.3$ Hz, $\text{CH}(\text{CH}_3)_2$). ${}^{31}\text{P}\{^1\text{H}\}$ NMR (202.5 MHz, benzene- d_6): δ 86.6. ${}^{29}\text{Si}$ NMR (99.4 MHz, benzene- d_6): δ 48.3. HRMS (ESI): calculated (M) $^+$ [$\text{C}_{38}\text{H}_{44}\text{N}_2\text{PSi}$] $^+$: 587.3006; found: 587.2996.

Synthesis of (R,R)-(TADDOL)SiHCl. A Schlenk flask equipped with a stir bar was charged with (4*R*,5*R*)-2,2-dimethyl- α - α' - α' -tetraphenyldioxolane-4-5-dimethanol ((*R,R*)-(TADDOL)) (6.00 g, 12.9 mmol) and 100 mL THF. The flask was cooled in an ice bath and triethylamine (5.4 mL, 38.7 mmol) was added followed by dropwise addition of trichlorosilane (2.6 mL, 25.7 mmol). The reaction mixture was allowed to warm to room temperature and stirred for 2 hours. The volatile components of the reaction mixture were

removed *in vacuo* and the crude residue was extracted with *ca.* 100 mL diethyl ether and filtered through a pad of Celite. The filtrate was collected and the solvent was removed under reduced pressure. The remaining residue was washed with 2 × 3 mL pentane and 3 × 3 mL diethyl ether to afford the chlorosilane as an air and moisture sensitive white solid (4.7 g, 8.88 mmol, 69 % yield). ¹H NMR (400 MHz, benzene-*d*₆): δ 7.79 – 7.77 (m, 4 H, *H*_{arom}), 7.65 – 7.63 (m, 2 H, *H*_{arom}), 7.42 – 7.40 (m, 2 H, *H*_{arom}), 7.17 – 6.98 (overlapping resonances, 12 H, *H*_{arom}), 5.60 (d, ³*J*_{H-H} = 7.2 Hz, *CH*), 5.41 – 5.40 (overlapping resonances, 2 H, *CH*, *Si-H*), 0.63 (s, 6 H, *CH*₃). ¹³C {¹H} NMR (101 MHz, benzene-*d*₆): 146.9 (s, *C*_{arom}), 146.0 (s, *C*_{arom}), 141.7 (s, *C*_{arom}), 141.7 (*C*_{arom}), 129.6 (s, *CH*_{arom}), 129.4 (s, *CH*_{arom}), 128.7 (s, *CH*_{arom}), 128.5 (s, *CH*_{arom}), 128.2 (s, *CH*_{arom}), 128.2 (s, *CH*_{arom}), 127.7 (s, *CH*_{arom}), 127.6 (s, *CH*_{arom}), 127.5 (s, *CH*_{arom}), 127.5 (s, *CH*_{arom}), 127.4 (s, *CH*_{arom}), 127.3 (s, *CH*_{arom}), 114.8 (s, *C*(O₂Me₂), 85.8 (s, *C*(OSiH)Ph₂), 84.9 (s, *C*(OSiH)Ph₂), 82.3 (s, *CH*), 81.6 (s, *CH*), 27.4 (s, *CH*₃), 27.2 (s, *CH*₃). ²⁹Si NMR (79.5 MHz, benzene-*d*₆): δ 198.9.

Synthesis of 5-3 (*R,R*)-(TADDOLSi)H. A 4-dram vial containing a stir bar was charged with (2-bromophenyl)dichlohexylphosphine (0.07 g, 0.189 mmol) in *ca.* 4 mL diethyl ether. A second 4-dram vial containing a stir bar was charged with (*R,R*)-(TADDOL)SiHCl (0.100 g, 0.189 mmol) in *ca.* 2 mL diethyl ether. Both vials were cooled to -35 °C. ⁿBuLi (0.118 mL, 0.189 mmol) was then added dropwise to the solution containing (2-bromophenyl)dicyclohexylphosphine and the reaction mixture was magnetically stirred for 10 minutes at room temperature resulting in the formation of a precipitate. The suspension was then cooled to -35 °C and added dropwise to the vial containing (*R,R*)-(TADDOL)SiHCl. The reaction mixture was allowed to warm to room temperature. After 1 h, the reaction mixture was filtered through Celite and the filtrate was

collected. The volatile components of the reaction mixture were removed under reduced pressure. The resulting oily solid was triturated with 3×2 mL pentane resulting in a white solid that was used without further purification (0.140 g, 0.182 mmol, 96% yield). ^1H NMR (500 MHz, benzene- d_6): 8.09 – 8.07 (m, 4 H, H_{arom}), 8.01 – 8.00 (m, 1 H, H_{arom}), 7.86 – 7.85 (m, 2 H, H_{arom}), 7.75 – 7.74 (m, 2 H, H_{arom}), 7.44 – 7.43 (m, 1 H, H_{arom}), 7.44 – 6.97 (overlapping resonances, 19 H, H_{arom}), 6.16 (d, $^4J_{\text{H-P}} = 6.9$ Hz, 1 H, Si-H), 5.66 (d, $^3J_{\text{H-H}} = 7.8$ Hz, 1 H, CH), 5.51 (d, $^3J_{\text{H-H}} = 7.8$ Hz, 1 H, CH), 1.92 – 1.07 (overlapping resonances, 25 H), 0.51 (s, 3 H, CH_3). $^{31}\text{P}\{^1\text{H}\}$ NMR (202.5 MHz, benzene- d_6): δ –7.16.

Synthesis of 5-4 (*R,R*)-(DAPSi)Ni(COE-yl). Ni(COD) $_2$ (0.090 g, 0.341 mmol) was weighed into a 4-dram vial equipped with a stir and suspended in 4 mL of benzene. Ligand **5-1** (0.200 g, 0.341 mmol) was added as a benzene solution (ca. 2 mL) and the resulting orange reaction mixture was allowed to stir at room temperature for 18 h. The volatile components of the reaction mixture were then removed under reduced pressure and the crude residue was extracted with 10 mL pentane and filtered through Celite. The orange-yellow filtrate solution was collected and the solvent was removed *in vacuo* to afford **5-4** as a bright yellow solid (0.180 g, 0.239 mmol, 70% yield). **5-4** exists as a 1:1 mixture of isomers. ^1H NMR (500 MHz, benzene- d_6): δ 8.26 (t, $J = 7.0$ Hz, 2 H, H_{arom}), 7.90 (d, $J = 8.5$ Hz, 1 H, H_{arom}), 7.85 (d, $J = 7.2$ Hz, 1 H, H_{arom}), 7.85 – 7.77 (m, 3 H, H_{arom}), 7.79 – 7.74 (m, 1 H, H_{arom}), 7.76 – 7.66 (m, 3 H, H_{arom}), 7.69 – 7.49 (m, 9 H, H_{arom}), 7.48 (d, $J = 8.3$ Hz, 1 H, H_{arom}), 7.43 (d, $J = 8.2$ Hz, 1 H, H_{arom}), 7.37 (dd, $J = 8.2, 7.1$ Hz, 1 H, H_{arom}), 7.37 – 7.10 (m, 15 H, H_{arom}), 6.17 (ddd, $J = 23.2, 11.2, 3.4$ Hz, 2 H, CH), 6.06 (dd, $J = 10.7, 3.4$ Hz, 1 H, CH), 5.96 (dd, $J = 10.5, 3.4$ Hz, 1 H, CH), 5.60 – 5.45 (m, 2 H, CH), 5.35 – 5.29 (m, 1 H, CH), 5.09 – 4.99 (m, 1 H, CH), 4.92 (dddq, $J = 12.3, 6.9, 4.9, 2.3$ Hz,

1 H, *CH*), 4.80 – 4.70 (m, 1 H, *CH*), 4.52 (t, $J = 8.5$ Hz, 1 H, *CH*), 4.44 – 4.34 (m, 1 H, *CH*), 4.14 – 4.05 (m, 1 H, *CH*), 3.67 (t, $J = 8.5$ Hz, 1 H, *CH*), 2.49 (ddt, $J = 12.9, 8.5, 4.3$ Hz, 1 H, *CH*), 2.23 (ddt, $J = 12.9, 8.2, 4.2$ Hz, 1 H, *CH*), 2.15 – 2.08 (m, 1 H, *CH*), 2.08 – 1.92 (m, 3 H), 1.92 – 1.78 (m, 1 H), 1.78 – 1.56 (m, 5 H), 1.59 – 1.22 (m, 21 H), 1.25 – 1.17 (m, 1 H), 1.17 (dd, $J = 7.0, 3.4$ Hz, 3 H), 1.17 – 1.06 (m, 3 H), 1.09 – 0.98 (m, 6 H), 0.95 (d, $J = 7.3$ Hz, 3 H), 0.95 – 0.84 (m, 3 H), 0.80 (d, $J = 7.4$ Hz, 3 H), 0.70 (s, 1 H). $^{13}\text{C}\{^1\text{H}\}$ NMR (126 MHz, benzene- d_6): δ 156.45 (dd, $J = 37.7, 34.9$ Hz, C_{arom}), 151.35 (dd, $J = 64.0, 38.0$ Hz, C_{arom}), 142.17 (dd, $J = 13.3, 4.5$ Hz, C_{arom}), 134.75 – 134.53 (m), 134.38 – 133.75 (m), 131.18 (d, $J = 5.3$ Hz, CH_{arom}), 129.75 (dd, $J = 5.4, 3.4$ Hz, CH_{arom}), 129.58 (d, $J = 6.6$ Hz, CH_{arom}), 129.48 (d, $J = 2.9$ Hz, CH_{arom}), 124.46 (d, $J = 7.4$ Hz, CH_{arom}), 124.15 (d, $J = 8.0$ Hz, CH_{arom}), 117.09 (d, $J = 18.1$ Hz, CH_{arom}), 110.77 (d, $J = 35.8$ Hz, CH_{arom}), 82.05 (d, $J = 60.7$ Hz, C=C), 61.06 (d, $J = 27.1$ Hz, C=C), 59.62 (d, $J = 27.8$ Hz, C=C), 53.87 (d, $J = 14.5$ Hz), 51.99 (dd, $J = 37.5, 13.4$ Hz, C=C), 33.12 (d, $J = 4.0$ Hz), 32.41 (d, $J = 3.7$ Hz), 32.19 (d, $J = 6.1$ Hz), 31.91 (d, $J = 5.2$ Hz), 24.05 (d, $J = 6.6$ Hz), 23.77 (d, $J = 5.7$ Hz, CH_2), 22.98 (d, $J = 5.7$ Hz, CH_3), 21.00 (d, $J = 3.0$ Hz, CH_3). $^{31}\text{P}\{^1\text{H}\}$ NMR (202.5 MHz, benzene- d_6): δ 147.3 (s), 145.8 (s). ^{29}Si NMR (99.4 MHz, benzene- d_6): δ 61.4, 60.3.

Synthesis of 5-5 (*R,R*)-(TADDOLSi)Ni(benzyl). $\text{NiCl}_2(\text{dme})$ (0.010 g, 0.052 mmol) was weighed into a 4-dram vial equipped with a stir and suspended in ca. 2 mL of benzene. Ligand **5-3** (0.040 g, 0.052 mmol) was added as a benzene solution (ca. 2 mL) and the reaction mixture was allowed to stir for 10 minutes. BnMgCl (0.104 mL, 1.0 M, 0.104 mmol) was then added dropwise and the resulting dark orange suspension was magnetically stirred for one hour at room temperature. The volatile components of the reaction mixture

were then removed under reduced pressure and the crude residue was triturated with 2×3 mL pentane. The residue was then extracted with ca. 8 mL pentane and filtered through Celite. The dark orange filtrate solution was collected and the solvent was removed under reduced pressure. The remaining residue was triturated with 2×2 mL pentane to afford **5-5** as an orange solid that was used without further purification (0.04 g, 0.018 mmol, 56% yield). ^1H NMR (400 MHz, benzene- d_6): δ 8.04 – 8.02 (m, 4 H, H_{arom}), 7.88 – 7.86 (m, 4 H, H_{arom}), 7.47 – 7.45 (m, 1 H, H_{arom}), 7.36 – 6.94 (overlapping resonances, 19 H), 6.70 (m, 1 H, H_{arom}), 6.18 (d, $J_{\text{H-P}} = 7.5$ Hz, 1 H, CH_2Ph), 6.10 (d, $^3J_{\text{H-H}} = 7.3$ Hz, 1 H, CH), 6.00 (d, $^3J_{\text{H-H}} = 7.3$ Hz, CH), 5.44 (d, $J_{\text{H-P}} = 7.4$ Hz, CH_2Ph), 1.82 – 0.82 (overlapping resonances, 28 H). $^{31}\text{P}\{^1\text{H}\}$ NMR (162 MHz, benzene- d_6): 68.3.

Synthesis of 5-6 (*R,R*)-(IndolSi)H. A 4-dram vial equipped with a stir bar was charged with a solution of (*R,R*)-(TADDOL)SiHCl (0.627 g, 1.18 mmol) in ca. 5 mL benzene. The lithium salt of diisopropyl(3-methylindolyl)phosphine (0.300 g, 1.18 mmol), prepared *via* treatment of diisopropyl(3-methylindolyl)phosphine with 1 equiv. $^n\text{BuLi}$, was dissolved in ca. 4 mL benzene and added dropwise to the solution of (*R,R*)-(TADDOL)SiHCl. The mixture was allowed to magnetically stir for 18 h at room temperature. The resulting suspension was filtered through Celite and the clear, colorless filtrate solution was collected. The solvent was removed under reduced pressure to afford **5-6** as a white solid after prolonged exposure to vacuum (0.786 g, 1.06 mmol, 90% yield). ^1H NMR (300 MHz, toluene- d_8 , 353K): δ 7.77 – 7.63 (overlapping resonances, 8 H), 7.43 – 7.41 (m, 1 H, H_{arom}), 7.14 – 6.93 (overlapping resonances, 16 H), 6.28 (d, $^4J_{\text{H-P}} = 6.5$ Hz, 1 H, Si-H), 5.67 (d, $^3J_{\text{H-H}} = 7.7$ Hz, 1 H, CH), 5.41 (d, $^3J_{\text{H-H}} = 7.7$ Hz, 1 H, CH), 2.46 – 2.22 (overlapping resonances, 5 H), 1.11 (dd, $^3J_{\text{H-P}} = 6.9$ Hz, $^3J_{\text{H-H}} = 0.9$ Hz, 3 H, $\text{CH}(\text{CH}_3)_2$), 1.06 (dd, $^3J_{\text{H-P}}$

= 6.8 Hz, $^3J_{\text{H-H}} = 1.8$ Hz, 3 H, $\text{CH}(\text{CH}_3)_2$), 0.91 – 0.80 (overlapping resonances, 9 H), 0.64 (s, 3 H, CH_3 acetal). $^{13}\text{C}\{^1\text{H}\}$ NMR (101 MHz, benzene- d_6 , 298K): 147.1 (s, C_{arom}), 146.8 (s, C_{arom}), 142.9 (s, C_{arom}), 142.8 (d, $J_{\text{C-P}} = 5.9$ Hz, C_{arom}), 142.3 (s, C_{arom}), 129.9 (d, $J_{\text{C-P}} = 18.9$ Hz, CH_{arom}), 128.5 (s, CH_{arom}), 128.0 (s, CH_{arom}), 127.6 (s, CH_{arom}), 127.5 (s, CH_{arom}), 123.5 (s, CH_{arom}), 121.0 (s, CH_{arom}), 119.2 (br s, CH_{arom}), 114.6 (s, CH_{arom}), 113.7 (br s, CH_{arom}), 85.6 (s, $\text{C}(\text{OSiH})\text{Ph}_2$), 83.4 (s, $\text{C}(\text{OSiH})\text{Ph}_2$), 82.9 (s, CH), 81.9 (s, CH), 27.7 (s, CH_3), 26.9 (s, CH_3), 26.0 (d, $J_{\text{C-P}} = 9.9$ Hz, $\text{CH}(\text{CH}_3)_2$), 25.6 (d, $J_{\text{C-P}} = 9.3$ Hz, $\text{CH}(\text{CH}_3)_2$), 22.0 (d, $J_{\text{C-P}} = 25.7$ Hz, $\text{CH}(\text{CH}_3)_2$), 21.1 (d, $J_{\text{C-P}} = 9.9$ Hz, $\text{CH}(\text{CH}_3)_2$). $^{31}\text{P}\{^1\text{H}\}$ NMR (121.5 MHz, toluene- d_8 , 353K): δ -6.13. ^{29}Si NMR (79.5 MHz, benzene- d_6 , 298K): δ 176.9. HRMS (ESI): calculated (M) $^+$ [$\text{C}_{46}\text{H}_{51}\text{NO}_4\text{PSi}$] $^+$: 740.3319; found: 740.3319.

Synthesis of 5-7 (*R,R*)-(IndolSi)Ni(benzyl). $\text{NiCl}_2(\text{dme})$ (0.074 g, 0.338 mmol) was weighed into a 4-dram vial equipped with a stir and suspended in ca. 4 mL of benzene. Ligand **5-6** (0.250 g, 0.338 mmol) was added as a benzene solution (ca. 2 mL) and the mixture was allowed to stir for 10 minutes. BnMgCl (0.676 mL, 1.0 M, 0.676 mmol) was then added dropwise and the resulting dark orange suspension was magnetically stirred for one hour at room temperature. The volatile components of the reaction mixture were then removed under reduced pressure and the crude residue was triturated with 2×3 mL pentane. The residue was then extracted with ca. 12 mL pentane and filtered through Celite. The bright orange filtrate solution was collected and the solvent was removed under reduced pressure. The remaining residue was triturated with 2×2 mL pentane. The resulting orange solid was washed with an additional 2×2 mL pentane to afford **5-7** as a light orange solid (0.194 g, 0.218 mmol, 65% yield). ^1H NMR (400 MHz, benzene- d_6): δ 8.20 – 8.16 (m, 3 H, H_{arom}), 8.05 – 7.95 (m, 6 H, H_{arom}), 7.64 – 7.62 (m, 1 H, H_{arom}), 7.26 –

6.86 (overlapping resonances, 18 H), 6.71 – 6.67 (m, 1 H, H_{arom}), 6.41 (d, $J_{\text{H-P}} = 7.5$ Hz, 1 H, CH_2Ph), 5.95 (d, $^3J_{\text{H-H}} = 7.6$ Hz, 1 H, CH), 5.82 (d, $^3J_{\text{H-H}} = 7.6$ Hz, 1 H, CH), 5.07 (d, $J_{\text{H-P}} = 7.2$ Hz, 1 H, CH_2Ph), 2.31 – 2.24 (overlapping resonances, 4 H), 1.84 (m, 1 H, $\text{CH}(\text{CH}_3)_2$), 1.30 (s, 3 H, CH_3), 0.86 – 0.66 (overlapping resonances 15 H). $^{13}\text{C}\{\text{H}\}$ NMR (101 MHz, benzene- d_6): δ 150.5 (s, C_{arom}), 148.7 (s, C_{arom}), 145.9 (s, C_{arom}), 143.4 (s, C_{arom}), 140.2 (d, $J_{\text{C-P}} = 13.6$ Hz, C_{arom}), 136.4 (d, $J_{\text{C-P}} = 7.1$ Hz, C_{arom}), 134.0 (s, CH_{arom}), 132.3 (s, CH_{arom}), 132.3 (s, CH_{arom}), 130.0 (s, CH_{arom}), 129.5 (s, CH_{arom}), 128.6 (s, CH_{arom}), 128.1 (s, CH_{arom}), 128.0 (s, CH), 127.6 (s, CH_{arom}), 127.5 (s, CH_{arom}), 127.3 (s, CH_{arom}), 127.0 (s, CH_{arom}), 126.9 (s, CH_{arom}), 123.7 (s, CH_{arom}), 122.3 (s, CH_{arom}), 120.2 (d, $J_{\text{C-P}} = 25.0$ Hz, CH_{arom}), 119.0 (s, CH_{arom}), 118.0 (s, C_{arom}), 117.1 (s, CH_{arom}), 116.9 (d, $J_{\text{C-P}} = 2.8$ Hz, C_{arom}), 112.9 (s, C_{arom}), 111.3 (s, CH_{arom}), 84.6 (s, CH), 83.9 (s, CH), 83.1 (s, $\text{C}(\text{Ph}_2\text{OSi})$), 81.8 (s, $\text{C}(\text{Ph}_2\text{OSi})$), 27.9 (s, CH_3), 27.0 (s, CH_3), 26.8 (s, $\text{CH}(\text{CH}_3)_2$), 25.4 (d, $J_{\text{C-P}} = 25.2$ Hz, $\text{CH}(\text{CH}_3)_2$), 20.4 – 20.2 (overlapping resonances), 19.9 (s, CH_3 acetal), 19.5 (d, $J_{\text{C-P}} = 6.6$ Hz, $\text{CH}(\text{CH}_3)_2$). $^{31}\text{P}\{\text{H}\}$ NMR (162 MHz, benzene- d_6): δ 52.6. ^{29}Si NMR (80 MHz, benzene- d_6): δ 193.3.

General Procedure for Catalytic Asymmetric Hydrogenation. The catalyst (complex **5-4**, **5-5**, or **5-7**, 0.005 mmol) was weighed into a 1-dram vial and 1.0 mL of a freshly prepared 0.1 M stock solution of the substrate in the specified solvent was added *via* microsyringe. The vial was equipped with a stirbar and closed with a screw cap featuring a PTFE septum. A needle was then inserted through the septum to allow for the introduction of H_2 gas. The vial was subsequently transferred to a Parr reactor which was sealed and pressurized to the required H_2 pressure. The Parr reactor was heated to the specified temperature in an oil bath for the duration of the reaction time. Afterward, the Parr reactor was removed from the oil bath and depressurized. The volatile components of the reaction were removed *in vacuo* and the crude mixture was dissolved in hexanes and

loaded on to a silica filter. The filter was washed with 3 × 3 mL 10% diethyl ether in hexanes and the filtrate solution was discarded. The product was then eluted off the silica with 100% diethyl ether. The ether filtrate was collected and the solvent was removed under reduced pressure. Conversion was then assessed *via* ¹H NMR spectroscopy relative to residual alkene. Enantioselectivity was determined by chiral HPLC analysis on a Chiralpak AD-H column using the specified conditions.

General Procedure for Catalytic Asymmetric Hydrogenation Using *In Situ* Generated Catalyst. 0.5 mL of a freshly prepared 0.015 M stock solution of **5-6** in THF was dispensed into a 1-dram vial equipped with a stir bar. 0.5 mL of a freshly prepared 0.01 M stock solution of Ni(COD)₂ in THF was then added to the same vial and the mixture was magnetically stirred for 30 minutes. The volatile components of the reaction mixture were then removed *in vacuo* and 1.0 mL of a freshly prepared 0.1 M stock solution of the substrate in MeOH was added *via* microsyringe. The vial was closed with a screw cap featuring a PTFE septum and a needle was inserted through the septum to allow for the introduction of H₂ gas. The vial was subsequently transferred to a Parr reactor which was sealed and pressurized to the required H₂ pressure. The Parr reactor was heated to the specified temperature in an oil bath for the duration of the reaction time. Afterward, the Parr reactor was removed from the oil bath and depressurized. The volatile components of the reaction were removed *in vacuo* and the crude residue was dissolved in hexanes and loaded on to a silica filter. The filter was washed with 3 × 3 mL 10% diethyl ether in hexanes and the filtrate solution was discarded. The product was then eluted off the silica with 100% diethyl ether. The ether filtrate was collected and the solvent was removed under reduced pressure. Conversion was then assessed *via* ¹H NMR spectroscopy relative

to residual alkene. Enantioselectivity was determined by chiral HPLC analysis on a Chiralpak AD-H column using the specified conditions.

Chapter 6: Conclusions and Future Work

6.1 Summary and Conclusions

As outlined in Chapter 1 of this document, there is a global demand for the development of sustainable first-row transition metal catalysts that can complement and possibly replace existing second- and third-row metal catalyst technology that is currently utilized in chemical synthesis. The design of ligands tailored to the unique properties of the first-row metals has emerged as a powerful strategy to overcome their often-inferior reactivity when compared to the platinum group metals. The incorporation of redox non-innocent motifs or electronegative elements into the ligand architecture to facilitate metal-ligand cooperativity are demonstrated approaches for taming the reactivity of the 3*d*-metals. With such design strategies in mind, an alternative ligand design approach based on phosphino(silyl) ligation has been pursued in the Turculet group. Phosphino(silyl) ligands have been shown to engage in cooperative behavior involving the electropositive Si donor in conjunction with 3*d*-metals. This reactivity, in concert with the incorporation of strong-field donors in a multidentate ligand framework, has been demonstrated to support active and selective hydrogenation catalysts featuring Earth-abundant 3*d*-metals.

In Chapter 2, significant improvements in the catalytic performance of (Cy-PSiP)Co^I complexes in alkene hydrogenation reactivity has been described. The synthesis of (Cy-PSiP)Co^I complexes lacking exogenous phosphine donors was targeted, as it was hypothesized that such ligands were inhibiting catalyst turnover. Complexes of the form (Cy-PSiP)Co^I(alkyne) (**2-1**; alkyne = 2-butyne, **2-2**; alkyne = diphenylacetylene) were isolated in high yield as diamagnetic, crystalline solids that could be readily purified. These complexes were characterized by multinuclear NMR spectroscopy, X-ray crystallography,

and elemental analysis. When applying complex **2-2** as a catalyst for alkene hydrogenation it was found that exceptionally mild conditions could be employed (1 atm H₂, 0.1 – 7.5 mol% **2-2**, 25 – 50 °C, 4 h) for a broad scope of substituted alkenes.

Exposing either complex **2-1** or **2-2** to an atm of H₂ led to the generation of a highly fluxional polyhydride species that could only be observed under an atmosphere of H₂. Low temperature NMR experiments did not aid in elucidating the structure of this polyhydride complex, as no decoalescence phenomena were observed at temperatures down to -80 °C. DFT calculations were then performed, and three possible isomers of the polyhydride complex with comparable energies were identified. A possible mechanism by which **2-2** could perform alkene hydrogenation was calculated, and it was found that the intermediacy of Co(σ -silane) complexes was crucial for catalytic turnover, consistent with the premise that metal-Si interactions in phosphino(silyl) ligated complexes play a key role in facilitating hydrofunctionalization reactivity.

Chapter 3 of this document expands the repertoire of catalytic reactions that (PSiP)Ni complexes can facilitate. While the hydrogenation of alkenes was targeted initially, complex **1-32** provided relatively poor performance for the hydrogenation of simple alkenes. Attempts to expand the scope to include alkynes led to the discovery that the hydrogenation of diphenylacetylene proceeded with exclusive selectivity for the (*E*)-alkene. This reaction could be made general for a broad scope of substituted diarylacetylenes and SiMe₃-protected terminal arylacetylenes. Exceptional selectivity for the (*E*)-alkene (>99:1 *E:Z*) was observed employing 1-2.5 mol% **1-32** under 1 atm of H₂ at room temperature for most substrates. Substrates featuring electron-withdrawing groups or those with *o*-substitution required a mild increase in temperature (50 °C) to achieve full

conversion and similarly high selectivity. Alkyne substrates bearing heterocyclic substituents (*i.e.*, pyridine, thiophene) could also be hydrogenated with high selectivity. Strongly electron withdrawing substituents such as nitro or cyano substitution led to a reversal in selectivity, with exclusive selectivity for the (*Z*)-alkene observed instead. Aldehyde substituents as well as direct carbonyl substitution on the alkyne were found to be incompatible with **1-32**, leading instead to catalyst decomposition. Mechanistic experiments wherein (*Z*)-stilbene was exposed to a catalytic amount of **1-32** led to near instantaneous isomerization to (*E*)-stilbene. Exposure of **1-32** to one equivalent of diphenylacetylene allowed for the isolation of complex **3-1**, a (PSiP)Ni(alkenyl) complex arising from insertion of the alkyne into the Ni-H. Exposure of **3-1** to 1 atm H₂ led to regeneration of **1-32** and liberation of (*E*)-stilbene, presumably through isomerization of unobserved (*Z*)-stilbene. On the basis of these data, a mechanism involving initial formation of the (*Z*)-alkene and subsequent isomerization to afford the (*E*)-product was proposed. The exquisite (*E*)-selectivity observed for this Ni-catalyzed semihydrogenation catalysis is synthetically useful, as such selectivity is challenging to obtain in transition metal catalyzed reactivity where the (*Z*)-isomer is typically formed and full reduction to the alkane product is often a competing reaction. The use of a Ni-based catalyst at low loading and low H₂ pressure is a highly desirable feature of this reactivity, contributing to both atom economy and sustainability.

In Chapter 4 of this document, the utility of the PhenDalPhos family of ligands was extended to include Co-catalyzed asymmetric hydrogenation. The enantiopure ligand (*S*)-Ph-PhenDalPhos was readily synthesized from commercially available starting materials and was coordinated to Co. The corresponding Co^{II} halide **4-1**, Co^{II} dialkyl **4-2**, and

cationic Co^I **4-3** complexes were synthesized and applied towards the asymmetric hydrogenation of α -dehydroamino acid derivatives. Pre-catalyst **4-3** was found to afford high enantioselectivity for a broad scope of phenylalanine derivatives featuring electron withdrawing and donating substituents. Substrates featuring *o*-substitution were challenging for **4-3**, requiring high catalyst loading (10 mol%) to achieve moderate enantioselectivity (*o*-F, *er* = 88:12, *o*-MeO, *er* = 76:24). This represents a rare example of the direct hydrogenation of α -dehydroamino acids by a 3*d*-metal catalyst, noteworthy due to the prevalence of such amino acid motifs in the pharmaceutical industry. Unlike previously reported examples that require stoichiometric Zn(0) as an additive, the system developed herein can operate effectively in the absence of added Zn(0), which is a significant improvement with respect to atom economy in such asymmetric hydrogenation catalysis.

Substrates bearing 2- and 3-thiophene substitution could also be hydrogenated with high enantioselectivity (>99:1 and 99:1 *er* respectively), as could (*Z*)-*dehydro-N*-acetyl-(4-acetoxy-3-methoxy) phenylalanine, the precursor to *L*-DOPA. While **4-3** provided selectivity for *D*-DOPA (99:1 *er*), this substrate was notable as its hydrogenation by Knowles and co-workers led to the first commercial route to *L*-DOPA.^{1, 197-198} When D₂ was employed instead of H₂ for the hydrogenation of (*Z*)-*dehydro-N*-acetyl-phenylalanine, deuterium was incorporated in the position resulting from *cis*-D₂ addition. Only a single isotopomer was observed, supporting the possibility of a Co^{III} dihydride mechanism resulting from oxidative addition of H₂ to the cationic Co(I) complex **4-3**.

Lastly, in Chapter 5 of this document, chiral bidentate (phosphino)silyl ligands were developed for the Ni-catalyzed asymmetric hydrogenation of tri-substituted carbocyclic

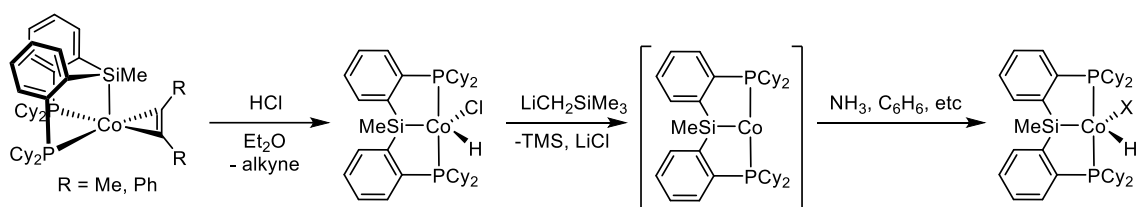
alkenes. The chiral products of these reactions are found in a variety of pharmaceuticals such as Tametraline, Sertraline, Rotigotine, and Rasagiline. However, platinum group metal catalysts have struggled to achieve high enantioselectivity for these substrates, and they have represented a notable challenge in asymmetric hydrogenation.⁶⁹ Work by Turculet group member Tyler Saunders has identified bidentate P₂Si supported Ni complexes as competent catalysts for the hydrogenation of tri- and tetra-substituted alkenes. To extend this reactivity to include asymmetric hydrogenation, several motifs were investigated featuring chirality at both the phosphino and silyl donor positions. Chirality was derived from readily commercially available materials such as a diazaphospholene derived from (*R*)-1-(1-naphthyl)ethylamine, a phosphonite derived from (*R,R*)-TADDOL, or a siloxane also derived from (*R,R*)-TADDOL. While most ligands screened for the asymmetric hydrogenation of *N*-(1-(3,4-dihydro)naphthalen-1-yl)-tert-butyl amide led to racemic hydrogenation, the use of **5-6** and Ni(COD)₂ led to quantitative conversion and 97:3 *er*. The (phosphino)silyl-based catalyst system employing **5-6** was found to significantly outperform the P,P-phosphoramidite analog in this reactivity, demonstrating a unique new approach to ligand design for asymmetric hydrofunctionalization catalysis based on Earth-abundant metals, wherein chirality at Si can provide high enantioselectivity while also facilitating catalytic turnover.

6.2 Future Work

The research in Chapters 2 of this document described the synthesis of reactive (Cy-PSiP)Co^I alkyne complexes for the catalytic hydrogenation of alkenes. While these complexes were designed with hydrogenation catalysis in mind, they are uniquely poised to be applied towards other forms of hydroelementation catalysis such as hydroboration or

hydrosilylation. Furthermore, while the chemistry of Chapter 2 focused on accessing reactive Co^{I} complexes through reduction from Co^{II} , an investigation into *oxidation* to Co^{III} would be informative as coordinatively unsaturated $(\text{PSiP})\text{Co}^{\text{III}}$ complexes have yet to be reported in the literature. Such complexes would be a valuable platform to investigate chemistry akin to what was previously reported with heavier group 9 $(\text{PSiP})\text{M}$ complexes.³⁷⁻³⁸

Co^{III} hydrido halide complexes of the form $(\text{PSiP})\text{Co}(\text{H})(\text{X})$ ($\text{X} = \text{halide}$) would be direct analogs to the Rh and Ir complexes employed in fundamental studies on the oxidative addition of benzene and ammonia by the Turculet group.³⁷⁻³⁸ Accessing these complexes might be achieved through reaction of complexes **2-1** and **2-2** with ethereal HCl, as Peters and co-workers have demonstrated that a similar strategy allowed access to a $(\text{P}_3\text{Si})\text{FeCl}$ complex without destruction of the Si-M bond.³³ Dehydrohalogenation from these complexes would allow for controlled access to the highly reactive Co^{I} intermediate without the presence of excess reductant.



Scheme 6.2.1. Potential synthetic route towards $(\text{PSiP})\text{Co}^{\text{III}}$ complexes for bond activation chemistry.

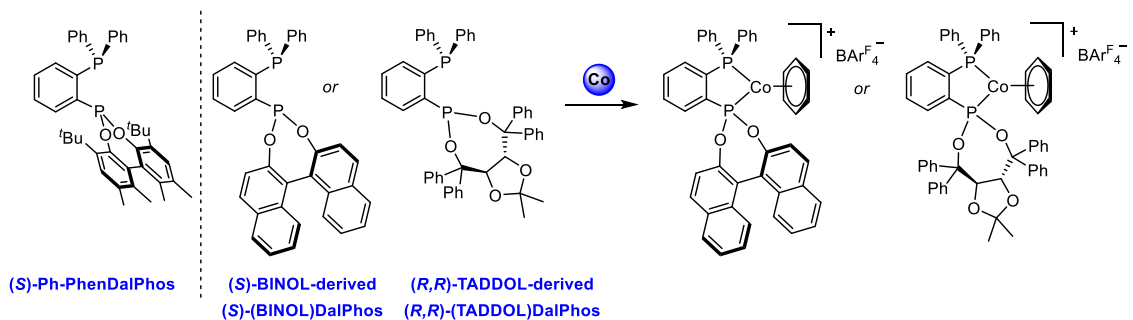
Work described in Chapter 4 of this document described the utility of (*S*)-PhenDalPhos supported Co complexes for the asymmetric hydrogenation of α -dehydroamino acid derivatives. Complex **4-3**, a well-defined and readily prepared cationic Co^{I} complex, was noted as being particularly reactive and provided the highest

enantioselectivity among the complexes that were synthesized. Applying complex **4-3** towards the asymmetric hydrogenation of other substrate classes would increase the versatility associated with the readily prepared PhenDalPhos family of ligands. Notable substrates that could be targeted include simple *N*-(arylethenyl)acetamide derivatives, dehydroamino acid esters, as well as α -enamido and α -enol phosphonates, as these are well established in Rh catalysis.²²³

Furthermore, the capabilities of the PhenDalPhos class of ligands should be interrogated through catalysis with substrates that have been previously subjected to asymmetric hydrogenation with Co and a privileged chiral bis(phosphine). Substrates such as conjugated enynes,⁶⁸ α/β -unsaturated carboxylic acids,⁶⁶⁻⁶⁷ and minimally functionalized alkenes lacking coordinating groups such as amides are proposed targets.^{20, 192} This would serve to establish the generality of the PhenDalPhos ligands for base-metal catalyzed asymmetric hydrogenation.

Modification of the phosphonite substituents is also proposed as a method to interrogate the generality of the mixed phosphine/phosphonite motif in supporting asymmetric catalysis. While the enantiopure Phen diol is commercially available, it is relatively expensive which precludes larger scale preparation of the Phen-DalPhos ligands. To that end, introduction of less costly chiral diols may allow for the synthesis of a scalable and readily modified ligand. The enantiopure diols BINOL and TADDOL are both commercially available and are relatively inexpensive when compared to the enantiopure Phen diol. A BINOL-derived ligand would bear similar structural features to the Phen-DalPhos ligands as its chirality is also derived from atropisomerism (Scheme 6.2.2). Ligands derived from TADDOL would feature a large steric profile, and TADDOL

derivatives can be easily prepared from the ethyl ester of *d/l*-tartrate.²¹⁸ These ligands are expected to have similar electronic properties to (*S*)-Ph-PhenDalPhos and would further expand the space of ligands that can support Co catalyzed asymmetric hydrogenation.

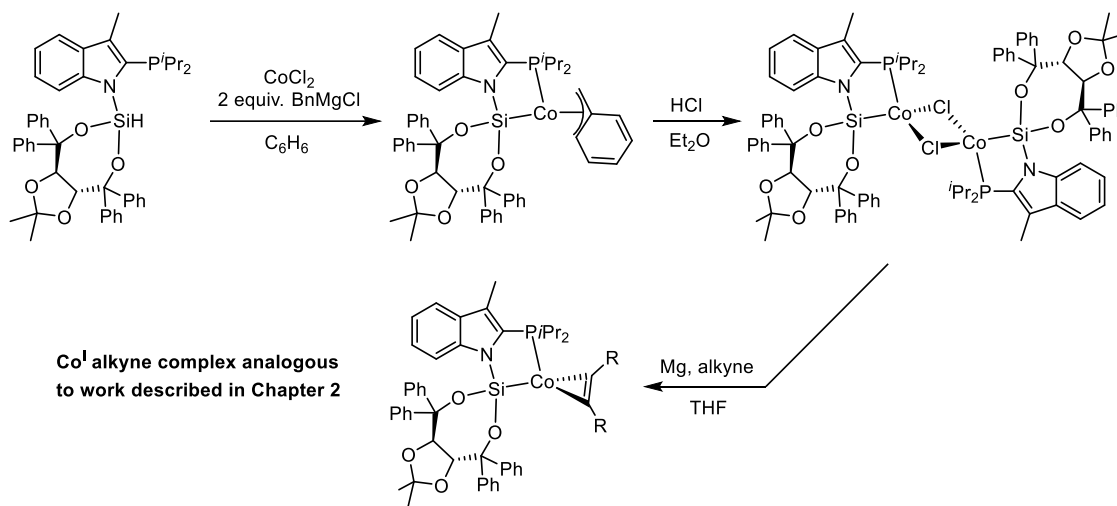


Scheme 6.2.2. Proposed mixed phosphine/phosphonite ligands for Co-catalyzed asymmetric hydrogenation.

Finally, in Chapter 5 of this document, the synthesis of a new class of chiral ligand that employs a chiral silyl donor was described. Screening these ligands for the asymmetric hydrogenation of (*Z*)-2-acetamido-3-phenylacrylate and *N*-(3,4-dihydro-1-naphthalenyl)acetamide led largely to racemic hydrogenation with Ni. However, a ligand derivative featuring a diisopropyl(3-methylindolyl)phosphine combined with a silyl donor derived from (*R,R*)-TADDOL led to selective asymmetric hydrogenation. Future work should involve investigation of the coordination chemistry of ligand **5-6** with Co and potentially Fe. Most of the examples of base-metal mediated asymmetric hydrogenation discussed in this document featured Co (*vide supra*), and work described in Chapter 2 of this document has established the high catalytic activity of (PSiP)Co^I alkyne complexes towards alkene hydrogenation. To that end, establishing chiral (phosphino)silyl ligation with Co is likely to lead to productive catalysis.

Co^{II} halide complexes of the form (PSi)CoX (X = Cl, Br, I) could be accessed *via* dehydrohalogenation of the corresponding Co salt and the PSi ligand. Ongoing work in the

Turculet group has found that the coordination of achiral P*Si* ligands has not proceeded analogously to P*Si*P ligands, and as a result a more roundabout approach may need to be taken in order to prepare isolable Co complexes. Accessing a Co^{II} benzyl complex utilizing 2 equiv. of BnMgCl may lead to a catalytically competent Co^{II} benzyl species (Scheme 6.2.3). Furthermore, such a complex could be reacted with one equiv. of HCl in ether to afford the corresponding Co^{II} chloride complex, which could then be subjected to Mg reduction in the presence of an alkyne. This would provide a three-coordinate Co^I alkyne complex analogous to the (Cy-P*Si*P)Co^I complexes described in Chapter 2 (Scheme 3.2.3).

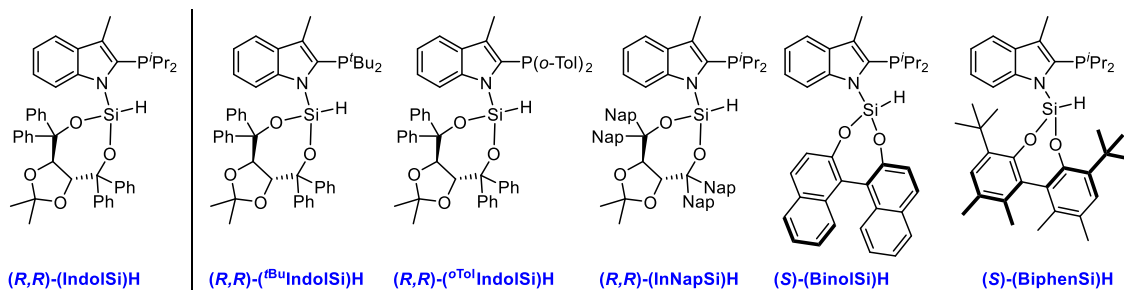


Scheme 6.2.3. Proposed synthesis of chiral P*Si*-supported Co^I and Co^{II} complexes.

Further work with the chiral (phosphino)silyl ligand framework should include modifications of the ligand architecture to improve enantioselectivity with challenging substrates, as well as to establish a library of such ligands that can be screened for a given transformation. The diisopropyl(3-methylindole)phosphine derived ligand features several handles that can be modified to tune reactivity. First, the steric and electronic features of the phosphino donor can be readily changed *via* reaction with various substituted

chlorophosphines. Di(*t*-butyl)phosphine and di(*o*-tolyl)phosphine are proposed as targets for future ligand design, as these respectively increase the steric bulk of the ligand and reduce the electron donating ability of the phosphine while maintaining steric bulk.

As noted above, the TADDOL moiety can also be readily modified through reaction of the *d/l*-tartrate ethyl ester with different protecting groups and Grignard reagents (Scheme 6.2.4). The introduction of 1-naphthyl moieties is proposed as a method to increase the crystallinity and decrease the solubility of these ligands, a noted problem in Chapter 5. Furthermore, 1-naphthyl substitution would increase the steric bulk of the silyl donor, potentially increasing enantioselectivity. Finally, Reek and co-workers have noted that BINOL-derived mixed phosphine/phosphoramidite ligands typically outperform their TADDOL-derived analogs.²²³ To that end, chiral PSi ligands that features BINOL or Phen-diol substitution are proposed to further improve on the results described in Chapter 5.



Scheme 6.2.4. Proposed derivatives of the chiral (phosphino)silyl framework.

References

1. Knowles, W. S. Asymmetric hydrogenations (Nobel lecture) *Angew. Chem. Int. Ed.* **2002**, *41*, 1999-2007.
2. Noyori, R. Asymmetric catalysis: science and opportunities (Nobel lecture) *Angew. Chem. Int. Ed.* **2002**, *41*, 2008-22.
3. Sharpless, K. B. Searching for new reactivity (Nobel lecture) *Angew. Chem. Int. Ed.* **2002**, *41*, 2024-32.
4. Schrock, R. R. Multiple metal-carbon bonds for catalytic metathesis reactions (Nobel Lecture) *Angew. Chem. Int. Ed.* **2006**, *45*, 3748-59.
5. Grubbs, R. H. Olefin-metathesis catalysts for the preparation of molecules and materials (Nobel Lecture) *Angew. Chem. Int. Ed.* **2006**, *45*, 3760-5.
6. Chauvin, Y. Olefin metathesis: the early days (Nobel Lecture) *Angew. Chem. Int. Ed.* **2006**, *45*, 3740-7.
7. Wu, X. F.; Anbarasan, P.; Neumann, H.; Beller, M. From noble metal to Nobel Prize: palladium-catalyzed coupling reactions as key methods in organic synthesis *Angew. Chem. Int. Ed.* **2010**, *49*, 9047-50.
8. Bauer, I.; Knolker, H. J. Iron catalysis in organic synthesis *Chem. Rev.* **2015**, *115*, 3170-387.
9. Murphy, L. J.; Ruddy, A. J.; McDonald, R.; Ferguson, M. J.; Turculet, L. Activation of Molecular Hydrogen and Oxygen by PSiP Complexes of Cobalt *Eur. J. Inorg. Chem.* **2018**, *2018*, 4481-4493.
10. Murphy, L. J.; Hollenhorst, H.; McDonald, R.; Ferguson, M.; Lumsden, M. D.; Turculet, L. Selective Ni-Catalyzed Hydroboration of CO₂ to the Formaldehyde Level Enabled by New PSiP Ligation *Organometallics* **2017**, *36*, 3709-3720.
11. McGuire, R. T.; Paffile, J. F. J.; Zhou, Y.; Stradiotto, M. Nickel-Catalyzed C–N Cross-Coupling of Ammonia, (Hetero)anilines, and Indoles with Activated (Hetero)aryl Chlorides Enabled by Ligand Design *ACS Catal.* **2019**, *9*, 9292-9297.

12. Yu, R. P.; Darmon, J. M.; Hoyt, J. M.; Margulieux, G. W.; Turner, Z. R.; Chirik, P. J. High-Activity Iron Catalysts for the Hydrogenation of Hindered, Unfunctionalized Alkenes *ACS Catal* **2012**, *2*, 1760-1764.
13. Tokmic, K.; Markus, C. R.; Zhu, L.; Fout, A. R. Well-Defined Cobalt(I) Dihydrogen Catalyst: Experimental Evidence for a Co(I)/Co(III) Redox Process in Olefin Hydrogenation *J. Am. Chem. Soc.* **2016**, *138*, 11907-13.
14. Lyaskovskyy, V.; de Bruin, B. Redox Non-Innocent Ligands: Versatile New Tools to Control Catalytic Reactions *ACS Catal.* **2012**, *2*, 270-279.
15. Alig, L.; Fritz, M.; Schneider, S. First-Row Transition Metal (De)Hydrogenation Catalysis Based On Functional Pincer Ligands *Chem. Rev.* **2019**, *119*, 2681-2751.
16. Chirik, P. J. Iron- and Cobalt-Catalyzed Alkene Hydrogenation: Catalysis with Both Redox-Active and Strong Field Ligands *Acc Chem Res* **2015**, *48*, 1687-95.
17. Russell, S. K.; Lobkovsky, E.; Chirik, P. J. Iron-catalyzed intermolecular [2pi+2pi] cycloaddition *J. Am. Chem. Soc.* **2011**, *133*, 8858-61.
18. Obligacion, J. V.; Chirik, P. J. Bis(imino)pyridine cobalt-catalyzed alkene isomerization-hydroboration: a strategy for remote hydrofunctionalization with terminal selectivity *J. Am. Chem. Soc.* **2013**, *135*, 19107-10.
19. Monfette, S.; Turner, Z. R.; Semproni, S. P.; Chirik, P. J. Enantiopure C1-symmetric bis(imino)pyridine cobalt complexes for asymmetric alkene hydrogenation *J. Am. Chem. Soc.* **2012**, *134*, 4561-4.
20. Friedfeld, M. R.; Shevlin, M.; Margulieux, G. W.; Campeau, L. C.; Chirik, P. J. Cobalt-Catalyzed Enantioselective Hydrogenation of Minimally Functionalized Alkenes: Isotopic Labeling Provides Insight into the Origin of Stereoselectivity and Alkene Insertion Preferences *J. Am. Chem. Soc.* **2016**, *138*, 3314-24.
21. Bart, S. C.; Lobkovsky, E.; Chirik, P. J. Preparation and molecular and electronic structures of iron(0) dinitrogen and silane complexes and their application to catalytic hydrogenation and hydrosilation *J. Am. Chem. Soc.* **2004**, *126*, 13794-807.

22. Trovitch, R. J.; Lobkovsky, E.; Bill, E.; Chirik, P. J. Functional Group Tolerance and Substrate Scope in Bis(imino)pyridine Iron Catalyzed Alkene Hydrogenation *Organometallics* **2008**, *27*, 1470-1478.
23. Bowman, A. C.; Milsmann, C.; Atienza, C. C.; Lobkovsky, E.; Wieghardt, K.; Chirik, P. J. Synthesis and molecular and electronic structures of reduced bis(imino)pyridine cobalt dinitrogen complexes: ligand versus metal reduction *J. Am. Chem. Soc.* **2010**, *132*, 1676-84.
24. Khusnutdinova, J. R.; Milstein, D. Metal-ligand cooperation *Angew. Chem. Int. Ed.* **2015**, *54*, 12236-73.
25. Gunanathan, C.; Milstein, D. Metal-ligand cooperation by aromatization-dearomatization: a new paradigm in bond activation and "green" catalysis *Acc Chem Res* **2011**, *44*, 588-602.
26. Langer, R.; Leitus, G.; Ben-David, Y.; Milstein, D. Efficient hydrogenation of ketones catalyzed by an iron pincer complex *Angew. Chem. Int. Ed.* **2011**, *50*, 2120-4.
27. Langer, R.; Diskin-Posner, Y.; Leitus, G.; Shimon, L. J.; Ben-David, Y.; Milstein, D. Low-pressure hydrogenation of carbon dioxide catalyzed by an iron pincer complex exhibiting noble metal activity *Angew. Chem. Int. Ed.* **2011**, *50*, 9948-52.
28. Zhang, Y.; MacIntosh, A. D.; Wong, J. L.; Bielinski, E. A.; Williard, P. G.; Mercado, B. Q.; Hazari, N.; Bernskoetter, W. H. Iron catalyzed CO(2) hydrogenation to formate enhanced by Lewis acid co-catalysts *Chem. Sci.* **2015**, *6*, 4291-4299.
29. Lin, T. P.; Peters, J. C. Boryl-mediated reversible H₂ activation at cobalt: catalytic hydrogenation, dehydrogenation, and transfer hydrogenation *J. Am. Chem. Soc.* **2013**, *135*, 15310-3.
30. Lin, T. P.; Peters, J. C. Boryl-metal bonds facilitate cobalt/nickel-catalyzed olefin hydrogenation *J. Am. Chem. Soc.* **2014**, *136*, 13672-83.
31. Corey, J. Y. Reactions of Hydrosilanes with Transition Metal Complexes *Chem. Rev.* **2016**, *116*, 11291-11435.

32. Gossage, R. A.; McLennan, G. D.; Stobart, S. R. (Phosphinoalkyl)silanes. 3.(1) Poly(o-(diphenylphosphino)benzyl)silanes: Synthesis, Spectroscopic Properties, and Complexation at Platinum or Iridium *Inorg. Chem.* **1996**, *35*, 1729-1732.
33. Mankad, N. P.; Whited, M. T.; Peters, J. C. Terminal FeI-N₂ and FeII...H-C interactions supported by tris(phosphino)silyl ligands *Angew. Chem. Int. Ed.* **2007**, *46*, 5768-71.
34. Whited, M. T.; Mankad, N. P.; Lee, Y.; Oblad, P. F.; Peters, J. C. Dinitrogen complexes supported by tris(phosphino)silyl ligands *Inorg. Chem.* **2009**, *48*, 2507-17.
35. Lee, Y.; Mankad, N. P.; Peters, J. C. Triggering N₂ uptake via redox-induced expulsion of coordinated NH₃ and N₂ silylation at trigonal bipyramidal iron *Nat. Chem.* **2010**, *2*, 558.
36. MacInnis, M. C.; MacLean, D. F.; Lundgren, R. J.; McDonald, R.; Turculet, L. Synthesis and Reactivity of Platinum Group Metal Complexes Featuring the New Pincer-like Bis(phosphino)silyl Ligand [κ^3 -(2-Ph₂PC₆H₄)₂SiMe]⁻ ([PSiP]): Application in the Ruthenium-Mediated Transfer Hydrogenation of Ketones *Organometallics* **2007**, *26*, 6522-6525.
37. Morgan, E.; MacLean, D. F.; McDonald, R.; Turculet, L. Rhodium and Iridium Amido Complexes Supported by Silyl Pincer Ligation: Ammonia N-H Bond Activation by a [PSiP]Ir Complex *Journal of the American Chemical Society* **2009**, *131*, 14234-14236.
38. MacLean, D. F.; McDonald, R.; Ferguson, M. J.; Caddell, A. J.; Turculet, L. Room temperature benzene C-H activation by a new [PSiP]Ir pincer complex *Chem. Commun.* **2008**, 5146-8.
39. MacInnis, M. C.; McDonald, R.; Ferguson, M. J.; Tobisch, S.; Turculet, L. Four-coordinate, 14-electron Ru(II) complexes: unusual trigonal pyramidal geometry enforced by bis(phosphino)silyl ligation *J. Am. Chem. Soc.* **2011**, *133*, 13622-33.
40. Murphy, L. J.; Ferguson, M. J.; McDonald, R.; Lumsden, M. D.; Turculet, L. Synthesis of Bis(phosphino)silyl Pincer-Supported Iron Hydrides for the Catalytic Hydrogenation of Alkenes *Organometallics* **2018**, *37*, 4814-4826.

41. Mitton, S. J.; McDonald, R.; Turculet, L. Nickel and palladium silyl pincer complexes: unusual structural rearrangements that involve reversible Si-C(sp³) and Si-C(sp²) bond activation *Angew. Chem. Int. Ed.* **2009**, *48*, 8568-71.
42. Charboneau, D. J.; Balcells, D.; Hazari, N.; Lant, H. M. C.; Mayer, J. M.; Melvin, P. R.; Mercado, B. Q.; Morris, W. D.; Repisky, M.; Suh, H.-W. Dinitrogen-Facilitated Reversible Formation of a Si-H Bond in a Pincer-Supported Ni Complex *Organometallics* **2016**, *35*, 3154-3162.
43. Suh, H. W.; Guard, L. M.; Hazari, N. A mechanistic study of allene carboxylation with Co₂ resulting in the development of a Pd(II) pincer complex for the catalytic hydroboration of CO₂ *Chem. Sci.* **2014**, *5*, 3859-3872.
44. Nova, A.; Suh, H. W.; Schmeier, T. J.; Guard, L. M.; Eisenstein, O.; Hazari, N.; Maseras, F. An unusual example of hypervalent silicon: a five-coordinate silyl group bridging two palladium or nickel centers through a nonsymmetrical four-center two-electron bond *Angew. Chem. Int. Ed.* **2014**, *53*, 1103-8.
45. Suh, H.-W.; Guard, L. M.; Hazari, N. Synthesis and reactivity of a masked PSiP pincer supported nickel hydride *Polyhedron* **2014**, *84*, 37-43.
46. Suh, H.-W.; Schmeier, T. J.; Hazari, N.; Kemp, R. A.; Takase, M. K. Experimental and Computational Studies of the Reaction of Carbon Dioxide with Pincer-Supported Nickel and Palladium Hydrides *Organometallics* **2012**, *31*, 8225-8236.
47. Takaya, J.; Iwasawa, N. Reaction of bis(o-phosphinophenyl)silane with M(PPh₃)₄ (M = Ni, Pd, Pt): synthesis and structural analysis of eta²-(Si-H) metal(0) and pentacoordinate silyl metal(II) hydride complexes of the Ni triad bearing a PSiP-pincer ligand *Dalton Trans.* **2011**, *40*, 8814-21.
48. Wu, S.; Li, X.; Xiong, Z.; Xu, W.; Lu, Y.; Sun, H. Synthesis and Reactivity of Silyl Iron, Cobalt, and Nickel Complexes Bearing a [PSiP]-Pincer Ligand via Si-H Bond Activation *Organometallics* **2013**, *32*, 3227-3237.
49. Kim, J.; Kim, Y.; Sinha, I.; Park, K.; Kim, S. H.; Lee, Y. The unusual hydricity of a cobalt bound Si-H moiety *Chem. Commun.* **2016**, *52*, 9367-70.
50. Xiong, Z.; Li, X.; Zhang, S.; Shi, Y.; Sun, H. Synthesis and Reactivity of N-Heterocyclic PSiP Pincer Iron and Cobalt Complexes and Catalytic Application of Cobalt Hydride in Kumada Coupling Reactions *Organometallics* **2016**, *35*, 357-363.

51. Imayoshi, R.; Nakajima, K.; Takaya, J.; Iwasawa, N.; Nishibayashi, Y. Synthesis and Reactivity of Iron - and Cobalt - Dinitrogen Complexes Bearing PSiP - Type Pincer Ligands toward Nitrogen Fixation *Eur. J. Inorg. Chem.* **2017**, *2017*, 3769-3778.
52. Luo, X.-L.; Howard, J. A. K.; Crabtree, R. H. ¹H NMR T₁(min) data and structure in a series of rhenium polyhydride complexes and the contribution of M-H dipole-dipole relaxation *Magn. Reson. Chem.* **1991**, *29*, S89-S93.
53. Heinekey, D. M.; van Roon, M. Dihydride Complexes of the Cobalt and Iron Group Metals: An Investigation of Structure and Dynamic Behavior *Journal of the American Chemical Society* **1996**, *118*, 12134-12140.
54. Desrosiers, P. J.; Cai, L.; Lin, Z.; Richards, R.; Halpern, J. Assessment of the " T₁ criterion" for distinguishing between classical and nonclassical transition-metal hydrides: hydride relaxation rates in tris (triarylphosphine) osmium tetrahydrides and related polyhydrides *Journal of the American Chemical Society* **1991**, *113*, 4173-4184.
55. Morris, R. H. Dihydrogen, dihydride and in between: NMR and structural properties of iron group complexes *Coord. Chem. Rev.* **2008**, *252*, 2381-2394.
56. Maltby, P. A.; Schlaf, M.; Steinbeck, M.; Lough, A. J.; Morris, R. H.; Klooster, W. T.; Koetzle, T. F.; Srivastava, R. C. Dihydrogen with Frequency of Motion Near the ¹H Larmor Frequency. Solid-State Structures and Solution NMR Spectroscopy of Osmium Complexes trans-[Os(H·H)X(PPh₂CH₂CH₂PPh₂)₂]⁺ (X = Cl, Br) *Journal of the American Chemical Society* **1996**, *118*, 5396-5407.
57. Gründemann, S.; Limbach, H.-H.; Buntkowsky, G.; Sabo-Etienne, S.; Chaudret, B. Distance and Scalar HH-Coupling Correlations in Transition Metal Dihydrides and Dihydrogen Complexes *The Journal of Physical Chemistry A* **1999**, *103*, 4752-4754.
58. Gelabert, R.; Moreno, M.; Lluch, J. M.; Lledos, A.; Pons, V.; Heinekey, D. M. Synthesis and properties of compressed dihydride complexes of iridium: theoretical and spectroscopic investigations *J. Am. Chem. Soc.* **2004**, *126*, 8813-22.
59. Lachaize, S.; Sabo - Etienne, S. σ - Silane Ruthenium Complexes: The Crucial Role of Secondary Interactions *Eur. J. Inorg. Chem.* **2006**, *2006*, 2115-2127.

60. Chirik, P.; Morris, R. Getting Down to Earth: The Renaissance of Catalysis with Abundant Metals *Acc Chem Res* **2015**, *48*, 2495.
61. Friedfeld, M. R.; Shevlin, M.; Hoyt, J. M.; Krska, S. W.; Tudge, M. T.; Chirik, P. J. Cobalt precursors for high-throughput discovery of base metal asymmetric alkene hydrogenation catalysts *Science* **2013**, *342*, 1076-80.
62. Shevlin, M.; Friedfeld, M. R.; Sheng, H.; Pierson, N. A.; Hoyt, J. M.; Campeau, L. C.; Chirik, P. J. Nickel-Catalyzed Asymmetric Alkene Hydrogenation of α,β -Unsaturated Esters: High-Throughput Experimentation-Enabled Reaction Discovery, Optimization, and Mechanistic Elucidation *J. Am. Chem. Soc.* **2016**, *138*, 3562-9.
63. Friedfeld, M. R.; Zhong, H.; Ruck, R. T.; Shevlin, M.; Chirik, P. J. Cobalt-catalyzed asymmetric hydrogenation of enamides enabled by single-electron reduction *Science* **2018**, *360*, 888-893.
64. Zhong, H.; Friedfeld, M. R.; Chirik, P. J. Syntheses and Catalytic Hydrogenation Performance of Cationic Bis(phosphine) Cobalt(I) Diene and Arene Compounds *Angew. Chem. Int. Ed.* **2019**, *58*, 9194-9198.
65. Zuo, Z.; Xu, S.; Zhang, L.; Gan, L.; Fang, H.; Liu, G.; Huang, Z. Cobalt-Catalyzed Asymmetric Hydrogenation of Vinylsilanes with a Phosphine–Pyridine–Oxazoline Ligand: Synthesis of Optically Active Organosilanes and Silacycles *Organometallics* **2019**, *38*, 3906-3911.
66. Du, X.; Xiao, Y.; Huang, J. M.; Zhang, Y.; Duan, Y. N.; Wang, H.; Shi, C.; Chen, G. Q.; Zhang, X. Cobalt-catalyzed highly enantioselective hydrogenation of α,β -unsaturated carboxylic acids *Nat. Commun.* **2020**, *11*, 3239.
67. Zhong, H.; Shevlin, M.; Chirik, P. J. Cobalt-Catalyzed Asymmetric Hydrogenation of α,β -Unsaturated Carboxylic Acids by Homolytic H(2) Cleavage *J. Am. Chem. Soc.* **2020**, *142*, 5272-5281.
68. Hu, Y.; Zhang, Z.; Liu, Y.; Zhang, W. Cobalt-Catalyzed Chemo- and Enantioselective Hydrogenation of Conjugated Enynes *Angew. Chem. Int. Ed.* **2021**, *60*, 16989-16993.

69. Chakraborty, S.; Konieczny, K.; de Zwart, F. J.; Bobylev, E. O.; Barath, E.; Tin, S.; Muller, B. H.; Reek, J. N. H.; de Bruin, B.; de Vries, J. G. Cobalt-Catalyzed Enantioselective Hydrogenation of Trisubstituted Carbocyclic Olefins: An Access to Chiral Cyclic Amides *Angew. Chem. Int. Ed.* **2023**, e202301329.
70. MacNeil, C. S.; Zhong, H.; Pabst, T. P.; Shevlin, M.; Chirik, P. J. Cationic Bis(phosphine) Cobalt(I) Arene Complexes as Precatalysts for the Asymmetric Synthesis of Sitagliptin *ACS Catal.* **2022**, *12*, 4680-4687.
71. Shultz, C. S.; Krska, S. W. Unlocking the potential of asymmetric hydrogenation at Merck *Acc Chem Res* **2007**, *40*, 1320-6.
72. Guan, Y. Q.; Han, Z.; Li, X.; You, C.; Tan, X.; Lv, H.; Zhang, X. A cheap metal for a challenging task: nickel-catalyzed highly diastereo- and enantioselective hydrogenation of tetrasubstituted fluorinated enamides *Chem. Sci.* **2019**, *10*, 252-256.
73. Hu, Y.; Chen, J.; Li, B.; Zhang, Z.; Gridnev, I. D.; Zhang, W. Nickel-Catalyzed Asymmetric Hydrogenation of 2-Amidoacrylates *Angew. Chem. Int. Ed.* **2020**, *59*, 5371-5375.
74. Blaser, H.-U.; Malan, C.; Pugin, B.; Spindler, F.; Steiner, H.; Studer, M. Selective Hydrogenation for Fine Chemicals: Recent Trends and New Developments *Adv. Synth. Catal.* **2003**, *345*, 103-151.
75. Yu, R. P.; Darmon, J. M.; Milsmann, C.; Margulieux, G. W.; Stieber, S. C.; DeBeer, S.; Chirik, P. J. Catalytic hydrogenation activity and electronic structure determination of bis(arylimidazol-2-ylidene)pyridine cobalt alkyl and hydride complexes *J. Am. Chem. Soc.* **2013**, *135*, 13168-84.
76. Friedfeld, M. R.; Margulieux, G. W.; Schaefer, B. A.; Chirik, P. J. Bis(phosphine)cobalt dialkyl complexes for directed catalytic alkene hydrogenation *J. Am. Chem. Soc.* **2014**, *136*, 13178-81.
77. Viereck, P.; Krautwald, S.; Pabst, T. P.; Chirik, P. J. A Boron Activating Effect Enables Cobalt-Catalyzed Asymmetric Hydrogenation of Sterically Hindered Alkenes *J. Am. Chem. Soc.* **2020**, *142*, 3923-3930.

78. Muhammad, S. R.; Nugent, J. W.; Tokmic, K.; Zhu, L.; Mahmoud, J.; Fout, A. R. Electronic Ligand Modifications on Cobalt Complexes and Their Application toward the Semi-Hydrogenation of Alkynes and Para-Hydrogenation of Alkenes *Organometallics* **2019**, *38*, 3132-3138.
79. Tokmic, K.; Fout, A. R. Alkyne Semihydrogenation with a Well-Defined Nonclassical Co-H(2) Catalyst: A H(2) Spin on Isomerization and E-Selectivity *J. Am. Chem. Soc.* **2016**, *138*, 13700-13705.
80. Sandl, S.; Maier, T. M.; van Leest, N. P.; Kröncke, S.; Chakraborty, U.; Demeshko, S.; Koszinowski, K.; de Bruin, B.; Meyer, F.; Bodensteiner, M.; Herrmann, C.; Wolf, R.; Jacobi von Wangelin, A. Cobalt-Catalyzed Hydrogenations via Olefin Cobaltate and Hydride Intermediates *ACS Catal.* **2019**, *9*, 7596-7606.
81. Anferov, S. W.; Filatov, A. S.; Anderson, J. S. Cobalt-Catalyzed Hydrogenation Reactions Enabled by Ligand-Based Storage of Dihydrogen *ACS Catal.* **2022**, *12*, 9933-9943.
82. Hale, D. J.; Ferguson, M. J.; Turculet, L. (PSiP)Ni-Catalyzed (E)-Selective Semihydrogenation of Alkynes with Molecular Hydrogen *ACS Catal.* **2021**, *12*, 146-155.
83. Dong, Y.; Xie, S.; Zhang, P.; Fan, Q.; Du, X.; Sun, H.; Li, X.; Fuhr, O.; Fenske, D. Selectivity Reverse of Hydrosilylation of Aryl Alkenes Realized by Pyridine N-Oxide with [PSiP] Pincer Cobalt(III) Hydride as Catalyst *Inorg. Chem.* **2021**, *60*, 4551-4562.
84. Dong, Y.; Zhang, P.; Fan, Q.; Du, X.; Xie, S.; Sun, H.; Li, X.; Fuhr, O.; Fenske, D. The Effect of Substituents on the Formation of Silyl [PSiP] Pincer Cobalt(I) Complexes and Catalytic Application in Both Nitrogen Silylation and Alkene Hydrosilylation *Inorg. Chem.* **2020**, *59*, 16489-16499.
85. Becke, A. D.; Johnson, E. R. Exchange-hole dipole moment and the dispersion interaction revisited *J Chem Phys* **2007**, *127*, 154108.
86. Becke, A. D. Density - functional thermochemistry. III. The role of exact exchange *The Journal of Chemical Physics* **1993**, *98*, 5648-5652.

87. Whited, M. T.; Trenerry, M. J.; DeMeulenaere, K. E.; Taylor, B. L. H. Computational and Experimental Investigation of Alkene Hydrogenation by a Pincer-Type [P2Si]Rh Complex: Alkane Release via Competitive σ -Bond Metathesis and Reductive Elimination *Organometallics* **2019**, *38*, 1493-1501.
88. Frisch, M. J.; Trucks, G. W.; Schlegel, H. B.; Scuseria, G. E.; Robb, M. A.; Cheeseman, J. R.; Scalmani, G.; Barone, V.; Petersson, G. A.; Nakatsuji, H.; Li, X.; Caricato, M.; Marenich, A. V.; Bloino, J.; Janesko, B. G.; Gomperts, R.; Mennucci, B.; Hratchian, H. P.; Ortiz, J. V.; Izmaylov, A. F.; Sonnenberg, J. L.; Williams; Ding, F.; Lipparini, F.; Egidi, F.; Goings, J.; Peng, B.; Petrone, A.; Henderson, T.; Ranasinghe, D.; Zakrzewski, V. G.; Gao, J.; Rega, N.; Zheng, G.; Liang, W.; Hada, M.; Ehara, M.; Toyota, K.; Fukuda, R.; Hasegawa, J.; Ishida, M.; Nakajima, T.; Honda, Y.; Kitao, O.; Nakai, H.; Vreven, T.; Throssell, K.; Montgomery Jr., J. A.; Peralta, J. E.; Ogliaro, F.; Bearpark, M. J.; Heyd, J. J.; Brothers, E. N.; Kudin, K. N.; Staroverov, V. N.; Keith, T. A.; Kobayashi, R.; Normand, J.; Raghavachari, K.; Rendell, A. P.; Burant, J. C.; Iyengar, S. S.; Tomasi, J.; Cossi, M.; Millam, J. M.; Klene, M.; Adamo, C.; Cammi, R.; Ochterski, J. W.; Martin, R. L.; Morokuma, K.; Farkas, O.; Foresman, J. B.; Fox, D. J. *Gaussian 16 Rev. C.01*, Wallingford, CT, 2016.
89. Lee, C.; Yang, W.; Parr, R. G. Development of the Colle-Salvetti correlation-energy formula into a functional of the electron density *Physical review. B, Condensed matter* **1988**, *37*, 785-789.
90. Molnár, Á.; Sárkány, A.; Varga, M. Hydrogenation of carbon-carbon multiple bonds: chemo-, regio- and stereo-selectivity *J. Mol. Catal. A: Chem.* **2001**, *173*, 185-221.
91. Kluwer, A. M.; Elsevier, C. J., Homogeneous Hydrogenation of Alkynes and Dienes. In *Handbook of Homogeneous Hydrogenation*, de Vries, J. G.; Elsevier, C. J., Eds. Wiley-VCH: Weinheim, 2007; pp 375-411.
92. Crespo-Quesada, M.; Cárdenas-Lizana, F.; Dessimoz, A.-L.; Kiwi-Minsker, L. Modern Trends in Catalyst and Process Design for Alkyne Hydrogenations *ACS Catal.* **2012**, *2*, 1773-1786.
93. Ager, D., 8.17 Homogeneous Catalytic Hydrogenation of C=C and C \equiv C. In *Comprehensive Organic Synthesis II*, Knochel, P., Ed. Elsevier: Amsterdam, 2014; pp 605-631.

94. Chinchilla, R.; Najera, C. Chemicals from alkynes with palladium catalysts *Chem. Rev.* **2014**, *114*, 1783-826.
95. Thomas, S. P.; Greenhalgh, M. D., 8.16 Heterogeneous Hydrogenation of CC and CC Bonds. In *Comprehensive Organic Synthesis II*, Knochel, P., Ed. Elsevier: Amsterdam, 2014; pp 564-604.
96. Delgado, J. A.; Benkirane, O.; Claver, C.; Curulla-Ferre, D.; Godard, C. Advances in the preparation of highly selective nanocatalysts for the semi-hydrogenation of alkynes using colloidal approaches *Dalton Trans.* **2017**, *46*, 12381-12403.
97. Lei, J.; Su, L.; Zeng, K.; Chen, T.; Qiu, R.; Zhou, Y.; Au, C.-T.; Yin, S.-F. Recent advances of catalytic processes on the transformation of alkynes into functional compounds *Chem. Eng. Sci.* **2017**, *171*, 404-425.
98. de Vries, J. G., 1.5 Catalytic Reduction of Alkynes and Allenes. In *Catalytic Reduction in Organic Synthesis I*, de Vries, J. G., Ed. Georg Thieme Verlag: Stuttgart, 2018.
99. Swamy, K. C. K.; Reddy, A. S.; Sandeep, K.; Kalyani, A. Advances in chemoselective and/or stereoselective semihydrogenation of alkynes *Tetrahedron Lett.* **2018**, *59*, 419-429.
100. Decker, D.; Drexler, H.-J.; Heller, D.; Beweries, T. Homogeneous catalytic transfer semihydrogenation of alkynes – an overview of hydrogen sources, catalysts and reaction mechanisms *Catalysis Science & Technology* **2020**, *10*, 6449-6463.
101. Siau, W. Y.; Zhang, Y.; Zhao, Y. Stereoselective synthesis of Z-alkenes *Top Curr Chem* **2012**, *327*, 33-58.
102. Michaelides, I. N.; Dixon, D. J. Catalytic stereoselective semihydrogenation of alkynes to E-alkenes *Angew. Chem. Int. Ed.* **2013**, *52*, 806-8.
103. Oger, C.; Balas, L.; Durand, T.; Galano, J. M. Are alkyne reductions chemo-, regio-, and stereoselective enough to provide pure (Z)-olefins in polyfunctionalized bioactive molecules? *Chem. Rev.* **2013**, *113*, 1313-50.
104. Lindlar, H.; Dubuis, R. Palladium Catalyst for Partial Reduction of Acetylenes *Org. Synth.* **1966**, *46*, 89.

105. Savoia, D.; Tagliavini, E.; Trombini, C.; Umani-Ronchi, A. Active metals from potassium-graphite. Highly dispersed nickel on graphite as a new catalyst for the stereospecific semihydrogenation of alkynes *The Journal of Organic Chemistry* **2002**, *46*, 5340-5343.
106. Choudary, B. M.; Sharma, G. V. M.; Bharathi, P. A Highly Selective Montmorillonite Catalyst for Hydrogenation of Alkynes, Alkenynes, and Alkadienes** *Angewandte Chemie International Edition in English* **1989**, *28*, 465-466.
107. Choi, J.; Yoon, N. M. An excellent nickel boride catalyst for the cis-selective semihydrogenation of acetylenes *Tetrahedron Lett.* **1996**, *37*, 1057-1060.
108. Trost, B. M.; Ball, Z. T.; Joge, T. A chemoselective reduction of alkynes to (E)-alkenes *J. Am. Chem. Soc.* **2002**, *124*, 7922-3.
109. Barrios-Francisco, R.; Garcia, J. J. Stereoselective hydrogenation of aromatic alkynes using water, triethylsilane, or methanol, mediated and catalyzed by Ni(0) complexes *Inorg. Chem.* **2009**, *48*, 386-93.
110. Luo, F.; Pan, C.; Wang, W.; Ye, Z.; Cheng, J. Palladium-catalyzed reduction of alkynes employing HSiEt₃: stereoselective synthesis of *trans*- and *cis*-alkenes *Tetrahedron* **2010**, *66*, 1399-1403.
111. Belger, C.; Plietker, B. Aryl-aryl interactions as directing motifs in the stereodivergent iron-catalyzed hydrosilylation of internal alkynes *Chem. Commun.* **2012**, *48*, 5419-21.
112. Semba, K.; Fujihara, T.; Xu, T.; Terao, J.; Tsuji, Y. Copper-Catalyzed Highly Selective Semihydrogenation of Non-Polar Carbon-Carbon Multiple Bonds using a Silane and an Alcohol *Adv. Synth. Catal.* **2012**, *354*, 1542-1550.
113. Whittaker, A. M.; Lalic, G. Monophasic catalytic system for the selective semireduction of alkynes *Org Lett* **2013**, *15*, 1112-5.
114. Greenhalgh, M. D.; Frank, D. J.; Thomas, S. P. Iron-Catalysed Chemo-, Regio-, and Stereoselective Hydrosilylation of Alkenes and Alkynes using a Bench-Stable Iron(II) Pre-Catalyst *Adv. Synth. Catal.* **2014**, *356*, 584-590.

115. Hall, J. W.; Unson, D. M. L.; Brunel, P.; Collins, L. R.; Cybulski, M. K.; Mahon, M. F.; Whittlesey, M. K. Copper-NHC-Mediated Semihydrogenation and Hydroboration of Alkynes: Enhanced Catalytic Activity Using Ring-Expanded Carbenes *Organometallics* **2018**, *37*, 3102-3110.
116. Johnson, C.; Albrecht, M. Z-Selective alkyne semi-hydrogenation catalysed by piano-stool *N*-heterocyclic carbene iron complexes *Catalysis Science & Technology* **2018**, *8*, 2779-2783.
117. Tani, K.; Iseki, A.; Yamagata, T. Efficient transfer hydrogenation of alkynes and alkenes with methanol catalysed by hydrido(methoxo)iridium(III) complexes *Chem. Commun.* **1999**, 1821-1822.
118. Wang, Y.; Huang, Z.; Huang, Z. Catalyst as colour indicator for endpoint detection to enable selective alkyne trans-hydrogenation with ethanol *Nature Catalysis* **2019**, *2*, 529-536.
119. Yang, J.; Wang, C.; Sun, Y.; Man, X.; Li, J.; Sun, F. Ligand-controlled iridium-catalyzed semihydrogenation of alkynes with ethanol: highly stereoselective synthesis of *E*- and *Z*-alkenes *Chem. Commun.* **2019**, *55*, 1903-1906.
120. Kaicharla, T.; Zimmermann, B. M.; Oestreich, M.; Teichert, J. F. Using alcohols as simple H(2)-equivalents for copper-catalysed transfer semihydrogenations of alkynes *Chem. Commun.* **2019**, *55*, 13410-13413.
121. Gong, D.; Hu, B.; Yang, W.; Kong, D.; Xia, H.; Chen, D. A Bidentate Ru(II)-NC Complex as a Catalyst for Semihydrogenation of Alkynes to (*E*)-Alkenes with Ethanol *Organometallics* **2020**, *39*, 862-869.
122. Shen, R.; Chen, T.; Zhao, Y.; Qiu, R.; Zhou, Y.; Yin, S.; Wang, X.; Goto, M.; Han, L. B. Facile regio- and stereoselective hydrometalation of alkynes with a combination of carboxylic acids and group 10 transition metal complexes: selective hydrogenation of alkynes with formic acid *J. Am. Chem. Soc.* **2011**, *133*, 17037-44.
123. Wienhofer, G.; Westerhaus, F. A.; Jagadeesh, R. V.; Junge, K.; Junge, H.; Beller, M. Selective iron-catalyzed transfer hydrogenation of terminal alkynes *Chem. Commun.* **2012**, *48*, 4827-9.
124. Richmond, E.; Moran, J. Ligand Control of *E/Z* Selectivity in Nickel-Catalyzed Transfer Hydrogenative Alkyne Semireduction *J Org Chem* **2015**, *80*, 6922-9.

125. Musa, S.; Ghosh, A.; Vaccaro, L.; Ackermann, L.; Gelman, D. Efficient E-Selective Transfer Semihydrogenation of Alkynes by Means of Ligand-Metal Cooperating Ruthenium Catalyst *Adv. Synth. Catal.* **2015**, *357*, 2351-2357.
126. Kusy, R.; Grela, K. E- and Z-Selective Transfer Semihydrogenation of Alkynes Catalyzed by Standard Ruthenium Olefin Metathesis Catalysts *Org Lett* **2016**, *18*, 6196-6199.
127. Schabel, T.; Belger, C.; Plietker, B. A mild chemoselective Ru-catalyzed reduction of alkynes, ketones, and nitro compounds *Org Lett* **2013**, *15*, 2858-61.
128. Shirakawa, E.; Otsuka, H.; Hayashi, T. Reduction of alkynes into 1,2-dideuterioalkenes with hexamethyldisilane and deuterium oxide in the presence of a palladium catalyst *Chem. Commun.* **2005**, 5885-6.
129. Li, J.; Hua, R. Stereodivergent ruthenium-catalyzed transfer semihydrogenation of diaryl alkynes *Chem. Eur. J.* **2011**, *17*, 8462-5.
130. Fu, S.; Chen, N. Y.; Liu, X.; Shao, Z.; Luo, S. P.; Liu, Q. Ligand-Controlled Cobalt-Catalyzed Transfer Hydrogenation of Alkynes: Stereodivergent Synthesis of Z- and E-Alkenes *J. Am. Chem. Soc.* **2016**, *138*, 8588-94.
131. Korytiakova, E.; Thiel, N. O.; Pape, F.; Teichert, J. F. Copper(i)-catalysed transfer hydrogenations with ammonia borane *Chem. Commun.* **2017**, *53*, 732-735.
132. Brzozowska, A.; Azofra, L. M.; Zubar, V.; Atodiresei, I.; Cavallo, L.; Rueping, M.; El-Sepelgy, O. Highly Chemo- and Stereoselective Transfer Semihydrogenation of Alkynes Catalyzed by a Stable, Well-Defined Manganese(II) Complex *ACS Catal.* **2018**, *8*, 4103-4109.
133. Zhou, Y. P.; Mo, Z.; Luecke, M. P.; Driess, M. Stereoselective Transfer Semihydrogenation of Alkynes to E-Olefins with N-Heterocyclic Silylene-Manganese Catalysts *Chem. Eur. J.* **2018**, *24*, 4780-4784.
134. Landge, V. G.; Pitchaimani, J.; Midya, S. P.; Subramanian, M.; Madhu, V.; Balaraman, E. Phosphine-free cobalt pincer complex catalyzed Z-selective semihydrogenation of unbiased alkynes *Catalysis Science & Technology* **2018**, *8*, 428-433.

135. Osborn, J. A.; Jardine, F. H.; Young, J. F.; Wilkinson, G. The preparation and properties of tris(triphenylphosphine)halogenorhodium(I) and some reactions thereof including catalytic homogeneous hydrogenation of olefins and acetylenes and their derivatives *Journal of the Chemical Society A: Inorganic, Physical, Theoretical* **1966**, 1711-1732.
136. Schrock, R. R.; Osborn, J. A. Catalytic hydrogenation using cationic rhodium complexes. II. The selective hydrogenation of alkynes to cis olefins *Journal of the American Chemical Society* **2002**, *98*, 2143-2147.
137. Crabtree, R. H.; Gautier, A.; Giordano, G.; Khan, T. The preparation and some catalytic properties of a number of rhodium(I) diolefin complexes *J. Organomet. Chem.* **1977**, *141*, 113-121.
138. Albers, M. O.; Singleton, E.; Viney, M. M. The homogeneous hydrogenation of alkynes and alkenes catalyzed by the cationic ruthenium(II)-phosphine complex [RuH(dppb)₂]⁺PF₆⁻ *J. Mol. Catal.* **1985**, *33*, 77-82.
139. Albers, M. O.; Singleton, E.; Viney, M. M. The selective homogeneous hydrogenation of alkynes in the presence of alkenes catalyzed by [RuH(PMe₂Ph)₅]⁺PF₆⁻ *J. Mol. Catal.* **1985**, *30*, 213-217.
140. Suarez, T.; Fontal, B. Hydrogenation reactions with RuCl₂(TRIPHOS) *J. Mol. Catal.* **1988**, *45*, 335-344.
141. Blum, Y.; Czarkie, D.; Rahamim, Y.; Shvo, Y. (Cyclopentadienone)ruthenium carbonyl complexes - a new class of homogeneous hydrogenation catalysts *Organometallics* **2002**, *4*, 1459-1461.
142. Sodeoka, M.; Shibasaki, M. New functions of (arene)tricarbonylchromium(0) complexes as hydrogenation catalysts: stereospecific semihydrogenation of alkynes and highly chemoselective hydrogenation of .alpha.,.beta.-unsaturated carbonyl compounds *The Journal of Organic Chemistry* **2002**, *50*, 1147-1149.
143. Sodeoka, M.; Shibasaki, M. Arene Chromium Tricarbonyl Catalyzed Reactions in Organic Synthesis *Synthesis* **1993**, *1993*, 643-658.
144. van Laren, M. W.; Elsevier, C. J. Selective Homogeneous Palladium(0)-Catalyzed Hydrogenation of Alkynes to (Z)-Alkenes *Angew. Chem. Int. Ed.* **1999**, *38*, 3715-3717.

145. van Laren, M. W.; Duin, M. A.; Klerk, C.; Naglia, M.; Rogolino, D.; Pelagatti, P.; Bacchi, A.; Pelizzi, C.; Elsevier, C. J. Palladium(0) Complexes with Unsymmetric Bidentate Nitrogen Ligands for the Stereoselective Hydrogenation of 1-Phenyl-1-propyne to (Z)-1-Phenyl-1-propene *Organometallics* **2002**, *21*, 1546-1553.
146. Costa, M.; Pelagatti, P.; Pelizzi, C.; Rogolino, D. Catalytic activity of palladium(II) complexes with tridentate nitrogen ligands in the hydrogenation of alkenes and alkynes *J. Mol. Catal. A: Chem.* **2002**, *178*, 21-26.
147. Kluwer, A. M.; Koblenz, T. S.; Jonischkeit, T.; Woelk, K.; Elsevier, C. J. Kinetic and spectroscopic studies of the [palladium(Ar-bian)]-catalyzed semi-hydrogenation of 4-octyne *J. Am. Chem. Soc.* **2005**, *127*, 15470-80.
148. La Pierre, H. S.; Arnold, J.; Toste, F. D. Z-selective semihydrogenation of alkynes catalyzed by a cationic vanadium bisimido complex *Angew. Chem. Int. Ed.* **2011**, *50*, 3900-3.
149. Wakamatsu, T.; Nagao, K.; Ohmiya, H.; Sawamura, M. Copper-Catalyzed Semihydrogenation of Internal Alkynes with Molecular Hydrogen *Organometallics* **2016**, *35*, 1354-1357.
150. Tseng, K. N.; Kampf, J. W.; Szymczak, N. K. Modular Attachment of Appended Boron Lewis Acids to a Ruthenium Pincer Catalyst: Metal-Ligand Cooperativity Enables Selective Alkyne Hydrogenation *J. Am. Chem. Soc.* **2016**, *138*, 10378-81.
151. Chen, C.; Huang, Y.; Zhang, Z.; Dong, X.-Q.; Zhang, X. Cobalt-catalyzed (Z)-selective semihydrogenation of alkynes with molecular hydrogen *Chem. Commun.* **2017**, *53*, 4612-4615.
152. Gorgas, N.; Brunig, J.; Stoger, B.; Vanicek, S.; Tilset, M.; Veiros, L. F.; Kirchner, K. Efficient Z-Selective Semihydrogenation of Internal Alkynes Catalyzed by Cationic Iron(II) Hydride Complexes *J. Am. Chem. Soc.* **2019**, *141*, 17452-17458.
153. Alawisi, H.; Arman, H. D.; Tonzetich, Z. J. Catalytic Hydrogenation of Alkenes and Alkynes by a Cobalt Pincer Complex: Evidence of Roles for Both Co(I) and Co(II) *Organometallics* **2021**, *40*, 1062-1070.

154. Garbe, M.; Budweg, S.; Papa, V.; Wei, Z.; Hornke, H.; Bachmann, S.; Scalone, M.; Spannenberg, A.; Jiao, H.; Junge, K.; Beller, M. Chemoselective semihydrogenation of alkynes catalyzed by manganese(i)-PNP pincer complexes *Catalysis Science & Technology* **2020**, *10*, 3994-4001.
155. Pasto, D. J., Reductions of C=C and C≡C by Noncatalytic Chemical Methods. In *Comprehensive Organic Synthesis*, Trost, B. M.; Fleming, I., Eds. Pergamon Press: Oxford, U.K., 1991; Vol. 8, pp 471-488.
156. Liu, Y.; Hu, L.; Chen, H.; Du, H. An alkene-promoted borane-catalyzed highly stereoselective hydrogenation of alkynes to give Z- and E-alkenes *Chem. Eur. J.* **2015**, *21*, 3495-501.
157. Furukawa, S.; Yokoyama, A.; Komatsu, T. Efficient Catalytic System for Synthesis of *trans*-Stilbene from Diphenylacetylene Using Rh-Based Intermetallic Compounds *ACS Catal.* **2014**, *4*, 3581-3585.
158. Furukawa, S.; Komatsu, T. Selective Hydrogenation of Functionalized Alkynes to (*E*)-Alkenes, Using Ordered Alloys as Catalysts *ACS Catal.* **2016**, *6*, 2121-2125.
159. Karunananda, M. K.; Mankad, N. P. *E*-Selective Semi-Hydrogenation of Alkynes by Heterobimetallic Catalysis *J. Am. Chem. Soc.* **2015**, *137*, 14598-601.
160. Schleyer, D.; Niessen, H. G.; Bargon, J. In situ ¹H-PHIP-NMR studies of the stereoselective hydrogenation of alkynes to (*E*)-alkenes catalyzed by a homogeneous [Cp**Ru*]⁺ catalyst *New J. Chem.* **2001**, *25*, 423-426.
161. Neumann, K. T.; Klimczyk, S.; Burhardt, M. N.; Bang-Andersen, B.; Skrydstrup, T.; Lindhardt, A. T. Direct *trans*-Selective Ruthenium-Catalyzed Reduction of Alkynes in Two-Chamber Reactors and Continuous Flow *ACS Catal.* **2016**, *6*, 4710-4714.
162. Yadav, S.; Dutta, I.; Saha, S.; Das, S.; Pati, S. K.; Choudhury, J.; Bera, J. K. An Annelated Mesoionic Carbene (MIC) Based Ru(II) Catalyst for Chemo- and Stereoselective Semihydrogenation of Internal and Terminal Alkynes *Organometallics* **2020**, *39*, 3212-3223.

163. Maazaoui, R.; Abderrahim, R.; Chemla, F.; Ferreira, F.; Perez-Luna, A.; Jackowski, O. Catalytic Chemoselective and Stereoselective Semihydrogenation of Alkynes to E-Alkenes Using the Combination of Pd Catalyst and ZnI(2) *Org Lett* **2018**, *20*, 7544-7549.
164. Higashida, K.; Mashima, K. E-Selective Semi-hydrogenation of Alkynes with Dinuclear Iridium Complexes under Atmospheric Pressure of Hydrogen *Chem. Lett.* **2016**, *45*, 866-868.
165. Radkowski, K.; Sundararaju, B.; Furstner, A. A functional-group-tolerant catalytic trans hydrogenation of alkynes *Angew. Chem. Int. Ed.* **2013**, *52*, 355-60.
166. Leutzsch, M.; Wolf, L. M.; Gupta, P.; Fuchs, M.; Thiel, W.; Fares, C.; Furstner, A. Formation of ruthenium carbenes by gem-hydrogen transfer to internal alkynes: implications for alkyne trans-hydrogenation *Angew. Chem. Int. Ed.* **2015**, *54*, 12431-6.
167. Guthertz, A.; Leutzsch, M.; Wolf, L. M.; Gupta, P.; Rummelt, S. M.; Goddard, R.; Fares, C.; Thiel, W.; Furstner, A. Half-Sandwich Ruthenium Carbene Complexes Link *trans*-Hydrogenation and *gem*-Hydrogenation of Internal Alkynes *J. Am. Chem. Soc.* **2018**, *140*, 3156-3169.
168. Biberger, T.; Gordon, C. P.; Leutzsch, M.; Peil, S.; Guthertz, A.; Coperet, C.; Furstner, A. Alkyne *gem*-Hydrogenation: Formation of Pianostool Ruthenium Carbene Complexes and Analysis of Their Chemical Character *Angew. Chem. Int. Ed.* **2019**, *58*, 8845-8850.
169. Bullock, R. M. Chemistry. Abundant metals give precious hydrogenation performance *Science* **2013**, *342*, 1054-5.
170. Ludwig, J. R.; Schindler, C. S. Catalyst: Sustainable Catalysis *Chem-Us* **2017**, *2*, 313-316.
171. Zweig, J. E.; Kim, D. E.; Newhouse, T. R. Methods Utilizing First-Row Transition Metals in Natural Product Total Synthesis *Chem. Rev.* **2017**, *117*, 11680-11752.
172. Hayler, J. D.; Leahy, D. K.; Simmons, E. M. A Pharmaceutical Industry Perspective on Sustainable Metal Catalysis *Organometallics* **2018**, *38*, 36-46.

173. Srimani, D.; Diskin-Posner, Y.; Ben-David, Y.; Milstein, D. Iron pincer complex catalyzed, environmentally benign, E-selective semi-hydrogenation of alkynes *Angew. Chem. Int. Ed.* **2013**, *52*, 14131-4.
174. Gramigna, K. M.; Dickie, D. A.; Foxman, B. M.; Thomas, C. M. Cooperative H₂ Activation across a Metal–Metal Multiple Bond and Hydrogenation Reactions Catalyzed by a Zr/Co Heterobimetallic Complex *ACS Catal.* **2019**, *9*, 3153-3164.
175. Angulo, I. M.; Kluwer, A. M.; Bouwman, E. Fast and selective homogeneous hydrogenation with nickel(II) phosphane catalysts *Chem. Commun.* **1998**, 2689-2690.
176. Angulo, I. M.; Bouwman, E. Kinetics of the hydrogenation of 1-octene catalyzed by
by
[Ni(o-MeO-dppp)(OAc)₂] *J. Mol. Catal. A: Chem.* **2001**, *175*, 65-72.
177. Angulo, I. M.; Bouwman, E.; Lutz, M.; Mul, W. P.; Spek, A. L. Autoionization of homogeneous nickel(II) diphosphane hydrogenation catalysts. An NMR study and crystal structures of [Ni(o-MeO-dppe)I₂] and [Ni(o-MeO-dppe)I₂](PF₆)₂ *Inorg. Chem.* **2001**, *40*, 2073-82.
178. Wu, J.; Faller, J. W.; Hazari, N.; Schmeier, T. J. Stoichiometric and Catalytic Reactions of Thermally Stable Nickel(0) NHC Complexes *Organometallics* **2012**, *31*, 806-809.
179. Mooibroek, T. J.; Wenker, E. C.; Smit, W.; Mutikainen, I.; Lutz, M.; Bouwman, E. Homogeneous hydrogenation and isomerization of 1-octene catalyzed by nickel(II) complexes with bidentate diarylphosphane ligands *Inorg. Chem.* **2013**, *52*, 8190-201.
180. Eberhardt, N. A.; Guan, H. Nickel Hydride Complexes *Chem. Rev.* **2016**, *116*, 8373-426.
181. Zaramello, L.; Albuquerque, B. L.; Domingos, J. B.; Philippot, K. Kinetic investigation into the chemoselective hydrogenation of alpha,beta-unsaturated carbonyl compounds catalyzed by Ni(0) nanoparticles *Dalton Trans.* **2017**, *46*, 5082-5090.
182. Léonard, N. G.; Chirik, P. J. Air-Stable α -Diimine Nickel Precatalysts for the Hydrogenation of Hindered, Unactivated Alkenes *ACS Catal.* **2017**, *8*, 342-348.

183. Maier, T. M.; Sandl, S.; Melzl, P.; Zweck, J.; Jacobi von Wangelin, A.; Wolf, R. Heterogeneous Olefin Hydrogenation Enabled by a Highly-Reduced Nickel(-II) Catalyst Precursor *Chem. Eur. J.* **2020**, *26*, 6113-6117.
184. Murugesan, K.; Bheeter, C. B.; Linnebank, P. R.; Spannenberg, A.; Reek, J. N. H.; Jagadeesh, R. V.; Beller, M. Nickel-Catalyzed Stereodivergent Synthesis of *E*- and *Z*-Alkenes by Hydrogenation of Alkynes *ChemSusChem* **2019**, *12*, 3363-3369.
185. Thiel, N. O.; Kaewmee, B.; Tran Ngoc, T.; Teichert, J. F. A Simple Nickel Catalyst Enabling an *E*-Selective Alkyne Semihydrogenation *Chem. Eur. J.* **2020**, *26*, 1597-1603.
186. Ramirez, B. L.; Lu, C. C. Rare-Earth Supported Nickel Catalysts for Alkyne Semihydrogenation: Chemo- and Regioselectivity Impacted by the Lewis Acidity and Size of the Support *J. Am. Chem. Soc.* **2020**, *142*, 5396-5407.
187. Turculet, L., PSiP Transition-Metal Pincer Complexes: Synthesis, Bond Activation, and Catalysis. In *Pincer and Pincer-Type Complexes: Applications in Organic Synthesis and Catalysis*, Szabó, K. J.; Wendt, O. F., Eds. Wiley-VCH: Weinheim, 2014; pp 149-188.
188. Zhang, P.; Li, X.; Qi, X.; Sun, H.; Fuhr, O.; Fenske, D. Transfer hydrogenation of aldehydes catalyzed by silyl hydrido iron complexes bearing a [PSiP] pincer ligand *Rsc Adv* **2018**, *8*, 14092-14099.
189. Wang, Y.; Zhang, H.; Xie, S.; Sun, H.; Li, X.; Fuhr, O.; Fenske, D. An Air-Stable N-Heterocyclic [PSiP] Pincer Iron Hydride and an Analogous Nitrogen Iron Hydride: Synthesis and Catalytic Dehydration of Primary Amides to Nitriles *Organometallics* **2020**, *39*, 824-833.
190. Charboneau, D. J.; Balcells, D.; Hazari, N.; Lant, H. M. C.; Mayer, J. M.; Melvin, P. R.; Mercado, B. Q.; Morris, W. D.; Repisky, M.; Suh, H. W. Dinitrogen-Facilitated Reversible Formation of a Si-H Bond in a Pincer-Supported Ni Complex *Organometallics* **2016**, *35*, 3154-3162.
191. Mavridis, A.; Moustakali-Mavridis, I. A reinvestigation of tolane *Acta Crystallographica Section B Structural Crystallography and Crystal Chemistry* **1977**, *33*, 3612-3615.

192. Seo, C. S. G.; Morris, R. H. Catalytic Homogeneous Asymmetric Hydrogenation: Successes and Opportunities *Organometallics* **2018**, *38*, 47-65.
193. Lu, P.; Wang, H.; Mao, Y.; Hong, X.; Lu, Z. Cobalt-Catalyzed Enantioconvergent Hydrogenation of Minimally Functionalized Isomeric Olefins *J. Am. Chem. Soc.* **2022**, *144*, 17359-17364.
194. Mendelsohn, L. N.; Pavlovic, L.; Zhong, H.; Friedfeld, M. R.; Shevlin, M.; Hopmann, K. H.; Chirik, P. J. Mechanistic Investigations of the Asymmetric Hydrogenation of Enamides with Neutral Bis(phosphine) Cobalt Precatalysts *J. Am. Chem. Soc.* **2022**, *144*, 15764-15778.
195. Pavlovic, L.; Mendelsohn, L. N.; Zhong, H.; Chirik, P. J.; Hopmann, K. H. Cobalt-Catalyzed Asymmetric Hydrogenation of Enamides: Insights into Mechanisms and Solvent Effects *Organometallics* **2022**, *41*, 1872-1882.
196. Xiao, G.; Xie, C.; Guo, Q.; Zi, G.; Hou, G.; Huang, Y. Nickel-Catalyzed Asymmetric Hydrogenation of gamma-Keto Acids, Esters, and Amides to Chiral gamma-Lactones and gamma-Hydroxy Acid Derivatives *Org Lett* **2022**, *24*, 2722-2727.
197. Vineyard, B. D.; Knowles, W. S.; Sabacky, M. J.; Bachman, G. L.; Weinkauff, D. J. Asymmetric hydrogenation. Rhodium chiral bisphosphine catalyst *Journal of the American Chemical Society* **2002**, *99*, 5946-5952.
198. Knowles, W. S.; Sabacky, M. J.; Vineyard, B. D.; Weinkauff, D. J. Asymmetric hydrogenation with a complex of rhodium and a chiral bisphosphine *Journal of the American Chemical Society* **2002**, *97*, 2567-2568.
199. Hoge, G.; Wu, H. P.; Kissel, W. S.; Pflum, D. A.; Greene, D. J.; Bao, J. Highly selective asymmetric hydrogenation using a three hindered quadrant bisphosphine rhodium catalyst *J. Am. Chem. Soc.* **2004**, *126*, 5966-7.
200. Burk, M. J.; De Koning, P. D.; Grote, T. M.; Hoekstra, M. S.; Hoge, G.; Jennings, R. A.; Kissel, W. S.; Le, T. V.; Lennon, I. C.; Mulhern, T. A.; Ramsden, J. A.; Wade, R. A. An enantioselective synthesis of (S)-(+)-3-aminomethyl-5-methylhexanoic acid via asymmetric hydrogenation *J Org Chem* **2003**, *68*, 5731-4.

201. Morrison, K. M.; McGuire, R. T.; Ferguson, M. J.; Stradiotto, M. CgPhen-DalPhos Enables the Nickel-Catalyzed O-Arylation of Tertiary Alcohols with (Hetero)Aryl Electrophiles *ACS Catal.* **2021**, *11*, 10878-10884.
202. Chen, J.; Chen, C.; Ji, C.; Lu, Z. Cobalt-Catalyzed Asymmetric Hydrogenation of 1,1-Diarylethenes *Org Lett* **2016**, *18*, 1594-7.
203. Fernandez-Perez, H.; Etayo, P.; Panossian, A.; Vidal-Ferran, A. Phosphine-phosphinite and phosphine-phosphite ligands: preparation and applications in asymmetric catalysis *Chem. Rev.* **2011**, *111*, 2119-76.
204. Tamura, K.; Sugiya, M.; Yoshida, K.; Yanagisawa, A.; Imamoto, T. Enantiopure 1,2-bis(tert-butylmethylphosphino)benzene as a highly efficient ligand in rhodium-catalyzed asymmetric hydrogenation *Org Lett* **2010**, *12*, 4400-3.
205. van den Berg, M.; Minnaard, A. J.; Haak, R. M.; Leeman, M.; Schudde, E. P.; Meetsma, A.; Feringa, B. L.; de Vries, A. H. M.; Maljaars, C. E. P.; Willans, C. E.; Hyett, D.; Boogers, J. A. F.; Henderickx, H. J. W.; de Vries, J. G. Monodentate Phosphoramidites: A Breakthrough in Rhodium-Catalysed Asymmetric Hydrogenation of Olefins *Adv. Synth. Catal.* **2003**, *345*, 308-323.
206. Detellier, C.; Gelbard, G.; Kagan, H. B. Asymmetric catalysis with chiral complexes of rhodium-O-isopropylidene-2,3-dihydroxy-1,4-bis(diphenylphosphino)butane. 6. On the mechanism of reduction of (E,Z)- α -acylaminoacinnamic acids with homogeneous rhodium catalysts *Journal of the American Chemical Society* **2002**, *100*, 7556-7561.
207. Koenig, K. E.; Knowles, W. S. Use of deuterium to investigate E-Z isomerizations during rhodium-catalyzed reduction. Asymmetric induction and mechanistic implications *Journal of the American Chemical Society* **2002**, *100*, 7561-7564.
208. Wong, H. N. C.; Xu, Z. L.; Chang, H. M.; Lee, C. M. A Modified Synthesis of (\pm)- β -Aryllactic acids *Synthesis* **1992**, *1992*, 793-797.
209. Hoyt, J. M.; Shevlin, M.; Margulieux, G. W.; Krska, S. W.; Tudge, M. T.; Chirik, P. J. Synthesis and Hydrogenation Activity of Iron Dialkyl Complexes with Chiral Bidentate Phosphines *Organometallics* **2014**, *33*, 5781-5790.
210. Guo, S.; Wang, X.; Zhou, J. S. Asymmetric Umpolung Hydrogenation and Deuteration of Alkenes Catalyzed by Nickel *Org Lett* **2020**, *22*, 1204-1207.

211. Imamoto, T.; Tamura, K.; Zhang, Z.; Horiuchi, Y.; Sugiya, M.; Yoshida, K.; Yanagisawa, A.; Gridnev, I. D. Rigid P-chiral phosphine ligands with tert-butylmethylphosphino groups for rhodium-catalyzed asymmetric hydrogenation of functionalized alkenes *J. Am. Chem. Soc.* **2012**, *134*, 1754-69.
212. Salomo, E.; Prades, A.; Riera, A.; Verdaguer, X. Dialkylammonium tert-Butylmethylphosphinites: Stable Intermediates for the Synthesis of P-Stereogenic Ligands *J Org Chem* **2017**, *82*, 7065-7069.
213. Verdaguer, X.; Riera, A.; Salomó, E.; Orgué, S. Efficient Preparation of (S)- and (R)-tert-Butylmethylphosphine–Borane: A Novel Entry to Important P-Stereogenic Ligands *Synthesis* **2016**, *48*, 2659-2663.
214. Lundrigan, T.; Welsh, E. N.; Hynes, T.; Tien, C. H.; Adams, M. R.; Roy, K. R.; Robertson, K. N.; Speed, A. W. H. Enantioselective Imine Reduction Catalyzed by Phosphenium Ions *J. Am. Chem. Soc.* **2019**, *141*, 14083-14088.
215. Adams, M. R.; Tien, C. H.; McDonald, R.; Speed, A. W. H. Asymmetric Imine Hydroboration Catalyzed by Chiral Diazaphospholenes *Angew. Chem. Int. Ed.* **2017**, *56*, 16660-16663.
216. Gatién, A. V.; Lavoie, C. M.; Bennett, R. N.; Ferguson, M. J.; McDonald, R.; Johnson, E. R.; Speed, A. W. H.; Stradiotto, M. Application of Diazaphospholidine/Diazaphospholene-Based Bisphosphines in Room-Temperature Nickel-Catalyzed C(sp²)-N Cross-Couplings of Primary Alkylamines with (Hetero)aryl Chlorides and Bromides *ACS Catal.* **2018**, *8*, 5328-5339.
217. DeMott, J. C.; Gu, W.; McCulloch, B. J.; Herbert, D. E.; Goshert, M. D.; Walensky, J. R.; Zhou, J.; Ozerov, O. V. Silyl–Silylene Interplay in Cationic PSiP Pincer Complexes of Platinum *Organometallics* **2015**, *34*, 3930-3933.
218. Seebach, D.; Beck, A. K.; Heckel, A. TADDOLs, Their Derivatives, and TADDOL Analogues: Versatile Chiral Auxiliaries *Angew. Chem. Int. Ed.* **2001**, *40*, 92-138.
219. Schmitz, C.; Leitner, W.; Francio, G. Ni-Catalyzed Asymmetric Cycloisomerization of Dienes by Using TADDOL Phosphoramidites *Chem. Eur. J.* **2015**, *21*, 10696-702.

220. Minnaard, A. J.; Feringa, B. L.; Lefort, L.; de Vries, J. G. Asymmetric hydrogenation using monodentate phosphoramidite ligands *Acc Chem Res* **2007**, *40*, 1267-77.
221. Bernsmann, H.; van den Berg, M.; Hoen, R.; Minnaard, A. J.; Mehler, G.; Reetz, M. T.; De Vries, J. G.; Feringa, B. L. PipPhos and MorfPhos: privileged monodentate phosphoramidite ligands for rhodium-catalyzed asymmetric hydrogenation *J Org Chem* **2005**, *70*, 943-51.
222. Khumsubdee, S.; Burgess, K. Comparison Of Asymmetric Hydrogenations Of Unsaturated- Carboxylic Acids And -Esters *ACS Catal* **2013**, *3*, 237-249.
223. Wassenaar, J.; Reek, J. N. Asymmetric hydrogenation of enamides, alpha-enol and alpha-enamido ester phosphonates catalyzed by IndolPhos-Rh complexes *J Org Chem* **2009**, *74*, 8403-6.
224. Wassenaar, J.; van Zutphen, S.; Mora, G.; Le Floch, P.; Siegler, M. A.; Spek, A. L.; Reek, J. N. H. INDOLPhosphole and INDOLPhos Palladium–Allyl Complexes in Asymmetric Allylic Alkylations *Organometallics* **2009**, *28*, 2724-2734.
225. Wassenaar, J.; Kuil, M.; Reek, J. N. H. Asymmetric Synthesis of the Roche Ester and its Derivatives by Rhodium - INDOLPHOS - Catalyzed Hydrogenation *Adv. Synth. Catal.* **2008**, *350*, 1610-1614.
226. Burk, M. J.; Casy, G.; Johnson, N. B. A Three-Step Procedure for Asymmetric Catalytic Reductive Amidation of Ketones *J Org Chem* **1998**, *63*, 6084-6085.
227. Wu, H.; Yang, J.; Peters, B. B. C.; Massaro, L.; Zheng, J.; Andersson, P. G. Asymmetric Full Saturation of Vinylarenes with Cooperative Homogeneous and Heterogeneous Rhodium Catalysis *J. Am. Chem. Soc.* **2021**, *143*, 20377-20383.
228. Eisch, J. J.; Dutta, S. Carbon–Carbon Bond Formation in the Surprising Rearrangement of Diorganylzirconium Dialkoxides: Linear Dimerization of Terminal Olefins *Organometallics* **2005**, *24*, 3355-3358.
229. Espinal-Viguri, M.; Neale, S. E.; Coles, N. T.; Macgregor, S. A.; Webster, R. L. Room Temperature Iron-Catalyzed Transfer Hydrogenation and Regioselective Deuteration of Carbon-Carbon Double Bonds *J. Am. Chem. Soc.* **2019**, *141*, 572-582.

230. Mehta, M.; Holthausen, M. H.; Mallov, I.; Perez, M.; Qu, Z. W.; Grimme, S.; Stephan, D. W. Catalytic Ketone Hydrodeoxygenation Mediated by Highly Electrophilic Phosphonium Cations *Angew. Chem. Int. Ed.* **2015**, *54*, 8250-4.
231. Len, C.; Bruniaux, S.; Luart, D. Continuous-Flow Reductive Alkylation: Synthesis of Bio-based Symmetrical and Disymmetrical Ethers *Synthesis* **2018**, *50*, 1849-1856.
232. Gatto, M.; Belanzoni, P.; Belpassi, L.; Biasiolo, L.; Del Zotto, A.; Tarantelli, F.; Zuccaccia, D. Solvent-, Silver-, and Acid-Free NHC-Au-X Catalyzed Hydration of Alkynes. The Pivotal Role of the Counterion *ACS Catal.* **2016**, *6*, 7363-7376.
233. Ekonomie, A.; Lefevre, G.; Fensterbank, L.; Lacote, E.; Malacria, M.; Ollivier, C.; Jutand, A. Iron-catalyzed reductive radical cyclization of organic halides in the presence of NaBH₄: evidence of an active hydrido iron(I) catalyst *Angew. Chem. Int. Ed.* **2012**, *51*, 6942-6.
234. Tseng, H.-C.; Shen, C.-T.; Matsumoto, K.; Shih, D.-N.; Liu, Y.-H.; Peng, S.-M.; Yamaguchi, S.; Lin, Y.-F.; Chiu, C.-W. [η⁵-Cp*B-Mes]⁺: A Masked Potent Boron Lewis Acid *Organometallics* **2019**, *38*, 4516-4521.
235. Manbeck, G. F.; Lipman, A. J.; Stockland, R. A., Jr.; Freidl, A. L.; Hasler, A. F.; Stone, J. J.; Guzei, I. A. Organosoluble copper clusters as precatalysts for carbon-heteroelement bond-forming reactions: microwave and conventional heating *J Org Chem* **2005**, *70*, 244-50.
236. Rock, C. L.; Groy, T. L.; Trovitch, R. J. Carbonyl and ester C-O bond hydrosilylation using kappa(4)-diimine nickel catalysts *Dalton Trans.* **2018**, *47*, 8807-8816.
237. Kalkhambkar, R. G.; Waters, S. N.; Laali, K. K. Highly efficient synthesis of amides via Ritter chemistry with ionic liquids *Tetrahedron Lett.* **2011**, *52*, 867-871.
238. Battilocchio, C.; Hawkins, J. M.; Ley, S. V. Mild and selective heterogeneous catalytic hydration of nitriles to amides by flowing through manganese dioxide *Org Lett* **2014**, *16*, 1060-3.

239. Sunada, Y.; Ogushi, H.; Yamamoto, T.; Uto, S.; Sawano, M.; Tahara, A.; Tanaka, H.; Shiota, Y.; Yoshizawa, K.; Nagashima, H. Disilaruthena- and Ferracyclic Complexes Containing Isocyanide Ligands as Effective Catalysts for Hydrogenation of Unfunctionalized Sterically Hindered Alkenes *J. Am. Chem. Soc.* **2018**, *140*, 4119-4134.

Appendix A: Crystallographic Experimental Details

Table A1. Crystallographic experimental details for **2-1**.

<i>A. Crystal Data</i>	
formula	C ₄₃ H ₆₆ CoO _{0.50} P ₂ Si
formula weight	739.91
crystal dimensions (mm)	0.46 × 0.07 × 0.04
crystal system	triclinic
space group	$P\bar{1}$ (No. 2)
unit cell parameters ^a	
<i>a</i> (Å)	9.8294(2)
<i>b</i> (Å)	10.7259(2)
<i>c</i> (Å)	19.6454(4)
α (deg)	97.7756(9)
β (deg)	91.6804(8)
γ (deg)	99.3174(11)
<i>V</i> (Å ³)	2022.30(7)
<i>Z</i>	2
ρ_{calcd} (g cm ⁻³)	1.215
μ (mm ⁻¹)	4.568
<i>B. Data Collection and Refinement Conditions</i>	
diffractometer	Bruker D8/APEX II CCD ^b
radiation (λ [Å])	Cu K α (1.54178) (microfocus source)
temperature (°C)	-100
scan type	ω and ϕ scans (1.0°) (5 s exposures)
data collection 2θ limit (deg)	148.36
total data collected	14772 ($-12 \leq h \leq 12$, $-13 \leq k \leq 13$, $-24 \leq l \leq 24$)
independent reflections	7918 ($R_{\text{int}} = 0.0305$)
number of observed reflections (<i>NO</i>)	7591 [$F_o^2 \geq 2\sigma(F_o^2)$]
structure solution method	intrinsic phasing (<i>SHELXT-2014</i> ^c)
refinement method	full-matrix least-squares on F^2 (<i>SHELXL-2017</i> ^d)
absorption correction method	Gaussian integration (face-indexed)
range of transmission factors	0.9999–0.3616
data/restraints/parameters	7918 / 28 ^e / 456
goodness-of-fit (<i>S</i>) ^f [all data]	1.045
final <i>R</i> indices ^g	
R_1 [$F_o^2 \geq 2\sigma(F_o^2)$]	0.0415
wR_2 [all data]	0.1131

largest difference peak and hole

0.754 and $-0.691 \text{ e } \text{\AA}^{-3}$

Table A1. Crystallographic experimental details for **2-1**.

^aObtained from least-squares refinement of 9687 reflections with $8.44^\circ < 2\theta < 147.90^\circ$.

^bPrograms for diffractometer operation, data collection, data reduction and absorption correction were those supplied by Bruker.

^cSheldrick, G. M. *Acta Crystallogr.* **2015**, *A71*, 3–8. (*SHELXT-2014*)

^dSheldrick, G. M. *Acta Crystallogr.* **2015**, *C71*, 3–8. (*SHELXL-2017*)

^eThe following distance restraints were applied to the inversion disordered solvent diethylether molecule: 1.43(1) Å O1S–C1S, O1S–C3S; 1.53(1) Å C1S–C2S, C3S–C4S; 2.42(2) Å O1S⋯C2S, O1S⋯C4S; 2.34(2) Å C1S⋯C3S. Additionally, the anisotropic displacement parameters for the atoms of the solvent molecule were restrained by use of the *SHELXL RIGU* instruction.

$$fS = [\Sigma w(F_o^2 - F_c^2)^2 / (n - p)]^{1/2} \quad (n = \text{number of data}; p = \text{number of parameters varied}; w = [\sigma^2(F_o^2) + (0.0839P)^2 + 0.1961P]^{-1} \text{ where } P = [\text{Max}(F_o^2, 0) + 2F_c^2]/3).$$

$$gR_1 = \Sigma ||F_o| - |F_c|| / \Sigma |F_o|; wR_2 = [\Sigma w(F_o^2 - F_c^2)^2 / \Sigma w(F_o^4)]^{1/2}.$$

Table A2. Crystallographic experimental details for **2-2**.

<i>A. Crystal Data</i>	
formula	C ₅₄ H ₆₈ CoP ₂ Si
formula weight	866.04
crystal dimensions (mm)	0.22 × 0.17 × 0.12
crystal system	triclinic
space group	<i>P</i> $\bar{1}$ (No. 2)]
unit cell parameters ^a	
<i>a</i> (Å)	9.6285(2)
<i>b</i> (Å)	13.6722(3)
<i>c</i> (Å)	18.5205(4)
α (deg)	101.1811(10)
β (deg)	97.6467(12)
γ (deg)	102.4770(10)
<i>V</i> (Å ³)	2296.04(9)
<i>Z</i>	2
ρ_{calcd} (g cm ⁻³)	1.253
μ (mm ⁻¹)	4.097
<i>B. Data Collection and Refinement Conditions</i>	
diffractometer	Bruker D8/APEX II CCD ^b
radiation (λ [Å])	Cu K α (1.54178) (microfocus source)
temperature (°C)	-100
scan type	ω and ϕ scans (1.0°) (5 s exposures)
data collection 2θ limit (deg)	148.46
total data collected	105925 ($-11 \leq h \leq 12$, $-17 \leq k \leq 17$, $-23 \leq l \leq$
23)	
independent reflections	8953 ($R_{\text{int}} = 0.0412$)
number of observed reflections (<i>NO</i>)	8699 [$F_o^2 \geq 2\sigma(F_o^2)$]
structure solution method	intrinsic phasing (<i>SHELXT-2014</i> ^c)
refinement method	full-matrix least-squares on F^2 (<i>SHELXL-</i>
<i>2017</i> ^d)	
absorption correction method	multi-scan (<i>SADABS</i>)
range of transmission factors	0.7481–0.5396
data/restraints/parameters	8953 / 0 / 523
goodness-of-fit (<i>S</i>) ^e [all data]	1.074
final <i>R</i> indices ^f	
R_1 [$F_o^2 \geq 2\sigma(F_o^2)$]	0.0270
wR_2 [all data]	0.0745
largest difference peak and hole	0.243 and -0.348 e Å ⁻³

Table A2. Crystallographic experimental details for **2-2** (continued).

^aObtained from least-squares refinement of 9842 reflections with $4.94^\circ < 2\theta < 147.68^\circ$.

^bPrograms for diffractometer operation, data collection, data reduction and absorption correction were those supplied by Bruker.

^cSheldrick, G. M. *Acta Crystallogr.* **2015**, *A71*, 3–8. (*SHELXT-2014*)

^dSheldrick, G. M. *Acta Crystallogr.* **2015**, *C71*, 3–8. (*SHELXL-2017*)

^e $S = [\sum w(F_o^2 - F_c^2)^2 / (n - p)]^{1/2}$ (n = number of data; p = number of parameters varied; $w = [\sigma^2(F_o^2) + (0.0453P)^2 + 0.4287P]^{-1}$ where $P = [\text{Max}(F_o^2, 0) + 2F_c^2]/3$).

^f $R_1 = \sum ||F_o| - |F_c|| / \sum |F_o|$; $wR_2 = [\sum w(F_o^2 - F_c^2)^2 / \sum w(F_o^4)]^{1/2}$.

Table A1. Crystallographic experimental details for **3-1**.

<i>A. Crystal Data</i>	
formula	C _{47.50} H ₆₂ N ₂ NiP ₂ Si
formula weight	809.73
crystal dimensions (mm)	0.15 × 0.10 × 0.06
crystal system	monoclinic
space group	<i>C2/c</i> (No. 15)
unit cell parameters ^a	
<i>a</i> (Å)	44.6555(10)
<i>b</i> (Å)	13.3640(3)
<i>c</i> (Å)	14.6990(3)
β (deg)	95.8471(9)
<i>V</i> (Å ³)	8726.4(3)
<i>Z</i>	8
ρ_{calcd} (g cm ⁻³)	1.233
μ (mm ⁻¹)	1.847
<i>B. Data Collection and Refinement Conditions</i>	
diffractometer	Bruker D8/APEX II CCD ^b
radiation (λ [Å])	Cu K α (1.54178) (microfocus source)
temperature (°C)	-100
scan type	ω and ϕ scans (1.0°) (5 s exposures)
data collection 2θ limit (deg)	144.72
total data collected	191173 ($-55 \leq h \leq 55$, $-16 \leq k \leq 16$, $-18 \leq l \leq 18$)
independent reflections	8624 ($R_{\text{int}} = 0.0395$)
number of observed reflections (<i>NO</i>)	8018 [$F_o^2 \geq 2\sigma(F_o^2)$]
structure solution method	intrinsic phasing (<i>SHELXT-2014</i> ^c)
refinement method	full-matrix least-squares on F^2 (<i>SHELXL-2018</i> ^d)
absorption correction method	Gaussian integration (face-indexed)
range of transmission factors	0.9377–0.7080
data/restraints/parameters	8624 / 30 ^e / 508
goodness-of-fit (S) ^f [all data]	1.033
final <i>R</i> indices ^g	
R_1 [$F_o^2 \geq 2\sigma(F_o^2)$]	0.0313
wR_2 [all data]	0.0881
largest difference peak and hole	0.302 and -0.323 e Å ⁻³

Table A1. Crystallographic experimental details for **3-1** (continued)

^aObtained from least-squares refinement of 9708 reflections with $7.96^\circ < 2\theta < 144.54^\circ$.

^bPrograms for diffractometer operation, data collection, data reduction and absorption correction were those supplied by Bruker.

^cSheldrick, G. M. *Acta Crystallogr.* **2015**, *A71*, 3–8. (*SHELXT-2014*)

^dSheldrick, G. M. *Acta Crystallogr.* **2015**, *C71*, 3–8. (*SHELXL-2018/3*)

^eThe C–C distances within the inversion disordered solvent pentane molecule were restrained to be approximately the same by use of the *SHELXL SADI* instruction; the C···C distances were similarly restrained. Additionally, the anisotropic displacement parameters for the carbon atoms of the pentane molecule were restrained by use of the rigid-bond restraint **RIGU**.

$fS = [\sum w(F_o^2 - F_c^2)^2 / (n - p)]^{1/2}$ (n = number of data; p = number of parameters varied; $w = [\sigma^2(F_o^2) + (0.0434P)^2 + 8.0340P]^{-1}$ where $P = [\text{Max}(F_o^2, 0) + 2F_c^2]/3$).

$gR_1 = \sum ||F_o| - |F_c|| / \sum |F_o|$; $wR_2 = [\sum w(F_o^2 - F_c^2)^2 / \sum w(F_o^4)]^{1/2}$.

Table A3. Crystal data and structure refinement for **L4-1**.

Empirical formula	C ₄₂ H ₄₆ O ₂ P ₂	
Formula weight	644.73	
Temperature	150(2) K	
Wavelength	1.54178 Å	
Crystal system	Orthorhombic	
Space group	<i>P</i> 2 ₁ 2 ₁ 2 ₁	
Unit cell dimensions	<i>a</i> = 8.9608(4) Å	$\alpha = 90^\circ$
	<i>b</i> = 17.0401(7) Å	$\beta = 90^\circ$
	<i>c</i> = 23.7511(9) Å	$\gamma = 90^\circ$
Volume	3626.6(2) Å ³	
<i>Z</i>	4	
Density (calculated)	1.181 Mg/m ³	
Absorption coefficient	1.343 mm ⁻¹	
F(000)	1376	
Crystal size	0.203 x 0.025 x 0.025 mm ³	
Theta range for data collection	3.192 to 68.205°	
Index ranges	-10 ≤ <i>h</i> ≤ 10, -20 ≤ <i>k</i> ≤ 20, -28 ≤ <i>l</i> ≤ 28	
Reflections collected	41010	
Independent reflections	6634 [R(int) = 0.2054]	
Completeness to theta = 67.679°	99.9 %	
Absorption correction	Semi-empirical from equivalents	
Max. and min. transmission	0.7538 and 0.5118	
Refinement method	Full-matrix least-squares on F ²	
Data / restraints / parameters	6634 / 0 / 426	
Goodness-of-fit on F ²	1.030	
Final R indices [I > 2σ(I)]	R1 = 0.0630, wR2 = 0.1481	
R indices (all data)	R1 = 0.0941, wR2 = 0.1708	
Absolute structure parameter	0.05(2)	
Extinction coefficient	0.0031(4)	
Largest diff. peak and hole	0.375 and -0.398 e.Å ⁻³	

The crystal chosen was attached to the tip of a MicroLoop with Paratone-N oil.

Measurements were made on a Bruker D8 VENTURE diffractometer equipped with a

PHOTON III CMOS detector using monochromated Cu K α radiation ($\lambda = 1.54178 \text{ \AA}$) from an Incoatec micro-focus sealed tube at 125 K. The initial orientation and unit cell were indexed using a least-squares analysis of the reflections collected from a 180° phi-scan, 10 seconds per frame and 1° per frame. For data collection, a strategy was calculated to maximize data completeness and multiplicity, in a reasonable amount of time, and then implemented using the Bruker Apex 3 software suite. The crystal to detector distance was set to 4.0 cm and 60 second frames were collected. Cell refinement and data reduction were performed with the Bruker SAINT software, which corrects for beam inhomogeneity, possible crystal decay, Lorentz and polarisation effects. A multi-scan absorption correction was applied (SADABS). The structure was solved using SHELXT-2014 and was refined using a full-matrix least-squares method on F^2 with SHELXL-2018. The non-hydrogen atoms were refined anisotropically. The hydrogen atoms bonded to carbon were included at geometrically idealized positions and were not refined. The isotropic thermal parameters of these hydrogen atoms were fixed at $1.2U_{\text{eq}}$ of the parent carbon atom or $1.5U_{\text{eq}}$ for methyl hydrogens.

An extinction parameter was refined and gave a final value of 0.0032(5).

Data was collected to a maximum θ angle of 74.63° (0.80 \AA resolution). The data was cut off at a resolution of 0.83 \AA (68.21°) using a SHEL instruction during the refinement.

The crystals of this sample were very tiny rods that grew together in fan-shaped clumps. The small size of the crystal made it difficult to center for analysis in the X-ray beam and long frame times had to be used to collect the data to the resolution chosen. Even so the data were weak which resulted in R_{int} (merging R) being larger than normal (0.205) and created a level B alert that could not be resolved in the final checkcif file.

The molecule was found to crystallize in the chiral space group $P2_12_12_1$. The absolute structure was reliably determined. Using the program Platon the refined structure was calculated to have a Hooft parameter of 0.06(2). This value agrees with the Parson's value calculated by the program SHELXL, 0.06(2) from 1534 selected quotients, and with the similarly calculated Flack parameter of 0.05(4).

Table A4. Crystal data and structure refinement for **4-2**.

Empirical formula	$C_{50}H_{68}CoO_2P_2Si_2$	
Formula weight	878.09	
Temperature	125(2) K	
Wavelength	0.71073 Å	
Crystal system	Orthorhombic	
Space group	$P2_12_12_1$	
Unit cell dimensions	$a = 13.0270(6)$ Å	$\alpha = 90^\circ$
	$b = 14.3814(6)$ Å	$\beta = 90^\circ$
	$c = 26.0220(9)$ Å	$\gamma = 90^\circ$
Volume	$4875.1(3)$ Å ³	
Z	4	
Density (calculated)	1.196 Mg/m ³	
Absorption coefficient	0.503 mm ⁻¹	
F(000)	1876	
Crystal size	0.091 x 0.067 x 0.058 mm ³	
Theta range for data collection	1.618 to 28.280°	
Index ranges	$-17 \leq h \leq 17$, $-19 \leq k \leq 19$, $-34 \leq l \leq 34$	
Reflections collected	75827	
Independent reflections	12095 [R(int) = 0.1092]	
Completeness to theta = 25.242°	100.0 %	
Absorption correction	Semi-empirical from equivalents	
Max. and min. transmission	0.7461 and 0.5921	
Refinement method	Full-matrix least-squares on F ²	
Data / restraints / parameters	12095 / 0 / 530	
Goodness-of-fit on F ²	1.052	
Final R indices [$I > 2\sigma(I)$]	R1 = 0.0629, wR2 = 0.1494	
R indices (all data)	R1 = 0.0954, wR2 = 0.1677	
Absolute structure parameter	0.021(9)	
Extinction coefficient	n/a	
Largest diff. peak and hole	0.773 and -0.601 e.Å ⁻³	

The crystal chosen was attached to the tip of a MicroLoop with paratone-N oil.

Measurements were made on a Bruker D8 VENTURE diffractometer equipped with a

PHOTON III CMOS detector using monochromated Mo $K\alpha$ radiation ($\lambda = 0.71073 \text{ \AA}$) from an Incoatec microfocus sealed tube at 125 K. The initial orientation and unit cell were indexed using a least-squares analysis of the reflections collected from a complete 180° phi-scan, 10 seconds per frame and 1° per frame. For data collection, a strategy was calculated to maximize data completeness and multiplicity, in a reasonable amount of time, and then implemented using the Bruker Apex 3 software suite. The data were collected with 60 sec frame times and the crystal to detector distance was set to 5 cm. Cell refinement and data reduction were performed with the Bruker SAINT software, which corrects for beam inhomogeneity, possible crystal decay, Lorentz and polarisation effects. A multi-scan absorption correction was applied (SADABS). The structure was solved using SHELXT-2014 and was refined using a full-matrix least-squares method on F^2 with SHELXL-2018. The refinement was unremarkable. The non-hydrogen atoms were refined anisotropically. The hydrogen atoms bonded to carbon were included at geometrically idealized positions and were not refined. The isotropic thermal parameters of these hydrogen atoms were fixed at $1.2U_{\text{eq}}$ of the parent carbon atom or $1.5U_{\text{eq}}$ for methyl hydrogens.

Data was integrated to a maximum resolution of 0.70 \AA . However, during the final refinement a SHEL instruction was used to limit the resolution to 0.75 \AA ($\theta_{\text{max}} = 28.3^\circ$). The largest peak in the final Fourier difference map (0.77 e\AA^{-3}) suggested that C44 might be disordered and need to be split. However, no model could be found that improved the overall results by doing so.

The molecule was found to crystallize in the chiral space group $P2_12_12_1$. The absolute structure of the molecule was reliably determined. Using the program Platon the refined structure was calculated to have a Hooft parameter of 0.010(9). This value agrees with the Parson's value calculated by the program SHELXL, 0.021(9) from 3084 selected quotients.

Table A5. Crystal data and structure refinement for **4-3**.

Empirical formula	C ₈₄ H ₇₂ BCoF ₂₄ O ₃ P ₂	
Formula weight	1717.09	
Temperature	150(2) K	
Wavelength	0.71073 Å	
Crystal system	Monoclinic	
Space group	P2 ₁	
Unit cell dimensions	$a = 13.4622(10) \text{ \AA}$	$\alpha = 90^\circ$
	$b = 17.2624(13) \text{ \AA}$	$\beta = 100.806(2)^\circ$
	$c = 17.5264(12) \text{ \AA}$	$\gamma = 90^\circ$
Volume	4000.7(5) Å ³	
Z	2	
Density (calculated)	1.425 Mg/m ³	
Absorption coefficient	0.359 mm ⁻¹	
F(000)	1756	
Crystal size	0.124 x 0.105 x 0.041 mm ³	
Theta range for data collection	2.111 to 26.367°	
Index ranges	-16 ≤ h ≤ 16, -21 ≤ k ≤ 21, -21 ≤ l ≤ 21	
Reflections collected	31583	
Independent reflections	16315 [R(int) = 0.0426]	
Completeness to theta = 25.242°	99.9 %	
Absorption correction	Semi-empirical from equivalents	
Max. and min. transmission	0.7454 and 0.6661	
Refinement method	Full-matrix least-squares on F ²	
Data / restraints / parameters	16315 / 2329 / 1390	
Goodness-of-fit on F ²	1.034	
Final R indices [I > 2σ(I)]	R1 = 0.0454, wR2 = 0.0945	
R indices (all data)	R1 = 0.0566, wR2 = 0.0988	
Absolute structure parameter	0.039(14)	
Extinction coefficient	n/a	
Largest diff. peak and hole	0.322 and -0.305 e.Å ⁻³	

The crystal chosen was attached to the tip of a MicroLoop with paratone-N oil.

Measurements were made on a Bruker D8 VENTURE diffractometer equipped with a

PHOTON III CMOS detector using monochromated Mo $K\alpha$ radiation ($\lambda = 0.71073 \text{ \AA}$) from an Incoatec microfocus sealed tube at 150 K. The initial orientation and unit cell were indexed using a least-squares analysis of the reflections collected from a complete 180° phi-scan, 3 seconds per frame and 1° per frame. For data collection, a strategy was calculated to maximize data completeness and multiplicity, in a reasonable amount of time, and then implemented using the Bruker Apex 3 software suite. The data were collected with 30 sec frame times and the crystal to detector distance was set to 4 cm. Cell refinement and data reduction were performed with the Bruker SAINT software, which corrects for beam inhomogeneity, possible crystal decay, and Lorentz and polarisation effects. A multi-scan absorption correction was applied (TWINABS). The structure was solved using SHELXT-2014 and was refined using a full-matrix least-squares method on F^2 with SHELXL-2018. The refinement was unremarkable. The non-hydrogen atoms were refined anisotropically. The hydrogen atoms bonded to carbon were included at geometrically idealized positions and were not refined. The isotropic thermal parameters of these hydrogen atoms were fixed at $1.2U_{\text{eq}}$ of the parent carbon atom or $1.5U_{\text{eq}}$ for methyl hydrogens.

The only crystal in the sample deemed large enough for analysis was observed to be an aggregate of several smaller components when viewed under the microscope. It was treated as a three-component twin (as determined using Cell Now on the original unit cell data) throughout the final data collection and processing. Refinement of the twin model was carried out using both the hklf4 and hklf5 files generated during the data scaling using TWINABS as implemented in APEX 4. The results were better using the hklf4 data so they

are reported here. In the hklf4 file generation the fractions for the twin components calculated were 0.486, 0.271 and 0.244.

Data was integrated to a maximum resolution of 0.80 Å ($\theta_{max} = 26.37^\circ$). All of this data was included in the refinement. Two reflections (1 1 0 and 1 -1 0) were removed from the final refinement because they were partially obscured by the beam stop resulting in poor agreement between F_{obs}^2 and F_{calc}^2 .

The compound was found to crystallize in the non-centrosymmetric Monoclinic space group, $P2_1$, with 1 independent cation and anion in the asymmetric unit. The CF₃ groups of the anion were disordered (rotating around their respective CC bonds) while the cation was well ordered. The crystal was also found to contain one molecule of disordered tetrahydrofuran solvate in the asymmetric unit. The P2 center was determined to have S chirality. The Flack parameter, calculated during the refinement, was determined to be 0.039(14), while the Hooft parameter calculated using the program Platon was found to be 0.028(5). Both values suggest that the correct absolute configuration has been chosen.

All of the CF₃ groups in the anion were found to be disordered, which was modelled using 2 or 3 parts depending on the amount of residual motion in each particular group. Only the fluorine atoms were split and their occupancies were not refined; they were set to 0.50 for atoms involved in a 2 part disorder and 0.33 for atoms involved in a 3 part disorder. The geometries of each part of a disordered group were restrained to be similar. All of the fluorine atoms were restrained to have similar anisotropic displacement parameters and

they were also restrained to keep these parameters more isotropic. A similar approach was used to model the disorder of the THF solvent molecule. Its atoms were split over two positions, with each part restrained to have similar geometries. All of the heavy atoms of the solvent were restrained to have similar anisotropic displacement parameters. The occupancies of the two parts of the solvent were refined to total one, and gave final values of 69.3(16) % and 30.7 % for parts A and B respectively. Finally, enhanced rigid bond restraints were placed over all of the atoms in the structure.

Appendix B: Selected NMR Spectra and HPLC Chromatograms for Reported Compounds

Selected NMR Spectra of Compounds Reported in Chapter 2

Figure B1. ^1H NMR (500 MHz, C_6D_6) for hydrogenation of 1-octene (0.5 mol% catalyst, 1 atm H_2 , 25 °C, 4 h).²²⁸

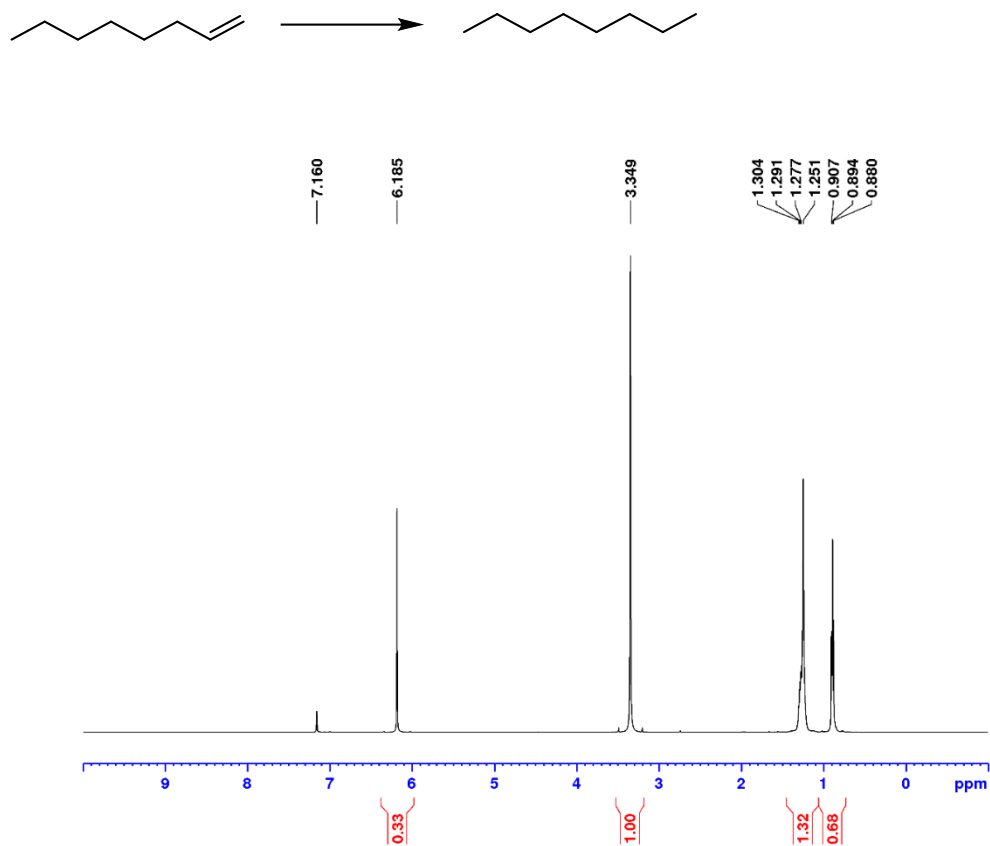


Figure B2. ^1H NMR (500 MHz, C_6D_6) for hydrogenation of *trans*-4-octene (0.5 mol% catalyst, 1 atm H_2 , 25 $^\circ\text{C}$, 4 h).²²⁸

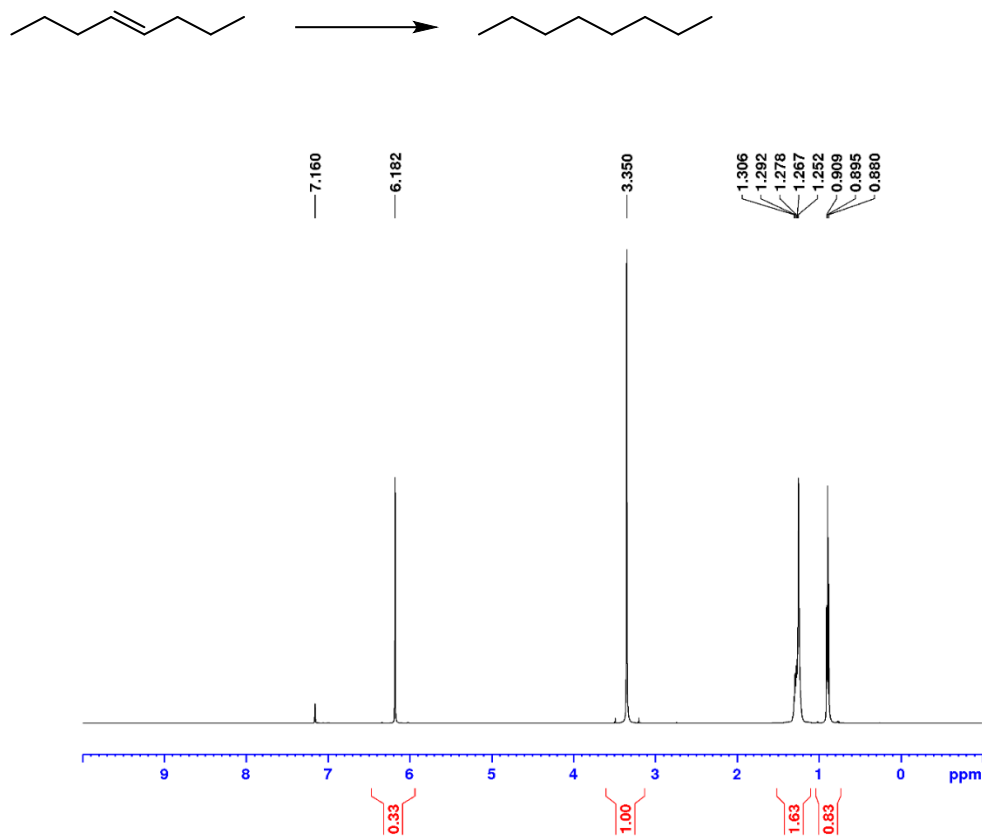


Figure B3. ^1H NMR (500 MHz, C_6D_6) for hydrogenation of *cis*-4-octene (0.5 mol% catalyst, 1 atm H_2 , 25 $^\circ\text{C}$, 4 h).²²⁸

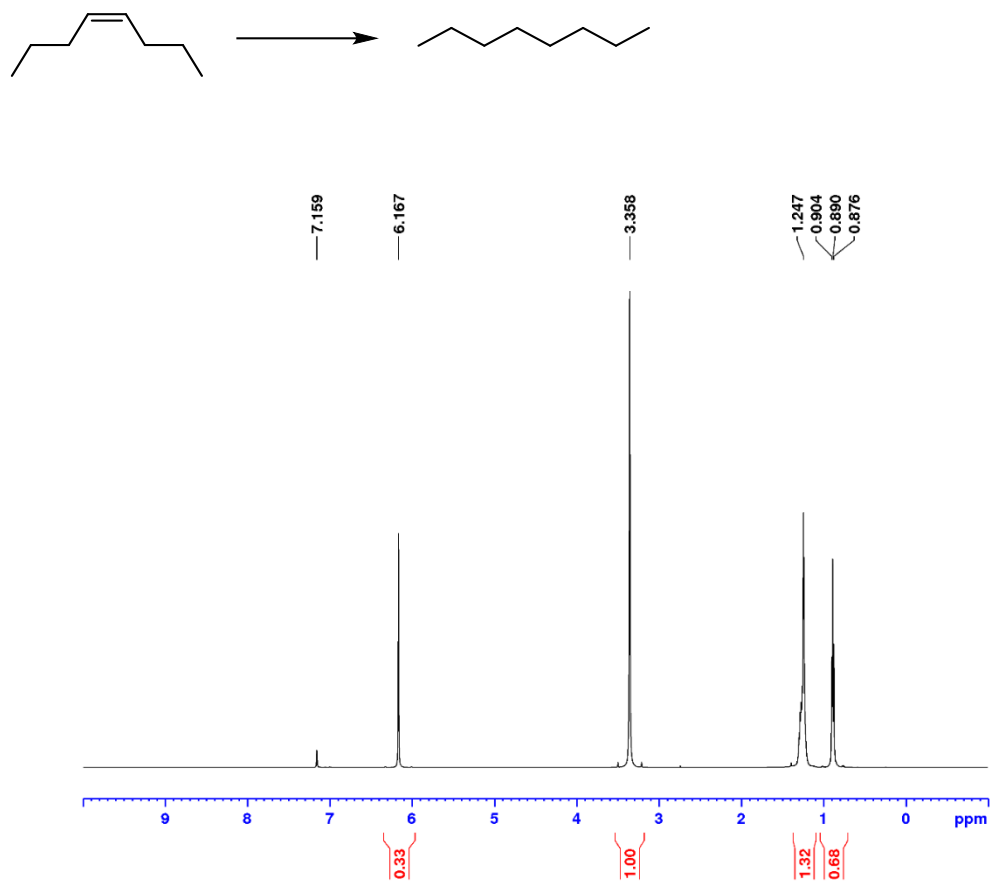


Figure B4. ^1H NMR (500 MHz, C_6D_6) for hydrogenation of *alpha*-methylstyrene (1.0 mol% catalyst, 1 atm H_2 , 25 $^\circ\text{C}$, 4 h).²²⁹

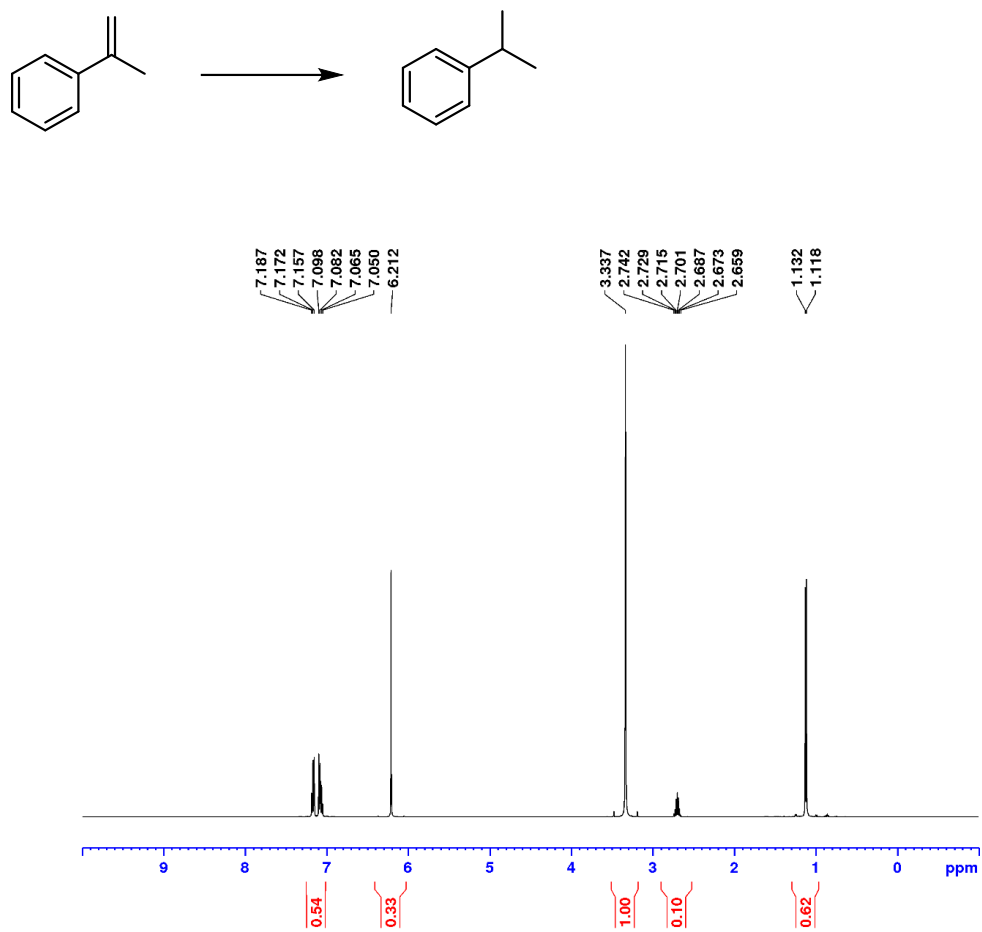


Figure B5. ^1H NMR (500 MHz, C_6D_6) for hydrogenation of *cis*-stilbene (1.0 mol% catalyst, 1 atm H_2 , 25 $^\circ\text{C}$, 4 h).²²⁹

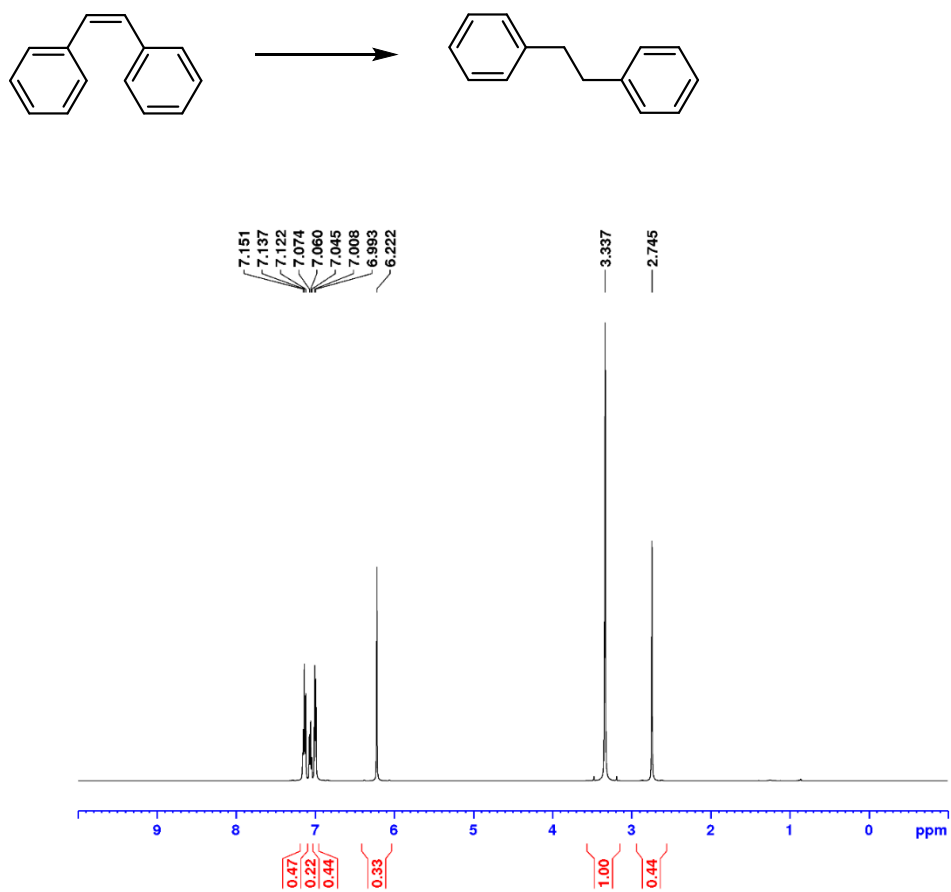


Figure B6. ^1H NMR (300 MHz, C_6D_6) for hydrogenation of ethylenecyclohexane (1.0 mol% catalyst, 1 atm H_2 , 25 $^\circ\text{C}$, 4 h).²³⁰

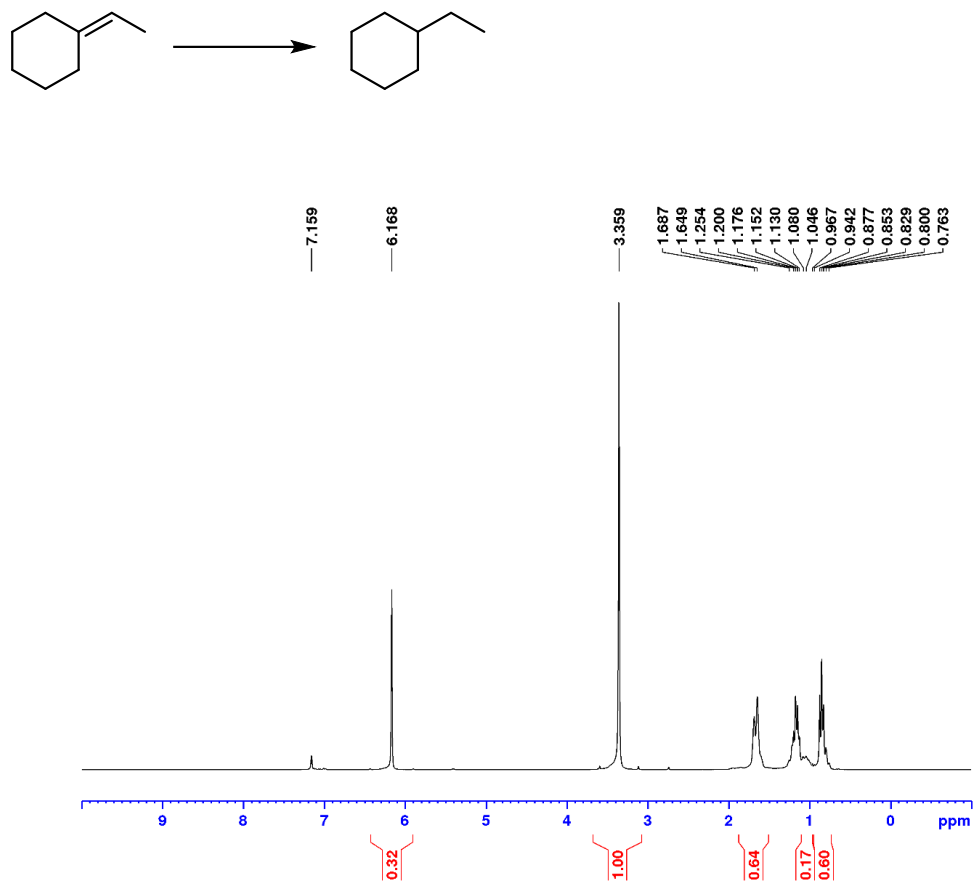


Figure B7. ^1H NMR (300 MHz, C_6D_6) for hydrogenation of allyl butyl ether (0.5 mol% catalyst, 1 atm H_2 , 25 $^\circ\text{C}$, 4 h).²³¹

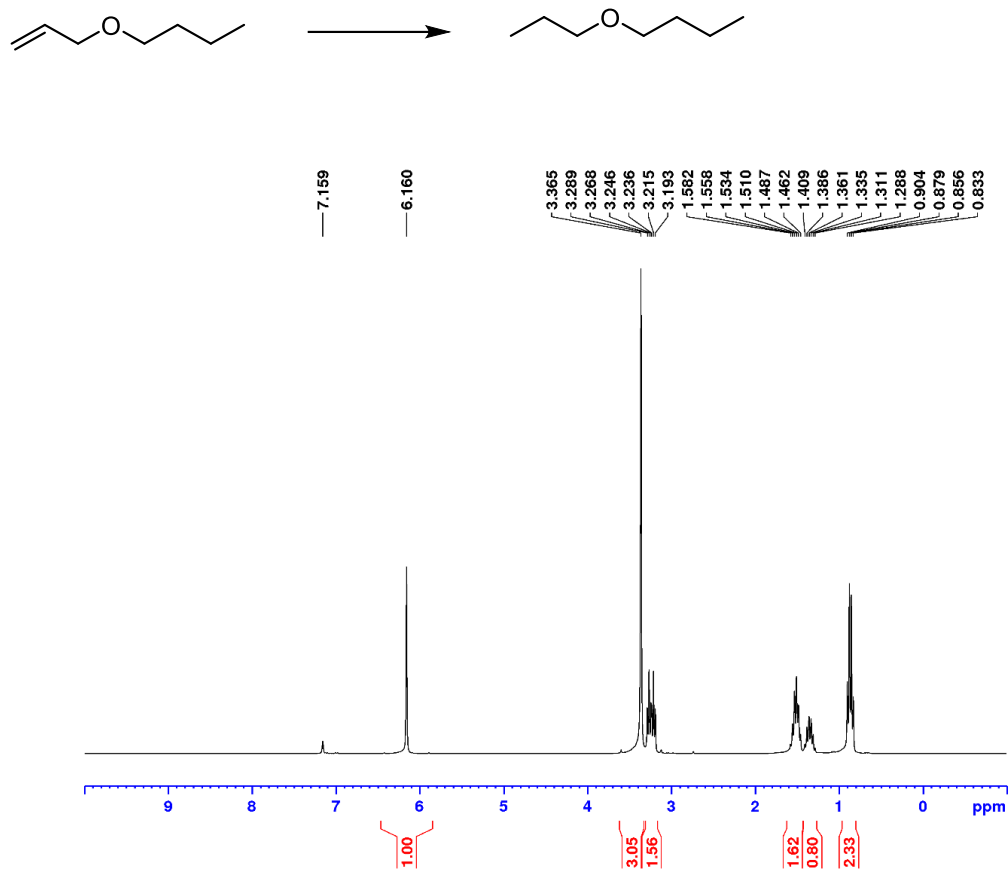


Figure B8. ^1H NMR (300 MHz, C_6D_6) for hydrogenation of 5-hexen-2-one (1.0 mol% catalyst, 1 atm H_2 , 25 $^\circ\text{C}$, 4 h).²³²

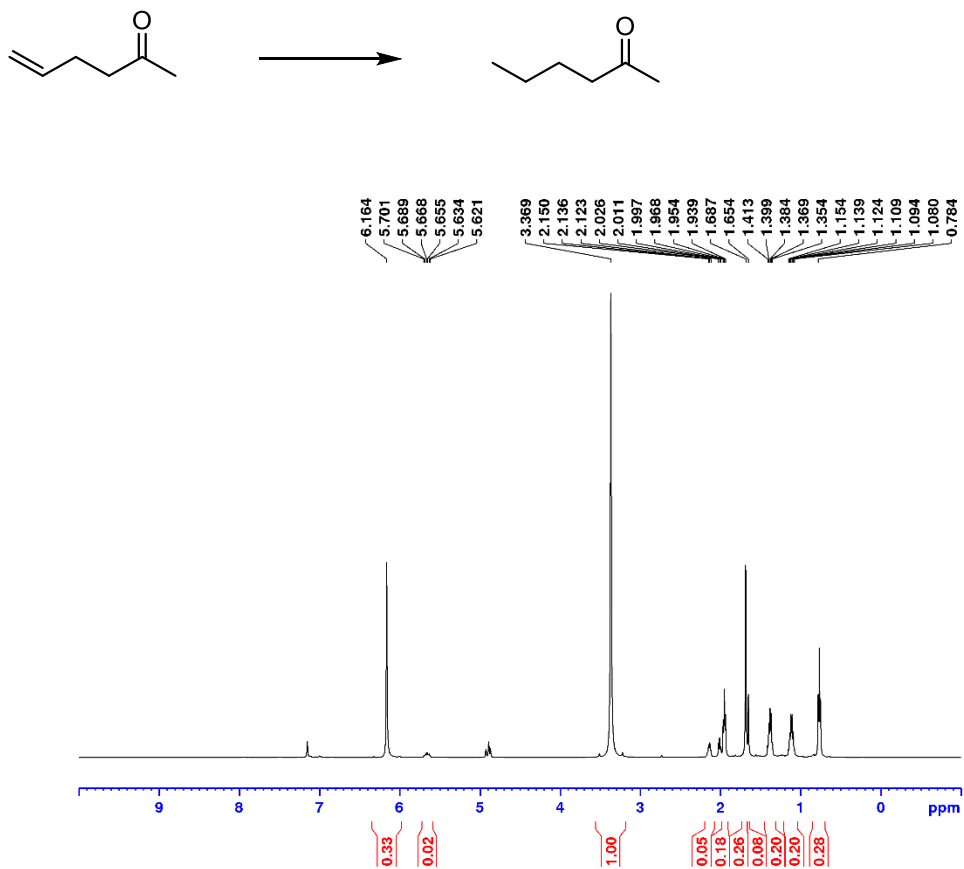


Figure B9. ^1H NMR (300 MHz, C_6D_6) for hydrogenation of ethyl crotonate (1.0 mol% catalyst, 1 atm H_2 , 25 $^\circ\text{C}$, 4 h).²³³

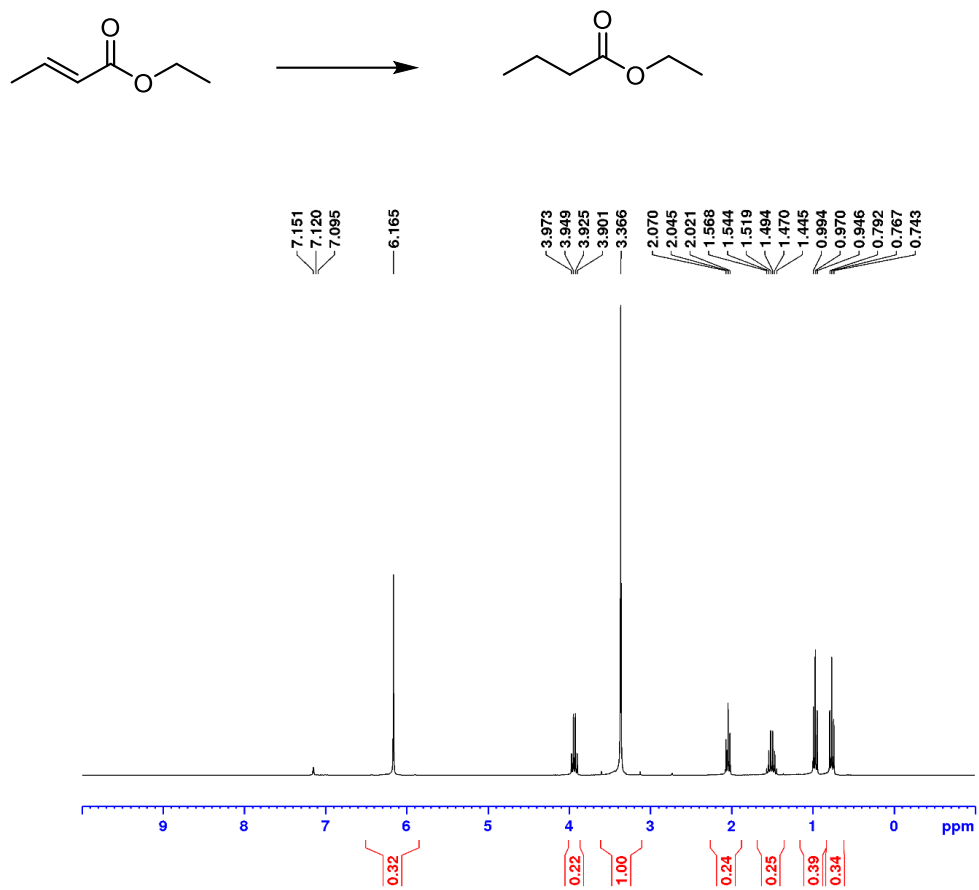


Figure B10. ^1H NMR (500 MHz, C_6D_6) for hydrogenation of pentafluorostyrene (1.0 mol% catalyst, 1 atm H_2 , 25 $^\circ\text{C}$, 4 h).²³⁴

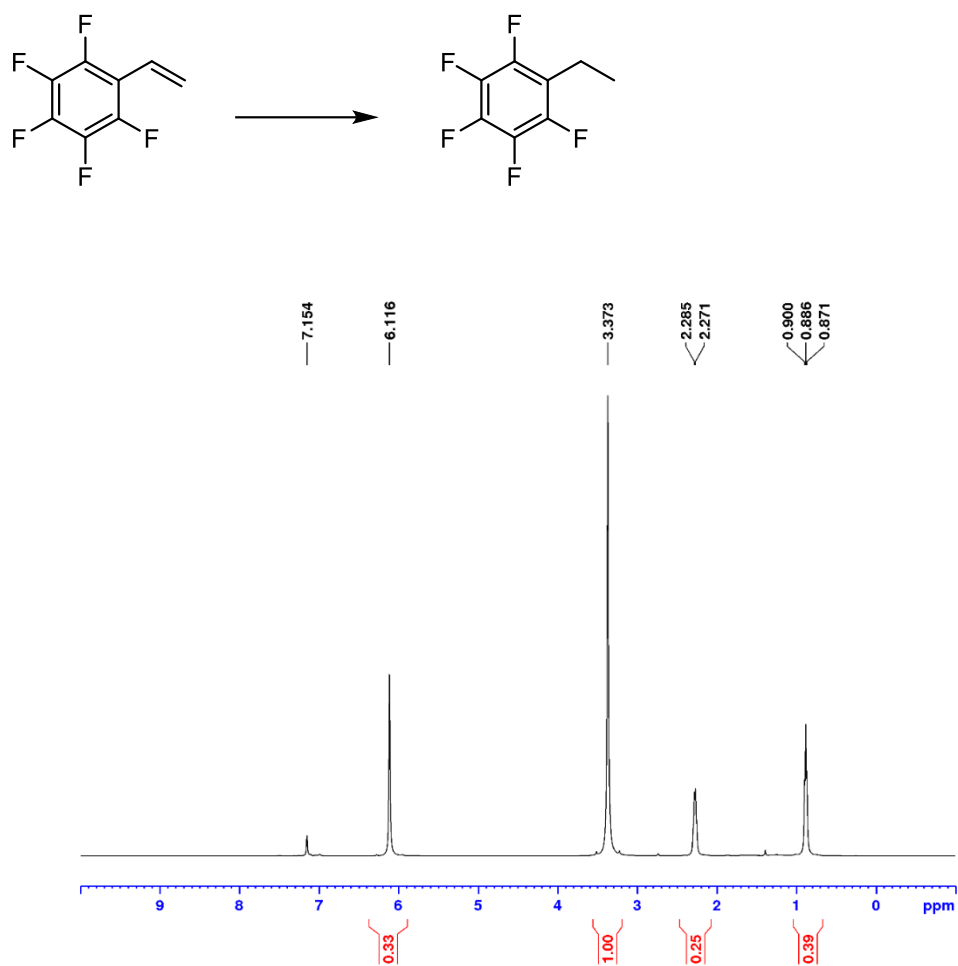


Figure B11. ^1H NMR (500 MHz, C_6D_6) for hydrogenation of allyl phenyl ether (1.0 mol% catalyst, 1 atm H_2 , 25 $^\circ\text{C}$, 4 h).²³⁵

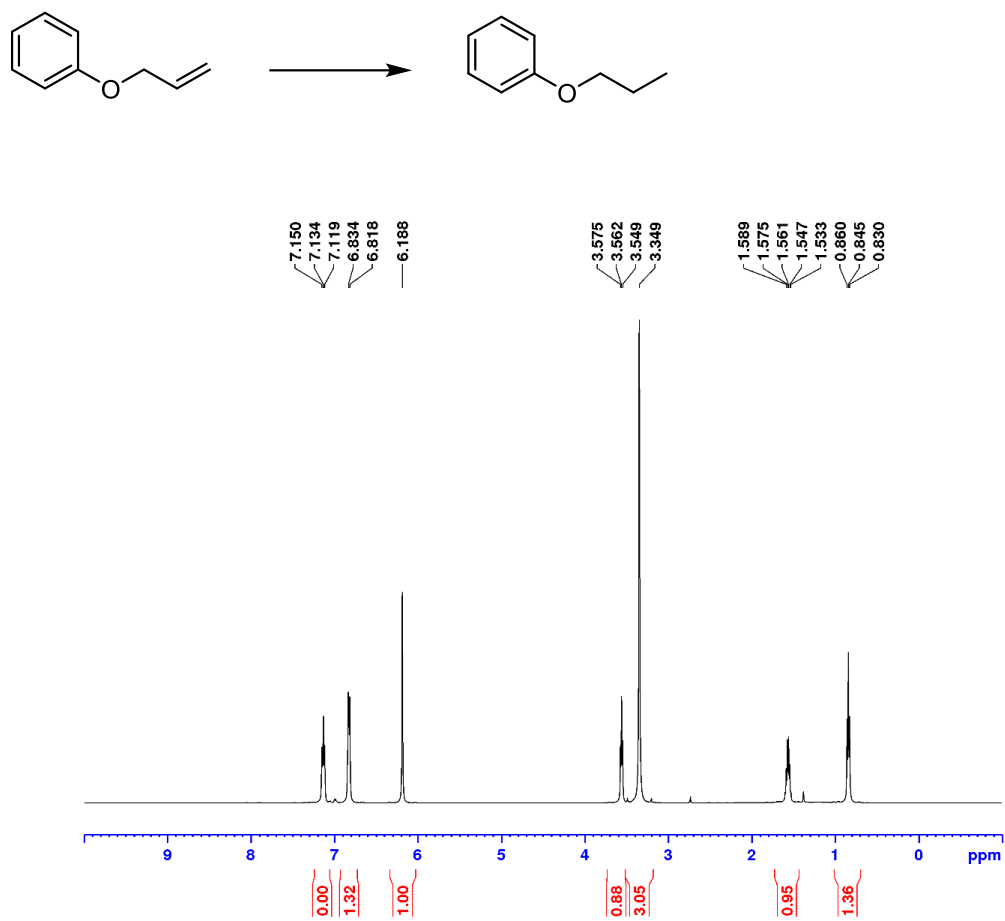


Figure B12. ^1H NMR (500 MHz, C_6D_6) for hydrogenation of 5-hexen-1-ol (1.0 mol% catalyst, 1 atm H_2 , 25 $^\circ\text{C}$, 4 h).²³⁶

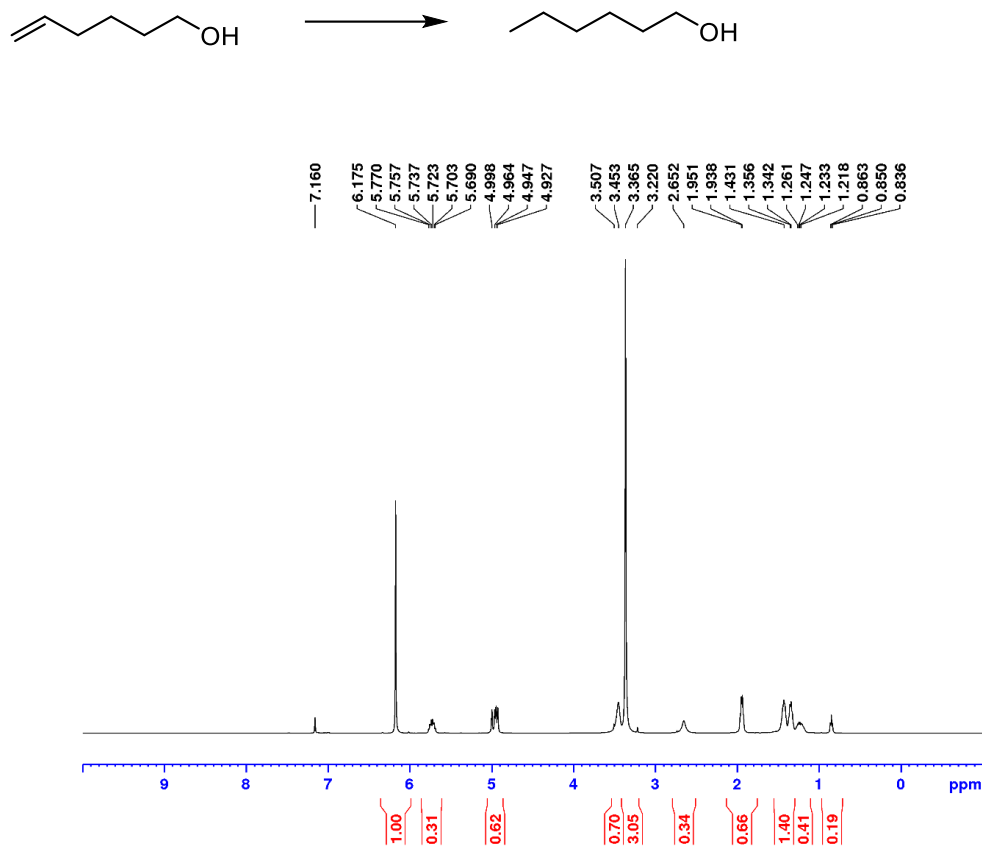


Figure B13. ^1H NMR (500 MHz, Acetone - d_6) for hydrogenation of *N*-tert-butylacrylamide (2.0 mol% catalyst, 1 atm H_2 , 25 $^\circ\text{C}$, 4 h).²³⁷

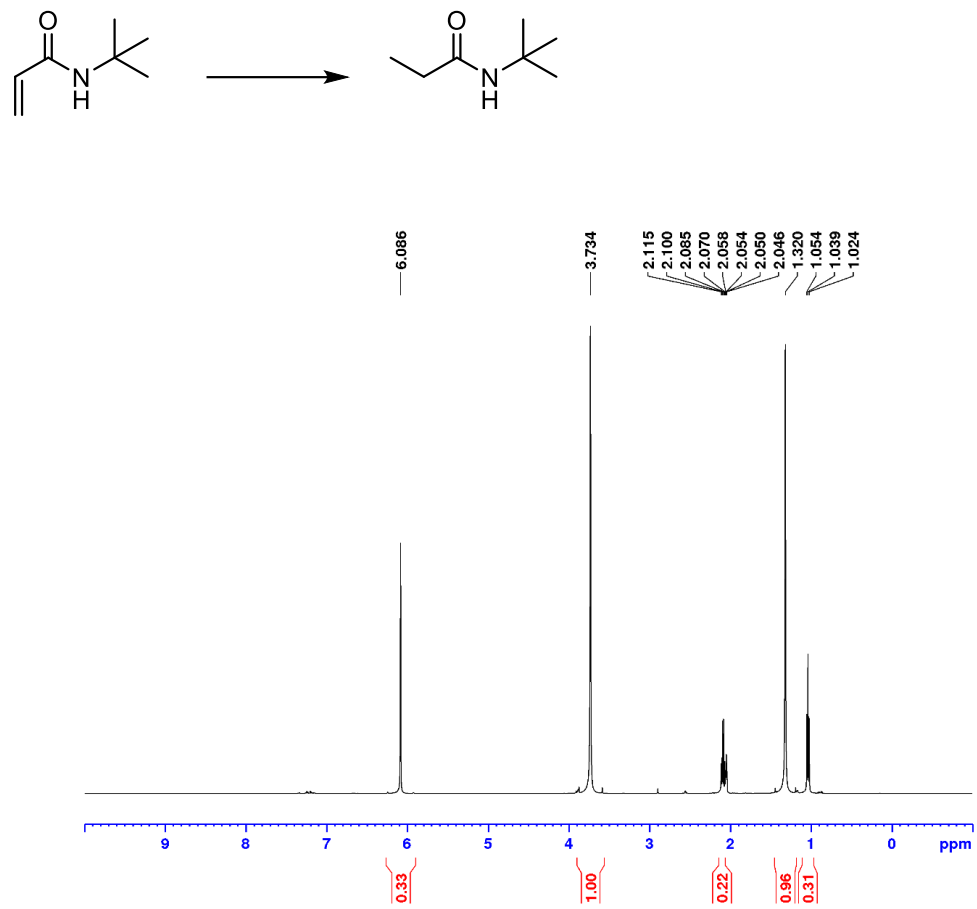


Figure B14. ^1H NMR (500 MHz, Acetone - d_6) for hydrogenation of acrylamide (1.0 mol% catalyst, 1 atm H_2 , 25 $^\circ\text{C}$, 4 h).²³⁸

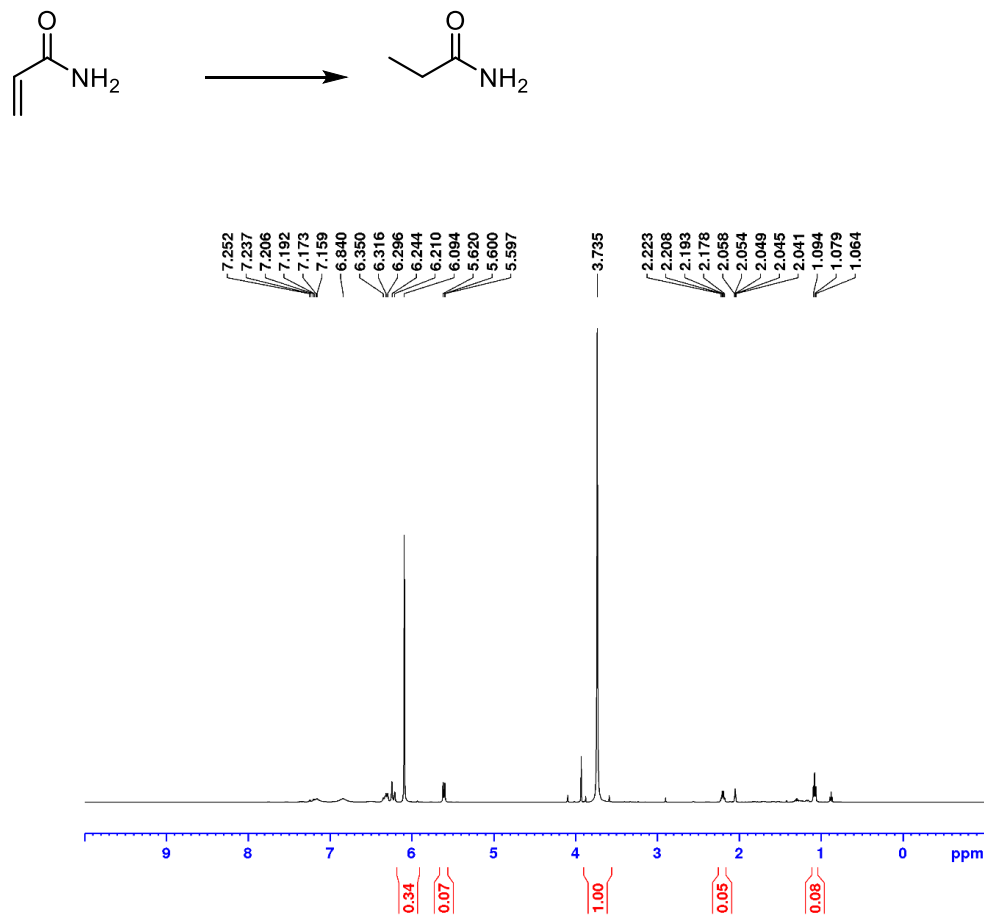


Figure B15. ^1H NMR (300 MHz, C_6D_6) for hydrogenation of *trans* methyl stilbene (7.5 mol% catalyst, 10 atm H_2 , 65 $^\circ\text{C}$, 24 h).⁶¹

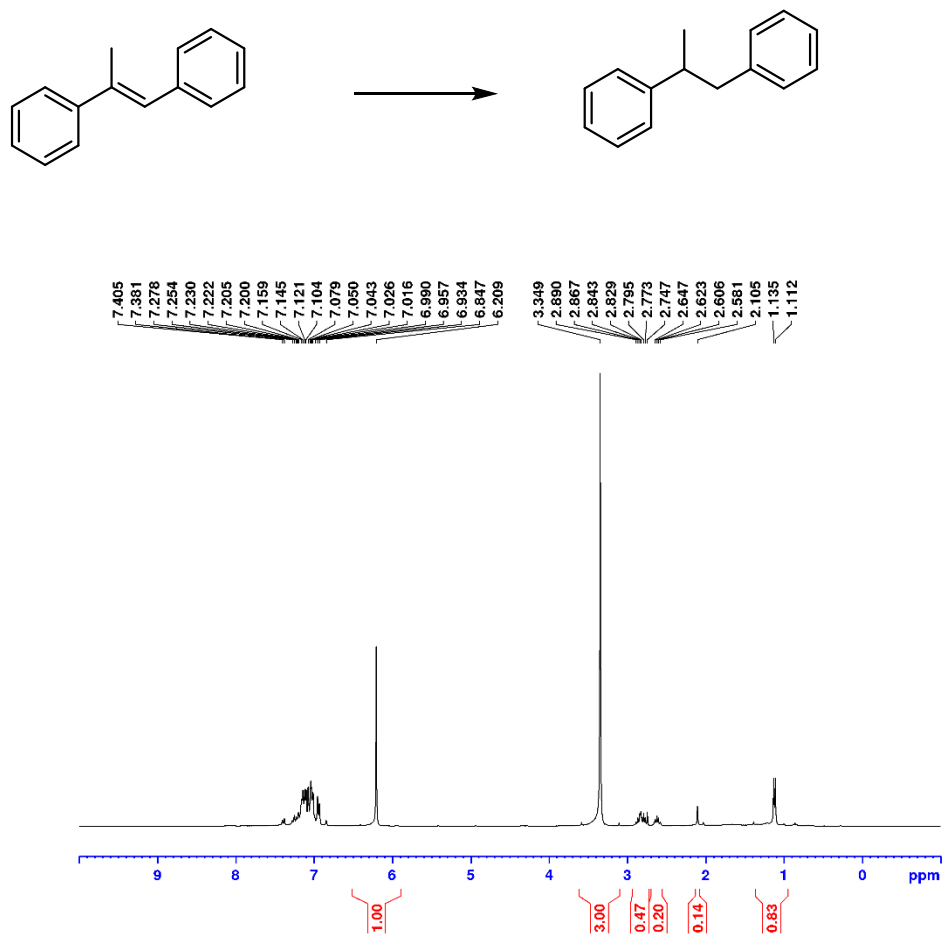


Figure B16. ^1H NMR (300 MHz, C_6D_6) for hydrogenation of methyl cyclohexene (5 mol% catalyst, 10 atm H_2 , 65 $^\circ\text{C}$, 24 h). ¹⁸²

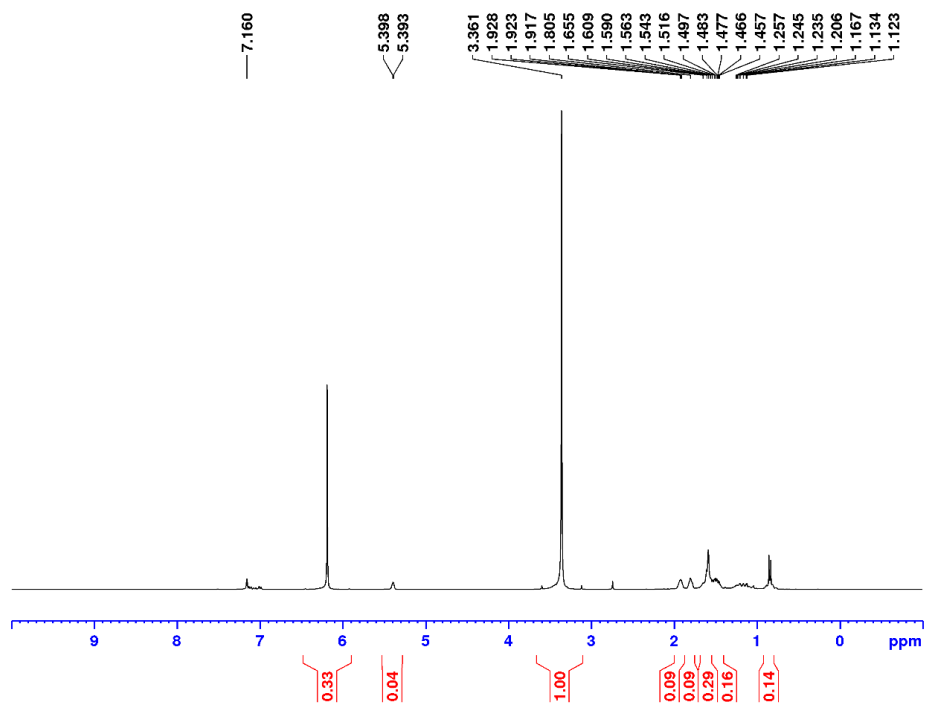
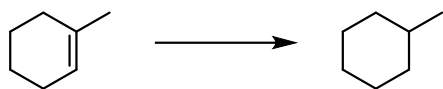


Figure B17. ^1H NMR (300 MHz, C_6D_6) for hydrogenation of 3,3-dimethylacrylate (2 mol% catalyst, 20 atm H_2 , 80 $^\circ\text{C}$, 4 h).²³⁹

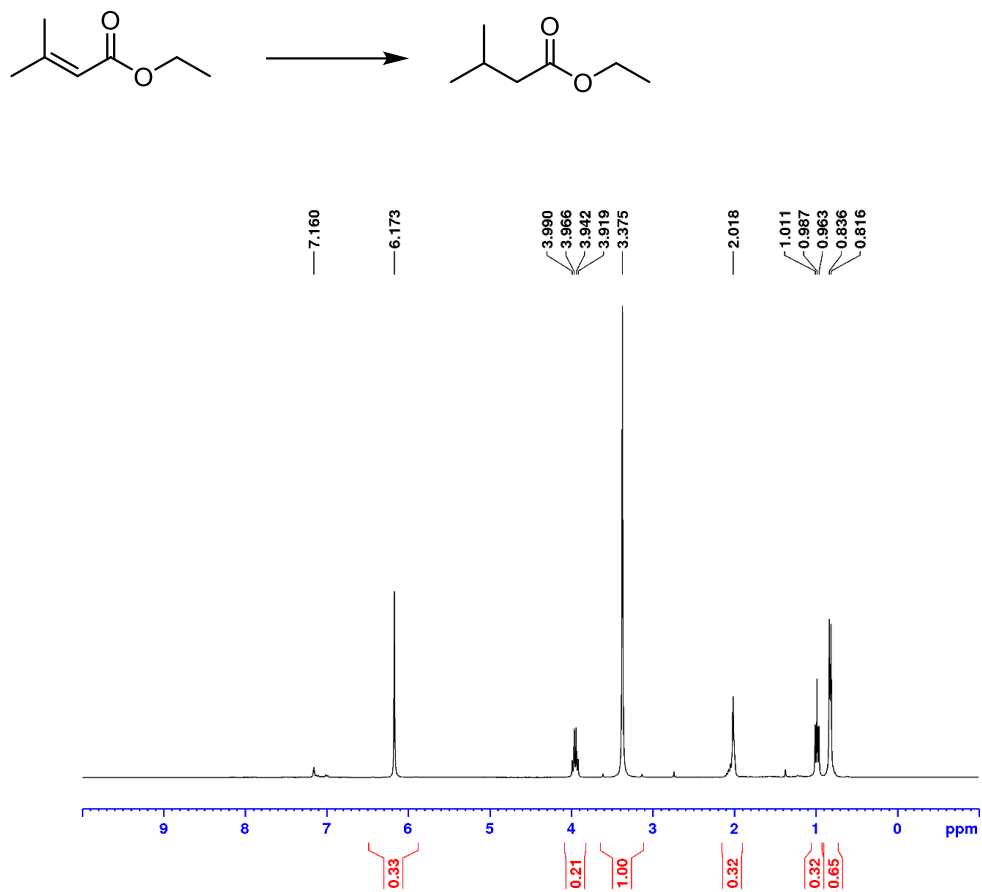


Figure B18. ^1H NMR spectrum (500 MHz, C_6D_6) of **2-2**. The resonance at 1.42 ppm is due to residual cyclohexane.

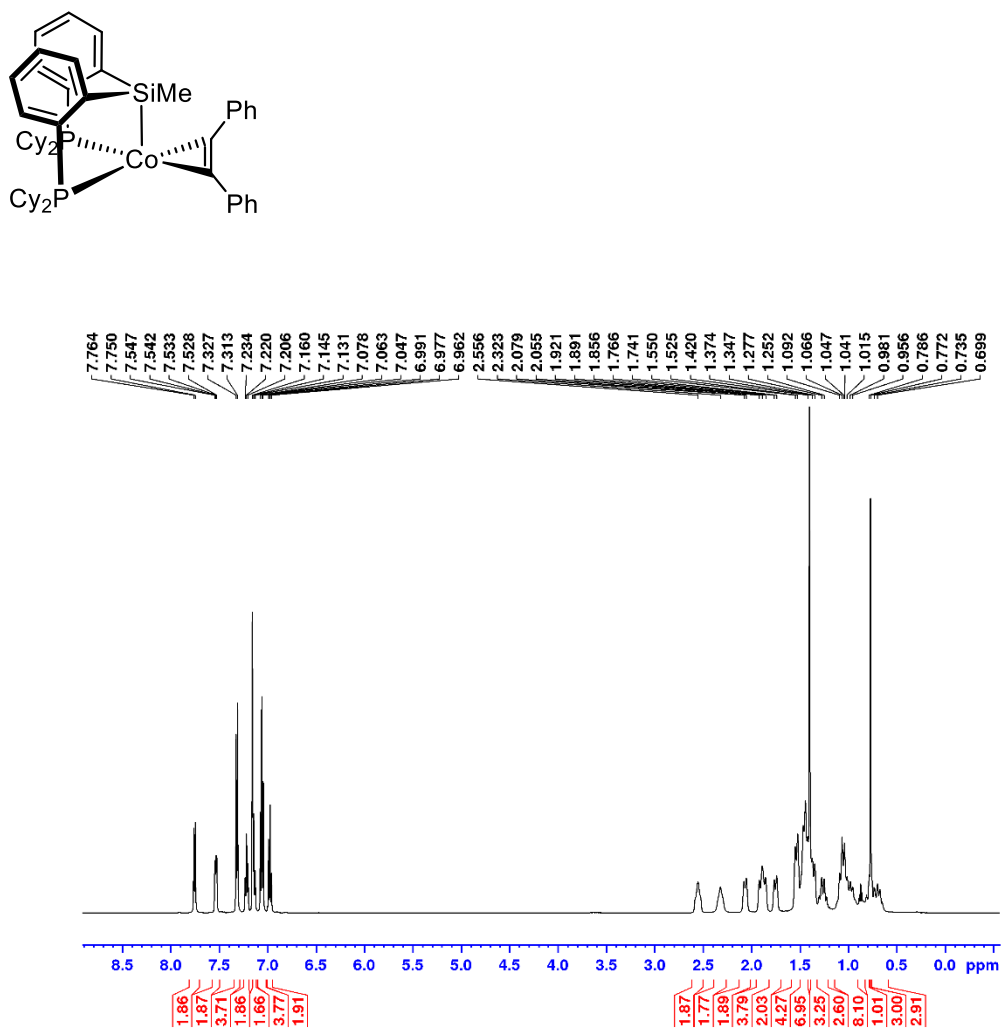


Figure B19. $^{31}\text{P}\{^1\text{H}\}$ NMR spectrum (202 MHz, C_6D_6) of **2-2**.

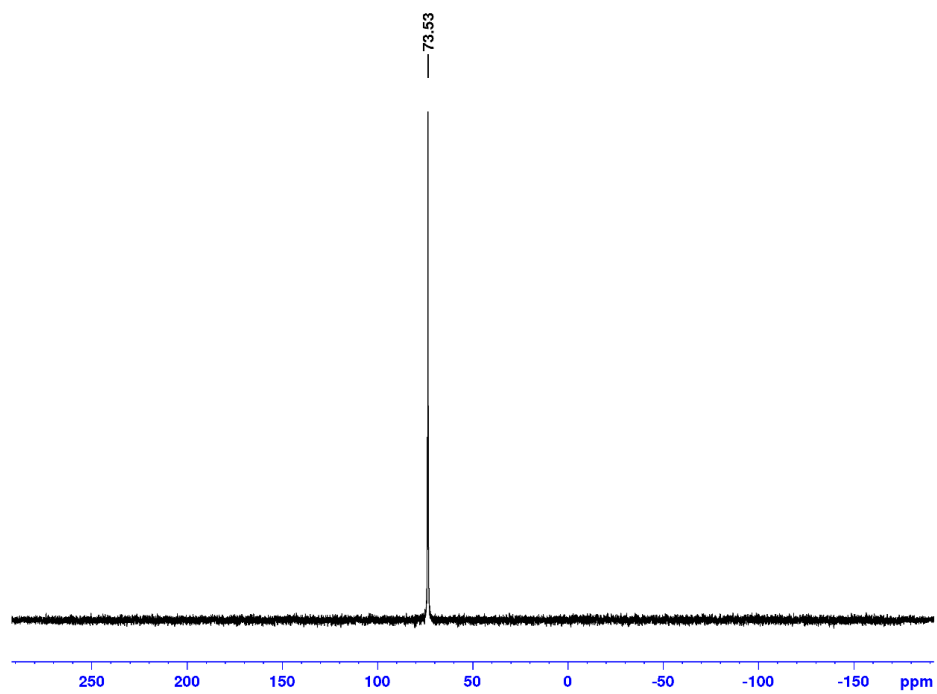
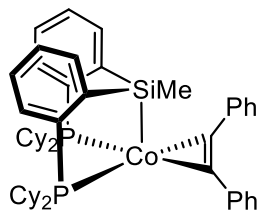


Figure B20. $^{13}\text{C}\{^1\text{H}\}$ NMR spectrum (125 MHz, C_6D_6) of **2-2**.

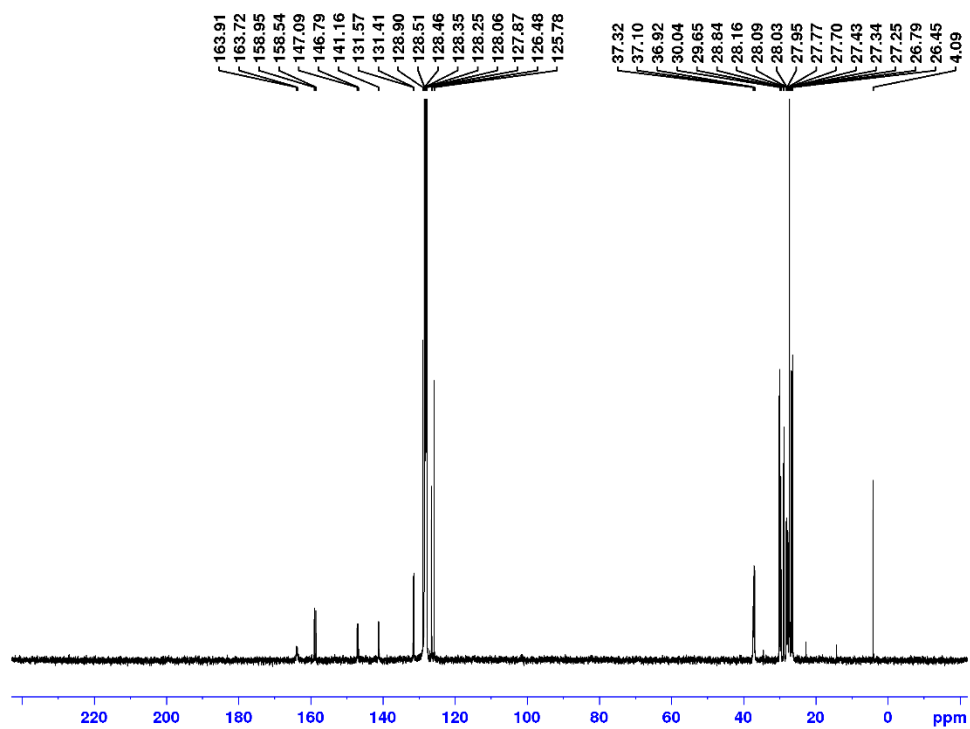
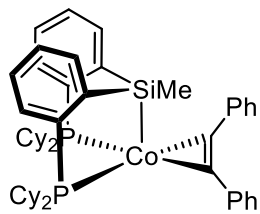


Figure B21. ^1H NMR spectrum (500 MHz, C_6D_6) of **2-1**. The resonance at 1.42 ppm is due to residual cyclohexane.

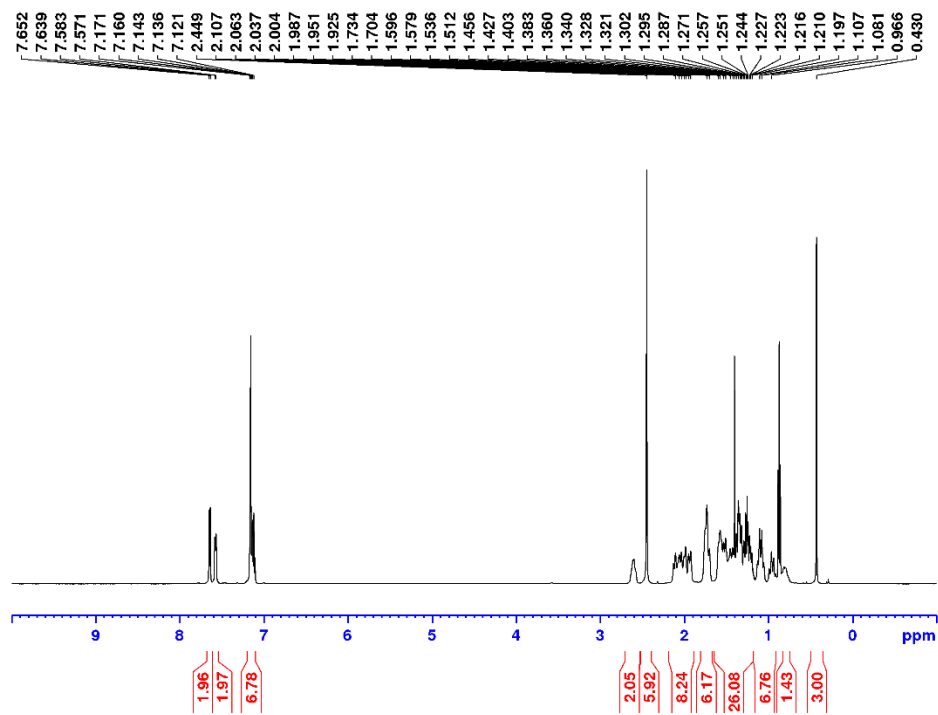
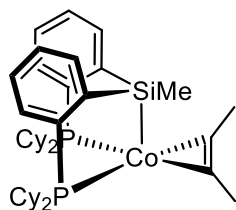


Figure B22. $^{31}\text{P}\{^1\text{H}\}$ NMR spectrum (202 MHz, C_6D_6) of **2-1**.

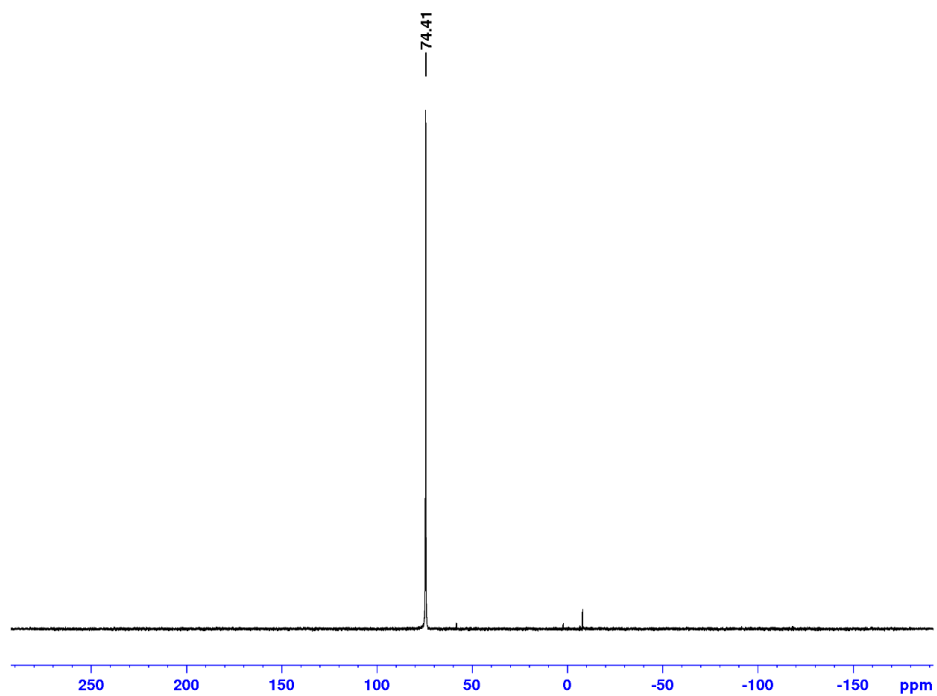
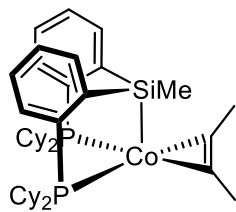
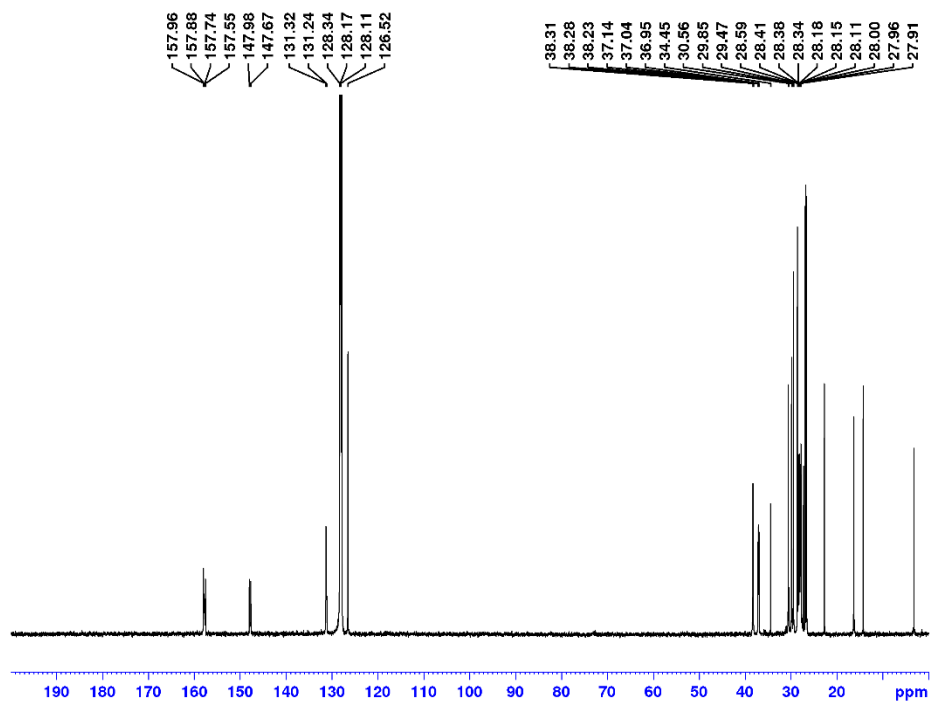
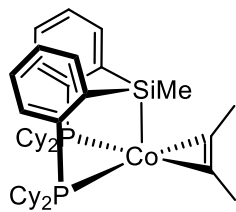


Figure B23. $^{13}\text{C}\{^1\text{H}\}$ NMR spectrum (125 MHz, C_6D_6) of **2-1**.



Selected NMR Spectra of Compounds Reported in Chapter 3

Figure B24. ^1H NMR (500 MHz, C_6D_6) spectrum for the semihydrogenation of diphenylacetylene to afford **3-1a** (1.0 mol% catalyst, 1 atm H_2 , 1.0 M, 25 °C, 4 h; 96% conversion, $E:Z > 99:1$). ^1H NMR (500 MHz, benzene- d_6): δ 7.33 – 7.31 (apparent d, 4 H, H_{arom}), 7.16 – 7.14 (overlapping resonances, 4 H, H_{arom}), 7.08 – 7.06 (m, 2 H, H_{arom}), 6.99 (s, 2 H, $\text{HC}=\text{C}$).

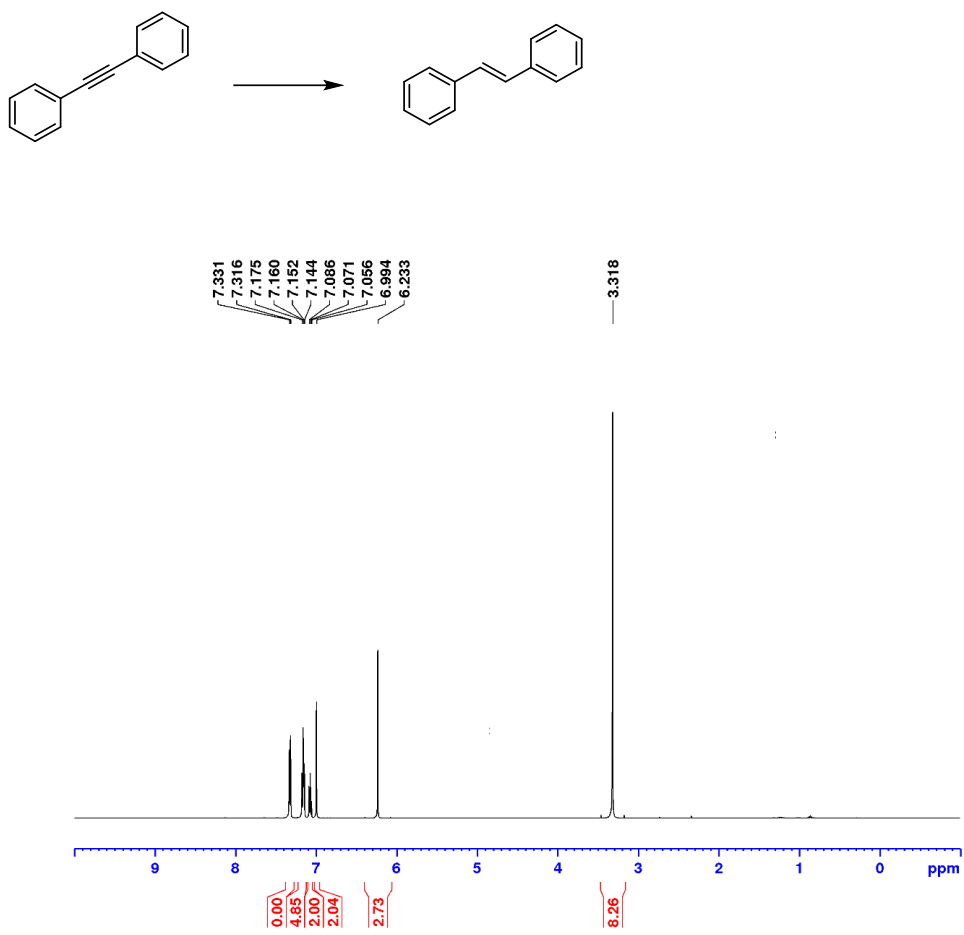


Figure B25. ^1H NMR (500 MHz, C_6D_6) spectrum for the semihydrogenation of 1-naphthyl-2-phenyl-ethyne to afford **3-1b** (1.0 mol% catalyst, 1 atm H_2 , 1.0 M, 25 $^\circ\text{C}$, 4 h; 91% conversion, $E:Z > 99:1$). ^1H NMR (500 MHz, benzene- d_6): δ 7.67 – 7.60 (overlapping resonances, 4 H, *Harom*), 7.56 – 7.54 (m, 1 H, *Harom*), 7.41 – 7.39 (m, 2 H, *Harom*), 7.31 – 7.24 (m, 2 H, *Harom*), 7.22 – 7.19 (m, 2 H, *Harom*), 7.14 – 7.09 (overlapping resonances, 2 H).

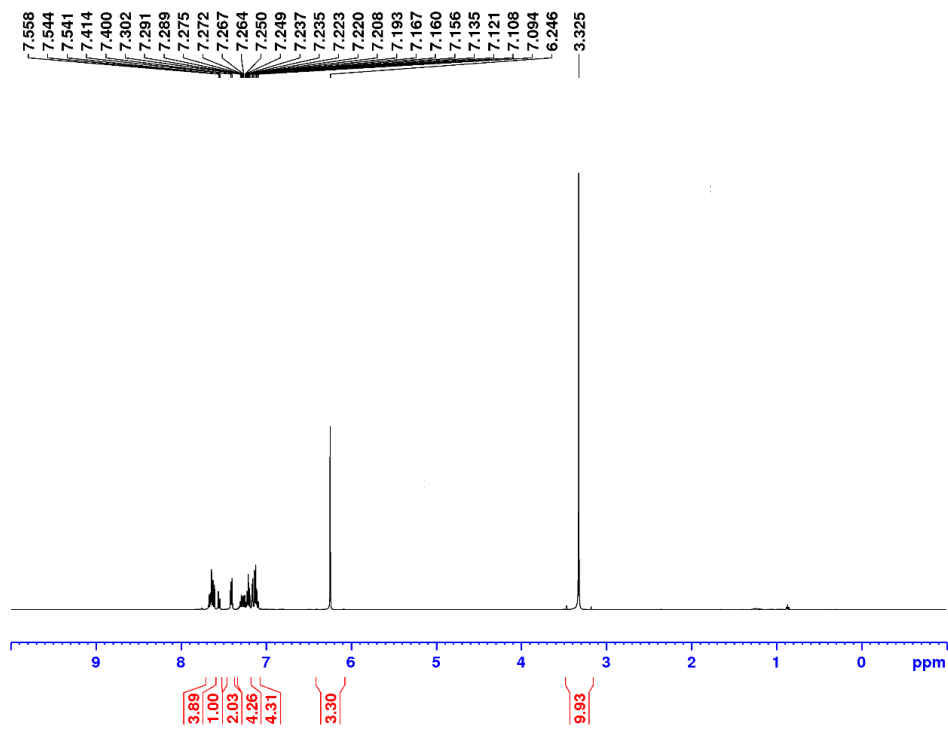
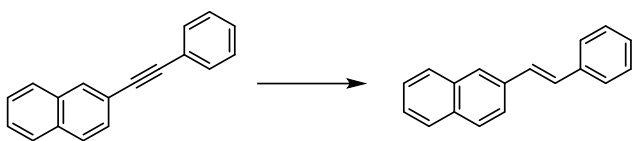


Figure B26. ^1H NMR (500 MHz, C_6D_6) spectrum for the semihydrogenation of 1-(2-phenylethynyl)-4-trimethylsilylbenzene to afford **3-1c** (1.0 mol% catalyst, 1 atm H_2 , 1.0 M, 25 $^\circ\text{C}$, 4 h; 96% conversion, $E:Z > 99:1$).

^1H NMR (500 MHz, benzene- d_6): δ 7.50 – 7.49 (apparent d, 2 H, *Harom*), 7.43 – 7.42 (apparent d, 2 H, *Harom*), 7.36 – 7.34 (apparent d, 2 H, *Harom*), 7.19 – 7.16 (overlapping resonances, 2 H, *Harom*), 7.11 (d, 1 H, $J = 16.4$ Hz, $\text{HC}=\text{C}$), 7.10 – 7.09 (m, 1 H, *Harom*), 7.05 (d, 1 H, $J = 16.4$ Hz, $\text{HC}=\text{C}$), 0.25 (s, 9 H, SiMe_3).

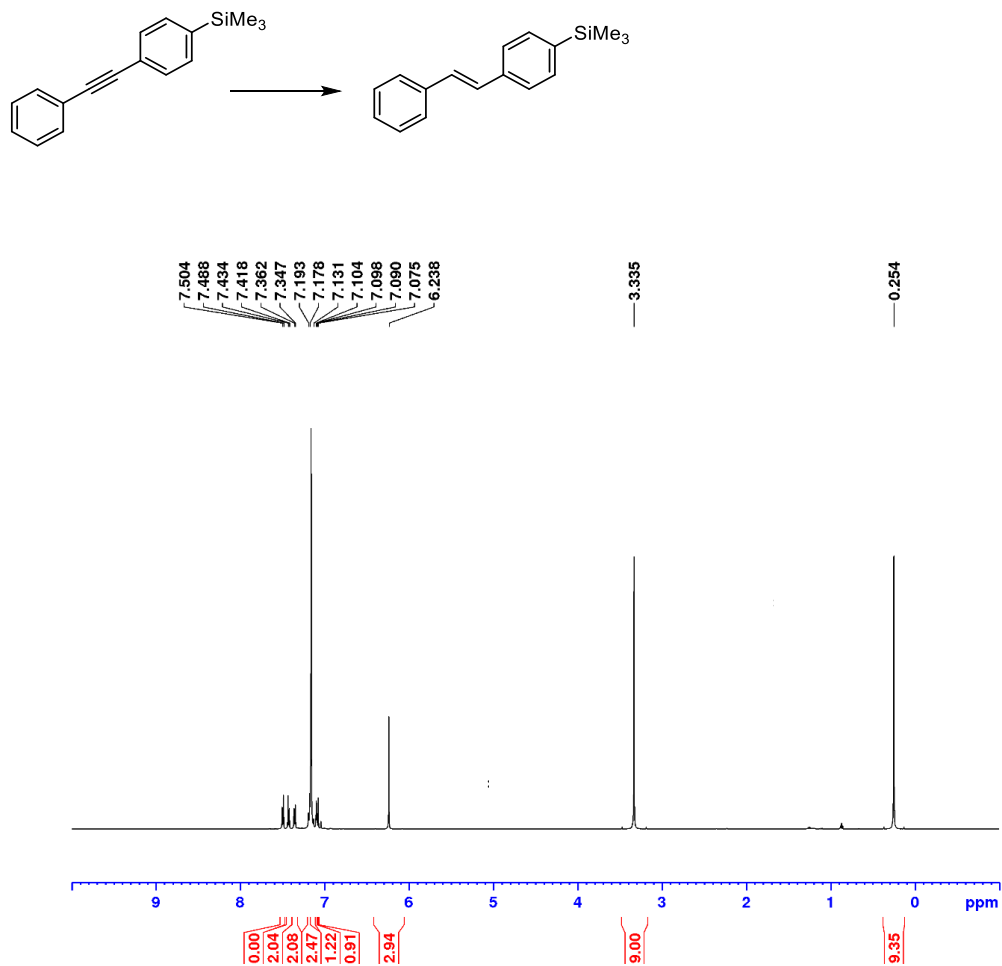


Figure B27. ^1H NMR (500 MHz, C_6D_6) spectrum for the semihydrogenation of 1,4-dimethyl-2-(2-phenylethynyl)benzene to afford **3-1d** (2.5 mol% catalyst, 1 atm H_2 , 1.0 M, 50 °C, 4 h; 98% conversion, $E:Z > 99:1$). ^1H NMR (500 MHz, benzene- d_6): δ 7.40 – 7.39 (overlapping resonances, 3 H, H_{arom}), 7.33 (d, 1 H, $J = 16.2$ Hz, $\text{H}_{\text{C}=\text{C}}$), 7.19 – 7.15 (m, 2 H, H_{arom}), 7.10 – 7.07 (m, 1 H, H_{arom}), 6.98 – 6.94 (overlapping resonances, 2 H), 6.92 – 6.90 (m, 1 H, H_{arom}), 2.19 (s, 6 H, CMe).

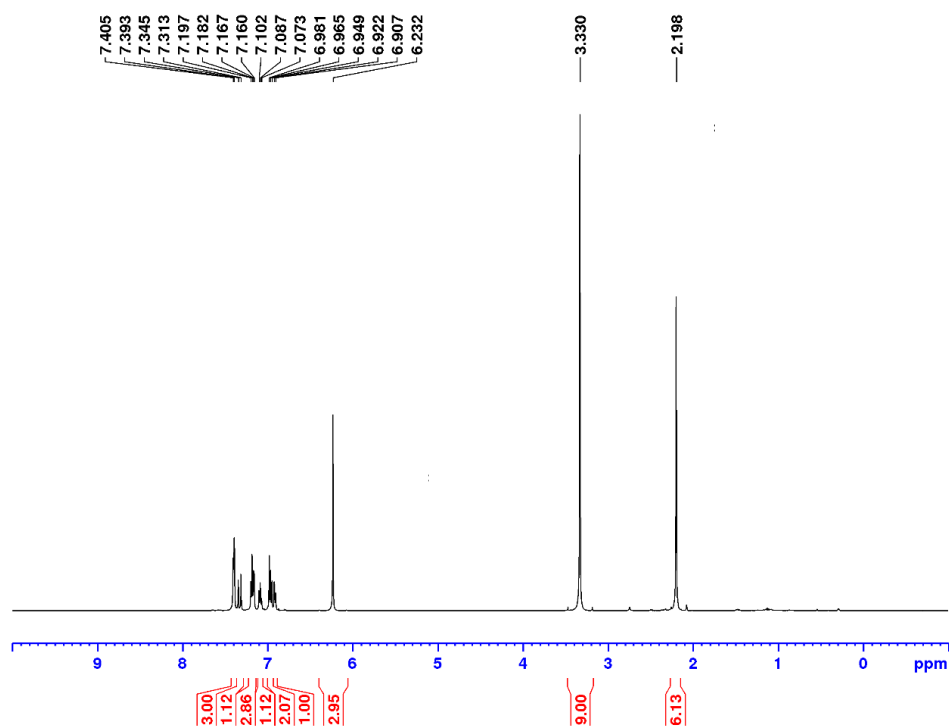
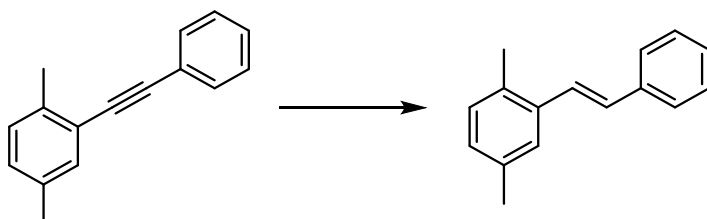


Figure B28. ^1H NMR (300 MHz, C_6D_6) spectrum for the hydrogenation of 1-methoxy-2-(2-phenylethynyl)benzene to afford **3-1e** (2.5 mol% catalyst, 1 atm H_2 , 1.0 M, 50 $^\circ\text{C}$, 4 h; >99% conversion, $E:Z > 99:1$). ^1H NMR (500 MHz, benzene- d_6): δ 7.78 (d, 1 H, $J = 16.5$ Hz, $\text{HC}=\text{C}$), 7.53 – 7.51 (m, 1 H, *Harom*), 7.43 – 7.41 (m, 2 H, *Harom*), 7.16 – 7.01 (overlapping resonances, 6 H), 6.90 – 6.85 (m, 1 H, *Harom*), 3.32 (s, 3 H, *OMe*).

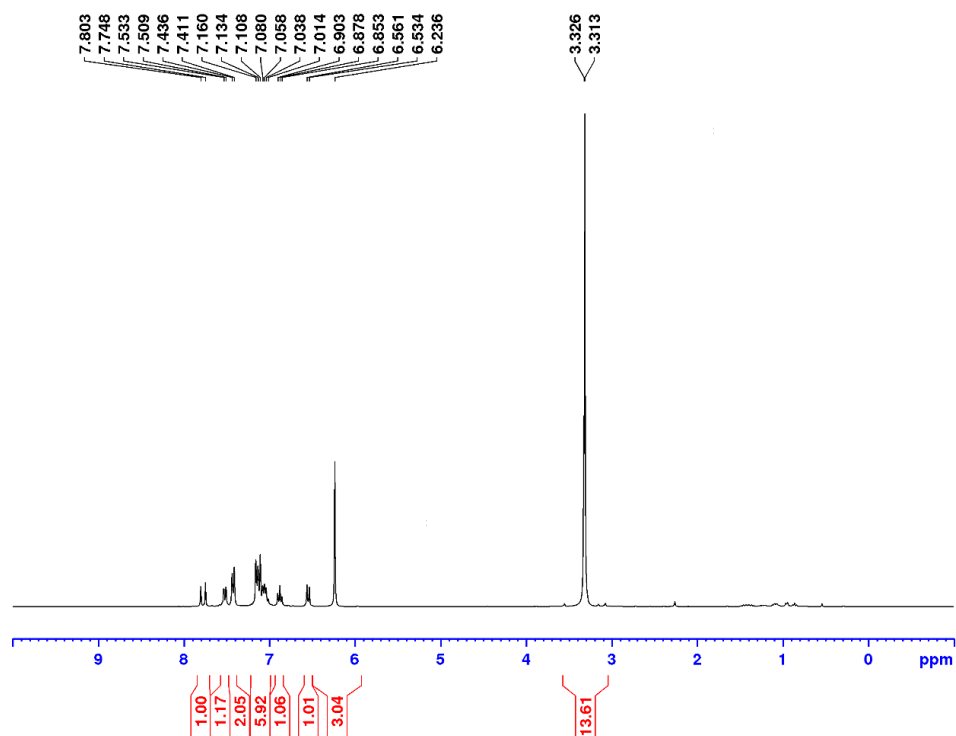
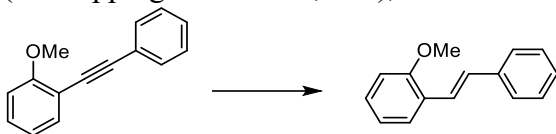


Figure B29. ^1H NMR (500 MHz, C_6D_6) spectrum for the semihydrogenation of 1-ethyl-4[2-(4-methoxyphenyl)ethynyl]benzene to afford **3-1f** (1.0 mol% catalyst, 1 atm H_2 , 1.0 M, 25 $^\circ\text{C}$, 4 h; 84% conversion, $E:Z > 99:1$).

^1H NMR (500 MHz, benzene- d_6): δ 7.38 – 7.37 (m, 2 H, *Harom*), 7.33 – 7.31 (m, 2 H, *Harom*), 7.08 – 7.06 (m, 2 H, *Harom*), 7.05 (d, 1 H, $J = 16.7$ Hz, $\text{HC}=\text{C}$), 6.98 (d, 1 H, $J = 16.3$ Hz, $\text{HC}=\text{C}$), 6.81 – 6.78 (m, 2H, *Harom*), 2.49 (q, 2 H, $J = 7.6$ Hz, CH_2CH_3), 1.12 (t, 3 H, $J = 7.6$ Hz, CH_2CH_3).

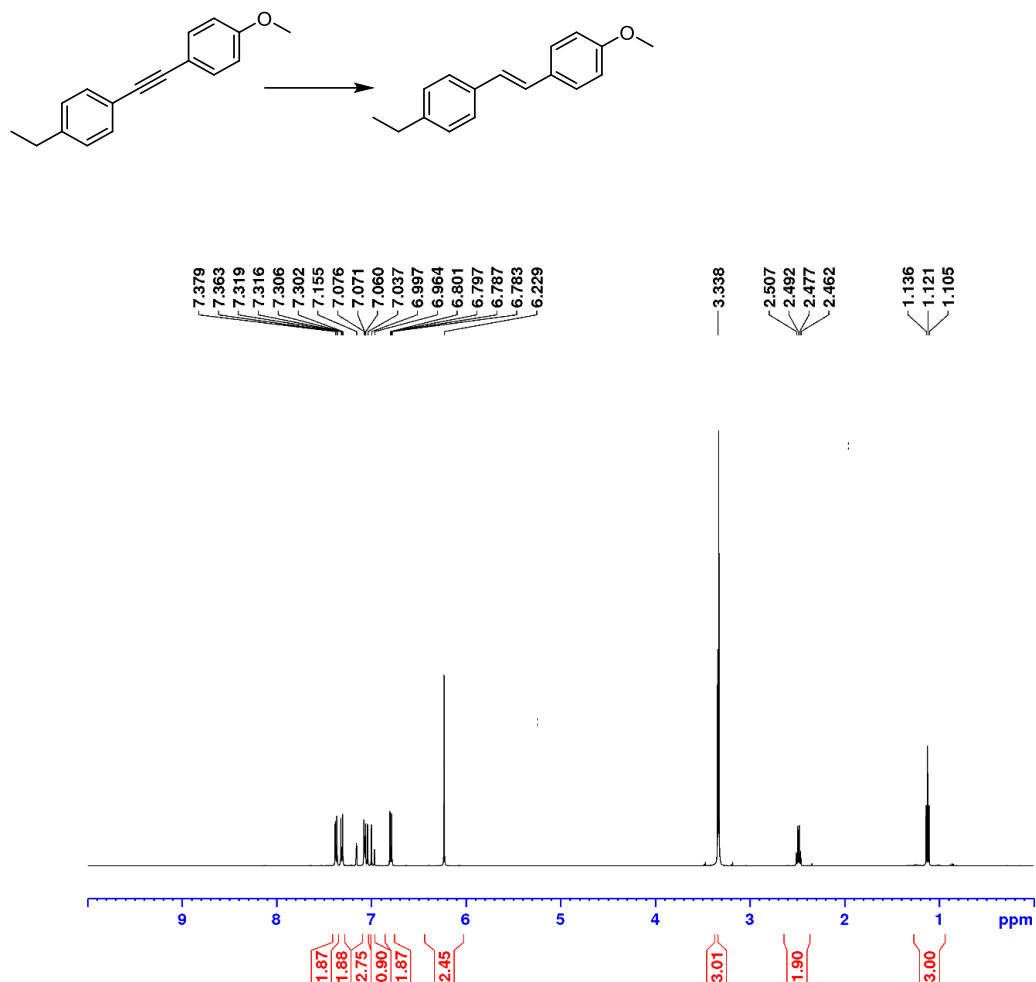


Figure B30. ^1H NMR (500 MHz, C_6D_6) spectrum for the semihydrogenation of 2-[4-[2-(4-methoxyphenyl)ethynyl]phenyl]boronic acid pinacol ester to afford **3-1g** (1.0 mol% catalyst, 1 atm H_2 , 1.0 M, 25 $^\circ\text{C}$, 4 h; 87% conversion, $E:Z > 99:1$).

^1H NMR (500 MHz, benzene- d_6): δ 8.19 – 8.17 (apparent d, 2 H, *Harom*), 7.42 – 7.40 (apparent d, 2 H, *Harom*), 7.27 – 7.26 (apparent d, 2 H, *Harom*), 7.01 (d, 1 H, $^3J_{\text{H-H}} = 16.3$ Hz, $\text{HC}=\text{C}$), 6.89 (d, 1 H, $^3J_{\text{H-H}} = 16.3$ Hz, $\text{HC}=\text{C}$), 6.78 -6.76 (m, 2 H, *Harom*), 3.33 (s, 3 H, *OMe*), 1.16 (s, 12 H, *BPin*).

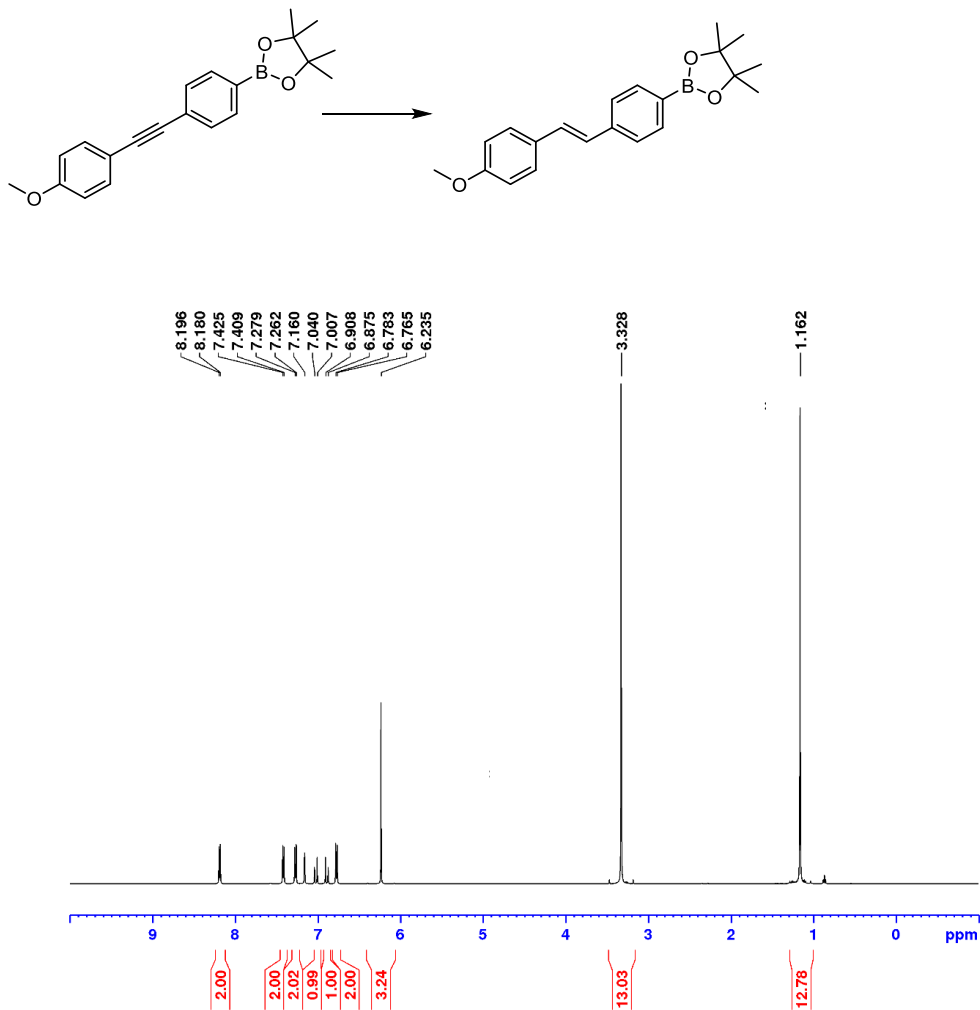


Figure 31. ^{11}B NMR (160 MHz, C_6D_6) spectrum for the semihydrogenation of 2-[4-[2-(4-methoxyphenyl)ethynyl]phenyl]boronic acid pinacol ester to afford **3-1g** (1.0 mol% catalyst, 1 atm H_2 , 1.0 M, 25 °C, 4 h; 87% conversion, $E:Z > 99:1$).

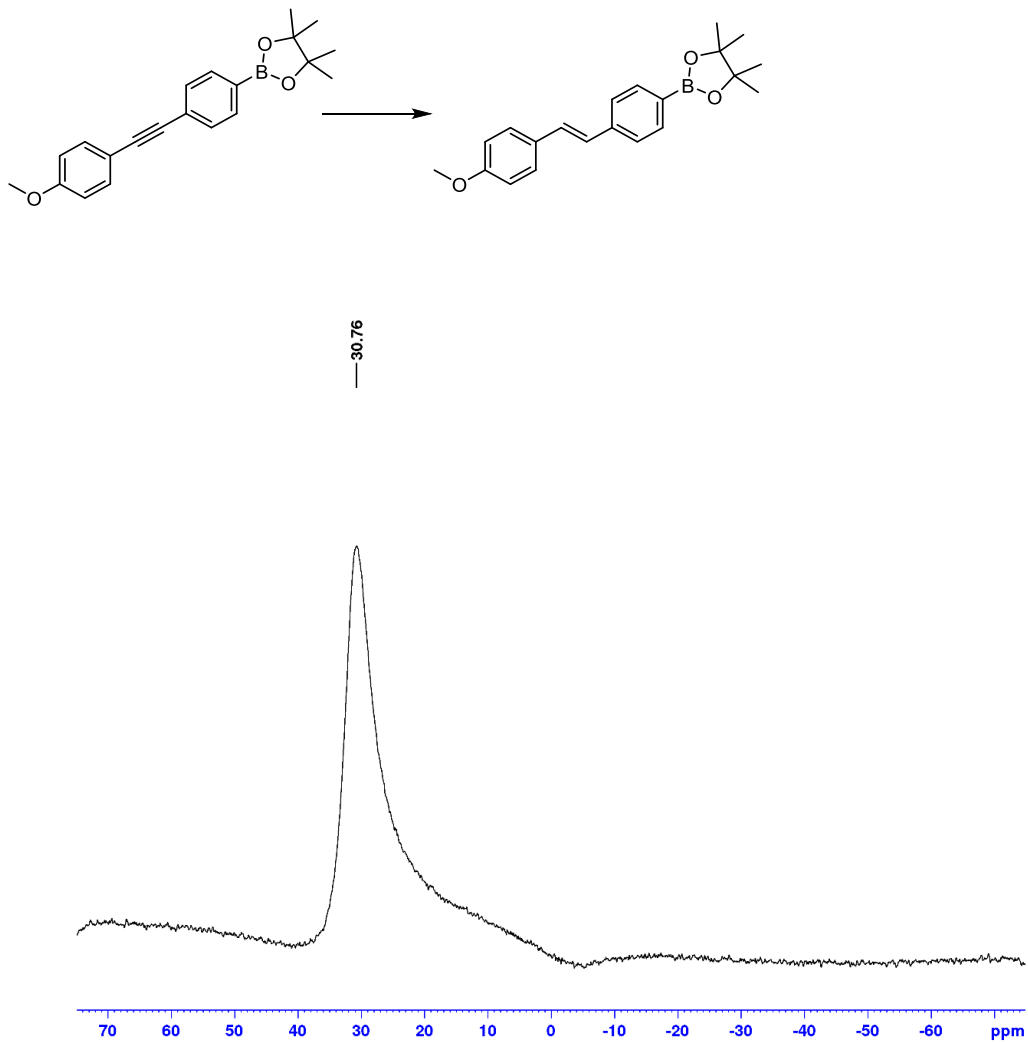


Figure B32. ^1H NMR (500 MHz, C_6D_6) spectrum for the semihydrogenation of 4-[2-[4-(4,4,5,5-tetramethyl-1,3,2-dioxaborolan-2-yl)phenyl]ethynyl]benzoic acid methyl ester to afford **3-1h** (1.0 mol% catalyst, 1 atm H_2 , 1.0 M, 25 $^\circ\text{C}$, 4 h; 96% conversion, $E:Z > 99:1$). ^1H NMR (500 MHz, benzene- d_6): δ 8.15 – 8.09 (overlapping resonances, 4 H, *Harom*), 7.35 – 7.34 (m, 2 H, *Harom*), 7.21 – 7.19 (m, 2 H, *Harom*), 6.90 (d, 1 H, $J = 16.3$ Hz, $\text{HC}=\text{C}$), 6.85 (d, 1 H, $J = 16.3$ Hz, $\text{HC}=\text{C}$), 3.55 (s, 3 H, COOMe), 1.16 (s, 12 H, *BPin*).

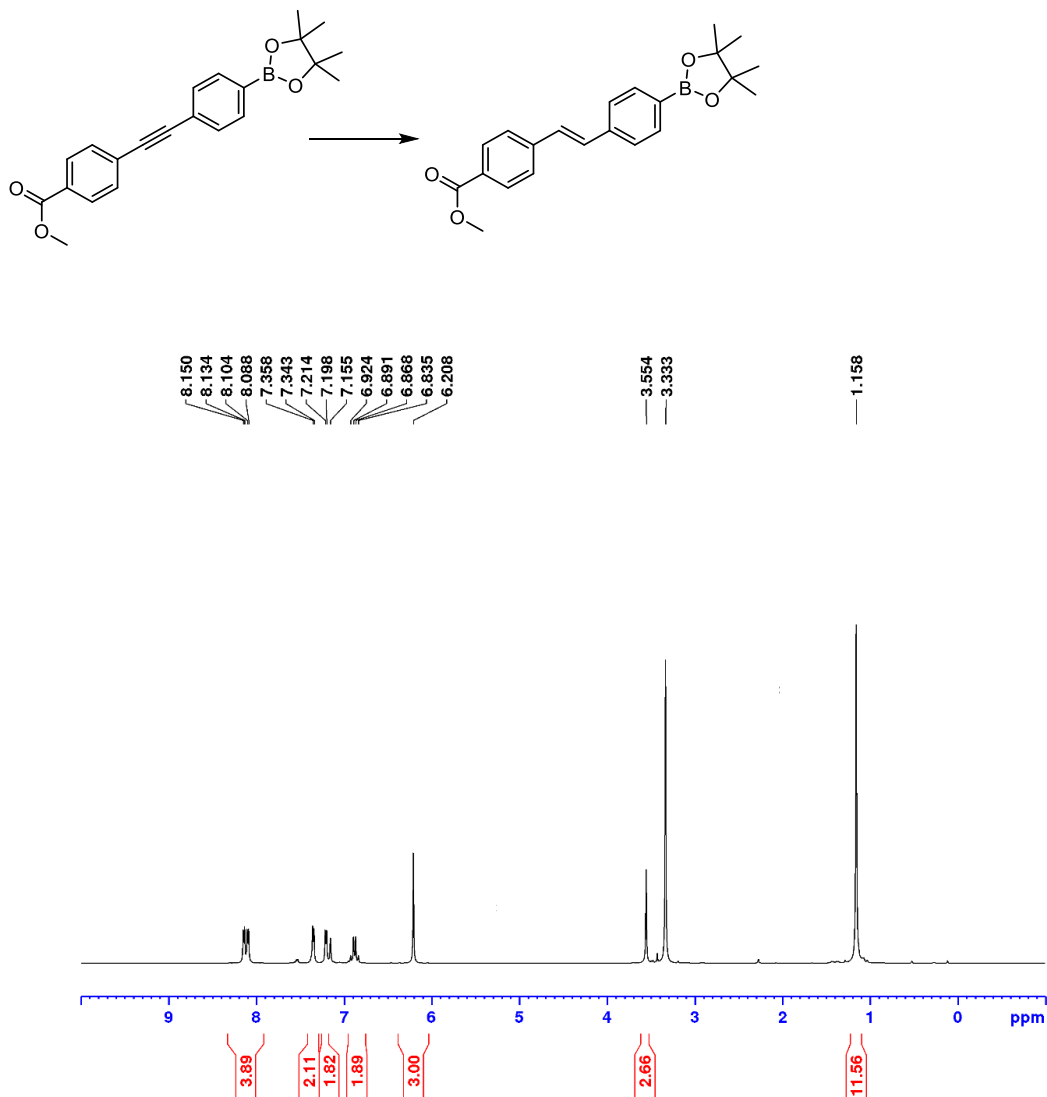


Figure B33. ^1H NMR (500 MHz, C_6D_6) spectrum for the semihydrogenation of 2-(2-phenylethynyl)aniline to afford **3-1i** (1.0 mol% catalyst, 1 atm H_2 , 1.0 M, 25 $^\circ\text{C}$, 4 h; 97% conversion, $E:Z > 99:1$).

^1H NMR (500 MHz, benzene- d_6): δ 7.35 – 7.34 (apparent d, 1 H, *Harom*), 7.31 – 7.29 (apparent d, 2 H, *Harom*), 7.17 – 7.14 (overlapping resonances, 2 H, *Harom*), 7.08 – 7.01 (overlapping resonances, 3 H), 6.90 (d, 1 H, $J = 16.0$ Hz, $\text{HC}=\text{C}$), 6.75 – 6.72 (apparent t, 1 H, *Harom*), 6.37 – 6.35 (apparent d, 1 H, *Harom*).

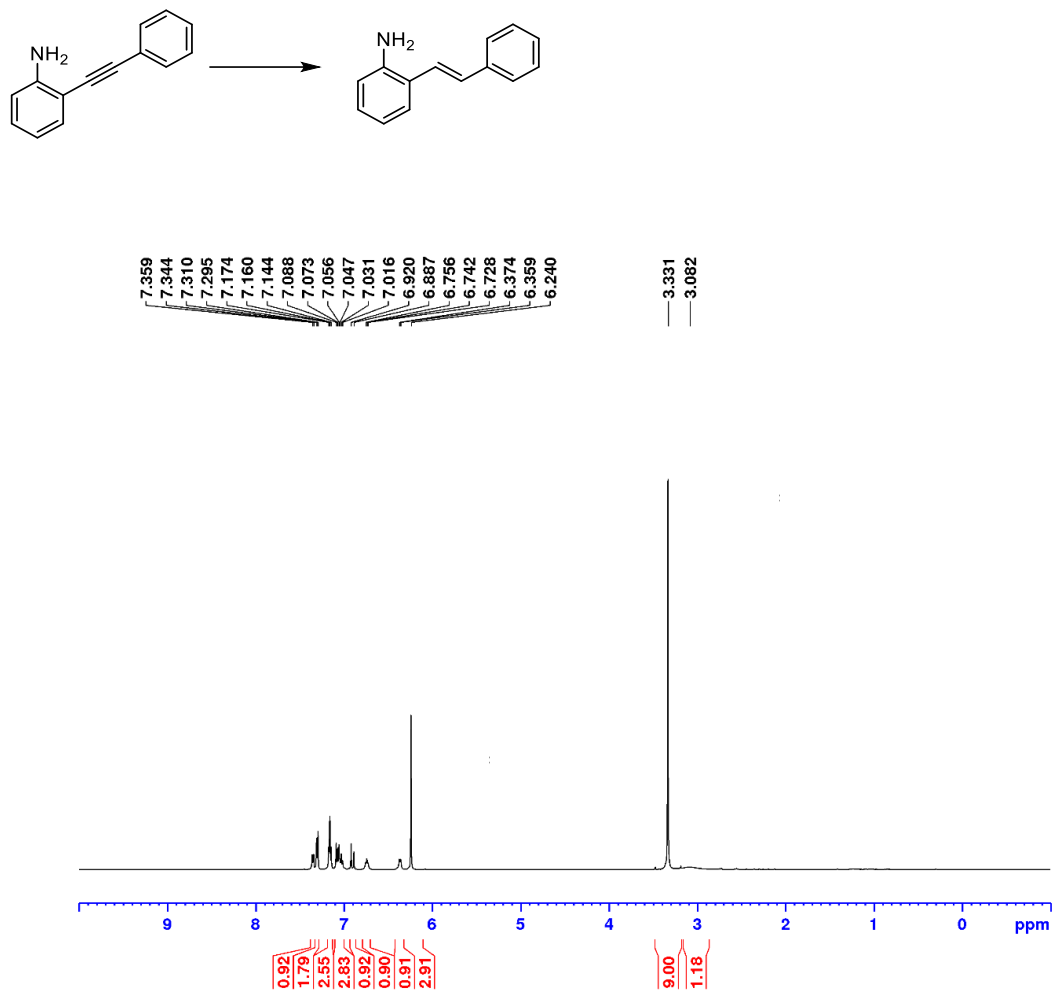


Figure B34. ^1H NMR (300 MHz, C_6D_6) spectrum for the hydrogenation of 1-chloro-2-(2-phenylethynyl)benzene to afford **3-1j** (2.5 mol% catalyst, 1 atm H_2 , 1.0 M, 50 $^\circ\text{C}$, 4 h; >99% conversion, $E:Z > 99:1$). ^1H NMR (300 MHz, benzene- d_6): δ 7.64 (d, 1 H, $J = 16.2$ Hz, $\text{HC}=\text{C}$), 7.37 – 7.31 (m, 3 H, *Harom*), 7.21 – 7.06 (m, 4 *Harom*), 6.91 – 6.84 (overlapping resonances, 2 H), 6.80 – 6.75 (m, 1 H, *Harom*).

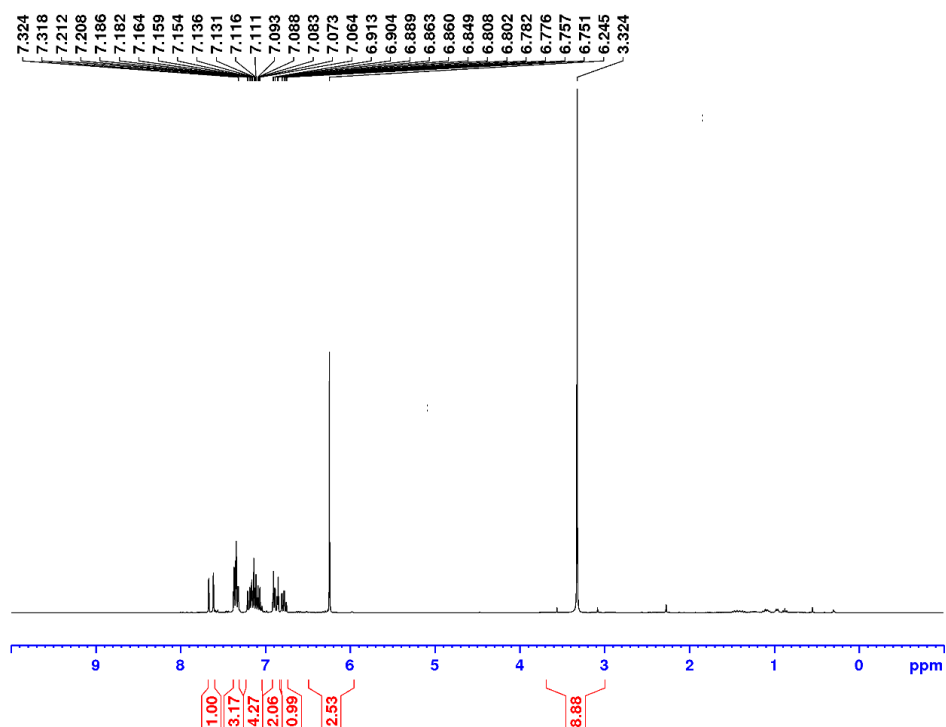
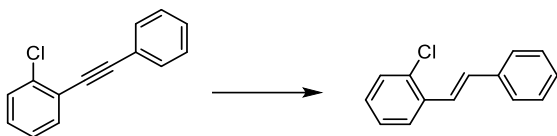


Figure B35. ^1H NMR (500 MHz, C_6D_6) spectrum for the semihydrogenation of 1-chloro-4-(2-phenylethynyl)benzene to afford the (*Z*)-isomer of **3-1k** (1.0 mol% catalyst, 1 atm H_2 , 1.0 M, 25 °C, 4 h; 90% conversion, *E:Z* > 1:99).

^1H NMR (500 MHz, benzene- d_6): δ 7.17 – 7.12 (m, 2 H, *Harom*), 7.02 – 6.96 (overlapping resonances, 3 H, *Harom*), 6.94 – 6.93 (overlapping resonances, 4 H, *Harom*), 6.41 (d, 1 H, $J = 12.3$ Hz, $\text{HC}=\text{C}$), 6.25 (d, 1 H, $J = 12.3$ Hz, $\text{HC}=\text{C}$).

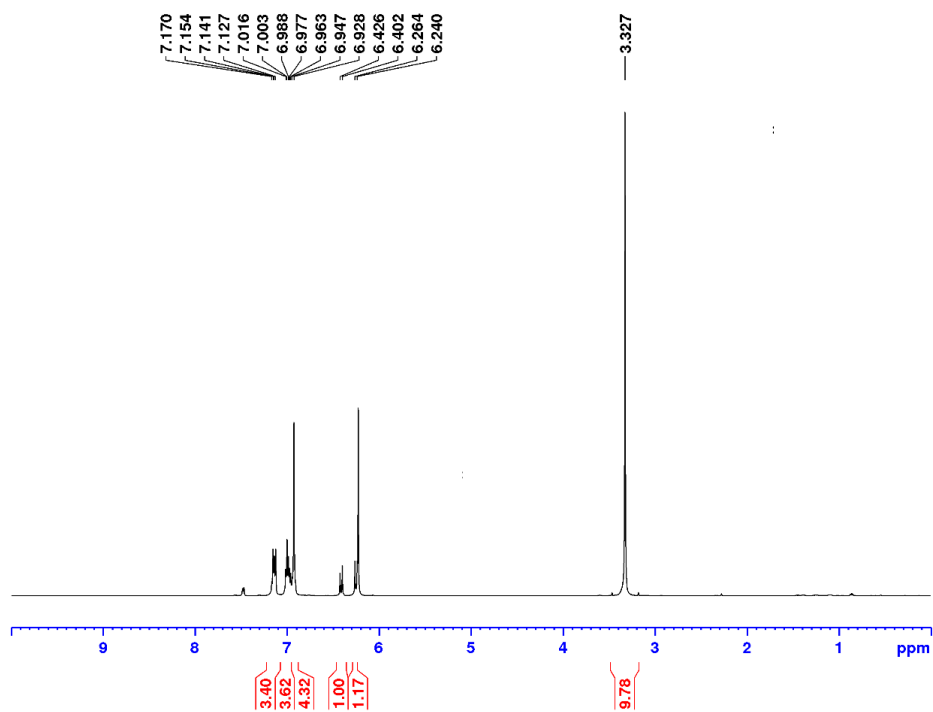
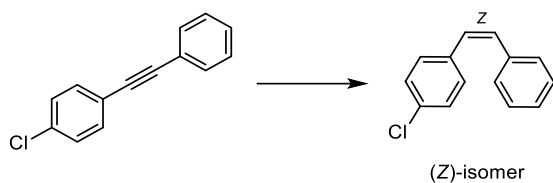


Figure B36. ^1H NMR (500 MHz, toluene- d_8) spectrum for the semihydrogenation of 1-chloro-4-(2-phenylethynyl)benzene to afford the (*E*)-isomer of **3-1k** (2.5 mol% catalyst, 1 atm H_2 , 1.0 M, 90 °C, 4 h; >99% conversion, *E*:*Z* > 99:1). ^1H NMR (500 MHz, benzene- d_6): δ 7.26 (apparent d, 2 H, Harom), 7.14 (overlapping resonances, 2 H, Harom), 7.06 (m, 3 H, Harom), 6.99 (overlapping resonances, 2 H, Harom) 6.78 (d, 1 H, $J = 16.3$ Hz, $\text{HC}=\text{C}$) 6.73 (d, 1 H, $J = 16.3$ Hz, $\text{HC}=\text{C}$).

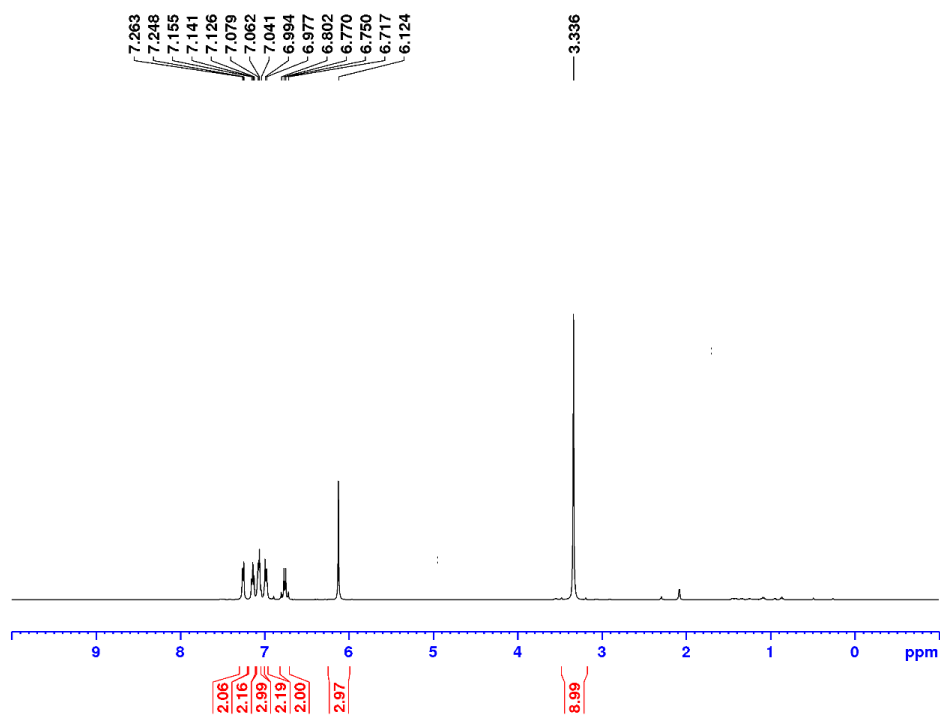
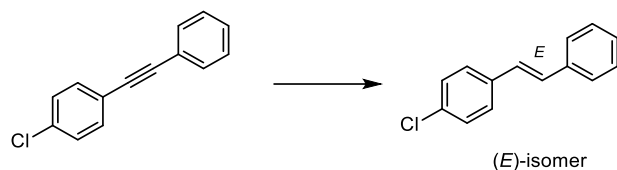


Figure B37. ^1H NMR (500 MHz, C_6D_6) spectrum for the semihydrogenation of 1-[4-(2-phenylethynyl)phenyl]ethanone (2.5 mol% catalyst, 1 atm H_2 , 1.0 M, 50 $^\circ\text{C}$, 4 h; 49% conversion). A mixture of the (*E*)- and (*Z*)-isomers of **3-11** in a 1:1 ratio was found; no starting material remained. The chemical shifts and coupling constants for the respective alkene protons of the (*E*)- and (*Z*)-isomers are as follows:

^1H NMR (500 MHz, benzene- d_6): δ 7.03 (d, 1 H, $J = 16.2$ Hz, (*E*) – $\text{HC}=\text{C}$), 6.91 (d, 1 H, $J = 16.2$ Hz, (*E*) – $\text{HC}=\text{C}$), 6.50 (d, 1 H, $J = 12.2$ Hz, (*Z*) – $\text{HC}=\text{C}$), 6.36 (d, 1 H, $J = 12.2$ Hz, (*Z*) – $\text{HC}=\text{C}$).

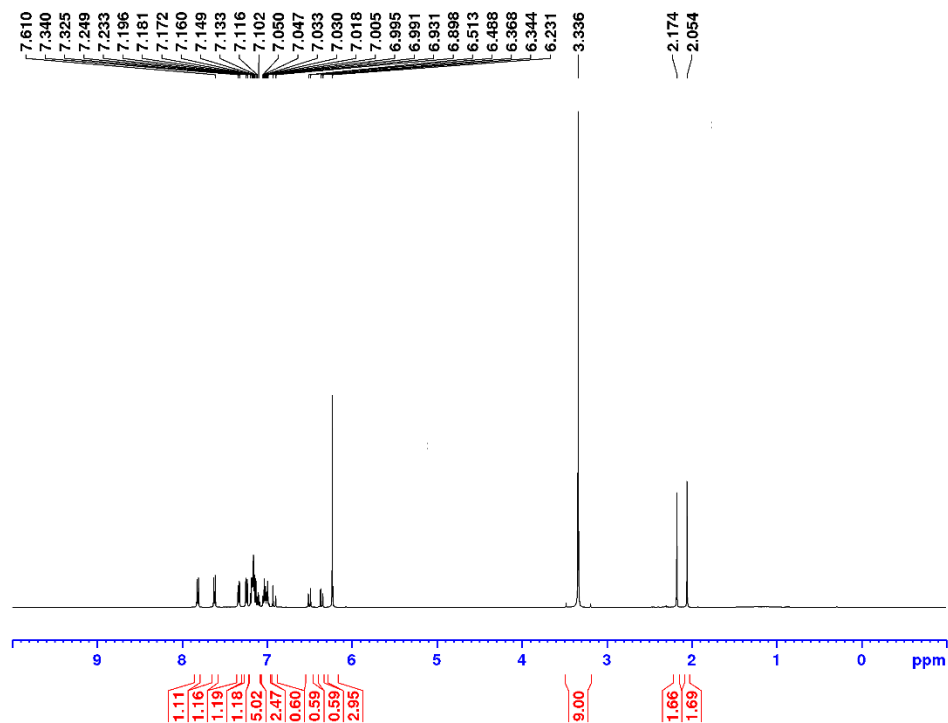
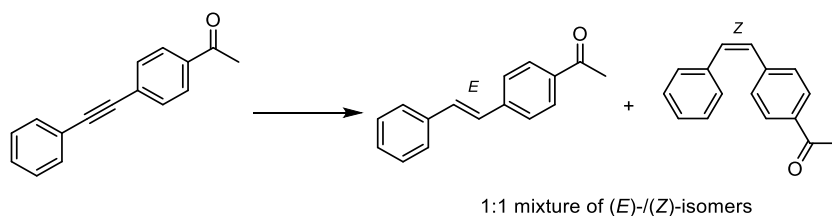


Figure B38. ^1H NMR (500 MHz, toluene- d_8) spectrum for the semihydrogenation of 1-[4-(2-phenylethynyl)phenyl]ethanone to afford the (*E*)-isomer of **3-II** (2.5 mol% catalyst, 1 atm H_2 , 1.0 M, 90 °C, 4 h; 78% conversion, *E*:*Z* > 99:1).

^1H NMR (500 MHz, toluene- d_8): δ 7.76 (apparent d, *H*Arom), 7.29 – 7.10 (overlapping resonances, 10 H), 7.01 – 6.95 (overlapping resonances, 3 H) 6.86 (d, 1 H, J = 16.4 Hz, (*E*) – *HC=C*), 2.16 (s, 3 H, *H*MeC=O).

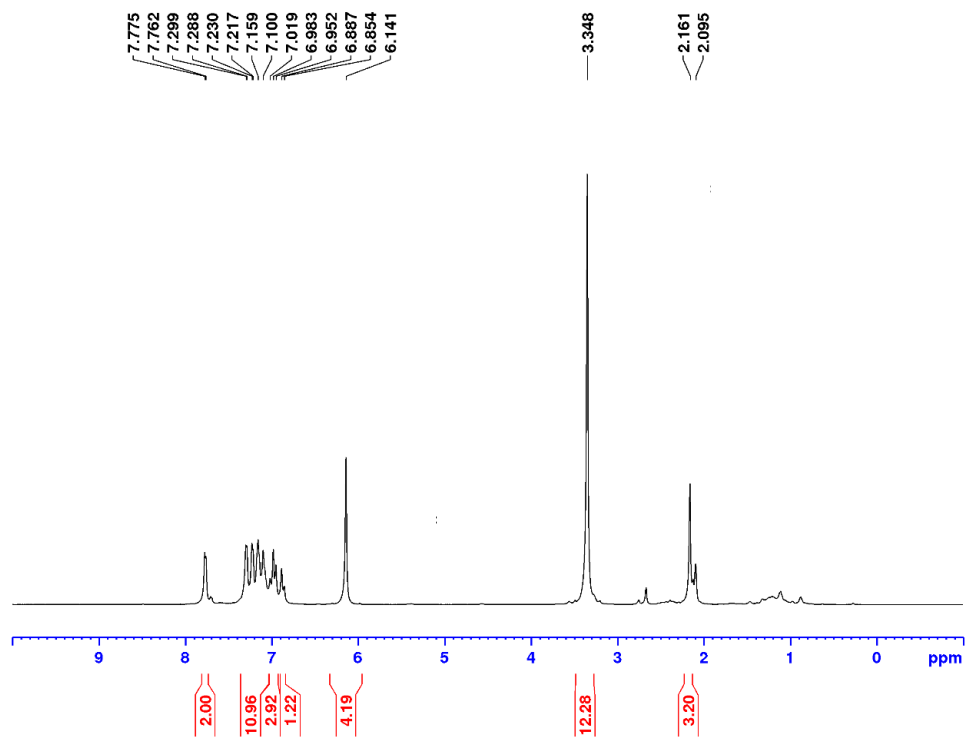
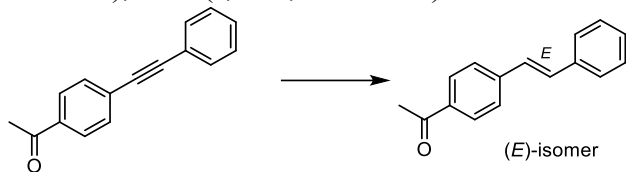


Figure B39. ^1H NMR (500 MHz, C_6D_6) spectrum for the semihydrogenation of 3-(2-phenylethynyl)thiophene to afford **3-1m** (2.5 mol% catalyst, 1 atm H_2 , 1.0 M, 50 $^\circ\text{C}$, 4 h; 96% conversion, $E:Z > 99:1$).

^1H NMR (500 MHz, benzene- d_6): δ 7.29 – 7.28 (apparent d, 2 H, *Harom*), 7.17 – 7.14 (overlapping resonances, 2 H, *Harom*), 7.08 – 7.05 (m, 2 H, *Harom*), 6.94 (d, 1 H, $J = 16.3$ Hz, $\text{HC}=\text{C}$), 6.88 – 6.87 (m, 1 H, *Harom*), 6.85 – 6.84 (m, 1 H, *Harom*), 6.82 (d, 1 H, $J = 16.3$ Hz, $\text{HC}=\text{C}$).

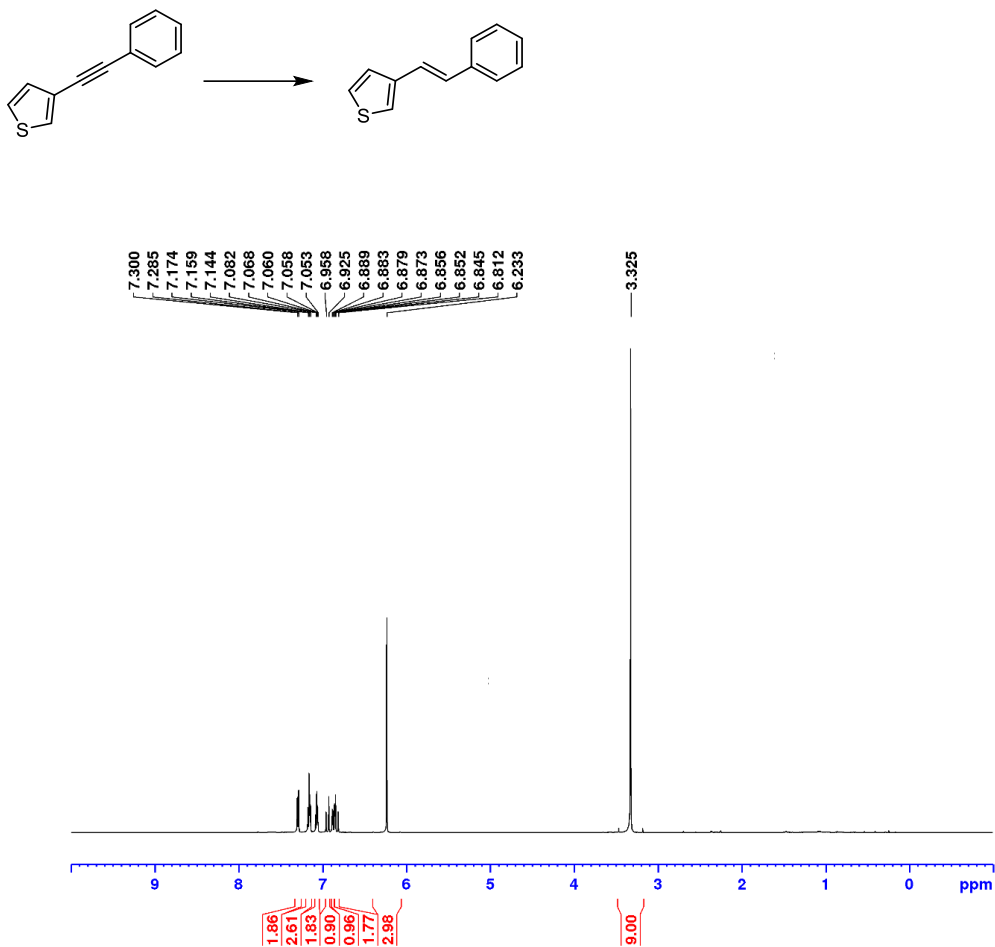


Figure B40. ^1H NMR (500 MHz, C_6D_6) spectrum for the semihydrogenation of 3-(2-phenylethynyl)pyridine to afford **3-1n** (2.5 mol% catalyst, 1 atm H_2 , 1.0 M, 25 °C, 4 h; 85% conversion, $E:Z > 99:1$). ^1H NMR (500 MHz, benzene- d_6): δ 8.74 (broad s, 1 H, *Harom*), 8.47 (broad s, 1 H, *Harom*), 7.26 – 7.24 (overlapping resonances, 3 H, *Harom*), 7.17 – 7.14 (overlapping resonances, 2 H, *Harom*), 6.85 (d, 1 H, $J = 16.4$ Hz, $\text{HC}=\text{C}$), 6.76 – 6.74 (overlapping resonances, 2 H).

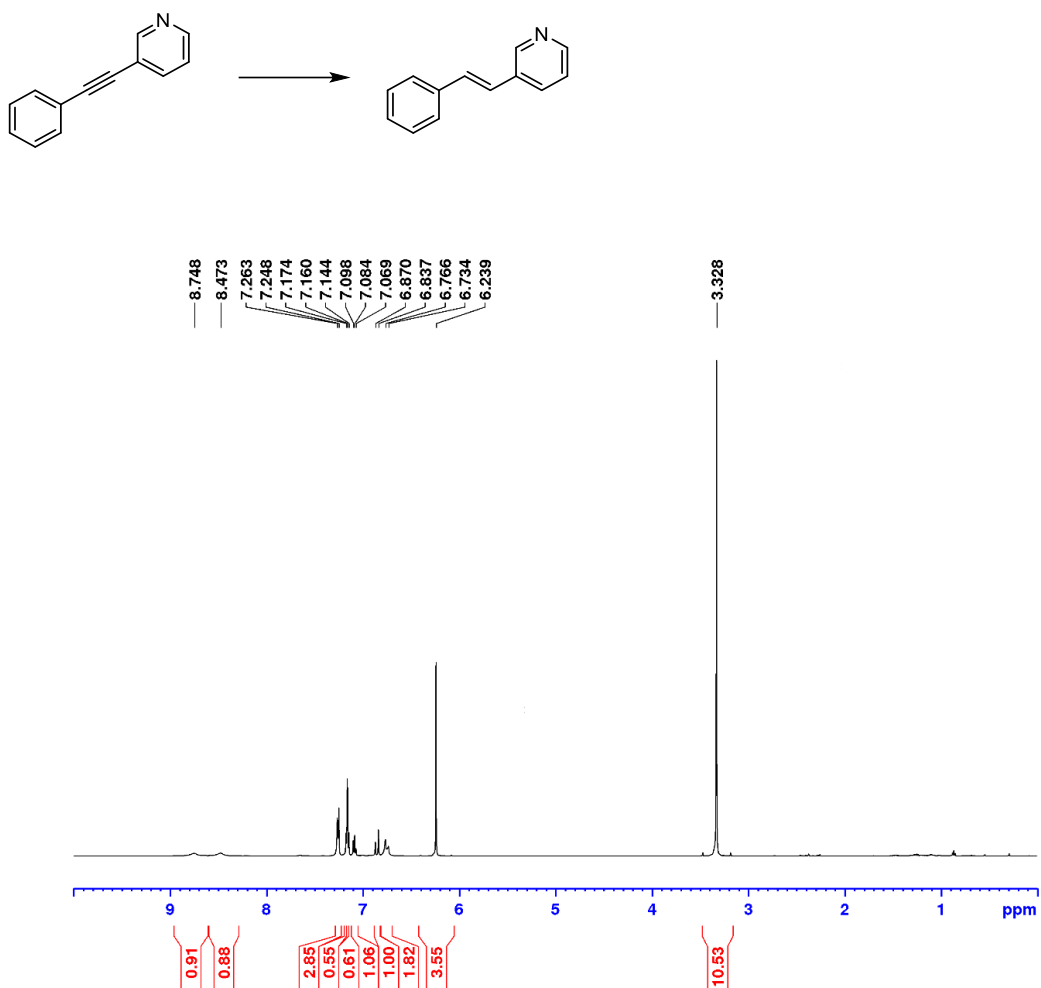


Figure B41. ^1H NMR (500 MHz, C_6D_6) spectrum for the semihydrogenation of [2-(trimethylsilyl)ethynyl]benzene to afford **3-1o** (1.0 mol% catalyst, 1 atm H_2 , 1.0 M, 25 °C, 4 h; 98% conversion, $E:Z > 99:1$). ^1H NMR (500 MHz, benzene- d_6): δ 7.34 – 7.32 (m, 2 H, *Harom*), 7.15 – 7.05 (m, 2 H, *Harom*), 7.08 – 7.05 (m, 1 H, *Harom*), 6.93 (d, 1 H, $J = 19.2$ Hz, $\text{HC}=\text{C}$), 6.47 (d, 1 H, $J = 19.2$ Hz, $\text{HC}=\text{C}$), 0.14 (s, 9 H, SiMe_3).

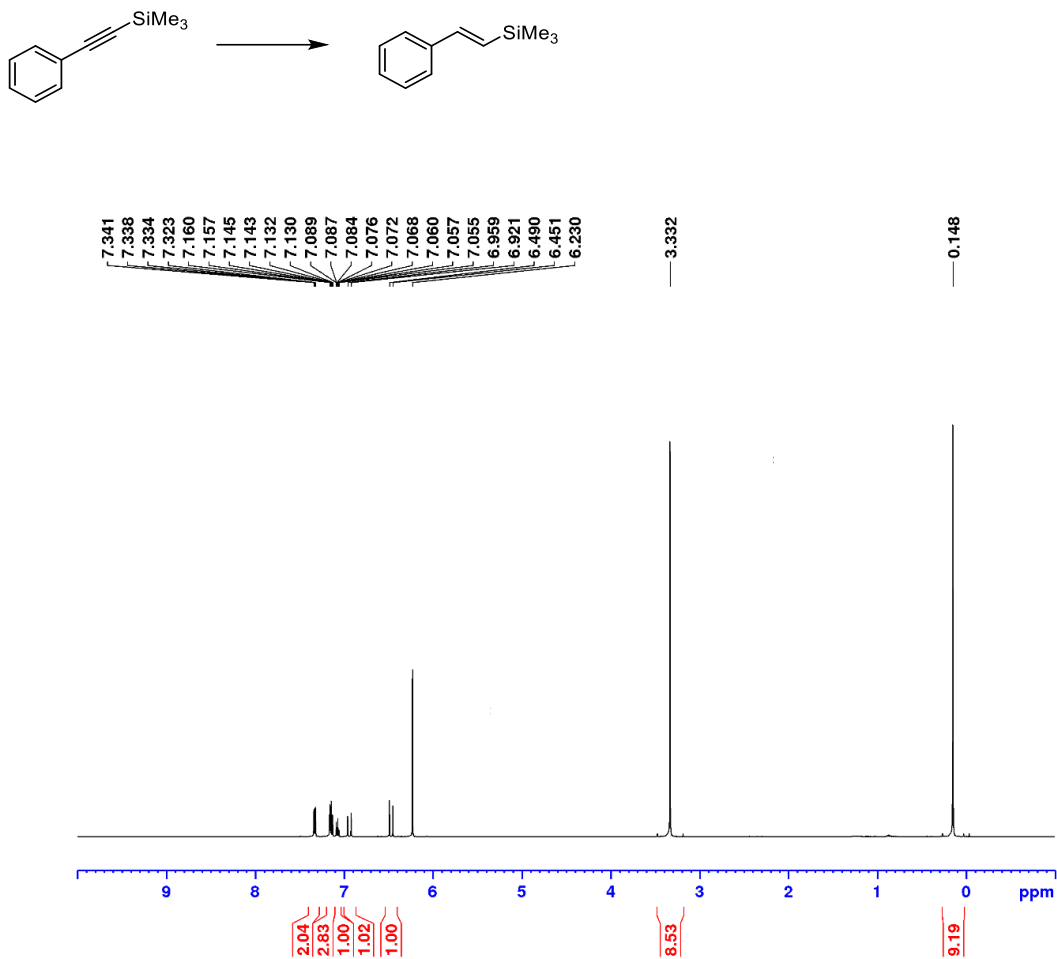


Figure B42. ^1H NMR (500 MHz, C_6D_6) spectrum for the semihydrogenation of 1,4-bis[2-(trimethylsilyl)ethynyl]benzene to afford **3-1p** (1.0 mol% catalyst, 1 atm H_2 , 1.0 M, 25 $^\circ\text{C}$, 4 h; 94% conversion, $E,E:Z,Z > 99:1$). ^1H NMR (500 MHz, benzene- d_6): δ 7.32 (s, 4 H, *Harom*), 6.94 (d, 2 H, $J = 19.2$ Hz, $\text{HC}=\text{C}$), 6.49 (d, 2 H, $J = 19.2$ Hz, $\text{HC}=\text{C}$), 0.17 (s, 18 H, SiMe_3).

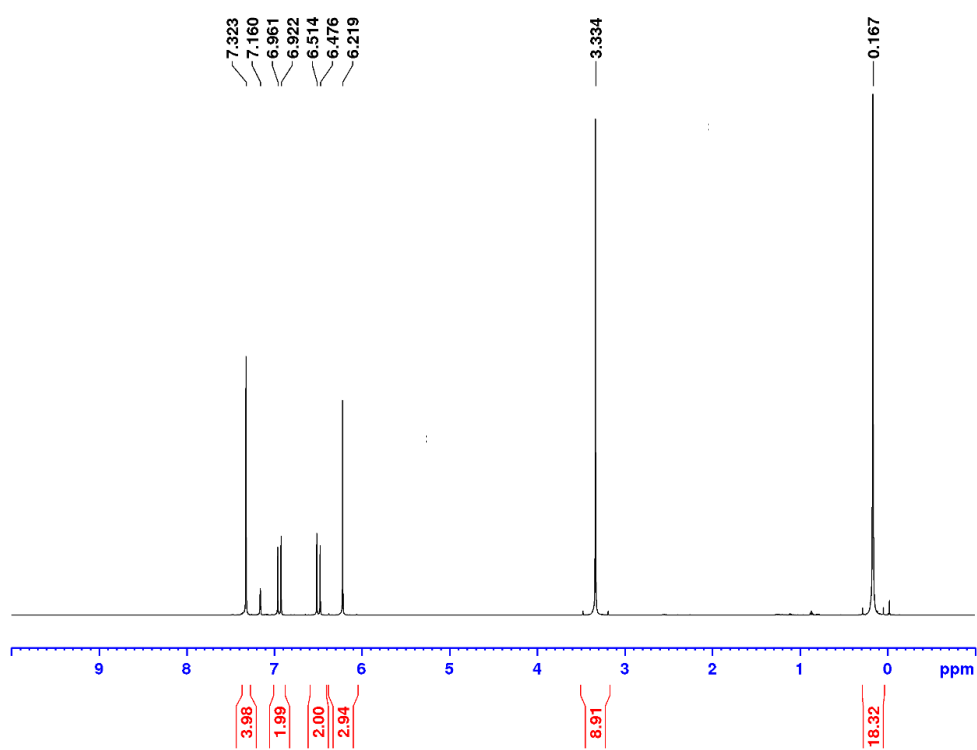
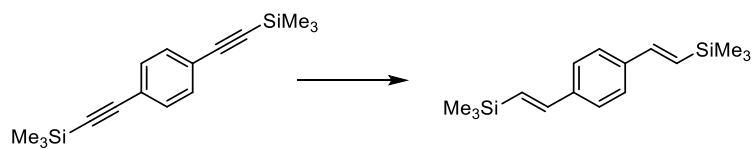


Figure B43. ^1H NMR (500 MHz, C_6D_6) spectrum for the semihydrogenation of 1-(trifluoromethyl)-4-[2-(trimethylsilyl)ethynyl]benzene to afford **3-1q** (1.0 mol% catalyst, 1 atm H_2 , 1.0 M, 25 $^\circ\text{C}$, 4 h; 85% conversion, $E:Z > 99:1$).

^1H NMR (500 MHz, benzene- d_6): δ 7.35 – 7.33 (apparent d, 2 H, Harom), 7.09 – 7.07 (apparent d, 2 H, Harom), 6.75 (d, 2 H, $J = 19.2$ Hz, $\text{HC}=\text{C}$), 6.41 (d, 2 H, $J = 19.2$ Hz, $\text{HC}=\text{C}$), 0.13 (s, 9 H, SiMe_3).

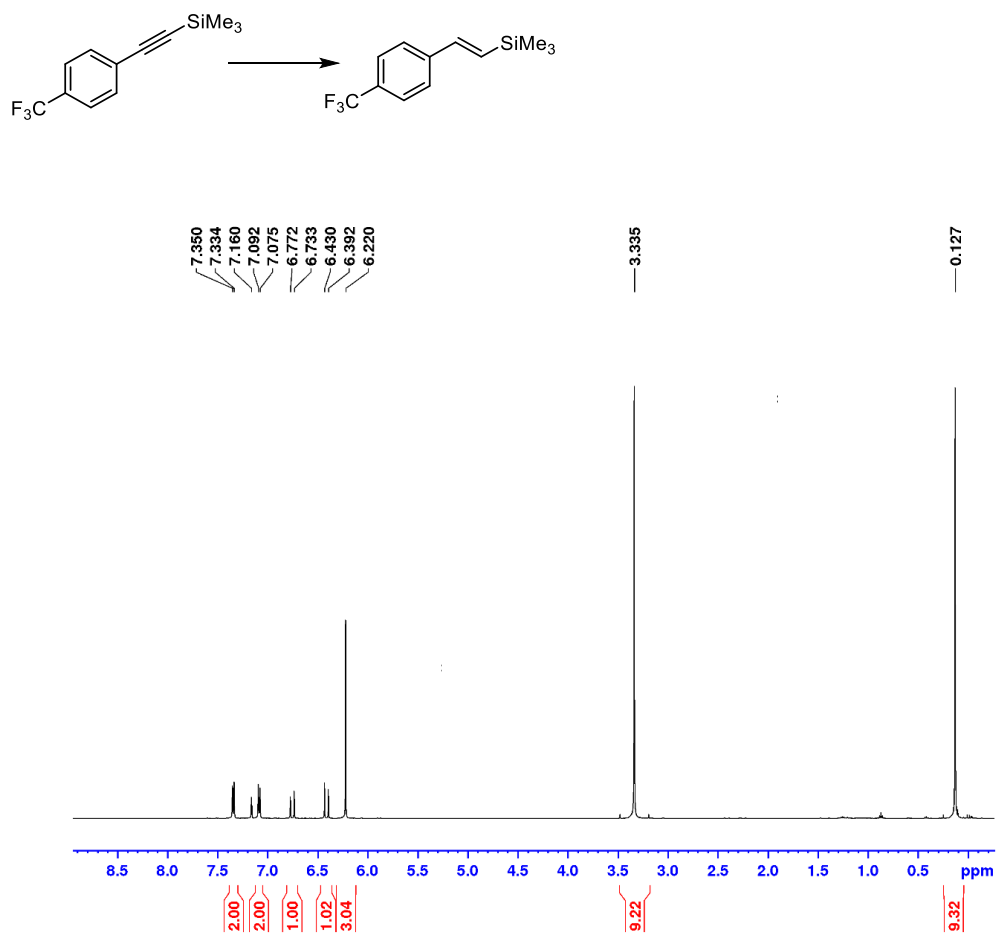


Figure B44. ^{19}F NMR (470 MHz, C_6D_6) spectrum for the semihydrogenation of 1-(trifluoromethyl)-4-[2-(trimethylsilyl)ethynyl]benzene to afford **3-1q** (1.0 mol% catalyst, 1 atm H_2 , 1.0 M, 25 $^\circ\text{C}$, 4 h; 85% conversion, $E:Z > 99:1$).

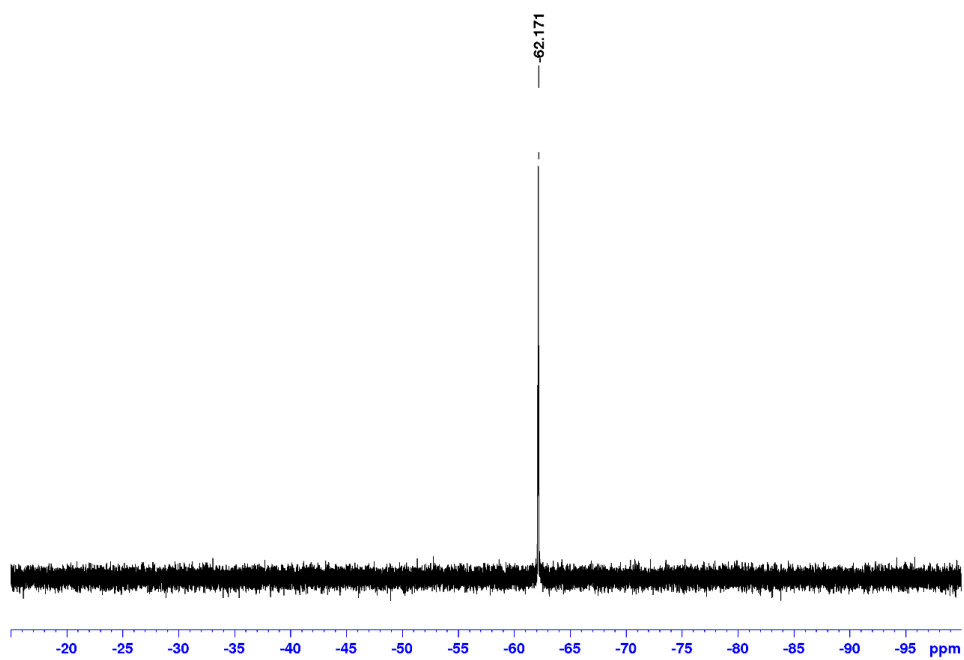
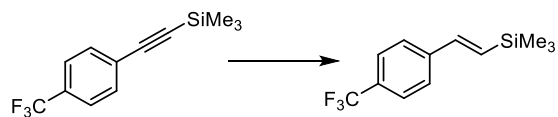


Figure B45. ^1H NMR (500 MHz, C_6D_6) spectrum for the semihydrogenation of 1,3-difluoro-5-[2-(trimethylsilyl)ethynyl]benzene to afford **3-1r** (2.5 mol% catalyst, 1 atm H_2 , 1.0 M, 25 $^\circ\text{C}$, 4 h; >99% conversion, $E:Z > 99:1$). ^1H NMR (500 MHz, benzene- d_6): δ 6.69 – 6.65 (m, 2 H, *Harom*), 6.55 (d, 1 H, $J = 19.1$ Hz, $\text{HC}=\text{C}$), 6.45 – 6.41 (m, 1 H, *Harom*), 6.25 (d, 1 H, $J = 19.1$ Hz, $\text{HC}=\text{C}$), 0.08 (s, 9 H, SiMe_3).

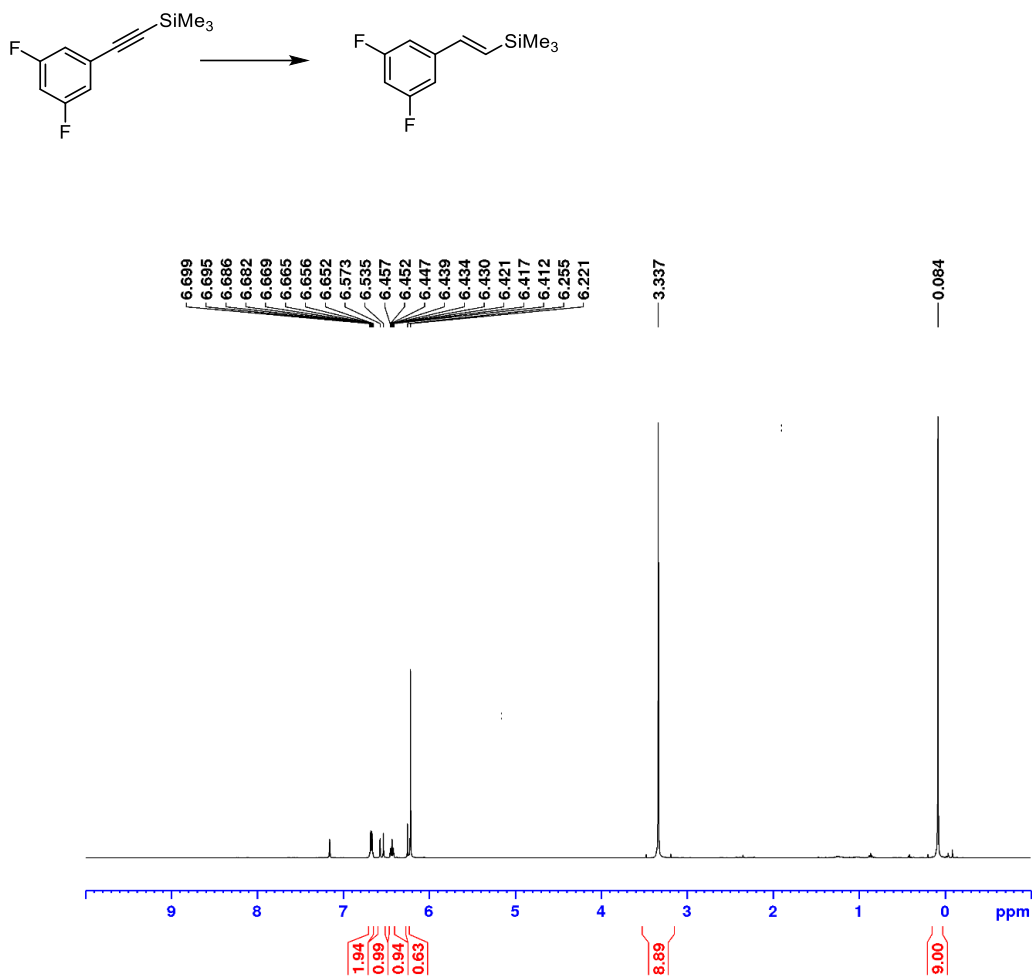


Figure B46. ^{19}F NMR (470 MHz, C_6D_6) spectrum for the semihydrogenation of 1,3-difluoro-5-[2-(trimethylsilyl)ethynyl]benzene to afford **3-1r** (2.5 mol% catalyst, 1 atm H_2 , 1.0 M, 25 °C, 4 h; >99% conversion, $E:Z > 99:1$).

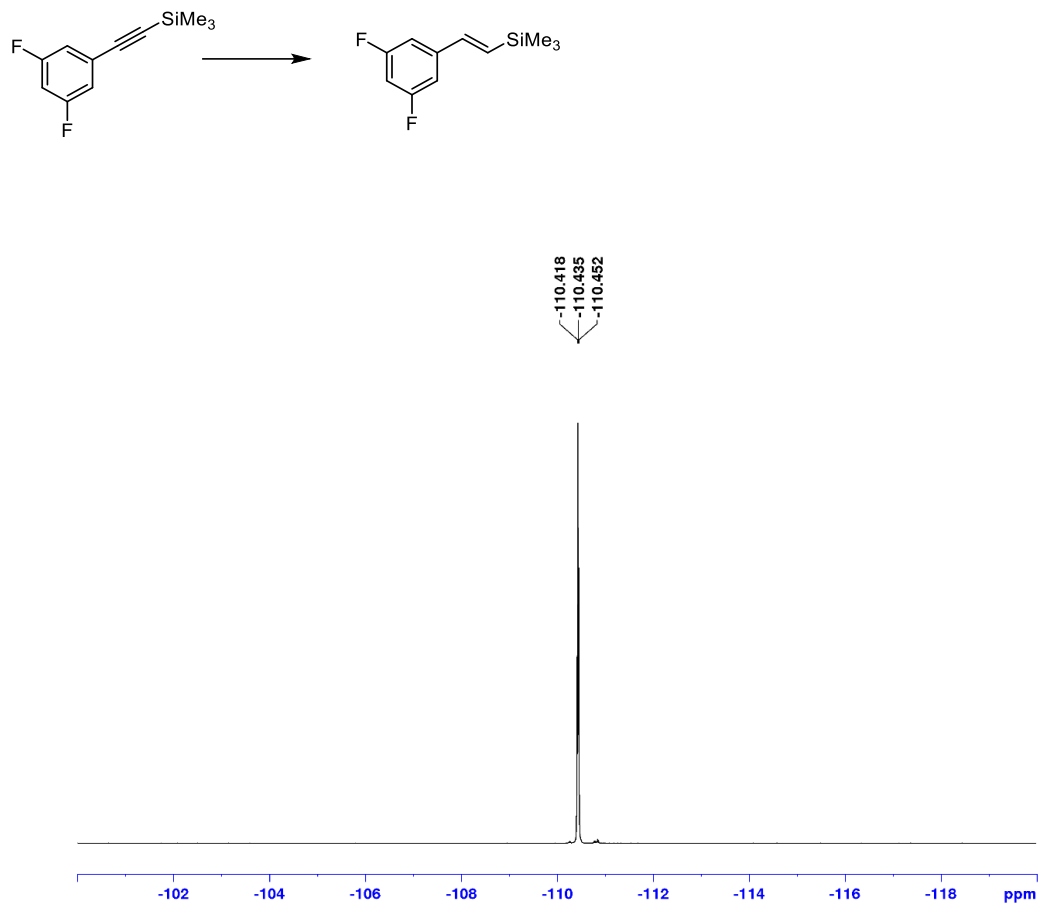


Figure B47. ^1H NMR (500 MHz, C_6D_6) spectrum for the semihydrogenation of 1-chloro-3-[2-(trimethylsilyl)ethynyl]benzene to afford **3-1s** (1.0 mol% catalyst, 1 atm H_2 , 1.0 M, 25 °C, 4 h; 98% conversion, $E:Z > 99:1$). ^1H NMR (500 MHz, benzene- d_6): δ 7.34 – 7.33 (m, 1 H, *Harom*), 7.04 – 7.02 (m, 1 H, *Harom*), 6.98 – 6.97 (m, 1 H, *Harom*), 6.83 – 6.81 (m, 1 H, *Harom*), 6.68 (d, 1 H, $J = 19.2$ Hz, $\text{HC}=\text{C}$), 6.32 (d, 1 H, $J = 19.2$ Hz, $\text{HC}=\text{C}$), 0.11 (s, 9 H, SiMe_3).

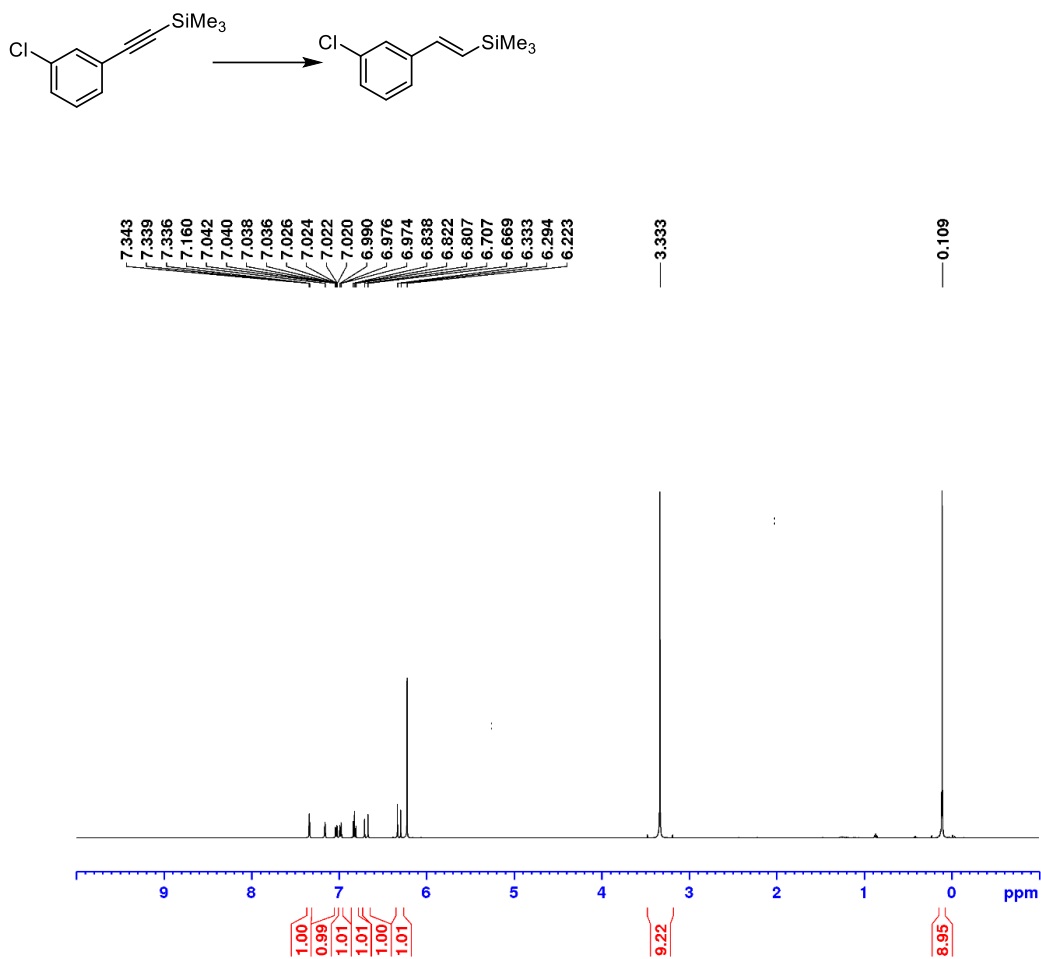


Figure B48. ^1H NMR (500 MHz, C_6D_6) spectrum for the semihydrogenation of 1-methyl-2-[2-(trimethylsilyl)ethynyl]benzene to afford **3-1t** (2.5 mol% catalyst, 1 atm H_2 , 1.0 M, 50 $^\circ\text{C}$, 4 h; 96% conversion, $E:Z > 99:1$).

^1H NMR (500 MHz, benzene- d_6): δ 7.52 – 7.49 (m, 1 H, *Harom*), 7.21 (d, 1 H, $J = 19.0$ Hz, $\text{HC}=\text{C}$), 7.11 – 7.02 (overlapping resonances, 2 H), 6.99 – 6.96 (m, 1 H, *Harom*), 6.39 (d, 1 H, $J = 19.0$ Hz, $\text{HC}=\text{C}$), 2.17 (s, 3 H, *CMe*), 0.16 (s, 9 H, SiMe_3).

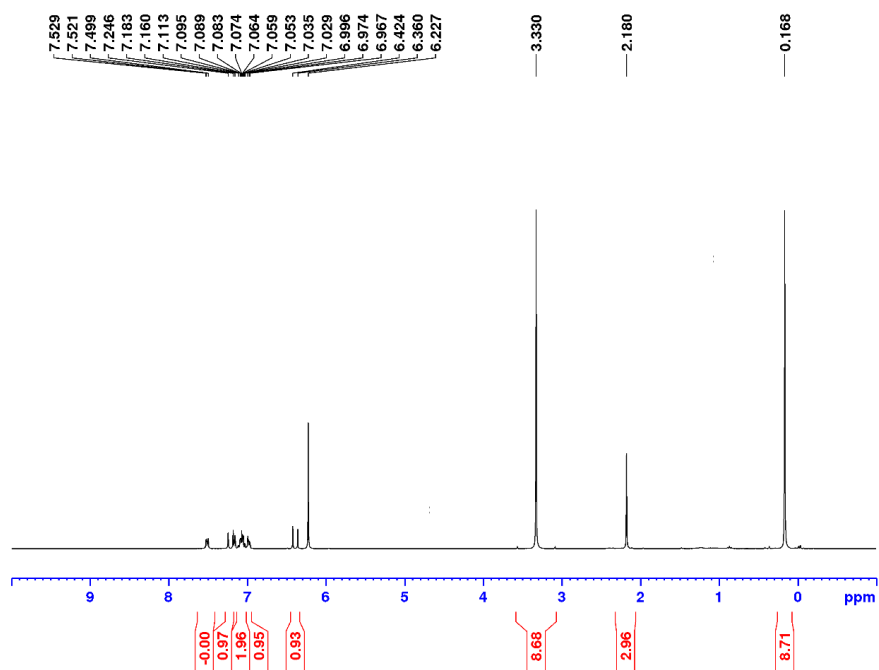
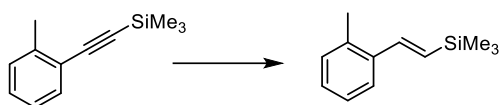


Figure B49. ^1H NMR (500 MHz, C_6D_6) spectrum for the semihydrogenation of 1-methoxy-4-[2-(trimethylsilyl)ethynyl]benzene to afford **3-1u** (1.0 mol% catalyst, 1 atm H_2 , 1.0 M, 25 $^\circ\text{C}$, 4 h; 99% conversion, $E:Z > 99:1$). ^1H NMR (500 MHz, benzene- d_6): δ 7.30 – 7.29 (apparent d, 2 H, *Harom*), 6.95 (d, 1 H, $J = 19.2$ Hz, $\text{HC}=\text{C}$), 6.76 – 6.74 (m, 2 H, *Harom*), 6.36 (d, 1 H, $J = 19.2$ Hz, $\text{HC}=\text{C}$), 3.30 (s, 3 H, *OMe*), 0.17 (s, 9 H, SiMe_3).

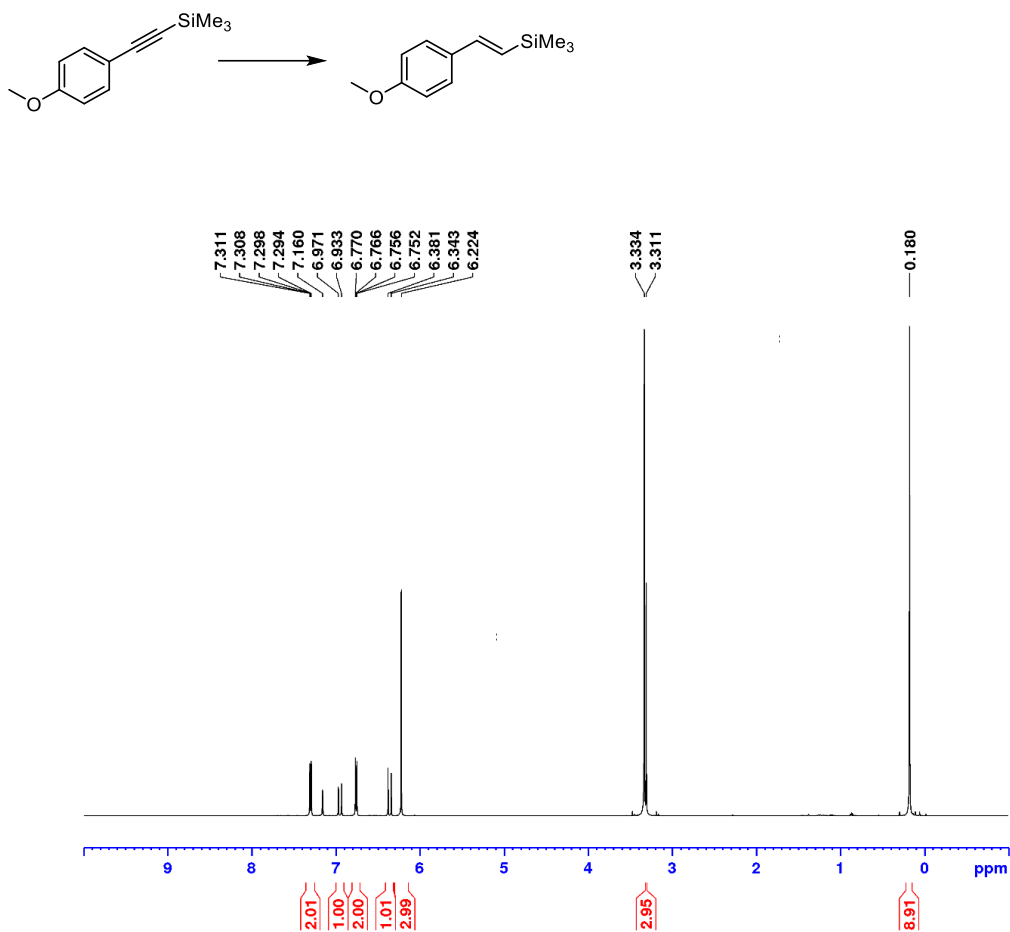


Figure B50. ^1H NMR (500 MHz, C_6D_6) spectrum for the semihydrogenation of **2v** 1,3-dimethoxy-5-[2-(trimethylsilyl)ethynyl]benzene to afford **3-1v** (1.0 mol% catalyst, 1 atm H_2 , 1.0 M, 25 $^\circ\text{C}$, 4 h; 95% conversion, $E:Z > 99:1$). ^1H NMR (500 MHz, benzene- d_6): δ 6.94 (d, 1 H, $J = 19.1$ Hz, $\text{HC}=\text{C}$), 6.76 – 6.75 (overlapping resonances, 2 H, *Harom*), 6.55 (d, 1 H, $J = 19.1$ Hz, $\text{HC}=\text{C}$), 6.52 – 6.51 (m, 1 H, *Harom*), 3.36 (s, 6 H, *OMe*), 0.15 (s, 9 H, SiMe_3).

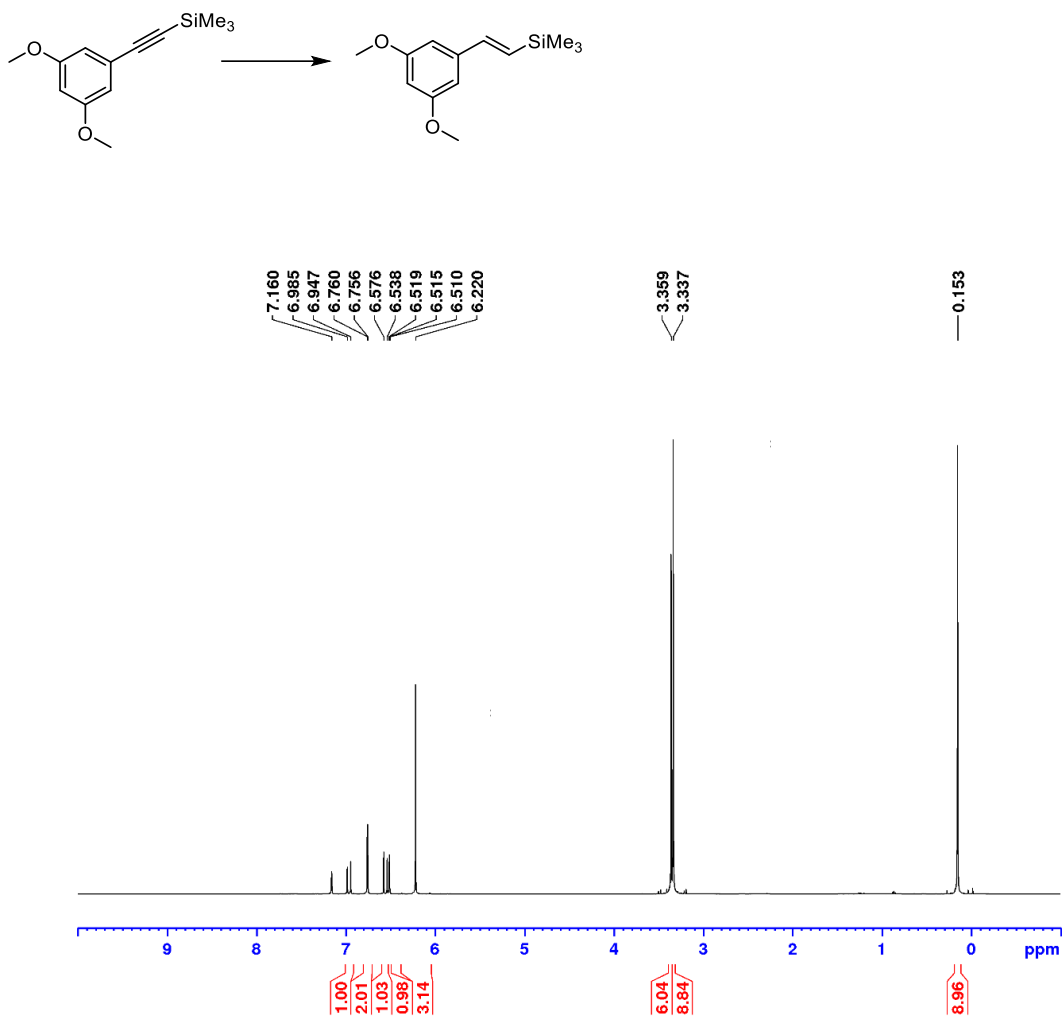


Figure B51. ^1H NMR (300 MHz, C_6D_6) spectrum for the semihydrogenation of 2-[2-(trimethylsilyl)ethynyl]aniline to afford **3-1w** (2.5 mol% catalyst, 1 atm H_2 , 1.0 M, 50 $^\circ\text{C}$, 4 h; 98% conversion, $E:Z > 99:1$). ^1H NMR (300 MHz, benzene- d_6): δ 7.37 – 7.34 (apparent d, 1 H, *Harom*), 7.03 – 6.97 (overlapping resonances, 2 H, *Harom* & $\text{HC}=\text{C}$ ($J = 18.8$ Hz)), 6.76 – 6.71 (m, 1 H, *Harom*), 6.38 – 6.32 (overlapping resonances, 2 H, *Harom* & $\text{HC}=\text{C}$ ($J = 18.8$ Hz)), 0.13 (s, 9 H, SiMe_3).

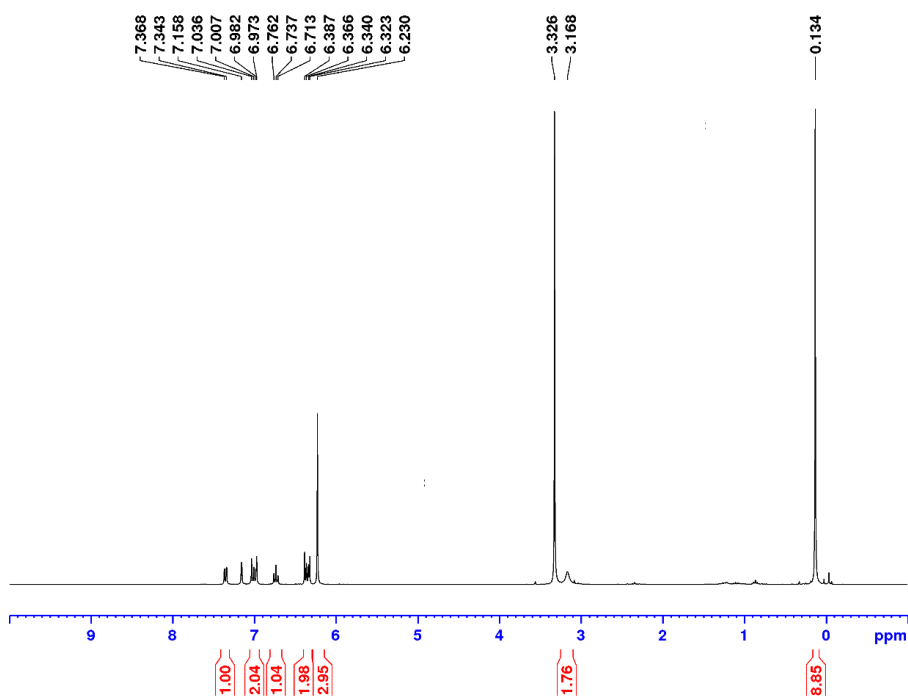
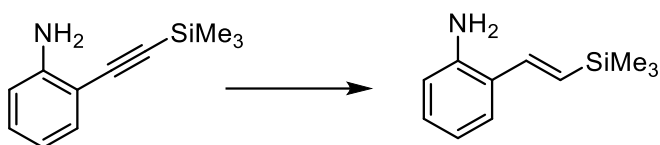


Figure B52. ^1H NMR (500 MHz, C_6D_6) spectrum for the semihydrogenation of 3-[2-(trimethylsilyl)ethynyl]thiophene to afford **3-1x** (1.0 mol% catalyst, 1 atm H_2 , 1.0 M, 25 $^\circ\text{C}$, 4 h; 92% conversion, $E:Z > 99:1$).

^1H NMR (500 MHz, benzene- d_6): δ 7.10 – 7.09 (m, 1 H, *Harom*), 6.86 (d, 1H, $J = 18.8$ Hz, $\text{HC}=\text{C}$), 6.86 – 6.83 (m, 2 H, *Harom*), 6.22 (d, 1H, $J = 18.8$ Hz, $\text{HC}=\text{C}$), 0.13 (s, 9 H, SiMe_3).

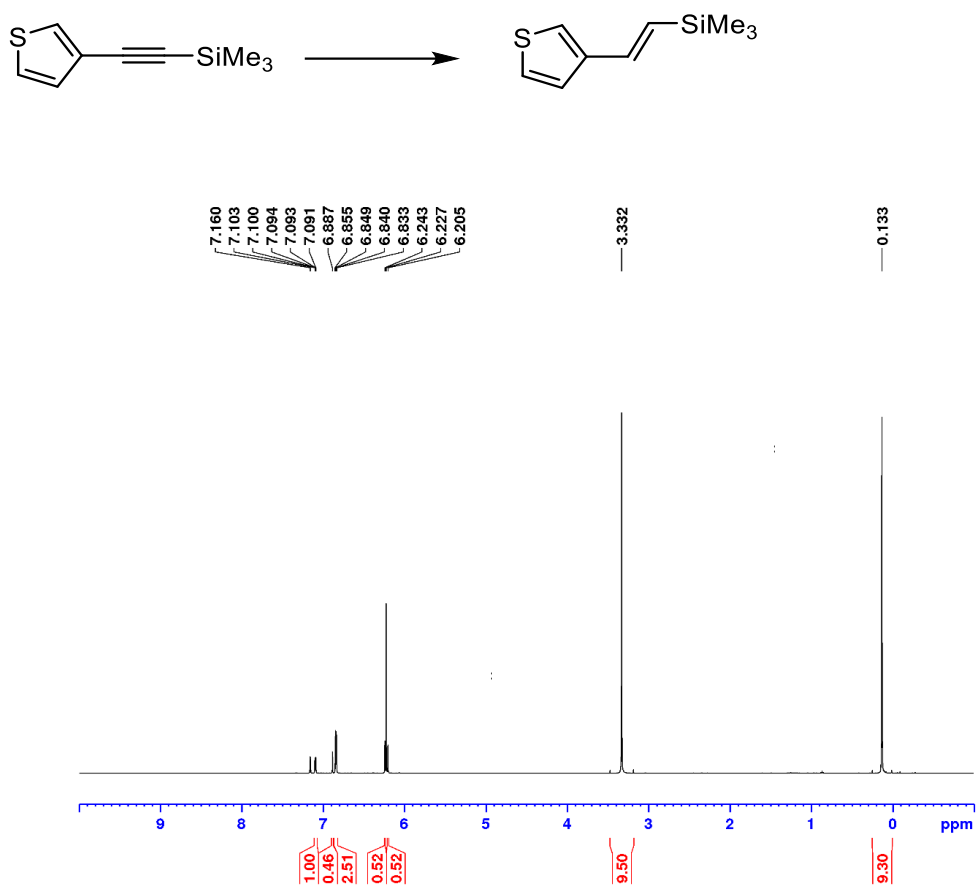


Figure B53. ^1H NMR (500 MHz, C_6D_6) spectrum for the semihydrogenation of 2-[2-(trimethylsilyl)ethynyl]thiophene to afford **3-1y** (1.0 mol% catalyst, 1 atm H_2 , 1.0 M, 25 $^\circ\text{C}$, 4 h; 97% conversion, $E:Z > 99:1$). ^1H NMR (500 MHz, benzene- d_6): δ 6.98 (d, 1 H, $J = 18.9$ Hz, $\text{HC}=\text{C}$), 6.79 – 6.76 (m, 2 H, *Harom*), 6.70 – 6.68 (m, 1 H, *Harom*), 6.34 (d, 1 H, $J = 18.9$ Hz, $\text{HC}=\text{C}$), 0.07 (s, 9 H, SiMe_3).

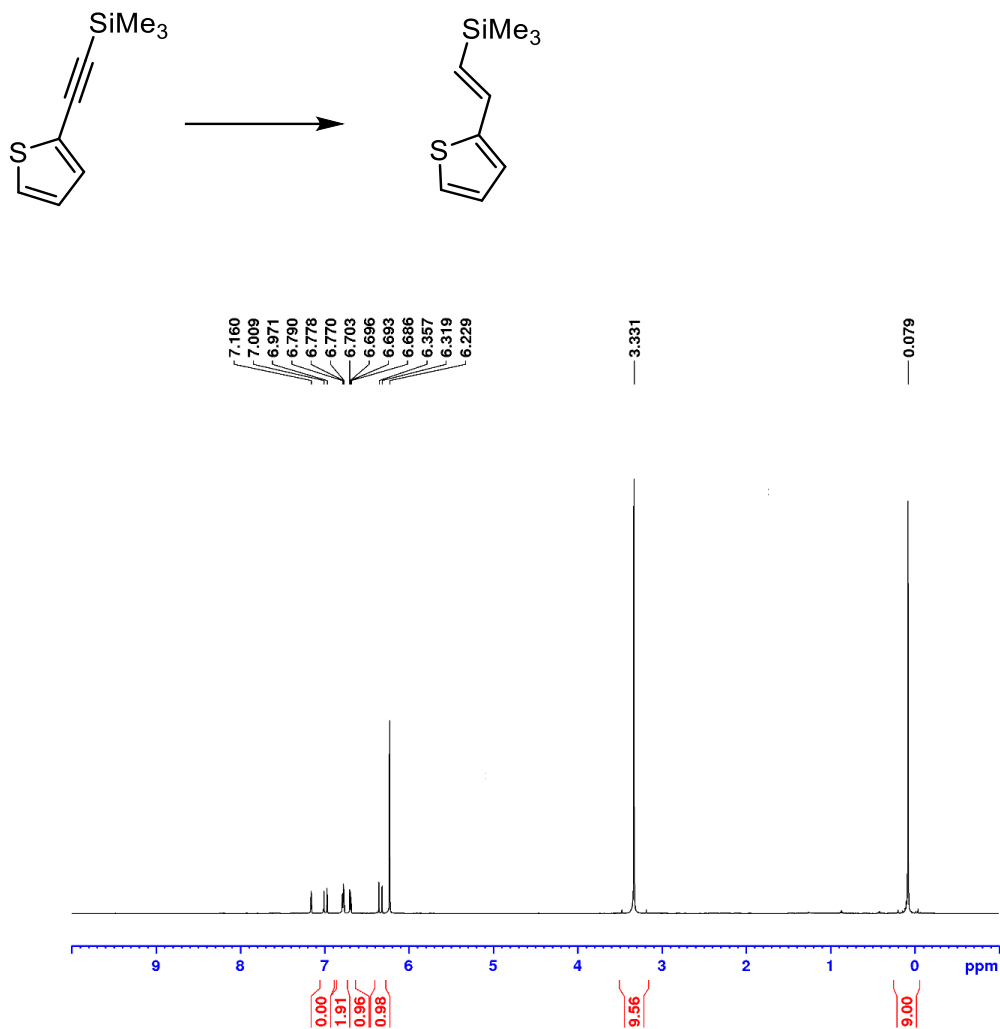


Figure B54. ^1H NMR (500 MHz, C_6D_6) spectrum for the semihydrogenation of 3-[2-(trimethylsilyl)ethynyl]pyridine to afford **3-1z** (1.0 mol% catalyst, 1 atm H_2 , 1.0 M, 25 $^\circ\text{C}$, 4 h; 97% conversion, $E:Z > 99:1$). ^1H NMR (500 MHz, benzene- d_6): δ 8.70 (s, 1 H, *Harom*), 8.44 (s, 1 H, *Harom*), 7.28 – 7.27 (m, 1 H, *Harom*), 6.75 – 6.71 (overlapping resonances, 2 H), 6.38 (d, 1 H, $J = 19.2$ Hz, $\text{HC}=\text{C}$), 0.10 (s, 9 H, SiMe_3).

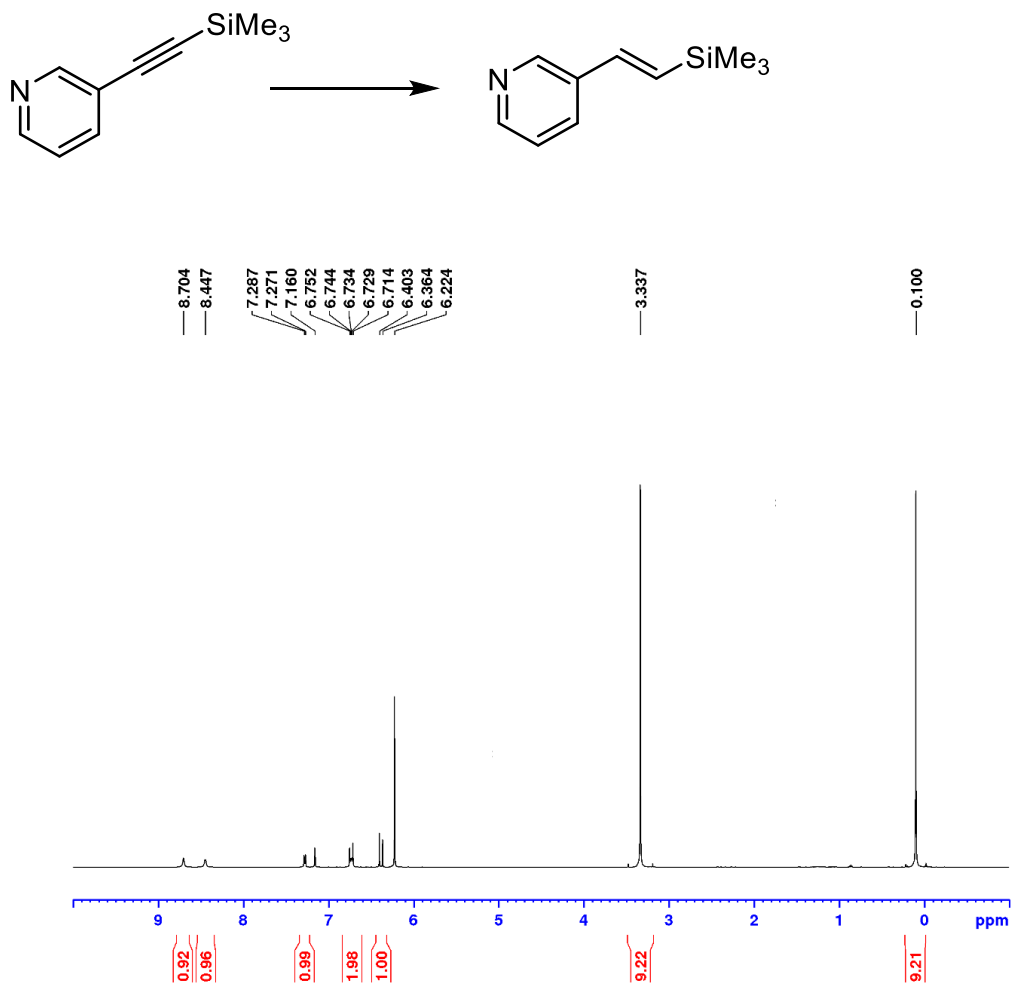


Figure B55. ^1H NMR (300 MHz, C_6D_6) spectrum for the semihydrogenation of 4,4,5,5-tetramethyl-2-(2-phenylethynyl)-1,3,2-dioxaborolane to afford **3-1aa** (2.5 mol% catalyst, 1 atm H_2 , 1.0 M, 50 $^\circ\text{C}$, 4 h; 83% conversion, $E:Z > 99:1$). ^1H NMR (500 MHz, benzene- d_6): δ 7.74 (d, 1 H, $J = 18.4$ Hz, $\text{H}_{\text{C}=\text{C}}$), 7.33 – 7.30 (m, 2 H, H_{arom}), 7.06 – 6.99 (m, 3 H, $\text{H}_{\text{C}=\text{C}}$), 6.44 (d, 1 H $J = 18.4$ Hz, $\text{H}_{\text{C}=\text{C}}$), 1.12 (s, 12 H, BPin).

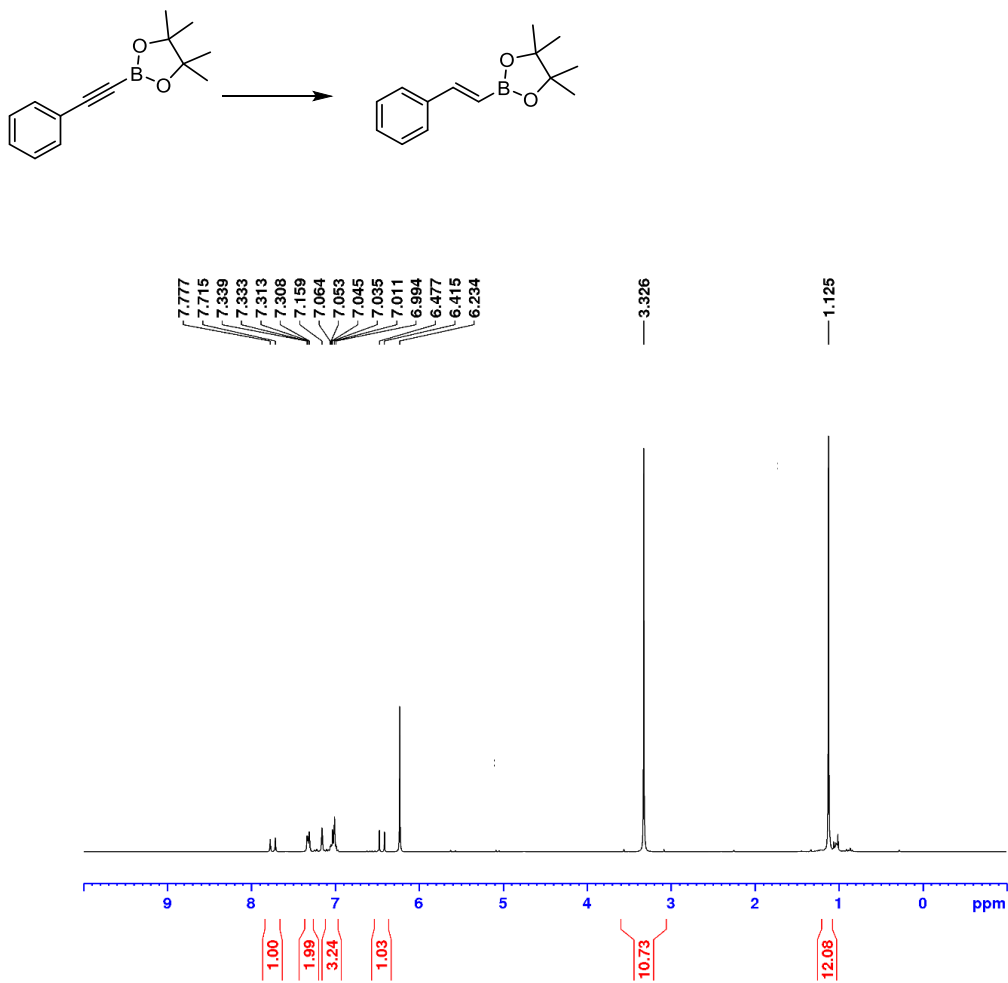


Figure B56. ^{11}B NMR (96.3 MHz, C_6D_6) spectrum for the semihydrogenation of 4,4,5,5-tetramethyl-2-(2-phenylethynyl)-1,3,2-dioxaborolane to afford **3-1aa** (2.5 mol% catalyst, 1 atm H_2 , 1.0 M, 50 $^\circ\text{C}$, 4 h; 83% conversion, $E:Z > 99:1$).

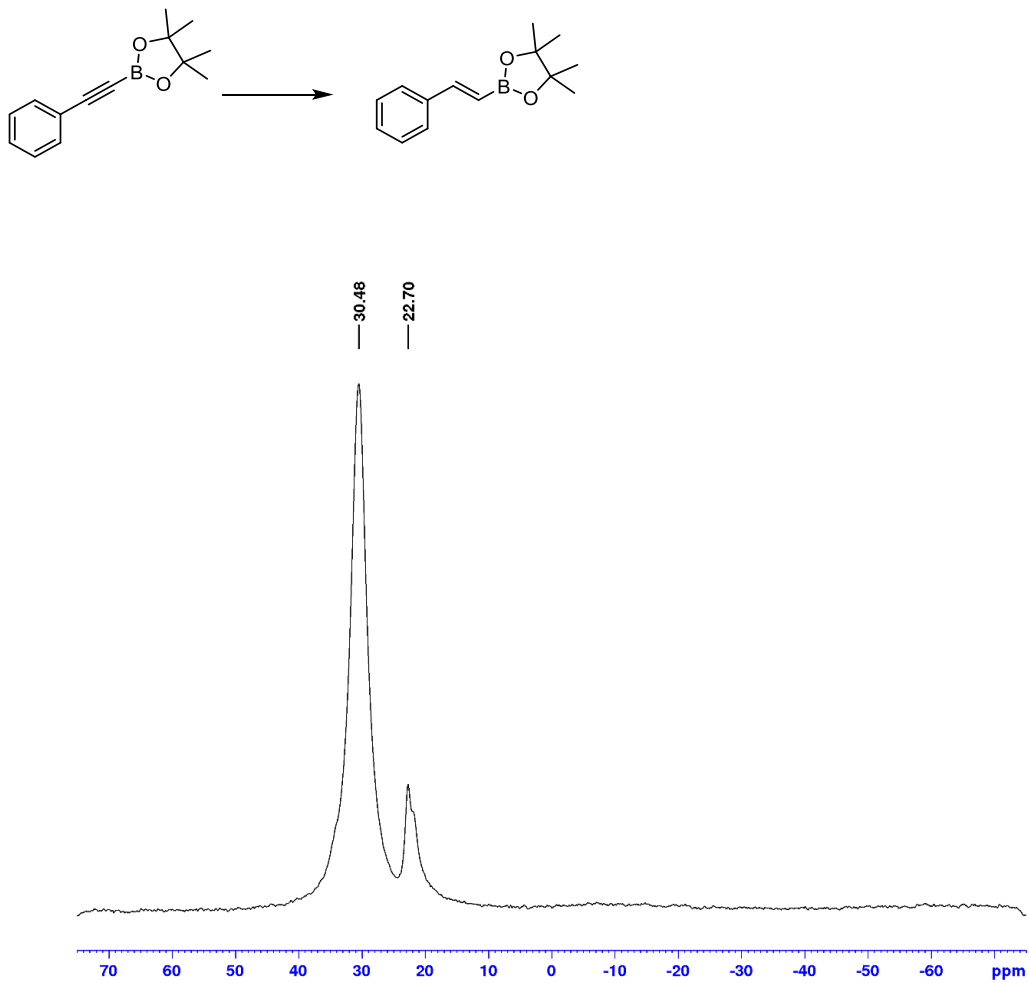


Figure B57. ^1H NMR (500 MHz, C_6D_6) spectrum for the semihydrogenation of 1-phenyl-1-butyne to afford **3-1bb** (1.0 mol% catalyst, 1 atm H_2 , 1.0 M, 25 $^\circ\text{C}$, 4 h; 95% conversion, $E:Z > 99:1$). ^1H NMR (500 MHz, benzene- d_6): δ 7.26 – 7.25 (m, 2 H, *Harom*), 7.16 – 7.13 (m, 2 H, *Harom*), 7.06 – 7.03 (m, 1 H, *Harom*), 6.31 (d, 1 H, $J_{\text{H-H}} = 15.8$ Hz, $\text{HC}=\text{C}$), 6.11 (dt, 1 H, $J_{\text{H-H}} = 15.8, 6.5$ Hz, $\text{HC}=\text{C}$), 2.06 – 2.00 (m, 2 H, CH_2), 0.94 (t, 3 H, $J_{\text{H-H}} = 7.5$ Hz, CH_2CH_3).

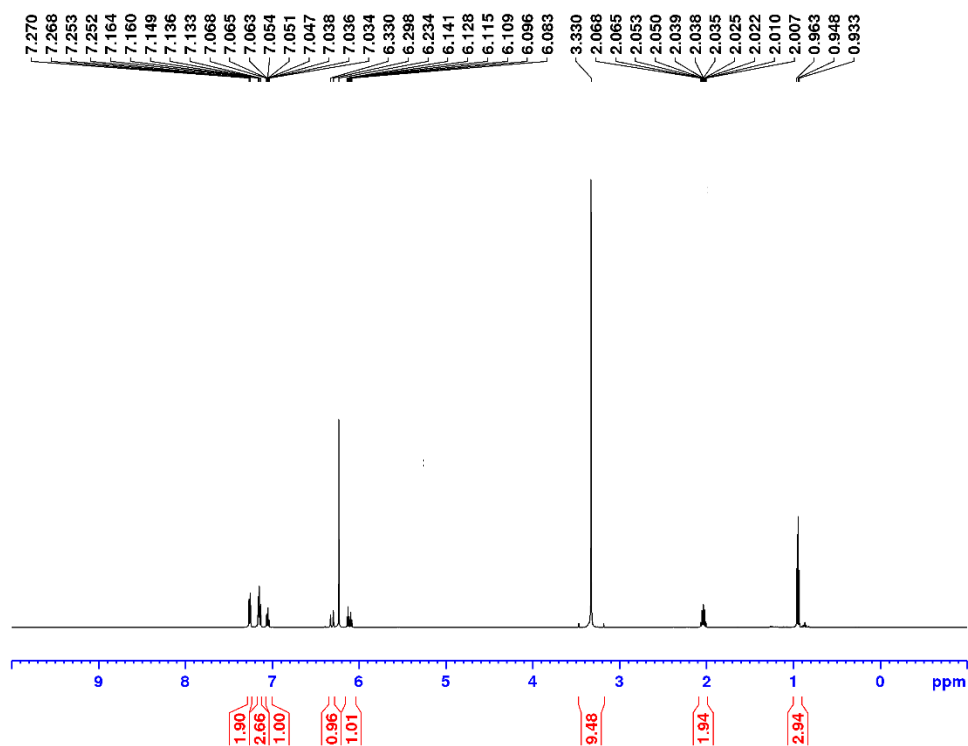
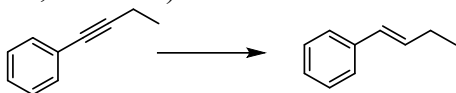


Figure B58. ^1H NMR (500 MHz, C_6D_6) spectrum for the semihydrogenation of 4-[2-(4-fluorophenyl)ethynyl]phenol to afford **3-1cc** (2.5 mol% catalyst, 1 atm H_2 , 1.0 M, 50 $^\circ\text{C}$, 4 h; 97% conversion, $E:Z > 1:99$).

^1H NMR (500 MHz, benzene- d_6): δ 7.04 – 7.03 (overlapping resonances, 4 H, *Harom*), 6.69 – 6.65 (m, 2 H, *Harom*), 6.45 – 6.43 (m, 2 H, *Harom*), 6.39 (d, 1 H, $J = 12.3$ Hz, $\text{HC}=\text{C}$), 6.26 (d, 1 H, $J = 12.3$ Hz, $\text{HC}=\text{C}$), 4.59 (broad s, 1 H, *OH*).

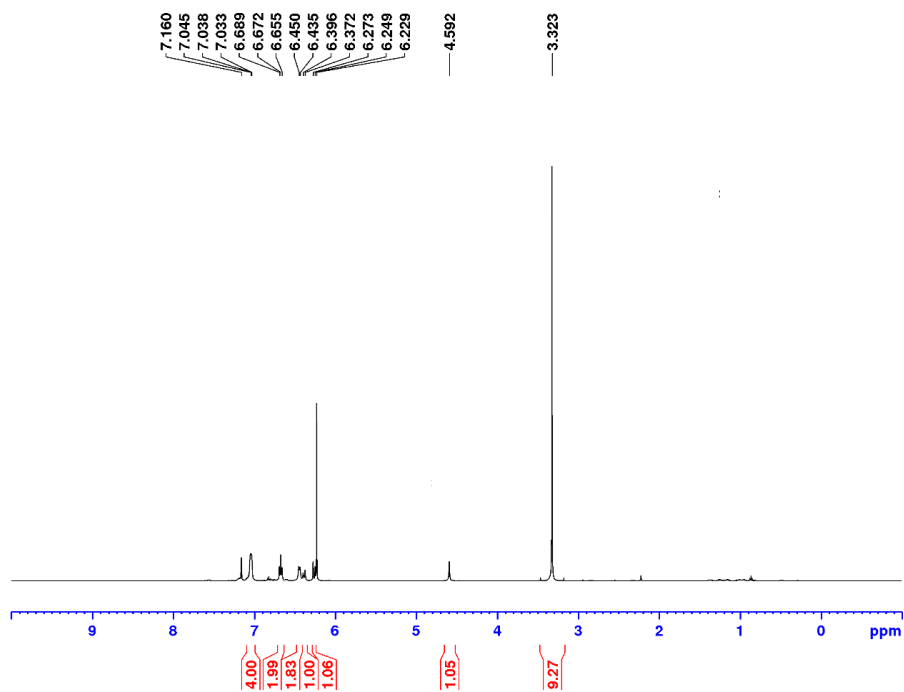
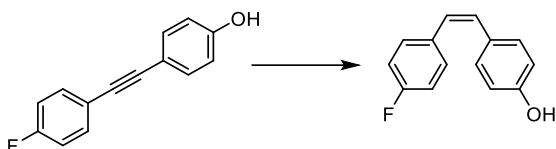


Figure B59. $^{19}\text{F}\{^1\text{H}\}$ NMR (470 MHz, C_6D_6) spectrum for the semihydrogenation of 4-[2-(4-fluorophenyl)ethynyl]phenol to afford **3-1cc** (2.5 mol% catalyst, 1 atm H_2 , 1.0 M, 50 $^\circ\text{C}$, 4 h; 97% conversion, $E:Z > 1:99$).

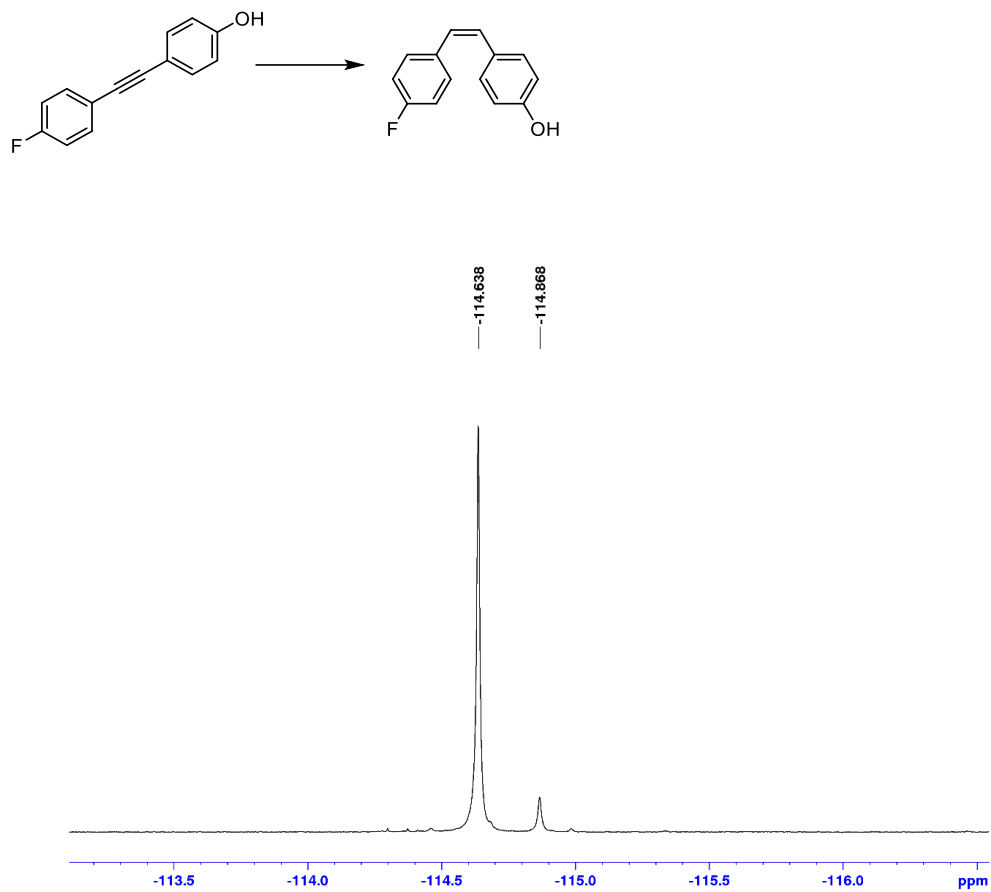


Figure B60. ^1H NMR (500 MHz, C_6D_6) spectrum for the semihydrogenation of 1-nitro-4-(2-phenylethynyl)benzene to afford **3-1dd** (1.0 mol% catalyst, 1 atm H_2 , 1.0 M, 50 $^\circ\text{C}$, 4 h; 82% conversion, $E:Z > 1:99$). ^1H NMR (500 MHz, benzene- d_6): δ 7.67 – 7.65 (m, 2 H, *Harom*), 7.03 – 6.99 (overlapping resonances, 5 H, *Harom*), 6.86 – 6.84 (m, 2 H, *Harom*), 6.45 (d, 1 H, $J = 12.2$ Hz, $\text{HC}=\text{C}$), 6.14 (d, 1 H, $J = 12.2$ Hz, $\text{HC}=\text{C}$).

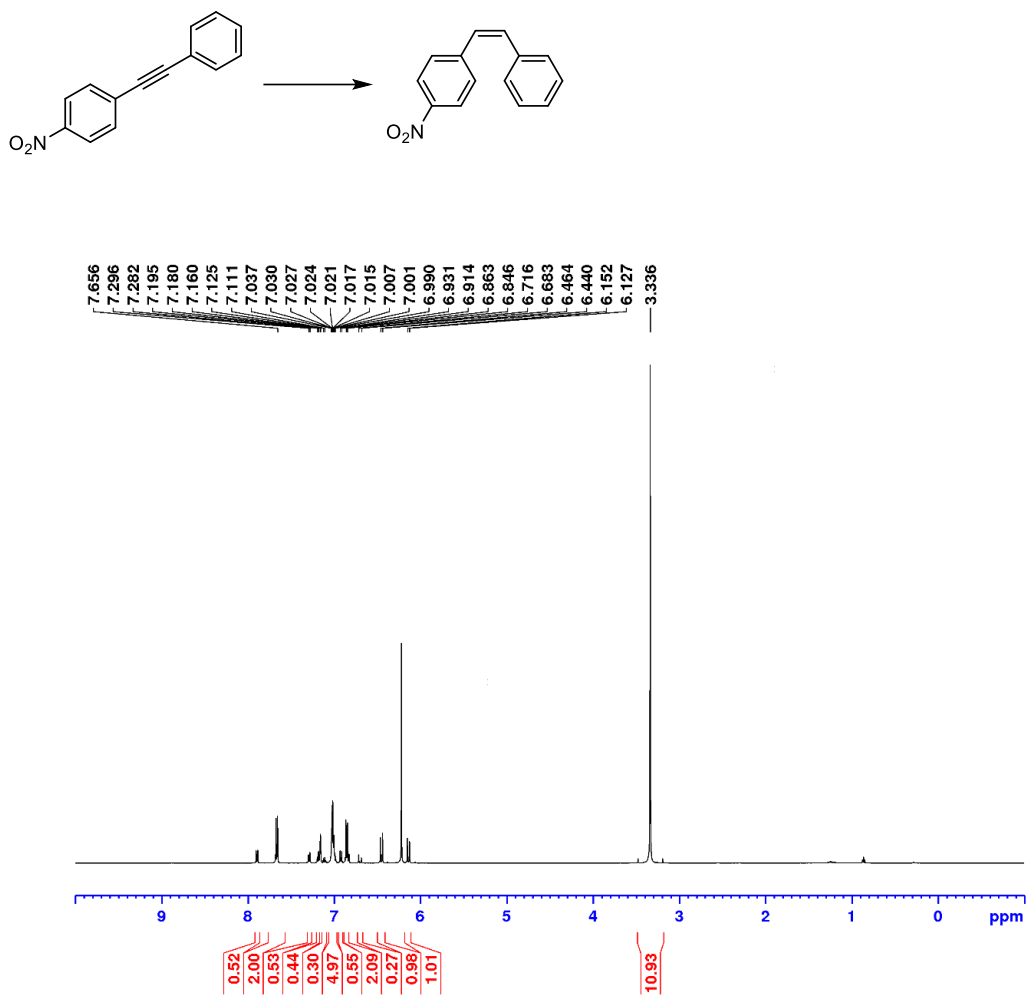


Figure B61. ^1H NMR (300 MHz, C_6D_6) spectrum for the semihydrogenation of 4-(2-phenylethynyl)benzonitrile to afford **3-1ee** (2.5 mol% catalyst, 1 atm H_2 , 1.0 M, 25 $^\circ\text{C}$, 4 h; 86% conversion, $E:Z > 1:99$). ^1H NMR (300 MHz, benzene- d_6): δ 7.16 (m, 1 H, *Harom*), 7.02 – 6.97 (overlapping resonances, 4 H, *Harom*), 6.87 – 6.79 (overlapping resonances, 4 H, *Harom*), 6.41 (d, 1 H, $J = 12.2$ Hz, $\text{HC}=\text{C}$), 6.12 (d, 1 H, $J = 12.2$ Hz, $\text{HC}=\text{C}$).

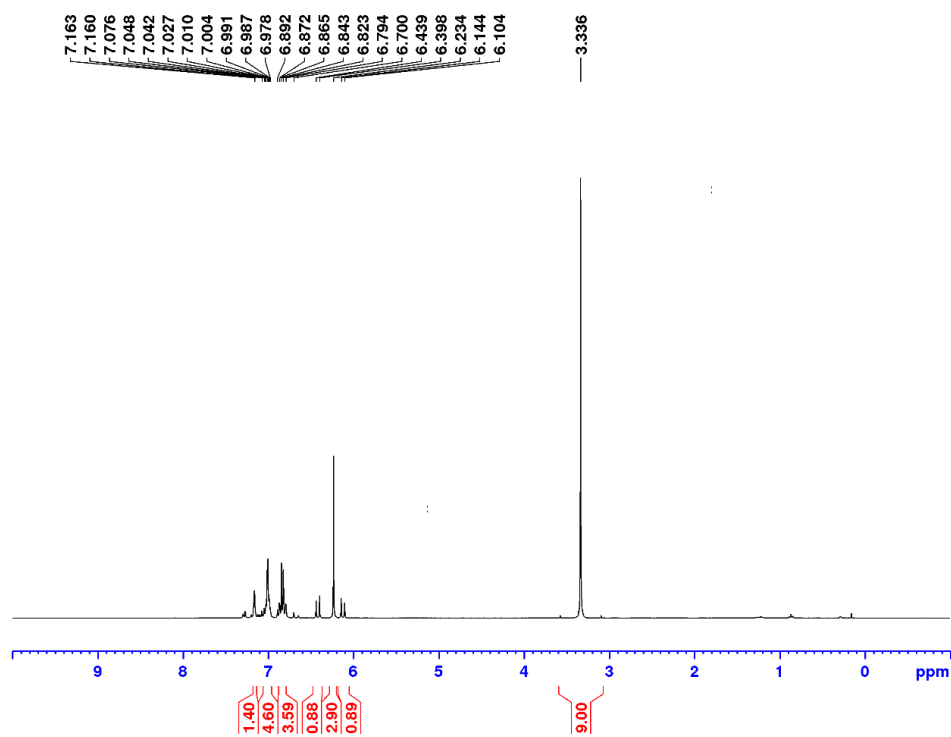
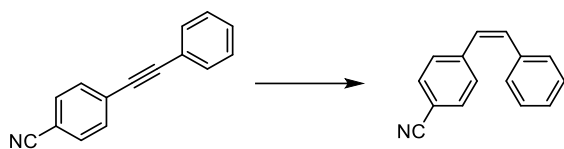


Figure B62. ^1H NMR (500 MHz, C_6D_6) spectrum for the semihydrogenation of 3-[2-(trimethylsilyl)ethynyl]furan (1.0 mol% catalyst, 1 atm H_2 , 1.0 M, 25 $^\circ\text{C}$, 4 h; 75% conversion). A mixture of the (*E*)- and (*Z*)-isomers of **3-1ff** in a 1:10 ratio was found. The chemical shifts and coupling constants for the alkene protons of the respective (*E*)- and (*Z*)-isomers are reported as follows:

^1H NMR (500 MHz, benzene- d_6): δ 6.97 (d, 1 H, $J = 15.2$ Hz, (*Z*) – $\text{HC}=\text{C}$), 6.72 (d, 1 H, $J = 19.1$ Hz, (*E*) – $\text{HC}=\text{C}$), 6.11 (d, 1 H, $J = 19.1$ Hz, (*E*) – $\text{HC}=\text{C}$), 5.73 (d, 1 H, $J = 15.2$ Hz, (*Z*) – $\text{HC}=\text{C}$).

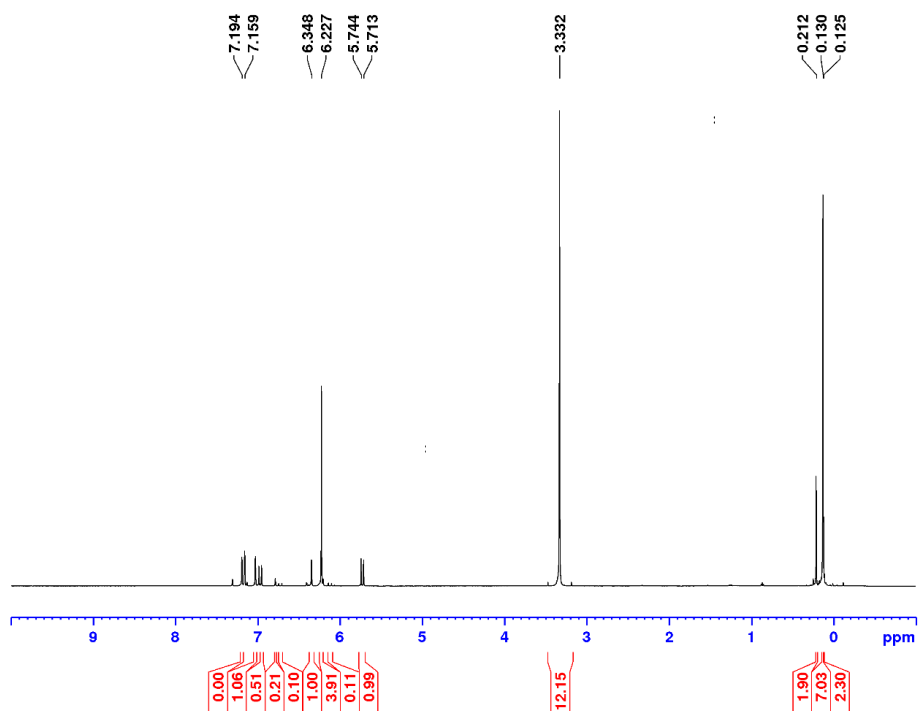
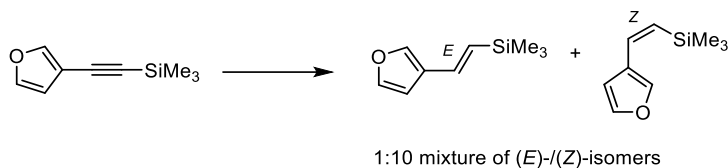


Figure B63. ^1H NMR (500 MHz, C_6D_6) spectrum for the semihydrogenation of 4-octyne to afford **3-1gg** (1.0 mol% catalyst, 1 atm H_2 , 1.0 M, 25 $^\circ\text{C}$, 4 h; 75% conversion, $E:Z > 1:99$). ^1H NMR (500 MHz, benzene- d_6): δ 5.42 (m, 2 H, $\text{HC}=\text{C}$), 1.99 (m, 4 H, CH_2), 1.33 (m, 4 H, CH_2), 0.87 (t, 3 H, CH_3).

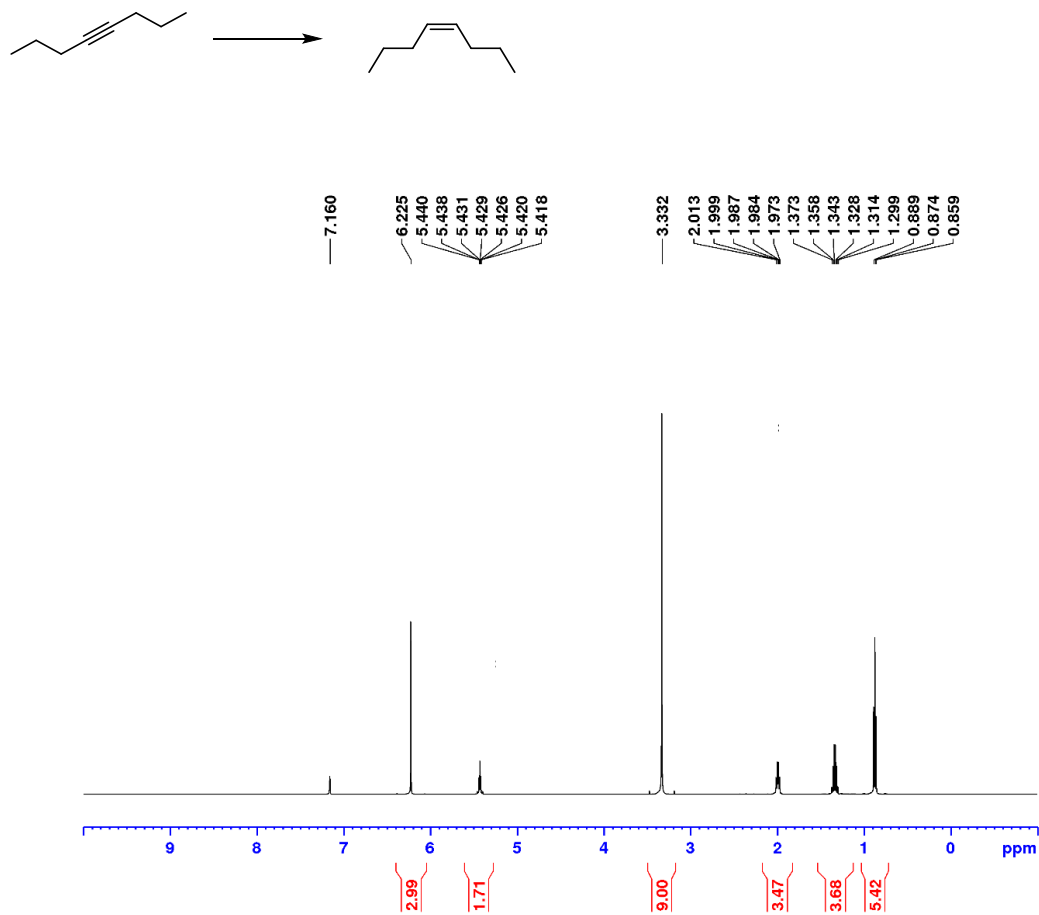


Figure B64. ^1H NMR (500 MHz, C_6D_6) spectrum for the semihydrogenation of (4-fluorophenyl)[4-(2-phenylethynyl)phenyl]methanone (2.5 mol% catalyst, 1 atm H_2 , 1.0 M, 50 $^\circ\text{C}$, 4 h; 28% conversion). A mixture of the (*E*)- and (*Z*)-isomers of **3-1hh** in a 1:1 ratio was found; no starting material remained. The chemical shifts and coupling constants for the alkene protons of the respective (*E*)- and (*Z*)-isomers are reported as follows:

^1H NMR (500 MHz, benzene- d_6): δ 6.93 (d, 1 H, $J = 16.4$ Hz, (*E*) – $\text{HC}=\text{C}$), 6.52 (d, 1 H, $J = 12.2$ Hz, (*Z*) – $\text{HC}=\text{C}$), 6.37 (d, 1 H, $J = 12.2$ Hz, (*Z*) – $\text{HC}=\text{C}$).

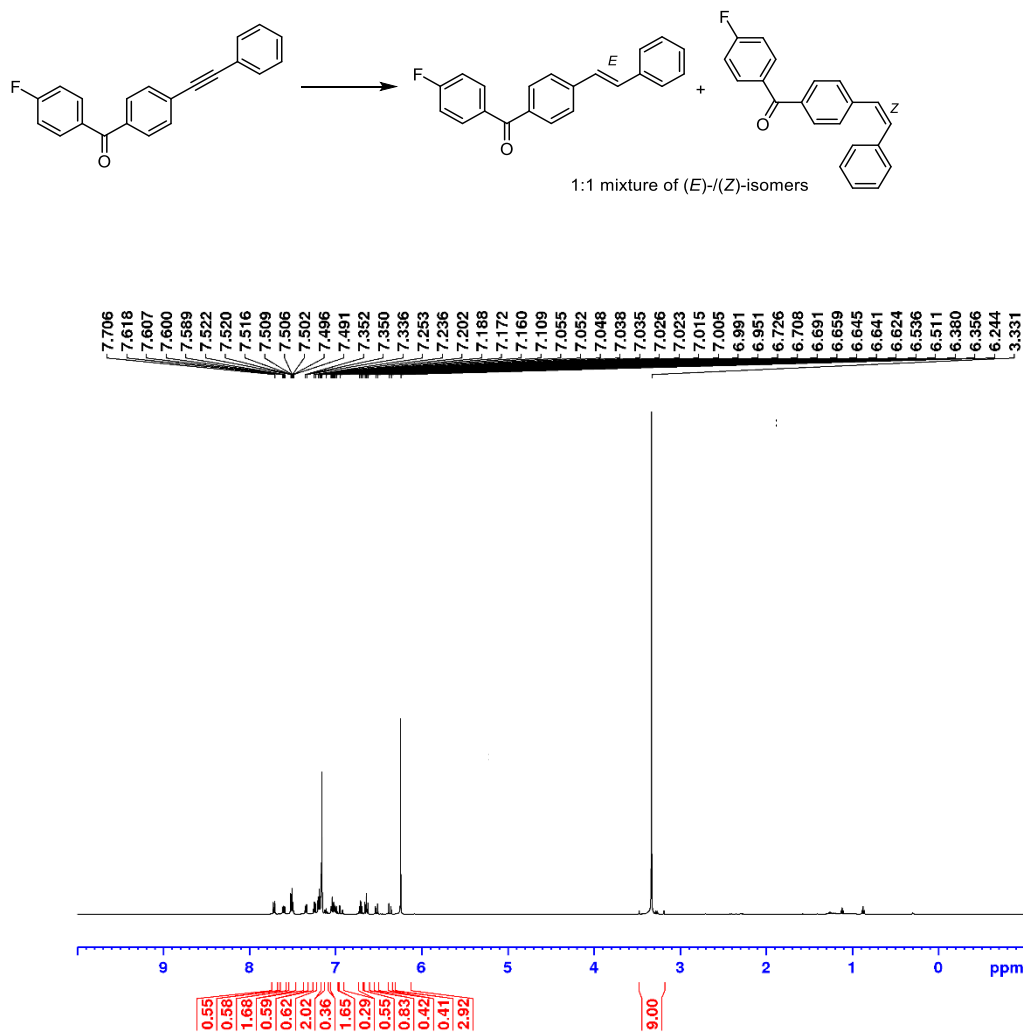


Figure B65. ^{19}F NMR (470 MHz, C_6D_6) spectrum for the semihydrogenation of **3-1hh** (4-fluorophenyl)[4-(2-phenylethynyl)phenyl]methanone (2.5 mol% catalyst, 1 atm H_2 , 1.0 M, 50 $^\circ\text{C}$, 4 h; 28% conversion, no starting material remained).

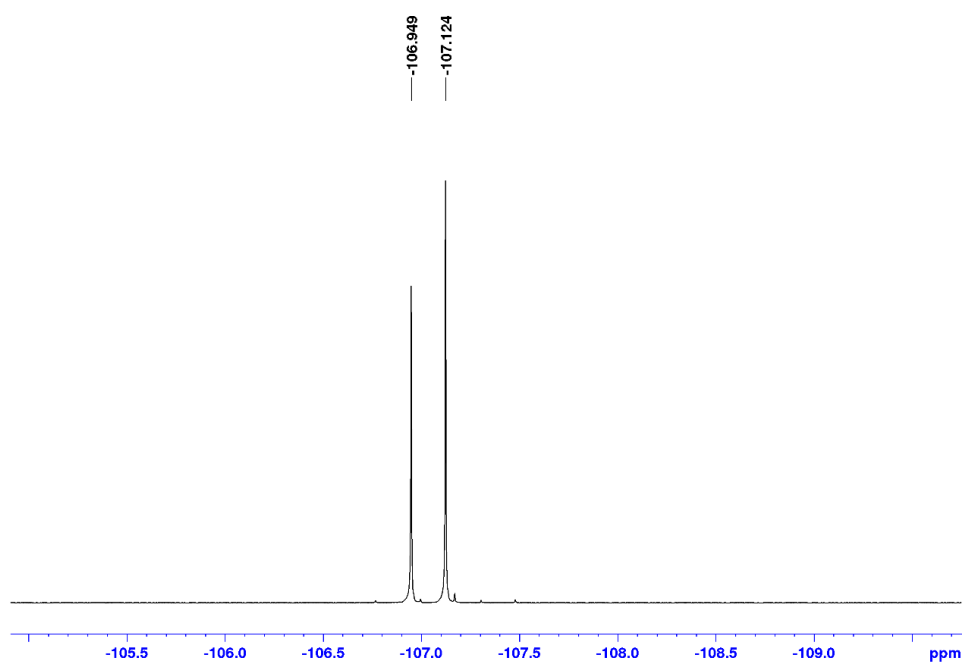
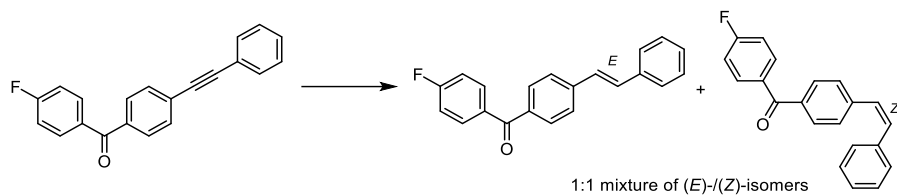


Figure B66. ^1H NMR (500 MHz, C_6D_6) spectrum for the semihydrogenation of 1-hexyn-1-yltrimethylsilane (1.0 mol% catalyst, 1 atm H_2 , 1.0 M, 25 $^\circ\text{C}$, 4 h). Ca. 15% conversion to **3-1ii** was observed.

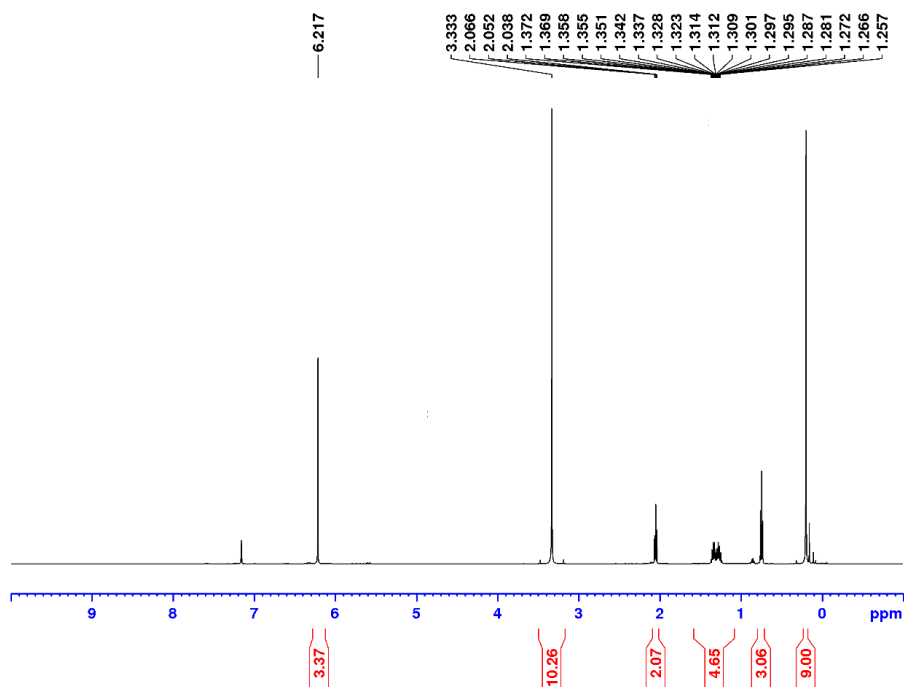
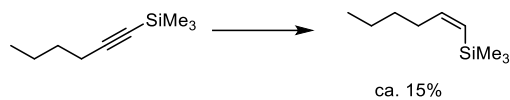


Figure B67. ^1H NMR (500 MHz, C_6D_6) spectrum for the semihydrogenation of 1-bromo-2-[2-(trimethylsilyl)ethynyl]benzene (2.5 mol% catalyst, 1 atm H_2 , 1.0M, 25 $^\circ\text{C}$, 4 h). Ca. 7% conversion to **3-1jj** was observed.

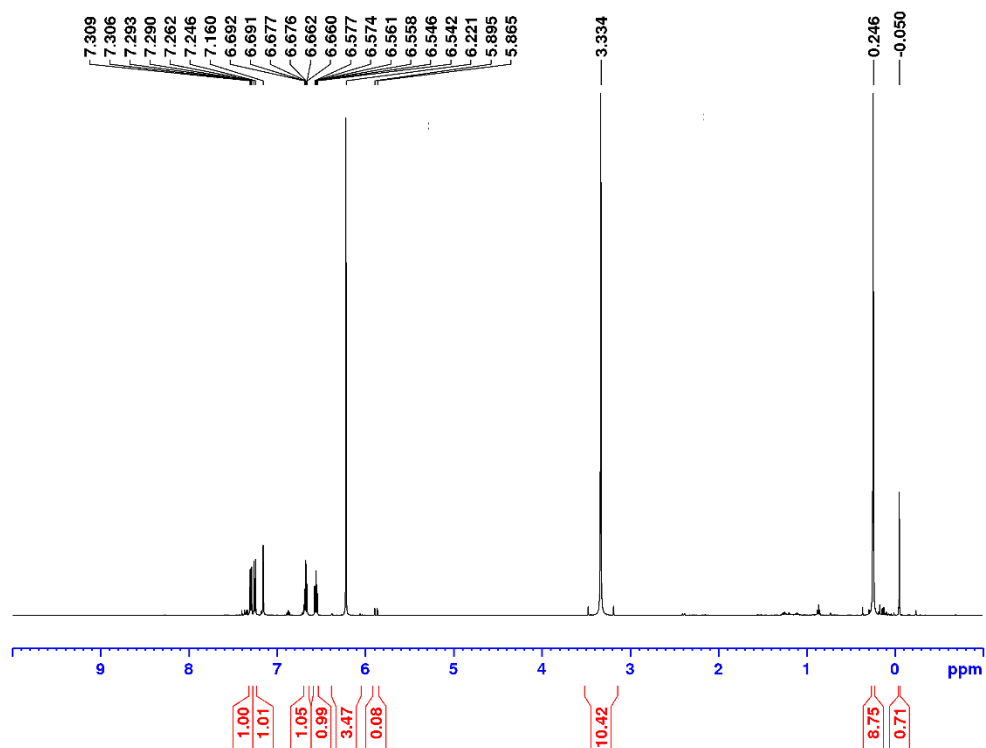
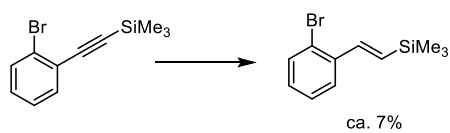


Figure B68. ^1H NMR (500 MHz, C_6D_6) spectrum for the semihydrogenation of 3-(trimethylsilyl)-2-propynal (1.0 mol% catalyst, 1 atm H_2 , 1.0 M, 25 $^\circ\text{C}$, 4 h). No conversion to **3-1kk** was observed.

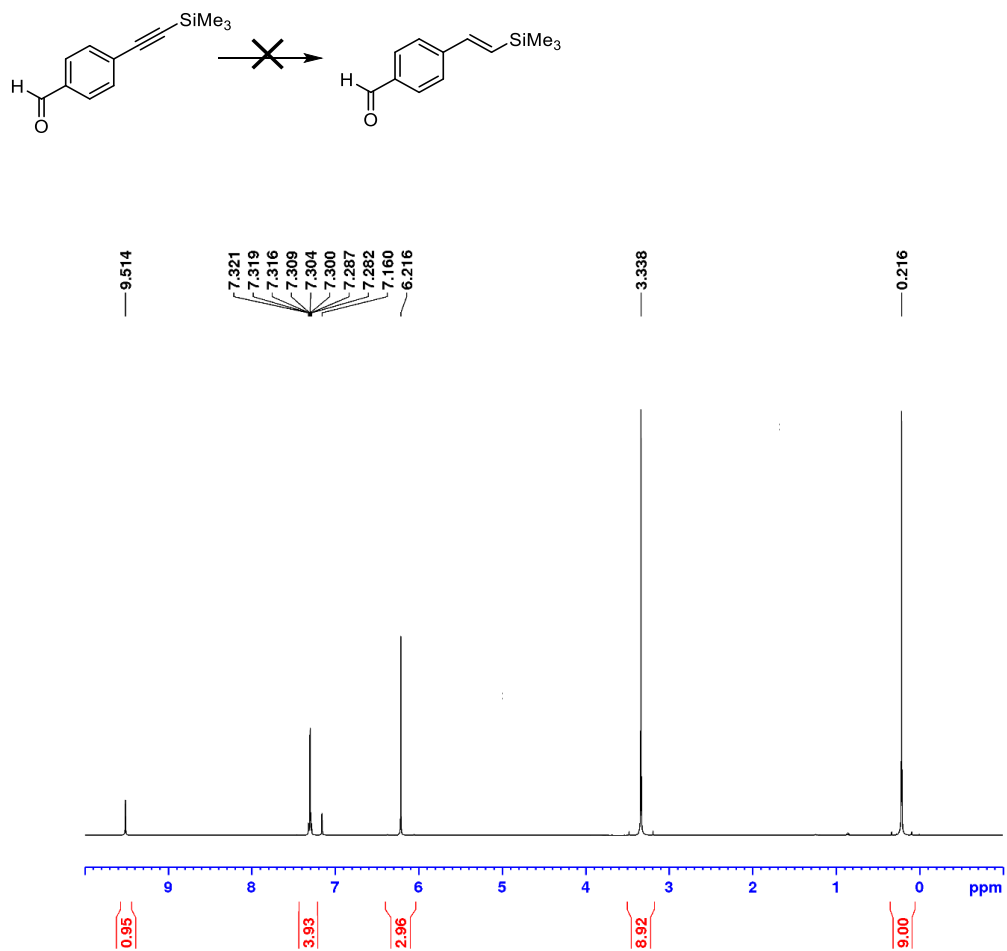


Figure B69. ^1H NMR (500 MHz, C_6D_6) spectrum for the semihydrogenation of 4-phenyl-3-butyne-2-one (1.0 mol% catalyst, 1 atm H_2 , 1.0 M, 25 $^\circ\text{C}$, 4 h). No conversion to **3-III** was observed.

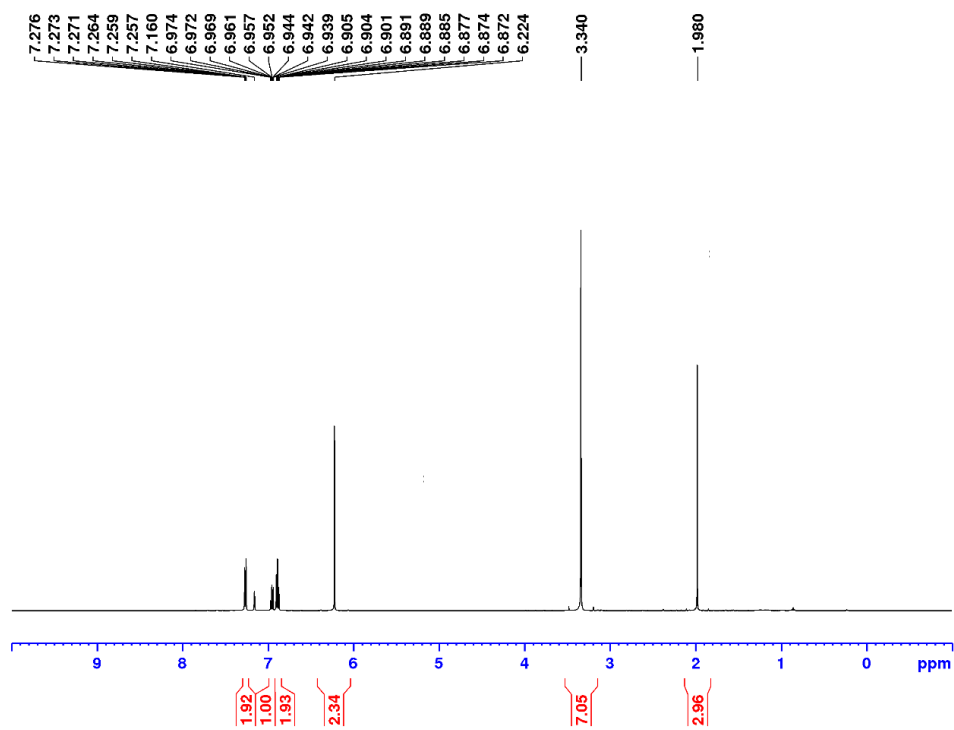
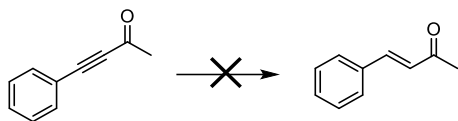


Figure B70. ^1H NMR (500 MHz, C_6D_6) spectrum for the semihydrogenation of 3-phenyl-2-propynoic acid ethyl ester (1.0 mol% catalyst, 1 atm H_2 , 1.0 M, 25 $^\circ\text{C}$, 4 h). No conversion to **3-1mm** was observed.

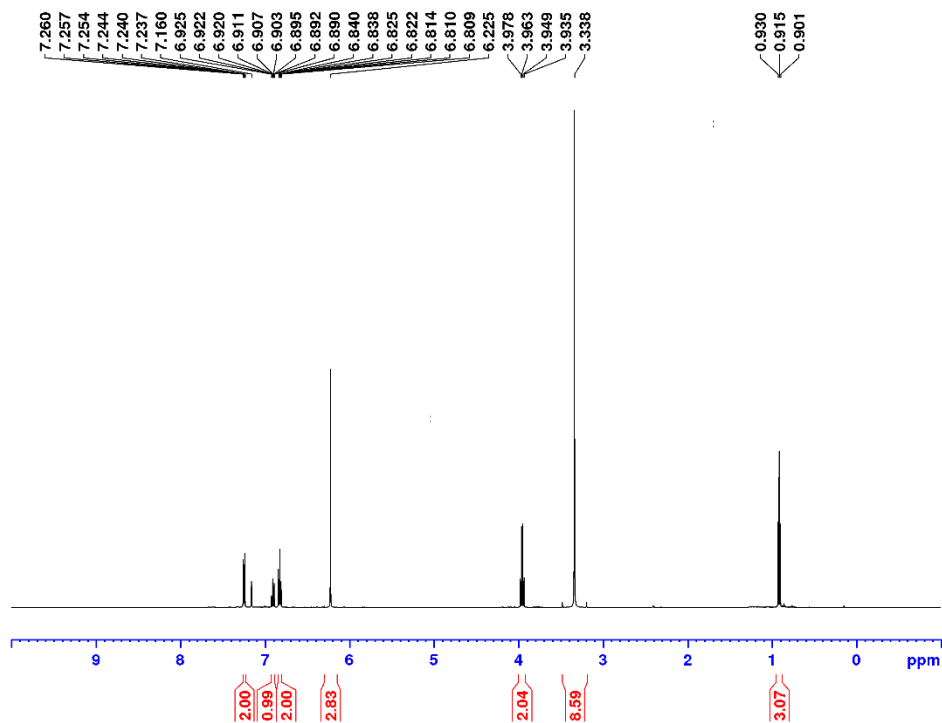
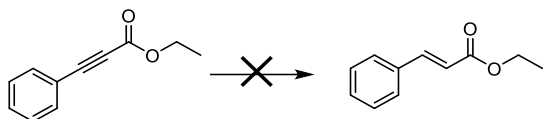


Figure B71. ^1H NMR (300 MHz, C_6D_6) spectrum for isolated (*E*)-**3-1f** (91% yield) resulting from the semihydrogenation of 1-ethyl-4[2-(4-methoxyphenyl)ethynyl]benzene (1.0 mmol scale, 1.0 mol% catalyst, 1 atm H_2 , 1.0 M, 25 $^\circ\text{C}$, 4 h).

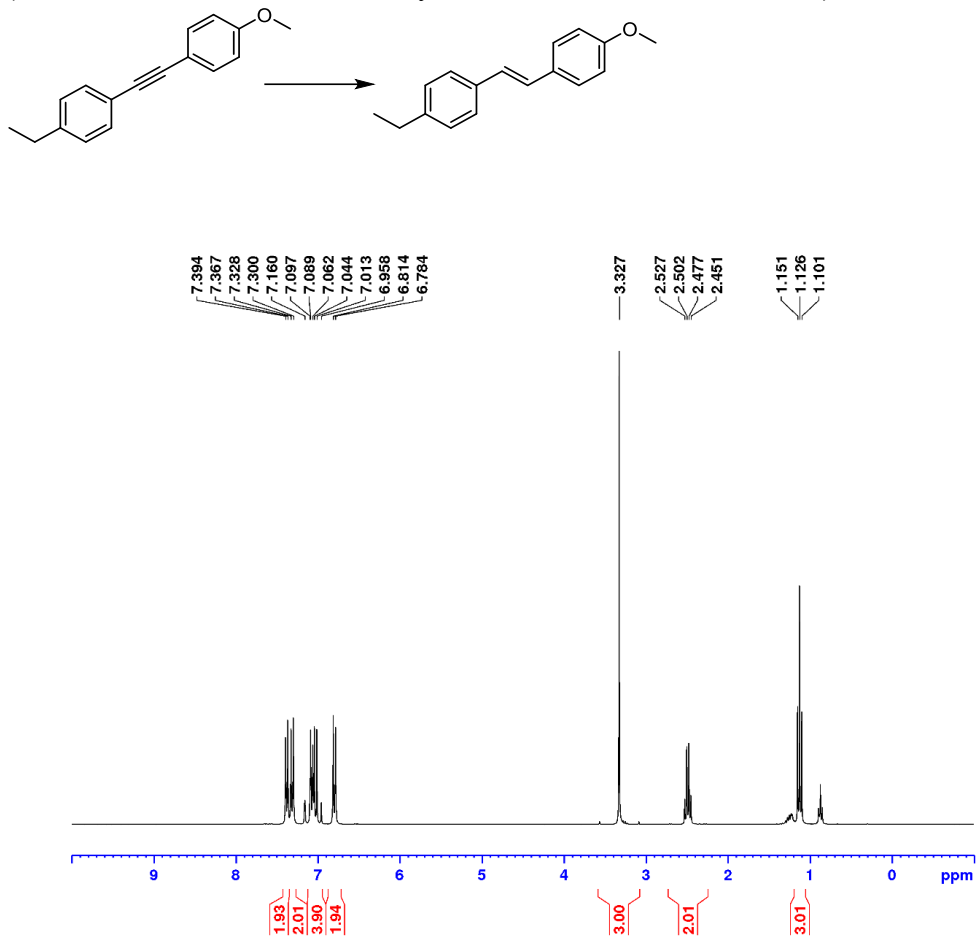


Figure B72. $^{13}\text{C}\{^1\text{H}\}$ NMR (75.5 MHz, C_6D_6) spectrum for isolated (*E*)-**3-1f** (91% yield) resulting from the semihydrogenation of 1-ethyl-4[2-(4-methoxyphenyl)ethynyl]benzene (1.0 mmol scale, 1.0 mol% catalyst, 1 atm H_2 , 1.0 M, 25 °C, 4 h).

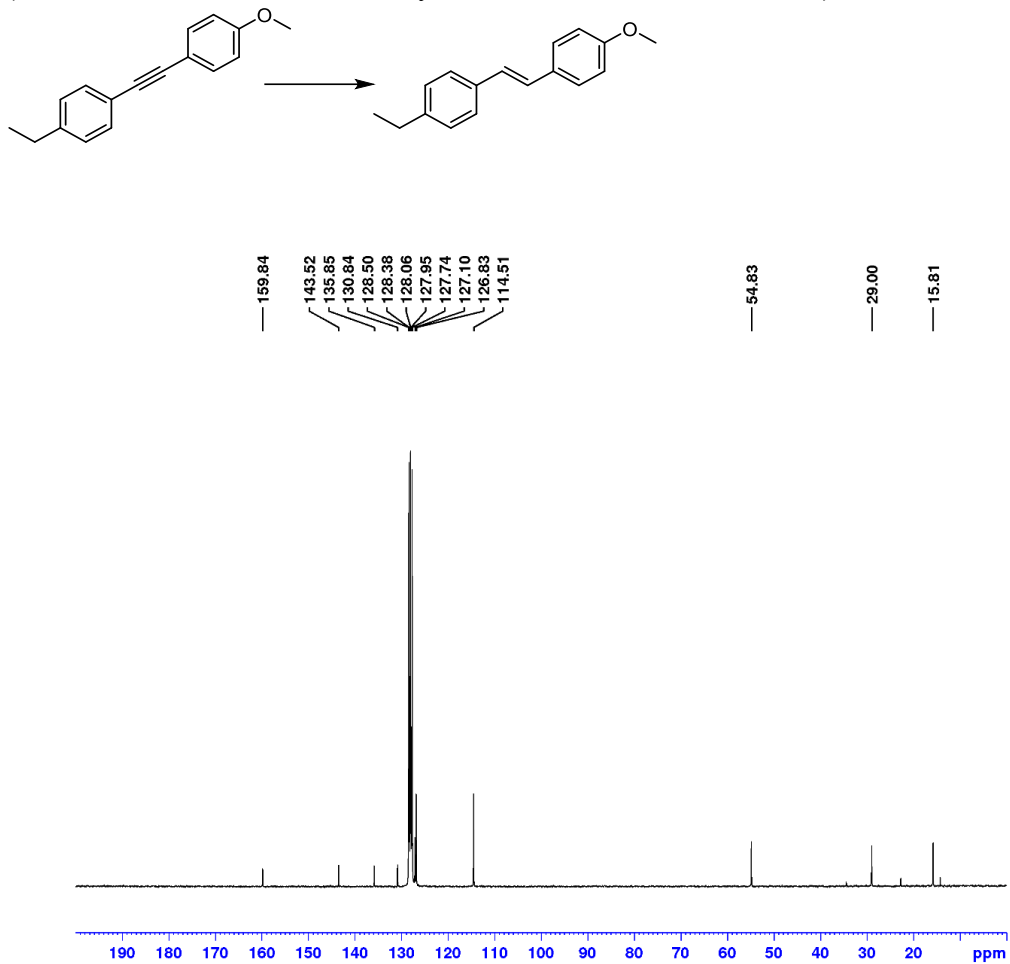


Figure B73. ^1H NMR (300 MHz, C_6D_6) spectrum for isolated (*E*)-**3-1g** (97% yield) resulting from the semihydrogenation of 2-[4-[2-(4-methoxyphenyl)ethynyl]phenyl]boronic acid pinacol ester (1.0 mmol scale, 1.0 mol% catalyst, 1 atm H_2 , 1.0 M, 25 $^\circ\text{C}$, 4 h).

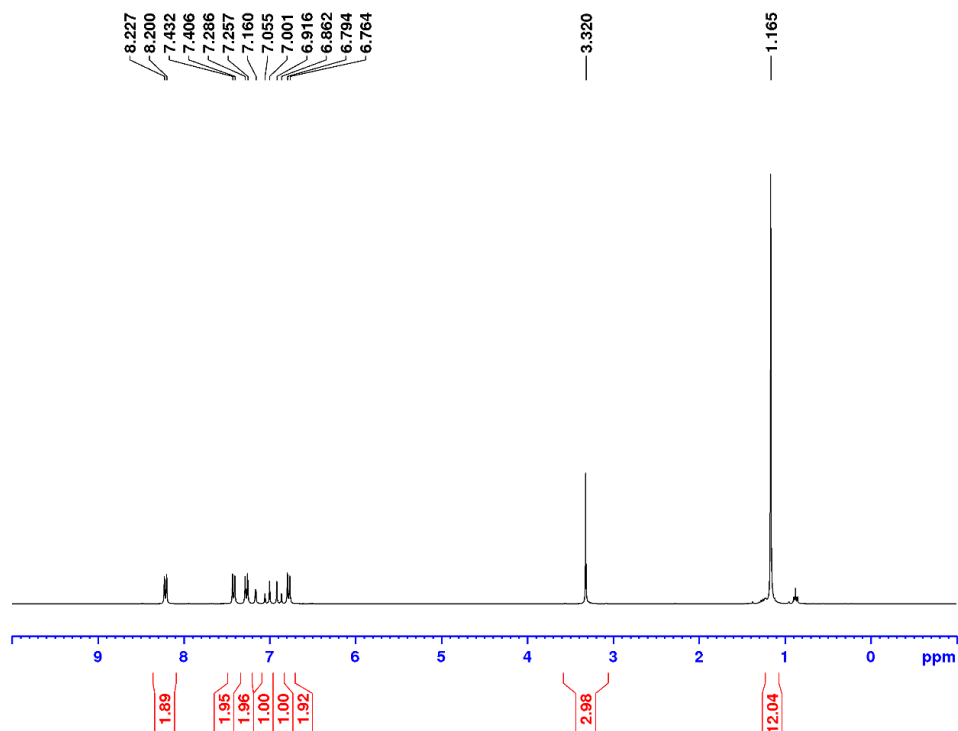
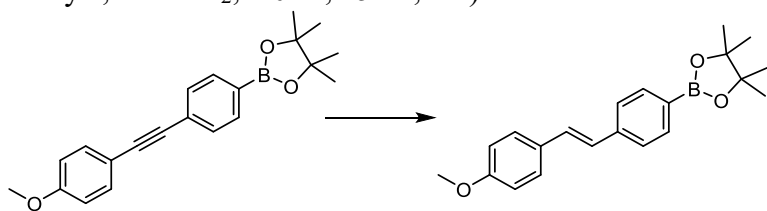


Figure B74. $^{13}\text{C}\{^1\text{H}\}$ NMR (75.5 MHz, C_6D_6) spectrum for isolated (*E*)-**3-1g** (97% yield) resulting from the semihydrogenation of 2-[4-[2-(4-methoxyphenyl)ethynyl]phenyl]boronic acid pinacol ester (1.0 mmol scale, 1.0 mol% catalyst, 1 atm H_2 , 1.0 M, 25 °C, 4 h).

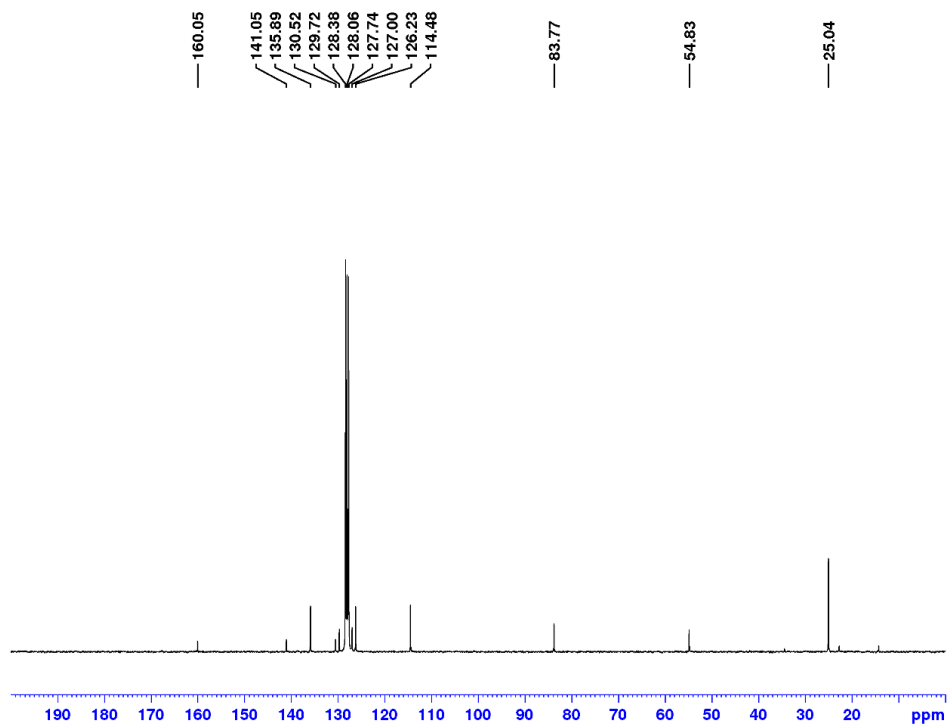
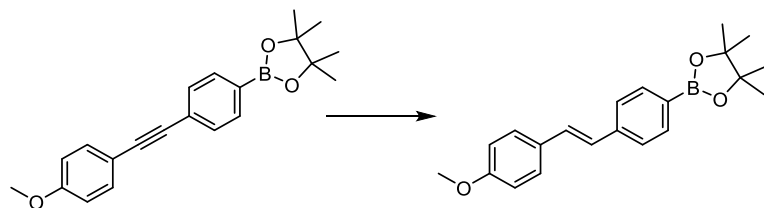


Figure B75. ^1H NMR (300 MHz, C_6D_6) spectrum for isolated (*E*)-**3-1p** (89% yield) resulting from the semihydrogenation of 1,4-bis[2-(trimethylsilyl)ethynyl]benzene (1.0 mmol scale, 1.0 mol% catalyst, 1 atm H_2 , 1.0 M, 25 $^\circ\text{C}$, 4 h).

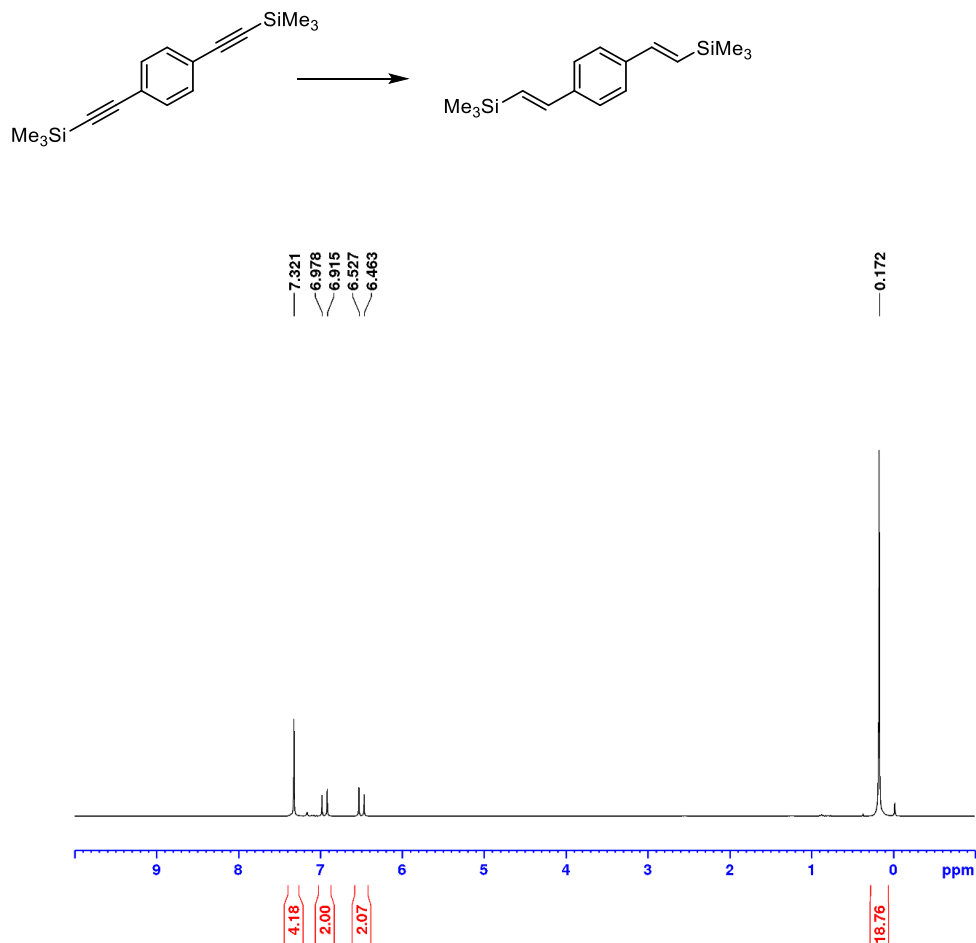


Figure B76. $^{13}\text{C}\{^1\text{H}\}$ NMR (75.5 MHz, C_6D_6) spectrum for isolated (*E*)-**3-1p** (89% yield) resulting from the semihydrogenation of 1,4-bis[2-(trimethylsilyl)ethynyl]benzene (1.0 mmol scale, 1.0 mol% catalyst, 1 atm H_2 , 1.0 M, 25 °C, 4 h).

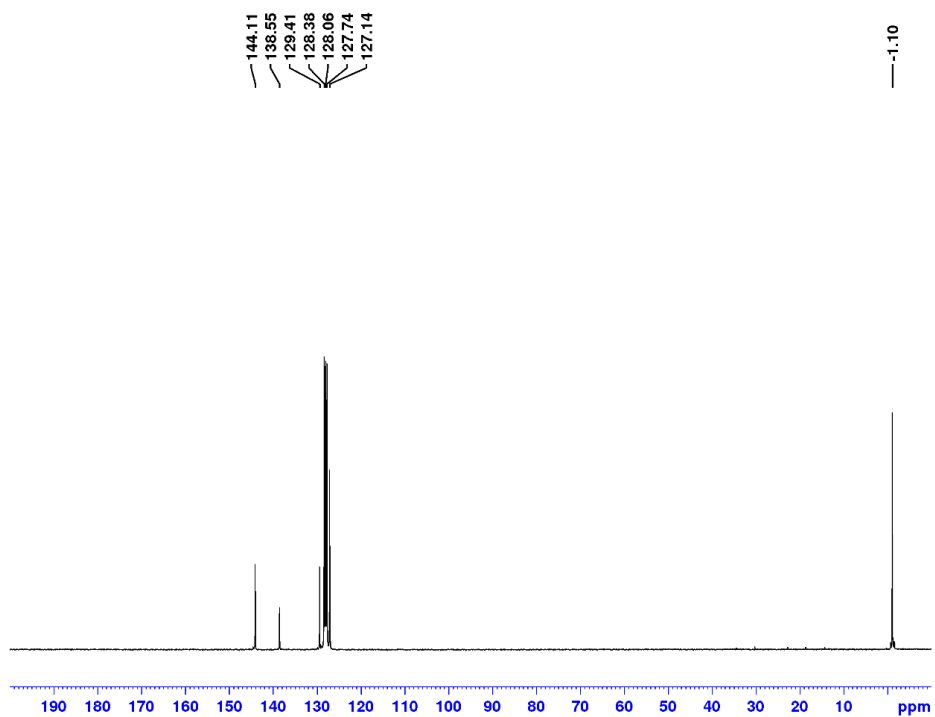
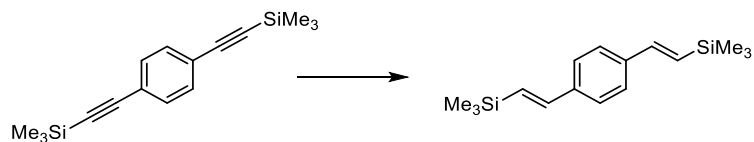


Figure B77. ^1H NMR (500 MHz, C_6D_6) spectrum for isolated *trans*-stilbene (*E*-**3-1a**, 71% yield) resulting from the semihydrogenation of diphenylacetylene (1.0 mol% catalyst, 1 atm H_2 , 1.0 M, 25 $^\circ\text{C}$, 4 h).

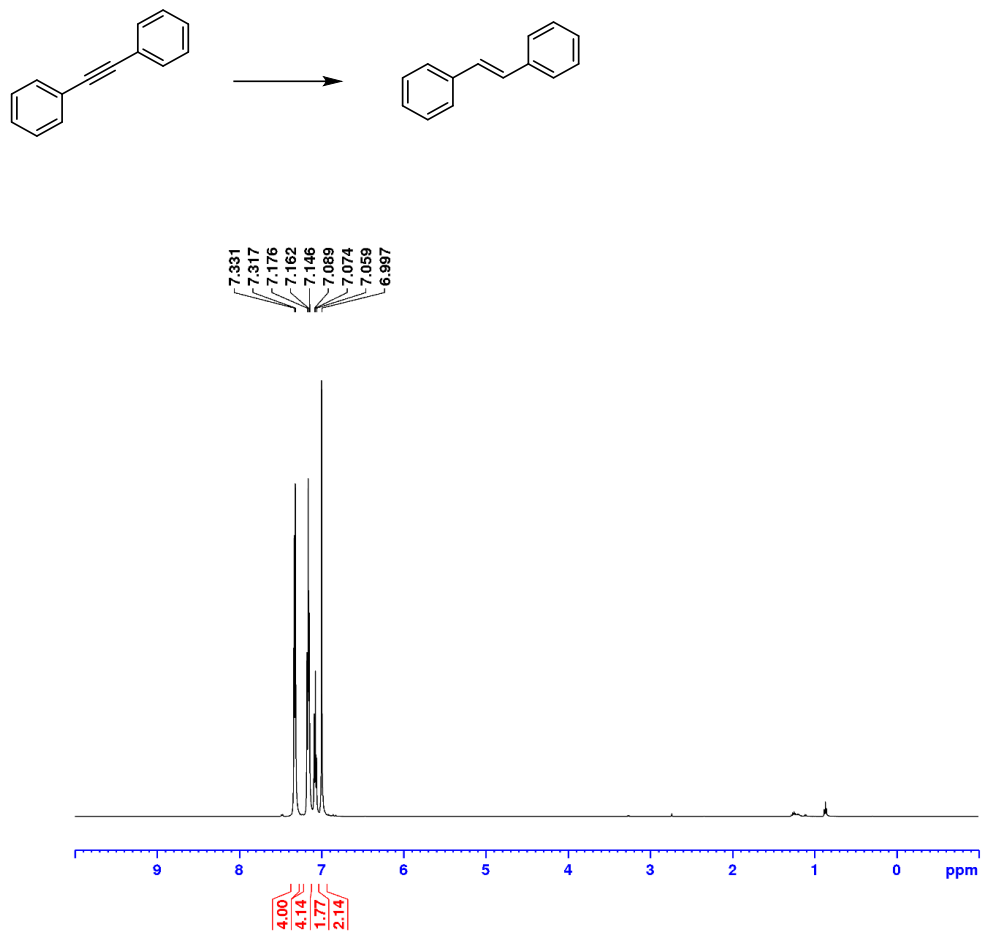


Figure B78. $^{31}\text{P}\{^1\text{H}\}$ NMR spectrum (202.5 MHz, C_6D_6) of complex **3-1**.

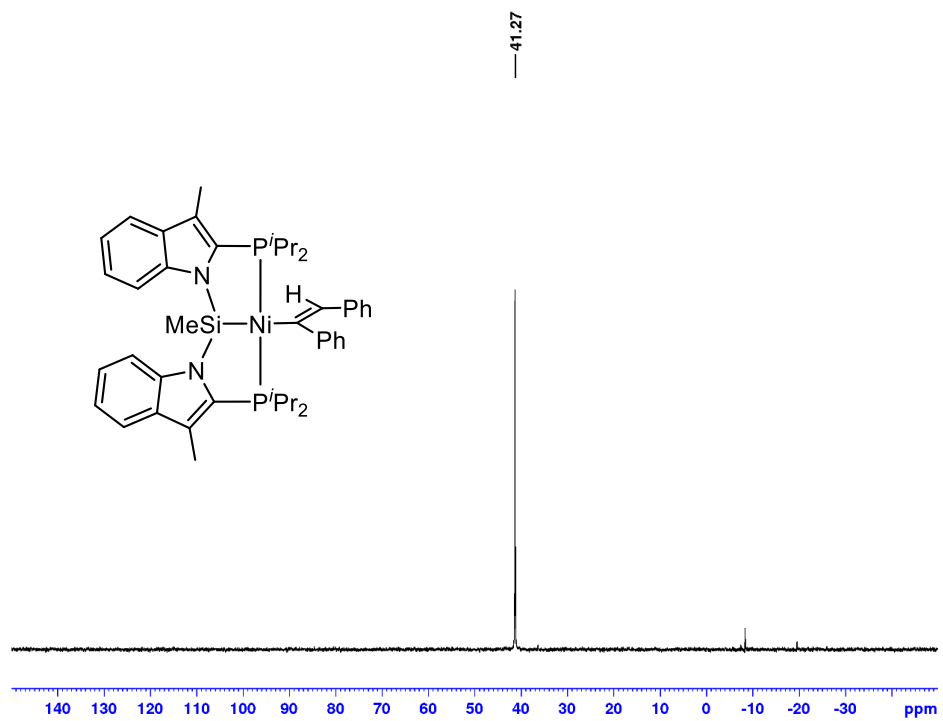


Figure B79. ^1H NMR spectrum (500 MHz, C_6D_6) of complex 3-1.

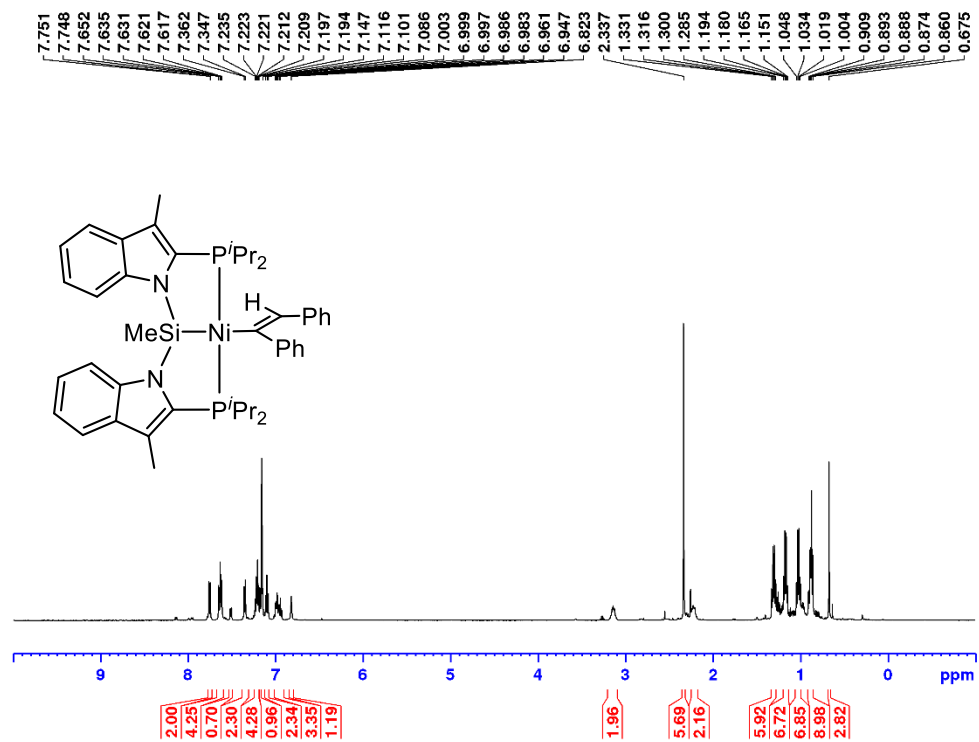
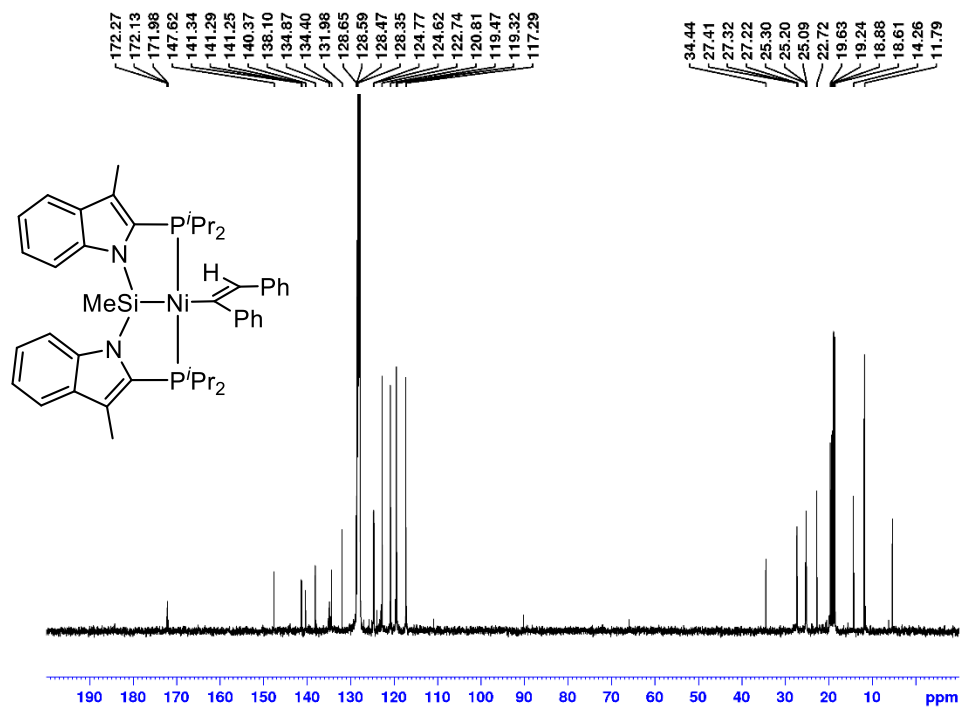
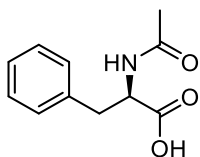


Figure B80. $^{13}\text{C}\{^1\text{H}\}$ NMR (125.8 MHz, C_6D_6) spectrum for complex **3-1**.



Selected NMR Spectra and HPLC Chromatograms for Compounds Reported in

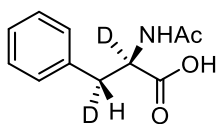
Chapter 4



(R)-N-acetyl-phenylalanine (4-1a). White solid (0.037 g, 89%

yield). $^1\text{H NMR}$ (500 MHz, MeOD- d_4): $^{13}\text{C}\{^1\text{H}\}$ NMR (125.7 MHz,

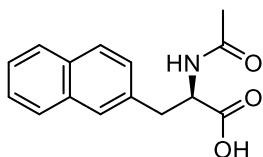
MeOD- d_4): Enantioselectivity was determined by chiral HPLC analysis on a Chiralpak AD-H column with a 91.5: 7.5: 1.0 Hexane: $^i\text{PrOH}$: Formic acid mobile phase at a 1.0 mL/min flow rate. $t_{\text{major}} = 15.425$ min, $t_{\text{min}} = 19.266$ min. Enantiomer ratio = 99:1.



(R)-N-acetyl-phenylalanine- d_2 (4-1a- d_2). White solid (0.040 g,

94% yield). $^1\text{H NMR}$ (500 MHz, MeOD- d_4): $^2\text{H NMR}$ (76.8 MHz,

MeOH): $^{13}\text{C}\{^1\text{H}\}$ NMR (125.7 MHz, MeOD- d_4): Enantioselectivity was determined by chiral HPLC analysis on a Chiralpak AD-H column with a 91.5: 7.5: 1.0 Hexane: $^i\text{PrOH}$: Formic acid mobile phase at a 1.0 mL/min flow rate. $t_{\text{major}} = 15.425$ min, $t_{\text{min}} = 19.266$ min. Enantiomer ratio = >99:1.

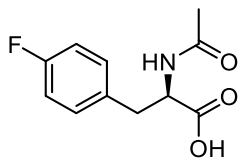


(R)-2-acetamido-3-(naphthalen-2-yl)propanoic acid (4-1b).

White solid (0.046 g, 90% yield). $^1\text{H NMR}$ (500 MHz, MeOD- d_4):

$^{13}\text{C}\{^1\text{H}\}$ NMR (125.7 MHz, MeOD- d_4):

Enantioselectivity was determined by chiral HPLC analysis on a Chiralpak AD-H column with a 91.5: 7.5: 1.0 Hexane: $^i\text{PrOH}$: Formic acid mobile phase at a 1.0 mL/min flow rate. $t_{\text{major}} = 24.959$ min, $t_{\text{min}} = 32.618$ min. Enantiomer ratio = 90:10.



(R)-2-acetamido-3-(4-fluorophenyl)propanoic acid (4-1c).

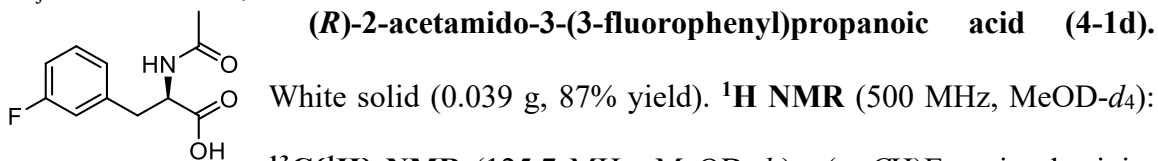
White solid (0.046 g, 90% yield). $^1\text{H NMR}$ (500 MHz, MeOD- d_4):

$^{13}\text{C}\{^1\text{H}\}$ NMR (125.7 MHz, MeOD- d_4): = 2.8 Hz, C_{arom}), 131.9 (d,

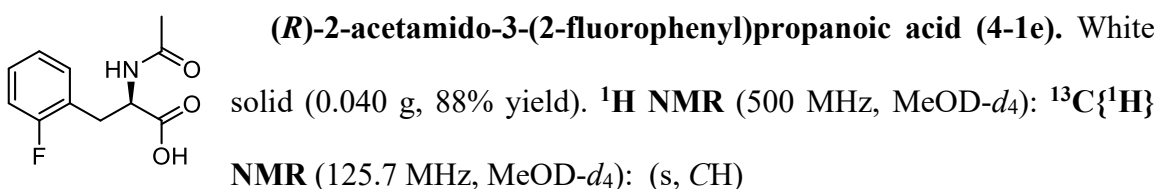
$^3J_{\text{C-F}} = 7.9$ Hz, CH_{arom}), 116.0 (d, $^2J_{\text{C-F}} = 21.5$ Hz, CH_{arom}), 55.1 (s, CH), 37.6 (s, CH_2), 22.3

(s, CH_3). $^{19}\text{F}\{^1\text{H}\}$ NMR (470.5 MHz, MeOD- d_4): -116.6 (s).

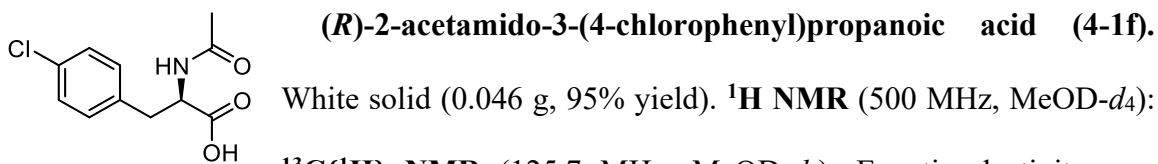
Enantioselectivity was determined by chiral HPLC analysis on a Chiralpak AD-H column with a 91.5: 7.5: 1.0 Hexane: *i*PrOH: Formic acid mobile phase at a 1.0 mL/min flow rate. $t_{\text{major}} = 17.676$ min, $t_{\text{min}} = 23.330$ min. Enantiomer ratio = 99:1.



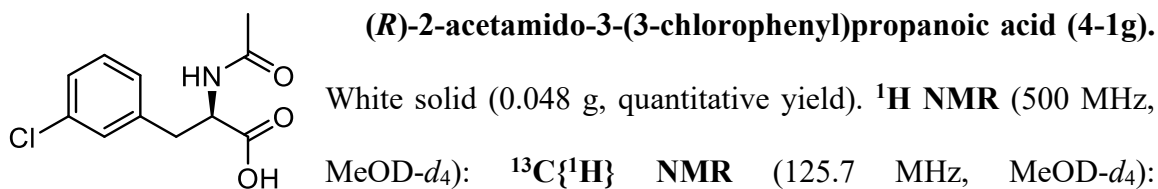
$^{13}\text{C}\{^1\text{H}\}$ NMR (125.7 MHz, MeOD- d_4): (s, CH) Enantioselectivity was determined by chiral HPLC analysis on a Chiralpak AD-H column with a 91.5: 7.5: 1.0 Hexane: *i*PrOH: Formic acid mobile phase at a 1.0 mL/min flow rate. $t_{\text{major}} = 15.877$ min, $t_{\text{min}} = 18.832$ min. Enantiomer ratio = 98:2.



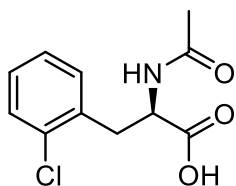
Enantioselectivity was determined by chiral HPLC analysis on a Chiralpak AD-H column with a 91.5: 7.5: 1.0 Hexane: *i*PrOH: Formic acid mobile phase at a 1.0 mL/min flow rate. $t_{\text{major}} = 20.460$ min, $t_{\text{min}} = 21.942$ min. Enantiomer ratio = 88:12.



$^{13}\text{C}\{^1\text{H}\}$ NMR (125.7 MHz, MeOD- d_4): Enantioselectivity was determined by chiral HPLC analysis on a Chiralpak AD-H column with a 91.5: 7.5: 1.0 Hexane: *i*PrOH: Formic acid mobile phase at a 1.0 mL/min flow rate. $t_{\text{major}} = 18.170$ min, $t_{\text{min}} = 23.409$ min. Enantiomer ratio = 98:2.



Enantioselectivity was determined by chiral HPLC analysis on a Chiralpak AD-H column with a 91.5: 7.5: 1.0 Hexane: *i*PrOH: Formic acid mobile phase at a 1.0 mL/min flow rate. $t_{\text{major}} = 15.492$ min, $t_{\text{min}} = 17.942$ min. Enantiomer ratio = >99:1.

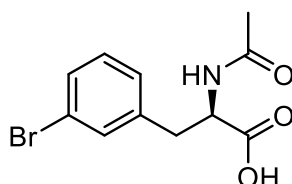


(R)-2-acetamido-3-(2-chlorophenyl)propanoic acid (4-1h).

White solid (0.041 g, 86% yield). $^1\text{H NMR}$ (500 MHz, $\text{MeOD-}d_4$):

$^{13}\text{C}\{^1\text{H}\}$ NMR (125.7 MHz, $\text{MeOD-}d_4$):

Enantioselectivity was determined by chiral HPLC analysis on a Chiralpak AD-H column with a 91.5: 7.5: 1.0 Hexane: i PrOH: Formic acid mobile phase at a 1.0 mL/min flow rate. $t_{\text{major}} = 21.919$ min, $t_{\text{min}} = 23.690$ min. Enantiomer ratio = 98:2.

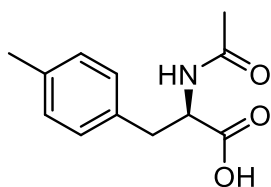


(R)-2-acetamido-3-(3-bromophenyl)propanoic acid (4-1i).

White solid (0.052 g, quantitative yield). $^1\text{H NMR}$ (500 MHz,

$\text{MeOD-}d_4$): $^{13}\text{C}\{^1\text{H}\}$ NMR (125.7 MHz, $\text{MeOD-}d_4$):

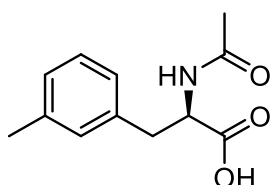
Enantioselectivity was determined by chiral HPLC analysis on a Chiralpak AD-H column with a 91.5: 7.5: 1.0 Hexane: i PrOH: Formic acid mobile phase at a 1.0 mL/min flow rate. $t_{\text{major}} = 16.618$ min, $t_{\text{min}} = 19.023$ min. Enantiomer ratio = >99:1.



(R)-2-acetamido-3-(p-tolyl)propanoic acid (4-1j). White

solid (0.028 g, 64% yield). $^1\text{H NMR}$ (500 MHz, $\text{MeOD-}d_4$):

$^{13}\text{C}\{^1\text{H}\}$ NMR (125.7 MHz, $\text{MeOD-}d_4$): Enantioselectivity was determined by chiral HPLC analysis on a Chiralpak AD-H column with a 94.0: 5.0: 1.0 Hexane: i PrOH: Formic acid mobile phase at a 1.0 mL/min flow rate. $t_{\text{major}} = 14.386$ min, $t_{\text{min}} = 20.978$ min. Enantiomer ratio = 99:1.

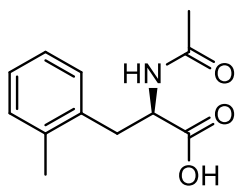


(R)-2-acetamido-3-(m-tolyl)propanoic acid (4-1k). White

solid (0.036 g, 95% yield). $^1\text{H NMR}$ (500 MHz, $\text{MeOD-}d_4$): 1 H,

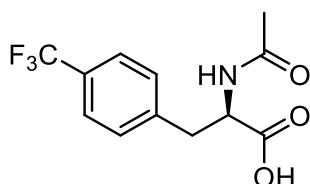
CH_2), 2.90 (dd, $^2J_{\text{H-H}} = 13.9$ Hz, $^3J_{\text{H-H}} = 8.8$ Hz, 1 H, CH_2), 2.30 (s,

3 H, CH_3), 1.89 (s, 3 H, CH_3). $^{13}\text{C}\{^1\text{H}\}$ NMR (125.7 MHz, $\text{MeOD-}d_4$): Enantioselectivity was determined by chiral HPLC analysis on a Chiralpak AD-H column with a 91.5: 7.5: 1.0 Hexane: i PrOH: Formic acid mobile phase at a 1.0 mL/min flow rate. $t_{\text{major}} = 13.040$ min, $t_{\text{min}} = 16.534$ min. Enantiomer ratio = 98:2.



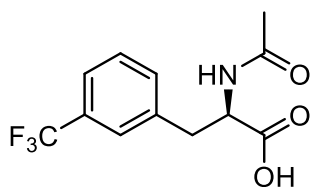
(R)-2-acetamido-3-(*o*-tolyl)propanoic acid (4-1l). White solid (0.030 g, 80% yield). $^1\text{H NMR}$ (500 MHz, $\text{MeOD-}d_4$): $^{13}\text{C}\{^1\text{H}\}$ NMR (125.7 MHz, $\text{MeOD-}d_4$):

Enantioselectivity was determined by chiral HPLC analysis on a Chiralpak AD-H column with a 91.5: 7.5: 1.0 Hexane: i PrOH: Formic acid mobile phase at a 1.0 mL/min flow rate. $t_{\text{major}} = 18.562$ min, $t_{\text{min}} = 22.077$ min. Enantiomer ratio = >99:1.



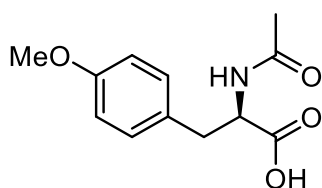
(R)-2-acetamido-3-(4-trifluoromethyl)phenyl)propanoic acid (4-1m). White solid (0.045 g, 82% yield). $^1\text{H NMR}$ (500 MHz, $\text{MeOD-}d_4$): $^{13}\text{C}\{^1\text{H}\}$ NMR (125.7 MHz, $\text{MeOD-}d_4$):

Enantioselectivity was determined by chiral HPLC analysis on a Chiralpak AD-H column with a 91.5: 7.5: 1.0 Hexane: i PrOH: Formic acid mobile phase at a 1.0 mL/min flow rate. $t_{\text{major}} = 15.381$ min, $t_{\text{min}} = 19.920$ min. Enantiomer ratio = 99:1.



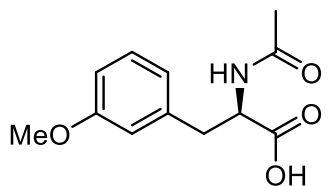
(R)-2-acetamido-3-(3-trifluoromethyl)phenyl)propanoic acid (4-1n). White solid (0.050 g, 95% yield). $^1\text{H NMR}$ (500 MHz, $\text{MeOD-}d_4$): $^{13}\text{C}\{^1\text{H}\}$ NMR (125.7 MHz, $\text{MeOD-}d_4$):

Enantioselectivity was determined by chiral HPLC analysis on a Chiralpak AD-H column with a 91.5: 7.5: 1.0 Hexane: i PrOH: Formic acid mobile phase at a 1.0 mL/min flow rate. $t_{\text{major}} = 12.298$ min, $t_{\text{min}} = 13.715$ min. Enantiomer ratio = 99:1.



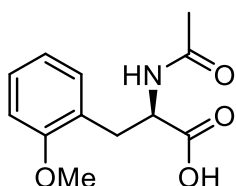
(R)-2-acetamido-3-(4-methoxyphenyl)propanoic acid (4-1o). White solid (0.040g, 84% yield). $^1\text{H NMR}$ (500 MHz, $\text{MeOD-}d_4$): $^{13}\text{C}\{^1\text{H}\}$ NMR (125.7 MHz, $\text{MeOD-}d_4$):

Enantioselectivity was determined by chiral HPLC analysis on a Chiralpak AD-H column with a 91.5: 7.5: 1.0 Hexane: i PrOH: Formic acid mobile phase at a 1.0 mL/min flow rate. $t_{\text{major}} = 24.111$ min, $t_{\text{min}} = 33.369$ min. Enantiomer ratio = 98:2.



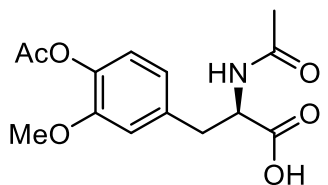
(R)-2-acetamido-3-(3-methoxyphenyl)propanoic acid (4-1p). White solid (0.043 g, 92% yield). $^1\text{H NMR}$ (500 MHz, MeOD- d_4): $^{13}\text{C}\{^1\text{H}\}$ NMR (125.7 MHz, MeOD- d_4):

Enantioselectivity was determined by chiral HPLC analysis on a Chiralpak AD-H column with a 91.5: 7.5: 1.0 Hexane: i PrOH: Formic acid mobile phase at a 1.0 mL/min flow rate. $t_{\text{major}} = 21.757$ min, $t_{\text{min}} = 29.156$ min. Enantiomer ratio = >99:1.



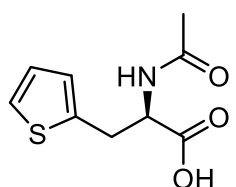
(R)-2-acetamido-3-(2-methoxyphenyl)propanoic acid (4-1q). White solid (0.034 g, 73% yield). $^1\text{H NMR}$ (500 MHz, MeOD- d_4): $^{13}\text{C}\{^1\text{H}\}$ NMR (125.7 MHz, MeOD- d_4):

Enantioselectivity was determined by chiral HPLC analysis on a Chiralpak AD-H column with a 91.5: 7.5: 1.0 Hexane: i PrOH: Formic acid mobile phase at a 1.0 mL/min flow rate. $t_{\text{major}} = 22.540$ min, $t_{\text{min}} = 24.967$ min. Enantiomer ratio = 76:24.



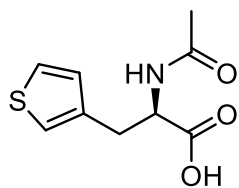
(R)-2-acetamido-3-(4-acetoxy-3-methoxyphenyl)propanoic acid (4-1r). White solid (0.050 g, 84% yield). $^1\text{H NMR}$ (500 MHz, MeOD- d_4): $^{13}\text{C}\{^1\text{H}\}$ NMR (125.7 MHz, MeOD- d_4):

Enantioselectivity was determined by chiral HPLC analysis on a Chiralpak AD-H column with a 91.5: 7.5: 1.0 Hexane: i PrOH: Formic acid mobile phase at a 1.0 mL/min flow rate. $t_{\text{major}} = 28.890$ min, $t_{\text{min}} = 31.222$ min. Enantiomer ratio = 99:1.



(R)-2-acetamido-3-(thiophen-2-yl)propanoic acid (4-1s). White solid (0.033 g, 77% yield). $^1\text{H NMR}$ (500 MHz, MeOD- d_4): $^{13}\text{C}\{^1\text{H}\}$ NMR (125.7 MHz, MeOD- d_4):

Enantioselectivity was determined by chiral HPLC analysis on a Chiralpak AD-H column with a 91.5: 7.5: 1.0 Hexane: i PrOH: Formic acid mobile phase at a 1.0 mL/min flow rate. $t_{\text{major}} = 22.794$ min, $t_{\text{min}} = 25.330$ min. Enantiomer ratio = >99:1.



(R)-2-acetamido-3-(thiophen-3-yl)propanoic acid (4-1t). White solid (0.038 g, 88% yield). $^1\text{H NMR}$ (500 MHz, $\text{MeOD-}d_4$): $^{13}\text{C}\{^1\text{H}\}$ NMR (125.7 MHz, $\text{MeOD-}d_4$):

Enantioselectivity was determined by chiral HPLC analysis on a Chiralpak AD-H column with a 91.5: 7.5: 1.0 Hexane: i PrOH: Formic acid mobile phase at a 1.0 mL/min flow rate. $t_{\text{major}} = 21.667$ min, $t_{\text{min}} = 29.106$ min. Enantiomer ratio = 99:1.

Figure B81. ^1H NMR spectrum of **4-1a** in $\text{MeOD-}d_4$.

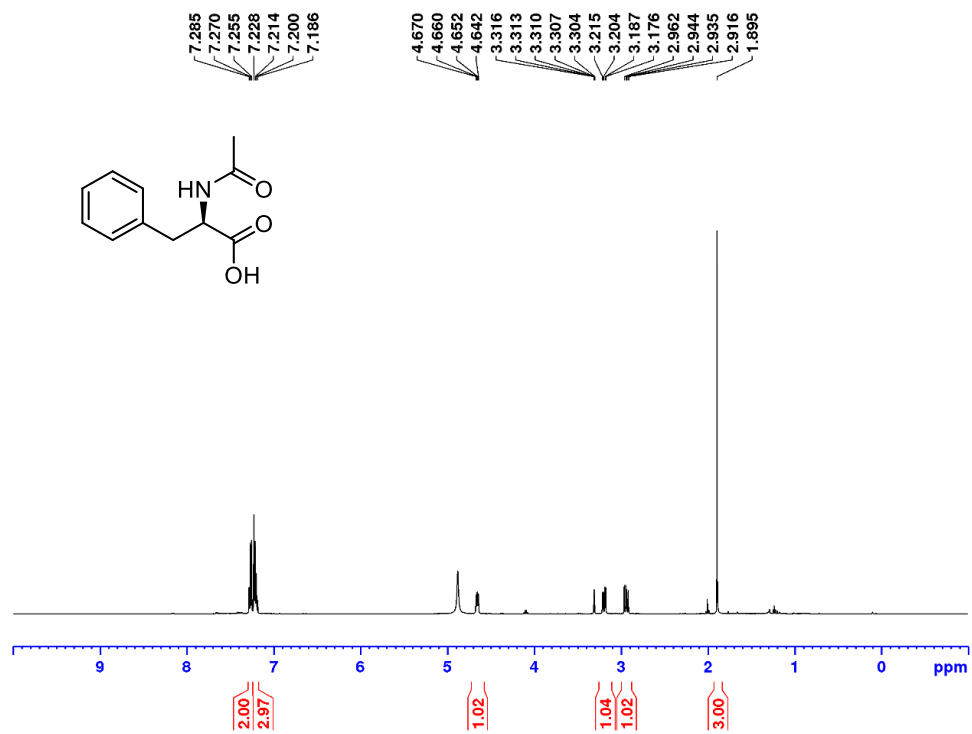


Figure B82. $^{13}\text{C}\{^1\text{H}\}$ NMR spectrum of **4-1a** in $\text{MeOD-}d_4$.

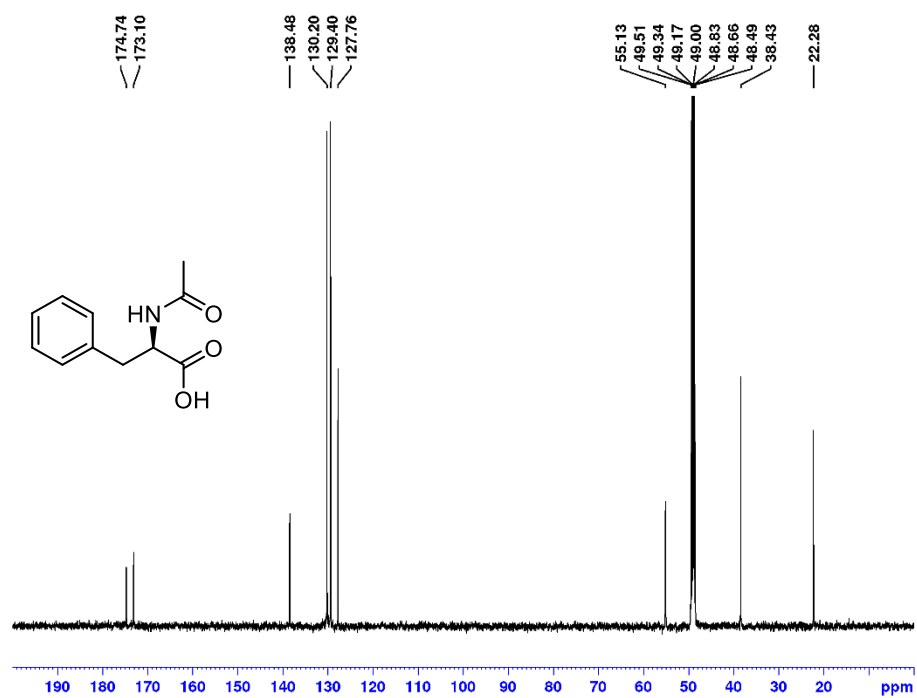


Figure B83. ^1H NMR spectrum of **4-1a- d_2** in $\text{MeOD-}d_4$

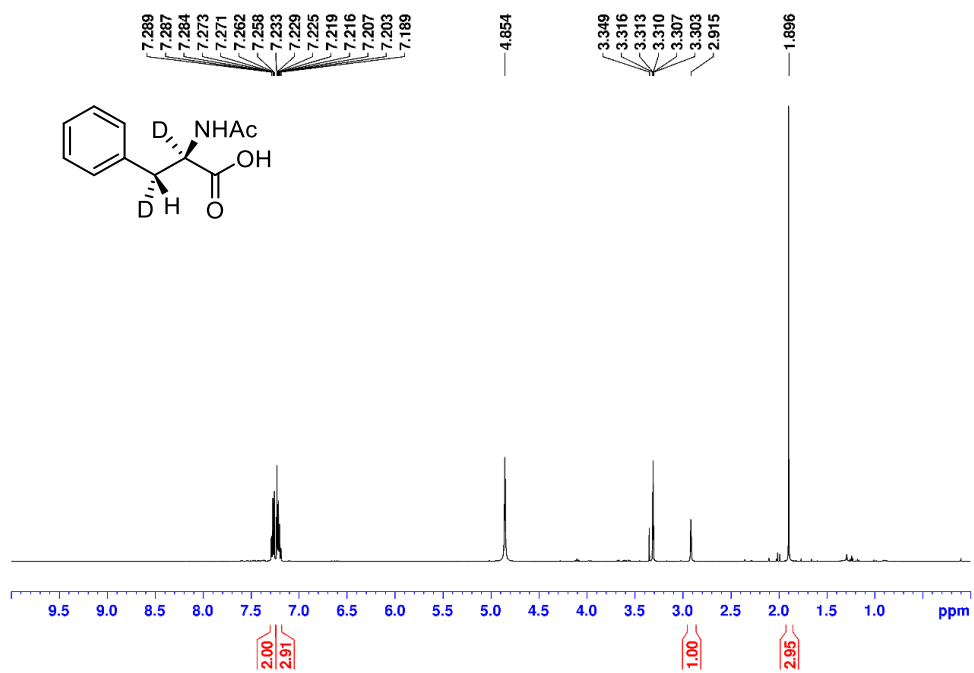


Figure B84. ^2H NMR spectrum of **4-1a-d₂** in MeOH.

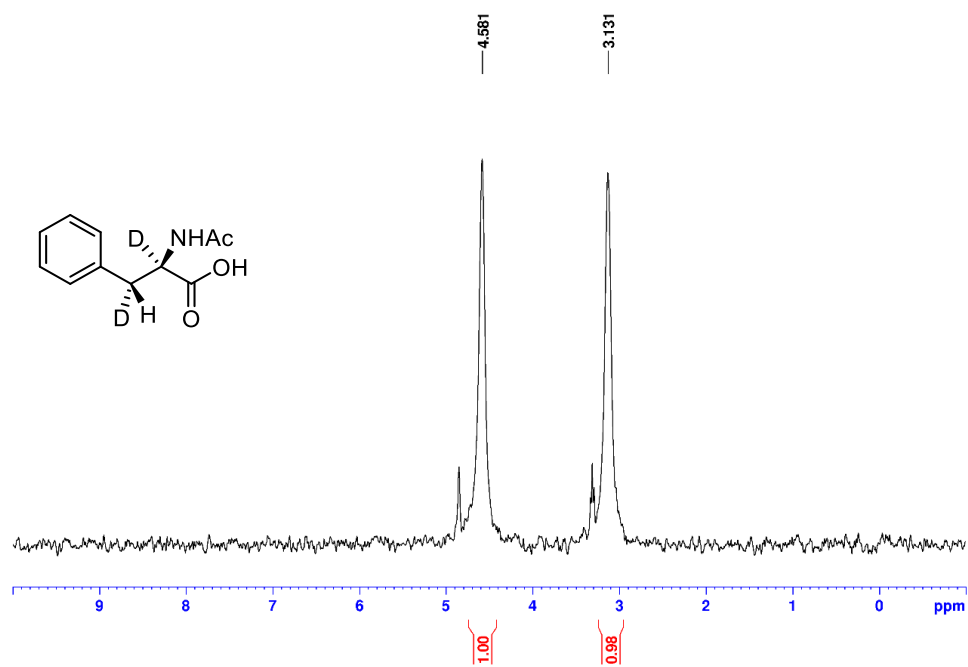


Figure B85. $^{13}\text{C}\{^1\text{H}\}$ NMR spectrum of **4-1a-d₂** in MeOD-*d*₄.

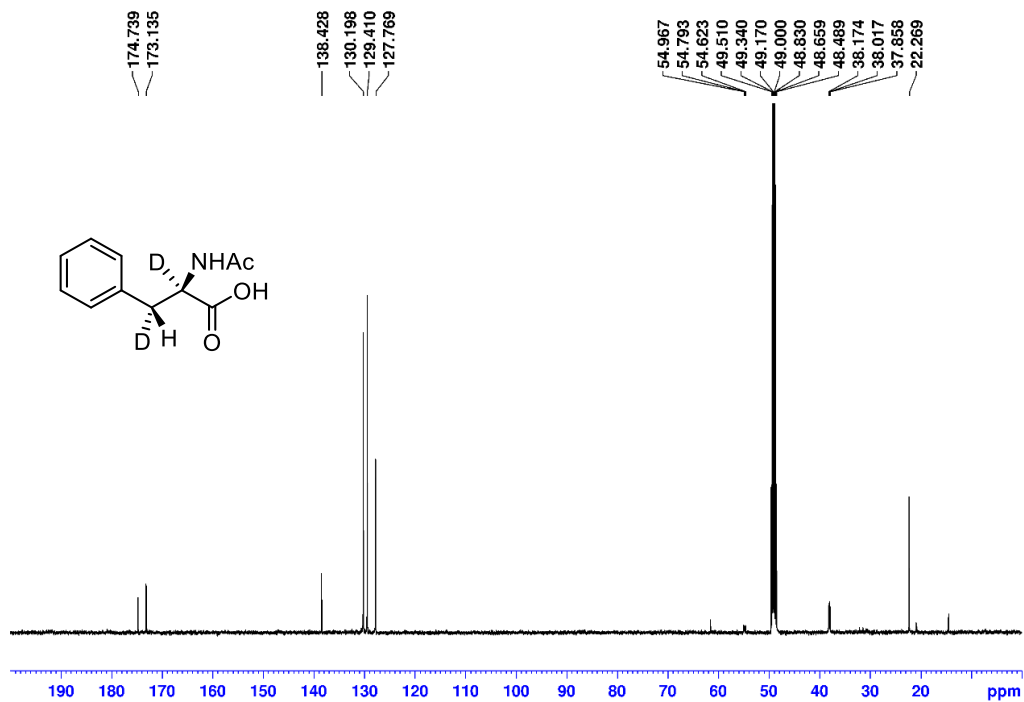


Figure B86. ^1H NMR spectrum of **4-1b** in $\text{MeOD-}d_4$.

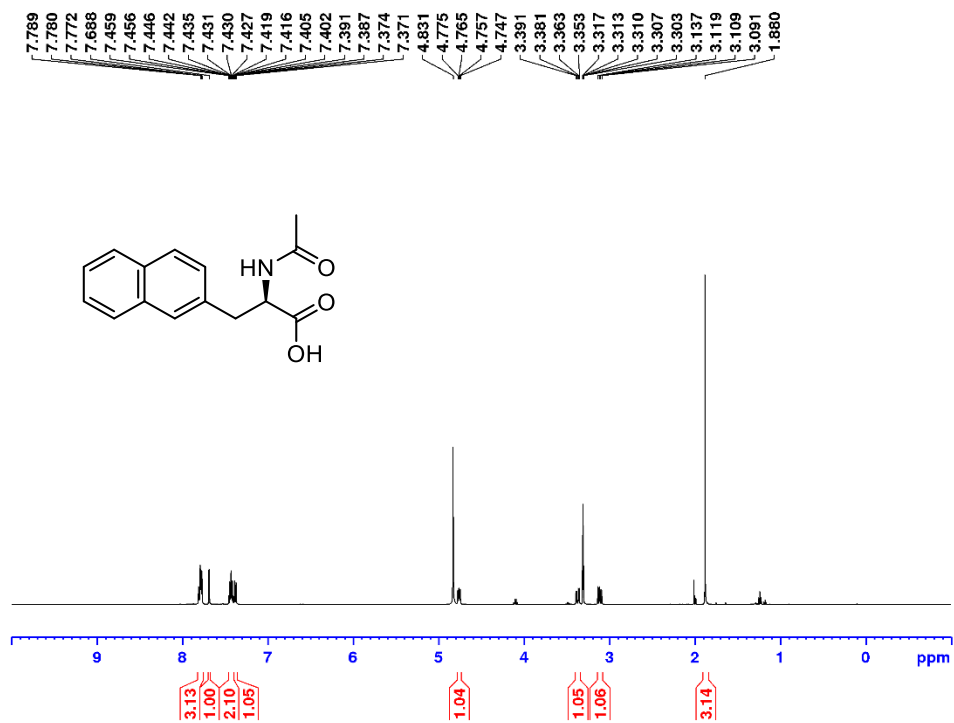


Figure B87. $^{13}\text{C}\{^1\text{H}\}$ NMR spectrum of **4-1b** in $\text{MeOD-}d_4$.

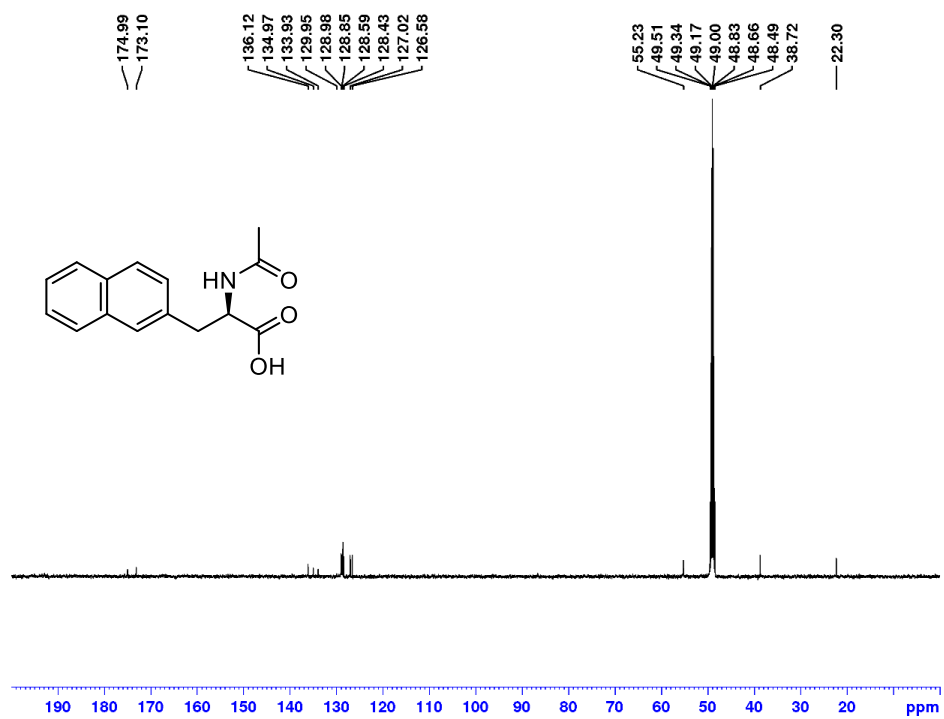


Figure B88. ^1H NMR spectrum of 4-1c in MeOD- d_4 .

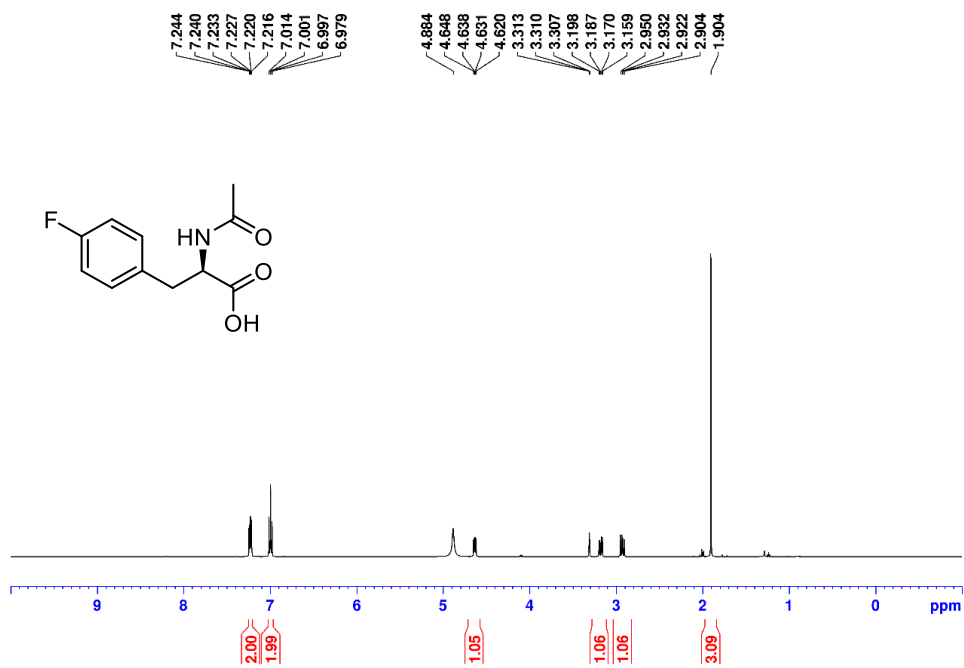


Figure B89. $^{13}\text{C}\{^1\text{H}\}$ NMR spectrum of **4-1c** in $\text{MeOD-}d_4$.

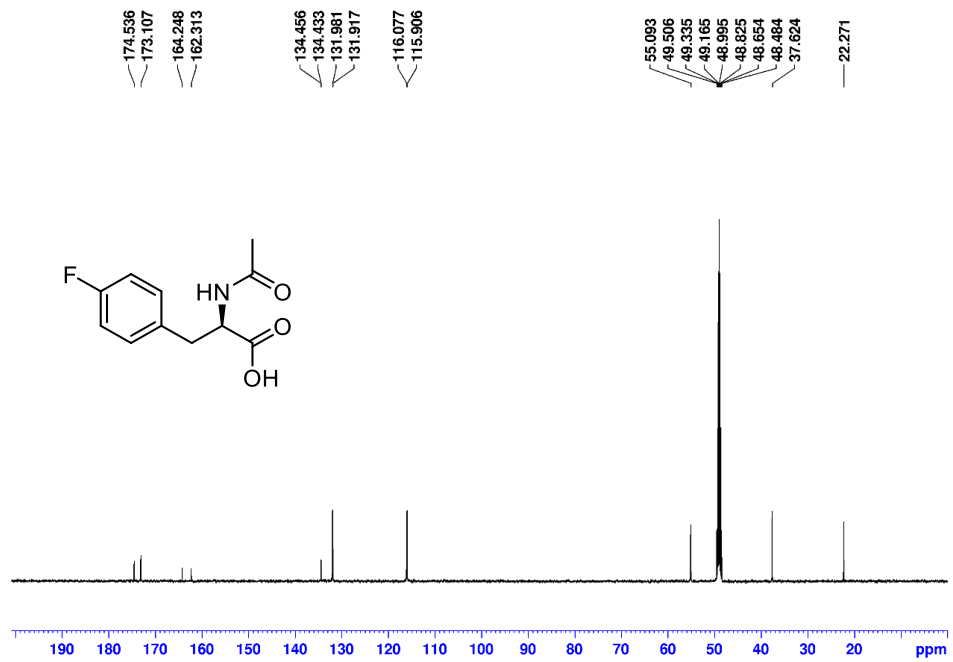


Figure B90. $^{19}\text{F}\{^1\text{H}\}$ NMR spectrum of **4-1c** in $\text{MeOD-}d_4$.

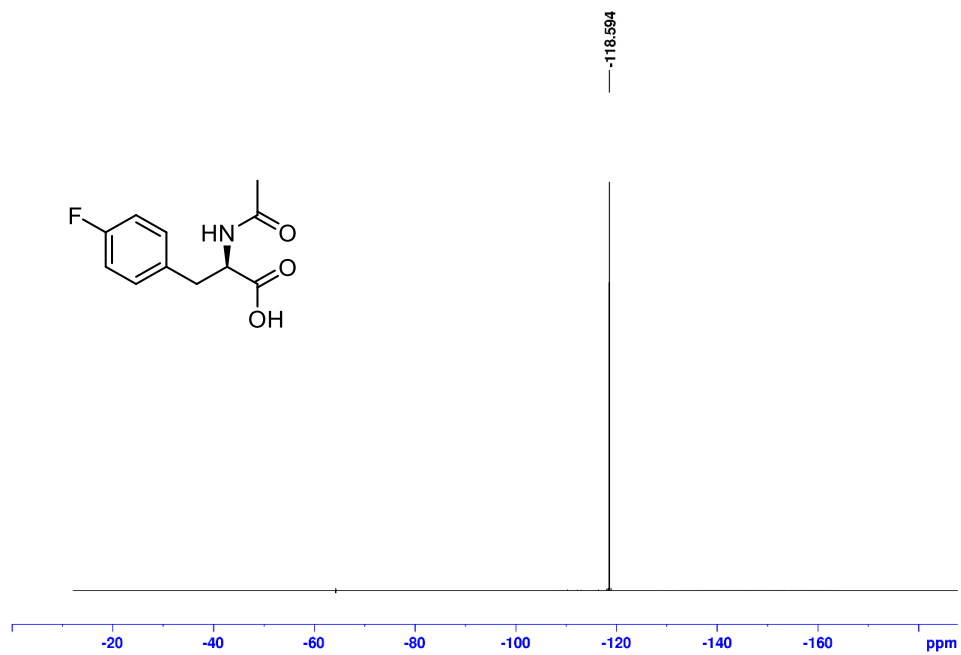


Figure B91. ^1H NMR spectrum of **4-1d** in $\text{MeOD-}d_4$.

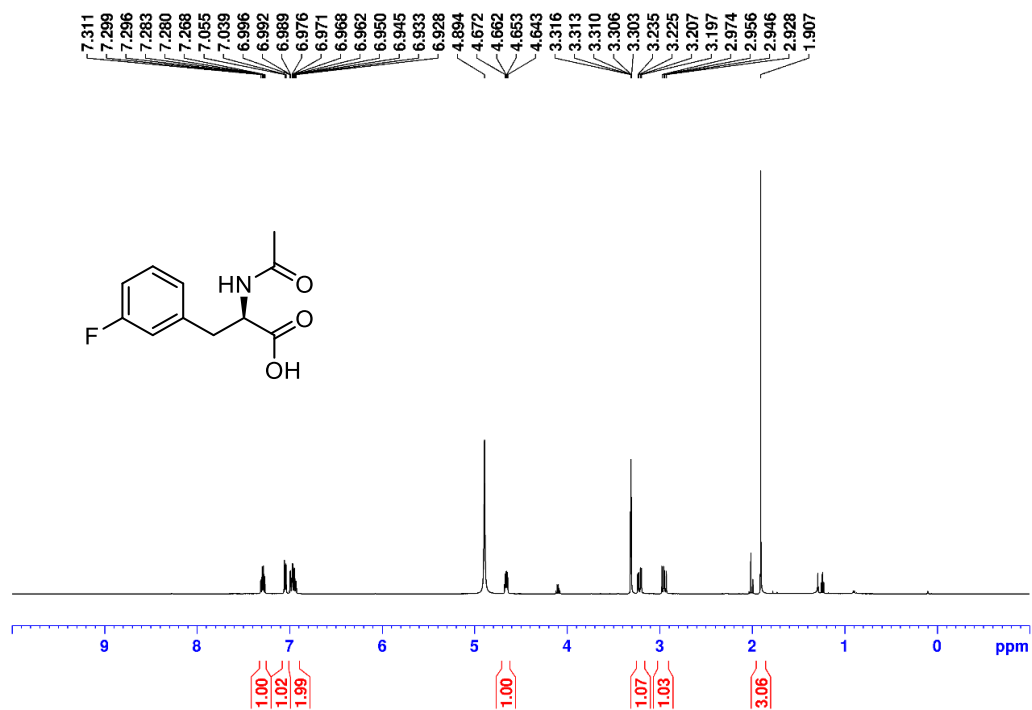


Figure B92. $^{13}\text{C}\{^1\text{H}\}$ NMR spectrum of 4-1d in MeOD- d_4 .

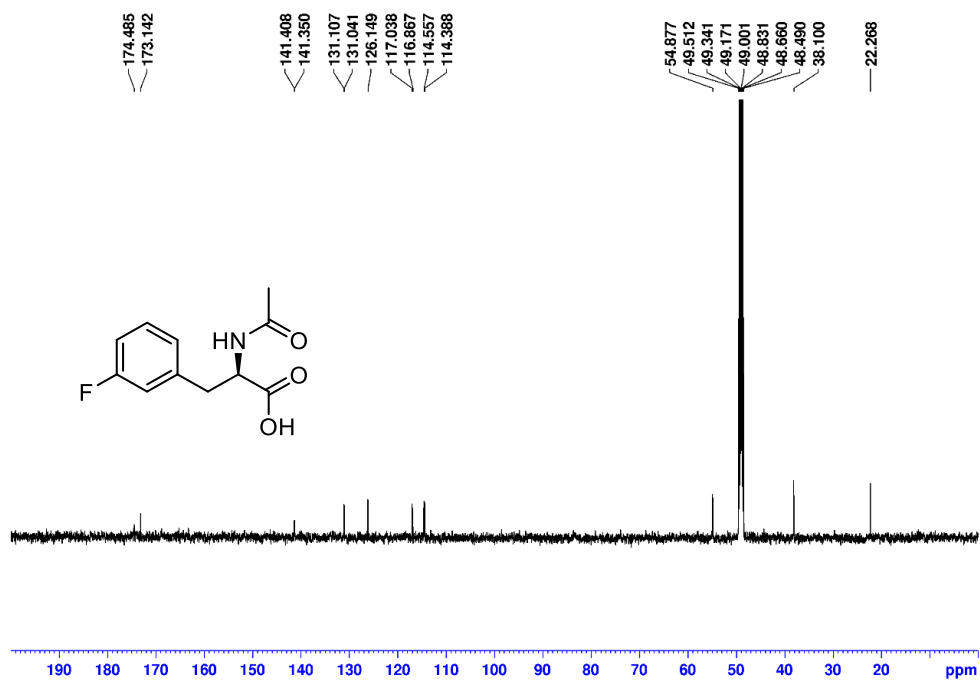


Figure B93 $^{19}\text{F}\{^1\text{H}\}$ NMR spectrum of **4-1d** in $\text{MeOD-}d_4$.

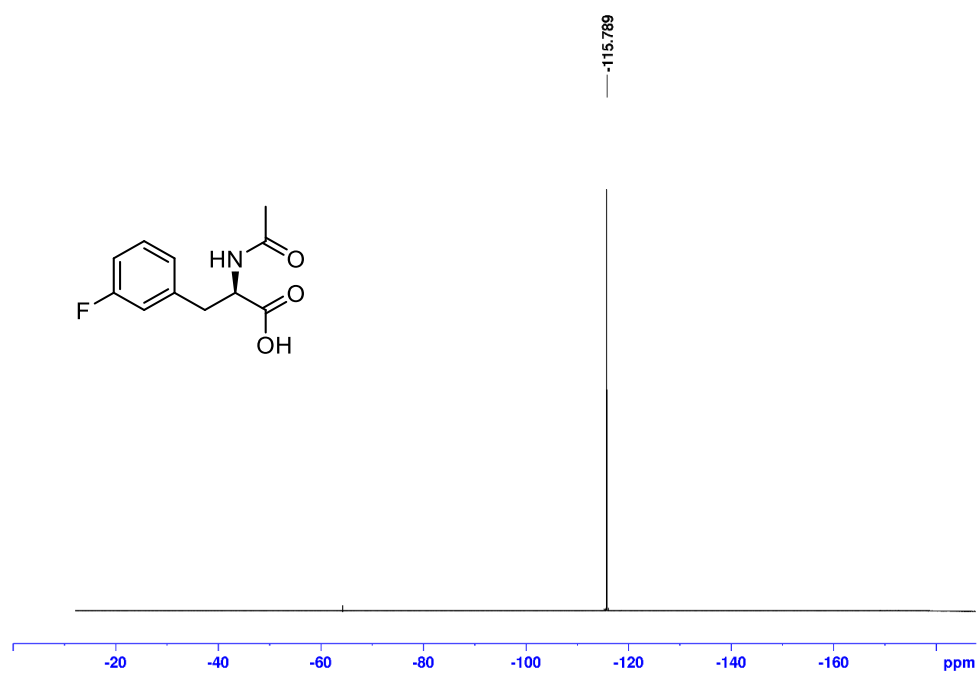


Figure B94. ^1H NMR spectrum of **4-1e** in $\text{MeOD-}d_4$.

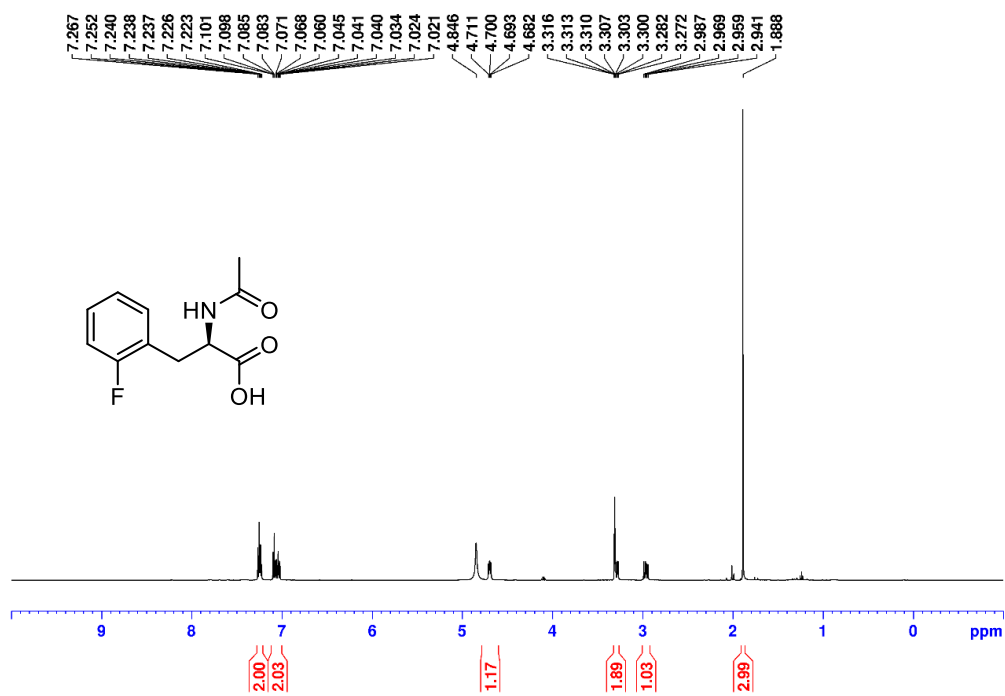


Figure B95. $^{13}\text{C}\{^1\text{H}\}$ NMR spectrum of **4-1e** in $\text{MeOD-}d_4$.

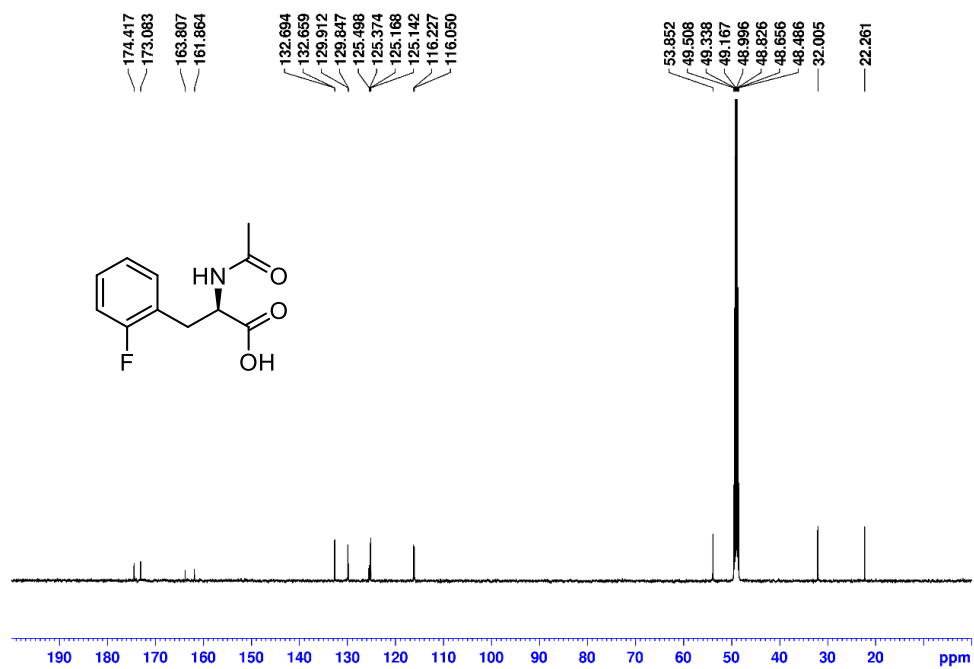


Figure B96. $^{19}\text{F}\{^1\text{H}\}$ NMR spectrum of **4-1e** in $\text{MeOD-}d_4$.

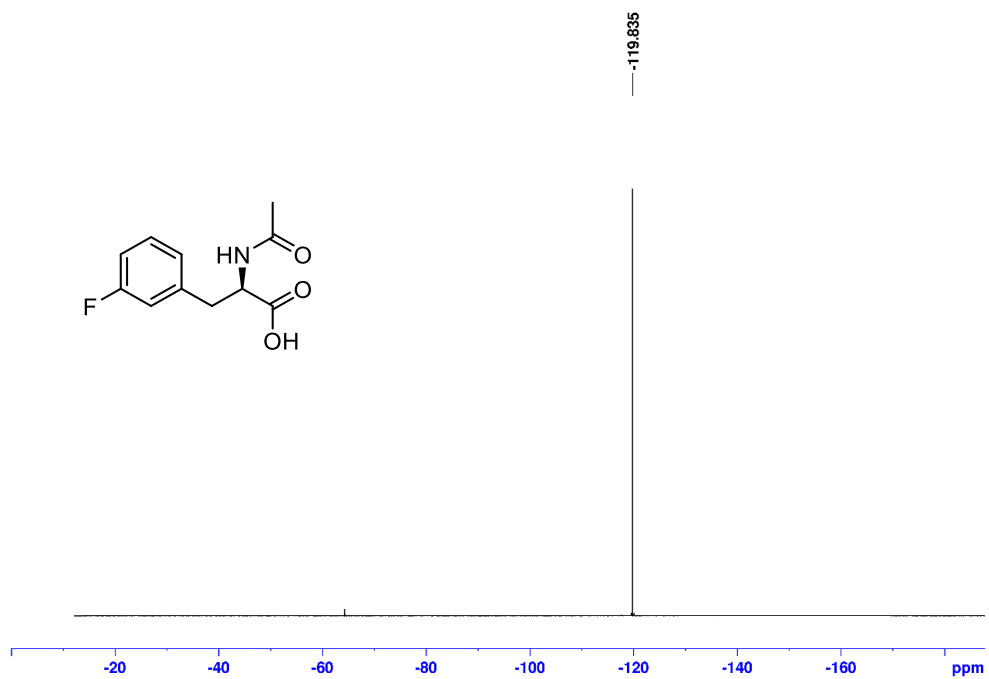


Figure B97. ^1H NMR spectrum of **4-1f** in $\text{MeOD-}d_4$.

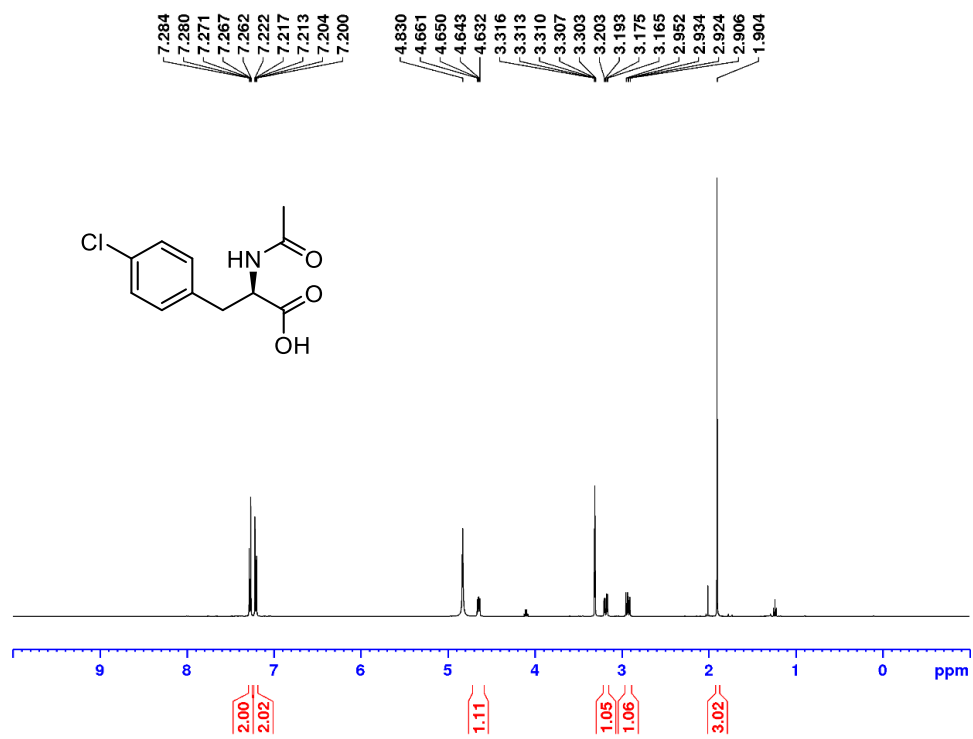


Figure B98. $^{13}\text{C}\{^1\text{H}\}$ NMR spectrum of **4-1f** in $\text{MeOD-}d_4$.

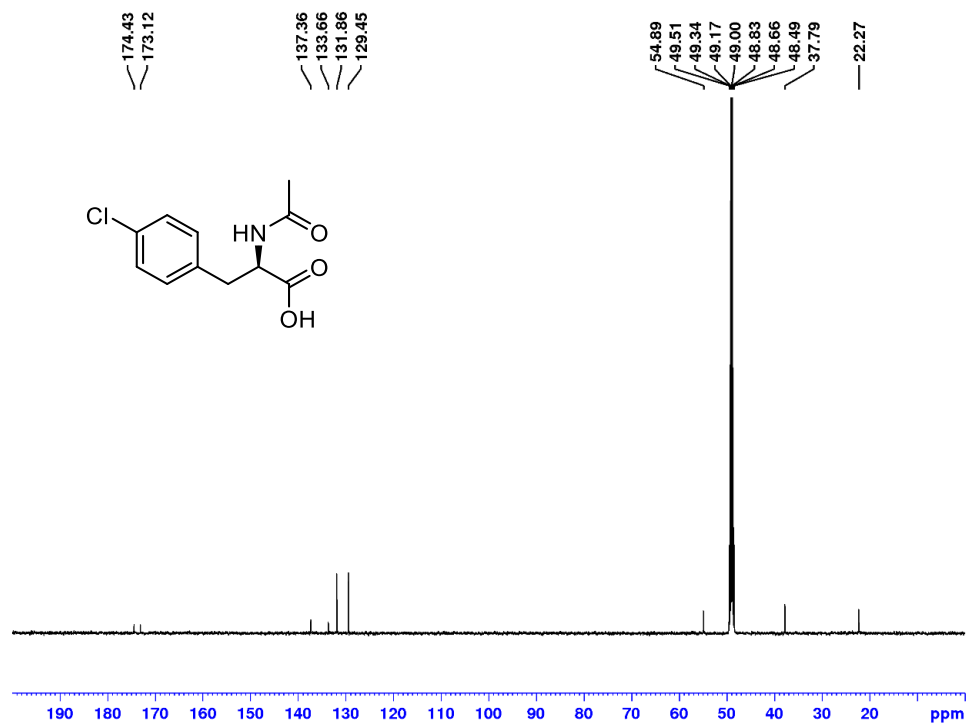


Figure B99. ^1H NMR spectrum of **4-1g** in $\text{MeOD-}d_4$.

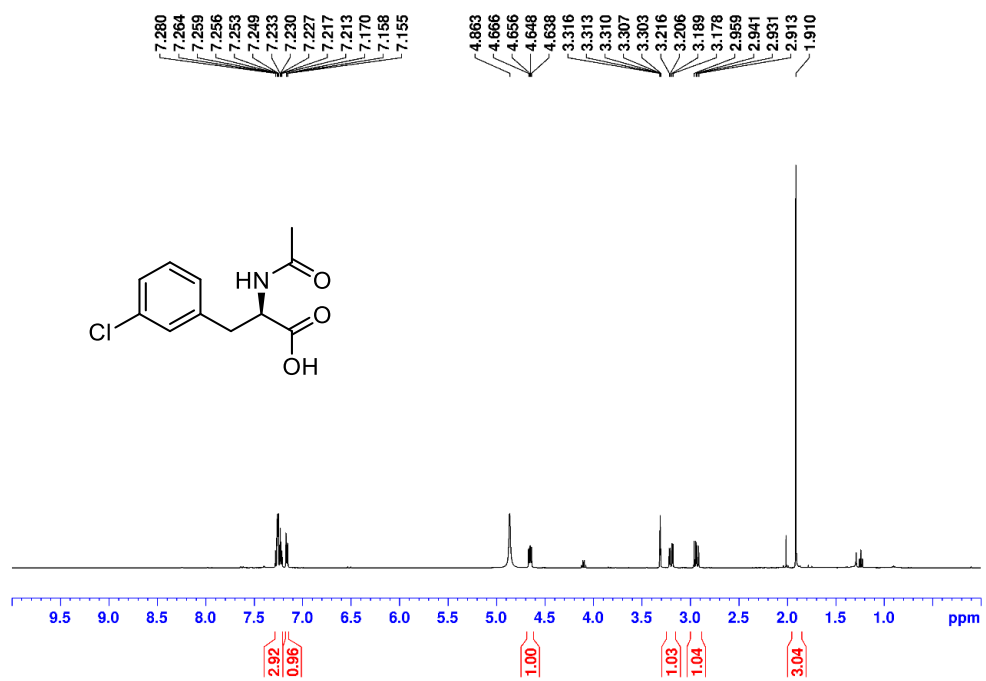


Figure B100. $^{13}\text{C}\{^1\text{H}\}$ NMR spectrum of **4-1g** in $\text{MeOD-}d_4$.

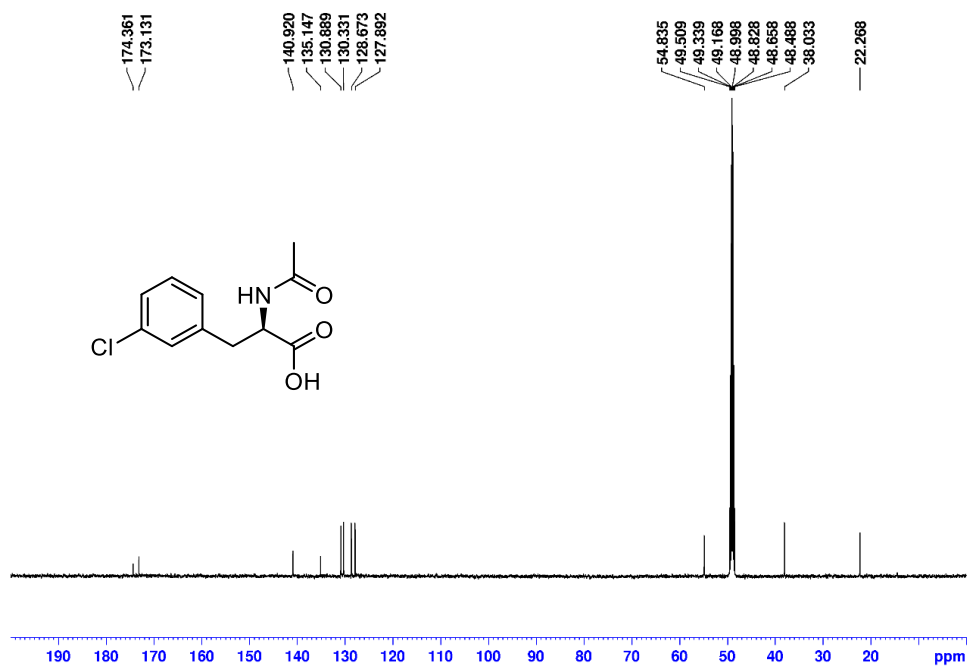


Figure B101. ^1H NMR spectrum of **4-1h** in $\text{MeOD-}d_4$.

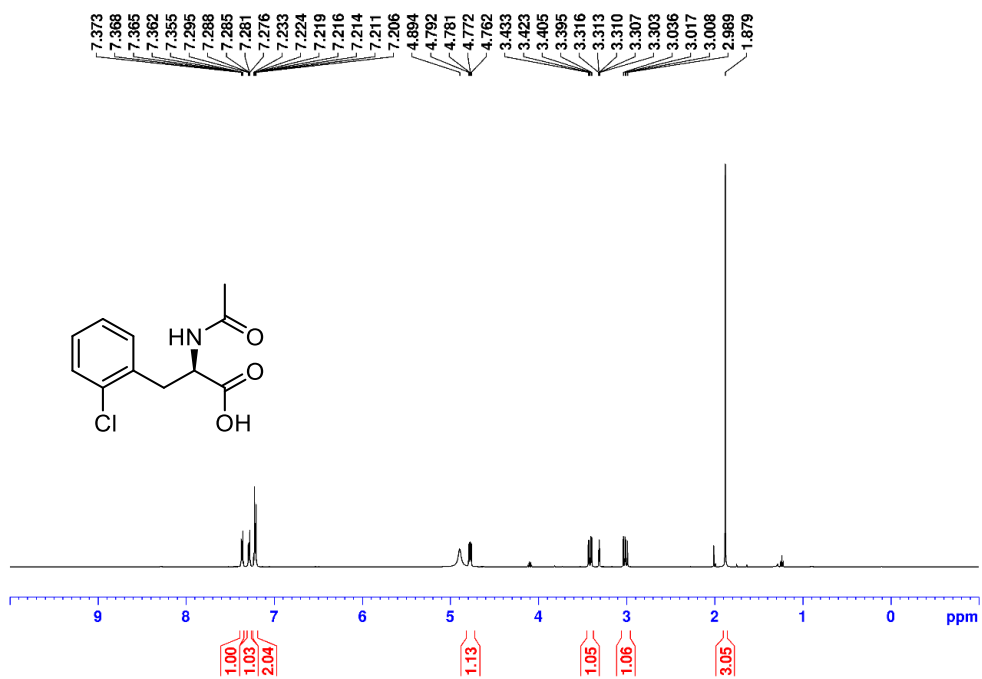


Figure B102. $^{13}\text{C}\{^1\text{H}\}$ NMR spectrum of 4-1h in $\text{MeOD-}d_4$.

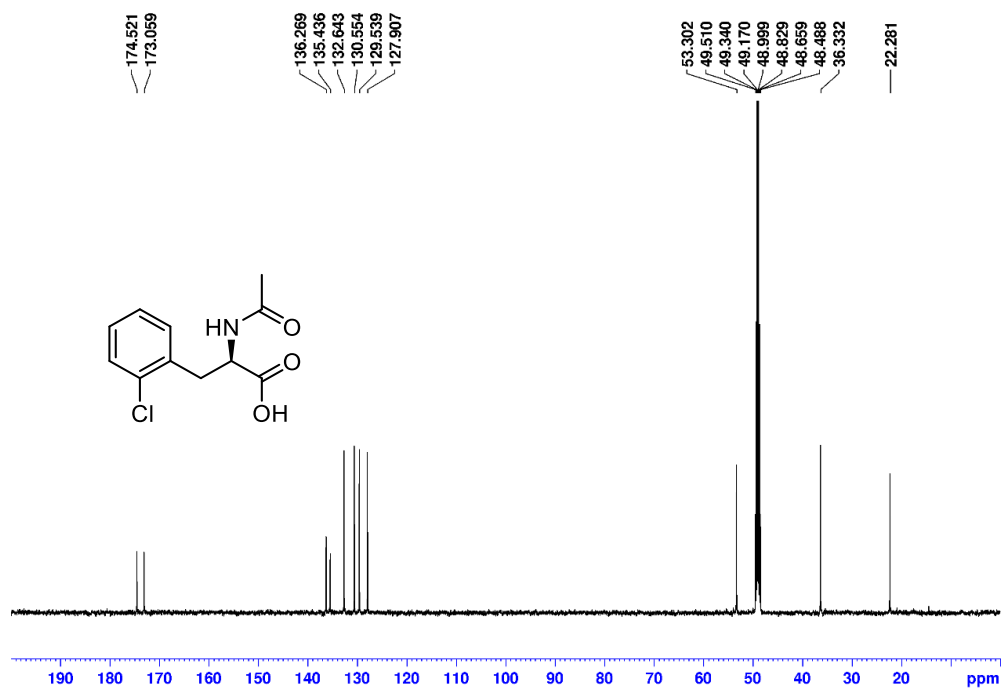


Figure B103. ^1H NMR spectrum of **4-1i** in $\text{MeOD-}d_4$.

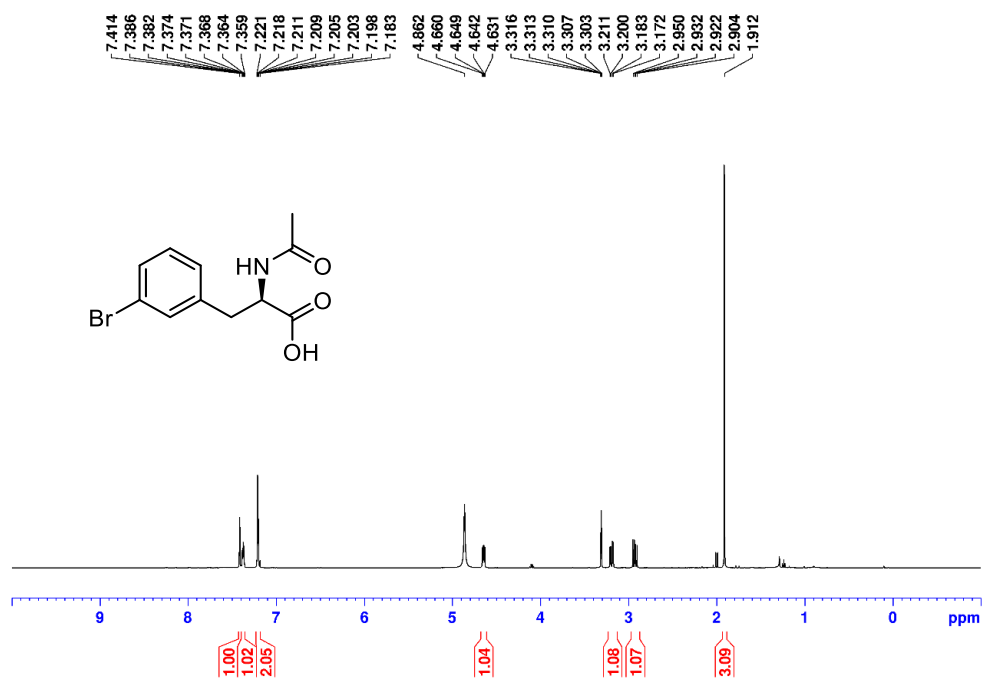


Figure B104. $^{13}\text{C}\{^1\text{H}\}$ NMR spectrum of **4-1i** in $\text{MeOD-}d_4$.

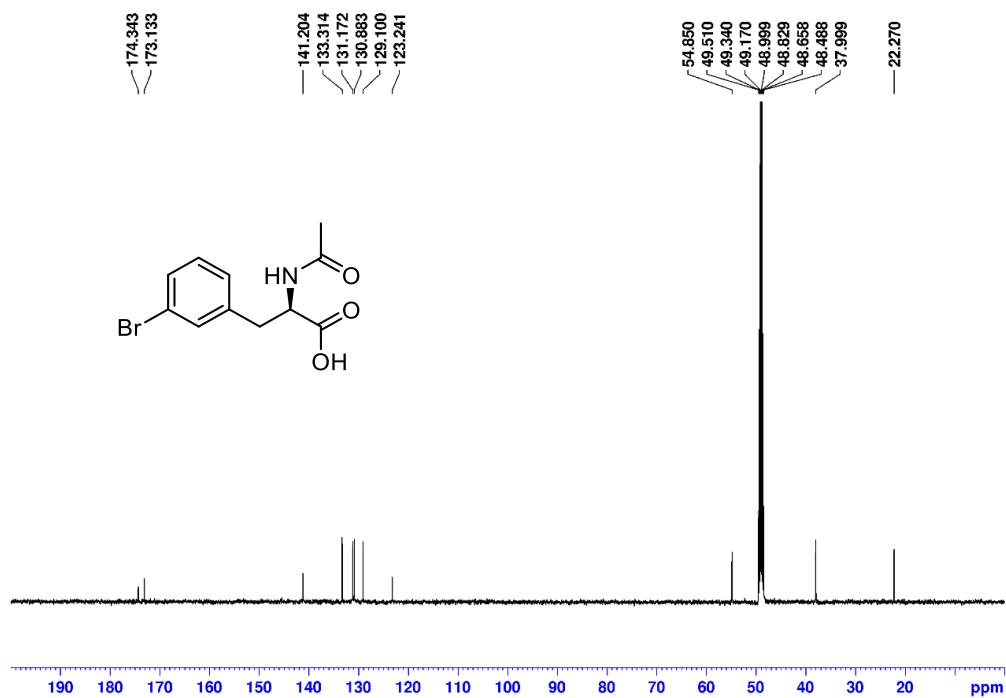


Figure B105. ^1H NMR spectrum of **4-1j** in $\text{MeOD-}d_4$.

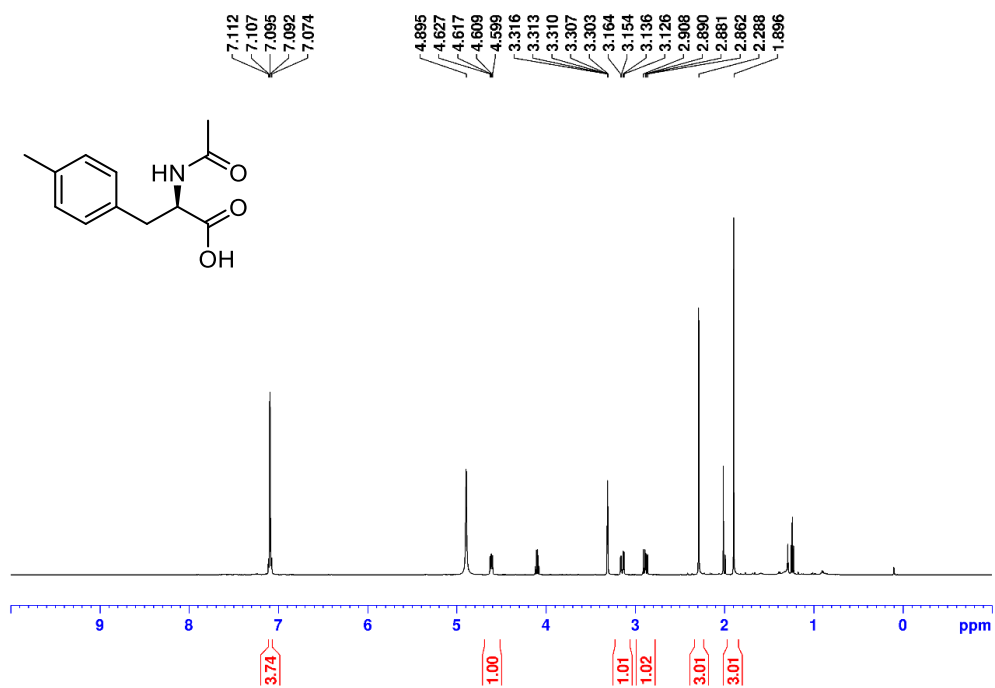


Figure B106. $^{13}\text{C}\{^1\text{H}\}$ NMR spectrum of 4-1j in MeOD- d_4 .

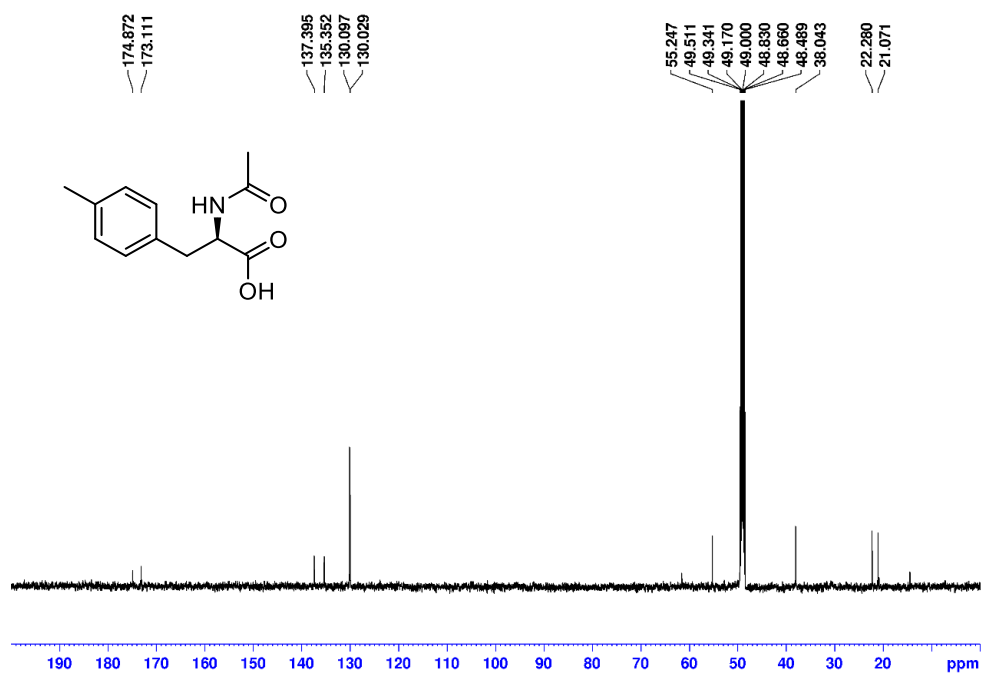


Figure B107. ^1H NMR spectrum of **4-1k** in $\text{MeOD-}d_4$.

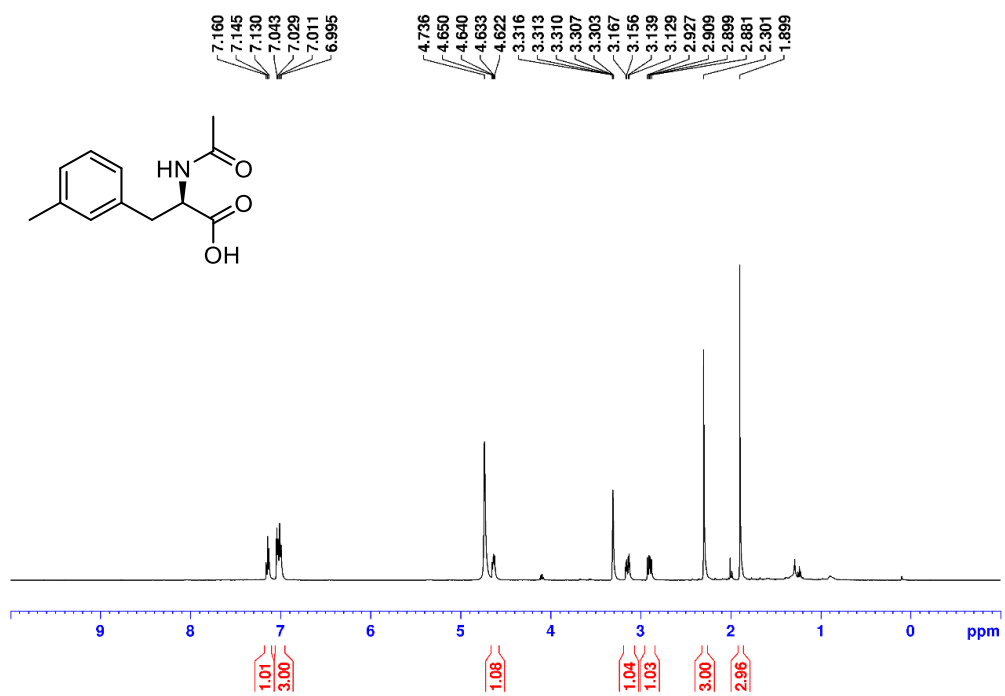


Figure B108. $^{13}\text{C}\{^1\text{H}\}$ NMR spectrum of 4-1k in MeOD- d_4 .

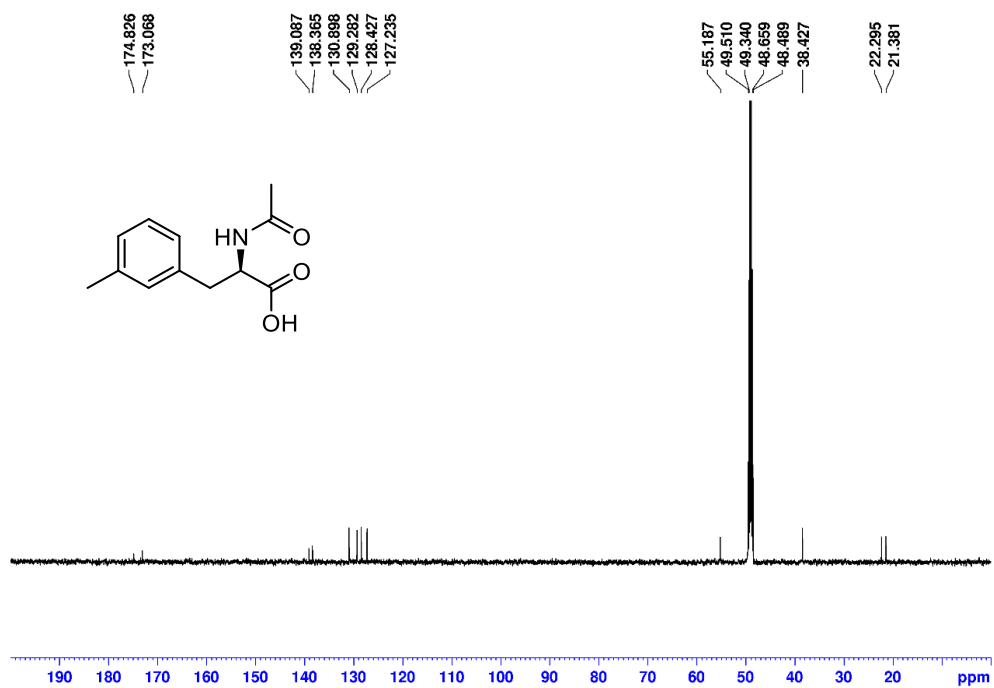


Figure B109. ^1H NMR spectrum of **4-11** in $\text{MeOD-}d_4$.

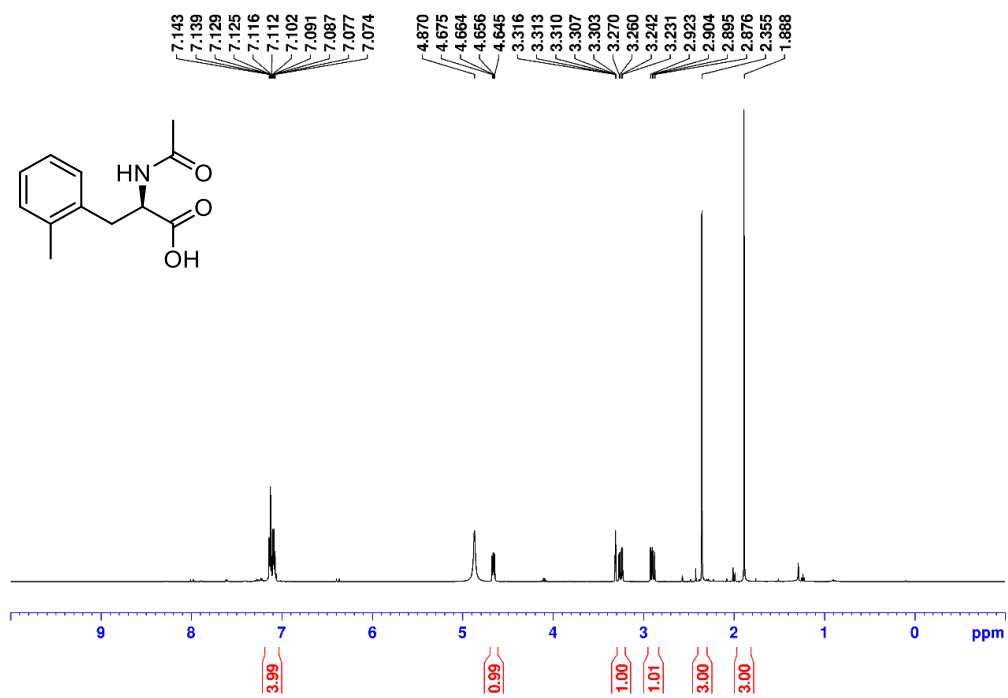


Figure B110. $^{13}\text{C}\{^1\text{H}\}$ NMR spectrum of 4-11 in MeOD- d_4 .

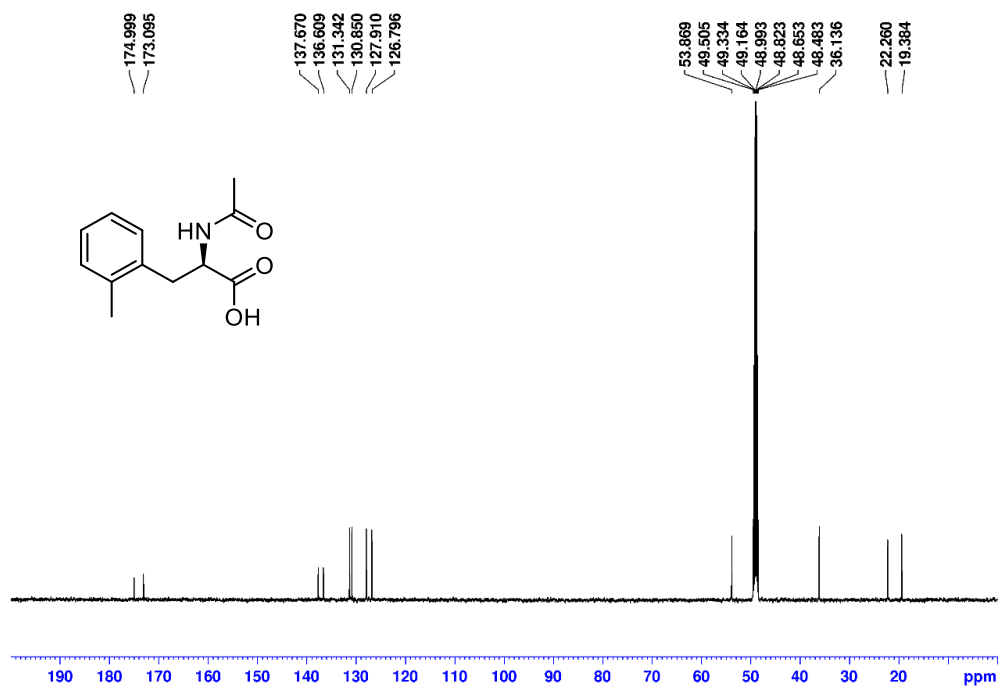


Figure B111. ^1H NMR spectrum of **4-1m** in $\text{MeOD-}d_4$.

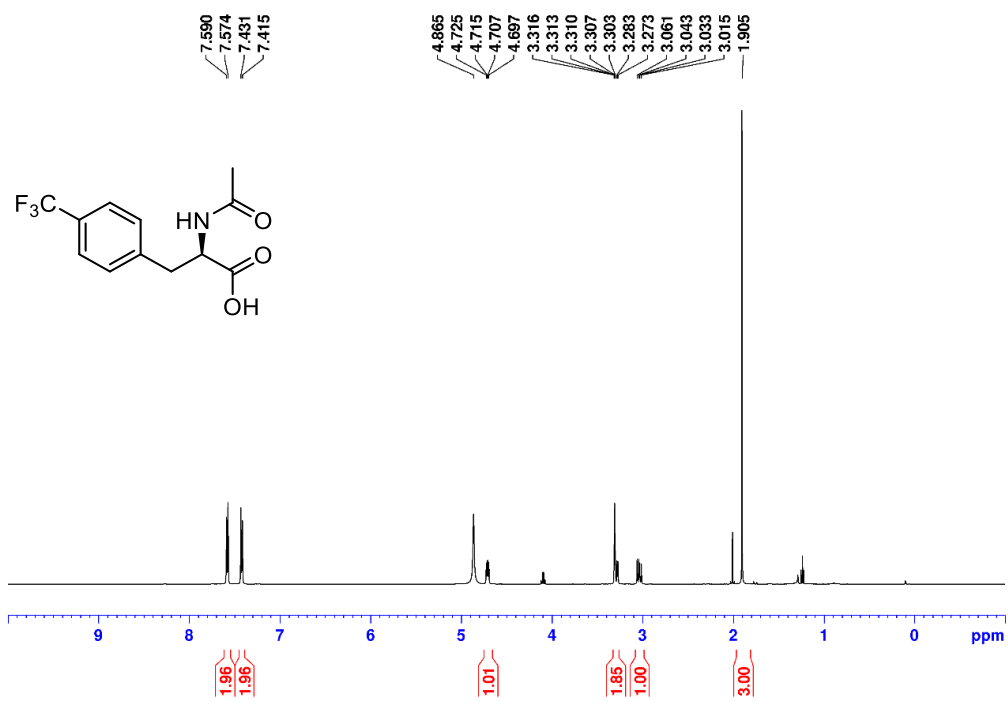


Figure B112. $^{13}\text{C}\{^1\text{H}\}$ NMR spectrum of **4-1m** in $\text{MeOD-}d_4$.

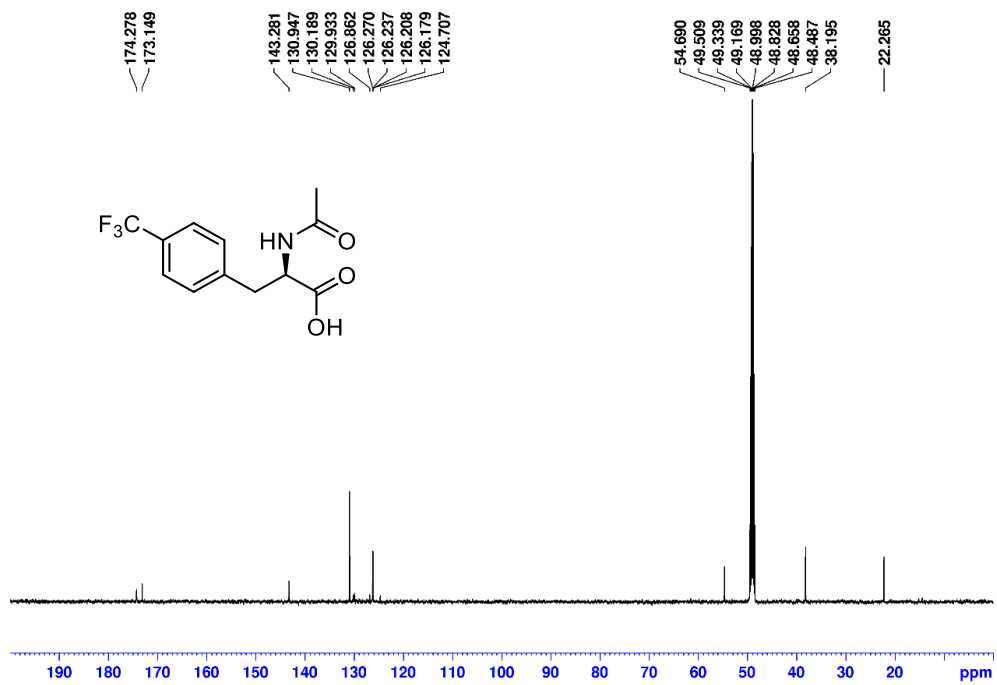


Figure B113. $^{19}\text{F}\{^1\text{H}\}$ NMR spectrum of **4-1m** in $\text{MeOD-}d_4$.

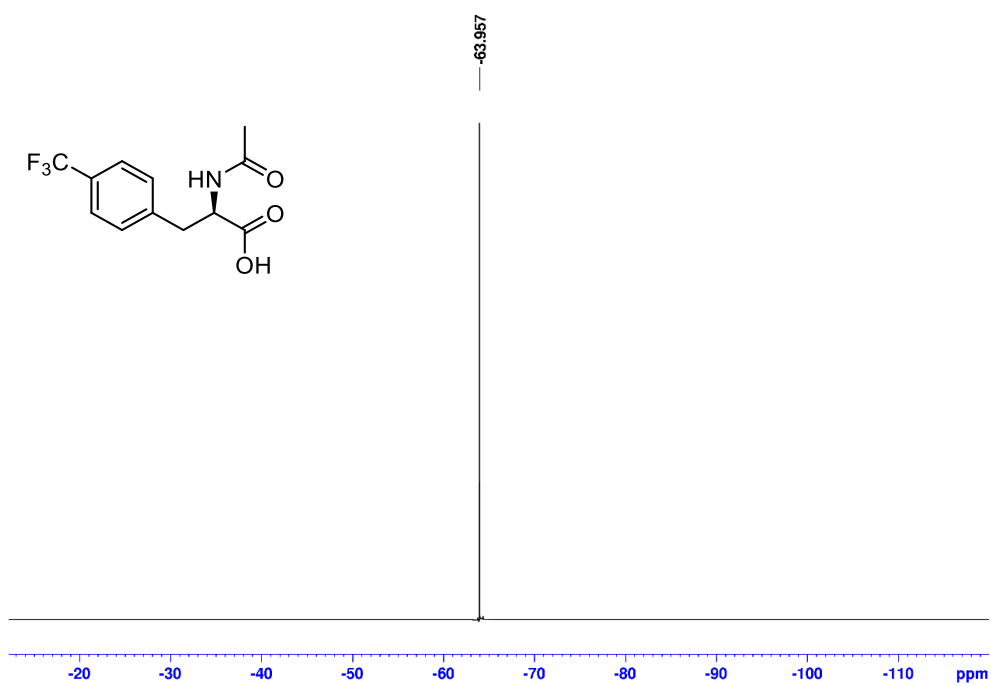


Figure B114. ^1H NMR spectrum of **4-1n** in $\text{MeOD-}d_4$.

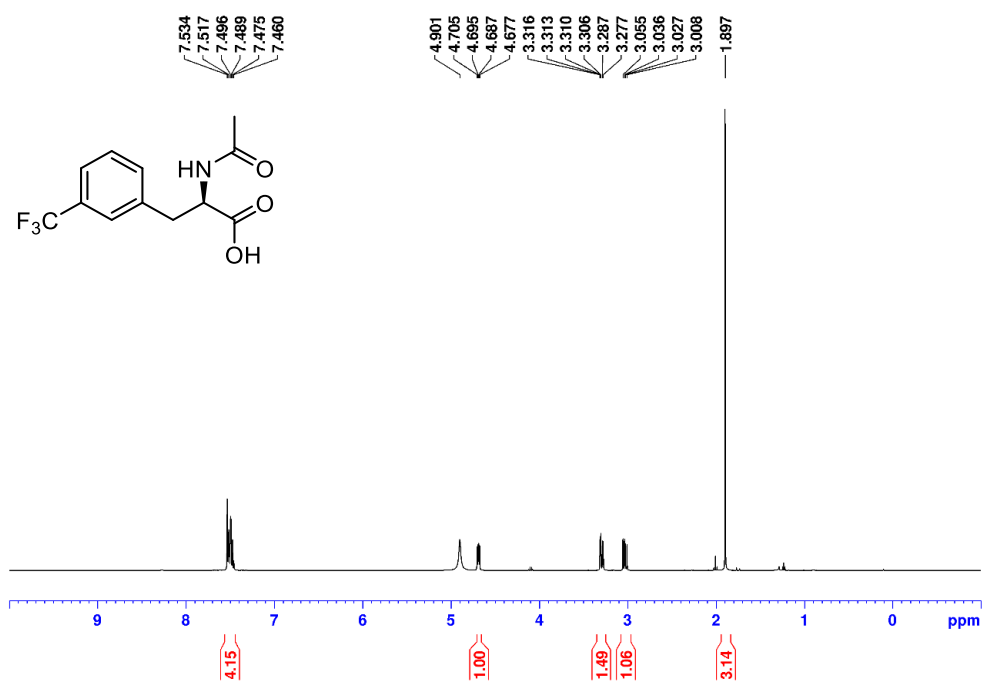


Figure B115. $^{13}\text{C}\{^1\text{H}\}$ NMR spectrum of **4-1n** in $\text{MeOD-}d_4$.

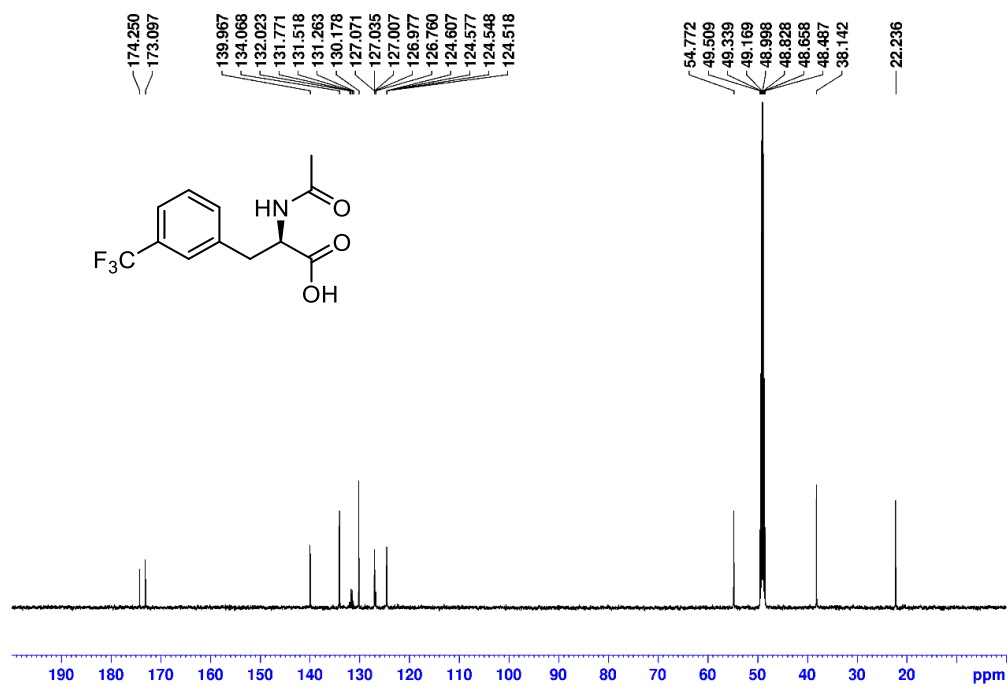


Figure B116. $^{19}\text{F}\{^1\text{H}\}$ NMR spectrum of **4-1n** in $\text{MeOD-}d_4$.



Figure B117. ^1H NMR spectrum of **4-1o** in $\text{MeOD-}d_4$.

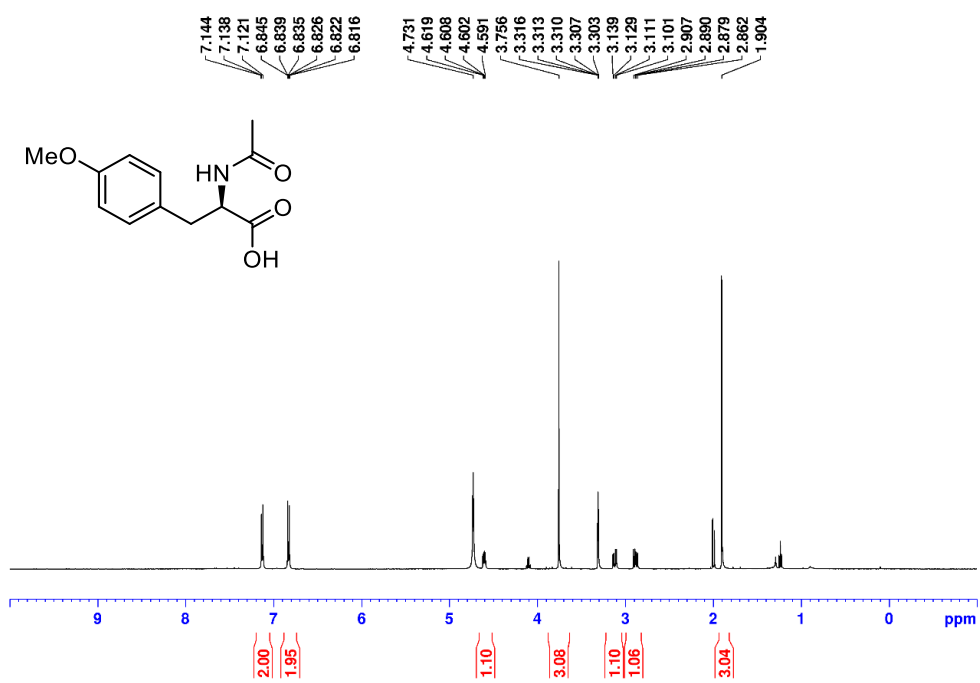


Figure B118. $^{13}\text{C}\{^1\text{H}\}$ NMR spectrum of **4-1o** in $\text{MeOD-}d_4$.

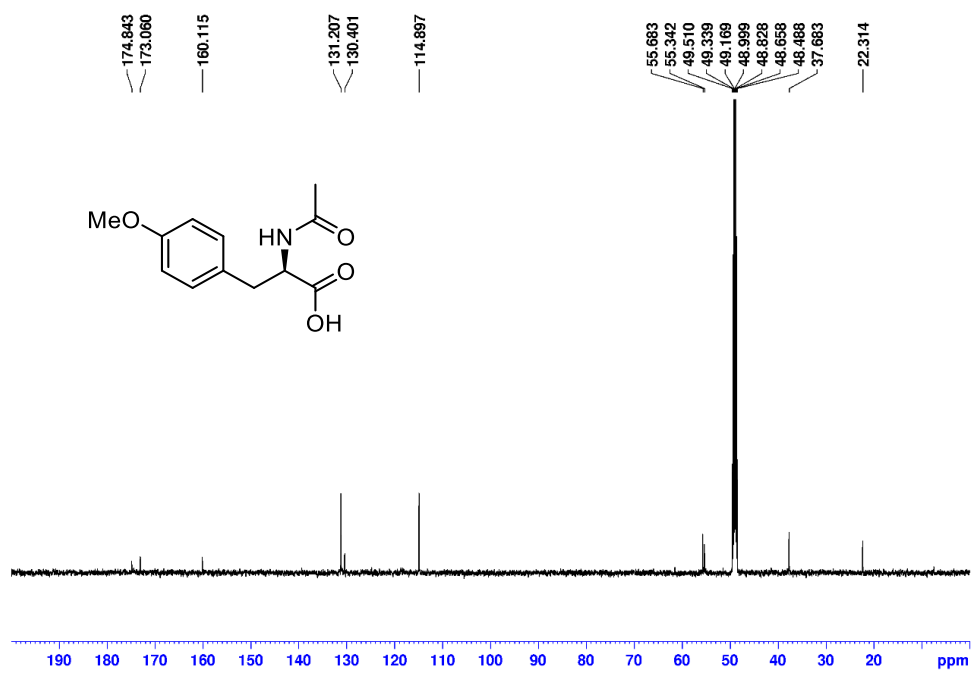


Figure B119. ^1H NMR spectrum of **4-1p** in $\text{MeOD-}d_4$.

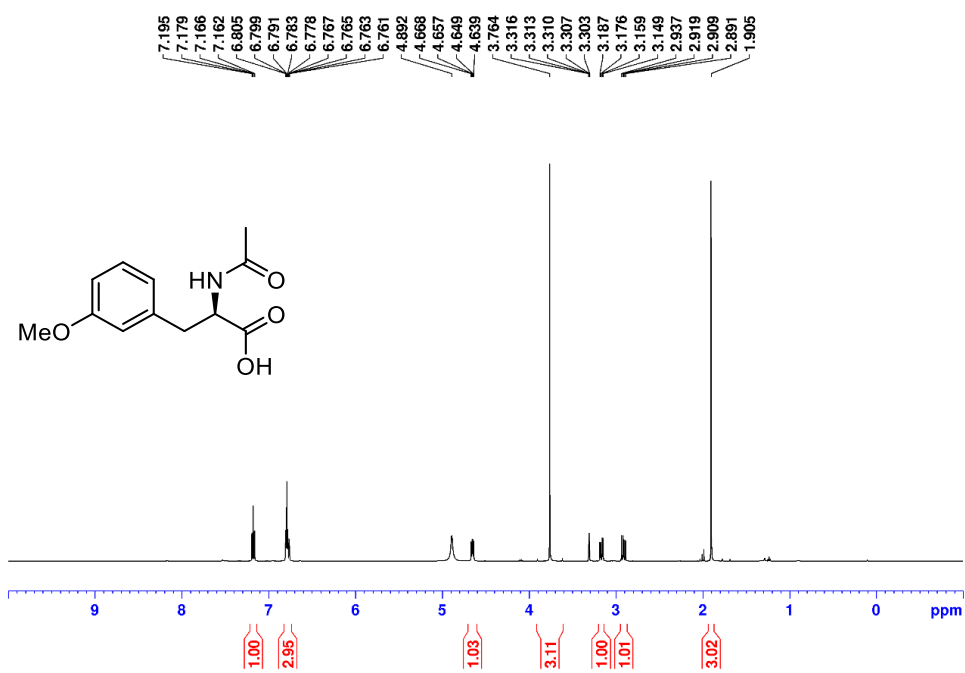


Figure B120. $^{13}\text{C}\{^1\text{H}\}$ NMR spectrum of **4-1p** in $\text{MeOD-}d_4$.

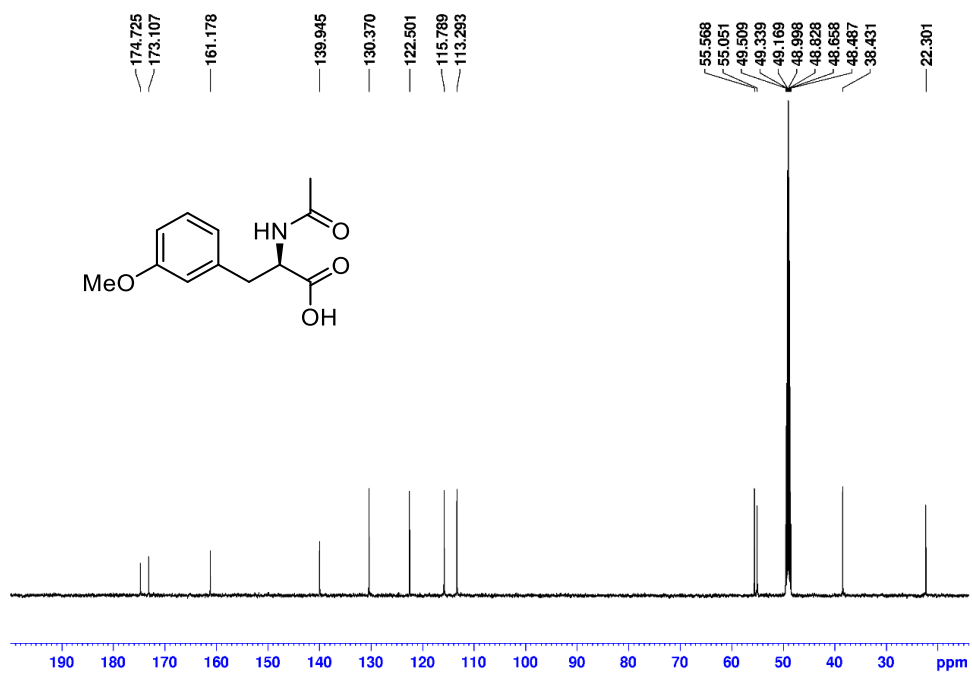


Figure B121. ^1H NMR spectrum of **4-1q** in $\text{MeOD-}d_4$.

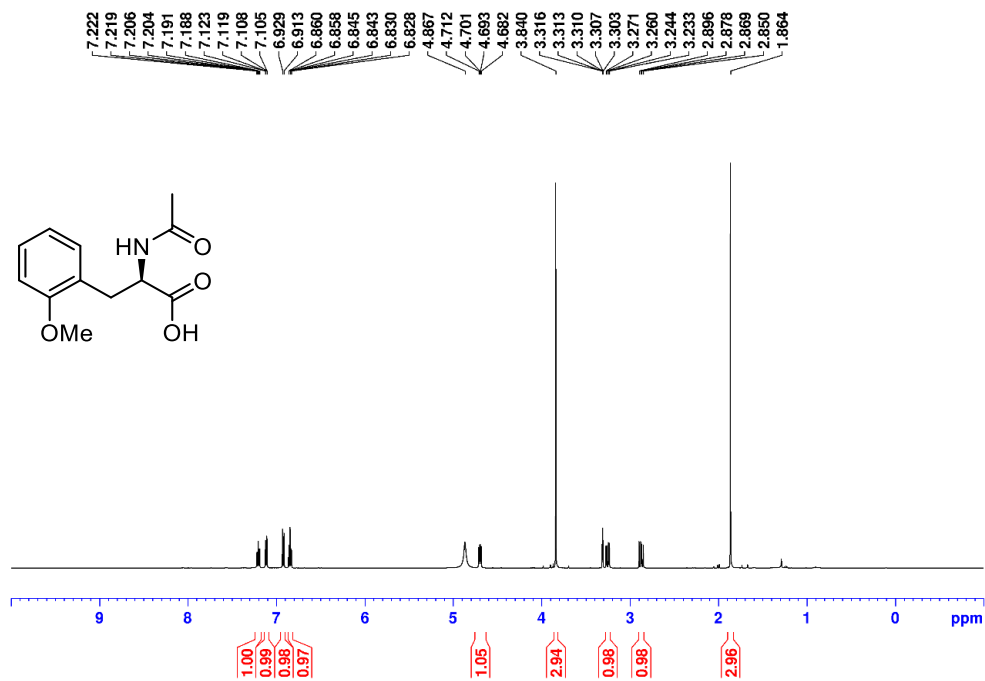


Figure B122. $^{13}\text{C}\{^1\text{H}\}$ NMR spectrum of **4-1q** in MeOD- d_4 .

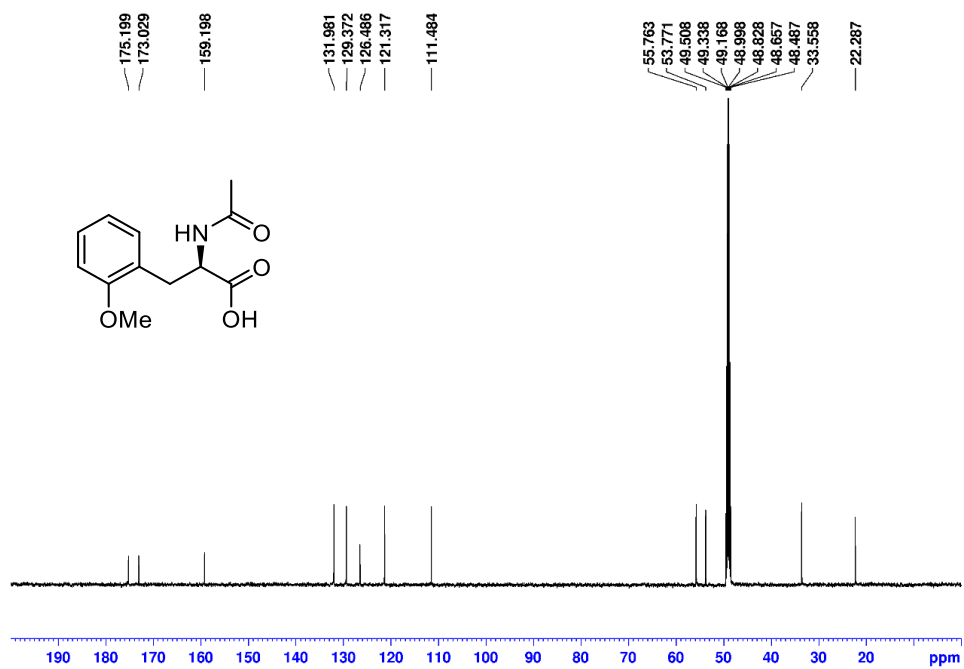


Figure B123. ^1H NMR spectrum of **4-1r** in $\text{MeOD-}d_4$.

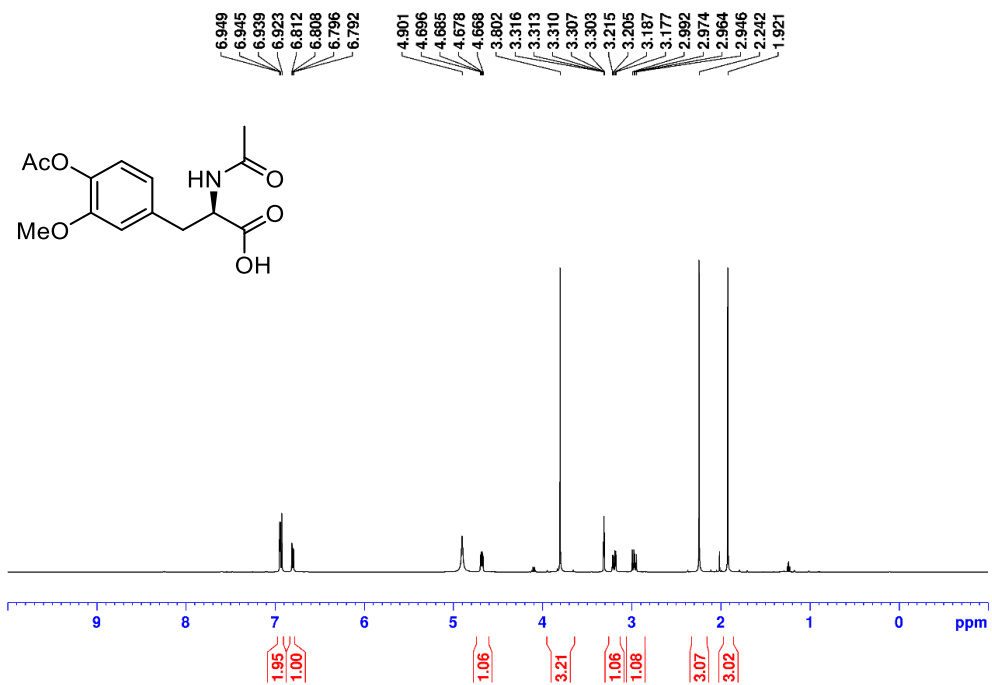


Figure B124. $^{13}\text{C}\{^1\text{H}\}$ NMR spectrum of **4-1r** in $\text{MeOD-}d_4$.

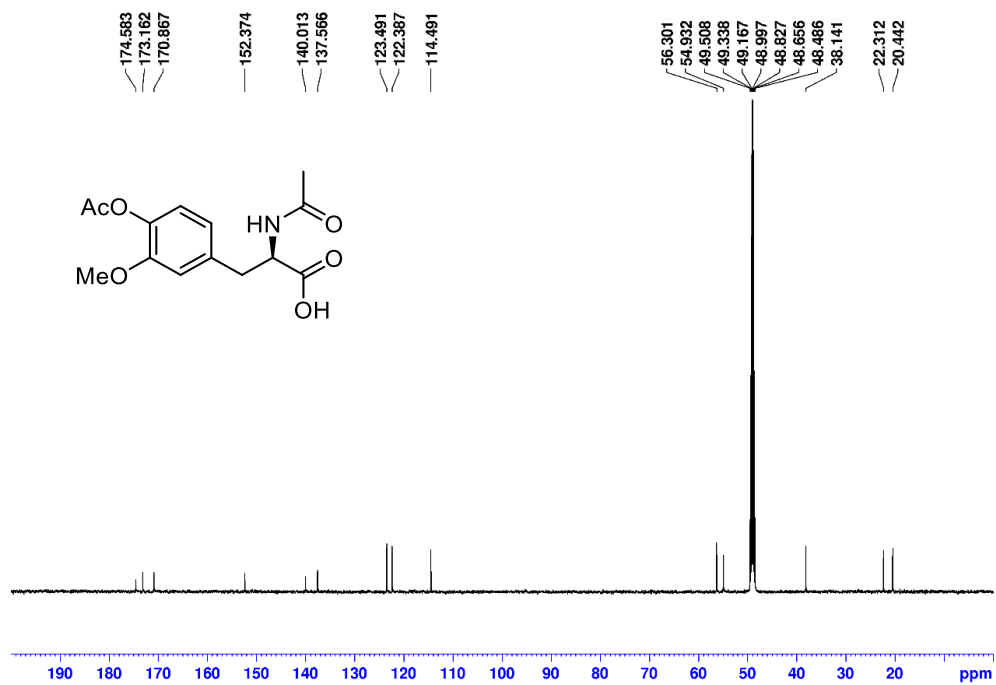


Figure B125. ^1H NMR spectrum of 4-1s in $\text{MeOD-}d_4$.

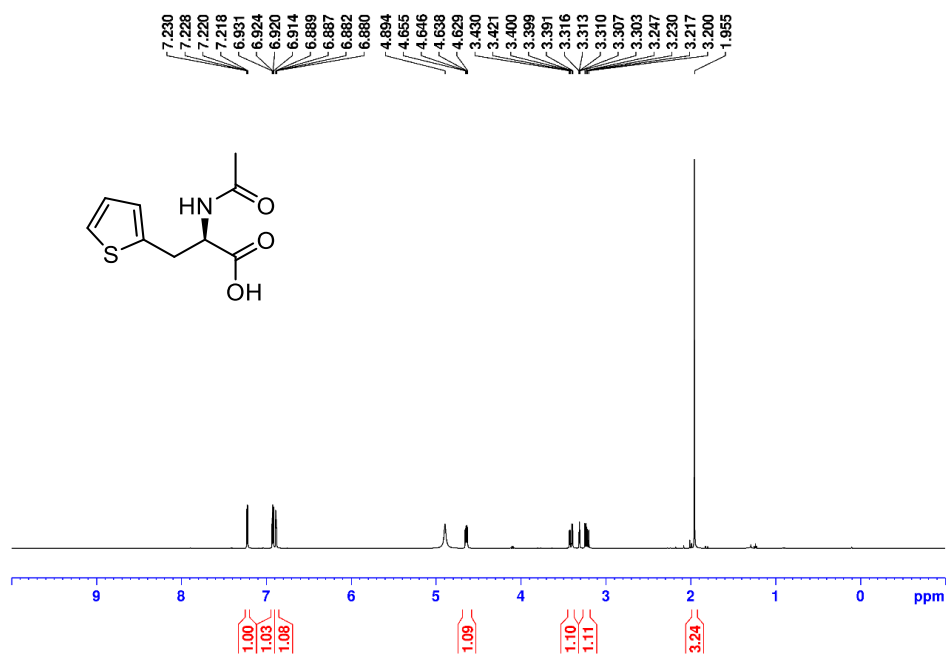


Figure B126. $^{13}\text{C}\{^1\text{H}\}$ NMR spectrum of 4-1s in MeOD- d_4 .

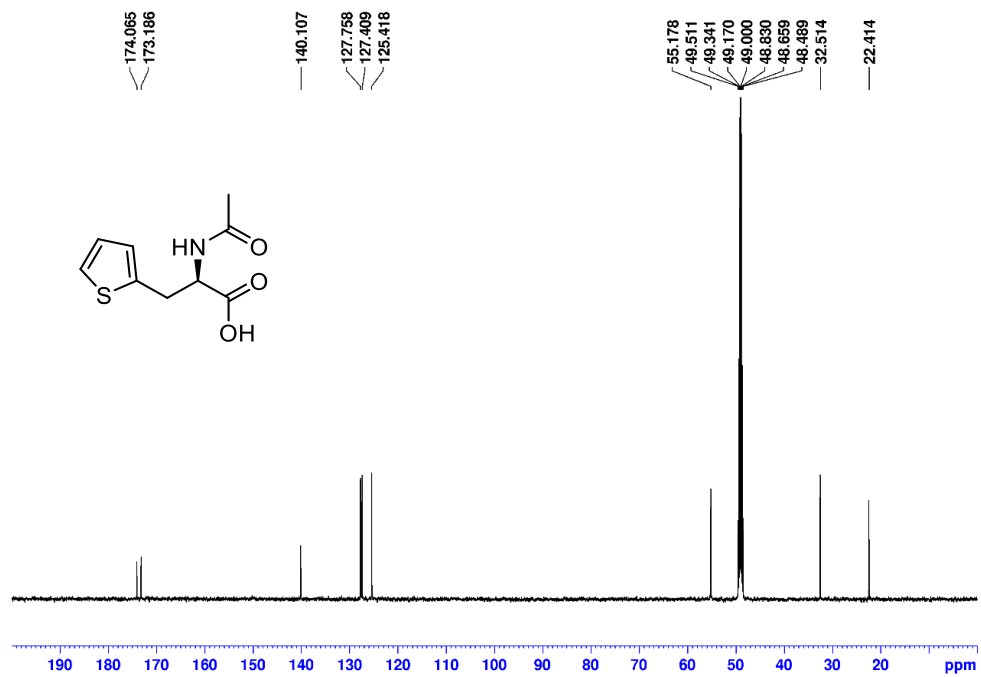


Figure B127. ^1H NMR spectrum of **4-1t** in $\text{MeOD-}d_4$.

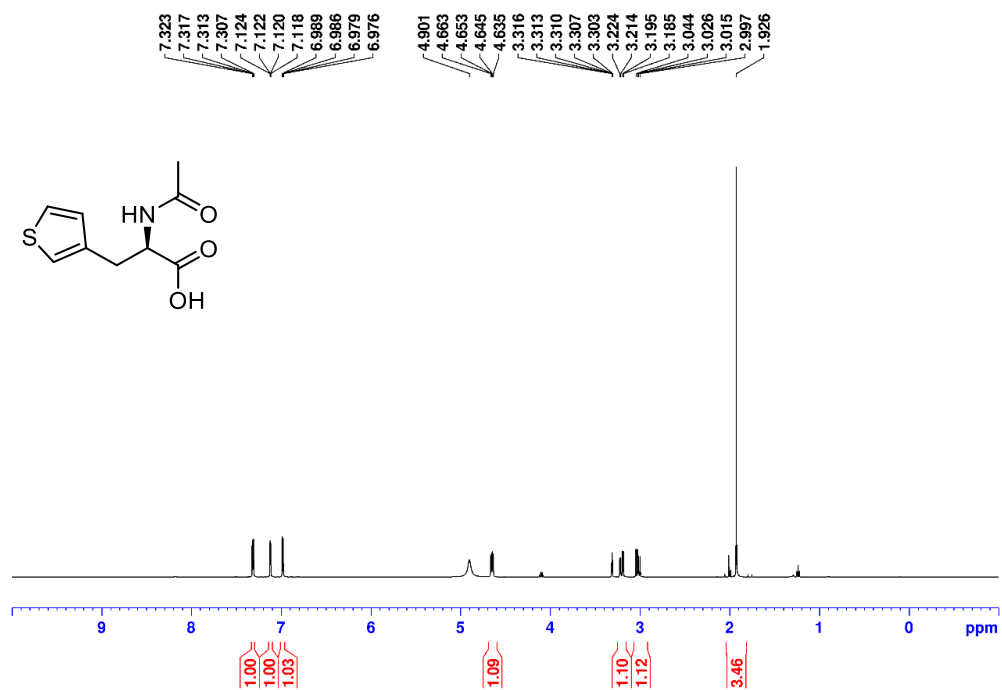


Figure B128. $^{13}\text{C}\{^1\text{H}\}$ NMR spectrum of **4-1t** in $\text{MeOD-}d_4$.

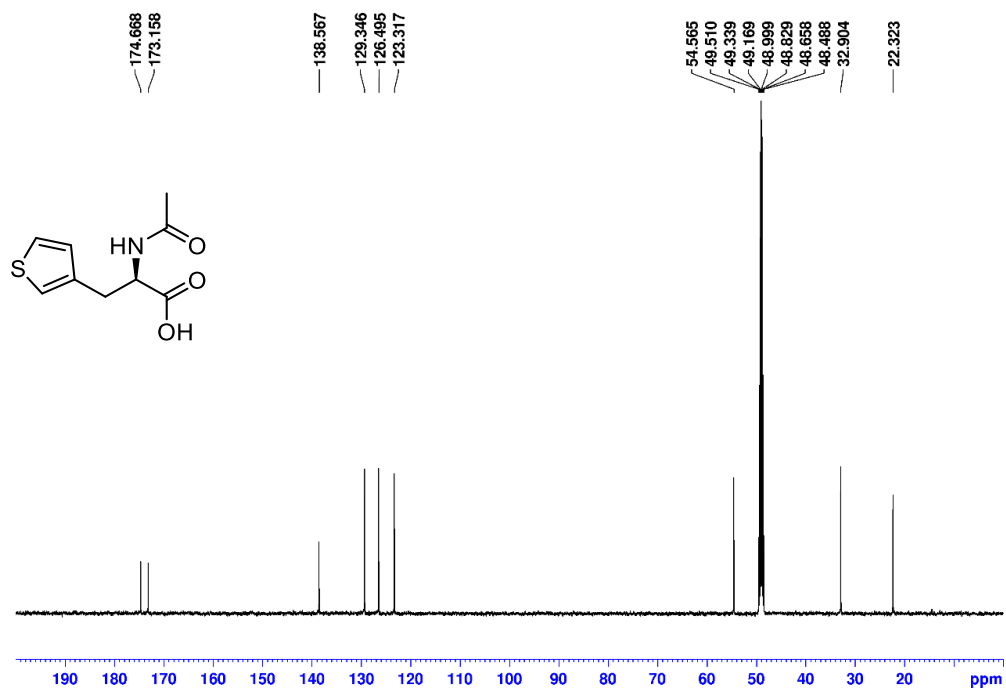


Figure B129. ^1H NMR spectrum of L4-1 in benzene- d_6 .

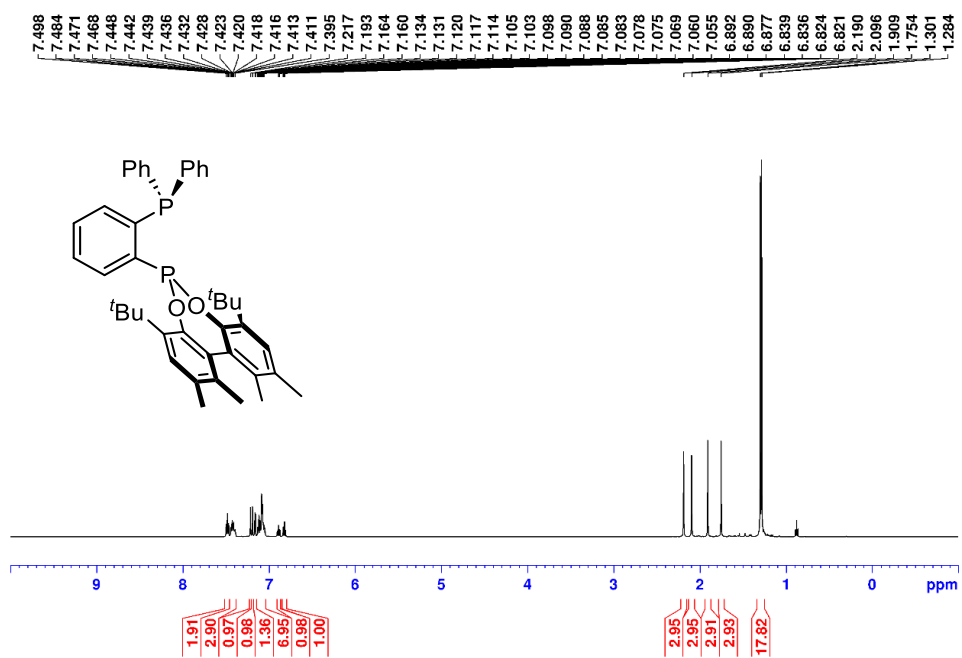


Figure B130. $^{13}\text{C}\{^1\text{H}\}$ NMR spectrum of L4-1 in benzene- d_6 .

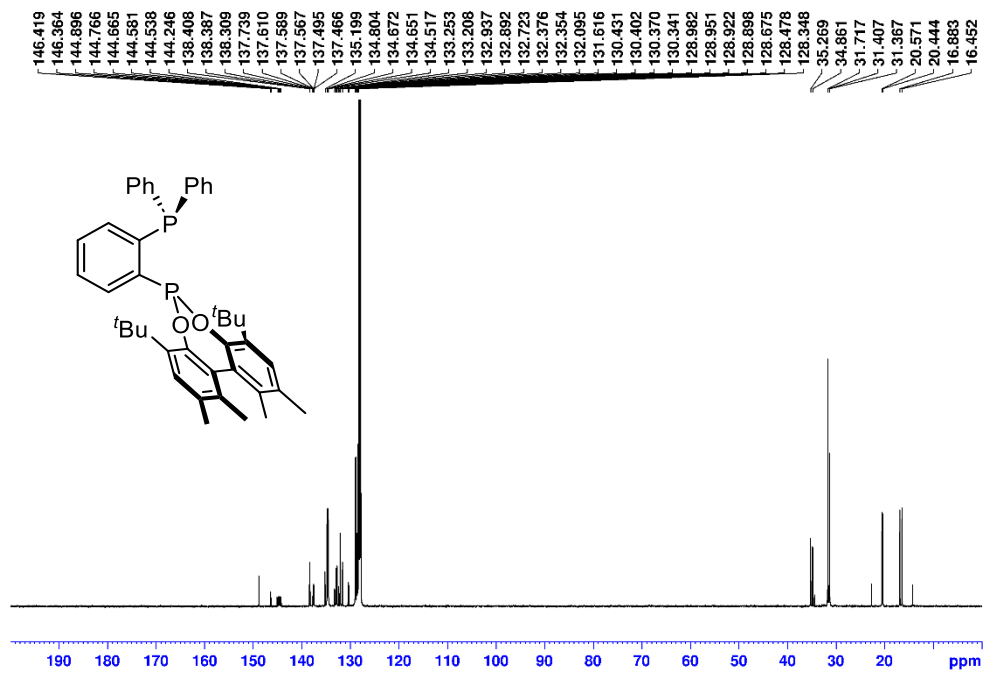


Figure B131. $^{31}\text{P}\{^1\text{H}\}$ NMR spectrum of **L4-1** in benzene- d_6 .

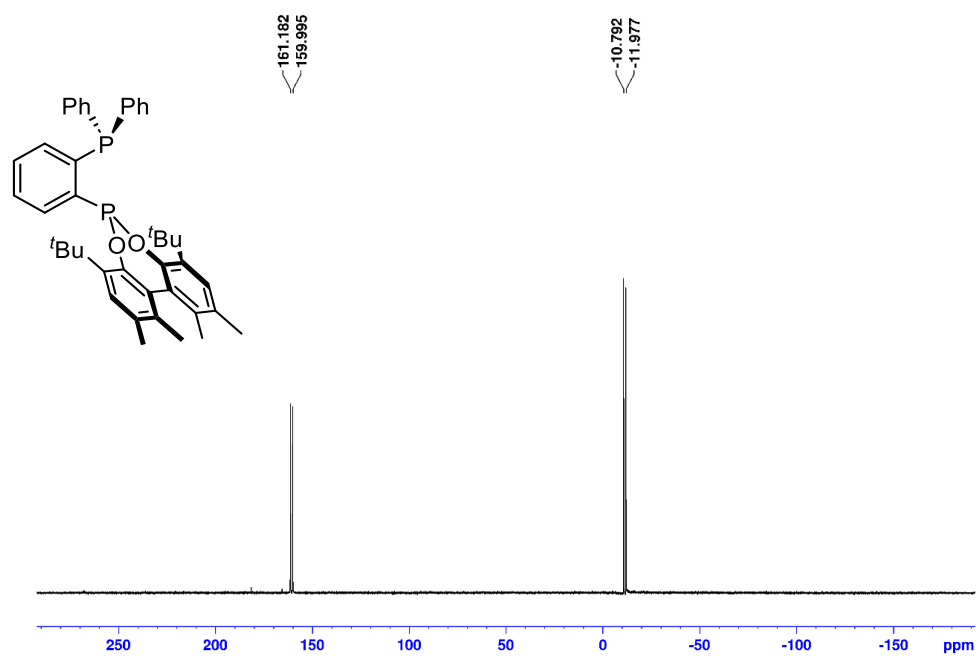


Figure B132. ^1H NMR spectrum of **4-1** in CD_2Cl_2 .

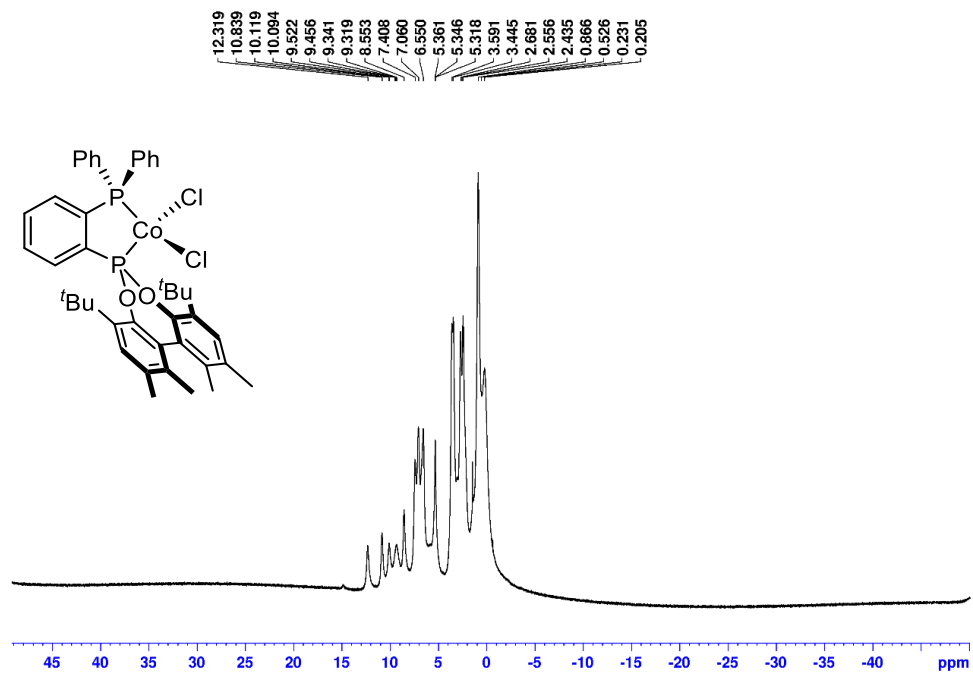


Figure B133. ^1H NMR spectrum of 4-2 in benzene- d_6 .

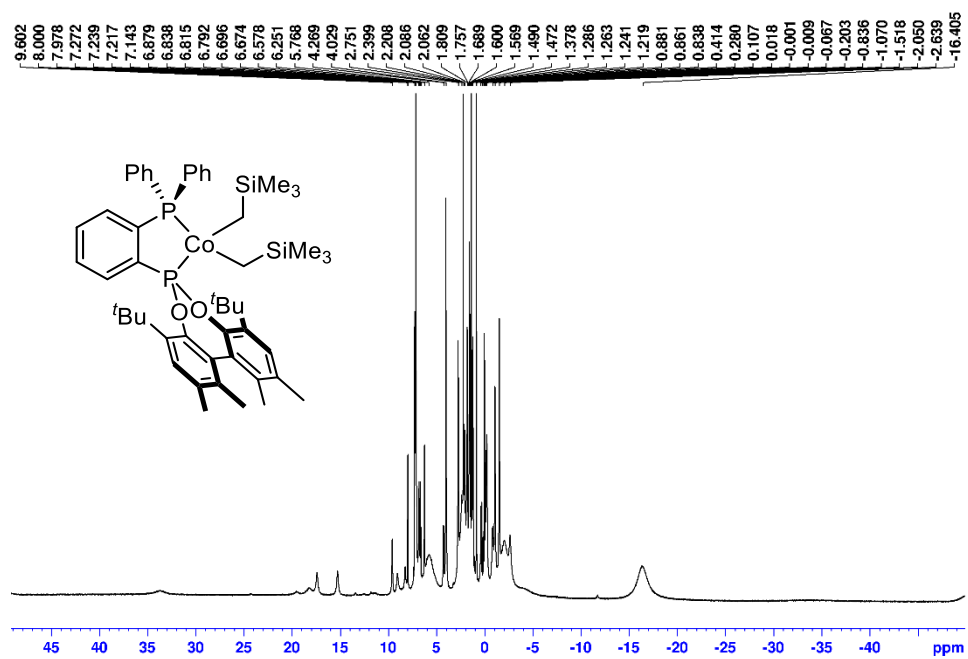


Figure B134. ^1H NMR spectrum of **4-3** in $\text{THF-}d_8$.

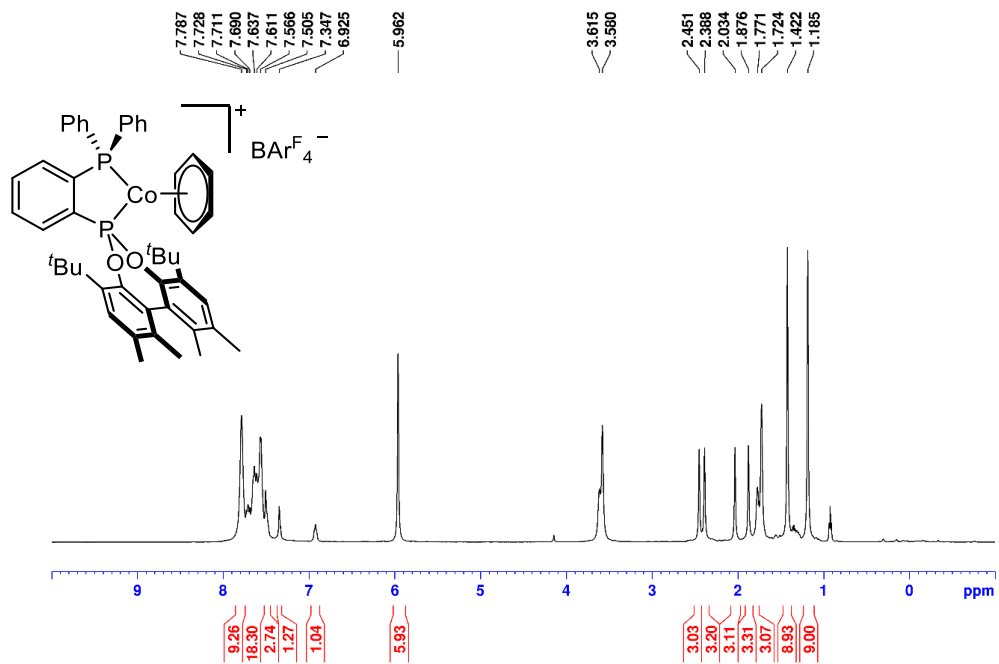


Figure B135. $^{13}\text{C}\{^1\text{H}\}$ NMR spectrum of 4-3 in $\text{THF-}d_8$.

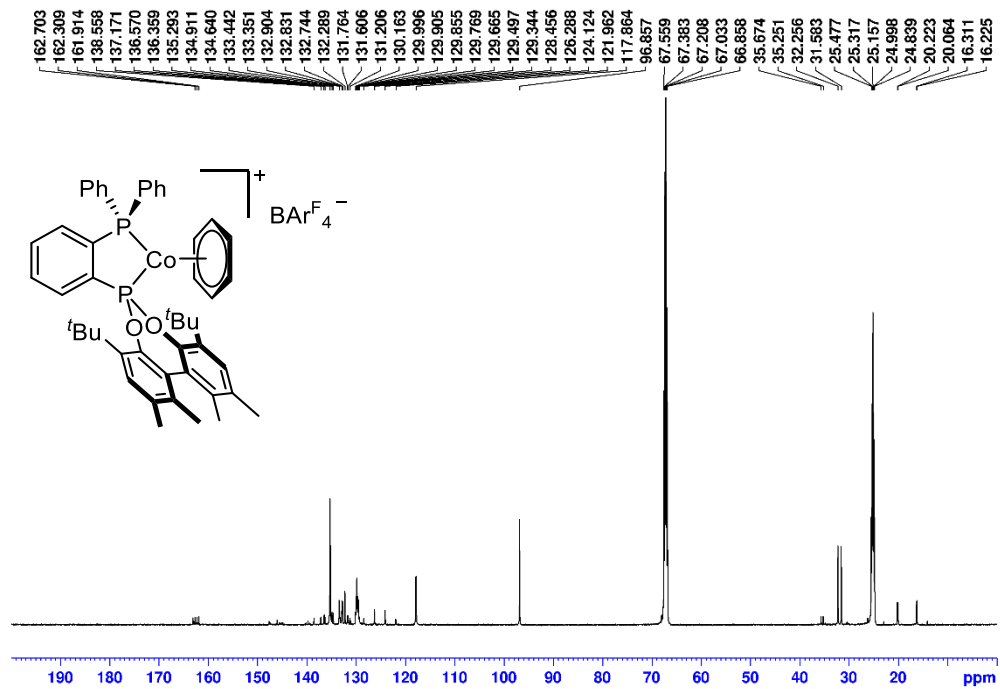


Figure B136. $^{31}\text{P}\{^1\text{H}\}$ NMR spectrum of **4-3** in $\text{THF-}d_8$.

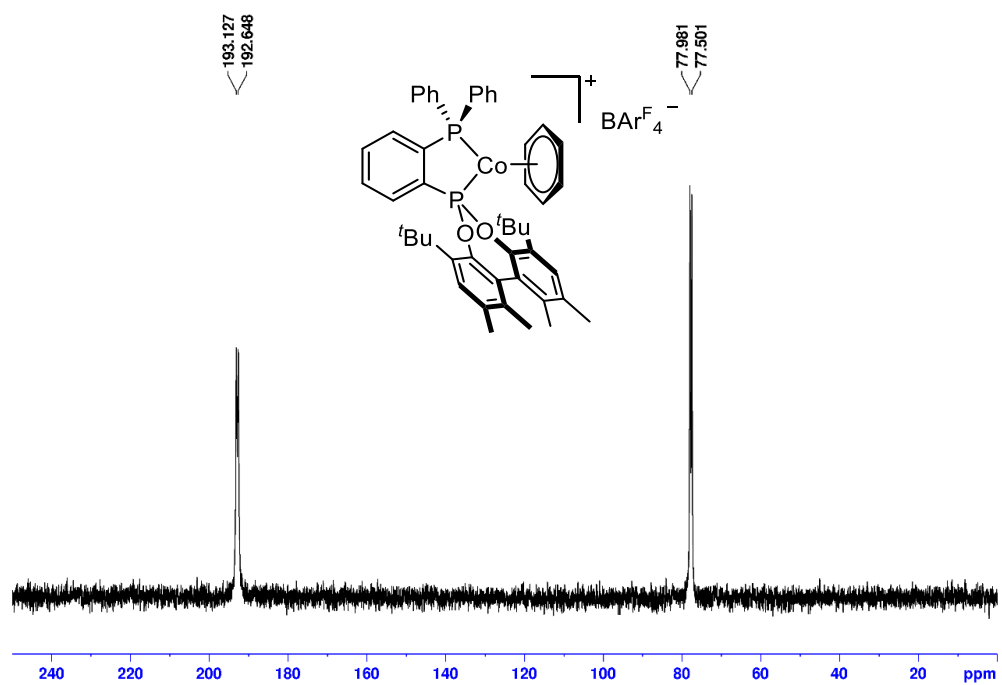


Figure B137. $^{19}\text{F}\{^1\text{H}\}$ NMR spectrum of **4-3** in $\text{THF-}d_8$.

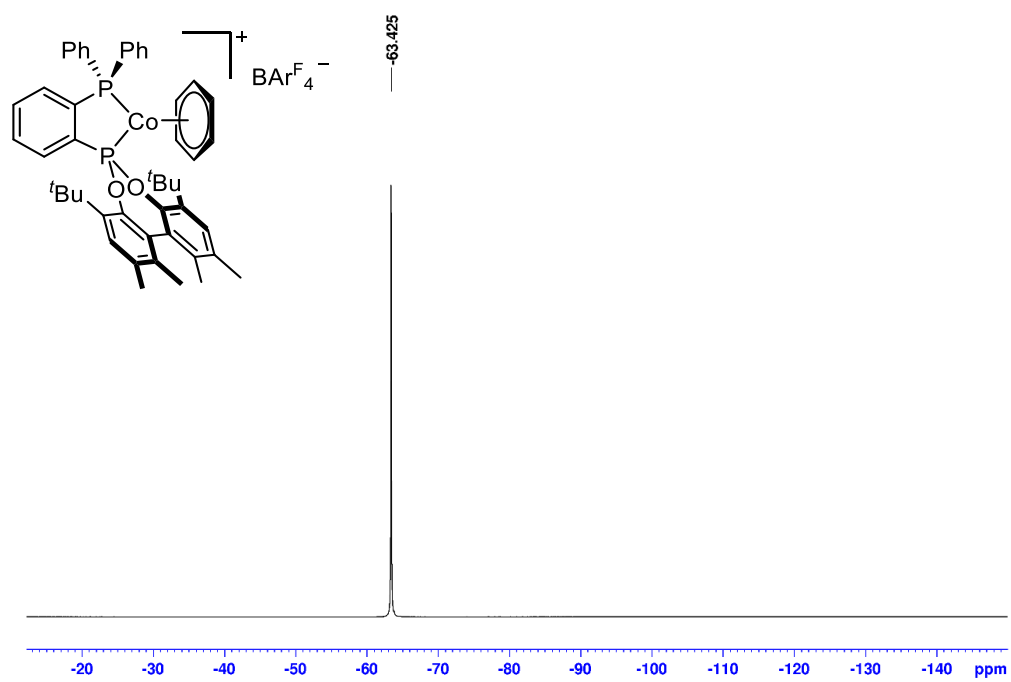
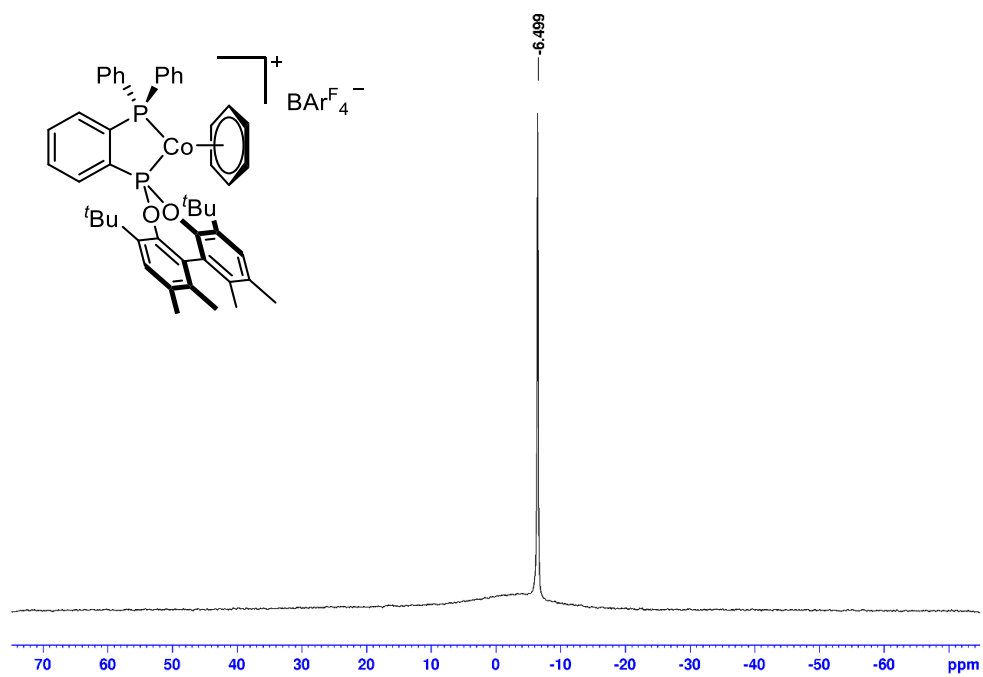
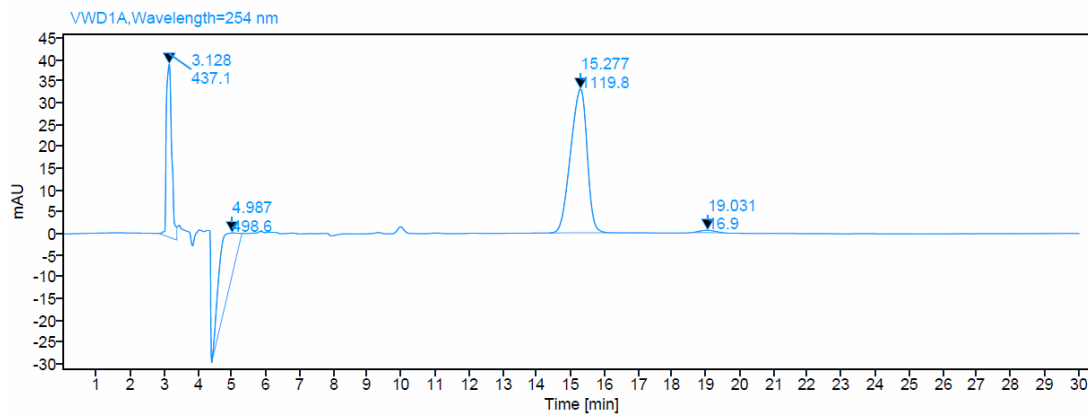
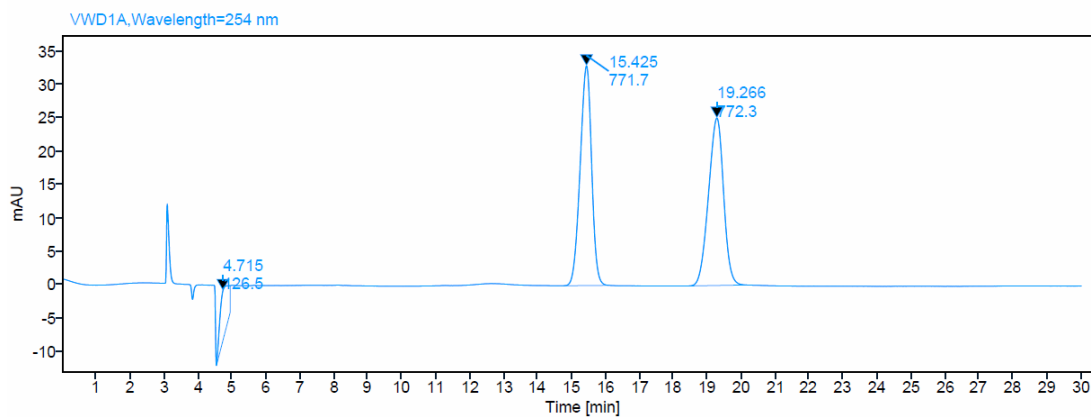
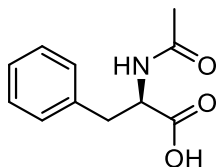


Figure B138. ^{11}B NMR spectrum of **4-3** in $\text{THF-}d_8$.



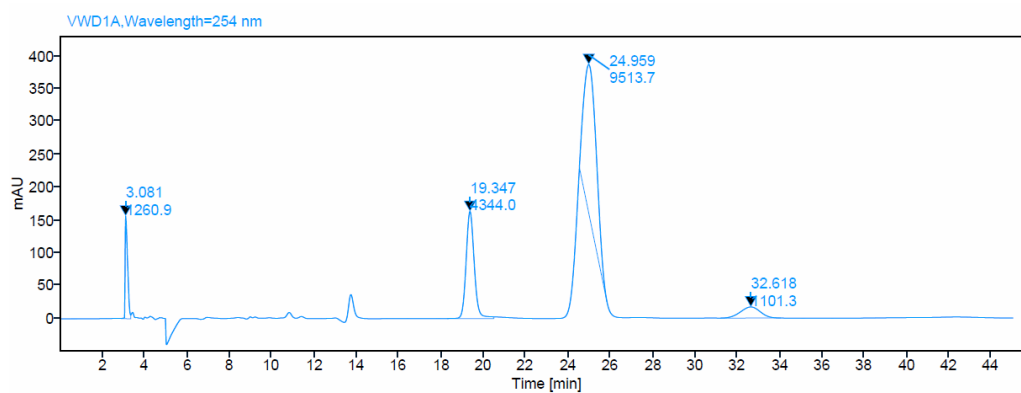
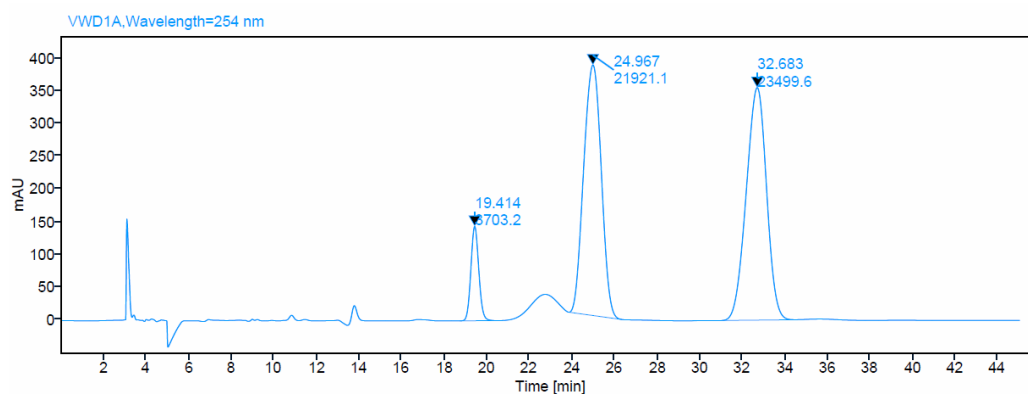
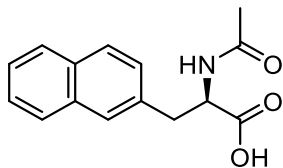
HPLC Chromatograms for Chiral Products Reported in Chapter 4

Figure B139. Chromatograms for 4-1a.



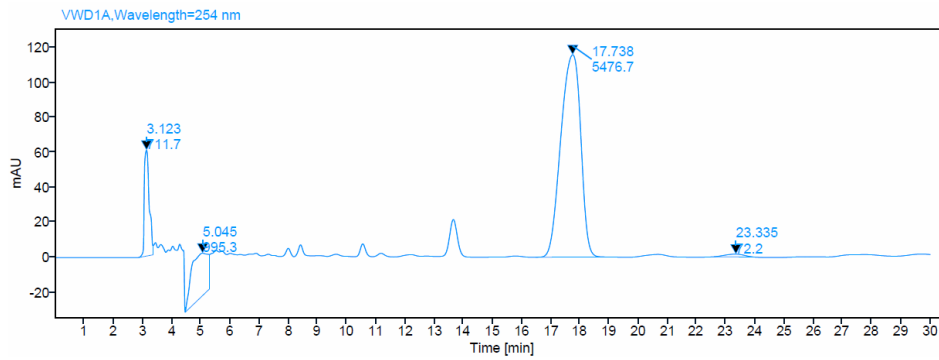
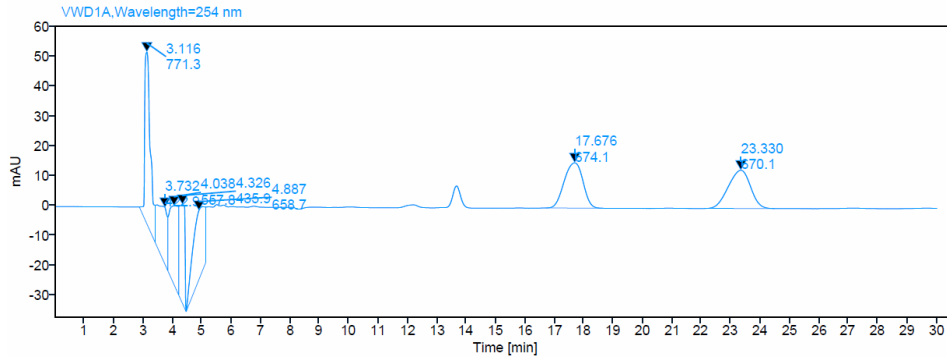
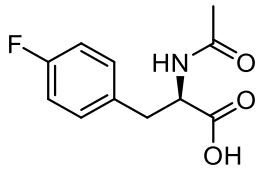
Retention Time	Area	Area%
15.277	1119.8	98.5
19.031	16.9	1.5

Figure B140. Chromatograms for **4-1b**.



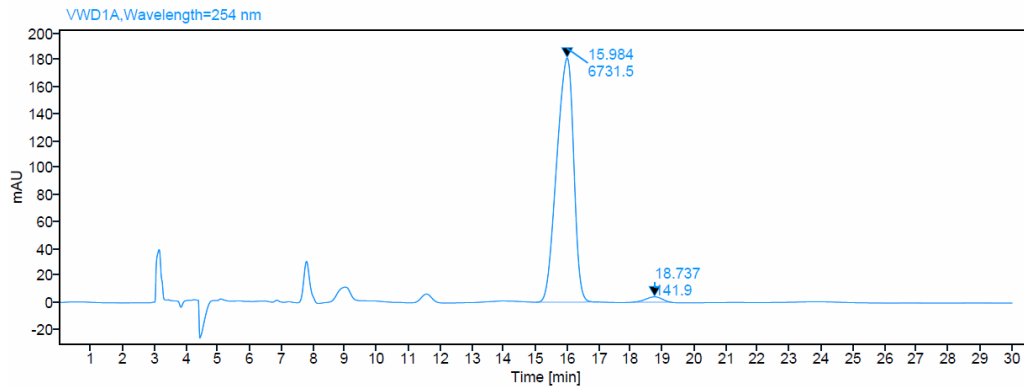
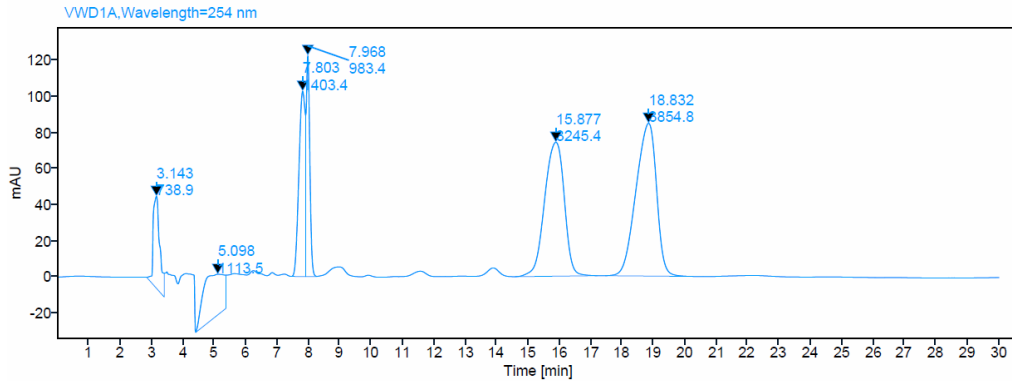
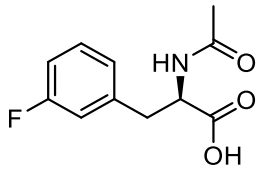
Retention Time	Area	Area%
24.959	9513.7	90.0
32.618	1101.3	10.0

Figure B141. Chromatograms for 4-1c.



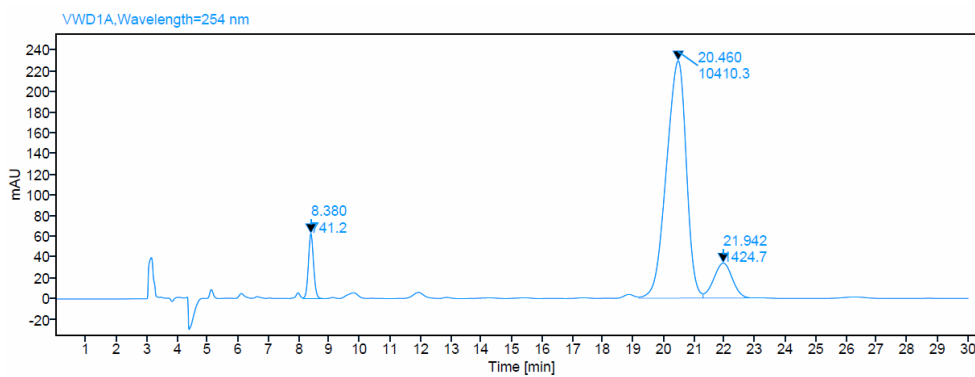
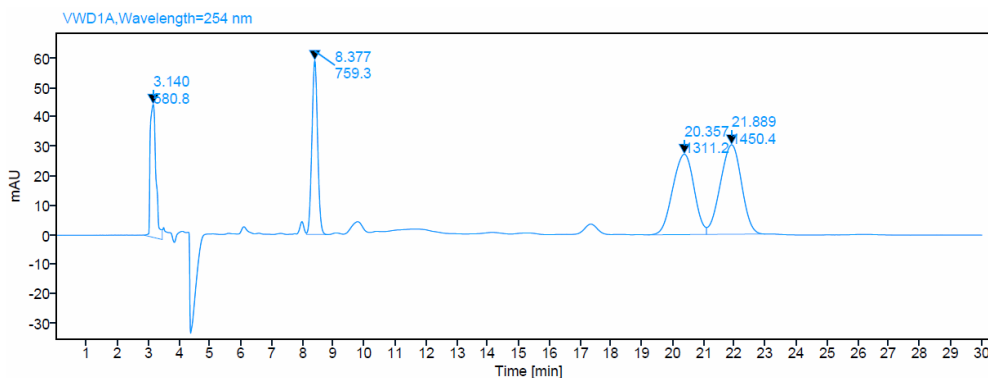
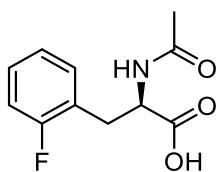
Retention Time	Area	Area%
17.738	5476.7	99.8
23.235	12.2	0.2

Figure B142. Chromatograms for **4-1d**.



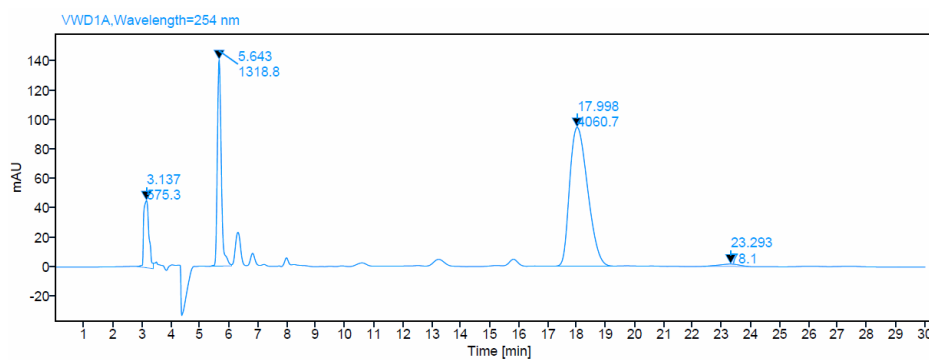
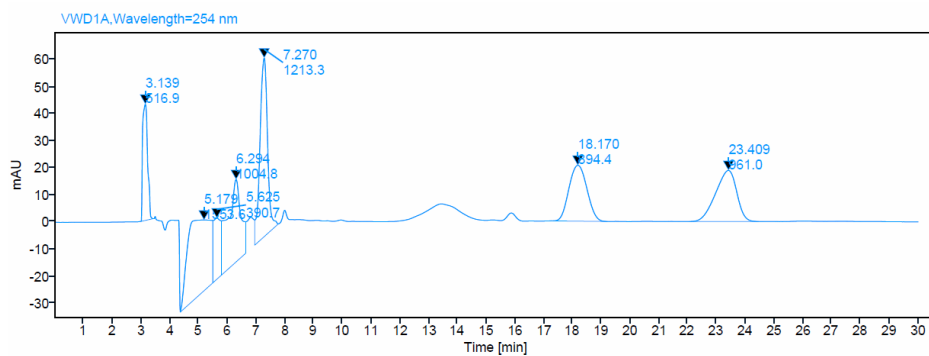
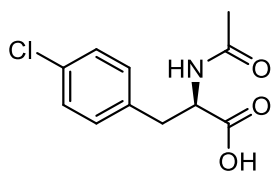
Retention Time	Area	Area%
15.984	6731.5	97.9
18.737	141.9	2.1

Figure B143. Chromatograms for **4-1e**.



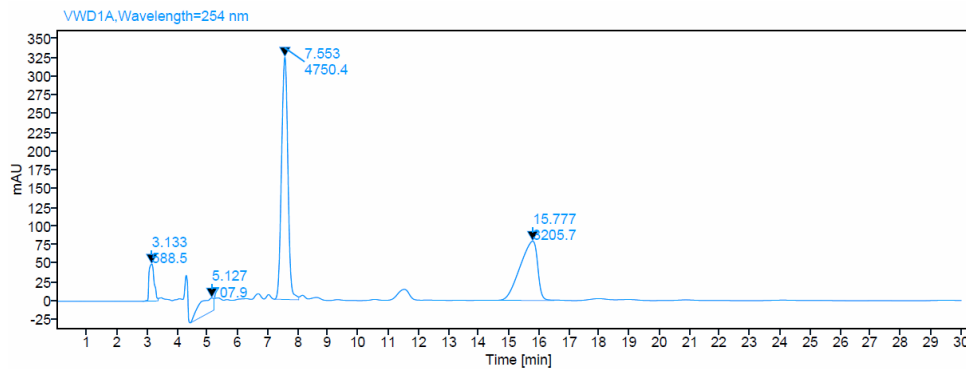
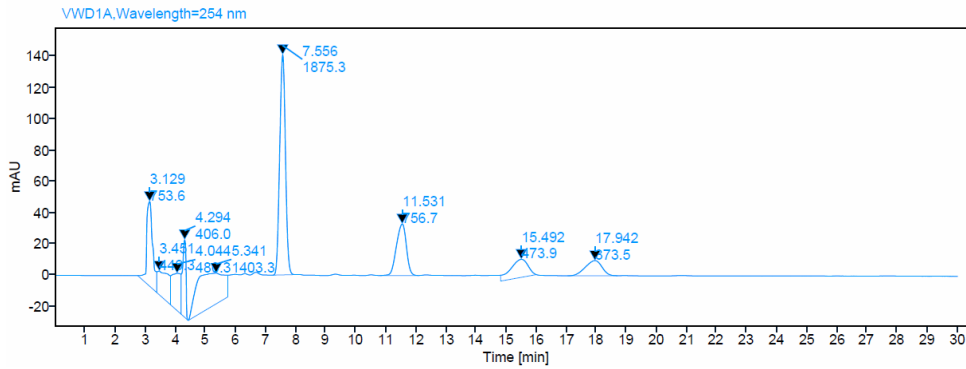
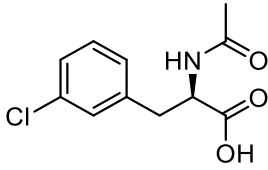
Retention Time	Area	Area%
20.460	10410.3	88.0
21.942	1424.7	12.0

Figure B144. Chromatograms for **4-1f**.



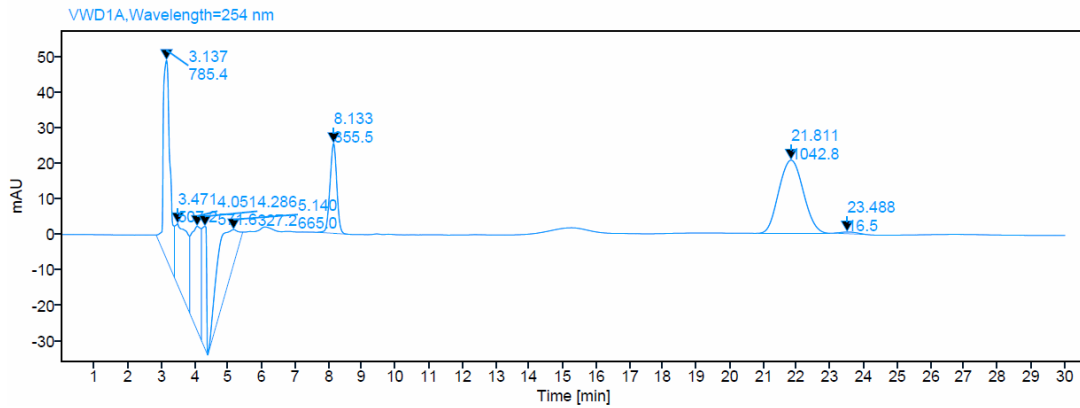
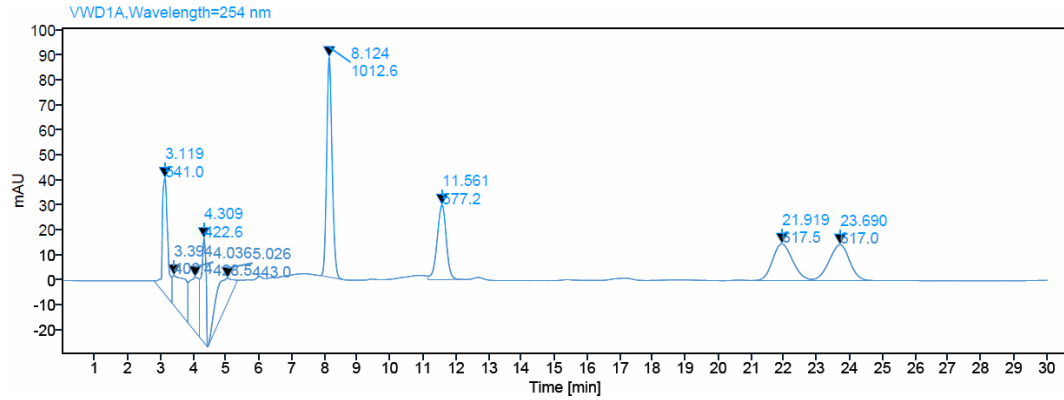
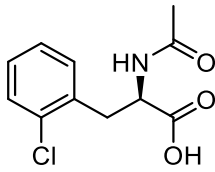
Retention Time	Area	Area%
17.998	4060.7	98.1
23.293	78.1	1.9

Figure B145. Chromatograms for **4-1g**.



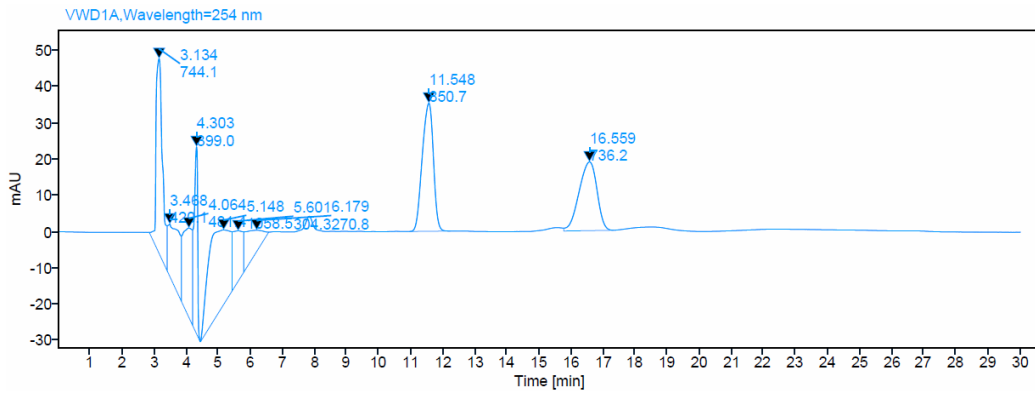
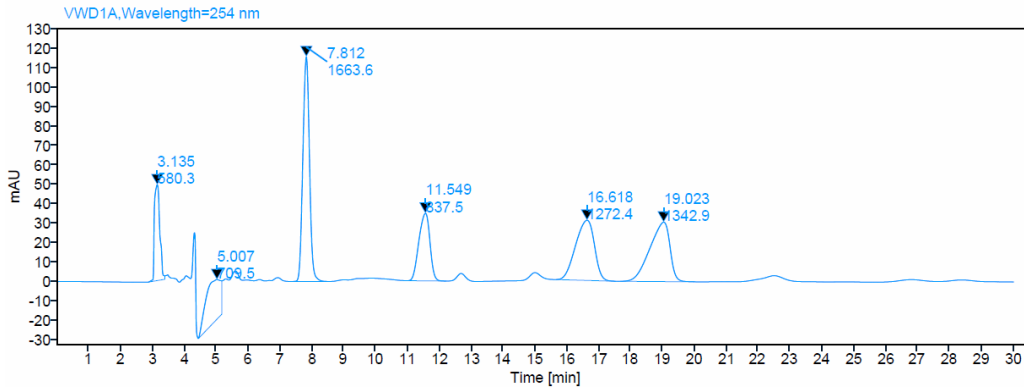
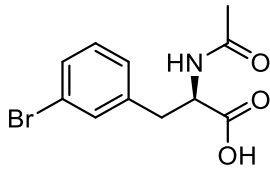
Retention Time	Area	Area%
15.777	3205.7	>99
17.942	None detected	-

Figure B146. Chromatograms for **4-1h**.



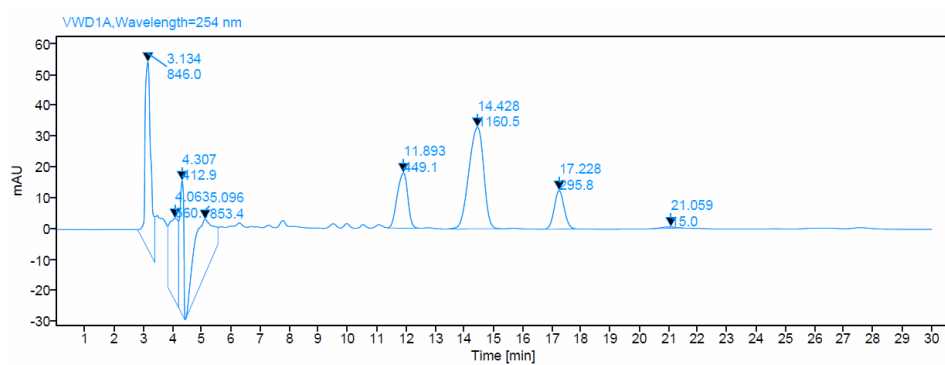
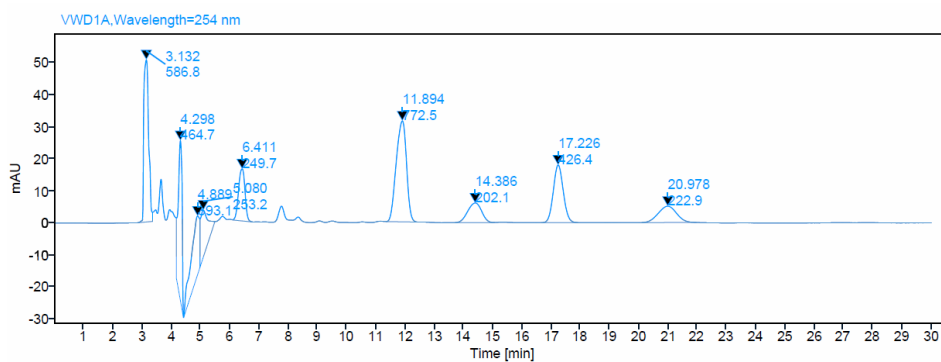
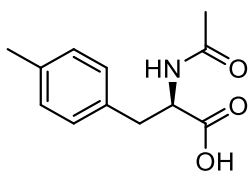
Retention Time	Area	Area%
21.811	1042.8	98.4
23.488	16.5	1.6

Figure B147. Chromatograms for **4-1i**.



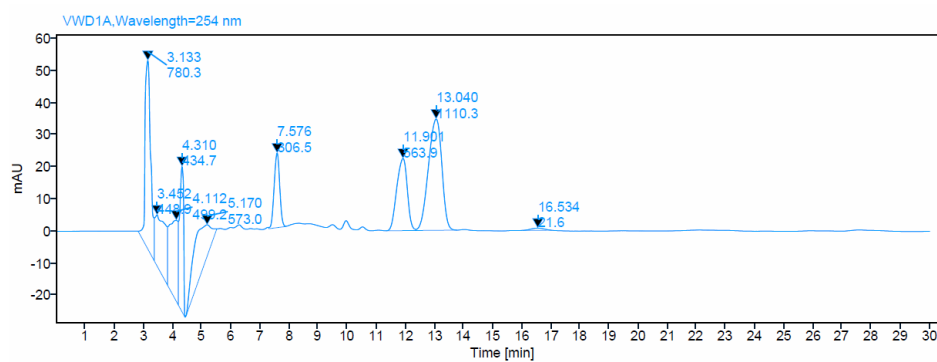
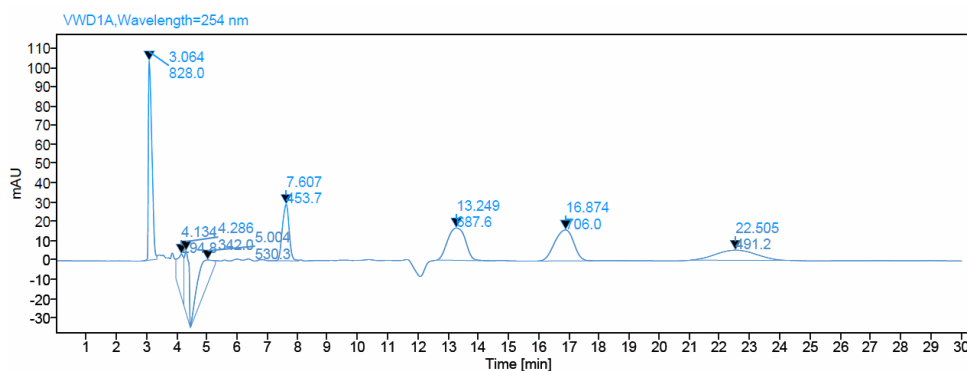
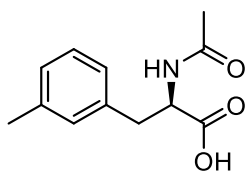
Retention Time	Area	Area%
16.559	3205.7	>99
19.023	None detected	-

Figure B148. Chromatograms for 4-1j.



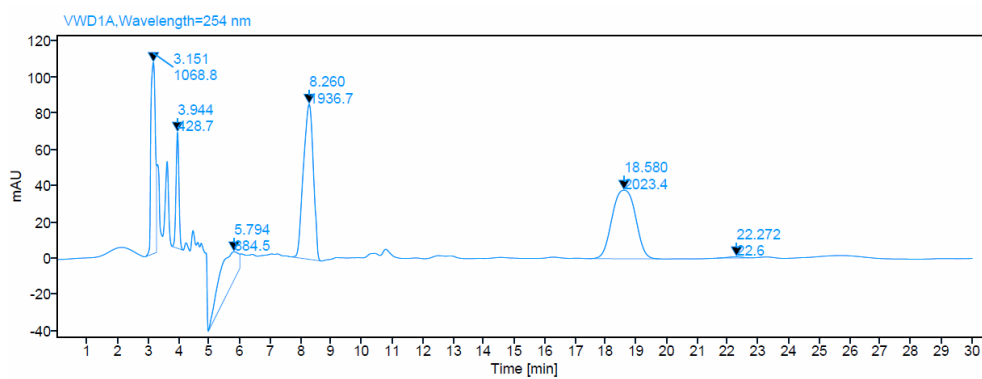
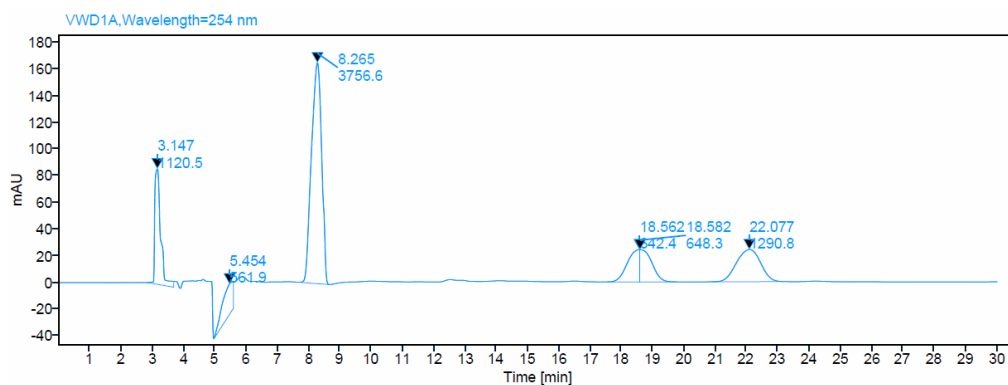
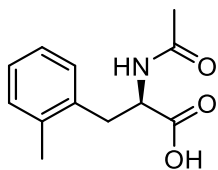
Retention Time	Area	Area%
14.428	1160.5	98.7
21.059	15.0	1.3

Figure B149. Chromatograms for 4-1k.



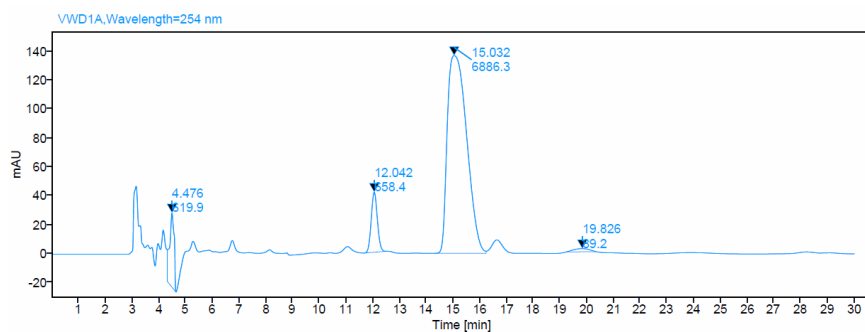
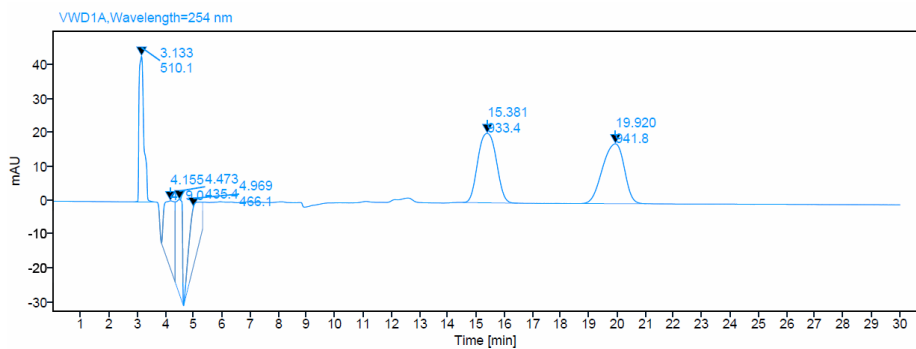
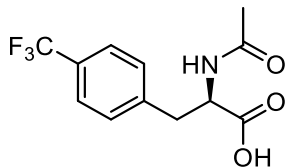
Retention Time	Area	Area%
13.040	1110.3	98.1
16.534	21.6	1.9

Figure B150. Chromatograms for 4-11.



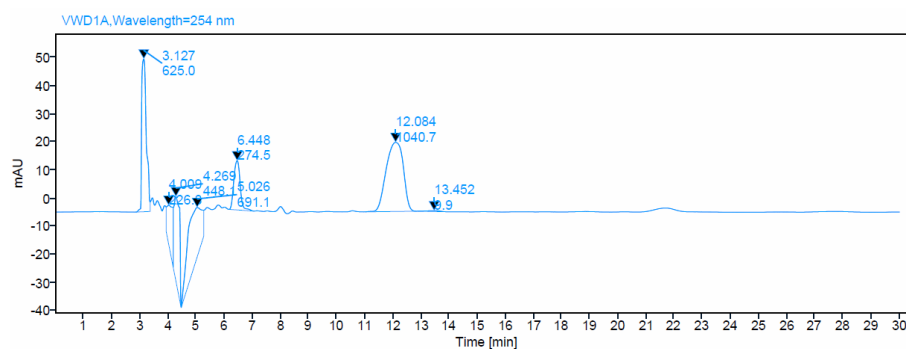
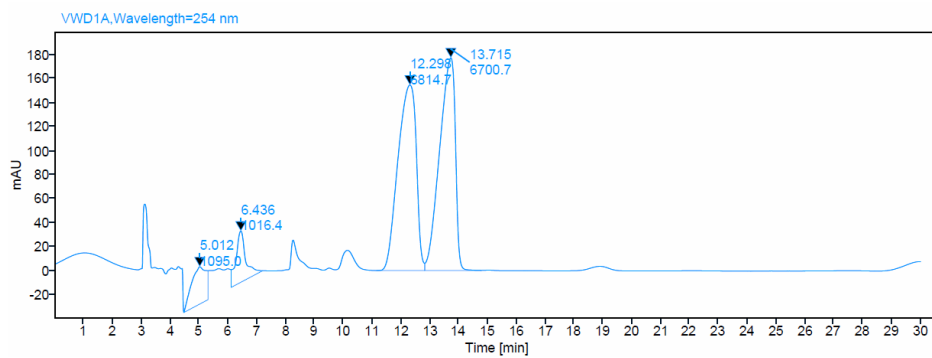
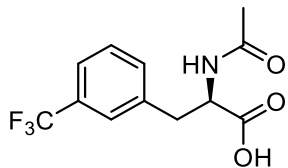
Retention Time	Area	Area%
18.580	2023.4	98.9
22.272	22.6	1.1

Figure B151. Chromatograms for **4-1m**.



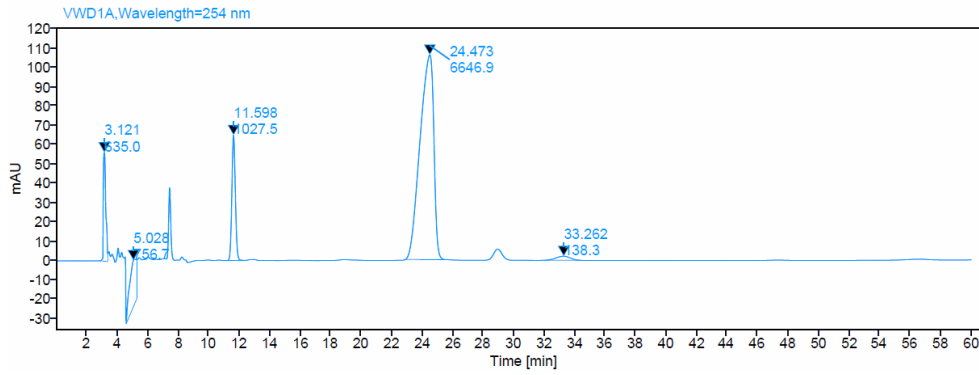
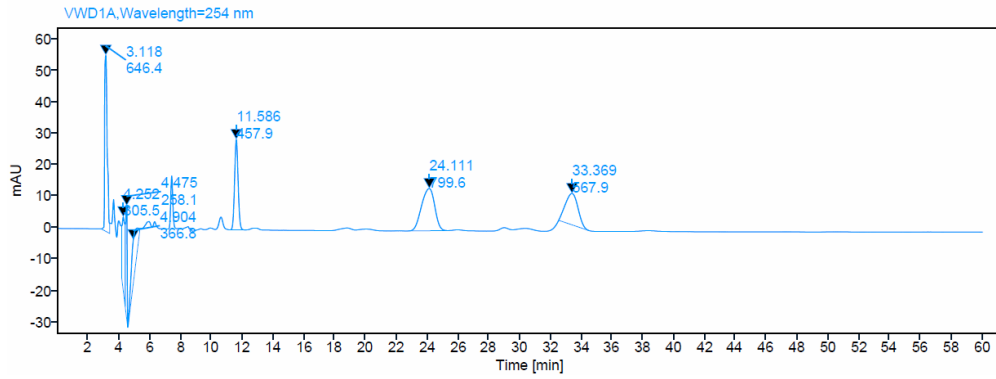
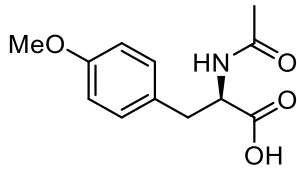
Retention Time	Area	Area%
15.032	2023.4	98.9
19.826	22.6	1.1

Figure B152. Chromatograms for **4-1n**.



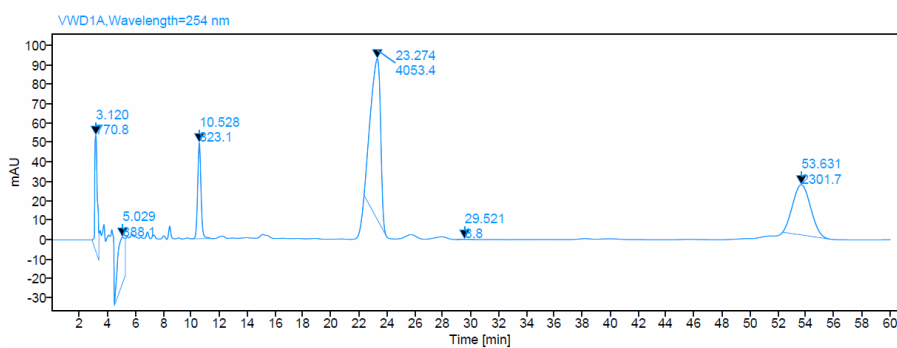
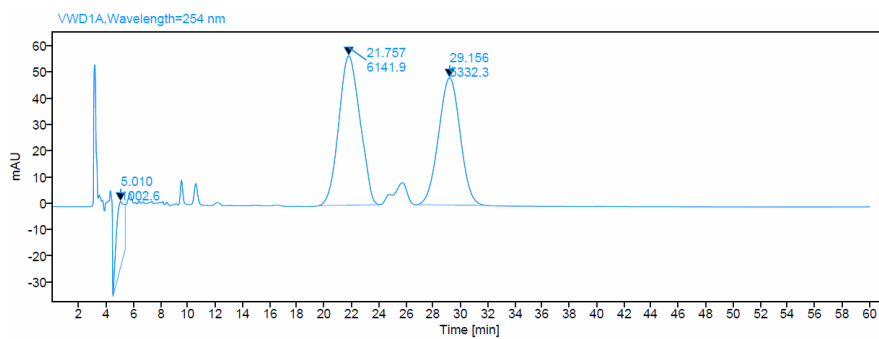
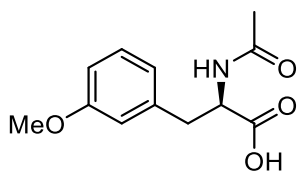
Retention Time	Area	Area%
12.084	1040.7	99.1
13.452	9.9	0.9

Figure B153. Chromatograms for **4-1o**.



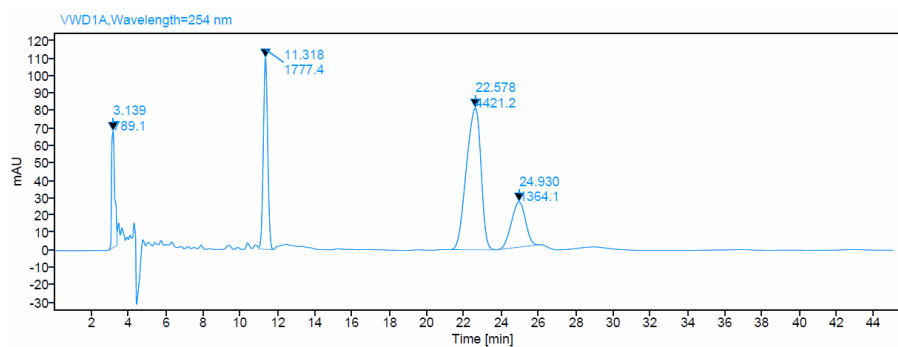
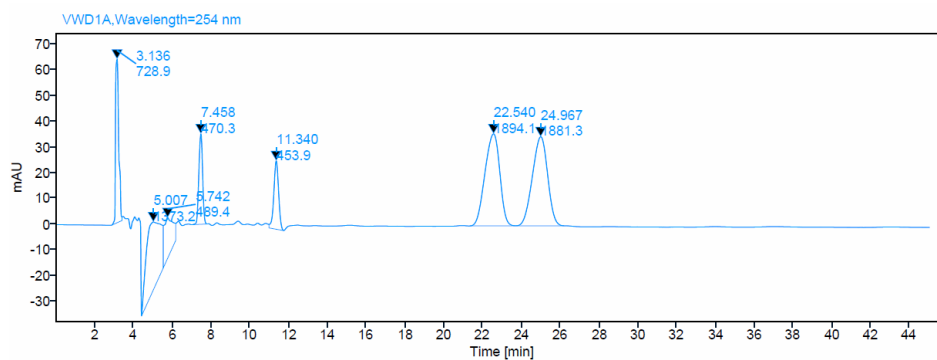
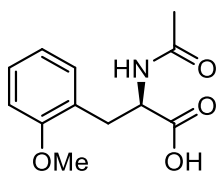
Retention Time	Area	Area%
24.111	6646.9	98.0
33.262	138.3	2.0

Figure B154. Chromatograms for **4-1p**.



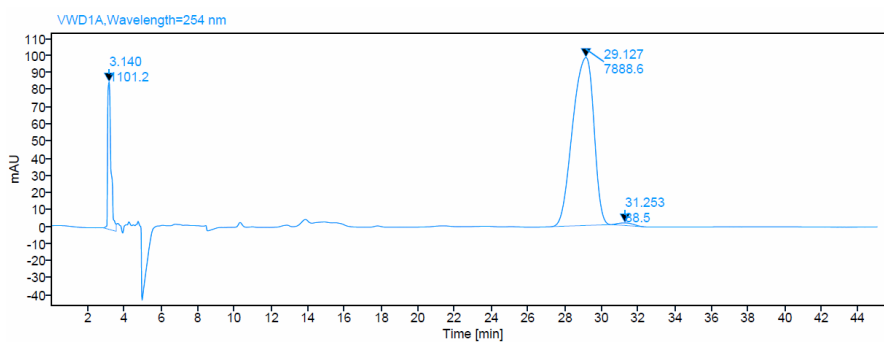
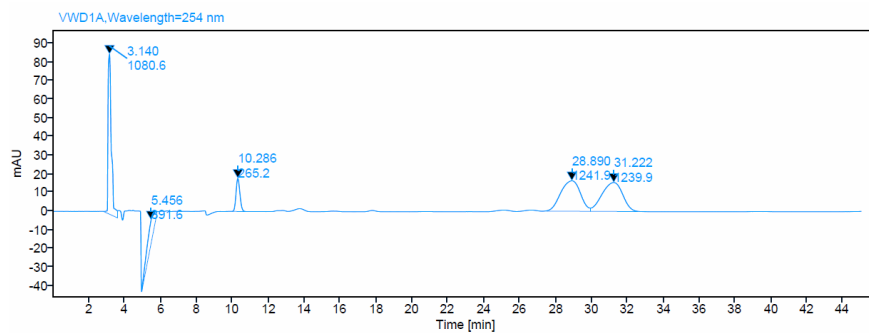
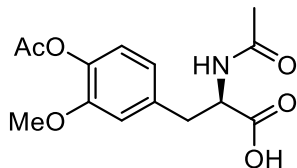
Retention Time	Area	Area%
23.274	4053.4	99.8
29.521	8.8	0.2

Figure B155. Chromatograms for **4-1q**.



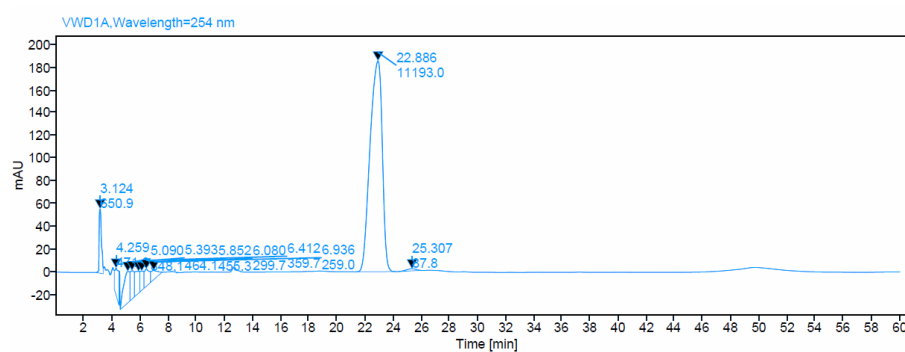
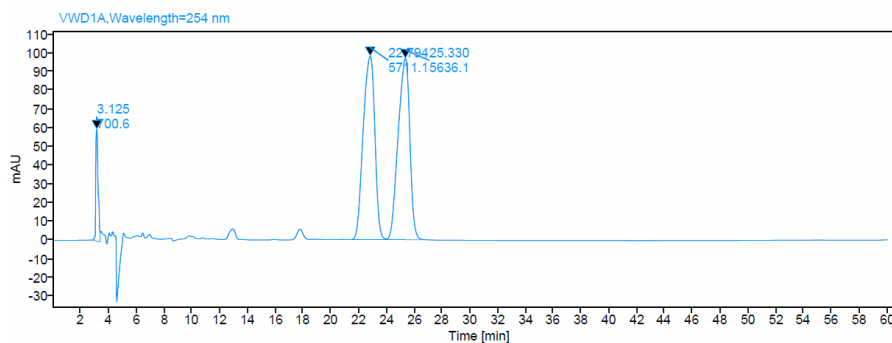
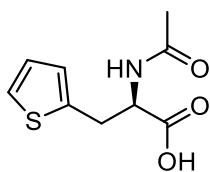
Retention Time	Area	Area%
22.578	4421.2	76.4
24.930	1364.1	23.6

Figure B156. Chromatograms for **4-1r**.



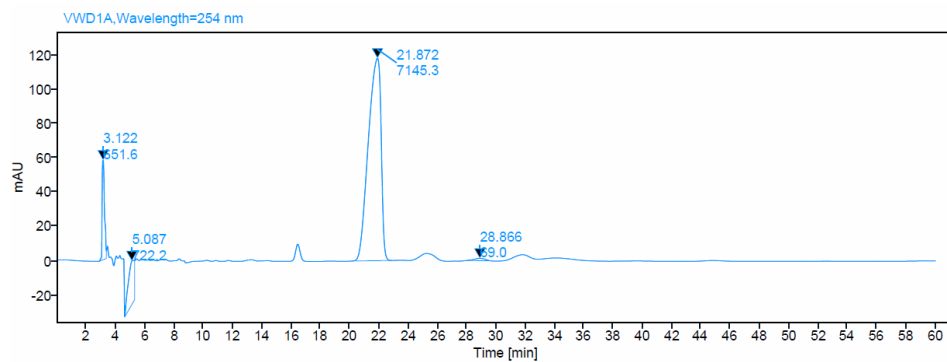
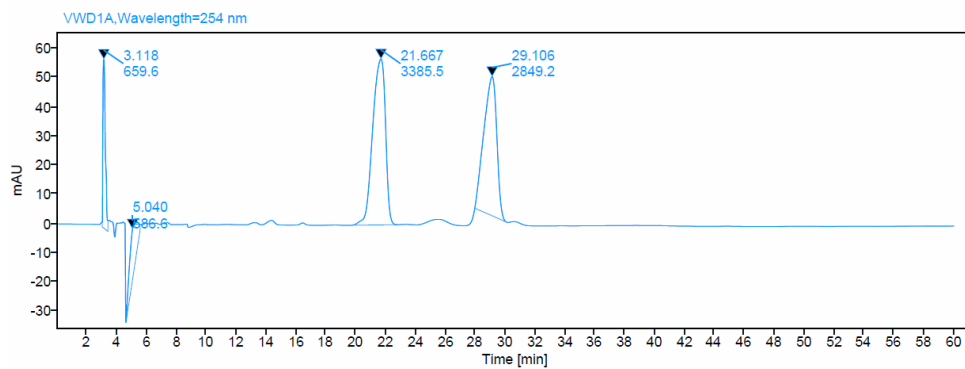
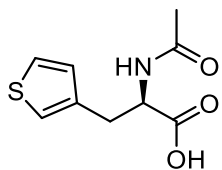
Retention Time	Area	Area%
29.127	7888.6	98.9
31.253	88.5	1.1

Figure B157. Chromatograms for **4-1s**.



Retention Time	Area	Area%
22.886	11193.0	99.2
25.307	87.8	0.8

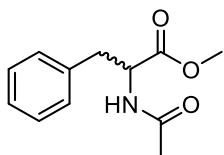
Figure B158. Chromatograms for 4-1r.



Retention Time	Area	Area%
21.872	7145.3	99.0
28.866	69.0	1.0

Selected NMR Spectra and HPLC Chromatograms for Compounds Reported in

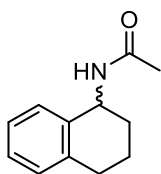
Chapter 5



***N*-acetyl-phenylalanine methyl ester.** ^1H NMR (400 MHz,

CDCl_3): Enantioselectivity was determined by chiral HPLC analysis on a Chiralpak AD-H column with a 90: 10 Hexane: $^i\text{PrOH}$ mobile phase at a 0.9 mL/min flow rate. $t_{\text{major}} = 11.721$ min, $t_{\text{min}} = 15.247$ min.

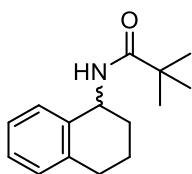
Enantiomer ratio = 94:6.



***N*-(1,2,3,4-tetrahydro-1-naphthalen)acetamide.** ^1H NMR (500 MHz,

CDCl_3): Enantioselectivity was determined by chiral HPLC analysis on a Chiralpak AD-H column with a 90: 10 Hexane: $^i\text{PrOH}$ mobile phase at a 0.9 mL/min flow rate. $t_{\text{major}} = 8.134$ min, $t_{\text{min}} = 10.544$ min. Enantiomer ratio =

60:40.



***N*-(1,2,3,4-tetrahydro-1-naphthalen)-*tert*-butylamide.** ^1H NMR

(500 MHz, CDCl_3): 7.22 – 7.09 (overlapping resonances, 4 H, H_{arom}), 5.80

– 5.78 (br m, 1 H, NH), 5.20 – 5.13 (m, 1 H, CH), 2.88 – 2.71 (m, 2 H,

CH_2), 2.10 – 2.01 (m, 1 H, CH_2), 1.87 – 1.70 (overlapping resonances, 3 H), 1.22 (s, 9 H,

tBu). Enantioselectivity was determined by chiral HPLC analysis on a Chiralpak AD-H column with a 98: 2 Hexane: $^i\text{PrOH}$ mobile phase at a 0.9 mL/min flow rate. $t_{\text{major}} = 10.835$ min, $t_{\text{min}} = 9.128$ min. Enantiomer ratio = 97:3.

Figure B159. ^1H NMR spectrum of *N*-acetyl-phenylalanine methyl ester in CDCl_3 .

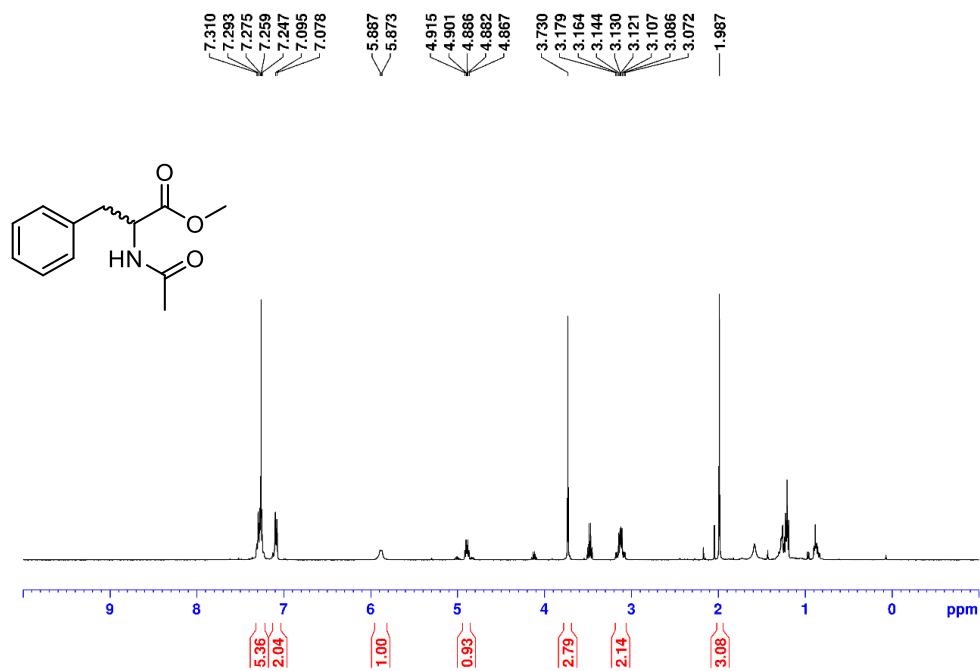


Figure B160. ^1H NMR spectrum of *N*-(1,2,3,4-tetrahydro-1-naphthalen)acetamide in CDCl_3 .

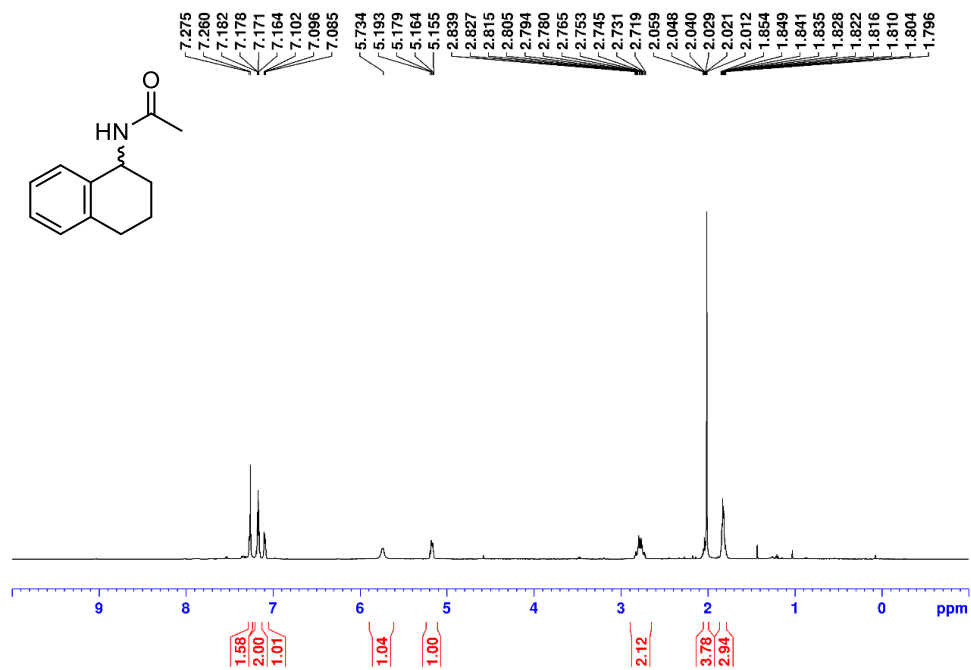


Figure B161. ^1H NMR spectrum of *N*-(1,2,3,4-tetrahydro-1-naphthalen)-*tert*-butylamide in CDCl_3

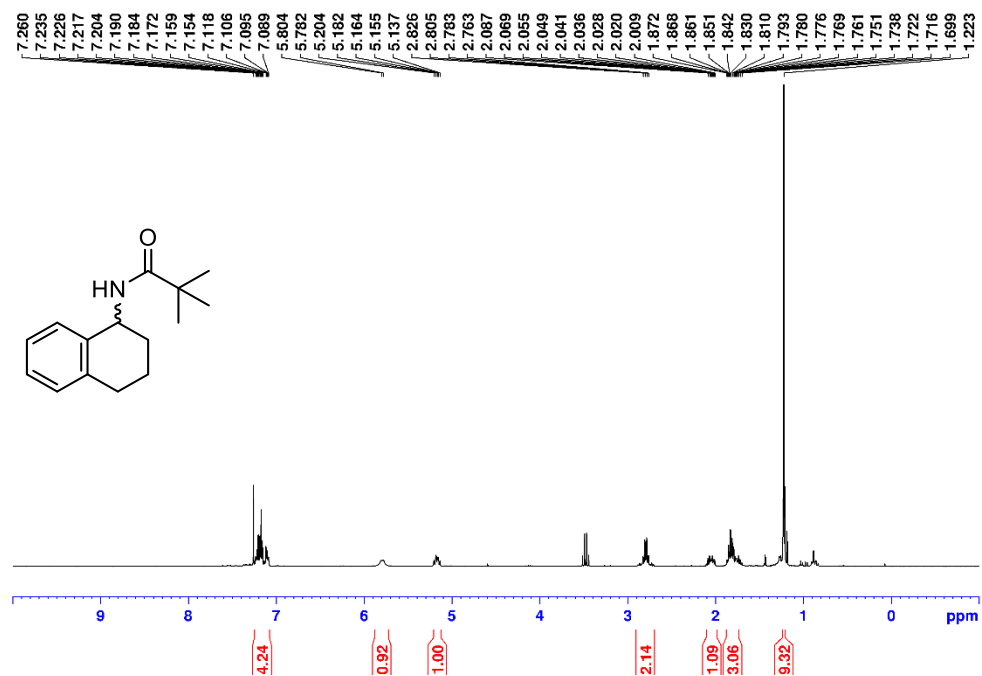


Figure B162. ^1H NMR spectrum of **5-1** in C_6D_6 .

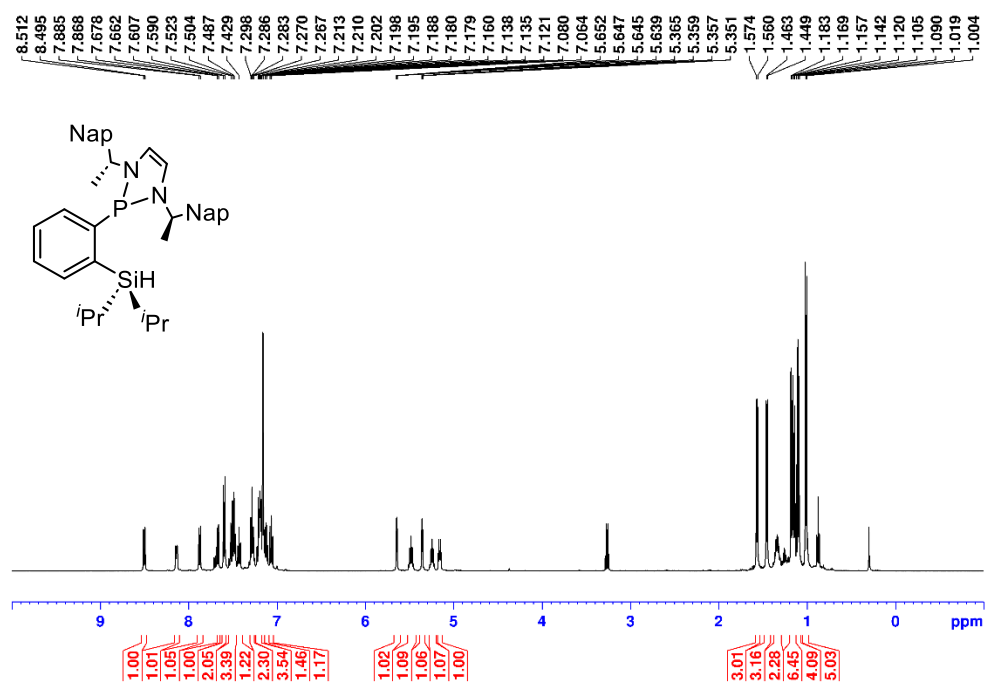


Figure B163. ^1H NMR spectrum of **5-1** in C_6D_6 (aromatic region).

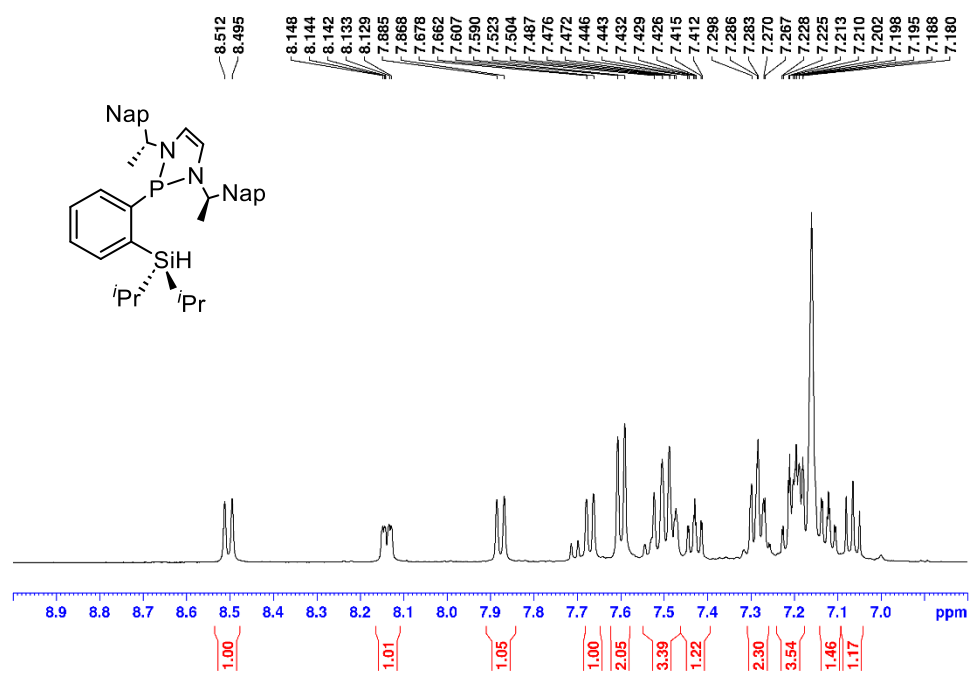


Figure B164. ^1H NMR spectrum of **5-1** in C_6D_6 (alkene region).

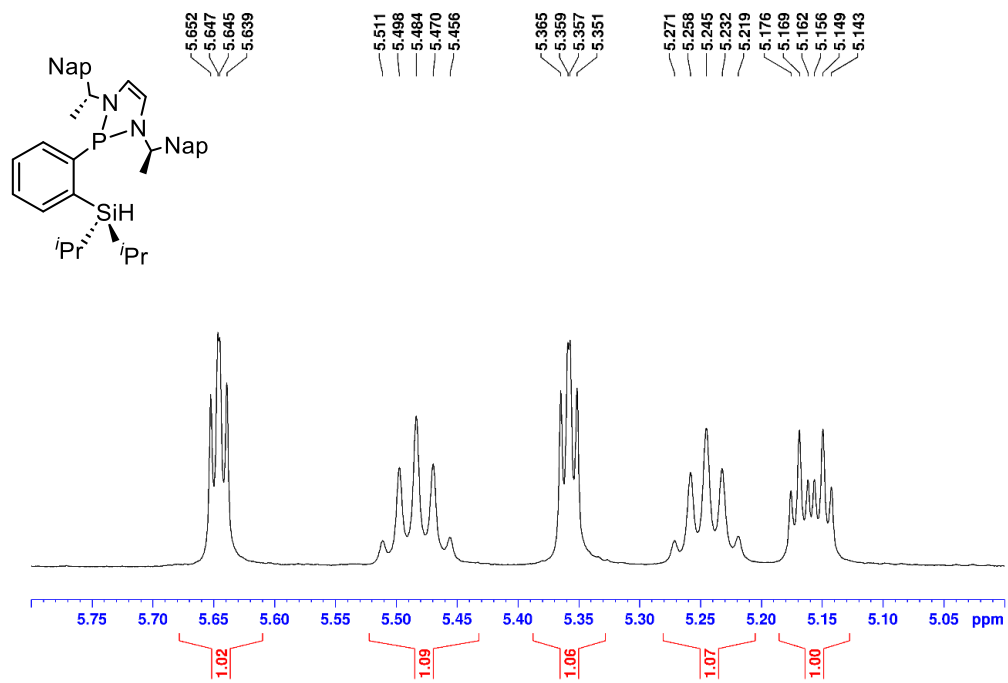


Figure B165. ^1H NMR spectrum of **5-1** in C_6D_6 (aliphatic region).

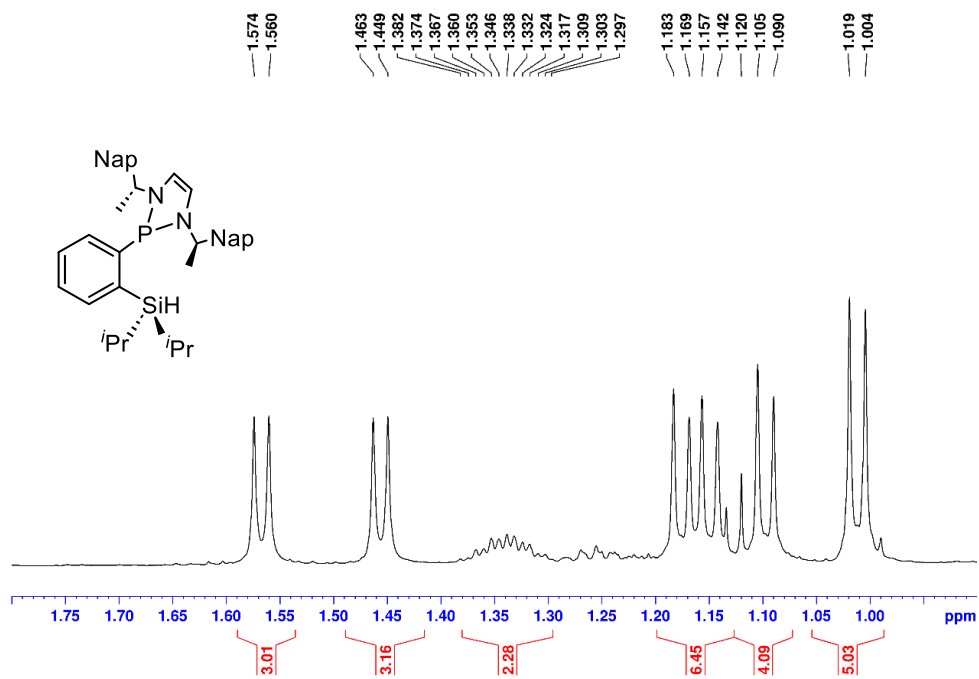


Figure B166. $^{31}\text{P}\{^1\text{H}\}$ NMR spectrum of **5-1** in C_6D_6 .

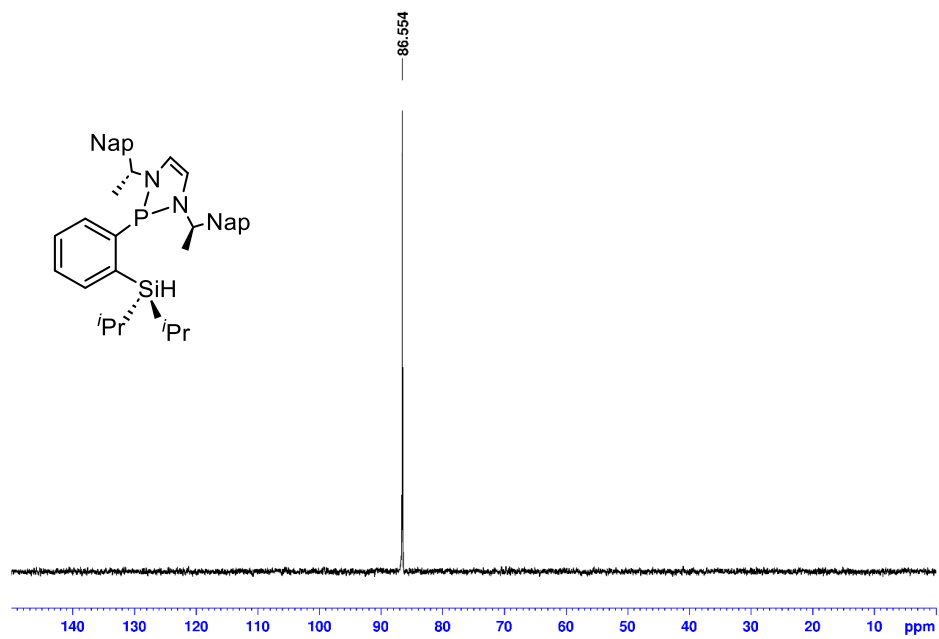


Figure B167. $^{13}\text{C}\{^1\text{H}\}$ NMR spectrum of **5-1** in C_6D_6 .

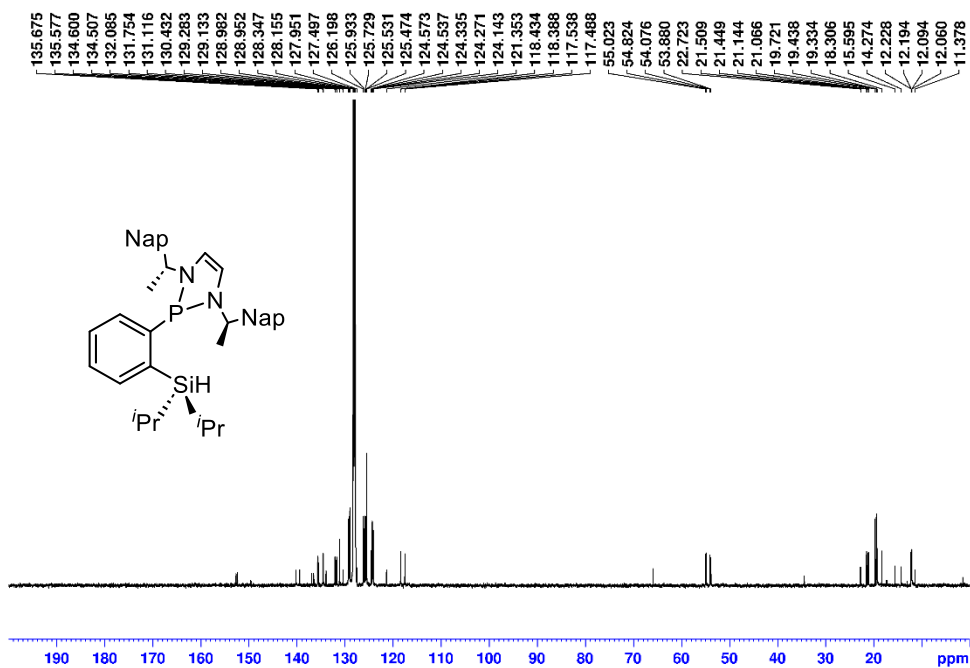


Figure B168. $^{13}\text{C}\{^1\text{H}\}$ NMR spectrum of **5-1** in C_6D_6 (aromatic region).

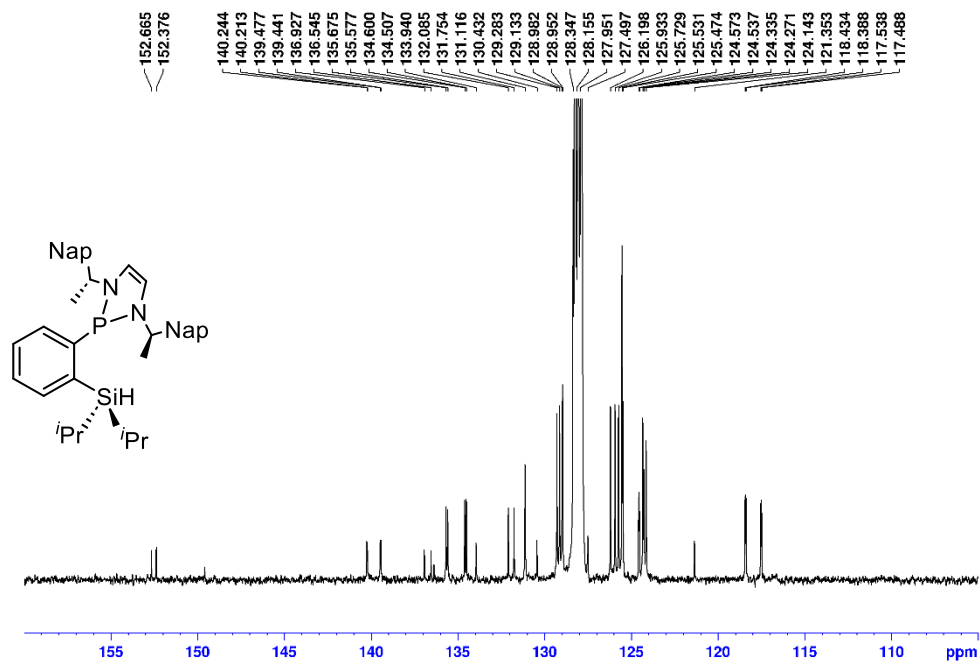


Figure B169. $^{13}\text{C}\{^1\text{H}\}$ NMR spectrum of **5-1** in C_6D_6 (aliphatic region).

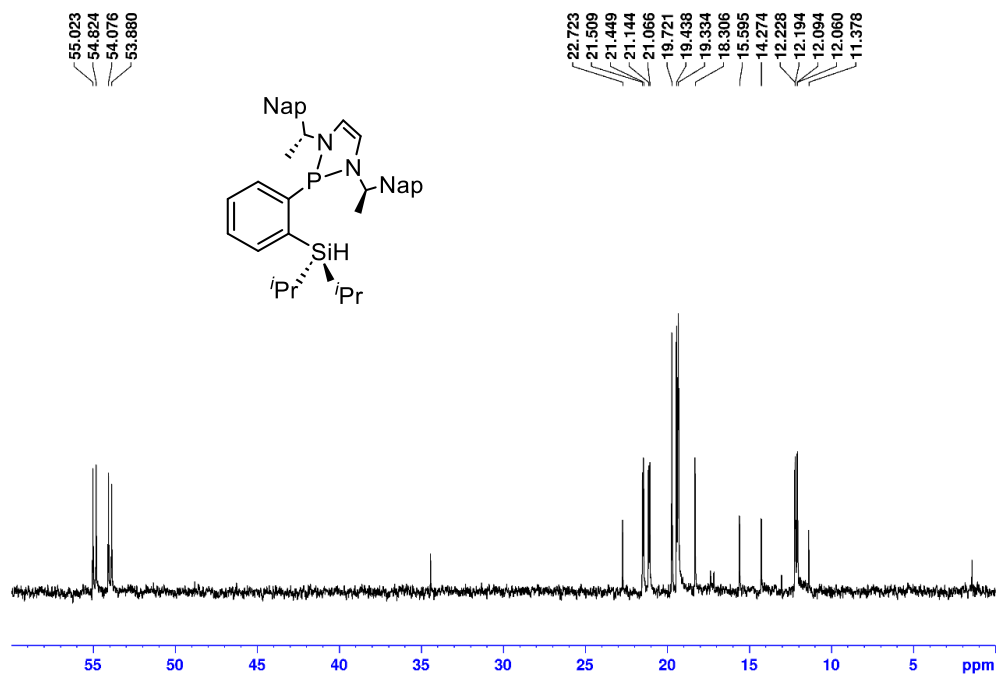


Figure B170. ^1H NMR spectrum of (*R,R*)-(TADDOL)SiHCl in C_6D_6 .

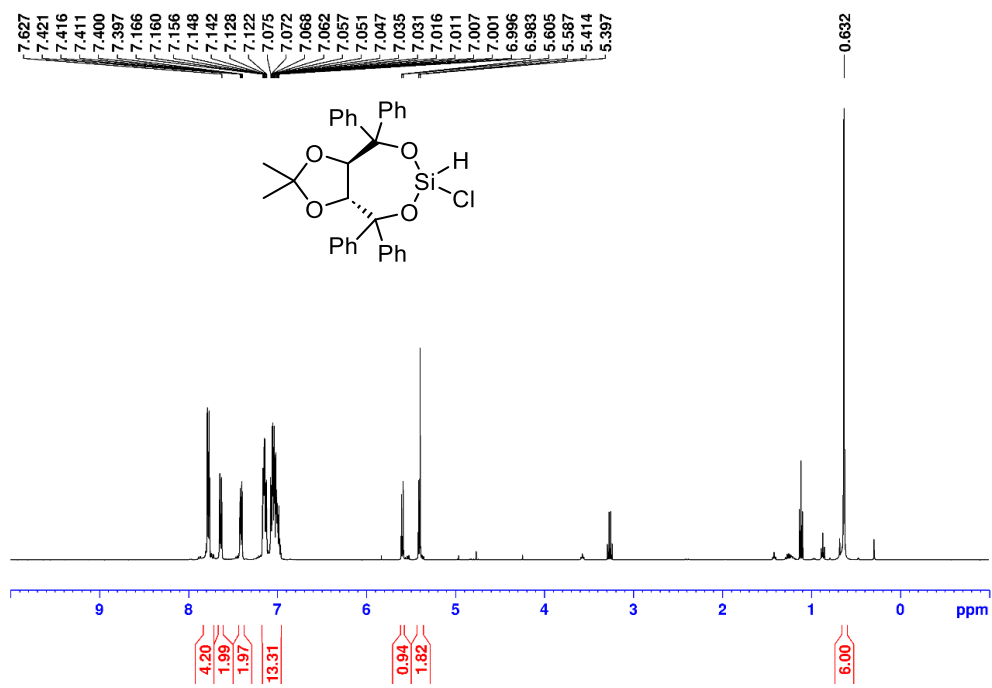


Figure B171. $^{13}\text{C}\{^1\text{H}\}$ NMR spectrum of (*R,R*)-(TADDOL)SiHCl in C_6D_6 .

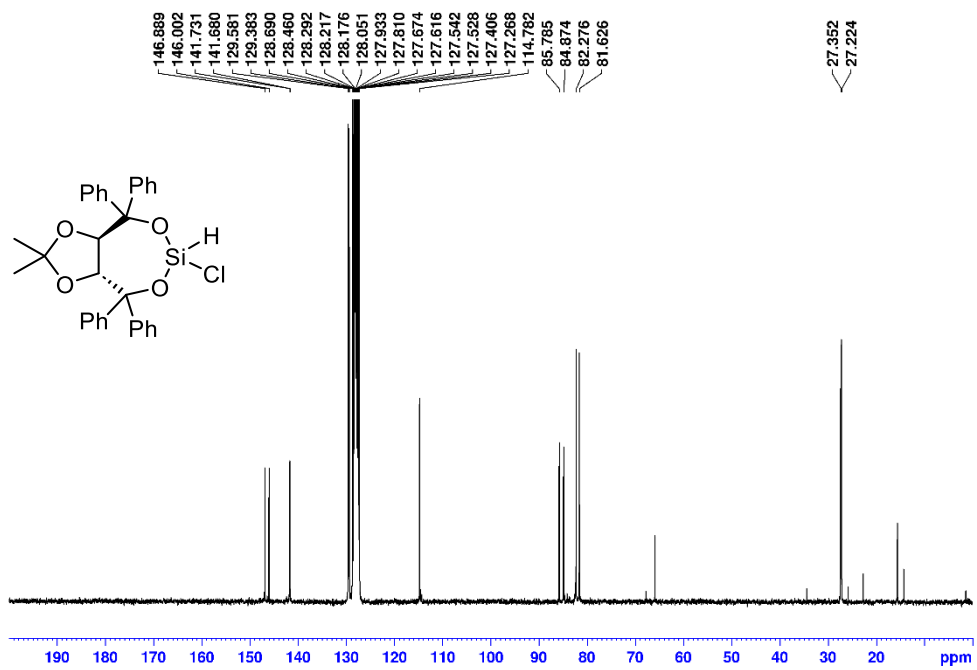


Figure B172. ^1H NMR spectrum of **5-3** in C_6D_6 .

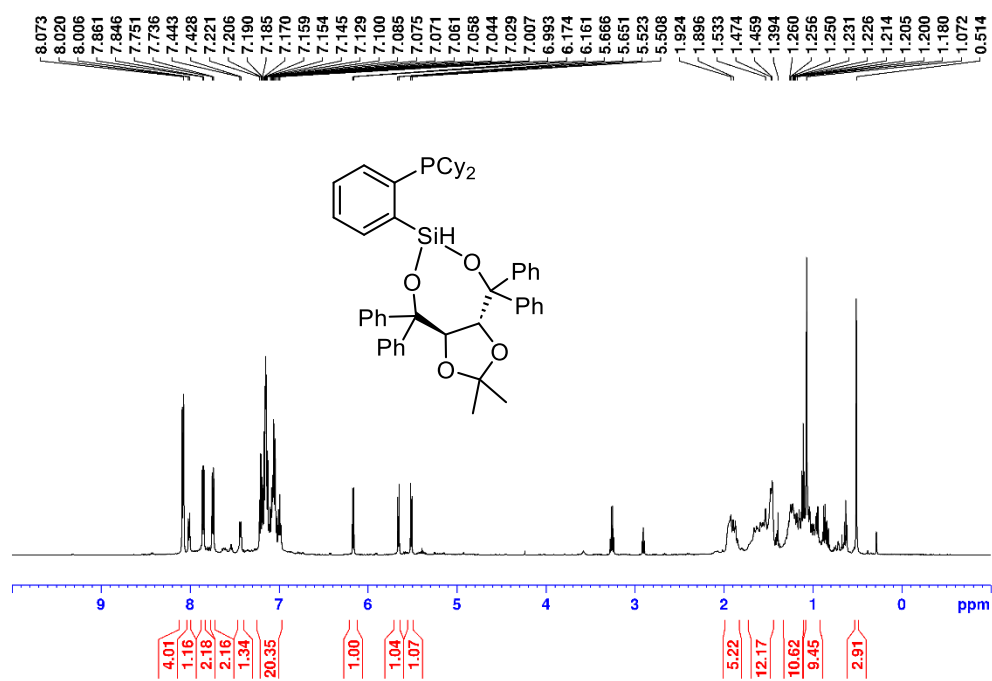


Figure B173. $^{31}\text{P}\{^1\text{H}\}$ NMR spectrum of **5-3** in C_6D_6 .

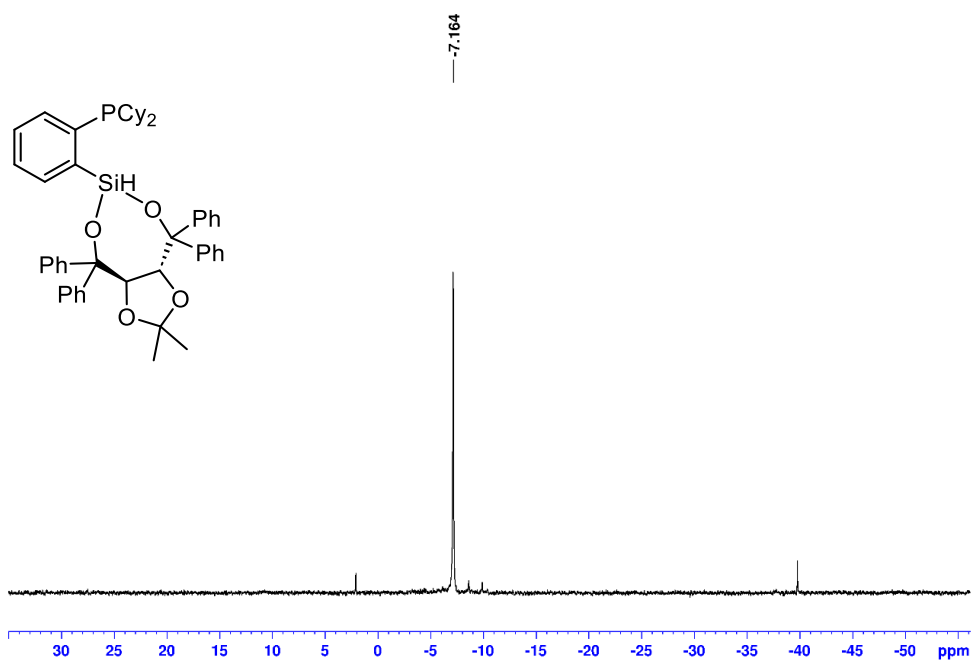


Figure B174. ^1H NMR spectrum of **5-4** in C_6D_6 .

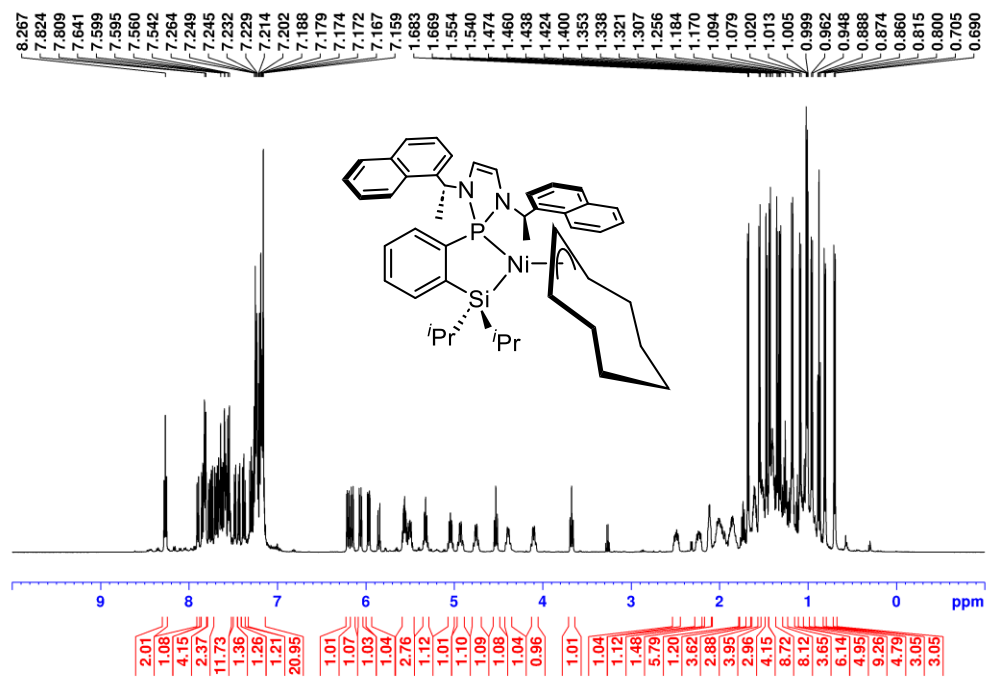


Figure B175. ^1H NMR spectrum of **5-4** in C_6D_6 (aromatic region).

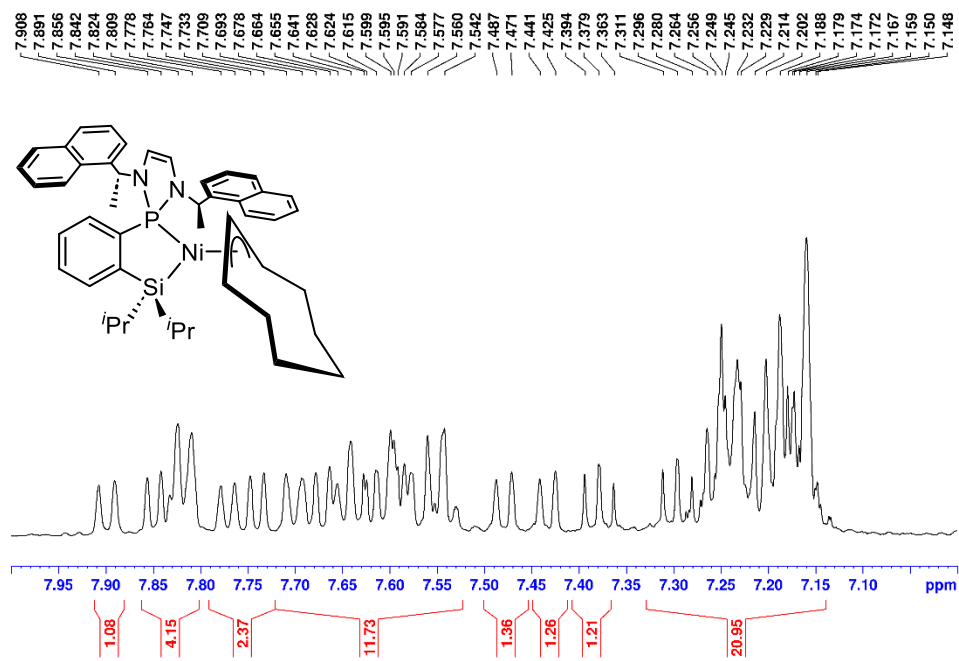


Figure B176. ^1H NMR spectrum of **5-4** in C_6D_6 (alkene region)

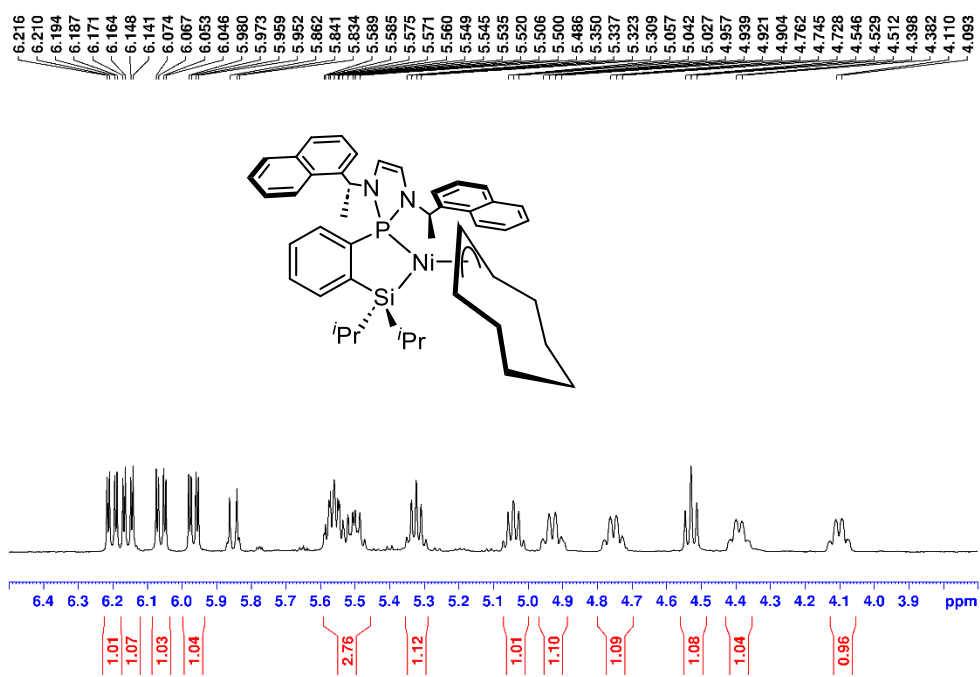


Figure B177. ^1H NMR spectrum of **5-4** in C_6D_6 (aliphatic region)

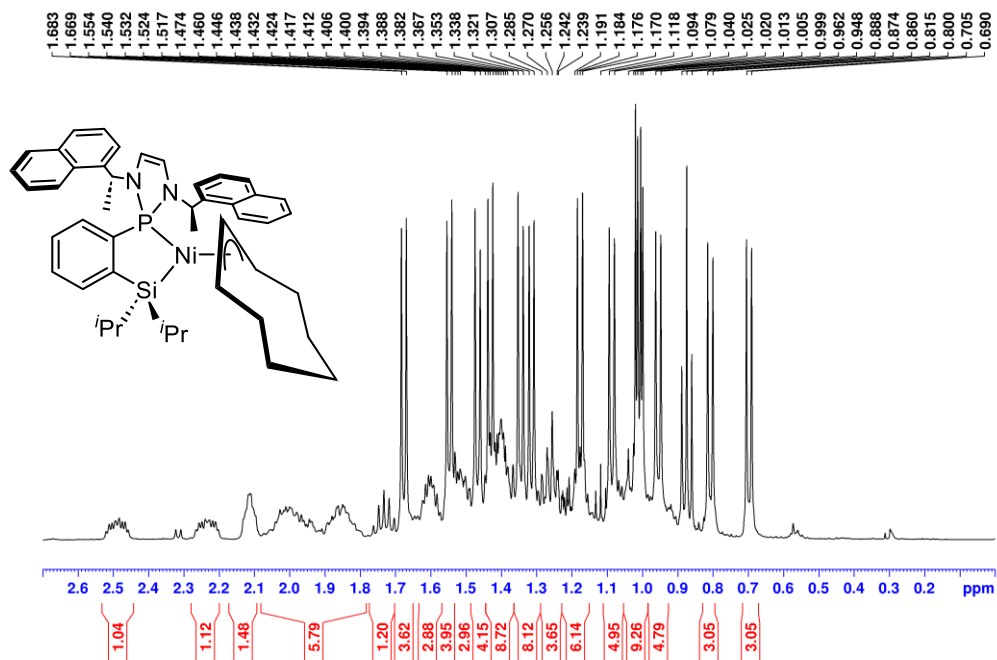


Figure B178. $^{13}\text{C}\{^1\text{H}\}$ NMR spectrum of **5-4** in C_6D_6

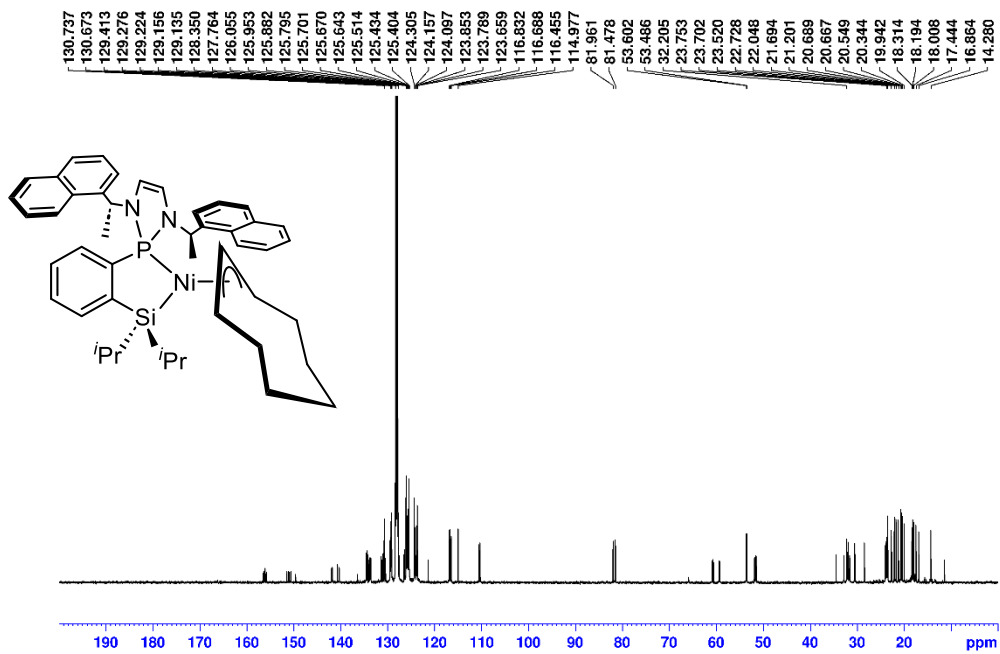


Figure B179. $^{13}\text{C}\{^1\text{H}\}$ NMR spectrum of **5-4** in C_6D_6 (aromatic region).

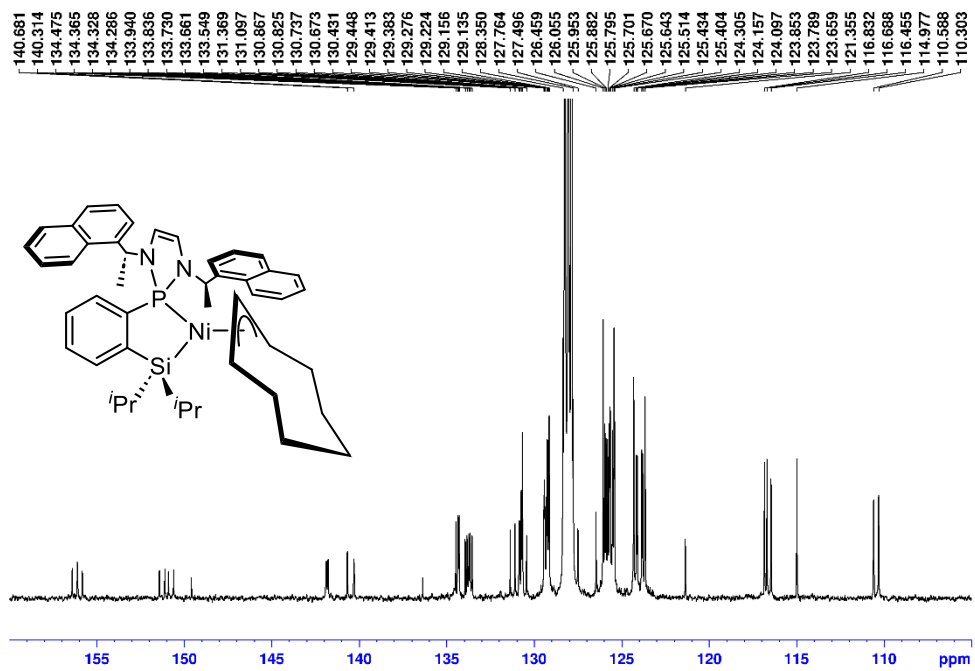


Figure B180. $^{13}\text{C}\{^1\text{H}\}$ NMR spectrum of **5-4** in C_6D_6 (aliphatic region).

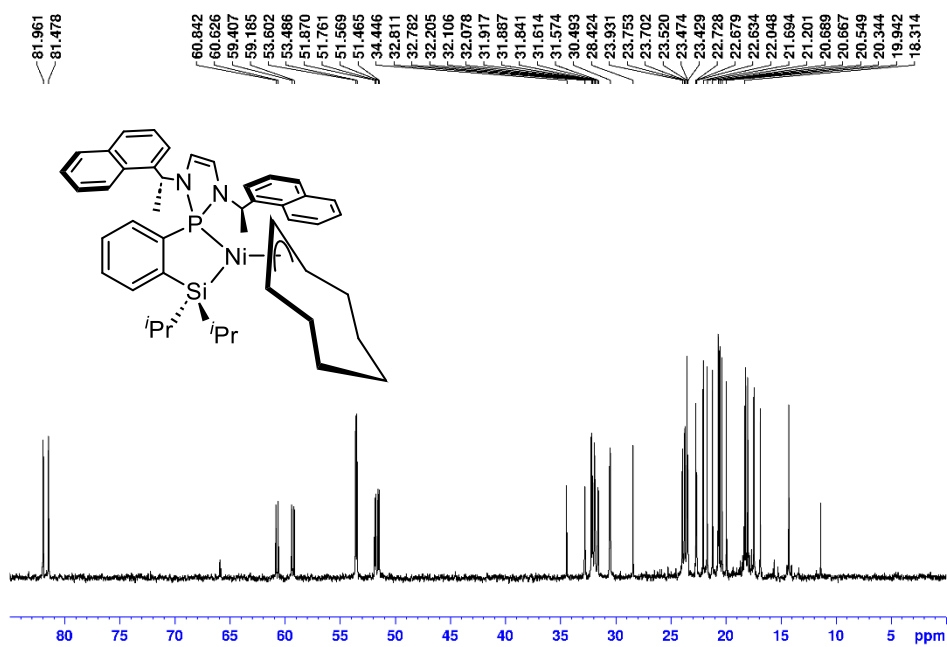


Figure B181. $^{31}\text{P}\{^1\text{H}\}$ NMR spectrum of **5-4** in C_6D_6 .

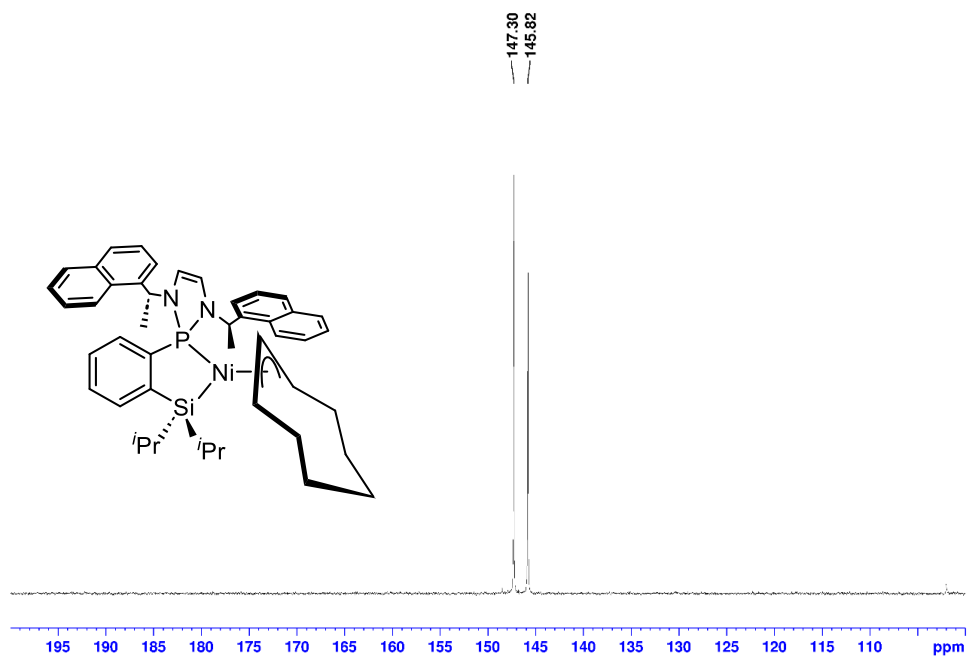


Figure B182. ^1H NMR spectrum of **5-5** in C_6D_6 .

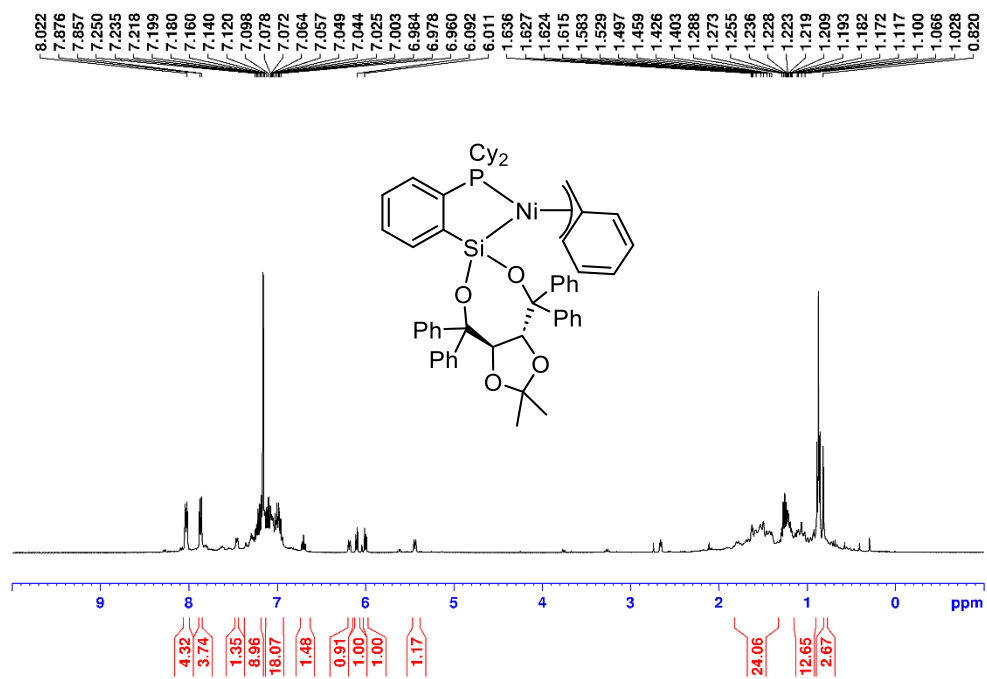


Figure B183. $^{31}\text{P}\{^1\text{H}\}$ NMR spectrum of **5-5** in C_6D_6 .

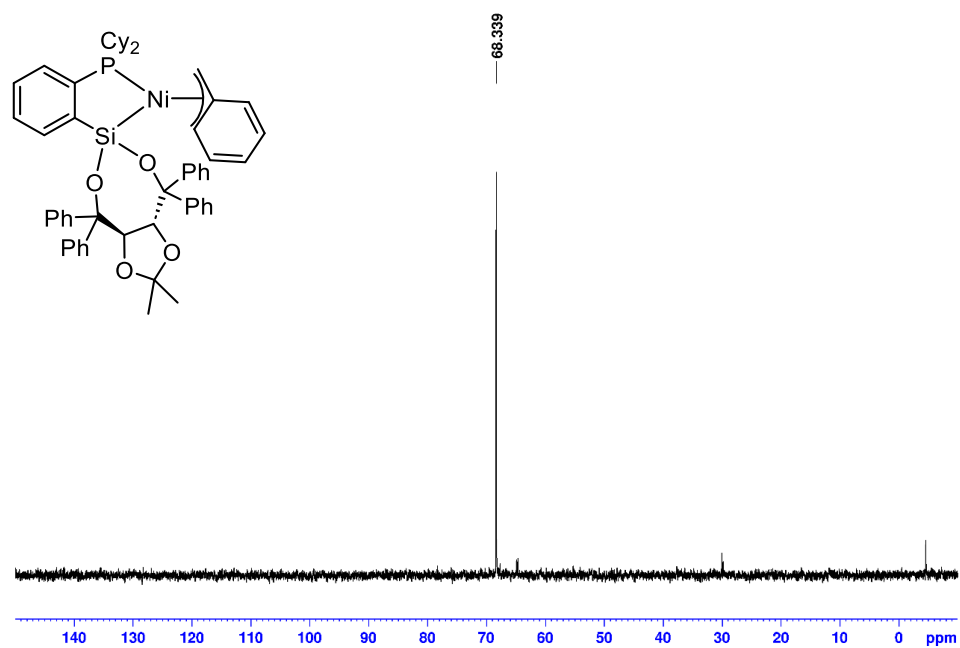


Figure B184. ^1H NMR spectrum of **5-6** in C_6D_6 at 298 K.

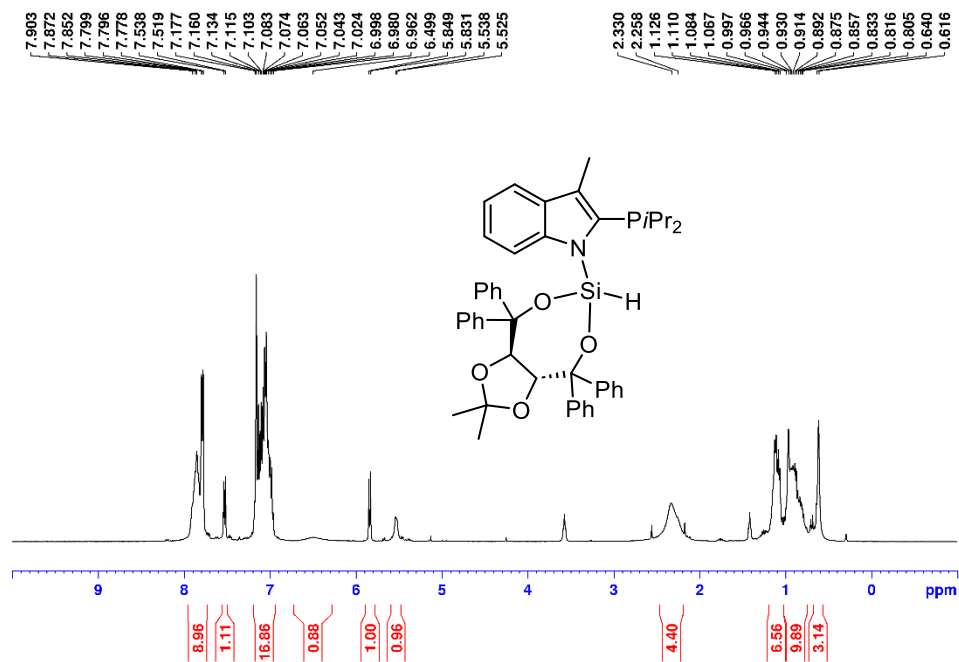


Figure B185. ^1H NMR spectrum of **5-6** in Toluene- d_8 at 353 K.

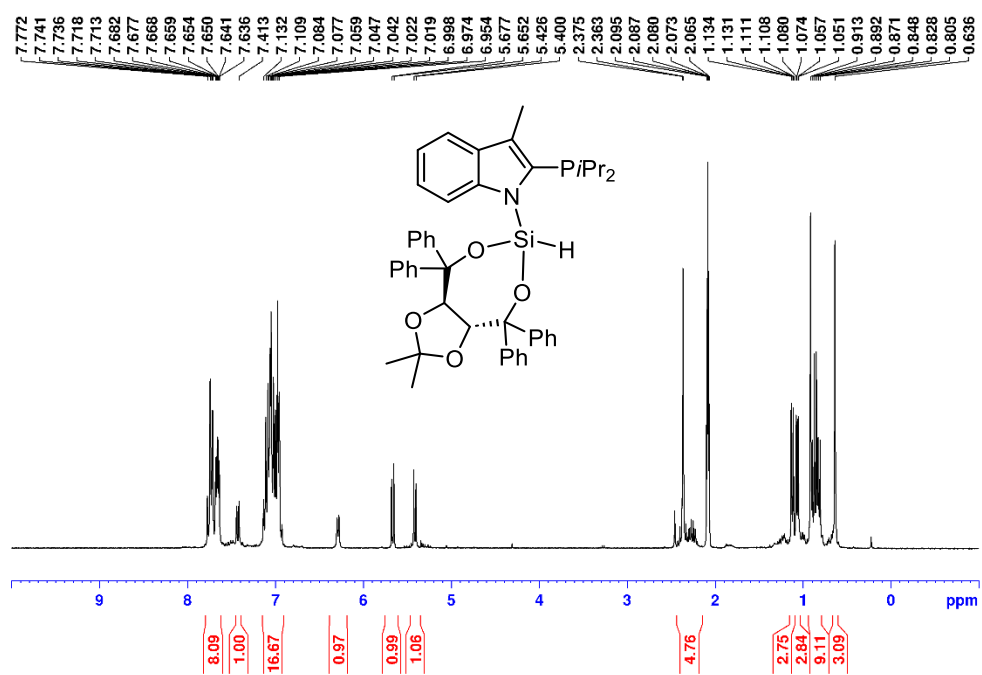


Figure B186. ^1H NMR spectrum of **5-6** in Toluene- d_8 at 353 K (aromatic region).

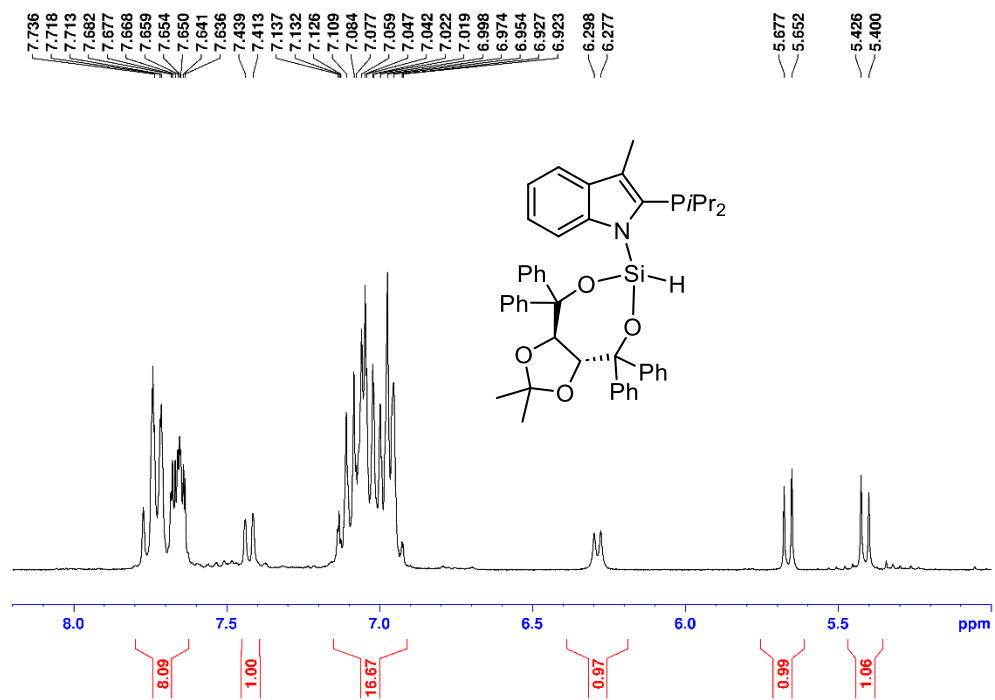


Figure B187. ^1H NMR spectrum of **5-6** in Toluene- d_8 at 353 K (aliphatic region).

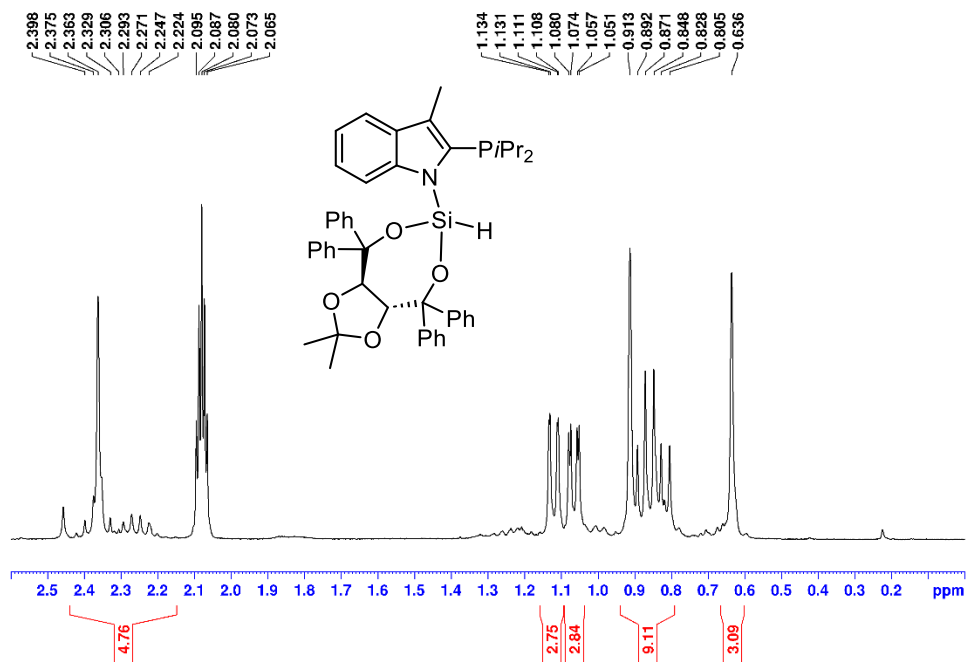


Figure B188. $^{13}\text{C}\{^1\text{H}\}$ NMR spectrum of **5-6** in C_6D_6 at 298 K.

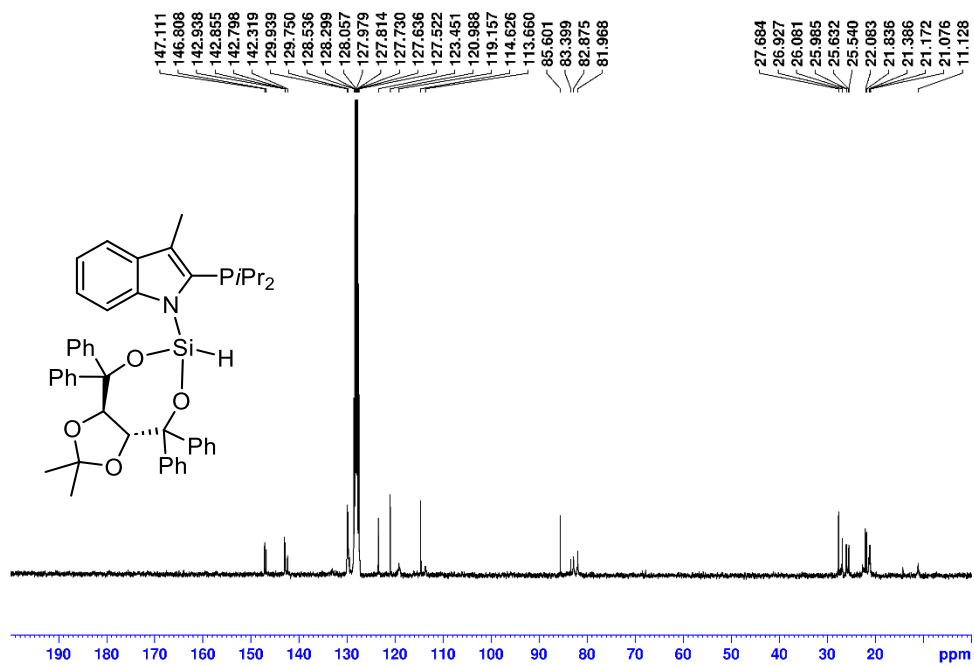


Figure B189. $^{31}\text{P}\{^1\text{H}\}$ NMR spectrum of **5-6** in C_6D_6 at 298 K.

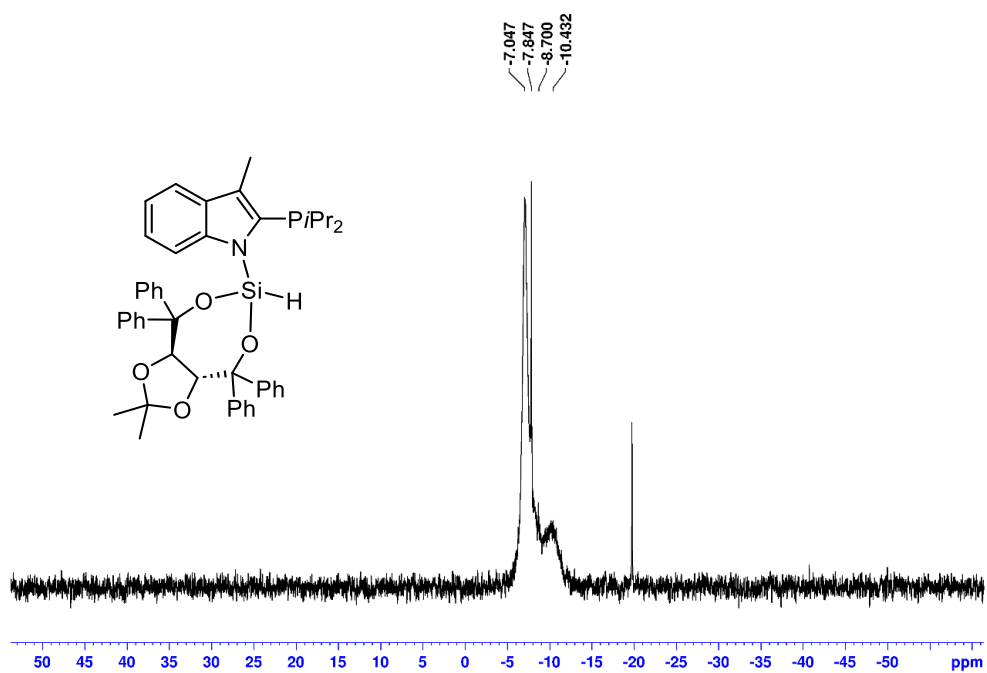


Figure B190. $^{31}\text{P}\{^1\text{H}\}$ NMR spectrum of **5-6** in Toluene- d_8 at 353 K.

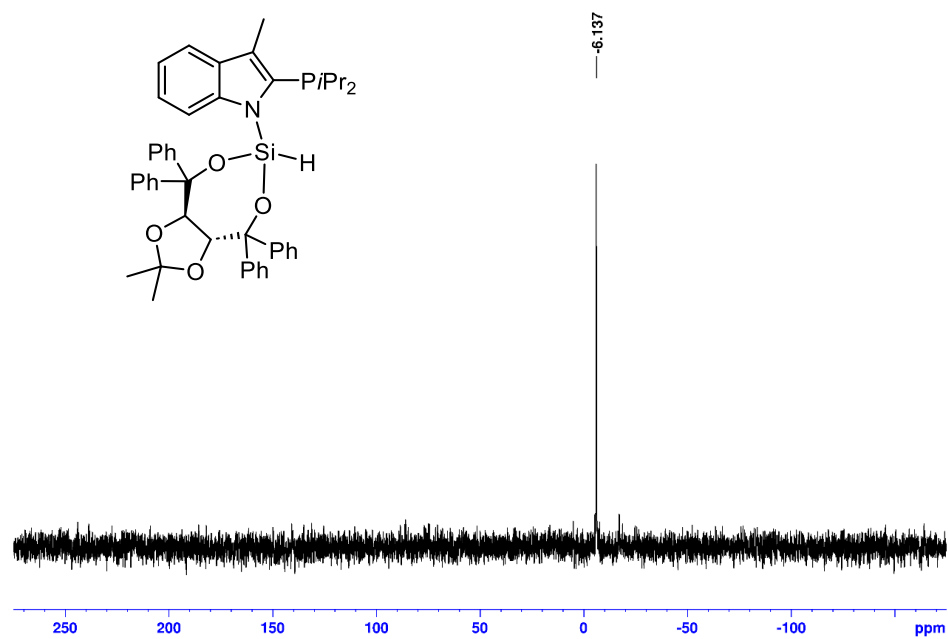


Figure B191. ^1H NMR spectrum of **5-7** in C_6D_6 .

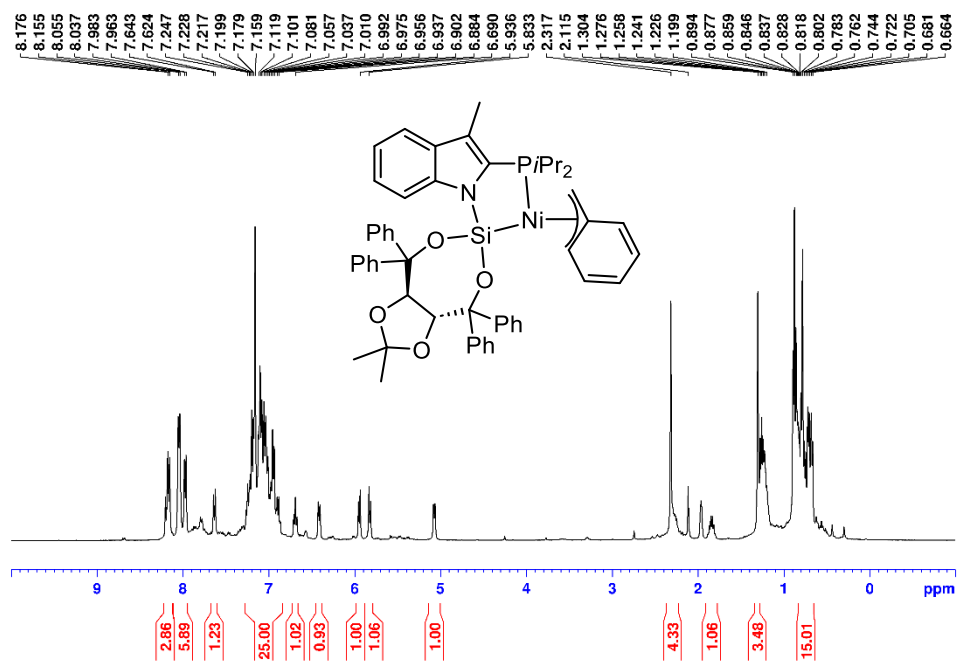


Figure B192. ^1H NMR spectrum of **5-7** in C_6D_6 (aromatic region).

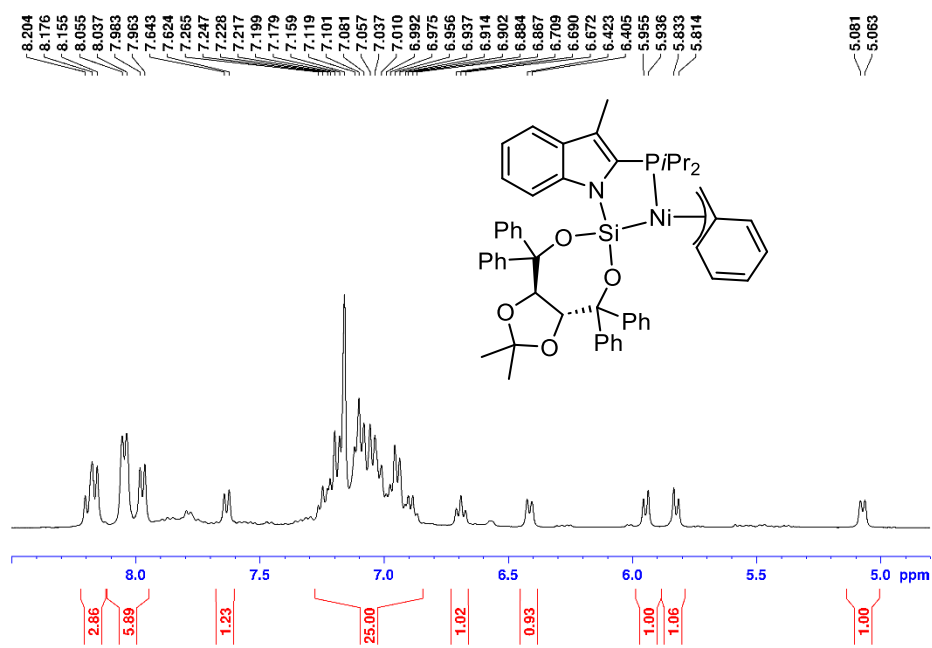


Figure B193. ^1H NMR spectrum of **5-7** in C_6D_6 (aliphatic region).

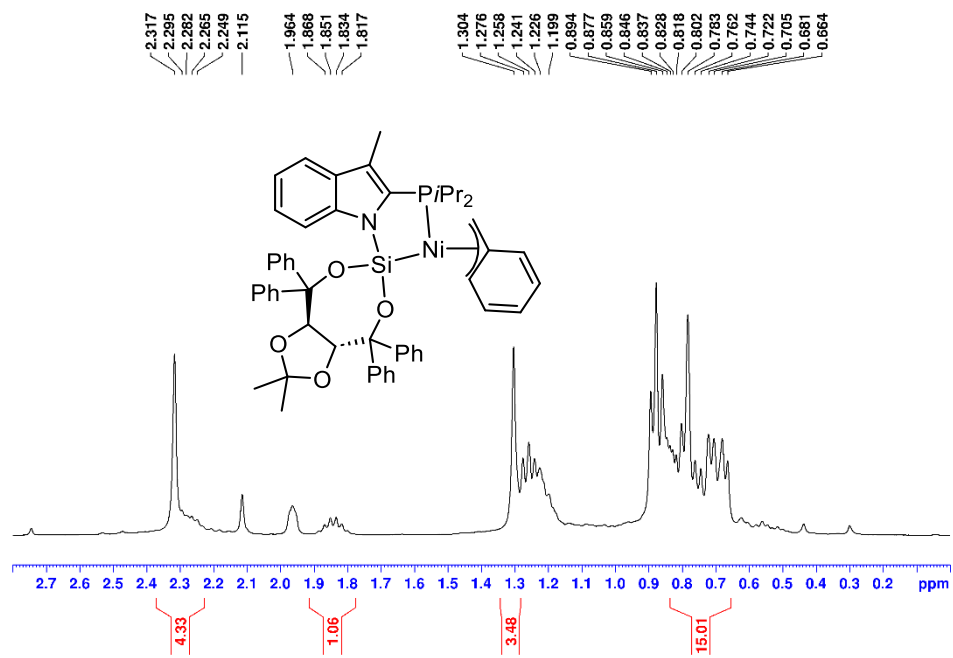


Figure B194. $^{13}\text{C}\{^1\text{H}\}$ NMR spectrum of 5-7 in C_6D_6 .

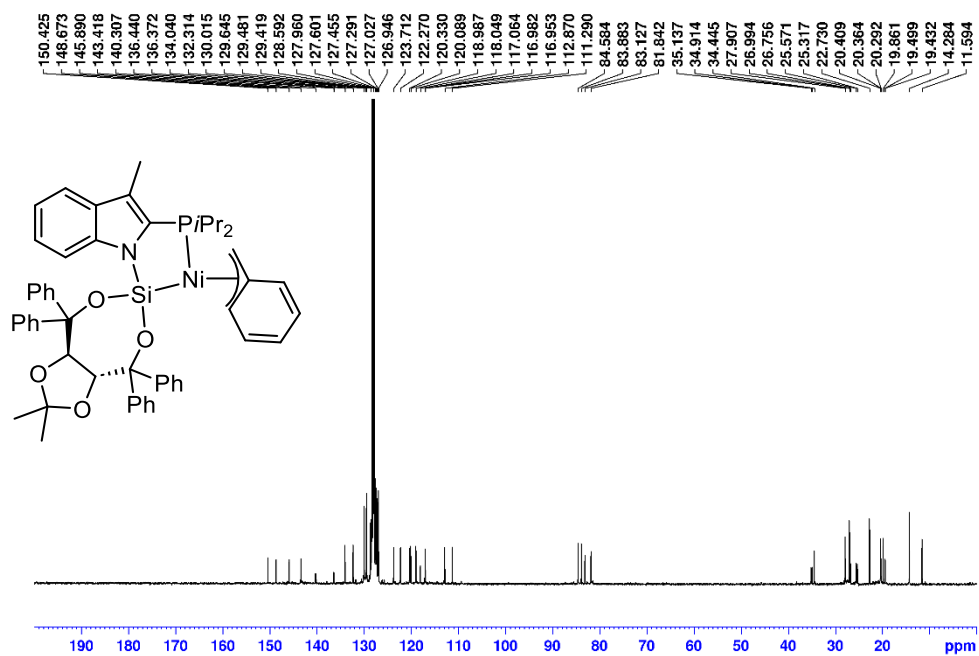


Figure B195. $^{13}\text{C}\{^1\text{H}\}$ NMR spectrum of **5-7** in C_6D_6 (aromatic region).

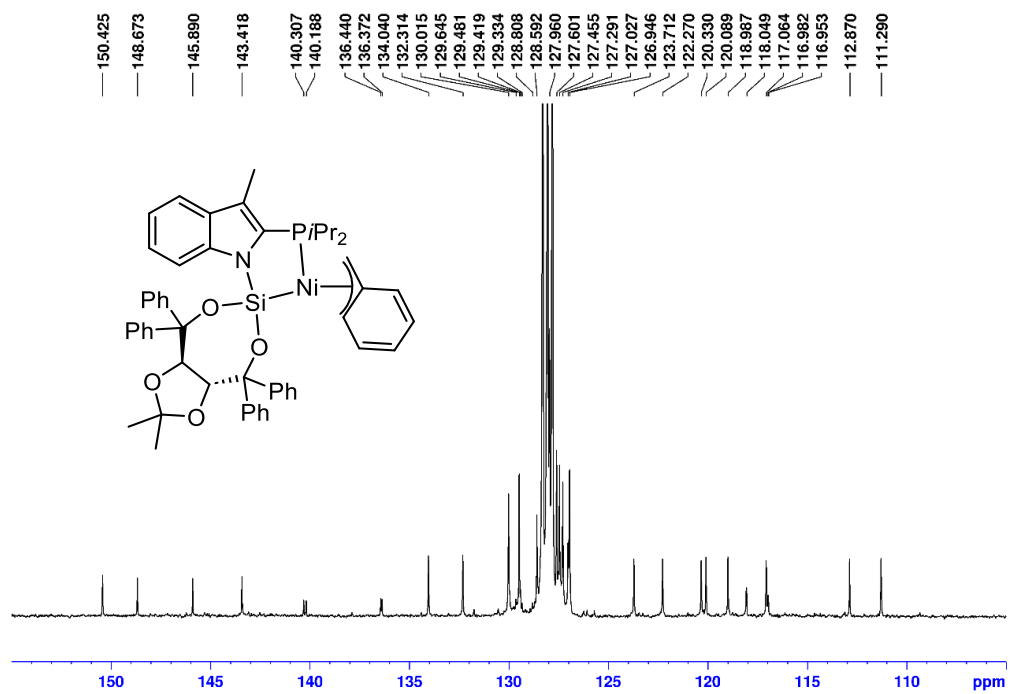


Figure B196. $^{13}\text{C}\{^1\text{H}\}$ NMR spectrum of 5-7 in C_6D_6 (aliphatic region).

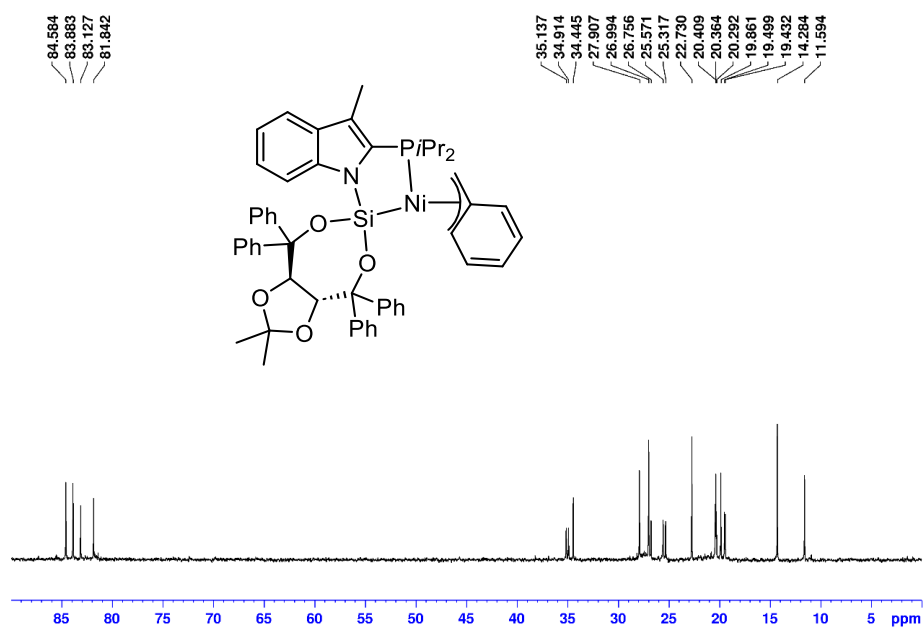


Figure B197. $^{31}\text{P}\{^1\text{H}\}$ NMR spectrum of **5-7** in C_6D_6 .

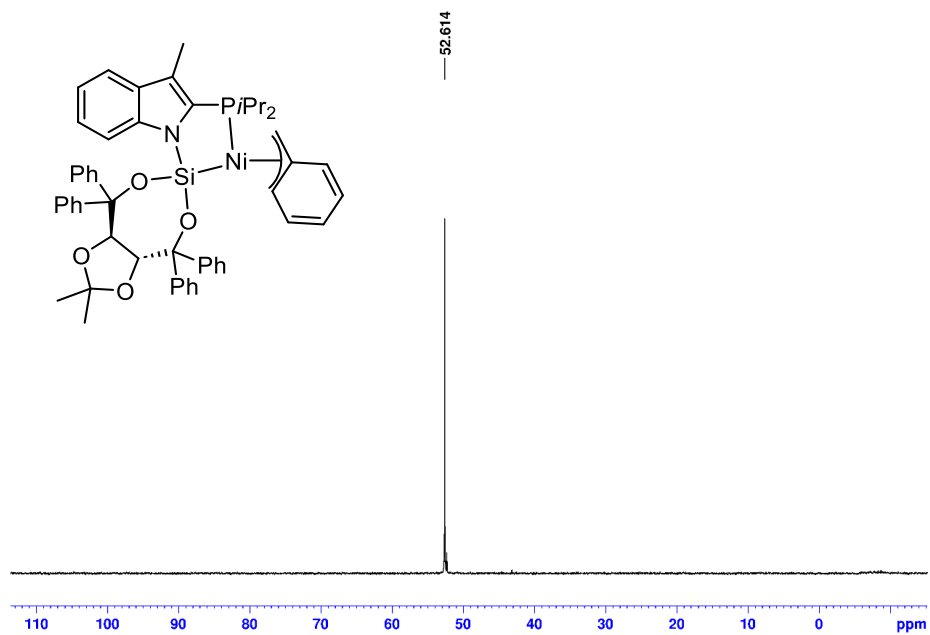


Figure B198. ^1H NMR spectrum of the mixture tentatively assigned as **5-8** in C_6D_6 .

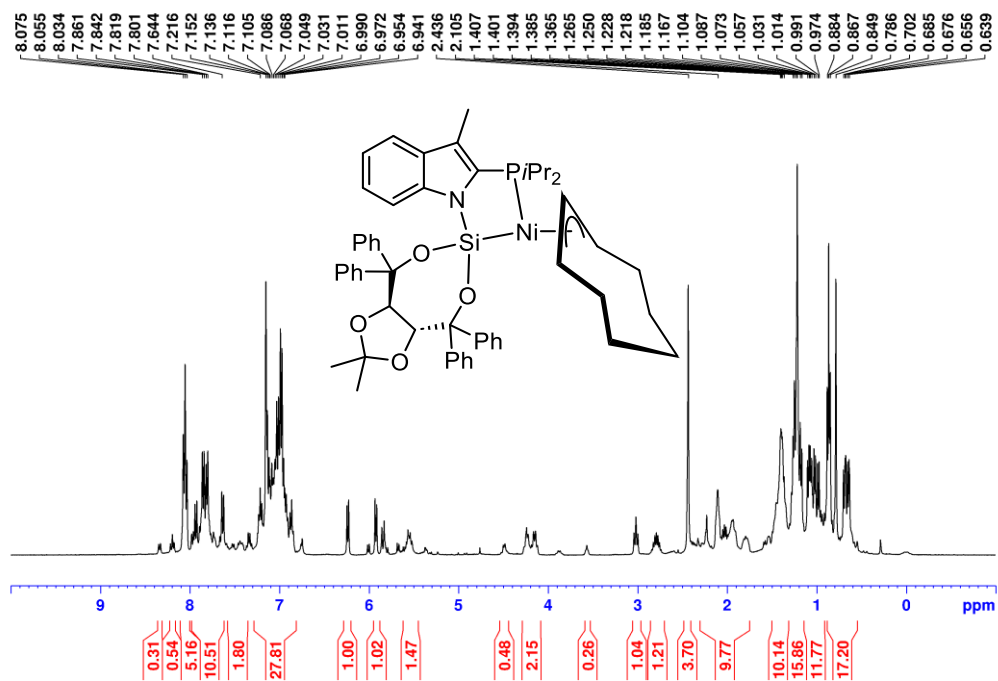


Figure B199. $^{31}\text{P}\{^1\text{H}\}$ NMR spectrum of the mixture tentatively assigned as **5-8** in C_6D_6 .

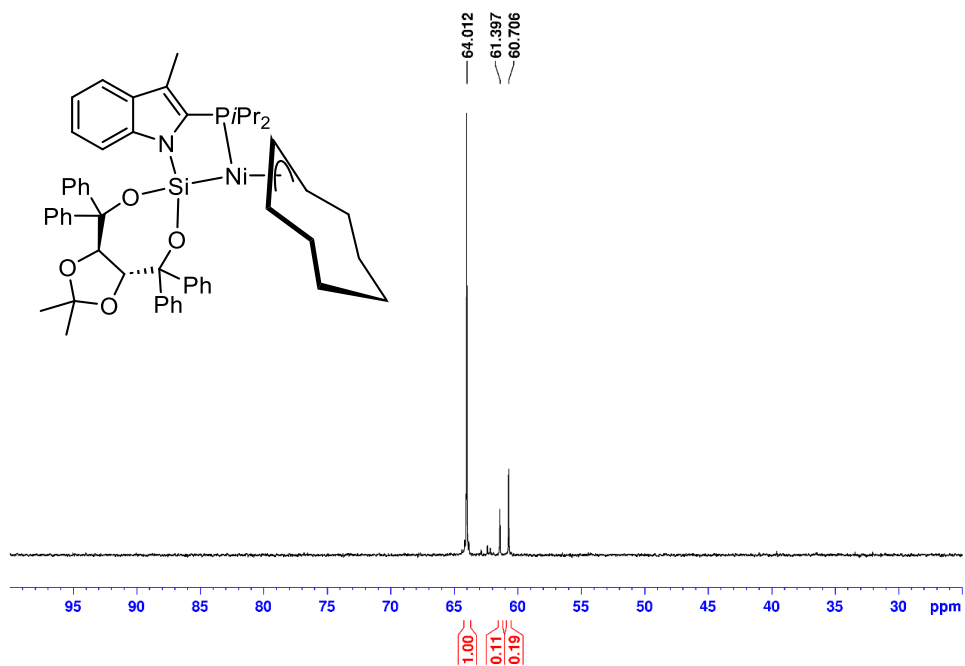
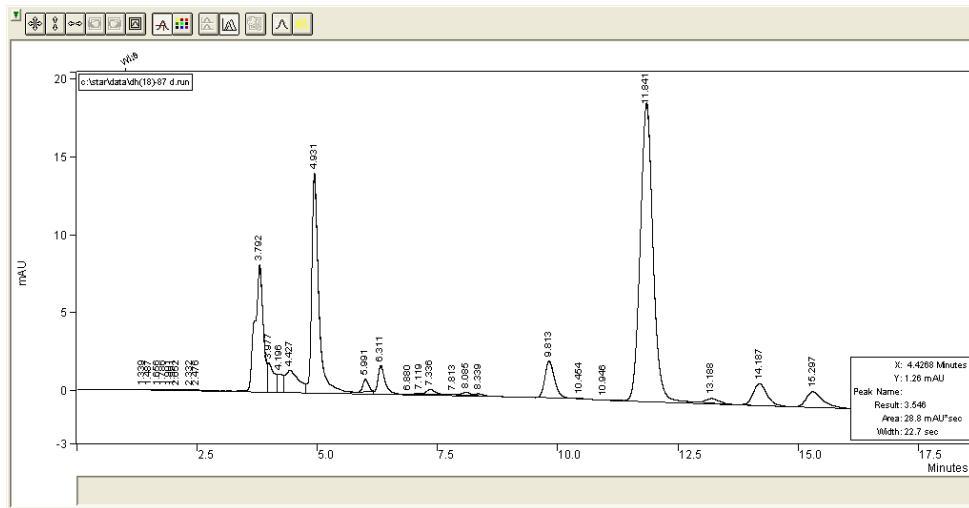
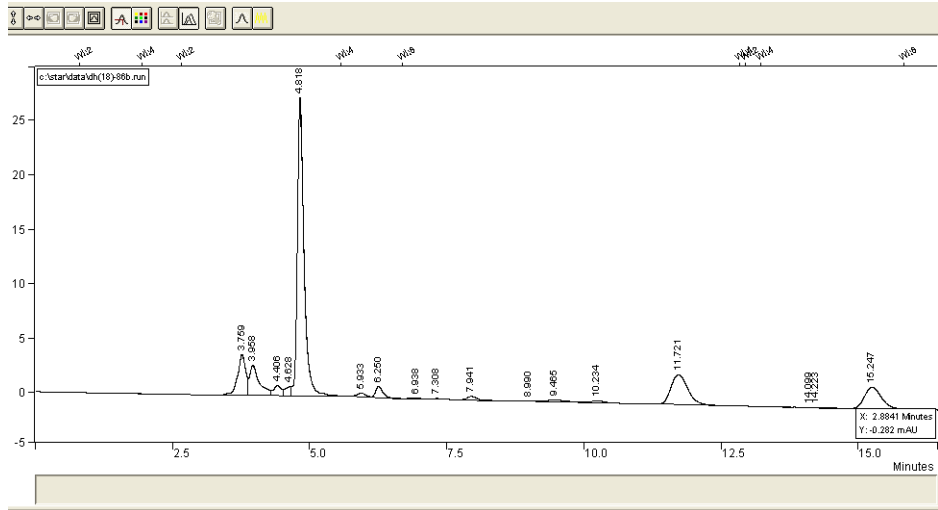
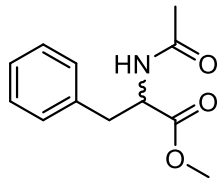
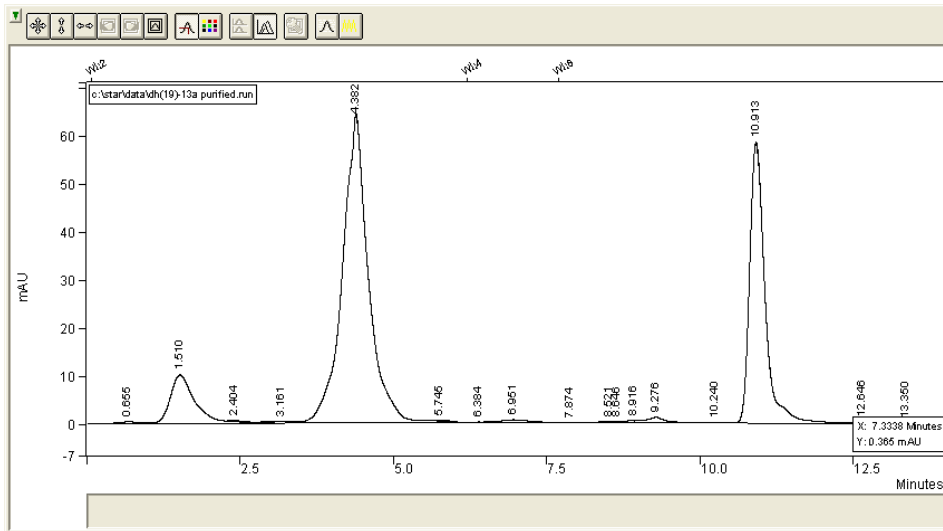
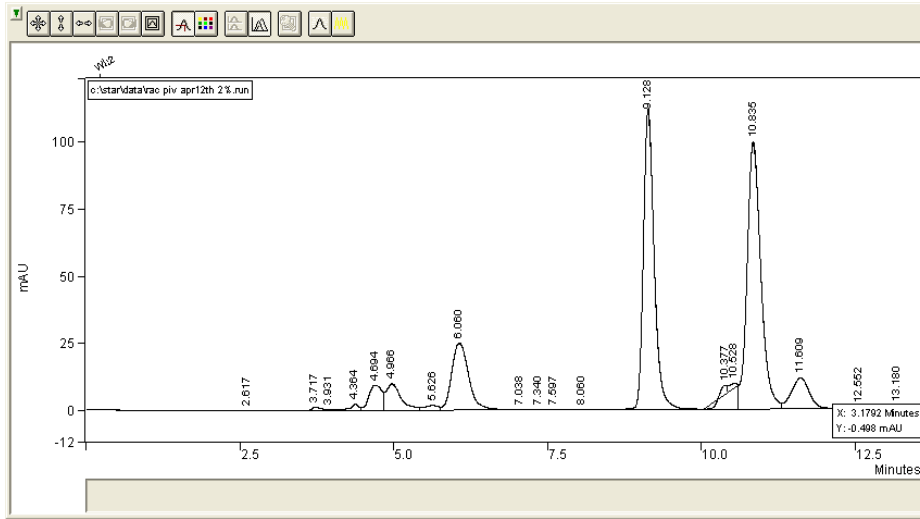
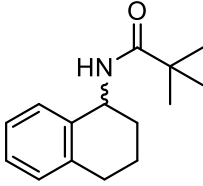


Figure B200. Chromatograms for *N*-acetyl-phenylalanine methyl ester.



Retention Time	Area	Area%
11.841	3589177	93.5
15.297	245534	6.5

Figure B201. Chromatograms for *N*-(1,2,3,4-tetrahydro-1-naphthalen)-*tert*-butylamide



Retention Time	Area	Area%
9.276	314732	3.0
10.913	10344976	97.0

Appendix C: Thermochemical Energies and Cartesian Coordinates for Computationally Modeled Compounds

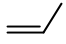
Below are the DFT calculated thermochemical energies and Cartesian coordinates for all modeled compounds reported in Chapter 2.

Dihydrogen

H-H
Zero-point correction= 0.010145 (Hartree/Particle)
Thermal correction to Energy= 0.012506
Thermal correction to Enthalpy= 0.013450
Thermal correction to Gibbs Free Energy= 0.001677
Sum of electronic and zero-point Energies= -1.165367
Sum of electronic and thermal Energies= -1.163006
Sum of electronic and thermal Enthalpies= -1.162062
Sum of electronic and thermal Free Energies= -1.173835
Single-point energy (6-311+G(2d,2p)) = -1.175511908084

H 0.0000000000 0.0000000000 0.3713900000
H 0.0000000000 0.0000000000 -0.3713900000

Propene


Zero-point correction= 0.080100 (Hartree/Particle)
Thermal correction to Energy= 0.084177
Thermal correction to Enthalpy= 0.085121
Thermal correction to Gibbs Free Energy= 0.058115
Sum of electronic and zero-point Energies= -117.828140
Sum of electronic and thermal Energies= -117.824063
Sum of electronic and thermal Enthalpies= -117.823119
Sum of electronic and thermal Free Energies= -117.850125
Single-point energy (6-311+G(2d,2p)) = -117.9082400018

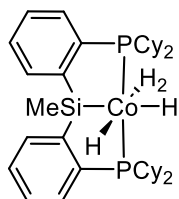
C 1.2829520000 0.2205670000 -0.0000090000
C 0.1337760000 -0.4559150000 0.0000350000
H 2.2452000000 -0.2844320000 -0.0000110000
H 1.3047930000 1.3088040000 -0.0002330000
C -1.2349170000 0.1629990000 -0.0000070000
H 0.1640190000 -1.5466160000 0.0000740000
H -1.1808690000 1.2569180000 -0.0005940000
H -1.8117620000 -0.1498190000 0.8809280000
H -1.8122470000 -0.1507590000 -0.8802750000

Propane

Zero-point correction= 0.104156 (Hartree/Particle)
Thermal correction to Energy= 0.108663
Thermal correction to Enthalpy= 0.109607
Thermal correction to Gibbs Free Energy= 0.081527
Sum of electronic and zero-point Energies= -119.041769
Sum of electronic and thermal Energies= -119.037262
Sum of electronic and thermal Enthalpies= -119.036318
Sum of electronic and thermal Free Energies= -119.064398
Single-point energy (6-311+G(2d,2p)) = -119.1459250758

C	-1.2768400000	-0.2600500000	-0.0000010000
C	0.0000000000	0.5869500000	-0.0000010000
H	-2.1758800000	0.3670900000	-0.0008110000
H	-1.3216300000	-0.9069300000	0.8850990000
H	-1.3208500000	-0.9081100000	-0.8842910000
C	1.2768400000	-0.2600500000	-0.0000010000
H	0.0000000000	1.2473800000	0.8777990000
H	0.0000000000	1.2474200000	-0.8777710000
H	1.3212100000	-0.9075800000	0.8846490000
H	2.1758800000	0.3670900000	0.0000790000
H	1.3212700000	-0.9074600000	-0.8847410000

Polyhydride Isomer A



Zero-point correction= 0.885477 (Hartree/Particle)
Thermal correction to Energy= 0.928147
Thermal correction to Enthalpy= 0.929091
Thermal correction to Gibbs Free Energy= 0.814899
Sum of electronic and zero-point Energies= -3799.663503
Sum of electronic and thermal Energies= -3799.620833
Sum of electronic and thermal Enthalpies= -3799.619889
Sum of electronic and thermal Free Energies= -3799.734082
Single-point energy (6-311+G(2d,2p)) = -3801.253147770

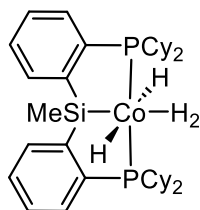
Co	-0.00001	0.03211	-0.56636
P	2.13966	0.15349	-0.22142
P	-2.13972	0.15315	-0.22134
Si	0.00008	-1.78640	0.78998

C	2.56407	-0.71199	1.35551
C	3.25225	-0.62980	-1.52298
C	2.85553	1.86742	0.00126
C	-2.56392	-0.71227	1.35568
C	-2.85572	1.86702	0.00152
C	-3.25230	-0.63008	-1.52296
C	-0.00013	-3.62802	0.26368
C	1.58798	-1.60680	1.84582
C	-1.58750	-1.60660	1.84625
C	3.77074	-0.52491	2.04584
H	2.95494	-0.12106	-2.45267
C	2.93120	-2.12817	-1.68569
C	4.76654	-0.42979	-1.32388
H	3.91048	1.74262	0.28332
C	2.80233	2.68391	-1.30403
C	2.14636	2.62036	1.14215
C	-3.77058	-0.52531	2.04606
H	-3.91059	1.74211	0.28383
C	-2.80294	2.68357	-1.30376
C	-2.14636	2.62001	1.14225
H	-2.95489	-0.12137	-2.45263
C	-2.93136	-2.12847	-1.68560
C	-4.76658	-0.42995	-1.32396
H	-0.00022	-4.28671	1.14255
H	0.88606	-3.87491	-0.33132
H	-0.88633	-3.87476	-0.33137
C	1.87609	-2.31547	3.02259
C	-1.87520	-2.31479	3.02340
H	4.51543	0.17563	1.67913
C	4.02301	-1.22601	3.22506
H	1.86062	-2.26766	-1.86220
H	3.16316	-2.64883	-0.74613
C	3.73811	-2.76155	-2.82927
C	5.57312	-1.06055	-2.47183
H	5.06964	-0.89554	-0.37676
H	5.01415	0.63492	-1.25017
H	1.75757	2.74837	-1.63263
H	3.35343	2.17346	-2.10374
C	3.37593	4.09666	-1.10787
C	2.73345	4.02584	1.33804
H	1.08180	2.70117	0.89670
H	2.21207	2.04729	2.07444
H	-4.51554	0.17484	1.67916
C	-4.02250	-1.22601	3.22560
H	-3.35419	2.17309	-2.10335
H	-1.75826	2.74815	-1.63262

C	-3.37663	4.09625	-1.10742
C	-2.73353	4.02543	1.33833
H	-2.21179	2.04691	2.07455
H	-1.08187	2.70092	0.89654
H	-1.86077	-2.26808	-1.86202
H	-3.16344	-2.64908	-0.74604
C	-3.73823	-2.76182	-2.82924
C	-5.57312	-1.06065	-2.47198
H	-5.01412	0.63477	-1.25027
H	-5.06980	-0.89569	-0.37688
C	3.07407	-2.12726	3.71241
H	1.15199	-3.02514	3.41623
C	-3.07316	-2.12667	3.71327
H	-1.15077	-3.02395	3.41733
H	4.95544	-1.06858	3.76109
H	3.50735	-3.83242	-2.89576
H	3.42470	-2.31322	-3.78403
C	5.24589	-2.54959	-2.64133
H	5.34441	-0.52907	-3.40769
H	6.64639	-0.92226	-2.28829
H	4.45190	4.02588	-0.88701
H	3.28662	4.66442	-2.04294
C	2.67522	4.83928	0.03790
H	3.77958	3.94552	1.67053
H	2.19087	4.54501	2.13847
H	-4.95494	-1.06869	3.76165
H	-3.28761	4.66406	-2.04250
H	-4.45254	4.02536	-0.88628
C	-2.67570	4.83892	0.03820
H	-2.19080	4.54463	2.13864
H	-3.77956	3.94501	1.67108
H	-3.42470	-2.31354	-3.78398
H	-3.50755	-3.83271	-2.89567
C	-5.24600	-2.54972	-2.64143
H	-6.64640	-0.92226	-2.28853
H	-5.34429	-0.52921	-3.40783
H	3.26807	-2.67781	4.62977
H	-3.26686	-2.67683	4.63093
H	5.80094	-2.96838	-3.49028
H	5.57881	-3.09660	-1.74681
H	3.12677	5.82903	0.18305
H	1.62247	5.00928	-0.23283
H	-3.12731	5.82862	0.18349
H	-1.62303	5.00901	-0.23279
H	-5.57905	-3.09669	-1.74693
H	-5.80102	-2.96848	-3.49042

H	-0.00041	1.42368	-1.15928
H	0.00012	0.68142	0.74071
H	0.00004	-1.00161	-1.79469
H	-0.00002	-0.22539	-2.14998

Polyhydride Isomer B



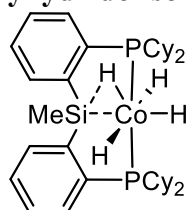
Zero-point correction=	0.884725 (Hartree/Particle)
Thermal correction to Energy=	0.927547
Thermal correction to Enthalpy=	0.928491
Thermal correction to Gibbs Free Energy=	0.813431
Sum of electronic and zero-point Energies=	-3799.661837
Sum of electronic and thermal Energies=	-3799.619015
Sum of electronic and thermal Enthalpies=	-3799.618071
Sum of electronic and thermal Free Energies=	-3799.733131
Single-point energy (6-311+G(2d,2p)) =	-3801.251108181

Co	-0.00006	0.03824	-0.55260
P	2.15457	0.13234	-0.21857
P	-2.15465	0.13213	-0.21859
Si	0.00012	-1.70194	0.84015
C	2.58567	-0.69687	1.36835
C	3.25897	-0.66621	-1.51778
C	2.89002	1.84777	-0.03246
C	-2.58508	-0.69618	1.36902
C	-2.89024	1.84763	-0.03326
C	-3.25948	-0.66706	-1.51703
C	-0.00056	-3.52771	0.28497
C	1.58906	-1.54543	1.89170
C	-1.58818	-1.54434	1.89258
C	3.80638	-0.52877	2.03774
H	2.94743	-0.16864	-2.44915
C	2.92428	-2.16222	-1.66439
C	4.77665	-0.47026	-1.34461
H	3.95483	1.70465	0.19872
C	2.80156	2.66427	-1.33611
C	2.26167	2.62835	1.13665
C	-3.80543	-0.52755	2.03890
H	-3.95502	1.70455	0.19811
C	-2.80194	2.66346	-1.33734
C	-2.26182	2.62884	1.13538

H	-2.94843	-0.16975	-2.44871
C	-2.92472	-2.16307	-1.66335
C	-4.77710	-0.47123	-1.34316
H	-0.00009	-4.19095	1.16044
H	0.88478	-3.76578	-0.31281
H	-0.88670	-3.76557	-0.31169
C	1.86603	-2.23317	3.08309
C	-1.86447	-2.23089	3.08480
H	4.56781	0.13810	1.64365
C	4.04889	-1.20576	3.23283
H	1.85004	-2.27945	-1.82906
H	3.16627	-2.67907	-0.72462
C	3.71133	-2.80912	-2.81372
C	5.56171	-1.11696	-2.49902
H	5.09378	-0.92803	-0.39803
H	5.03336	0.59364	-1.28701
H	1.74556	2.79219	-1.60846
H	3.27768	2.12869	-2.16645
C	3.45050	4.04858	-1.17363
C	2.92021	4.00631	1.30216
H	1.19008	2.75370	0.94558
H	2.34460	2.05275	2.06546
H	-4.56710	0.13893	1.64461
C	-4.04730	-1.20343	3.23476
H	-3.27818	2.12748	-2.16734
H	-1.74597	2.79119	-1.60991
C	-3.45084	4.04786	-1.17551
C	-2.92041	4.00685	1.30025
H	-2.34460	2.05371	2.06449
H	-1.19026	2.75418	0.94411
H	-1.85055	-2.28024	-1.82850
H	-3.16620	-2.67964	-0.72329
C	-3.71227	-2.81040	-2.81208
C	-5.56267	-1.11837	-2.49697
H	-5.03390	0.59265	-1.28575
H	-5.09368	-0.92875	-0.39628
C	3.07734	-2.06323	3.75417
H	1.12587	-2.90985	3.50323
C	-3.07542	-2.06034	3.75640
H	-1.12403	-2.90707	3.50523
H	4.99150	-1.06410	3.75521
H	3.47305	-3.87903	-2.86873
H	3.38580	-2.36660	-3.76705
C	5.22309	-2.60539	-2.65053
H	5.32105	-0.59262	-3.43597
H	6.63859	-0.98281	-2.33368

H	4.53088	3.92361	-1.00659
H	3.34292	4.62044	-2.10423
C	2.84294	4.82255	0.00439
H	3.97509	3.87813	1.58858
H	2.43814	4.55077	2.12408
H	-4.98963	-1.06131	3.75750
H	-3.34331	4.61924	-2.10642
H	-4.53121	3.92298	-1.00835
C	-2.84322	4.82244	0.00207
H	-2.43832	4.55173	2.12189
H	-3.97527	3.87877	1.58678
H	-3.38726	-2.36813	-3.76571
H	-3.47389	-3.88031	-2.86690
C	-5.22398	-2.60680	-2.64820
H	-6.63948	-0.98428	-2.33111
H	-5.32256	-0.59428	-3.43421
H	3.26466	-2.59465	4.68406
H	-3.26217	-2.59083	4.68693
H	5.76385	-3.03427	-3.50382
H	5.56653	-3.14640	-1.75620
H	3.34953	5.78835	0.12659
H	1.78856	5.04636	-0.21707
H	-3.34982	5.78830	0.12381
H	-1.78886	5.04615	-0.21955
H	-5.56690	-3.14758	-1.75354
H	-5.76510	-3.03600	-3.50110
H	-0.00018	-1.05540	-1.59785
H	-0.00014	0.90448	0.67662
H	0.00094	0.77584	-1.97057
H	-0.00015	1.41245	-1.40098

Polyhydride Isomer C



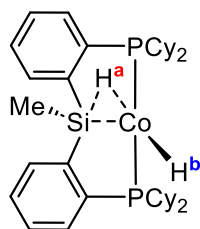
Zero-point correction=	0.885030 (Hartree/Particle)
Thermal correction to Energy=	0.927590
Thermal correction to Enthalpy=	0.928534
Thermal correction to Gibbs Free Energy=	0.813710
Sum of electronic and zero-point Energies=	-3799.662290
Sum of electronic and thermal Energies=	-3799.619730
Sum of electronic and thermal Enthalpies=	-3799.618786
Sum of electronic and thermal Free Energies=	-3799.733610
Single-point energy (6-311+G(2d,2p)) =	-3801.247495733

H	-0.00001	-1.51603	-0.72298
Co	-0.00001	-0.01732	-0.46180
P	2.14704	0.15407	-0.22806
P	-2.14707	0.15403	-0.22809
Si	-0.00001	-1.80835	0.96388
C	2.61433	-0.71162	1.33989
C	3.21339	-0.61978	-1.56387
C	2.83996	1.87485	-0.02020
C	-2.61432	-0.71158	1.33993
C	-2.84001	1.87481	-0.02026
C	-3.21342	-0.61987	-1.56388
C	-0.00018	-3.68131	0.57396
C	1.64101	-1.56996	1.89893
C	-1.64095	-1.56983	1.89904
C	3.85026	-0.54136	1.97899
H	2.89466	-0.08438	-2.47032
C	2.84381	-2.10335	-1.75415
C	4.73580	-0.45632	-1.40333
H	3.91133	1.77099	0.20331
C	2.69815	2.69521	-1.31758
C	2.17414	2.60024	1.16453
C	-3.85022	-0.54127	1.97907
H	-3.91138	1.77095	0.20325
C	-2.69817	2.69517	-1.31764
C	-2.17420	2.60021	1.16447
H	-2.89474	-0.08443	-2.47033
C	-2.84376	-2.10341	-1.75419
C	-4.73584	-0.45650	-1.40331
H	-0.00026	-4.27956	1.49430
H	0.88698	-3.96508	-0.00431
H	-0.88741	-3.96487	-0.00432
C	1.95530	-2.25458	3.08208
C	-1.95516	-2.25429	3.08231
H	4.59750	0.12741	1.56193
C	4.13039	-1.21048	3.17137
H	1.76643	-2.19288	-1.92015
H	3.07776	-2.65620	-0.83263
C	3.60971	-2.72995	-2.92927
C	5.49402	-1.07896	-2.58805
H	5.05764	-0.95100	-0.47719
H	5.00841	0.60177	-1.31215
H	1.63789	2.72849	-1.59815
H	3.22599	2.20423	-2.14433
C	3.23374	4.12519	-1.14217
C	2.72203	4.02500	1.33242

H	1.09398	2.64055	0.98715
H	2.31727	2.02705	2.08786
H	-4.59749	0.12743	1.56196
C	-4.13028	-1.21024	3.17155
H	-3.22600	2.20418	-2.14440
H	-1.63791	2.72844	-1.59819
C	-3.23376	4.12514	-1.14225
C	-2.72209	4.02497	1.33235
H	-2.31734	2.02703	2.08781
H	-1.09404	2.64053	0.98711
H	-1.76638	-2.19288	-1.92020
H	-3.07767	-2.65628	-0.83267
C	-3.60963	-2.73003	-2.92931
C	-5.49403	-1.07915	-2.58804
H	-5.00851	0.60157	-1.31211
H	-5.05764	-0.95122	-0.47719
C	3.18074	-2.07091	3.72386
H	1.23098	-2.93766	3.52063
C	-3.18058	-2.07056	3.72412
H	-1.23080	-2.93726	3.52093
H	5.08614	-1.05897	3.66626
H	3.35281	-3.79367	-3.01323
H	3.28196	-2.25370	-3.86515
C	5.12658	-2.55647	-2.77706
H	5.24938	-0.52312	-3.50540
H	6.57528	-0.96889	-2.43428
H	4.32095	4.08952	-0.97469
H	3.07963	4.69261	-2.06887
C	2.56599	4.83898	0.04083
H	3.78695	3.98085	1.60704
H	2.20621	4.52309	2.16329
H	-5.08602	-1.05869	3.66646
H	-3.07963	4.69255	-2.06895
H	-4.32097	4.08948	-0.97479
C	-2.56604	4.83895	0.04076
H	-2.20629	4.52306	2.16323
H	-3.78702	3.98082	1.60695
H	-3.28192	-2.25375	-3.86519
H	-3.35268	-3.79373	-3.01329
C	-5.12652	-2.55664	-2.77708
H	-6.57530	-0.96915	-2.43426
H	-5.24943	-0.52327	-3.50538
H	3.39441	-2.59504	4.65196
H	-3.39418	-2.59455	4.65231
H	5.64937	-2.97089	-3.64842
H	5.47069	-3.12843	-1.90237

H	2.98768	5.84436	0.16685
H	1.49498	4.97093	-0.17458
H	-2.98773	5.84432	0.16677
H	-1.49503	4.97090	-0.17464
H	-5.47059	-3.12864	-1.90240
H	-5.64929	-2.97107	-3.64845
H	0.00004	-0.09296	-1.96714
H	-0.00002	0.41451	0.97487
H	-0.00004	1.41187	-0.79565

Intermediate 2-4



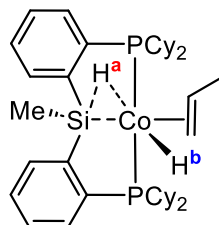
Zero-point correction=	0.866432 (Hartree/Particle)
Thermal correction to Energy=	0.909040
Thermal correction to Enthalpy=	0.909984
Thermal correction to Gibbs Free Energy=	0.793607
Sum of electronic and zero-point Energies=	-3798.480615
Sum of electronic and thermal Energies=	-3798.438007
Sum of electronic and thermal Enthalpies=	-3798.437063
Sum of electronic and thermal Free Energies=	-3798.553440
Single-point energy (6-311+G(2d,2p)) =	-3799.347047472

H	-0.00002	-0.34966	-1.91074
Co	-0.00001	0.03870	-0.40576
P	2.15753	0.09093	-0.20855
P	-2.15755	0.09113	-0.20866
Si	-0.00014	-1.58522	1.04100
C	2.63718	-0.67376	1.39980
C	3.21527	-0.71340	-1.52798
C	2.78604	1.85428	-0.13528
C	-2.63736	-0.67338	1.39972
C	-2.78581	1.85458	-0.13562
C	-3.21537	-0.71319	-1.52803
C	-0.00011	-3.39698	0.43170
C	1.62655	-1.43418	2.03058
C	-1.62687	-1.43402	2.03047
C	3.89189	-0.51581	2.00328
H	2.93461	-0.15384	-2.43292
C	2.77208	-2.17176	-1.74148
C	4.74147	-0.62913	-1.35094

H	3.88492	1.83024	-0.10025
C	2.35522	2.60721	-1.41220
C	2.28217	2.59138	1.12085
C	-3.89204	-0.51523	2.00318
H	-3.88470	1.83075	-0.10090
C	-2.35447	2.60741	-1.41243
C	-2.28216	2.59162	1.12064
H	-2.93477	-0.15364	-2.43298
C	-2.77223	-2.17155	-1.74154
C	-4.74155	-0.62888	-1.35085
H	-0.00035	-4.07096	1.30008
H	0.88624	-3.62458	-0.16705
H	-0.88619	-3.62452	-0.16748
C	1.92408	-2.04233	3.25802
C	-1.92455	-2.04219	3.25787
H	4.66076	0.08678	1.52755
C	4.15710	-1.11319	3.23667
H	1.68974	-2.19767	-1.90209
H	2.98204	-2.74895	-0.82910
C	3.50869	-2.81430	-2.92610
C	5.47469	-1.26587	-2.54431
H	5.02901	-1.15962	-0.43356
H	5.06820	0.41171	-1.23421
H	1.25843	2.57112	-1.49043
H	2.74214	2.10752	-2.30808
C	2.81826	4.07180	-1.39074
C	2.75612	4.05236	1.14003
H	1.18577	2.55903	1.13624
H	2.61764	2.07221	2.02513
H	-4.66080	0.08752	1.52746
C	-4.15738	-1.11261	3.23654
H	-2.74123	2.10777	-2.30841
H	-1.25767	2.57112	-1.49035
C	-2.81725	4.07209	-1.39112
C	-2.75583	4.05268	1.13967
H	-2.61800	2.07252	2.02483
H	-1.18577	2.55905	1.13636
H	-1.68990	-2.19748	-1.90227
H	-2.98210	-2.74874	-0.82915
C	-3.50897	-2.81410	-2.92609
C	-5.47490	-1.26562	-2.54413
H	-5.06825	0.41198	-1.23411
H	-5.02902	-1.15933	-0.43343
C	3.17247	-1.88046	3.86229
H	1.17244	-2.64672	3.76087
C	-3.17291	-1.88011	3.86213

H	-1.17304	-2.64677	3.76070
H	5.12713	-0.97786	3.70794
H	3.20088	-3.86255	-3.03071
H	3.20761	-2.30548	-3.85384
C	5.03224	-2.71866	-2.76601
H	5.26507	-0.67945	-3.45130
H	6.55928	-1.21593	-2.38277
H	3.91764	4.10305	-1.42422
H	2.46382	4.58612	-2.29310
C	2.32983	4.79964	-0.13106
H	3.85294	4.08041	1.22631
H	2.36068	4.55744	2.03047
H	-5.12739	-0.97711	3.70781
H	-2.46246	4.58633	-2.29339
H	-3.91662	4.10354	-1.42491
C	-2.32904	4.79985	-0.13131
H	-2.36054	4.55771	2.03021
H	-3.85267	4.08095	1.22564
H	-3.20797	-2.30529	-3.85387
H	-3.20118	-3.86235	-3.03072
C	-5.03250	-2.71842	-2.76585
H	-6.55947	-1.21565	-2.38249
H	-5.26535	-0.67923	-3.45116
H	3.37707	-2.34772	4.82244
H	-3.37761	-2.34738	4.82226
H	5.53783	-3.14041	-3.64404
H	5.34380	-3.32516	-1.90249
H	2.70734	5.82989	-0.11569
H	1.23183	4.86807	-0.15731
H	-2.70636	5.83018	-0.11607
H	-1.23102	4.86807	-0.15725
H	-5.34398	-3.32490	-1.90228
H	-5.53819	-3.14018	-3.64382
H	-0.00000	0.58054	1.00396

Intermediate 2-5



Zero-point correction=	0.951437 (Hartree/Particle)
Thermal correction to Energy=	0.997776
Thermal correction to Enthalpy=	0.998721
Thermal correction to Gibbs Free Energy=	0.877503

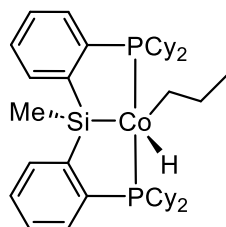
Sum of electronic and zero-point Energies= -3916.331291
 Sum of electronic and thermal Energies= -3916.284951
 Sum of electronic and thermal Enthalpies= -3916.284007
 Sum of electronic and thermal Free Energies= -3916.405224
 Single-point energy (6-311+G(2d,2p)) = -3918.028557919

H	-0.10200	-1.62217	-1.03779
Co	-0.00514	-0.16466	-0.65068
P	2.12666	0.12707	-0.13110
P	-2.10710	0.14491	-0.10539
Si	0.02704	-1.89708	0.80101
C	2.40774	-0.53584	1.56892
C	3.44246	-0.75645	-1.16006
C	2.82515	1.87361	-0.04110
C	-2.55842	-0.85827	1.37587
C	-2.65918	1.85933	0.43260
C	-3.40007	-0.37297	-1.38227
C	0.21004	-3.76140	0.41526
C	1.47353	-1.50341	1.98842
C	-1.61387	-1.82271	1.76679
C	3.47320	-0.17117	2.40456
H	3.37333	-0.27730	-2.14799
C	3.08596	-2.24120	-1.34607
C	4.89455	-0.61576	-0.66711
H	3.75707	1.79924	0.53546
C	3.20115	2.47846	-1.41003
C	1.87964	2.81419	0.72646
C	-3.76621	-0.72108	2.07800
H	-3.73324	1.76877	0.64669
C	-2.48928	2.93053	-0.65935
C	-1.97042	2.31014	1.73564
H	-3.04102	0.09069	-2.31209
C	-3.35045	-1.90378	-1.56943
C	-4.85461	0.08823	-1.17482
H	0.23145	-4.36161	1.33405
H	1.12790	-3.97883	-0.14013
H	-0.63692	-4.11061	-0.18865
C	1.65354	-2.10264	3.24444
C	-1.93310	-2.67014	2.84101
H	4.19655	0.57547	2.09146
C	3.61619	-0.75954	3.66146
H	2.06211	-2.33452	-1.71992
H	3.11346	-2.74058	-0.36774
C	4.06691	-2.94221	-2.29798
C	5.87917	-1.31073	-1.62322
H	4.98104	-1.06965	0.32850

H	5.17500	0.43847	-0.55889
H	2.31414	2.54123	-2.05104
H	3.91930	1.83939	-1.93464
C	3.80114	3.88526	-1.24602
C	2.48222	4.21746	0.88710
H	0.93198	2.88241	0.17992
H	1.63984	2.38836	1.70798
H	-4.48729	0.04028	1.79688
C	-4.05075	-1.55447	3.15834
H	-2.99888	2.63000	-1.58373
H	-1.42472	3.02124	-0.90179
C	-3.02230	4.29482	-0.19401
C	-2.49863	3.67580	2.20217
H	-2.11829	1.56310	2.52255
H	-0.89031	2.37409	1.56669
H	-2.31829	-2.23080	-1.72985
H	-3.69162	-2.38646	-0.64368
C	-4.24223	-2.35957	-2.73373
C	-5.74801	-0.36281	-2.34417
H	-4.91108	1.17824	-1.07837
H	-5.24824	-0.33879	-0.24337
C	2.70629	-1.73183	4.08100
H	0.95187	-2.85837	3.58858
C	-3.13432	-2.53943	3.53580
H	-1.23491	-3.44680	3.14403
H	4.43630	-0.46041	4.30914
H	3.80423	-4.00419	-2.38637
H	3.96373	-2.50943	-3.30447
C	5.51915	-2.78837	-1.82656
H	5.86424	-0.79556	-2.59548
H	6.90156	-1.21579	-1.23505
H	4.75741	3.80749	-0.70693
H	4.03275	4.30546	-2.23302
C	2.86117	4.81958	-0.47251
H	3.37809	4.16266	1.52372
H	1.76889	4.86914	1.40821
H	-4.98520	-1.43867	3.70153
H	-2.86694	5.04230	-0.98259
H	-4.10938	4.22754	-0.03634
C	-2.34866	4.74328	1.10988
H	-1.96929	3.98425	3.11274
H	-3.56092	3.58363	2.47476
H	-3.84308	-1.95862	-3.67729
H	-4.20910	-3.45311	-2.82076
C	-5.68932	-1.88204	-2.55151
H	-6.78202	-0.04047	-2.16551

H	-5.41722	0.14249	-3.26395
H	2.81544	-2.19392	5.05914
H	-3.35670	-3.19828	4.37160
H	6.20694	-3.25351	-2.54414
H	5.64779	-3.32441	-0.87450
H	3.32706	5.80437	-0.34083
H	1.94665	4.98088	-1.06269
H	-2.76764	5.69988	1.44732
H	-1.27874	4.91767	0.92080
H	-6.12623	-2.38250	-1.67459
H	-6.30103	-2.17211	-3.41524
H	0.02261	0.81751	0.47709
H	-0.20571	-2.07931	-3.51868
C	-0.48029	-1.02807	-3.65704
C	0.29939	-0.11177	-2.73853
C	-0.19268	1.12272	-2.29978
H	0.45767	1.97582	-2.14618
H	-1.21547	1.39101	-2.54962
H	1.37478	-0.20458	-2.87317
H	-1.55818	-0.94105	-3.50254
H	-0.27927	-0.76983	-4.70828

Intermediate 2-6



Zero-point correction=	0.954703 (Hartree/Particle)
Thermal correction to Energy=	1.000940
Thermal correction to Enthalpy=	1.001885
Thermal correction to Gibbs Free Energy=	0.880391
Sum of electronic and zero-point Energies=	-3916.336849
Sum of electronic and thermal Energies=	-3916.290611
Sum of electronic and thermal Enthalpies=	-3916.289667
Sum of electronic and thermal Free Energies=	-3916.411161
Single-point energy (6-311+G(2d,2p)) =	-3918.037581846

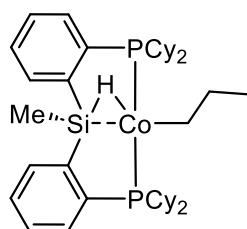
P	2.14569	0.12488	-0.11444
P	-2.08679	0.10248	-0.12421
Si	0.04052	-1.75860	1.00421
C	2.62023	-0.70554	1.46563
C	3.38377	-0.53362	-1.37407
C	2.70154	1.89113	0.20269

C	-2.39389	-0.46662	1.61352
C	-2.75709	1.85854	-0.09047
C	-3.40807	-0.80826	-1.11998
C	-0.06091	-3.63684	0.63551
C	1.66495	-1.59058	1.99913
C	-1.43913	-1.35818	2.14534
C	3.84730	-0.49971	2.11655
H	2.99404	-0.16141	-2.33322
C	3.32259	-2.07529	-1.40254
C	4.84650	-0.06485	-1.26490
C	2.43239	2.81311	-1.00002
C	-3.50447	-0.07868	2.37932
H	-3.76800	1.78609	0.33267
C	-2.88681	2.49729	-1.48547
C	-1.93893	2.78105	0.82988
H	-3.25903	-0.44195	-2.14574
C	-3.12723	-2.32230	-1.11230
C	-4.87579	-0.53901	-0.73887
H	-0.02079	-4.22973	1.55914
H	0.78278	-3.95073	0.00824
H	-0.98534	-3.90290	0.11246
C	1.99308	-2.28688	3.17453
C	-1.64636	-1.85718	3.44108
H	4.57304	0.20513	1.72169
C	4.14175	-1.18822	3.29189
H	2.28546	-2.41638	-1.48636
H	3.69741	-2.46314	-0.44581
C	4.16633	-2.65071	-2.54955
C	5.69555	-0.63728	-2.41381
H	5.27037	-0.39834	-0.30869
H	4.90895	1.02893	-1.28055
H	1.35506	2.81706	-1.20057
H	2.91652	2.42088	-1.90381
C	2.91546	4.24722	-0.73402
C	2.55039	3.90928	1.74419
H	-4.23556	0.62018	1.98471
C	-3.67890	-0.57475	3.67106
H	-3.47262	1.86004	-2.15932
H	-1.88802	2.59081	-1.92499
C	-3.53498	3.88886	-1.39579
C	-2.58197	4.17242	0.93537
H	-1.82923	2.33517	1.82526
H	-0.92963	2.88153	0.41508
H	-2.09303	-2.51429	-1.41132
H	-3.22874	-2.69759	-0.08458
C	-4.09255	-3.08749	-2.02949

C	-5.84127	-1.29813	-1.66561
H	-5.10250	0.53225	-0.78229
H	-5.04680	-0.86136	0.29622
C	3.21365	-2.09111	3.81875
H	1.28633	-2.99770	3.59673
H	5.09096	-1.02253	3.79513
H	4.12517	-3.74716	-2.52850
H	3.73249	-2.33896	-3.51165
C	5.62142	-2.16910	-2.46861
H	5.33551	-0.22177	-3.36690
H	6.73699	-0.30862	-2.30365
H	4.01103	4.25189	-0.62880
H	2.68219	4.88251	-1.59816
C	2.28361	4.82249	0.54030
H	-3.59853	4.33464	-2.39674
H	-4.56890	3.78564	-1.03302
C	-2.75547	4.81260	-0.44917
H	-1.96913	4.81691	1.57870
H	-3.56415	4.08630	1.42410
H	-3.91284	-2.78932	-3.07313
H	-3.88441	-4.16357	-1.97165
C	-5.55643	-2.80551	-1.66687
H	-6.87703	-1.10431	-1.35814
H	-5.74054	-0.90815	-2.68962
H	3.44343	-2.63538	4.73164
H	6.19869	-2.54780	-3.32156
H	6.08802	-2.58542	-1.56355
H	2.66414	5.83357	0.73382
H	1.19735	4.91783	0.39263
H	-3.25916	5.78386	-0.36305
H	-1.76214	5.01059	-0.87903
H	-5.76551	-3.21271	-0.66655
H	-6.23026	-3.32094	-2.36298
C	0.10068	0.66046	-2.44962
C	0.19482	-0.80175	-2.74191
H	0.98090	1.23638	-2.73349
H	-0.79982	1.12898	-2.84803
C	-0.82415	-1.39737	-3.71907
H	1.20174	-1.10553	-3.04060
H	-1.83975	-1.06796	-3.48671
H	-0.81235	-2.49433	-3.71309
H	-0.59273	-1.06099	-4.73617
C	2.07107	2.47265	1.48384
H	3.78775	1.84675	0.36411
H	2.05742	4.30455	2.64151
H	3.62980	3.90079	1.95904

H	2.30727	1.83889	2.34476
H	0.98019	2.46702	1.38380
C	-2.74938	-1.47166	4.20218
H	-0.92901	-2.55079	3.87288
H	-4.53618	-0.26023	4.26085
H	-2.88294	-1.86178	5.20834
Co	0.03261	-0.16438	-0.62410
H	0.05247	-1.44558	-1.75383
H	0.00019	0.94929	0.31231

Intermediate 2-5'



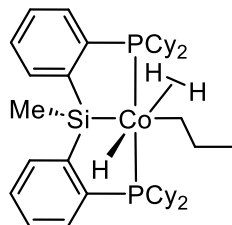
Zero-point correction=	0.954958 (Hartree/Particle)
Thermal correction to Energy=	1.001882
Thermal correction to Enthalpy=	1.002826
Thermal correction to Gibbs Free Energy=	0.877988
Sum of electronic and zero-point Energies=	-3916.308831
Sum of electronic and thermal Energies=	-3916.261907
Sum of electronic and thermal Enthalpies=	-3916.260963
Sum of electronic and thermal Free Energies=	-3916.385801
Single-point energy (6-311+G(2d,2p)) =	-3918.010197208

P	2.21893	0.01652	-0.07397
P	-2.21885	0.01642	-0.07395
Si	0.00014	-1.91426	0.88807
C	2.65363	-1.06496	1.37241
C	3.21733	-0.62948	-1.53091
C	3.13043	1.58323	0.41892
C	-2.65326	-1.06482	1.37274
C	-3.13103	1.58296	0.41829
C	-3.21707	-0.63039	-1.53070
C	0.00009	-3.72174	0.24473
C	1.61320	-1.86355	1.88751
C	-1.61277	-1.86340	1.88773
C	3.91761	-1.08684	1.98526
H	3.08297	0.15869	-2.28747
C	2.59210	-1.91809	-2.09792
C	4.72567	-0.82745	-1.29490
C	3.47891	2.53100	-0.74583
C	-3.91711	-1.08659	1.98585

H	-4.08823	1.25821	0.84623
C	-3.47938	2.53021	-0.74693
C	-2.34786	2.28421	1.54777
H	-3.08292	0.15757	-2.28753
C	-2.59153	-1.91901	-2.09731
C	-4.72536	-0.82867	-1.29463
H	0.00034	-4.43031	1.08280
H	0.88611	-3.93112	-0.36581
H	-0.88616	-3.93125	-0.36542
C	1.87126	-2.66204	3.01387
C	-1.87065	-2.66177	3.01422
H	4.73296	-0.48490	1.59796
C	4.14941	-1.87649	3.11020
H	1.52791	-1.75570	-2.29904
H	2.65402	-2.71294	-1.34072
C	3.30841	-2.37798	-3.37695
C	5.44013	-1.27050	-2.58280
H	4.86929	-1.59799	-0.52635
H	5.18903	0.09016	-0.91321
H	2.58127	2.80303	-1.30475
H	4.14261	2.02331	-1.45488
C	4.17409	3.80432	-0.23313
C	3.05384	3.56243	2.02290
H	-4.73252	-0.48466	1.59864
C	-4.14874	-1.87611	3.11091
H	-4.14290	2.02212	-1.45587
H	-2.58169	2.80210	-1.30583
C	-4.17486	3.80366	-0.23496
C	-3.05552	3.56277	2.02160
H	-2.22473	1.59261	2.39026
H	-1.33757	2.52355	1.19798
H	-1.52737	-1.75644	-2.29845
H	-2.65330	-2.71364	-1.33988
C	-3.30771	-2.37946	-3.37622
C	-5.43972	-1.27234	-2.58237
H	-5.18897	0.08894	-0.91326
H	-4.86878	-1.59899	-0.52581
C	3.12015	-2.66290	3.63179
H	1.08854	-3.29870	3.41812
H	5.13033	-1.87632	3.57843
H	2.86460	-3.31631	-3.73350
H	3.14145	-1.63204	-4.16826
C	4.81702	-2.55066	-3.15499
H	5.37257	-0.46604	-3.33030
H	6.50846	-1.42164	-2.38111
H	5.15900	3.53582	0.17867

H	4.36264	4.48397	-1.07383
C	3.35545	4.51208	0.85539
H	-4.36317	4.48296	-1.07599
H	-5.15990	3.53521	0.17658
C	-3.35671	4.51193	0.85360
H	-2.44111	4.06784	2.77783
H	-4.00016	3.29154	2.51692
H	-3.14095	-1.63369	-4.16773
H	-2.86363	-3.31776	-3.73250
C	-4.81627	-2.55250	-3.15419
H	-6.50800	-1.42372	-2.38062
H	-5.37241	-0.46809	-3.33012
H	3.29467	-3.27732	4.51154
H	5.31244	-2.83033	-4.09338
H	4.98665	-3.37886	-2.45086
H	3.89372	5.39805	1.21580
H	2.41086	4.87338	0.42481
H	-3.89523	5.39799	1.21343
H	-2.41199	4.87315	0.42325
H	-4.98566	-3.38054	-2.44983
H	-5.31161	-2.83258	-4.09250
C	0.00049	1.67400	-1.56771
C	-0.00038	3.16639	-1.21088
H	-0.87114	1.49454	-2.22151
H	0.87277	1.49558	-2.22090
C	-0.00079	4.09054	-2.43886
H	-0.86417	3.41962	-0.59112
H	0.88232	3.91126	-3.06607
H	-0.00129	5.15169	-2.15440
H	-0.88373	3.91046	-3.06609
C	2.34657	2.28396	1.54825
H	4.08756	1.25867	0.84716
H	2.43902	4.06714	2.77903
H	3.99829	3.29114	2.51855
H	2.22307	1.59204	2.39043
H	1.33645	2.52330	1.19796
C	-3.11941	-2.66252	3.63239
H	-1.08786	-3.29841	3.41838
H	-5.12956	-1.87586	3.57933
H	-3.29380	-3.27681	4.51225
Co	0.00016	0.00314	-0.39134
H	0.86316	3.42051	-0.59109
H	0.00020	-1.41302	-0.78916

Intermediate 2-7



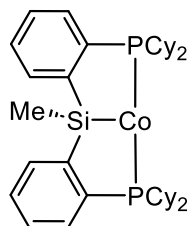
Zero-point correction=	0.972440 (Hartree/Particle)
Thermal correction to Energy=	1.019786
Thermal correction to Enthalpy=	1.020730
Thermal correction to Gibbs Free Energy=	0.896632
Sum of electronic and zero-point Energies=	-3917.497036
Sum of electronic and thermal Energies=	-3917.449690
Sum of electronic and thermal Enthalpies=	-3917.448746
Sum of electronic and thermal Free Energies=	-3917.572844
Single-point energy (6-311+G(2d,2p)) =	-3919.222611731

P	-2.17194	0.04414	0.10045
P	2.12224	0.02036	0.04857
Si	-0.04714	-2.04837	-0.55673
C	-2.67298	-1.21440	-1.16483
C	-3.31115	-0.25260	1.56960
C	-2.85001	1.59875	-0.71220
C	2.44210	-1.05743	-1.43311
C	2.84697	1.65638	-0.53290
C	3.38187	-0.57287	1.32190
C	0.04427	-3.74185	0.33723
C	-1.69316	-2.16515	-1.50974
C	1.45128	-2.01632	-1.73099
C	-3.93571	-1.24509	-1.77961
H	-2.93183	0.45510	2.32245
C	-3.11239	-1.67947	2.12127
C	-4.81333	0.02369	1.36741
C	-2.87749	2.86665	0.16080
C	3.59242	-0.96629	-2.23325
H	3.80393	1.39842	-1.00519
C	3.16408	2.67510	0.57830
C	1.96433	2.30279	-1.61651
H	3.23856	0.11740	2.16544
C	3.03728	-1.98859	1.81991
C	4.86131	-0.51193	0.89645
H	0.00102	-4.57063	-0.38197
H	-0.80122	-3.86277	1.02589
H	0.96839	-3.85423	0.91387
C	-2.02332	-3.14882	-2.45670

C	1.65542	-2.87147	-2.82532
H	-4.69176	-0.50564	-1.53582
C	-4.23491	-2.22098	-2.72857
H	-2.05044	-1.88059	2.29046
H	-3.45165	-2.40432	1.36801
C	-3.89529	-1.89435	3.42587
C	-5.59489	-0.17605	2.67735
H	-5.21101	-0.66575	0.61152
H	-4.98090	1.03980	0.99460
H	-1.85349	3.16854	0.39703
H	-3.37710	2.67758	1.11851
C	-3.58203	4.01584	-0.57920
C	-2.81649	3.04926	-2.79339
H	4.36090	-0.22945	-2.02362
C	3.76566	-1.81554	-3.32578
H	3.80969	2.23232	1.34514
H	2.23997	2.97526	1.07857
C	3.84416	3.92338	-0.00837
C	2.63237	3.55596	-2.20240
H	1.74786	1.58142	-2.41315
H	1.00125	2.57537	-1.17018
H	1.99701	-2.02869	2.15535
H	3.12606	-2.69551	0.98317
C	3.96650	-2.43009	2.96137
C	5.79079	-0.93846	2.04542
H	5.13443	0.49516	0.56220
H	5.01882	-1.18494	0.04403
C	-3.27586	-3.17906	-3.06693
H	-1.29298	-3.90926	-2.72308
H	-5.21305	-2.23379	-3.20258
H	-3.75786	-2.92569	3.77503
H	-3.47925	-1.24045	4.20673
C	-5.38767	-1.58530	3.24745
H	-5.25981	0.56897	3.41429
H	-6.66202	0.01347	2.50402
H	-4.63558	3.74889	-0.75333
H	-3.58719	4.91433	0.05098
C	-2.90290	4.31150	-1.92399
H	4.04636	4.64524	0.79317
H	4.82096	3.64209	-0.43053
C	2.98521	4.56924	-1.10460
H	1.97022	4.01565	-2.94736
H	3.54894	3.26420	-2.73691
H	3.79122	-1.78630	3.83622
H	3.71415	-3.45274	3.26969
C	5.44364	-2.34264	2.55632

H	6.83503	-0.90055	1.70937
H	5.70069	-0.21704	2.87122
H	-3.50708	-3.94395	-3.80427
H	-5.91766	-1.69287	4.20226
H	-5.82863	-2.32093	2.55848
H	-3.43896	5.10741	-2.45662
H	-1.88664	4.68847	-1.73568
H	3.50356	5.43560	-1.53490
H	2.05636	4.94991	-0.65453
H	5.64403	-3.07519	1.76043
H	6.08918	-2.61276	3.40159
C	-0.08222	1.70172	1.66867
C	0.74021	1.77100	2.96594
H	-1.11932	1.90632	1.96381
H	0.20289	2.53544	1.01376
C	0.67803	3.14073	3.65921
H	0.37949	1.00743	3.67368
H	1.07868	3.92919	3.00875
H	1.25202	3.15617	4.59554
H	-0.35894	3.41110	3.89647
C	-2.13515	1.89253	-2.04541
H	-3.89304	1.34981	-0.95297
H	-2.27105	3.26218	-3.72166
H	-3.83049	2.74196	-3.09054
H	-2.11418	0.99751	-2.67688
H	-1.09119	2.15453	-1.83907
C	2.79470	-2.77381	-3.62275
H	0.90885	-3.62335	-3.06879
H	4.65572	-1.72690	-3.94347
H	2.92600	-3.43768	-4.47377
Co	-0.02545	-0.05749	0.56061
H	1.79259	1.51924	2.78467
H	-0.02123	0.58687	-0.75193
H	-0.00573	-1.17201	1.74313
H	-0.06453	-0.44851	2.13835

Intermediate 2-6'



Zero-point correction=

0.850387 (Hartree/Particle)

Thermal correction to Energy=

0.892654

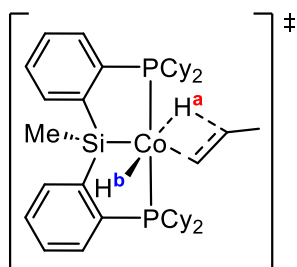
Thermal correction to Enthalpy= 0.893598
 Thermal correction to Gibbs Free Energy= 0.777158
 Sum of electronic and zero-point Energies= -3797.283646
 Sum of electronic and thermal Energies= -3797.241379
 Sum of electronic and thermal Enthalpies= -3797.240435
 Sum of electronic and thermal Free Energies= -3797.356875
 Single-point energy (6-311+G(2d,2p)) = -3798.820298441

Co	-0.00001	-0.02303	-0.56169
P	2.13419	0.12020	-0.23515
P	-2.13420	0.12021	-0.23512
Si	-0.00000	-1.71130	0.84227
C	2.56893	-0.66725	1.37301
C	3.28305	-0.66078	-1.50892
C	2.78004	1.87735	-0.09523
C	-2.56892	-0.66725	1.37304
C	-2.78003	1.87737	-0.09519
C	-3.28308	-0.66076	-1.50888
C	-0.00000	-3.54736	0.29477
C	1.58227	-1.52381	1.90949
C	-1.58226	-1.52381	1.90950
C	3.77509	-0.44692	2.05389
H	3.07890	-0.08283	-2.42380
C	2.83867	-2.11138	-1.77534
C	4.79404	-0.59811	-1.22771
H	3.87136	1.85547	0.03669
C	2.46272	2.65037	-1.39138
C	2.15676	2.58778	1.12144
C	-3.77509	-0.44693	2.05393
H	-3.87134	1.85549	0.03683
C	-2.46284	2.65034	-1.39139
C	-2.15664	2.58784	1.12139
H	-3.07897	-0.08277	-2.42375
C	-2.83866	-2.11134	-1.77536
C	-4.79406	-0.59815	-1.22762
H	-0.00000	-4.20812	1.17241
H	0.88583	-3.78817	-0.30213
H	-0.88584	-3.78817	-0.30213
C	1.86041	-2.16390	3.12726
C	-1.86039	-2.16391	3.12727
H	4.52304	0.22807	1.64672
C	4.01810	-1.08131	3.27229
H	1.76731	-2.12951	-2.00847
H	2.96966	-2.70070	-0.85659
C	3.65067	-2.75472	-2.90925
C	5.60340	-1.23609	-2.37009

H	5.00930	-1.13530	-0.29480
H	5.12167	0.43870	-1.08116
H	1.37681	2.60573	-1.57256
H	2.94205	2.17364	-2.25516
C	2.89774	4.12143	-1.30328
C	2.59310	4.05781	1.20887
H	1.06309	2.53063	1.03764
H	2.42073	2.05979	2.04393
H	-4.52304	0.22806	1.64676
C	-4.01809	-1.08133	3.27232
H	-2.94224	2.17357	-2.25512
H	-1.37694	2.60569	-1.57268
C	-2.89785	4.12140	-1.30332
C	-2.59297	4.05787	1.20881
H	-2.42053	2.05989	2.04393
H	-1.06298	2.53068	1.03749
H	-1.76730	-2.12942	-2.00854
H	-2.96960	-2.70069	-0.85663
C	-3.65067	-2.75466	-2.90927
C	-5.60344	-1.23612	-2.37000
H	-5.12172	0.43865	-1.08103
H	-5.00927	-1.13537	-0.29472
C	3.05979	-1.94588	3.80679
H	1.12974	-2.84237	3.56125
C	-3.05977	-1.94590	3.80681
H	-1.12972	-2.84239	3.56126
H	4.95007	-0.90173	3.80227
H	3.33774	-3.79768	-3.04664
H	3.42800	-2.23374	-3.85263
C	5.15922	-2.68117	-2.63499
H	5.46835	-0.64096	-3.28576
H	6.67421	-1.20285	-2.13074
H	3.99444	4.16840	-1.22903
H	2.62445	4.64658	-2.22754
C	2.27764	4.81949	-0.08561
H	3.67546	4.10576	1.40199
H	2.10266	4.53975	2.06426
H	-4.95005	-0.90175	3.80231
H	-2.62464	4.64651	-2.22763
H	-3.99453	4.16837	-1.22897
C	-2.27763	4.81951	-0.08574
H	-2.10245	4.53985	2.06413
H	-3.67531	4.10584	1.40203
H	-3.42805	-2.23365	-3.85264
H	-3.33772	-3.79761	-3.04671
C	-5.15922	-2.68117	-2.63496

H	-6.67424	-1.20291	-2.13061
H	-5.46843	-0.64095	-3.28565
H	3.24782	-2.44496	4.75444
H	-3.24779	-2.44498	4.75446
H	5.72264	-3.10490	-3.47609
H	5.39658	-3.29759	-1.75519
H	2.63338	5.85539	-0.01815
H	1.18641	4.87075	-0.21708
H	-2.63337	5.85541	-0.01828
H	-1.18641	4.87076	-0.21731
H	-5.39653	-3.29763	-1.75517
H	-5.72266	-3.10488	-3.47605

Transition State 2



Zero-point correction=	0.950851 (Hartree/Particle)
Thermal correction to Energy=	0.996887
Thermal correction to Enthalpy=	0.997831
Thermal correction to Gibbs Free Energy=	0.876971
Sum of electronic and zero-point Energies=	-3916.329685
Sum of electronic and thermal Energies=	-3916.283650
Sum of electronic and thermal Enthalpies=	-3916.282706
Sum of electronic and thermal Free Energies=	-3916.403566
Single-point energy (6-311+G(2d,2p)) =	-3918.026490793

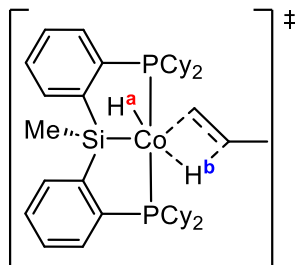
P	2.14595	0.12788	-0.11882
P	-2.07301	0.08591	-0.17046
Si	0.04452	-1.82210	0.91222
C	2.63559	-0.79312	1.40151
C	3.42254	-0.40046	-1.40423
C	2.64040	1.88354	0.33165
C	-2.34795	-0.46652	1.57695
C	-2.73672	1.84663	-0.13314
C	-3.44376	-0.81588	-1.11352
C	-0.12738	-3.69549	0.56734
C	1.68783	-1.71468	1.87984
C	-1.39771	-1.37644	2.08274
C	3.86358	-0.62318	2.06053

H	3.01214	-0.00911	-2.34717
C	3.44750	-1.94063	-1.50380
C	4.85759	0.14340	-1.27819
C	2.34055	2.88443	-0.79880
C	-3.42649	-0.05591	2.37513
H	-3.73071	1.77211	0.32720
C	-2.93092	2.47922	-1.52382
C	-1.89543	2.78329	0.75026
H	-3.31368	-0.47633	-2.15131
C	-3.19535	-2.33463	-1.08109
C	-4.89699	-0.51014	-0.70458
H	-0.10315	-4.27618	1.49853
H	0.70129	-4.04537	-0.06109
H	-1.06310	-3.93603	0.05356
C	2.02328	-2.48872	3.00290
C	-1.57264	-1.86963	3.38433
H	4.58445	0.10926	1.70955
C	4.16568	-1.38667	3.18646
H	2.42999	-2.33580	-1.59400
H	3.85440	-2.34968	-0.56933
C	4.31163	-2.41272	-2.68240
C	5.72865	-0.32591	-2.45724
H	5.30709	-0.21051	-0.34126
H	4.85972	1.23842	-1.24242
H	1.26334	2.86828	-1.00231
H	2.84021	2.58008	-1.72794
C	2.77057	4.31111	-0.42378
C	2.41448	3.77333	2.02025
H	-4.15685	0.65515	2.00168
C	-3.56938	-0.54426	3.67403
H	-3.52598	1.82911	-2.17659
H	-1.95240	2.60050	-2.00080
C	-3.60426	3.85703	-1.40887
C	-2.55617	4.16460	0.87945
H	-1.74023	2.34155	1.74135
H	-0.90410	2.89635	0.29766
H	-2.17116	-2.55166	-1.39383
H	-3.28926	-2.68844	-0.04500
C	-4.19242	-3.09481	-1.96769
C	-5.89787	-1.26528	-1.59685
H	-5.10580	0.56398	-0.76193
H	-5.05085	-0.81131	0.33962
C	3.24500	-2.32896	3.65452
H	1.32234	-3.23138	3.37795
H	5.11602	-1.25008	3.69623
H	4.33182	-3.50953	-2.71387

H	3.85307	-2.08024	-3.62583
C	5.73843	-1.85512	-2.58623
H	5.33924	0.11453	-3.38730
H	6.75129	0.05410	-2.33625
H	3.86505	4.34660	-0.31421
H	2.51585	5.00095	-1.23866
C	2.11675	4.76514	0.88791
H	-3.71963	4.29982	-2.40648
H	-4.61928	3.73205	-1.00246
C	-2.80358	4.79786	-0.49719
H	-1.92579	4.82192	1.49231
H	-3.51343	4.06425	1.41278
H	-4.02676	-2.81636	-3.01924
H	-4.00484	-4.17394	-1.89691
C	-5.64309	-2.77794	-1.58134
H	-6.92254	-1.04616	-1.26966
H	-5.81265	-0.89309	-2.62891
H	3.48167	-2.93221	4.52766
H	6.32899	-2.15922	-3.45973
H	6.23488	-2.28815	-1.70516
H	2.46146	5.77131	1.15868
H	1.02813	4.83376	0.74372
H	-3.32292	5.75871	-0.39007
H	-1.83458	5.01580	-0.97062
H	-5.84014	-3.16624	-0.57109
H	-6.34119	-3.28951	-2.25615
C	0.13000	0.72375	-2.51591
C	0.25380	-0.67154	-2.74646
H	1.00667	1.35673	-2.61057
H	-0.79346	1.20626	-2.82184
C	-0.77972	-1.43205	-3.55695
H	1.26008	-1.03943	-2.93497
H	-1.78833	-1.04813	-3.38783
H	-0.78005	-2.50437	-3.33408
H	-0.55866	-1.31385	-4.62677
C	1.98939	2.34323	1.65152
H	3.72752	1.86502	0.49237
H	1.90565	4.08164	2.94245
H	3.49307	3.78884	2.23877
H	2.25334	1.65651	2.46225
H	0.89966	2.30004	1.55029
C	-2.64187	-1.45767	4.17931
H	-0.85465	-2.57509	3.79606
H	-4.40097	-0.21032	4.28937
H	-2.75007	-1.84022	5.19138
Co	0.04896	-0.22971	-0.67757

H	-0.01693	0.92419	0.25512
H	0.12671	-1.58107	-1.35480

Transition State 2'



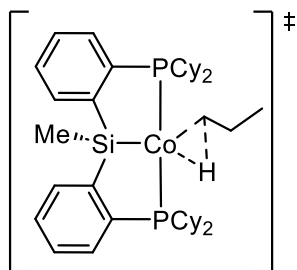
Zero-point correction=	0.951677 (Hartree/Particle)
Thermal correction to Energy=	0.997531
Thermal correction to Enthalpy=	0.998476
Thermal correction to Gibbs Free Energy=	0.875660
Sum of electronic and zero-point Energies=	-3916.316101
Sum of electronic and thermal Energies=	-3916.270246
Sum of electronic and thermal Enthalpies=	-3916.269302
Sum of electronic and thermal Free Energies=	-3916.392118
Single-point energy (6-311+G(2d,2p)) =	-3918.014136044

H	-0.78573	-1.82875	-0.96883
Co	-0.05935	-0.52386	-0.97296
P	1.91506	0.22858	-0.22865
P	-1.98705	0.08347	-0.04923
Si	0.11953	-2.03644	0.70157
C	2.12581	-0.19295	1.55167
C	3.46147	-0.59147	-0.99154
C	2.43972	2.03070	-0.37610
C	-2.48588	-1.07486	1.29931
C	-2.36447	1.73467	0.74987
C	-3.36849	-0.06244	-1.34189
C	0.57712	-3.87766	0.50115
C	1.34972	-1.28822	1.97626
C	-1.55056	-2.07466	1.61996
C	3.00917	0.44242	2.43542
H	3.39588	-0.34715	-2.06145
C	3.38625	-2.12093	-0.85866
C	4.83056	-0.09415	-0.48750
H	3.47716	2.09480	-0.02657
C	2.40986	2.47358	-1.85303
C	1.61688	2.99896	0.48237
C	-3.69531	-0.98285	2.00527
H	-3.41927	1.69010	1.05456
C	-2.21827	2.91314	-0.22890

C	-1.53420	1.93958	2.03031
H	-2.96857	0.51517	-2.18821
C	-3.53472	-1.52233	-1.80898
C	-4.75335	0.52148	-0.99502
H	0.63536	-4.37350	1.47868
H	1.54017	-4.02876	0.00683
H	-0.18936	-4.39506	-0.08826
C	1.49450	-1.73264	3.29913
C	-1.88027	-2.99851	2.62463
H	3.60939	1.28666	2.10732
C	3.11862	-0.00051	3.75429
H	2.43011	-2.47569	-1.24358
H	3.41932	-2.38944	0.20583
C	4.53944	-2.82430	-1.58891
C	5.99227	-0.79973	-1.21071
H	4.91036	-0.28203	0.59147
H	4.94135	0.98516	-0.63272
H	1.38022	2.38456	-2.22557
H	3.02486	1.80957	-2.47236
C	2.89059	3.92360	-2.02237
C	2.11530	4.44439	0.32832
H	0.57139	2.94450	0.17066
H	1.64794	2.70135	1.53596
H	-4.40573	-0.19154	1.78877
C	-3.99790	-1.90383	3.00755
H	-2.87341	2.77312	-1.09740
H	-1.19652	2.93728	-0.62440
C	-2.54920	4.25070	0.45378
C	-1.86645	3.28309	2.69901
H	-1.72837	1.12065	2.73125
H	-0.46792	1.88973	1.79152
H	-2.56189	-1.94921	-2.06494
H	-3.92619	-2.12053	-0.97416
C	-4.49040	-1.62881	-3.00710
C	-5.70682	0.43475	-2.20001
H	-4.68015	1.56474	-0.67192
H	-5.19196	-0.04200	-0.16195
C	2.36243	-1.09312	4.18566
H	0.90366	-2.57389	3.65446
C	-3.09107	-2.92164	3.31192
H	-1.18268	-3.79364	2.87746
H	3.79150	0.50497	4.44233
H	4.45526	-3.91029	-1.45338
H	4.45330	-2.63617	-2.66973
C	5.90151	-2.32535	-1.09329
H	5.97674	-0.51767	-2.27429

H	6.94719	-0.43903	-0.80678
H	3.95560	3.98504	-1.75311
H	2.81807	4.21868	-3.07704
C	2.09032	4.89037	-1.13956
H	3.14295	4.51834	0.71480
H	1.50447	5.11867	0.94214
H	-4.93840	-1.82806	3.54737
H	-2.38834	5.07825	-0.24921
H	-3.61881	4.26443	0.71203
C	-1.72205	4.46508	1.72958
H	-1.22354	3.43015	3.57622
H	-2.90093	3.25059	3.07325
H	-4.04430	-1.11300	-3.87086
H	-4.60494	-2.68098	-3.29766
C	-5.85888	-1.00783	-2.69833
H	-6.68525	0.85111	-1.92733
H	-5.31526	1.06289	-3.01427
H	2.44490	-1.43896	5.21323
H	-3.32668	-3.64697	4.08689
H	6.71600	-2.80114	-1.65432
H	6.03153	-2.61621	-0.04035
H	2.48183	5.91075	-1.23815
H	1.04722	4.91903	-1.48863
H	-2.02532	5.39798	2.22194
H	-0.66480	4.58580	1.45951
H	-6.35954	-1.60557	-1.92218
H	-6.50516	-1.04025	-3.58478
H	-0.29424	0.78787	-1.64579
H	0.80749	-3.43708	-2.45597
C	0.30171	-2.71426	-3.10474
C	0.65534	-1.28080	-2.75699
C	-0.23654	-0.21045	-3.03572
H	0.15734	0.69716	-3.48951
H	-1.25193	-0.43614	-3.35550
H	1.70959	-1.06114	-2.91244
H	-0.77490	-2.89470	-3.02170
H	0.59851	-2.94425	-4.13974

Transition State 3'



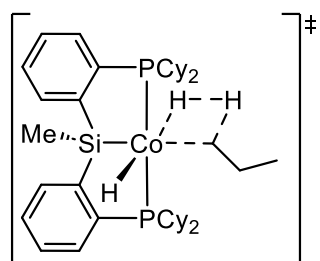
Zero-point correction=	0.953780 (Hartree/Particle)
Thermal correction to Energy=	0.999865
Thermal correction to Enthalpy=	1.000809
Thermal correction to Gibbs Free Energy=	0.879627
Sum of electronic and zero-point Energies=	-3916.323571
Sum of electronic and thermal Energies=	-3916.277485
Sum of electronic and thermal Enthalpies=	-3916.276541
Sum of electronic and thermal Free Energies=	-3916.397723
Single-point energy (6-311+G(2d,2p)) =	-3918.023045923

P	2.10585	0.11857	-0.08887
P	-2.05679	0.10844	-0.10272
Si	0.03192	-1.74642	0.98742
C	2.60331	-0.72030	1.47789
C	3.37969	-0.50842	-1.34172
C	2.65445	1.88551	0.24745
C	-2.37773	-0.44801	1.63413
C	-2.70075	1.87667	-0.07745
C	-3.42289	-0.77086	-1.08160
C	-0.08725	-3.61564	0.57614
C	1.65309	-1.62149	1.98855
C	-1.43145	-1.35543	2.14987
C	3.82636	-0.52056	2.13705
H	2.98756	-0.14663	-2.30496
C	3.35194	-2.05068	-1.37605
C	4.83272	-0.01285	-1.22697
C	2.42897	2.81431	-0.95862
C	-3.47294	-0.04556	2.41344
H	-3.70888	1.83916	0.35626
C	-2.82428	2.49814	-1.48067
C	-1.83672	2.77602	0.82117
H	-3.27137	-0.41160	-2.11074
C	-3.18150	-2.29127	-1.07734
C	-4.88004	-0.46527	-0.68921
H	-0.04009	-4.22343	1.48971
H	0.74948	-3.92160	-0.06418
H	-1.01825	-3.86817	0.05888

C	1.97989	-2.34719	3.14599
C	-1.63080	-1.86298	3.44313
H	4.54935	0.19713	1.76073
C	4.11966	-1.23401	3.29810
H	2.32210	-2.41310	-1.46150
H	3.73424	-2.43419	-0.42051
C	4.20861	-2.60520	-2.52381
C	5.69712	-0.56185	-2.37608
H	5.25980	-0.34457	-0.27158
H	4.87603	1.08202	-1.23420
H	1.36195	2.81358	-1.21353
H	2.96304	2.43830	-1.84117
C	2.86705	4.25582	-0.65672
C	2.38306	3.88957	1.79787
H	-4.19662	0.66755	2.03024
C	-3.63838	-0.54560	3.70521
H	-3.45652	1.88051	-2.13011
H	-1.83116	2.53347	-1.94525
C	-3.39293	3.92522	-1.41050
C	-2.39716	4.20371	0.90174
H	-1.74755	2.34389	1.82459
H	-0.82506	2.80681	0.40231
H	-2.15663	-2.50782	-1.39219
H	-3.27651	-2.66497	-0.04831
C	-4.17710	-3.03454	-1.98038
C	-5.87559	-1.20149	-1.60254
H	-5.08116	0.61123	-0.73196
H	-5.04838	-0.78086	0.34846
C	3.19703	-2.15747	3.79888
H	1.27679	-3.07338	3.54766
H	5.06504	-1.07306	3.81013
H	4.18994	-3.70247	-2.50760
H	3.77047	-2.29855	-3.48584
C	5.65365	-2.09468	-2.43899
H	5.33173	-0.14894	-3.32845
H	6.73181	-0.21347	-2.26180
H	3.95472	4.28174	-0.49201
H	2.66728	4.89460	-1.52680
C	2.15367	4.80354	0.58655
H	-3.44887	4.35374	-2.41951
H	-4.42455	3.88545	-1.02980
C	-2.54930	4.82285	-0.49456
H	-1.74154	4.82584	1.52477
H	-3.37737	4.18535	1.40143
H	-4.00349	-2.74331	-3.02720
H	-3.99512	-4.11547	-1.92284

C	-5.62914	-2.71550	-1.60155
H	-6.90281	-0.98037	-1.28469
H	-5.77630	-0.81789	-2.62923
H	3.42814	-2.72190	4.69911
H	6.23978	-2.45766	-3.29286
H	6.12718	-2.50594	-1.53523
H	2.49607	5.82300	0.80559
H	1.07456	4.87193	0.38212
H	-2.99468	5.82347	-0.42548
H	-1.55139	4.95348	-0.93983
H	-5.83615	-3.11372	-0.59718
H	-6.32387	-3.21669	-2.28757
C	0.11347	0.51169	-2.56504
C	0.18575	-0.97522	-2.81936
H	1.00231	1.05573	-2.88953
H	-0.77307	0.97679	-3.00017
C	-0.85724	-1.52815	-3.79757
H	1.18867	-1.26932	-3.14211
H	-1.86711	-1.21700	-3.51640
H	-0.83885	-2.62398	-3.82810
H	-0.66361	-1.15888	-4.81169
C	1.96443	2.43958	1.50900
H	3.73467	1.84975	0.44671
H	1.83326	4.26559	2.67019
H	3.44977	3.91305	2.06789
H	2.19877	1.80750	2.37189
H	0.87960	2.38588	1.37437
C	-2.71850	-1.46261	4.21913
H	-0.91941	-2.56993	3.86275
H	-4.48168	-0.21926	4.30870
H	-2.84643	-1.85571	5.22487
Co	0.02642	-0.21648	-0.70536
H	0.04561	-1.56833	-1.83242
H	0.00541	1.20663	-1.13753

Transition State 4



Zero-point correction=
Thermal correction to Energy=

0.970571 (Hartree/Particle)
1.017478

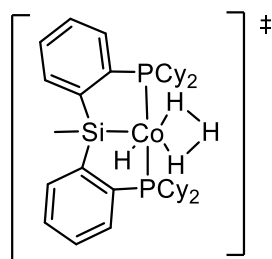
Thermal correction to Enthalpy= 1.018422
 Thermal correction to Gibbs Free Energy= 0.891915
 Sum of electronic and zero-point Energies= -3917.493453
 Sum of electronic and thermal Energies= -3917.446546
 Sum of electronic and thermal Enthalpies= -3917.445602
 Sum of electronic and thermal Free Energies= -3917.572109
 Single-point energy (6-311+G(2d,2p)) = -3919.218166957

P	-2.17469	0.06946	0.05930
P	2.10898	0.00430	-0.00401
Si	-0.07537	-2.05281	-0.46703
C	-2.67675	-1.21626	-1.16844
C	-3.30556	-0.20488	1.54103
C	-2.85669	1.62131	-0.74969
C	2.41490	-1.14090	-1.42852
C	2.85739	1.61243	-0.63272
C	3.35660	-0.54580	1.30011
C	-0.01499	-3.68316	0.52764
C	-1.71152	-2.20373	-1.44118
C	1.41992	-2.11440	-1.65336
C	-3.92681	-1.24655	-1.80715
H	-2.93561	0.52464	2.27743
C	-3.08200	-1.61354	2.12763
C	-4.81033	0.04893	1.33341
C	-2.79231	2.88072	0.13305
C	3.55597	-1.09569	-2.24438
H	3.82684	1.33489	-1.06753
C	3.14337	2.66277	0.45737
C	2.01147	2.23130	-1.76008
H	3.22376	0.18700	2.10883
C	2.98193	-1.92651	1.86802
C	4.83729	-0.53038	0.87654
H	-0.06418	-4.55346	-0.14045
H	-0.86770	-3.74222	1.21385
H	0.90123	-3.76683	1.11965
C	-2.04675	-3.22942	-2.34016
C	1.61426	-3.03763	-2.69254
H	-4.66777	-0.47633	-1.61665
C	-4.22920	-2.26358	-2.71100
H	-2.01528	-1.78052	2.29637
H	-3.40639	-2.36319	1.39211
C	-3.86490	-1.81132	3.43442
C	-5.59243	-0.14077	2.64470
H	-5.19741	-0.65492	0.58498
H	-4.99001	1.05845	0.94738
H	-1.74509	3.12387	0.33525

H	-3.27033	2.70516	1.10455
C	-3.45877	4.07646	-0.56666
C	-2.84973	3.09073	-2.81904
H	4.32417	-0.34516	-2.08747
C	3.71753	-2.01147	-3.28380
H	3.76642	2.24249	1.25470
H	2.20344	2.97844	0.92310
C	3.84039	3.89627	-0.14063
C	2.70452	3.46262	-2.36283
H	1.80978	1.48722	-2.53935
H	1.03722	2.52426	-1.35124
H	1.93905	-1.91912	2.19394
H	3.05898	-2.67674	1.06850
C	3.90103	-2.32843	3.03152
C	5.75698	-0.92244	2.04577
H	5.13007	0.45629	0.49981
H	4.98378	-1.24217	0.05395
C	-3.28747	-3.26167	-2.97478
H	-1.33067	-4.02015	-2.55083
H	-5.19619	-2.27810	-3.20728
H	-3.70962	-2.83125	3.80871
H	-3.46397	-1.13161	4.20122
C	-5.36205	-1.53420	3.24393
H	-5.27293	0.62415	3.36822
H	-6.66218	0.02685	2.46476
H	-4.53205	3.87100	-0.69737
H	-3.38639	4.96693	0.07077
C	-2.82326	4.34710	-1.93750
H	4.01416	4.64111	0.64646
H	4.83148	3.60412	-0.51948
C	3.02144	4.50894	-1.28529
H	2.07032	3.90024	-3.14441
H	3.63820	3.15218	-2.85550
H	3.73941	-1.63777	3.87274
H	3.62756	-3.32863	3.39123
C	5.37974	-2.29240	2.62398
H	6.80201	-0.92283	1.70987
H	5.68212	-0.16050	2.83606
H	-3.52252	-4.05939	-3.67521
H	-5.89486	-1.63175	4.19834
H	-5.78609	-2.29172	2.56817
H	-3.33543	5.17831	-2.43874
H	-1.77924	4.66268	-1.79254
H	3.55638	5.36132	-1.72303
H	2.07800	4.90448	-0.88025
H	5.56409	-3.06694	1.86477

H	6.02029	-2.53455	3.48153
C	-0.06708	1.69440	1.88697
C	0.83718	1.86944	3.10568
H	-1.09517	1.93932	2.17197
H	0.22248	2.37512	1.08078
C	0.78215	3.27732	3.70686
H	0.54942	1.13939	3.87733
H	1.12049	4.03014	2.98346
H	1.41689	3.35987	4.59864
H	-0.24233	3.53749	4.00181
C	-2.19478	1.89272	-2.11399
H	-3.91780	1.40695	-0.93954
H	-2.34053	3.28272	-3.77209
H	-3.89288	2.84268	-3.06684
H	-2.25167	1.00321	-2.75093
H	-1.12912	2.09654	-1.95900
C	2.74538	-2.98872	-3.50654
H	0.86709	-3.80445	-2.88084
H	4.59934	-1.96088	-3.91738
H	2.86877	-3.70539	-4.31485
Co	-0.03031	-0.02643	0.50395
H	1.87037	1.62529	2.84483
H	-0.01984	0.69238	-0.81197
H	-0.06323	0.43709	1.96003
H	-0.04198	-0.82505	1.79607

Polyhydride Exchange Transition State



Zero-point correction=	0.882223 (Hartree/Particle)
Thermal correction to Energy=	0.924888
Thermal correction to Enthalpy=	0.925832
Thermal correction to Gibbs Free Energy=	0.811381
Sum of electronic and zero-point Energies=	-3799.658731
Sum of electronic and thermal Energies=	-3799.616066
Sum of electronic and thermal Enthalpies=	-3799.615122
Sum of electronic and thermal Free Energies=	-3799.729573
Single-point energy (6-311+G(2d,2p)) =	-3801.242086135

Co	0.00000	0.02248	-0.53197
----	---------	---------	----------

P	2.14855	0.13623	-0.21801
P	-2.14855	0.13623	-0.21801
Si	-0.00000	-1.74267	0.85401
C	2.58921	-0.71421	1.35939
C	3.24363	-0.64389	-1.53271
C	2.86126	1.85474	-0.01462
C	-2.58921	-0.71421	1.35939
C	-2.86126	1.85474	-0.01462
C	-3.24363	-0.64389	-1.53271
C	0.00000	-3.57276	0.31208
C	1.60047	-1.57310	1.88455
C	-1.60047	-1.57310	1.88455
C	3.81232	-0.54550	2.02406
H	2.92267	-0.13832	-2.45599
C	2.92171	-2.14183	-1.69148
C	4.76065	-0.43742	-1.36364
H	3.92572	1.72926	0.22888
C	2.76652	2.67359	-1.31643
C	2.19918	2.61141	1.15178
C	-3.81232	-0.54550	2.02406
H	-3.92572	1.72926	0.22888
C	-2.76652	2.67359	-1.31643
C	-2.19918	2.61141	1.15178
H	-2.92267	-0.13832	-2.45599
C	-2.92171	-2.14183	-1.69148
C	-4.76065	-0.43742	-1.36364
H	0.00000	-4.23511	1.18799
H	0.88628	-3.81260	-0.28477
H	-0.88628	-3.81260	-0.28477
C	1.88838	-2.26705	3.06952
C	-1.88838	-2.26705	3.06952
H	4.56798	0.12816	1.63037
C	4.06557	-1.22842	3.21385
H	1.84850	-2.27173	-1.85400
H	3.17105	-2.66509	-0.75726
C	3.70994	-2.77124	-2.84996
C	5.54605	-1.06504	-2.52807
H	5.08562	-0.90303	-0.42360
H	5.00753	0.62803	-1.29486
H	1.71119	2.75850	-1.60560
H	3.27674	2.15773	-2.13901
C	3.36429	4.07888	-1.13988
C	2.80945	4.00977	1.32845
H	1.12664	2.70293	0.94878
H	2.29255	2.03529	2.07956
H	-4.56798	0.12816	1.63037

C	-4.06557	-1.22842	3.21385
H	-3.27674	2.15773	-2.13901
H	-1.71119	2.75850	-1.60560
C	-3.36429	4.07888	-1.13988
C	-2.80945	4.00977	1.32845
H	-2.29255	2.03529	2.07956
H	-1.12664	2.70293	0.94878
H	-1.84850	-2.27173	-1.85400
H	-3.17105	-2.66509	-0.75726
C	-3.70994	-2.77124	-2.84996
C	-5.54605	-1.06504	-2.52807
H	-5.00753	0.62803	-1.29486
H	-5.08562	-0.90302	-0.42361
C	3.10206	-2.09413	3.73578
H	1.15348	-2.95025	3.48897
C	-3.10206	-2.09413	3.73577
H	-1.15348	-2.95025	3.48897
H	5.01032	-1.08419	3.73162
H	3.48115	-3.84274	-2.91333
H	3.37622	-2.32314	-3.79775
C	5.22046	-2.55507	-2.69156
H	5.29598	-0.53409	-3.45874
H	6.62237	-0.92254	-2.36644
H	4.44646	3.99284	-0.95929
H	3.24798	4.64980	-2.06999
C	2.71549	4.82703	0.03264
H	3.86558	3.91650	1.62371
H	2.30172	4.53399	2.14812
H	-5.01032	-1.08419	3.73162
H	-3.24798	4.64980	-2.06999
H	-4.44646	3.99284	-0.95929
C	-2.71549	4.82703	0.03264
H	-2.30172	4.53399	2.14812
H	-3.86558	3.91650	1.62371
H	-3.37622	-2.32314	-3.79775
H	-3.48115	-3.84274	-2.91332
C	-5.22046	-2.55507	-2.69156
H	-6.62237	-0.92254	-2.36644
H	-5.29598	-0.53409	-3.45874
H	3.29698	-2.62939	4.66185
H	-3.29698	-2.62940	4.66185
H	5.76070	-2.97142	-3.55130
H	5.57299	-3.10107	-1.80384
H	3.18480	5.81045	0.16323
H	1.65594	5.01200	-0.19958
H	-3.18480	5.81045	0.16323

H	-1.65594	5.01200	-0.19958
H	-5.57300	-3.10107	-1.80384
H	-5.76070	-2.97142	-3.55130
H	-0.00000	1.38871	-1.13650
H	-0.00000	0.72145	0.78581
H	-0.00000	-1.18776	-1.39706
H	-0.00000	0.41888	-1.96474

Appendix D: Copyright Agreements



Home



Help ▾



Live Chat



Sign in



Create Account



(PSiP)Ni-Catalyzed (E)-Selective Semihydrogenation of Alkynes with Molecular Hydrogen

Author: Dylan J. Hale, Michael J. Ferguson, Laura Turculet

Publication: ACS Catalysis

Publisher: American Chemical Society

Date: Jan 1, 2022

Copyright © 2022, American Chemical Society

PERMISSION/LICENSE IS GRANTED FOR YOUR ORDER AT NO CHARGE

This type of permission/license, instead of the standard Terms and Conditions, is sent to you because no fee is being charged for your order. Please note the following:

- Permission is granted for your request in both print and electronic formats, and translations.
- If figures and/or tables were requested, they may be adapted or used in part.
- Please print this page for your records and send a copy of it to your publisher/graduate school.
- Appropriate credit for the requested material should be given as follows: "Reprinted (adapted) with permission from {COMPLETE REFERENCE CITATION}. Copyright {YEAR} American Chemical Society." Insert appropriate information in place of the capitalized words.
- One-time permission is granted only for the use specified in your RightsLink request. No additional uses are granted (such as derivative works or other editions). For any uses, please submit a new request.

If credit is given to another source for the material you requested from RightsLink, permission must be obtained from that source.

[BACK](#)

[CLOSE WINDOW](#)